University of Reading

Approaches to identifying Dansgaard-Oeschger events in pollen records and quantitative climate reconstructions

Doctor of Philosophy

School of Archaeology, Geography and Environmental Science

Mark Grenville Turner

1 November 2023

Declaration

I confirm that this is my own work and the use of all material from other sources has been properly and fully acknowledged.

Signed

Mark Grenville Turner

Abstract

The warmings associated with Dansgaard-Oeschger cycles (D-Os) during the last glacial were as fast as and of a similar magnitude to expected warming over the 21st century. Identifying these warmings in pollen records objectively may assist understanding of current and future climate change impacts. Identification of D-Os by age alone is hampered by dating uncertainties in both Greenland and pollen core age-depth models, so additional methods of identification are sought. Several statistical techniques applied directly to pollen series from the circum-Mediterranean area do not show D-Os clearly and consistently. An alternative approach using quantitative climate reconstructions made using WA-PLS and fxTWA-PLS is explored. First, the robustness of these methods is evaluated. A training set should sample a climate space which includes the target climate as comprehensively as possible. Actual distributions of taxon abundances along climate gradients often differ from the symmetrical unimodal shape assumed by WA-PLS and fxTWA-PLS, so many taxa are unsuited to a mean-based method, and many are weakly evidenced or even misleading. Calibrations made including and excluding such suspect taxa are indistinguishable, yet provide different reconstructions. Large differences between the balance of abundances in the training set and a fossil core lead to poorly evidenced reconstructions. A proposed alternative reconstruction method avoids a problem identified in WA-PLS (but fxTWA-PLS is unaffected). Potential D-Os are found in reconstructions by their similarity to the signature asymmetrical shape of D-Os warmings in Greenland ('pattern matching'). By combining the age uncertainties of the Greenland GIs and of the core age models, updated to IntCal20, many younger candidate D-Os can be assigned with high plausibility to specific GIs, and some rejected. Many older candidates are highly plausibly D-Os, being similar in number to the expected GIs, but cannot be firmly assigned.

Acknowledgments

I must thank my primary supervisor, Sandy Harrison, for her persistence in trying to mould me into a rigorous and coherent researcher, and my second supervisor, Alison Macleod, for moral support. My late Panel Chair, Jo Clarke, and her successor Steve Robinson, helped cut some Gordian knots.

Many members of Sandy's research group have helped in many ways, but especially Mengmeng Liu, and before her Dongyang Wei.

Without the combined efforts over many years of the palaeoclimate community, and in particular the dedicated souls who recovered all those pollen cores then counted all those grains, this work would have been impossible.

Great credit goes to my family for tolerating nearly 6 years of my effective unavailability, interspersed with unwelcome attempts to explain palaeoclimatic issues.

Contents

Abstract ii

Acknowledgments iii

Contents iv

List of Figures x

List of Tables xx

List of Abbreviations xxii

1 ..... Introduction 1

1.1 Why this is important 1

1.2 Characteristics of Dansgaard-Oeschger events 3

1.3 Palaeoclimate archives which include D-O events 4

1.3.1 Other archives 5

1.3.2 Ice archives 5

1.4 Pollen 9

1.4.1 Pollen as a palaeoclimate archive 9

1.4.2 How plants and pollen represent climate 11

1.4.3 Fossil pollen core age models 13

1.4.4 Underlying assumptions 14

1.4.5 Challenges in climate reconstruction from pollen 14

1.4.6 Registration of rapid climate change in pollen cores 15

1.4.7 Why Mediterranean pollen cores? 16

1.5 Climate reconstruction using pollen 17

1.5.1 Qualitative reconstructions 17

1.5.2 Quantitative climate reconstruction methods 17

1.5.3 Modern Analogue Technique (MAT) 19

1.5.4 Weighted Averaging Partial Least Squares (WA-PLS) 20

1.5.5 Comparisons of different methods 21

1.6 Sources of fossil pollen data 21

1.7 Sources of modern pollen and climate data 21

1.8 Analytical tools 22

1.9 Structure 22

1.10 References 24

2 ..... Identifying D-Os in pollen series 35

2.1 D-Os and pattern matching 35
2.2 Characteristics of D-Os 36
2.2.1 Definitions 36
2.2.2 Kindler temperature series 37
2.3 Consistency of D-O patterns in Kindler series 38
2.3.1 Defining a reference dating point in a D-O 40
2.3.2 Similarity of GI onsets: Superposed Epoch Analysis 40
2.4 Objective pattern matching using Euclidean distance 41
2.4.1 Distance measures 42
2.4.2 Methodological choices in pattern matching 43
2.4.3 Template widths and choices 43
2.4.4 Consistency of treatment 48
2.4.5 Combining distance curves 51
2.4.6 From distance curve to binary choice: D-O or not? 54
2.4.7 Summary of section 2.4: pattern matching 54
2.5 Application of pattern matching to identify D-Os in pollen time series 55
2.5.1 Selection of pollen core data 55
2.5.2 Testing whether sampling resolution affects the recognition of D-Os 57
2.6 Evidence of D-Os in fossil pollen data sets of reduced dimensions 59
2.6.1 Dimension reduction by PCA and DCA 59
2.6.2 Squared Chord Distance (SCD) 62
2.6.3 Grouping taxa 64
2.6.4 Dynamic Time Warping (DTW) 68
2.6.5 Other methods 71
2.7 Summary of chapter 77
2.8 References 79
3 The impact of methodological decisions on climate reconstructions using WA-PLS 81
3.1 Abstract 81
3.2 INTRODUCTION 82
3.3 METHODS 84
3.3.1 Modern climate data 85
3.3.2 Fossil pollen 87
3.3.3 Climate space analysis 87
3.3.4 Application of WA-PLS 88
3.4 RESULTS 89

3.4.1 Impact of choice of training data set 89
3.4.2 Impact of amalgamation of pollen taxa to higher taxonomic levels 93
3.4.3 Impact of number of taxa 93
3.5 DISCUSSION 98
3.6 CONCLUSIONS 104
3.7 ACKNOWLEDGMENTS 106
3.8 AUTHOR CONTRIBUTIONS 106
3.9 SUPPLEMENTARY MATERIAL 106
3.10 REFERENCES 106
3.11 Supplementary Information: The impact of methodological decisions on climate reconstructions using WA-PLS 116
4 ..... Examination of some algorithms in WA-PLS and fxTWA-PLS 140
4.1 WA-PLS 140
4.1.1 Calibration 141
4.1.2 Reconstruction ('prediction') 144
4.2 De-shrinking and reconstruction in WAPLS*rioja* 145
4.2.1 An alternative reconstruction algorithm 146
4.2.2 WAPLS*rioja* regression coefficients and taxon coefficients 147
4.2.3 Alternative method 148
4.2.4 Comparison of the methods 150
4.2.5 Conclusion on the alternative reconstruction method 154
4.2.6 Taxon abundance imbalance between training set and fossil set 155
4.3 Frequency weighted tolerance adjusted WA-PLS (fxTWA-PLS) 156
4.4 (Un)availability of effective optima 159
4.5 Chapter summary 160
4.6 References 161
5 ..... The representation of abundance and its application in the WA-PLS family 162
5.1 Gradient analysis and response patterns 162
5.2 Substitute for true optima 164
5.3 Distilling abundance along a gradient 164
5.3.1 Scatterplots 164
5.3.2 Shapes versus means 166
5.3.3 Simple 1-D case 166
5.3.4 Binning 167

5.3.5 Smoothing 169
5.3.6 Sampling frequency 171
5.4 Results of applying loess curves to abundant taxa 173
5.5 Do abundance distributions represent climate well? 183
5.5.1 Summary: reading the climate 186
5.6 Do abundance distributions support fxTWA-PLS transfer functions? 186
5.6.1 Skewness and tolerance 186
5.6.2 Components higher than 1 187
5.6.3 Mean versus mode 192
5.6.4 Should outliers be removed? 195
5.7 Applying learnings to reconstructions 196
5.7.1 Inclusion/exclusion of taxa in calibration 196
5.7.2 Identifying potentially unreliable taxa important in fossil record 197
5.7.3 Tolerance 200
5.7.4 Taxon characteristics and possible treatment 201
5.7.5 Results of exclusion of taxa from a training set 202
5.7.6 Exclusion of taxa from fossil core reconstructions 205
5.8 Chapter summary 205
6 ..... Identifying DOs in quantitative climate reconstructions 207
6.1 Methods: reconstructions 207
6.1.1 Bioclimatic variables 207
6.1.2 Treatment of suspect materials 207
6.1.3 Component selection 208
6.1.4 Testing the reliability of reconstructions 209
6.2 Results and discussion: reconstructions 211
6.2.1 Reliability of reconstructions 211
6.2.2 Full versus restricted set calibration 212
6.2.3 Modern climate comparison 214
6.2.4 Literature comparison 216
6.3 Methods: pattern matching 219
6.3.1 Choice of base reconstructions for pattern matching 219
6.3.2 Template and other pattern matching parameters 219
6.3.3 Core specific adjustments 221
6.3.4 SEA tests 222
6.3.5 Code availability 222

6.4 Results: pattern matching 222
6.4.1 Impact of filter settings 222
6.4.2 Pattern matching based on gdd reconstructions 224
6.4.3 Plausibility of selected D-O-like points (DOLPs) 225
6.4.4 Base reconstructions other than full set gdd 227
6.4.5 Restricted set gdd reconstructions 230
6.5 Age comparisons 232
6.5.1 Age-depth modelling 233
6.5.2 Matching DOLPS and GIs 233
6.6 Methods: age comparison 233
6.6.1 Consistent updated age-depth models 233
6.6.2 Uncertainty overlaps 235
6.7 Results: age comparisons 236
6.7.1 Potential matches: example 236
6.7.2 Potential matches: 12 cores 238
6.7.3 Events between GI 1 and GI 2 254
6.7.4 Age comparison section summary 255
6.8 Chapter summary 255
References 256
7 ..... Conclusions and Future Work 258
7.1 Pollen, climate, and training sets 258
7.2 WA-PLS and fxTWA-PLS 259
7.3 Reconstructions from fossil cores 262
7.4 Locating D-O-like responses 263
7.4.1 Direct use of pollen records 263
7.4.2 Pattern and age matching 264
7.5 What would make reconstructions better? 266
7.6 Possible future work 266
7.6.1 Improvements to reconstruction methods 266
7.6.2 Regional climate regime 267
7.6.3 Data-model comparisons 268
7.6.4 Matrix Profile 268
7.7 References 269
Appendix A: Mean binned abundances, loess curves and fxt optima of SMPDSv1 taxa with summed fractional abundance > 0.1 (n = 138) 272

Appendix B: Bootstrapped loess curves and fxt optima of SMPDSv1 taxa with summed fractional abundance > 0.1 (n = 138) 291
Appendix C: Reconstructions of tmin and gdd for 16 cores 310
Appendix D: Pattern matching filtering plots for 14 cores 314

List of Figures

Figure 1.1 CO_2 concentrations in ppmv in the Antarctic EPICA Dome C core (Bereiter et al., 2015). Red points are pre-industrial (1850) and current concentrations. Recent Greenland CO_2 does not match the instrumental record, seemingly affected by carbonate dust, and is discounted. Antarctic CO_2 is considered reliable (Brook, 2013) and is used to adjust plant-available moisture. 7
Figure 1.2 Rasmussen et al (2014) Fig 1: δ18O and dust flux records of the long Greenland ice cores GRIP, GISP2, and NGRIP, aligned by multiple match points. The close coincidence of all three provides great confidence in the records. δ18O is essentially a measure of temperature. Dust flux is an index of windiness and of aridity in the source regions of the dust. 8
Figure 1.3 The flow of information and processing in climate reconstruction using WA-PLS 18
Figure 2.1 NGRIP Kindler temperatures °C (red) and $\delta^{18}O_{ice}$ ‰ (blue). 37
Figure 2.2: Kindler temperatures for all GIs, not individually normalised, aligned on common point (x = 100), and mean of all GIs (thick red line), taken from normalised Kindler series. X axis is data points in Kindler series, intervals ~ 20 years, time range ~2750 years). 39
Figure 2.3 GI templates taken from normalised Kindler temperature then individually normalised; vertical lines denote midpoint of rise. Youngest on the left. Samples ~ 20 yrs apart, age range ~ 500 years. Headings are GI numbers. 39
Figure 2.4 SEA: composited mean of Kindler temperatures during GI initiations and early part of GIs for GIs 1 to 20, aligned on midpoint of rise. Script: SEA CoP v2 41
Figure 2.5 Standardised mean of means of Euclidean distances (smmdist) for a reconstructed GDD0 (growing degree days > 0 °C) time series from Lac du Bouchet. Blue line: smmdist. Red points: potential D-O, marking trough points where smmdist < 0.9 and nearest trough point is > ~ 1 ka distant, since D-Os do not occur that close together. .43
Figure 2.6 Pattern matching distance curve applied to detrended, normalised Kindler temperature series from which templates for GIs 1 to 20 were taken. Template width: 10 points younger to 15 older than GI date. Blue line: smmdist curve. Red points are troughs where smmdist < 0.7; these are candidate D-Os. Red figures: GI numbers. Black line: original Kindler series, arbitrarily scaled. 44
Figure 2.7 GI templates extracted from Kindler series from 10 data points younger to 15 older than the GI initiation date. 45
Figure 2.8 Pattern matching distance curve applied to Kindler temperature series from which templates for GIs 1 to 20 were taken. Template width: 37 points younger to 37 older than GI date. Blue line: smmdist curve. Red points are troughs where smmdist < 0.7, and grey where smmdist < 0.75; these are candidate D-Os. Red figures: GI numbers. Black line: original Kindler series, arbitrarily scaled. 45
Figure 2.9 GI templates extracted from Kindler series from 37 data points younger to 37 older than the GI initiation date. 46
Figure 2.10 Pattern matching distance curve applied to Kindler temperature series from which templates for GIs 1 to 20 were taken. Template width: 100 data points younger to 37 older than the GI initiation date. Blue line: smmdist curve. Red points are troughs where smmdist < 0.7, and grey where smmdist < 0.75; these are candidate D-Os. Red figures: GI numbers. Black line: original Kindler series, arbitrarily scaled. 46

Figure 2.11 Templates extracted from Kindler series from 100 data points younger to 37 older than the GI initiation date. 47
Figure 2.12 Detrending of normalised Kindler series. Black: normalised Kindler series; red: loess curve through normalised series, span = 0.1; blue: detrended curve, i.e. normalised less loess curve. 48
Figure 2.13 Upper panel: comparison of SSA residuals (red) and normalised and loess-detrended series for Kindler (black), both normalised. Lower panel: difference between (scaled) SSA residual and loess-based result. 49
Figure 2.14 Templates extracted from Kindler series for GIs 1 to 20. Headings are GI numbers. Orange data points are the rising part of the temperature change, and the vertical line denotes the midpoint of the rise. 50
Figure 2.15 Pattern matching distance curve applied to detrended, normalised Kindler temperature series using a single template (GI 5) . Blue line: smdist curve. Red figures: GI numbers. Black line: original Kindler series, arbitrarily scaled. 52
Figure 2.16 Pattern matching distance curve applied to detrended, normalised Kindler temperature series from which templates for GIs 1 to 20 were taken. Template width: 10 points before to 15 after GI date. Blue line: smmdist curve. Red points are troughs where smmdist < 0.7; these are candidate D-Os. Red figures: GI numbers. Black line: original Kindler series, arbitrarily scaled. 52
Figure 2.17 Pattern matching distance curve applied to detrended, normalised Kindler temperature series from which templates for GIs 1 to 24 were taken. Template width: 10 points before to 15 after GI date. Blue line: mdist = minimum of all template curves. Red figures: GI numbers. Black line: original Kindler series, arbitrarily scaled. 53
Figure 2.18 Age ranges of cores, according to age models provided with core data. 57
Figure 2.19 Sampling intervals of cores; horizontal lines at 250 and 500 years. Script: Sampling resolution all cores v2 58
Figure 2.20 Demonstration of sampling resolution: grey line: Kindler temperature series; coloured lines: Kindler series sampled only where core has samples; ages: ACER age models for cores, GICC05modelext for Kindler. 59
Figure 2.21 First 3 PCA (orange) and DCA (blue) components for Lac du Bouchet, all normalised for comparability. Top to bottom: First, second and third components 61
Figure 2.22 Euclidean distance curves (smmdist) for first 3 PCA components for Lac du Bouchet. Points are troughs (and peaks in case the series is inverted) in the curves. Age is from ACER age model. 62
Figure 2.23 Euclidean distance curves (smmdist) for first 3 DCA components for Lac du Bouchet. Points are trough points in the curves, most similar to templates. Age is from ACER age model. Script: # Pattern hunting DCA allT v2, pbx 62
Figure 2.24 SCD (blue) and rate of change in SCD (orange), both normalised and interpolated to the Kindler timescale, for Lac du Bouchet pollen series. 63
Figure 2.25 Orange line: detrended normalised SCD for Lac du Bouchet, on ACER age model scale; green line: arbitrarily scaled Kindler temperatures, on GICC05modelext chronology, with GI numbers and, below, ± 1 sigma error bar (MCE) in GI age (thick line) and ± 2 sigma error bar (thin line). 64
Figure 2.26 Heatmap of correlation matrix of taxon abundances for Lagaccione for 25 most abundance taxa (96% of total abundance) from 14 ka to 36.2 ka. 66

Figure 2.27 Heatmap of correlation matrix of taxon abundances for Lagaccione for 25 most abundance taxa (96% of total abundance) for age range 9.2 ka to 76.2 ka. 66
Figure 2.28 Stacked area plot of abundances of 10 most abundant PFTs covering 86% of total abundance at Lac du Bouchet over time. 67
Figure 2.29: Stacked area plot of abundances of 4 major PFTs covering 75% of total abundance at Ioannina over time (NB legend colours differ from Figure 2.28). 68
Figure 2.30 Ioannina distance matrix, with custom-built widening window and the path (blue) taken through it to minimise the cumulative distance (represented by colour). 'Reference' is the Kindler series, and 'Query' the interpolated points in the ACER age model for Ioannina, using a quantitative reconstruction of gdd as the time series to be matched. 70
Figure 2.31 Changes in Ioannina sample ages implied by DTW run shown in Figure 2.30 above. 71
Figure 2.32 4-state HMM for Kindler temperature (normalised and detrended), with transition matrix. States: 1 = blue, 2 = green , 3 = orange, 4 = red. 73
Figure 2.33 Lagaccione reconstruction mean: 3 states. Green = clear low peaks, orange = high amplitude peaks and troughs, blue = uneventful, near 0. Table is the heuristically found transition matrix. Script: Hidden Markov test2 73
Figure 2.34 First 20 principal components of SSA applied to the Kindler temperature series, plotted as time series; headings include % variation explained. 74
Figure 2.35 First 20 principal components of SSA applied to the Kindler temperature series, plotted in phase space 75
Figure 2.36 Reconstruction of components of the original series using the following combinations of principal components: F1 = (1,6), F2 = (2,3), F3 = (4,5), F4 = (7,8), F5 = (9,10), F 6 = (16,17). Residual is after these 6 series are extracted. X axis time steps are ~20 year intervals, so x = 5000 represents age = 100 ka; max age ~123ka. 75
Figure 2.37 Comparison of F2 and F3 components calculated by SSA from the Greenland Kindler series (Kindler et al., 2014) (bold) with (Laskar et al., 2004) obliquity and (inverted) precession (thin), both normalised, at 65 °N summer solstice. Script: Taxon metrics\DTW\Rssa v3.R 76
Figure 3.1 Distribution of modern pollen samples in climate space, represented by growing degree days above 0°C (GDD0) and mean temperature of the coldest month (MTCO), sampled by Eastern Mediterranean-Black Sea-Caspian Corridor Biomes (EMBSeCBIO) (labelled EMB), the European Modern Pollen Database (EMPD), and the full SMPDS data sets; SMPDS includes EMB and EMPD. The background shows the climate space for a rectangular area (latitude 29° N to 82° N, longitude 21° W to 150° E) enclosing the SMPDS data set, derived from the Climate Research Unit CRU CL 2.0 database (New et al., 2002). Stars indicate the present climate at the eight fossil sites used as examples. 86
Figure 3.2 Reconstructions of mean temperature of the coldest month (MTCO) during the last glacial period (80,000 to 10,000 calendar years before 2000) using the pollen record from Lake Ioannina, (a) using the Eastern Mediterranean-Black Sea-Caspian Corridor Biomes (EMBSeCBIO) (labelled EMB) and the European Modern Pollen Database (EMPD) as training data sets, and (b) using the full SMPDS data set. The reconstruction spread (±2σ) is obtained by resampling the training set 1,000 times. 90
Figure 3.3 (color online) Relationship between the number of occurrences of a taxon and the standard deviation (SD) of the bootstrapped taxon coefficients. The analysis was made using the full SMPDS data set. 92
Figure 3.4 Impact of reducing the sampling density of the modern training data set on reconstructions of mean temperature of the coldest month (MTCO) during the last glacial period (80,000 to 10,000 calendar years before 2000) using the pollen record from Lake Ioannina. The plots show the impact of randomly removing 70% of the modern samples while preserving the overall

range of climate space (see also Supplementary Figs. 7, 8, and 9) on the MTCO reconstructions compared to reconstructions made with the full SMPDS data set. 94
Figure 3.5 Impact of lack of continuity in sampling showing the effect on standard deviation (SD) of coefficients of the full set of taxa (n = 195), weighted by abundance, of removal of all samples in a given specified range of MTCO from the calibration data set. The red blocks (weighted [Wtd] SD of coefficients if block removed) show the impact of removing a specified number of samples (in this case 646 samples) contiguous in climate space. The low number of cold samples means that the first gap (samples 647–1293) starts at -14.6°C. The abundance-weighted SD using the full sample set (n = 6458) is indicated as a grey line for comparison, and the effect of removal of 646 randomly selected samples is indicated by a red line. 95
Figure 3.6 Climate space diagrams for individual taxa in the Asteroideae, based on Generalized Additive Models (GAMs). The plots are two dimensional representations of a three-dimensional space defined by mean temperature of the coldest month (MTCO, °C), growing degree days above a baseline of 0°C (GDD0, °C day), and the square root of a moisture index (MI, unitless), defined as the ratio of annual precipitation to annual potential evapotranspiration. The three columns show slices of the GAM at the points where GDD0 is 1000°C, 3000°C, and 5000°C day. The plots have been trimmed so that they only represent the sampled areas using convex hulls. The top four rows show the relative abundance on climate space of four of the most important taxa in the Asteroideae, the fifth row shows the relative abundance of Asteroideae where this was explicitly recorded as a taxon in the original pollen counts, and the bottom panels show the relative abundance for the amalgamated taxon Asteroideae, created by summing all named component taxa together. Two scales are used, distinguished by colour: the scale for the top four panels is shown in the Solidago row, and for the bottom two the scale is shown in the Amalgamated row. Supplementary Fig. 13 shows the abundance in the same climate space at the sample level. 97
Figure 3.7 (a) Change in the standard deviation (SD) of the reconstruction of mean temperature of the coldest month (MTCO) as increasing numbers of taxa are used in the Weighted Averaging Partial Least Squares (WA-PLS) regression, taken across the whole time series, and (b) the mean reconstructions at three example points. The specified number of taxa is randomly selected without replacement 100 times, and the WA-PLS reconstruction run. The SD is taken across the 100 runs. Three WA-PLS components were used, but only results with $p < 0.05$ in a random t-test were included in the means and SDs. 100
Figure 4.1 WA-PLS calibration: the weighted averaging and regression process..... 142
Figure 4.2 An example of the result of WA-PLS regression, and the de-shrinking requirement using SMPDS v1 and component 1 for MTCO in °C (temperature of coldest month).
..... 143
Figure 4.3 Observed ranges for Tmin (temperature of coldest month) in SMPDS (black lines and points) and ranges of Component 3 optima provided by WAPLSrioja (red dotted lines and points). Blue lines: maximum and minimum observed Tmin in SMPDS.
..... 146
Figure 4.4 Top panel: alternative (red open circles) v WAPLSrioja (black points) “prediction” of training set for Tmin (temperature of the coldest month) for Comp 3 in °C. Red line = 1:1 slope. Middle panel: difference between them. Lower panel: differences between them as violin plot, with quantiles shown as horizontal lines at 0.025, 0.5 and 0.975
..... 150
Figure 4.5 Upper panel: differences in mean fractional abundances in SMPDS and in Lac du Bouchet core. Lower panel: differences in °C between unmodified (“alternative”) and WAPLSrioja transfer coefficients for Tmin (temperature of the coldest month) for Comp 3, for the 40 most abundant taxa at Lac du Bouchet. 152

Figure 4.6 WAPLSrioja Tmin (temperature of the coldest month) Component 3 for Lac du Bouchet reconstruction (orange); blue = reconstructed by alternative. Red vertical line at 25.05 ka. 153
Figure 4.7 SMPDS fractional abundance of Thalictrum on Tmin (temperature of the coldest month) gradient: points are mean fractional abundance in each 0.5 °C bin; line is loess curve (span = 0.5) with ± 2 SD ribbon 154
Figure 4.8 fxTWA-PLS calibration Step 4: fitted (trial reconstructed) gdd (growing degree days > 0 °C) plotted against observed gdd in SMPDS, Component 4. Red line is 1:1 159
Figure 5.1 Upper panels: Abundance of Picea as fraction of total pollen count in a sample for each SMPDS sample including Picea, against modern climate at that point; gdd = growing degree days above 0 °C, Tmin = mean temperature of the coldest month (MTCO) in °C; sqrt(MI) = square root of Moisture Index, which is actual evapotranspiration / potential evapotranspiration. Orange vertical line: mean climate, weighted by abundance (awm). Lower panels: histograms of counts of samples in SMPDS (n = 6458) showing how densely the gradients are sampled at different points. Orange vertical line: mean climate, weighted by observations.
..... 165
Figure 5.2 Upper panel: Picea fractional abundance along Tmin gradient, with attempted summarisation by loess, span = 0.3 (red curve) and GAM (yellow curve). Orange vertical line: abundance-weighted mean Tmin. Lower panel: occurrence of Picea samples along gradient (binwidth 0.5 °C). 167
Figure 5.3 From the bottom: simple histogram of counts of occurrences of Picea in SMPDS, binned at 0.5 °C intervals; sums of fractional abundances in bins; means of fractional abundances in bins. Orange vertical line: abundance-weighted mean Tmin.
..... 168
Figure 5.4 Distribution of abundances of Picea in each bin: lower panel: mean binned abundance (fxab); upper panel, boxplots of distribution, on log scale. X axes not precisely aligned.
..... 169
Figure 5.5 Response curves of 9 abundant taxa in the SMPDS by abundance to Tmin (MTCO, temperature of the coldest month), using different loess spans. No weighting is applied. Numbers in headings are respectively the sum of fractional abundances of the taxon and the number of occurrences of the taxon in SMPDS (number of SMPDS samples = sum of fractional abundances = 6458). Points: fxabf (fractional mean binned abundance). Blue line: loess curve, span = 0.3; orange line: loess curve, span = 0.5; green line: loess curve, span = 0.75.
..... 171
Figure 5.6 Response curves of 9 abundant taxa in the SMPDS by abundance to Tmin (MTCO), using different loess weightings: span = 0.5 in all cases. Numbers in headings are respectively the sum of fractional abundances of the taxon and the number of occurrences of the taxon in SMPDS (number of SMPDS samples = sum of fractional abundances = 6458). Points: fxabf (mean binned fractional abundance). Blue line: loess curve, no weighting; orange line: loess curve, weighted by square root of frequency; green line: loess curve, weighted by frequency.
..... 172
Figure 5.7 Response curves of 9 abundant taxa in the SMPDS by abundance to Tmin (MTCO), using loess weighting = 1/square root of frequency, and span = 0.5. Numbers in headings are respectively the sum of fractional abundances of the taxon and the number of occurrences of the taxon in SMPDS (number of SMPDS samples = sum of fractional abundances = 6458). Points: fxabf (mean binned fractional abundance). Blue line: loess curve; ribbon = ± 2 SD provided by loess calculation.
..... 173
Figure 5.8 Response curves of top 24 taxa in the SMPDS by abundance to Tmin (MTCO). Numbers in taxon headings are respectively the sum of fractional abundances of the taxon and the number of

occurrences of the taxon in SMPDS (number of SMPDS samples and sum of fractional abundances = 6458). Points: fxabf (mean fractional binned abundance). Blue lines: loess curve, span = 0.3; orange lines; loess curve, span 0.5; grey lines: loess curve, span = 0.75. Vertical line: fxTWA-PLS abundance-weighted mean for component 1 (awm). 176
Figure 5.9 Response curves of top 24 taxa in the SMPDS by abundance to gdd. Numbers in taxon headings are respectively the sum of fractional abundances of the taxon and the number of occurrences of the taxon in SMPDS (number of SMPDS samples and sum of fractional abundances = 6458). Points: fxabf (mean fractional binned abundance). Blue lines: loess curve, span = 0.3; orange lines; loess curve, span 0.5; grey lines: loess curve, span = 0.75. . Vertical line: fxTWA-PLS abundance-weighted mean for component 1 (awm). 177
Figure 5.10 Response curves of top 24 taxa in the SMPDS by abundance to sqrt(Moisture Index). Numbers in taxon headings are respectively the sum of fractional abundances of the taxon and the number of occurrences of the taxon in SMPDS (number of SMPDS samples and sum of fractional abundances = 6458). Points: fxabf (mean fractional binned abundance). Blue lines: loess curve, span = 0.3; orange lines; loess curve, span 0.5; grey lines: loess curve, span = 0.75. Vertical line: fxTWA-PLS abundance-weighted mean for component 1 (awm). ... 178
Figure 5.11 Bootstrapped response curves of top 24 taxa in the SMPDS by abundance to Tmin (MTCO, temperature of coldest month). Numbers in taxon headings are respectively the sum of fractional abundances of the taxon and the number of occurrences of the taxon in SMPDS (number of SMPDS samples = sum of fractional abundances = 6458). Points: fxabf (mean fractional binned abundance of SMPDS set). Black line: loess curve, span = 0.5, weighting 1/square root of frequency. Blue ribbon: mean ± 2 SD of loess curve resulting from bootstrapping.
..... 180
Figure 5.12 Bootstrapped response curves of top 24 taxa in the SMPDS by abundance to gdd (growing degree days > 0 °C). Numbers in taxon headings are respectively the sum of fractional abundances of the taxon and the number of occurrences of the taxon in SMPDS (number of SMPDS samples = sum of fractional abundances = 6458). Points: fxabf (mean fractional binned abundance of SMPDS set). Black line: loess curve, span = 0.5, weighting 1/square root of frequency. Blue ribbon: mean ± 2 SD of loess curve resulting from bootstrapping.
..... 181
Figure 5.13 Bootstrapped response curves of top 24 taxa in the SMPDS by abundance to rtmi (square root of Moisture Index). Numbers in taxon headings are respectively the sum of fractional abundances of the taxon and the number of occurrences of the taxon in SMPDS (number of SMPDS samples = sum of fractional abundances = 6458). Points: fxabf (mean fractional binned abundance of SMPDS set). Black line: loess curve, span = 0.5, weighting 1/square root of frequency. Blue ribbon: mean ± 2 SD of loess curve resulting from bootstrapping.
..... 182
Figure 5.14 Red open circles: scaled Artemisia mean binned abundance on the rtmi (square root of Moisture Index) gradient by latitude band in degrees N, with blue loess curves span = 0.5, plotted against background (grey histogram) of SMPDS samples in the latitude band.
..... 185
Figure 5.15 (Scaled) Artemisia mean binned abundance on the gdd gradient by latitude band in degrees N (red points), with blue loess curves span = 0.5, plotted against background (grey histogram) of SMPDS samples in the latitude band. 185
Figure 5.16 Spread of tolerance factor t for all taxa in SMPDS with respect to Tmin (temperature of the coldest month in °C), gdd (growing degree days > 0 °C), and rtmi (square root of Moisture Index), provided by fxTWA-PLS for Components 1 (blue), 2 (orange) and 3 (purple).
..... 187

Figure 5.17 6 examples of taxa where the Component 2 Tmin increment is effectively zero in WA-PLSrioja. Histogram is residuals from previous regression, i.e. environmental vector for this component, for the samples which include this taxon; points are absolute values of product of abundance and environment i.e. elements contributing to coefficient increment; size of points is proportional to abundance; red line is resulting coefficient increment; movement is distance of red line from zero. 189
Figure 5.18 6 examples of taxa where Component 2 Tmin increment becomes colder. Histogram is residuals from previous regression, i.e. environmental vector for this component, for the samples which include this taxon; points are absolute values of product of abundance and environment i.e. elements contributing to coefficient increment; size of points is proportional to abundance; red line is resulting coefficient increment; movement is distance of red line from zero. 190
Figure 5.19 Response curves of top 24 taxa in the SMPDS by abundance to Tmin. Numbers in taxon headings are respectively the sum of fractional abundances of the taxon and the number of occurrences of the taxon in SMPDS (number of SMPDS samples = sum of fractional abundances = 6458). Blue points: fxabf (mean fractional binned abundance of SMPDS set). Orange line: loess curve, span = 0.5, weighting 1/square root of frequency. Red points: apparent modes; blue large points: 'best' mode (largest > 1800). Vertical line: fxTWA-PLS abundance-weighted mean for component 1 (awm). 193
Figure 5.20 Abundance of Artemisia (red points, size ~ abundance) in a 2D rtmi/gdd climate space. Background contours are density of SMPDS samples in the climate space. Purple points: fractional abundance> 0.75. 195
Figure 5.21 Fractional mean binned abundances (fxabf) of Artemisia along gdd gradient. Black open points: all Artemisia samples; grey line and pink ribbon mean: loess span = 0.5 curve, and bootstrapped ±2 SD limits. Red open points: Artemisia samples excluding samples with fractional abundance > 0.75; black line and blue ribbon: mean loess span = 0.5 curve, and bootstrapped ±2 SD limits. 196
Figure 5.22 Summed fractional abundances of taxa in the SMPDS in descending order. Top few taxa labelled. 198
Figure 5.23 Log/log plot of summed fractional abundance (as fraction of total abundance in the set) of SMPDS and a set of fossil cores (Villarquemado, Lac_du_Bouchet, Les_Echets_redone_2, Lagaccione, Stracciacappa, Castiglione, Lago_Grande_di_Monticchio, Ioannina, Lake_Xinias, Megali_Limni, Dead_Sea). Taxa where fossil abundance is greater than in SMPDS are highlighted in red and labelled. Point size proportional to $1/t^2$ for Tmin (temperature of the coldest month). Red line: 1:1. 198
Figure 5.24 Summed fractional abundance (as fraction of total abundance in the set) of SMPDS and a set of fossil cores (Villarquemado, Lac_du_Bouchet, Les_Echets_redone_2, Lagaccione, Stracciacappa, Castiglione, Lago_Grande_di_Monticchio, Ioannina, Lake_Xinias, Megali_Limni, Dead_Sea). Taxa where fossil abundance is greater than in SMPDS highlighted in red and labelled. Point size proportional to $1/t^2$ for Tmin (temperature of the coldest month). Red line: 1:1. 199
Figure 5.25 Differences in distributions on log scale of fractional abundances in samples between SMPDS (coloured, unfilled) and fossil set (dark grey with orange fill) for taxa with high abundance in SMPDS. 200
Figure 5.26 Left panel: fitted versus observed calibration result for gdd using full SMPDS set, Component 4. Right panel: using reduced set. 203
Figure 5.27 Reconstruction of gdd at Lac du Bouchet. Blue: using full SMPDS set of taxa (Component 4); orange: using restricted set (Component 3). 204

Figure 6.1 Comparison between gdd (growing degree days > 0 °C) reconstructed using the full set of 195 SMDS taxa (blue line) and using the restricted set (orange line) for the 16 selected cores. 213
Figure 6.2 Castiglione fraction of indeterminate pollen grains, up to hiatus. Script: Castiglione indeterminates 214
Figure 6.3 Bootstrapped (x 100) full SMPDS set reconstructions (ribbon width is ± 2 SD) for Tmin (temperature of the coldest month in °C) for the Holocene intervals (11.7 ka onwards) of the selected set of 16 cores (4 have no Holocene presence). Green points: CRU CL 2.0 modern climate at the site; pink open triangles: WorldClim modern climate at the site. 215
Figure 6.4 Bootstrapped (x 100) full SMPDS set reconstructions (ribbon width is ± 2 SD) for gdd (growing degree days > 0 °C) for the Holocene intervals of the selected set of 16 cores (4 have no Holocene presence). Green points: CRU CL 2.0 modern climate at the site; pink open triangles: WorldClim modern climate at the site. 216
Figure 6.5 Comparison of (Allen et al., 1999; Allen and Huntley, 2000) response surface reconstructions with those made using fxTWA-PLS full SMPDS for GDD (GDD0 for fxTWA-PLS, GDD5 for A&H). Blue: Allen reconstructions. Orange: fxTWA-PLS reconstructions. Source: Monty comparison.xlsx 217
Figure 6.6 Part of Fig 3 from (Parnell et al. (2016): Monticchio BClim reconstructions of GDD5 and MTCO. “The blue areas represent the 95% credible regions of the slice clouds whilst the red ribbons represent the 95% confidence intervals for each time grid point on a centennial time grid. Darker regions indicate the 75% and 50% regions.” 218
Figure 6.7 Cartoon showing the minimum number of physical samples defining a DOLP and a warm interval in a quantitative reconstruction. Orange point is DOLP at midpoint of rise, which except by accident is not a physical sample. The template-width window is the window which has identified the DOLP (interpolated points are in reality denser than shown, with 26 in the normal template-width window). 221
Figure 6.8 Pattern matching filtering process applied to gdd (growing degree days > 0 °C) reconstruction at Castiglione. Top panel: gdd reconstruction; red points = finally accepted DOLPs; blue points = rejected DOLPs; red segments of reconstruction = warm intervals following all potential DOLPs. Second panel: ED curve with troughs falling below threshold (ED = 0.75) shown as points, size inverse to ED. Third panel: increase in gdd from DOLP value to peak as black points, size inverse to ED; orange points = DOLPs already rejected on grounds of ED; red line: threshold for rise (rfilta) = 200 degree days. Fourth panel: area-under-the-curve traced by warm interval; orange points = DOLPs already rejected on ground of ED; blue line: threshold for area (afilta) = 1000. Fifth panel: count of physical samples defining the shape of the warm interval. Sixth panel: mean Hill’s N.2 for warm interval; red line = threshold for N.2 = 2 (n2filt). Bottom panel: repeat of gdd reconstruction with blue points indicating physical samples, with ±2 SD uncertainty added; red vertical lines mark finally accepted DOLPs, grey vertical lines mark rejected DOLPs; numbers are number of finally accepted DOLPs / number of GIs in apparent age range; numbers in triangles are GI numbers; GI dates on GICC05modelext scale. In all other panels, age is ACER age model. 223
Figure 6.9 As lower panel in Figure 6.8, up to 63 ka, with ±2 SD uncertainty added. 224
Figure 6.10 Superposed Epoch Analysis of potential warm intervals identified in the GDD0 (growing degree days > 0 °C) reconstructions made with full SMPDS. The centre-points of the rises (DOLPs) are aligned on year 0. The p value scale indicates the probability that this mean bin value arose by chance, and applies to all panels. 226

Figure 6.11 Superposed Epoch Analysis of potential warm intervals identified in the MTCO (tmin, temperature of the coldest month) reconstructions made with full SMPDS, using DOLP locations found using gdd as base reconstruction. The centre-points of the rises (DOLP) are aligned on year 0. The p value scale indicates the probability that this mean bin value arose by chance, and applies to all panels. 227
Figure 6.12 EDs (smmdist, standardised mean of mean distance) and DOLPs using full SMPDS set for 14 cores. Blue: using gdd (growing degree days > 0 °C) as base reconstruction; blue line = smmdist, blue points are final accepted DOLPs and open points on same line rejected DOLPs. Orange: using tmin (temperature of coldest month, °C) as base reconstruction; orange line = smmdist, orange points are final accepted DOLPs and open points on same line rejected DOLPs. Age is ACER or original given age. 229
Figure 6.13 Superposed Epoch Analysis of potential warm intervals identified in the MTCO (tmin, temperature of the coldest month) reconstructions made with full SMPDS, using DOLP locations found using MTCO as base reconstruction. The centre-points of the rises (DOLP) are aligned on year 0. The p value scale indicates the probability that this mean bin value arose by chance, and applies to all panels. 230
Figure 6.14 Blue line: smmdist using gdd (growing degree days > 0 °C) reconstruction for Lac du Bouchet using full SMPDS set as base reconstruction; blue points are final accepted DOLPs and open points on same line rejected DOLPs. Orange line: smmdist using restricted taxon set gdd as base reconstruction; orange points are final accepted DOLPs and open points on same line rejected DOLPs. Core age is ACER or original age. 232
Figure 6.15 Potential matches between DOLPs, using gdd reconstruction and the full SMPDS set, and GIs for Lagaccione. Main panel: age model; vertical red lines mark accepted DOLPs, with sequential identifying numbers; blue horizontal lines are GICC05modelext ages of GIs (less 50 years), red points are intersections of DOLP and rbacon age model median; blue ribbon: central line is rbacon age model median value, with 75% (darker) and (lighter) 95% uncertainties; green points and error bars are core dating points with uncertainties; blue points and error bars are ages and MCEs of those GIs which overlap with uncertainty of DOLP age. Orange curve: ACER age model. Purple circles with cross: 'events' determining ACER age model. Lower panel: gdd reconstruction for Lagaccione using full SMPDS taxon set, with accepted DOLPs marked by orange points; red segments of reconstruction are warm intervals; blue points are rejected DOLPs; vertical purple lines: 'event' locations in ACER age model. Vertical panel: Kindler Greenland temperature in °C on GICC05modelext scale, aligned with main panel. 236
Figure 6.16 Potential matches for Navarres between DOLPs using gdd reconstruction and the full SMPDS set, and GIs. Main panel: age model; vertical red lines mark accepted DOLP, with sequential identifying numbers; blue horizontal lines are GICC05modelext ages of GIs (less 50 years), red points are intersections of DOLP and rbacon age model median; blue ribbon: central line is rbacon age model median value, with 75% (darker) and (lighter) 95% uncertainties; green points and error bars are core dating points with uncertainties; blue points and error bars are ages and MCEs of those GIs which overlap with uncertainty of DOLP age. Grey ribbon: model extrapolation beyond last effective dating point. Orange curve: ACER age model. Lower panel: gdd reconstruction for Lagaccione using full SMPDS taxon set, with accepted DOLPs marked by orange points; red segments of reconstruction are warm intervals; blue points are rejected DOLPs. Vertical panel: Kindler Greenland temperature in °C on GICC05modelext scale, aligned with main panel. 239
Figure 6.17 Lac du Bouchet; otherwise as caption for Figure 6.16. 240
Figure 6.18 Les Echets: otherwise as caption for Figure 6.16. 241
Figure 6.19 Castiglione: otherwise as caption for Figure 6.16. 243
Figure 6.20 Stracciacappa: otherwise as caption for Figure 6.16. 244

Figure 6.21 Lago Grande di Monticchio: no rbacon model exists and the original age model (orange line) has no uncertainties. Otherwise as caption for Figure 6.16. 245
Figure 6.22 Ioannina: otherwise as caption for Figure 6.16. 246
Figure 6.23 Lake Xinias: otherwise as caption for Figure 6.16. 247
Figure 6.24 Megali Limni full core length: purple line: original age model; otherwise as caption for Figure 6.16. 248
Figure 6.25 Megali Limni, well dated section only: purple line: original age model; otherwise as caption for Figure 6.16. Script: Trial id GIs v4 ML 249
Figure 6.26 Dead Sea: Orange line is original, not ACER, model; otherwise as caption for Figure 6.16. Inset: locations of starts of hiatus marked by red points. 250
Figure 6.27 Ghab: otherwise as caption for Figure 6.16. 251
Figure 6.28 Zeribar: otherwise as caption for Figure 6.16. 252
Figure 6.29 Kindler series (black line) and NGRIP $\delta^{18}O_{ice}$ ‰ (blue line) with YD and GIs 1 and 2 (blue triangles). Red triangles mark small excursions picked up by pattern matching applied to the Kindler series. 254

List of Tables

Table 2-1 Pollen cores. 56
Table 2-2: % variation explained by PCA components at Lac du Bouchet 60
Table 3-1 Weighted Averaging Partial Least Squares (WA-PLS) model parameters for the reconstructions of mean temperature of the coldest month (MTCO, 0°C), growing degree days above a baseline of 0°C (GDD0, °day) and the square root of Moisture Index (√MI, unitless) using the Eastern Mediterranean-Black Sea-Caspian Corridor Biomes (EMBSeCBIO) (EMB), the European Modern Pollen Database (EMPD), and full SMPDS as training data sets, including the cross-validated r2, number of significant components ($p < 0.05$), root mean square error (RMSE), maximum bias, and number of samples. Supplementary Table 2 provides a complete list of WA-PLS model parameters for all data sets. 92
Table 3-2 Weighted Averaging Partial Least Squares (WA-PLS) model parameters for the reconstructions of mean temperature of the coldest month (MTCO), growing degree days above zero (GDD0) and the square root of Moisture Index (√MI) at Lake Ioannina using the full SMPDS data set and a version of this data set randomly reduced by 70% for the training data sets, including the cross-validated r2, number of significant components ($p < 0.05$), root mean square error (RMSE), maximum bias, and number of samples. Because the reduced sets are randomly chosen, different runs give different results; the standard deviations across 10 runs are given. The number of components is given as, for example, 2(7) meaning 7 runs allowed 2 significant components to be extracted; the balance allowed 3. 95
Table 3-3 Examples of the impact of amalgamating taxa to higher taxonomic levels on the bootstrapped standard deviation (SD) of transfer coefficients for mean temperature of the coldest month (MTCO). The mean SD of the component taxa (column 3) is weighted by abundance. Additional information on the component taxa and the transfer coefficients (climate optima) identified for the component taxa and the amalgamated taxon is given in Supplementary Tables 4 and 5. 99
Table 3-4 Checklist of issues, steps to identify them, and some potential solutions. 101
Table 4-1 WA-PLS calibration algorithms in ter Braak and Juggins and in rioja WAPLS() function. 143
Table 4-2 WA-PLS slope coefficient notation 148
Table 4-3 WAPLSrioja and alternative 'prediction' algorithms 149
Table 4-4 WAPLSrioja cross-validation and random t-test results reconstructing Tmin (temperature of the coldest month) 151
Table 4-5 Alternative leave-one-out cross-validation and random t test result for Tmin (temperature of the coldest month), simple linear regression 151
Table 4-6 Alternative leave-one-out cross-validation and random t test result for Tmin (temperature of the coldest month), multiple linear regression on incremental reconstructions. 151
Table 4-7 Different contributions of taxa to Tmin at 25.05 ka under WAPLSrioja and alternative methods 153
Table 4-8 fxTWA-PLS summary algorithms 157
Table 5-1 Thalictrum WA-PLS optima increments for Tmin °C (temperature of the coldest month) . 191
Table 5-2 Most obvious mode, abundance-weighted mean found by fxTWA-PLS, and the difference between them for gdd (growing degree days > 0 °C). 194

Table 5-3 Top 14 by SMPDS abundances. Fossil abundances greater than SMPDS abundances in bold red. t greater than the SMPDS mean and $1/t^2$ less than the SMPDS mean in bold. 201
Table 5-4 Characteristics of taxon abundance distributions, identification, effects, and possible responses. Grey boxes: condition not affected by characteristic. 202
Table 5-5 Taxa to exclude from test calibration 202
Table 5-6 Random t-test results for full and reduced SMPDS taxon set for gdd. 203
Table 6-1 Results of random t-test on leave-one-out cross-validation of fxTWA-PLS calibration for SMPDS full set. b0 , b1, b0.se, b .se are the intercept, slope, standard error of the intercept, and standard error of the slope of the regression, respectively. Selected components are in bold. 208
Table 6-2 Results of random t-test on leave-one-out cross-validation of fxTWA-PLS calibration for first 4 components of restricted set. b0 , b1, b0.se, b .se are the intercept, slope, standard error of the intercept, and standard error of the slope of the regression, respectively. Selected components are in bold. 209
Table 6-3 Settings applied to 14 cores, the age ranges of the cores, the number of GIs in those ranges, and the number of DOLPs accepted. 225
Table 6-4 Accumulation rates and thicknesses for preferred rbacon age models. 235
Table 6-5 'Event' based dating points at Lagaccione using GICC05modelext chronology 238
Table 6-6 Matches between DOLP numbers and GI numbers; 'X' denotes rejected DOLP; 'rej' denotes previously rejected DOLP now accepted; beyond the point where specific assignments are made, counts of available DOLPs and available GIs are given. 'GIs missed' are not registered in the core. Source: DOLPS v GIs.xlsx 253
Table 7-1 Characteristics of taxon abundance distributions, identification, effects, and possible responses. Grey boxes: condition not affected by characteristic (copy of Table 5-4). 262

List of Abbreviations

AMOC	Atlantic Meridional Overturning Circulation
AP	Arboreal pollen
awm	Abundance-weighted mean
DCA	Detrended Correspondence Analysis
D-O	Dansgaard-Oeschger (event)
DOLP	D-O-like point
DTW	Dynamic Time Warping
ED	Euclidean distance
fxTWA-PLS	Frequency-adjusted tolerance weighted weighted averaging partial least squares
GAM	Generalised Additive Model
GISP2	Greenland Ice Sheet Project 2 (core)
GRIP	Greenland Ice-core Project (core)
gdd/GDD0	Growing degree days above 0 °C
GI	Greenland Interstadial
GS	Greenland Stadial
GWR	Geographically weighted regression
HMM	Hidden Markov Model
MAT	Modern Analogue Technique
MI	Moisture index (actual divided by potential evaporation)
MTCO	Mean temperature of coldest month (here synonymous with Tmin and tmin)
NAP	Non-arboreal pollen
NEEM	North Greenland Eemian Ice Drilling (core)
NGRIP	North Greenland Ice-core Project (core)
PCA	Principal Components Analysis
PFT	Plant Functional Type
rtmi	Root mean square of Moisture index (MI)
SCD	Squared Chord Distance
SEA	Superposed Epoch Analysis

smmdist	Standardised mean of mean distances
SSA	Singular Spectrum Analysis
SST	Sea surface temperature
Tmin/tmin	Mean temperature of coldest month (here synonymous with MTCO)
WA-PLS	Weighted averaging partial least squares

1 Introduction

This thesis examines ways of identifying Dansgaard-Oeschger cycles in glacial pollen records extracted from lacustrine cores from the circum-Mediterranean region.

1.1 Why this is important

The impact of current climate change on vegetation has raised concerns that some terrestrial species may suffer extinctions. This is strongly expressed in the Climate Change 2014 Synthesis Report (Pachauri, Mayer and Intergovernmental Panel on Climate Change, 2015) Figure 2.5a, where even with a future rate of change in temperature as low as < 0.01 $^{o}C\ yr^{-1}$, which is less than that assumed in RCP2.6, the comment is made "Most trees and herbs can't keep up" (Fig 2.5, p 66). The rate of temperature change translates to a rate of poleward movement of isotherms, and the assumption made is that plants cannot migrate fast enough in response to avoid extinctions.

The IPCC comment is made plausible because there is no example in the instrumental or historical record of the impact on vegetation of a warming event of the scale and speed of current and projected climate change. Observations of current geospatial climate change and apparent changes in vegetation ranges cover only a few decades. Furthermore, climate velocity - the rate and direction of movement of constant temperature zones - is not a straightforward measure: the chosen spatial scale strongly influences its magnitude and direction, because of the influence of local topography, so studies can differ widely in the climate velocity given and their interpretations of its causal relationship with vegetation ranges (Loarie *et al.*, 2009; Dobrowski *et al.*, 2013; Dobrowski and Parks, 2016; Brito-Morales *et al.*, 2018; Burrows and Schoeman, no date).

During the glacial period, however, multiple rapid warmings occurred, and the response of vegetation to these warmings can improve the understanding of likely future vegetation behaviour. While these repeated events, associated with Dansgaard-Oeschger cycles (D-Os), were not caused by CO_2 increase as is

current warming, and started from a much colder base, they were of similar amplitude and speed to current and projected warming. They are evidenced in the Greenland ice cores (e.g. Rasmussen *et al.*, 2014) but also at many other sites and in many materials. There are multiple examples in glacial pollen records of repeated alternations between cold-climate vegetation such as grasslands and more forested warm-climate landscapes during the last glacial period, and these are usually considered to be responses to D-Os (e.g. Fletcher *et al.*, 2010). This behaviour suggests that under climate change plants are migrating repeatedly to suitable environments, not suffering wholesale extinction. There is only one known extinction of a tree in the Late Quaternary – *Picea critchfieldii* (Jackson and Weng, 1999) – and that occurred during the deglaciation.

Evidently during the glacial period processes were operating that are not captured in the modern observations which lead to the IPCC comment. Long distance transport mechanisms must exist to account for observed rates of range expansion in the past, for instance carriage by birds as food, in their guts or on their surfaces, or by water. This conclusion is described in Reid's paradox, which originated in the realisation that the rate of northward spread of oak trees at the end of the last glacial in Britain was far in excess of that which can reasonably be explained by the extension of the range by seed fall and local transport at the forest edge (Reid, 1899; Clark *et al.*, 1998).

The terrestrial evidence of changes in the glacial period can be interpreted qualitatively, for instance using pollen to describe changes in vegetation and the implied climate changes, and this is the most frequent style of description associated with a pollen core (e.g. Beaulieu and Reille, 1984; de Beaulieu, J.-L. and Reille, M.:, 1992; Pèrez-Obiol and Julià, 1994; Magri, 1999; Tzedakis, Hooghiemstra and Pälike, 2006; Djamali *et al.*, 2008; Margari *et al.*, 2009; Di Rita, Anzidei and Magri, 2013; Fletcher *et al.*, 2010). Terrestrial pollen can also be used to create quantitative reconstructions, providing time series of numerical climate values, but this is rarer (e.g. Allen and Huntley, 2009; Wei *et al.*, 2019).

1.2 Characteristics of Dansgaard-Oeschger events

Dansgaard-Oeschger (D-O) events are abrupt large-magnitude warmings registered in Greenland ice cores (Dansgaard et al, 1993; Huber *et al.*, 2006; Steffensen *et al.*, 2008; Rasmussen *et al.*, 2014) that occurred multiple times during the last glacial period (115 ka to 11.7 ka) and probably in previous glacials (Rousseau *et al.*, 2020).

As evidenced in the Greenland ice cores, during D-O events a cold period is ended by a phase of rapid warming over an interval of 10-200 years which varies in magnitude from 6 to 15 ^{o}C (Huber *et al.*, 2006; Kindler *et al.*, 2014a; Rasmussen *et al.*, 2014). This is followed by a period of decline in temperature, varying in duration from a few to many centuries, often ending with a sharper decline to a new cold state which then shows little variation over time. Warm periods are referred to interstadials (Greenland Interstadials, GIs) and cold periods as Greenland stadials (GSs). In addition to warmer conditions, interstadials are characterised by an increase in snow accumulation rate in Greenland, implying locally greater precipitation, and a reduction by orders of magnitude in the dust flux to the ice surface, implying lower wind speeds and/or a change in the atmospheric circulation.

The mechanism which triggers the abrupt warming at the beginning of a D-O and controls the progress of the interstadial is the subject of active research. Climate models have not to date succeeded consistently in replicating D-Os (Malmierca-Vallet *et al.*, 2023).

D-O events relate to changes in the transport to the North Atlantic of heat in the ocean and transferred from the ocean to the atmosphere. An index of this is the change in the strength and poleward extent of the Atlantic Meridional Overturning Circulation (AMOC). The salty surface branch of the AMOC extends to the north of the Greenland-Scotland ridge today, and having given up its heat to the atmosphere sinks there owing to its density to form North Atlantic Deep Water (NADW); this sinking is often interpreted as a driver of the AMOC (Broecker, 1992).

One explanation for abrupt warmings is as follows. During stadials, extensive sea-ice cover in the North Atlantic suppresses the release of heat and moisture from the ocean to the atmosphere, and the formation

of NADW; the AMOC is unable to transport heat very far into the North Atlantic (Broecker, 1992; Rahmstorf, 2002). The cause of the rapid warming event is a sudden reduction in sea-ice cover when a slow build-up of underlying warm surface water reaches the point it can melt the ice, causing a rapid release of heat and moisture to the atmosphere and the strengthening and poleward extension of the AMOC (Gildor and Tziperman, 2003; Dokken *et al.*, 2013; Lynch-Stieglitz, 2017; Sime, Hopcroft and Rhodes, 2019; Malmierca-Vallet *et al.*, 2023).

This is only one possible explanation; many different mechanisms affecting the AMOC have been invoked, including sea-ice fluctuations linked to ice-shelf growth and decay (Alley, Anandakrishnan and Jung, 2001; Petersen, Schrag and Clark, 2013; Boers, Ghil and Rousseau, 2018), shifts in atmospheric circulation associated with changes in the northern hemisphere ice sheets (Banderas *et al.*, 2015; Seager and Battisti, 2007) or changes in tropical climate modes (Clement, Cane and Seager, 2001; Seager and Battisti, 2007).

D-O events are registered strongly in the North Atlantic both in ice cores and marine sediment cores, but their effects are transmitted globally (Leuschner and Sirocko, 2000; Voelker, 2002; Harrison and Sánchez Goñi, 2010; Corrick *et al.*, 2020), and are clear in well-dated speleothem records in, for instance, China (e.g. Wang *et al.*, 2001). Vegetation records suggest that they are expressed through temperature changes in the extratropics and changes in moisture in the tropics (Harrison and Sánchez Goñi, 2010).

D-O events have been identified at many sites in the Mediterranean region, including from speleothem isotopic records (Corrick *et al.*, 2020), marine (Sánchez Goñi *et al.*, 2018) and terrestrial (Fletcher *et al.*, 2010) pollen records.

1.3 Palaeoclimate archives which include D-O events

Many natural archives and materials have been interpreted as evidence of past climate. The most significant for the purposes of this thesis are the Greenland ice cores, because they provide the most complete record of D-O cycles, and pollen, as the source of terrestrial information. Other major archives are briefly surveyed first.

1.3.1 Other archives

Oxygen stable isotopes incorporated in the $CaCO_3$ of foraminifera in marine cores demonstrate glacial/interglacial, orbital scale, and sometimes finer-resolution changes in the volume of the oceans, and hence of ice on land, and provide evidence of benthic and sea surface temperatures (Emiliani, 1955; Shackleton, 1987; Lisiecki and Raymo, 2005).

Loess sequences in China and Europe exhibit glacial/interglacial and DO cycles by the alternation of loess and palaeosol horizons, in which palaeosols represent warm intervals with sufficiently abundant vegetation to permit the development of soils (e.g. Antoine *et al.*, 2016; Tang, Du and Liu, 2017; Rousseau *et al.*, 2020).

Speleothems are calcium carbonate deposits in caves. Examples from across the world show changes in the oxygen stable isotope ratio ($\delta^{18}O_{calc}$) in $CaCO_3$ which clearly represent responses to the same climate changes as Greenland events, within dating error (Wang *et al.*, 2001; Genty *et al.*, 2005). Variations in $\delta^{18}O_{calc}$ denote changes in climate, principally temperature and precipitation. Partitioning the signal between the two is challenging, since many other factors than the isotopic content of meteoric water affect the result, such as the conditions in the ground through which the water has passed and the temperature in the cave (McDermott, 2004). Speleothems are often discontinuously deposited, and deposition may cease in cold conditions such as GSs. They typically contain uranium, so uranium-series disequilibrium radiometric dating is often available, which is more precise than ^{14}C, and has a useful age range to ~ 500 ka (Bradley, 2015).

1.3.2 Ice archives

Ice cores reaching back over 100 ka have been recovered from Greenland and reaching much further back from Antarctica. These provide evidence of past temperatures and atmospheric gas composition (e.g. Rasmussen *et al.*, 2014). The Greenland evidence is central to glacial climate science in the Northern Hemisphere. Ice sheets, where undisturbed by horizontal flow, provide a stratified record of past

precipitation, and variation in the oxygen stable isotope ratio of the ice ($\delta^{18}O_{ice}$) principally signals changes in the local air temperature at the point of precipitation (Jouzel et al., 2003). Lighter $\delta^{18}O_{ice}$ signifies lower temperature. Rayleigh distillation theory states that $\delta^{18}O_{ice}$ is also influenced by the $\delta^{18}O$ of the vapour-source, the evaporation conditions, the moisture lost *en route*, and the altitude when precipitated, but these do not undermine the basic relationship with temperature (Bradley, 2015).

$\delta^{18}O$ for water is calculated as

$$\delta^{18}O = \frac{(^{18}O/^{16}O)_{sample} - (^{18}O/^{16}O)_{vsmow}}{(^{18}O/^{16}O)_{vsmow,}} \times 1000$$

VSMOW being Vienna Standard Mean Ocean Water.

By combining borehole temperatures, which partially preserve original surface temperatures, with information from thermal fractionation of gas in the firn column at sudden warmings ($\delta^{15}N$), the oxygen isotope record has been translated to a more precise measure of temperature (Cuffey et al., 1994; Kindler *et al.*, 2014).

Ancient atmosphere is trapped in bubbles as snow compresses to ice, yielding information about past atmospheric gas concentrations. The atmospheric concentration of CO_2, now ~420 ppm, was at the last glacial maximum (LGM) ~185 ppm (Bereiter *et al.*, 2015) and varied during stadial/interstadial cycles by up to ~20 ppmv (Figure 1.1). An understanding of changing CO_2 concentrations is important both in demonstrating that CO_2 is a follower not a driver of Northern Hemisphere stadial/interstadial cycles (e.g. Ahn and Brook, 2007, 2008, 2014), and also in the reconstruction of plant-available moisture (the ratio of actual to potential evapotranspiration) from plant evidence, since the water demands of plants vary inversely with atmospheric CO_2 concentration (Prentice *et al.*, 1996 and 1.4.2 below).

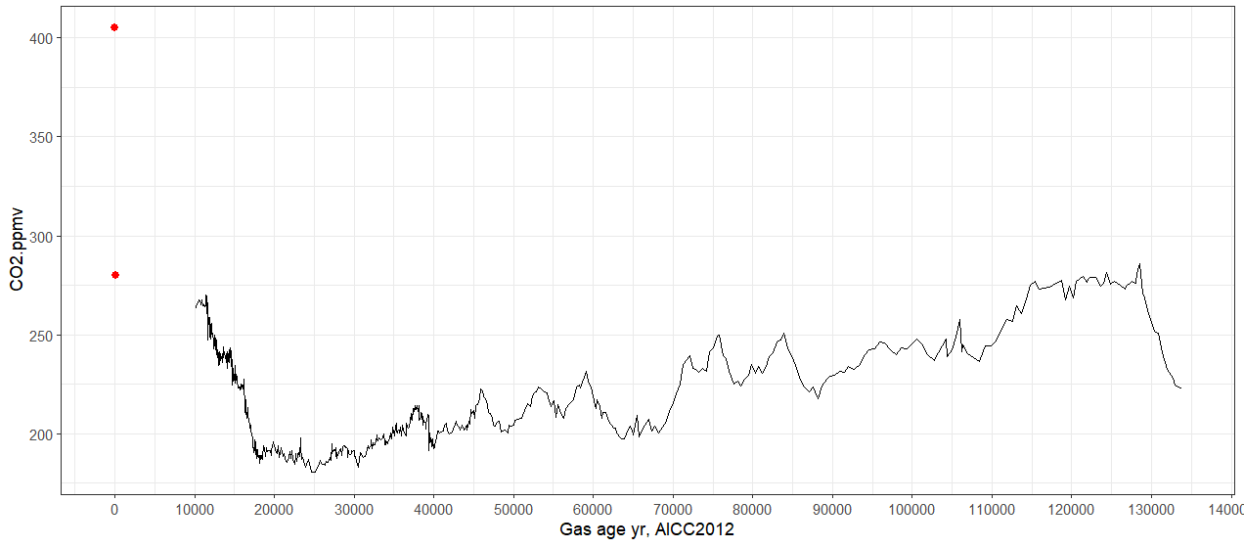

Figure 1.1 CO_2 concentrations in ppmv in the Antarctic EPICA Dome C core (Bereiter et al*., 2015). Red points are pre-industrial (1850) and current concentrations. Recent Greenland CO_2 does not match the instrumental record, seemingly affected by carbonate dust, and is discounted. Antarctic CO_2 is considered reliable (Brook, 2013)* ***and is used to adjust plant-available moisture.***

The Greenland ice cores contain information which can be used for dating (Seierstad *et al.*, 2014). Firstly, they show annual variations in layer thickness and geochemistry, indicating seasonal changes in precipitation, making layer counting possible to ~ 60 ka. Secondly, they contain many instances of identifiable and often datable tephra or the sulfate signature of volcanic activity, mainly Icelandic, so that the different cores (GISP2, GRIP, NGRIP, NEEM) can be correlated and dated. The result is the GICC05modelext age model (Seierstad *et al.*, 2014) which is the most comprehensive and precise age model available for events in the Northern Hemisphere (Figure 1.2). Comparisons with new high-resolution data from NEEM and EGRIP mean that the glacial section of this age model is now considered rather more accurate than originally assumed (Rasmussen *et al.*, 2023).

A large part of the GICC05 age model was compared with speleothem U/Th dates by Adolphi *et al* (2018), using cosmogenic nuclides found in both ice and speleothems; the two were found to be highly consistent, so that the dates of D-O signatures in both ice and speleothems are essentially identical.

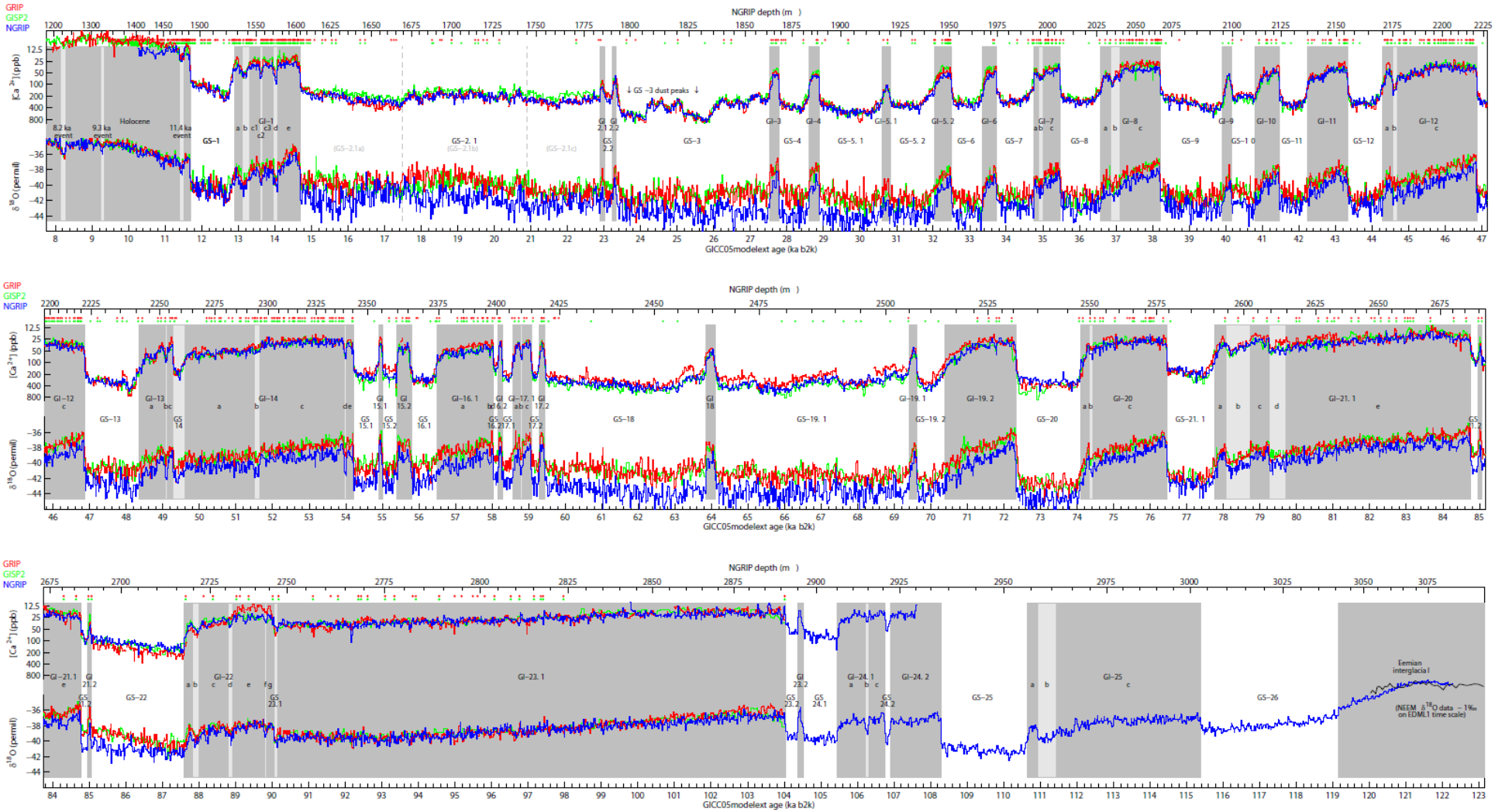

Fig. 1. 20-year average values of $\delta^{18}O$ and $[Ca^{2+}]$ (note the reversed logarithmic $[Ca^{2+}]$ scale; see text for data sources) from GRIP (red), GISP2 (green), and NGRIP (blue) on the GICC05modelext time scale. The dots just below the upper NGRIP depth axis show the position of the match points used to transfer the GICC05modelext time scale from NGRIP to the GRIP (red dots) and GISP2 (green dots) records. The proposed extension of the INTIMATE event stratigraphy scheme is shown with interstadials illustrated by grey shading (light grey indicates cold sub-events). In the Eemian interglacial, NGRIP data are extended by NEEM $\delta^{18}O$ data offset by 2‰ (NEEM community members, 2013). See main text for details on the numbering of stadial and interstadial events. Note the small time overlap between the three panels introduced to ease interpretation.

Figure 1.2 Rasmussen et al (2014) Fig 1: δ18O and dust flux records of the long Greenland ice cores GRIP, GISP2, and NGRIP, aligned by multiple match points. The close coincidence of all three provides great confidence in the records. δ18O is essentially a measure of temperature. Dust flux is an index of windiness and of aridity in the source regions of the dust.

1.4 Pollen

1.4.1 Pollen as a palaeoclimate archive

Pollen is the most commonly used material for terrestrial climate reconstruction, and is also found in marine sediments. Pollen is ubiquitous and is produced in high volumes, and sporopollenin, which forms the outer casing of pollen grains, is robust, almost chemically inert, and has high preservation potential in anoxic conditions (Birks and Birks, 1980; Fægri, Kaland and Krzywinski, 1989; Moore and Webb, 1991; Smol, Last and Birks, 2001).

The translation of pollen taxon abundances to climate or to vegetation cover is not straightforward (Birks and Birks, 1980; Fægri, Kaland and Krzywinski, 1989; Moore and Webb, 1991; Smol, Last and Birks, 2001).

Pollen taxonomy is morphological, that is, it is based on the shapes, sizes, aperture characteristics and surface sculpture of the grains (palynomorphs) (Tschudy and Scott, 1969; Moore and Webb, 1991; Punt *et al.*, 2007). Pollen taxonomy is not necessarily identical with plant taxonomy; related plants typically produce morphologically highly similar pollen, making it hard to distinguish between them, and while Scanning Electron Microscopy (SEM) permits more discrimination than light microscopy, it is not universally used (Birks and Birks, 1980; Moore and Webb, 1991). Pollen is collected for many purposes (Moore and Webb, 1991), so different palynologists, depending on their specific interests, skills, and available technology and time, will apply different levels of taxonomic discrimination, and may use different naming conventions. Pollen is therefore often recorded not at a species level but at genus, family or higher taxonomic level (e.g. Moore and Webb, 1991). When samples from different sources are involved, the nomenclature of pollen data can be mapped to a harmonised list of names, and pollen recorded at finer taxonomic resolutions may be amalgamated into a higher level (Harrison, 2019; Wei *et al.*, 2019; Turner *et al.*, 2020).

The relative abundance of pollen taxa is not directly indicative of the relative abundance of the parent plants (Birks and Birks, 1980; Fægri, Kaland and Krzywinski, 1989; Moore and Webb, 1991). Different plant species produce very different quantities of pollen, which in turn have different characteristics affecting their dispersal. While there are overlaps between these broad classes, anemophilous species tend to produce vast quantities of very light smooth-

surfaced pollen which is then very widely distributed; zoophilous plants invest in flowers and nectar to attract vectors, and many only produce small amounts pollen, which is not widely dispersed, and the pollen of cleistogamous plants such as *Viola* rarely leaves the flower (Birks and Birks, 1980; Fægri, Kaland and Krzywinski, 1989; Moore and Webb, 1991). Methods of adjusting for the production/dispersal bias have been developed (e.g. Sugita, 2007a; Hellman *et al.*, 2008; Gaillard *et al.*, 2010).

Pollen is known to be capable of being transported enormous distances from the source plant (e.g. Salas, 1983; Fægri, Kaland and Krzywinski, 1989; Campbell *et al.*, 1999; Rousseau *et al.*, 2008), so an important question is what catchment is sampled by a pollen core. Pollen source theory (Prentice, 1985; Prentice, I C, 1988; Sugita, 1994; Davis, 2000) considers how local and more distant sources contribute to pollen found in different sizes of lake, and distinguishes between local and regional pollen rain. This led to models such as REVEALS and LOVE (Sugita, 2007a, 2007b; tested by Hellman *et al.*, 2008) which estimate the local vegetation assemblage from pollen abundances. An important input is the relative pollen productivity of different taxa (RPP), which is not known for all taxa and can only be established by fieldwork (Broström *et al.*, 2008). In general, small lakes (e.g. ~ 1 km^2) tend to indicate local vegetation; larger lakes contain more regional signals (Prentice, 1985; Prentice, I C, 1988; Sugita, 1994).

Marine pollen is the extreme case of terrestrial pollen collected from a large area, since pollen reaches the ocean both by wind and in river outflow; it is often dominated by *Pinus,* and may be re-deposited by currents (e.g. Fægri, Kaland and Krzywinski, 1989). The pollen assemblage therefore may represent a wide variety of climates. Marine pollen can provide a general picture of terrestrial conditions, whose broad features may correlate with nearby terrestrial records, and the same core may contain other material such as foraminifera which provide additional information on ocean conditions and, by correlation with Greenland events, on dating (e.g. Goñi *et al.*, 2000; Sánchez Goñi, 2006; Naughton *et al.*, 2016). The sources and depositional environment of marine pollen are unlike those of lacustrine or bog pollen, and the pollen records of the two environments are not directly comparable (Birks *et al.*, 2010).

1.4.2 How plants and pollen represent climate

Plants can provide evidence of multiple aspects of climate. The ecophysiological factors which limit the ranges of plants are well understood (e.g. Harrison *et al.*, 2010). The principal factors are:

- the available solar radiation budget during the growing season, often approximated by GDD (growing degree days) above a certain temperature e.g. 0 ^{o}C (GDD0); this determines the amount of energy available for growth, repair and respiration;
- the minimum temperature and its duration, for which the mean temperature of the coldest month (MTCO) is a common proxy; plants have limits below which they cannot survive. These limits vary across a range of cold-tolerance mechanisms;
- the maximum temperature, for which the mean temperature of the warmest month (MTWA) is a common proxy; beyond a given temperature, heat damage occurs;
- plant-available moisture, which reflects the balance between actual and potential evapotranspiration, which depends ultimately on precipitation and warmth; some plants are water-loving and others prefer aridity;
- seasonal variation in these factors.

These are not simply limiting factors. Biota, including plants, exhibit environmental preferences not only by presence or absence but by their changing abundance along an environmental gradient, in response both to environmental factors and to competition. This distribution is often assumed to be approximately unimodal (Shelford, 1931; ter Braak, 1987; Ter Braak and Juggins, 1993), but other responses are well known (e.g. Huisman, Olff and Fresco, 1993). In the case of terrestrial plants, the gradients are the variables listed above. The location on the gradient of the peak abundance of a plant taxon therefore should represent its most preferred climate, or, more precisely, its preferred climate out of the range left available to it by competition. In practice, the pattern is rarely this neat, a subject examined in detail in Chapter 5.

The climate variables listed above are not all conventional meteorological variables, though they are often correlated with such, and while many quantitative studies reconstruct more common variables such as annual

precipitation (e.g. Feurdean, 2008), climate variables more closely related to the controlling factors of plant distributions are likely to yield better reconstructions. For the European region, three climate variables have been shown by Canonical Correspondence Analysis (CCA) to be important to the pattern of modern pollen abundances and to be capable of being independently reconstructed (e.g. Wei *et al.*, 2019). These are GDD0 (growing degree days above 0 °C), MTCO (mean temperature of the coldest month) and a measure of plant-available moisture, the square root of Moisture Index (MI), MI being the ratio of actual to potential evapotranspiration.

When making reconstructions of moisture, account needs to be taken of the fact that the moisture requirement of plants varies inversely with the CO_2 concentration in the atmosphere (Prentice *et al.*, 1996). Plants absorb CO_2 by allowing air to enter leaves passively via their stomata, but this simultaneously allows the escape of water vapour. When CO_2 is in low concentration, plants tend to open their stomata more and/or for longer, and for a given level of carbon uptake will lose more water that would be the case today. Guiot *et al.* (2000) found that inverse modelling of glacial vegetation required atmospheric CO_2 to be set to glacial levels if observed palaeovegetation was to be replicated well. An adjustment therefore needs to be made to the modern water requirement of each taxon, increasing it for lower CO_2 levels, using a physiology-based model (Prentice and Harrison, 2009; Prentice, Villegas-Diaz and Harrison, 2022).

Climate is the primary, but not the only, influence on plant abundances, since there are many other factors, such as the availability of soil nutrients, herbivory, disease, and chance. A probable case of non-climatic influence is the interstadial forest composition found in the Megali Limni core from Lesvos (Margari *et al.* 2009) which is unusual compared to other Greek and Italian cores. Margari *et al.* (2009) attribute this to the serpentinised ophiolitic bedrock, which provides a soil low in nutrients. The signal of plant and pollen abundance is not a pure climate signal (Fægri, Kaland and Krzywinski, 1989).

1.4.3 Fossil pollen core age models

A palaeoclimatic archive requires a sufficiently good age-depth model if it is to be set in a wider context. The Greenland GICC05modelext chronology (see 1.3.2) and the U/Th chronologies of speleothems are based on multiple radiometric and other dates and are sufficiently accurate and precise that their time series can be aligned with high confidence (Adolphi *et al.*, 2018).

In contrast, pollen cores covering the glacial period suffer from a comparative lack of dating points. Nearly all are ^{14}C, whose uncertainties expand rapidly towards ~ 40 ka, just at the time when D-Os are most common, and is unavailable beyond ~ 50 ka (Reimer *et al.*, 2020). Pollen itself has not normally been found capable of providing ^{14}C dates, and other biological material or carbon-rich bulk sediment are the normal dating material (Bradley, 2015). In some cores tephra dates are available, or floating chronologies developed from varves (e.g. Brauer *et al.* (2007) at Lago Grande di Monticchio; Margari *et al.* (2007) at Megali Limni). Beyond ~ 40 ka changes in pollen assemblages have been attributed to particular Greenland events, or Marine Isotope Stage (MIS) transitions, based on similarity of features. Features in marine core pollen dated using $\delta^{18}O$ in foraminifera (see 1.4.1) have been linked to terrestrial records (e.g. Fletcher and Sánchez Goñi, 2008).

Many age-depth modelling techniques exist, each with their strengths and weaknesses (Blockley, Bronk Ramsey and Pyle, 2008; Bronk Ramsey, 2009; Blaauw, 2010; Trachsel and Telford, 2017; Lacourse and Gajewski, 2020). All attempt to fit a curve through dating points at given depths, the ages of which points are known within radiometric uncertainties, or, in the case of visual similarities with another record, are taken from that other record, including uncertainties. Age models compromise between closeness of fit to the dating points and plausible sedimentation rates between them, but there is no single statistically correct answer and a degree of judgement is called for.

In most glacial-age pollen cores the lack of dating points leads to wide uncertainties whatever the method. So it is difficult reliably to find a DO in a pollen series by looking up the GICC05modelext date of the Greenland event (which itself has uncertainties) in the pollen core age model. This motivated the search by other means for the signature of D-Os in pollen records, which is central to this thesis.

1.4.4 Underlying assumptions

Extracting climate information from fossil pollen using the current relationship between pollen and climate makes several assumptions. These have been widely discussed in the literature, e.g. Birks *et al.* (2010), Huntley (2012) and references therein. Ignoring for a moment the questions specific to reconstruction methodology, two fundamental assumptions stand out:

- The taxa are related to the climate in which they live
- The taxa are the same entities, and respond to their environment in the same way now, as in the past.

They appear to be sufficiently reliable assumptions on which to proceed; pollen abundance can in general be demonstrated to vary with conditions, and the pollen taxa found in glacial cores are all recognisable in the modern. As noted in 1.1 only one tree is known to have gone extinct in the Late Quaternary; the same taxa appear to persist through the glacial. But there are several other issues to be aware of.

1.4.5 Challenges in climate reconstruction from pollen

1.4.5.1 Non-analogue and non-equilibrium conditions

In the past, different patterns of insolation owing to Milanković cycles, low and varying levels of CO_2, changing configurations and altitudes of ice sheets, and the lag time before vegetation responded fully to changing climate, combined at times to create climates and vegetation assemblages which are not found today (Williams, Shuman and Webb, 2001; Jackson and Williams, 2004; Williams and Jackson, 2007; Nogués-Bravo, 2009). Assemblages or biomes not known today are found in the late glacial/last termination (Overpeck, Webb and Webb, 1992; Behling, 1998; Correa-Metrio *et al.*, 2012) or very early Holocene (Cruz-Silva *et al.*, 2022) but fade away later in the Holocene. It is not clear to what extent such non-analogue assemblages existed during the earlier part of the glacial.

Plants, especially trees, take time to mature and produce pollen, so that both vegetation and pollen rain may on a decadal scale be out of equilibrium with climate (Lowe and Walker, 2015). More significant than maturation, though, is migration (see 1.1). When tracts of the Earth's surface become climatically suitable for, for instance, trees, the degree of disequilibrium depends on the migration rate of the trees. This is most pronounced under rapid climate

change, such as now and during D-Os. Nevertheless, Harrison and Sánchez Goñi (2010) found no lag, within the resolution of the records and the implied ages of the samples, between D-O warming and the vegetation response, so the theoretical concern that vegetation is at times too far out of equilibrium with climate to provide a valid reconstruction can be overstated.

1.4.5.2 Sampling the climate gradient

In a set of modern pollen samples used to establish the relationship between modern pollen and modern climate (a training set), taxa which are very infrequently found are unlikely to provide an adequate sampling of the climate gradient. One response is to set some limit to exclude these, say 5 or 10 occurrences, but this is necessarily arbitrary. In theory, if the realised niche of a taxon is known by other means, the adequacy of the sampling could be established, but this would require data which are not typically available. Another response is to rely on niche conservation (Ackerly, 2003) and combine thinly evidenced taxa into higher taxonomic levels of the same genus, sub-family, or family to provide a more comprehensive reading of the climate, subject to checking that the climate preferences of the component taxa appear sufficiently similar.

1.4.5.3 Taxa not representing climate, or missing

There are taxa whose abundance is not primarily determined by climate, such as obligate aquatics and carnivorous plants, and these are often excluded from consideration in climatic studies. Modern pollen is also strongly affected by human activity, since the vegetation found today is far from the natural cover. Humans have fragmented forests, introduced industrial scale monocultures, and moved species around the globe. So modern pollen includes introduced species and cultivars, and it is arguable that they should be ignored; the counter-argument is that if these plants produce pollen, then they are capable of reproduction, and must be adapted to the local climate, of which they are good indicators. Conversely human-induced impoverishment of plant biodiversity means that modern pollen samples may not include all the taxa that would naturally occur locally.

1.4.6 Registration of rapid climate change in pollen cores

There are a number of generic issues which mean that pollen core records have to be carefully screened if the response to D-Os is to be identifiable. A core may not be stratigraphically continuous, so either an interval is missed and/or its chronological order is disturbed, and there may be intervals with no, or insufficient, pollen grains. The

abrupt warming phase of a D-O is very short (< 150 years) and some interstadials are short (e.g. GI 3 and GI 4 ~ 400 years), so that sampling resolution is important; too coarse a resolution, or dearth of pollen, may mean that a rapid change is not seen. The age resolution of pollen cores varies greatly both along individual cores and between cores, and is always much coarser than that in, say, the Greenland ice cores, where the underlying annual resolution is often expressed as a 20-year mean based on a near-annual resolution (Rasmussen *et al.*, 2014).

Some pollen cores show little variation in composition over time (e.g. contrast reconstructions for Lac du Bouchet and Monticchio in Appendix C). In these cases it may be that the local climate was more stable than the regional climate, reducing the likelihood of locating D-Os.

1.4.7 Why Mediterranean pollen cores?

This thesis focuses on records from the circum-Mediterranean region for several reasons. This region hosts most of the European glacial lacustrine evidence, since during the glacial period, fresh water lakes persisted only south of the periglacial region fringing the ice sheets, and the cores have sampling resolutions offering a good chance of identifying D-Os. Many modern pollen samples are available from Eurasia to provide a training set consistent with the taxa found in the cores and the expected glacial climate. There are several lines of evidence independent of pollen that D-Os affected the climate of this region, including most obviously speleothems (e.g. Genty *et al.*, 2003; Lechleitner *et al.*, 2018), and many studies have identified changes in the Mediterranean pollen records as responses to D-Os (e.g. Fletcher *et al.*, 2010). Substantial changes in land cover occur between stadial and interstadial: Harrison and Sánchez Goñi (2010) took the examples of DOs 6, 8 and 19, and using multiple pollen records showed that in the Mediterranean region, grasslands dominate in stadials, are at least partially replaced by forest during interstadials, and return in the following stadial.

For these reasons, Mediterranean glacial pollen cores were expected to host good evidence of the impact of D-Os on pollen and vegetation, and were chosen as the material for this thesis.

1.5 Climate reconstruction using pollen

1.5.1 Qualitative reconstructions

Many pollen studies describe past climate qualitatively and comparatively, such as describing one interval as being warmer/wetter than another (e.g. Beaulieu and Reille, 1984; de Beaulieu, J.-L. and Reille, M.:, 1992; Pèrez-Obiol and Julià, 1994; Magri, 1999; Tzedakis, Hooghiemstra and Pälike, 2006; Djamali *et al.*, 2008; Margari *et al.*, 2009; Di Rita, Anzidei and Magri, 2013). This often makes use of indicator species, whose climate preferences are widely accepted, and may be supported by statistical techniques such as CONISS to subdivide the pollen series into pollen zones on the basis of some similarity measure (Bennett, 1996).

1.5.2 Quantitative climate reconstruction methods

Quantitative climate reconstructions provide time series of numerical values of bioclimatic variables in physical units such as ^{o}C or degree days. Relatively few quantitative reconstructions have been made from pollen in the Mediterranean area for the glacial period; exceptions are Allen and Huntley (2009); Sinopoli *et al.* (2019); Wei *et al.* (2019).

Figure 1.3 shows the context in which any training-set based statistical method is applied. Pollen accumulates in sediments; a core is extracted and the pollen identified; and a reconstruction method uses the training set to hypothesise the ancient climate.

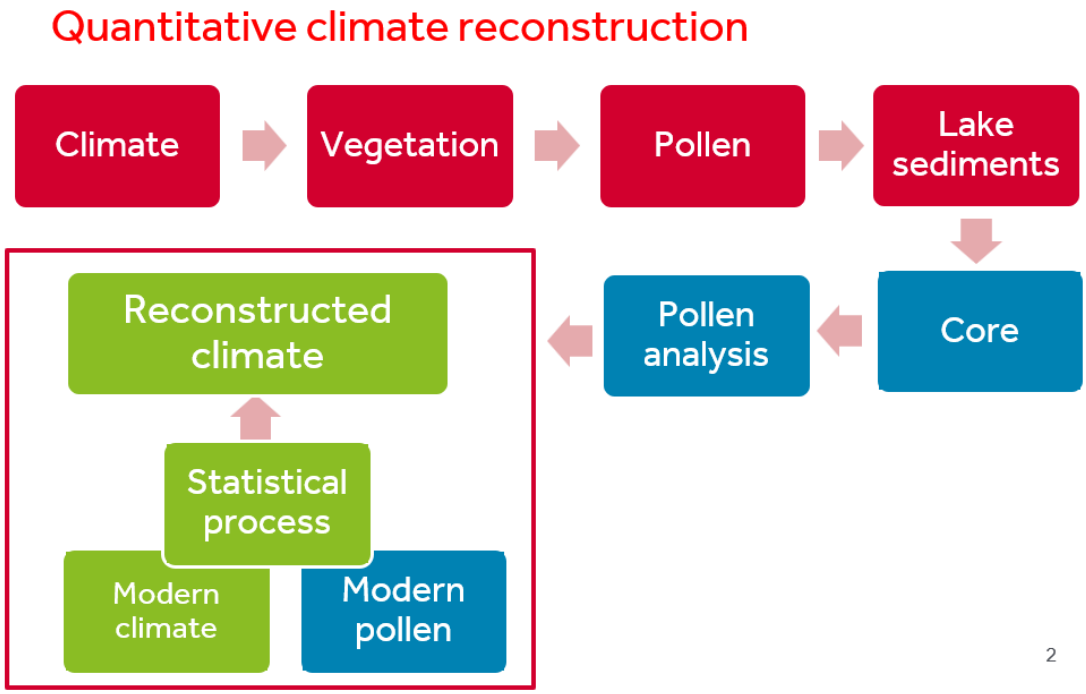

Figure 1.3 The flow of information and processing in climate reconstruction using WA-PLS.

There are several techniques for making quantitative climate reconstructions (e.g. Birks *et al.*, 2010; Bartlein *et al.*, 2011; Sweeney *et al.*, 2018; Chevalier *et al.*, 2020), of which the most widely-used are Modern Analogue Technique (MAT) and the WA-PLS family, both of which depend on a training set and are discussed specifically below; first, some other less-used quantitative methods are noted.

Artificial Neural Networks (ANNs) have been tried (e.g. in conjunction with other techniques Brewer *et al.*, 2008), but ANNS offer no means of understanding how their conclusions are arrived at.

Process-based vegetation modelling (e.g. Guiot *et al.*, 2000; Alfano *et al.*, 2003; Garreta *et al.*, 2010; Izumi and Bartlein, 2016) models how key plant physiological processes respond to a set of environmental conditions, providing as output the vegetation assemblage which can be expected to result from the conditions. This can be used in the forward or reverse directions, either taking reconstructed climate and comparing the modelled vegetation with that observed in pollen records, or taking the observed vegetation and deducing the required climate. These models operate at the level of ~ 30 or fewer Plant Functional Types (PFTs), providing lower resolution than methods which operate at a more precise taxonomic level such as MAT or WA-PLS. They require a mapping

between pollen abundance and vegetation abundance, which introduces further uncertainty (see 1.4.1). Perhaps most importantly, they rely heavily of the realism of the vegetation model.

Response surfaces (e.g. (Bartlein, Prentice and Webb, 1986; Birks *et al.*, 2010) fit a surface through a cloud of points representing abundance of a taxon in a training set on the z axis and two bioclimatic variables on the x and y axes. By stacking the surfaces of multiple taxa together, pollen assemblages for grid points in the climate space can be interpolated, and a nearest match then found with a fossil pollen sample, to estimate the past climate values for the available dimensions of climate. It can be thought of as MAT (see below) using smoothed surfaces (Birks *et al.*, 2010). However, dispersion of abundances in the z dimension, sparseness of the training set samples, and the choice of stiffness of the fit affect the precision with which the surface at any (x,y) point can represent climate. For these reasons, response surfaces are considered hard to interpret and the method has not commonly been applied in the recent literature.

1.5.3 Modern Analogue Technique (MAT)

Modern Analogue Technique (MAT) (Overpeck, Webb and Prentice, 1985; Guiot *et al.*, 1989; Overpeck, Webb and Webb, 1992, p. 192; Jackson and Williams, 2004; Juggins and Birks, 2012) compares the taxon abundances in a fossil sample with those in a training set, and finds the nearest modern sample, or group of samples, typically using Squared Chord Distance (SCD) as the distance measure. The climate associated with the selected samples in the training set is taken as the ancient climate. Taxa may be weighted by their apparent sensitivity (Sweeney *et al.*, 2018). It is a form of *k*-nearest neighbours analysis and requires a substantial training set to ensure sufficiently dense sampling of the possible assemblages (Birks *et al.*, 2010).

Since MAT considers the assemblage in each sample as a whole, large distances between fossil and modern samples can arise where fossil assemblages have no modern analogues; the inability to handle no-analogue assemblages, or to interpolate or extrapolate where there is no analogue, has led some to avoid the use of MAT (Finsinger *et al.*, 2007; Sweeney *et al.*, 2018). Large distances can lead to instability when a series of very similar fossil samples which are quite distant from all modern samples may become associated with two or more different modern samples

which themselves are very different in climate; but since the degree of similarity between the fossil and modern samples is quantified, the robustness of the reconstruction for each sample can be judged.

1.5.4 Weighted Averaging Partial Least Squares (WA-PLS)

Weighted Averaging Partial Least Squares (WA-PLS) (Ter Braak and Juggins, 1993)~~,~~ one of a number of regression-based methods, assumes that the distribution of abundances of taxa along an environmental gradient are at least approximately unimodal and Gaussian, and that the mode represents the taxon's most preferred environment.

By two-way weighted averaging of the taxon abundances with a bioclimatic variable, regressing the observed against the trial result, and looking in the residuals for further information, WA-PLS provides a transfer function for each taxon, which represent the optimum or strongest preference of that taxon for that environmental variable. The appropriate number of iterations of PLS is found by cross-validation and random *t*-testing of the skill in reconstructing the training set.

By weighting the optima by the abundance of the taxa in a fossil sample, a reconstructed bioclimatic value is found for the sample. Unlike MAT, WA-PLS provides no evidence of the robustness of its results at a sample level, but will aways provide a value. This technique is widely applied to pollen and to aquatic and marine biota. Some of its assumptions are discussed and tested in Chapters 3 to 5.

Frequency-adjusted tolerance weighted WA-PLS (fxTWA-PLS) (Liu *et al.*, 2020, 2023) is a development of WA-PLS designed to overcome issues in WA-PLS. WA-PLS implicitly assumes that all taxa have the same tolerance to a given environmental factor, that is, that the dispersion of their abundances along the gradient is the same, and this is patently not the case. In addition, the robustness of the reading of climate by a taxon depends partly on the frequency with each part of the climate gradient is sampled by the training set, a subject discussed in Turner *et al.* (2020), which forms Chapter 3. fxTWA-PLS adjusts for both tolerance and frequency, but expresses the transfer function in a manner in which the optima are not directly accessible.

1.5.5 Comparisons of different methods

Many studies have applied multiple quantitative techniques to the same material, and it is often the case that their results are different in some key respect such as amplitude of change and/or absolute value (e.g. Brewer *et al.*, 2008; Feurdean, 2008; Sinopoli *et al.*, 2019). The discrepancy is typically attributed to weak representation in the training set of climates like that being reconstructed.

1.6 Sources of fossil pollen data

Fossil data were obtained from the ACER database (Sánchez Goñi *et al.*, 2017), available at https://doi.org/10.1594/PANGAEA.870867, Pangaea (https://www.pangaea. de/), and Neotoma (https://apps.neotomadb.org/explorer/). It was found that the ACER record for Les Echets does not appear to replicate the originally published pollen spectra well, and was partially manually redigitised. The nomenclature of the fossil pollen data was harmonised and aggregated to the same taxonomic level as SMPDSv1 (see following section) amalgamated version, using the mapping provided with SMPDS v1 and restated as fractional abundances.

1.7 Sources of modern pollen and climate data

To apply statistical methods to fossil pollen from the Mediterranean, a corresponding training set of modern pollen samples is required which samples climate space as broadly and continuously as possible (Chapter 3; Turner *et al.*, 2020).

The modern pollen training set used is the amalgamated (number of taxa = 195) version 1 of the SPECIAL Modern Pollen Data Set (SMPDSv1: Harrison, 2019). This dataset combines counts of modern samples from the European Modern Pollen Database (EMPD) v3.0 (Davis et al., 2013), the Eastern Mediterranean-Black Sea-Caspian Corridor Biomes (EMBSeCBIO) database (Marinova *et al.*, 2018), the European Pollen Database (http://www.europeanpollendatabase.net/) or Pangaea (https://www.pangaea. de/) and 73 modern surface samples from Spain from Wei et al. (2019). The SMPDSv1 has 6,458 samples.

The modern climate at the SMPDS sample sites was derived from CRU CL 2.0 (New *et al.*, 2002) available from https://doi.org/10.3354/cr021001, by geographically weighted regression, using latitude, longitude and elevation as

predictors. CRU CL 2.0 has a resolution of 10 minutes, and in some analyses, this was compared with the WorldClim 30 second dataset, available from https://www.worldclim.org/data/worldclim21.html.

1.8 Analytical tools

The analyses and plotting in this project were performed principally with versions of R up to 4.3.1 (R Core Team, 2023).

1.9 Structure

The structure of this thesis is as follows.

Chapter 2 tests methods of locating D-Os in multi-taxon fossil pollen abundance records. The anatomy of a D-O cycle is described and defined. The pollen records are summarised by dimension reduction and other methods to provide a limited set of time series, and a method is developed which finds the intervals in a time series which are most similar to the characteristic asymmetrical rapid rise in temperature seen in the Greenland ice cores at the initiation of an interstadial ('pattern matching'). Other methods of matching the Greenland and pollen time series are examined. None perform very well, and all subsequent Chapters use time series made by quantitative climate reconstruction.

Chapter 3 consists of Turner et al (2020), "The impact of methodological decisions on climate reconstructions using WA-PLS". This paper deals with the treatment of a modern pollen and climate training set to be used for quantitative glacial climate reconstruction, illustrated by comparing the results of running WA-PLS using different components of the SMPDSv1. The key conclusion was that the climate space should be sampled as widely and continuously as possible.

Chapter 4 describes the algorithms used in WA-PLS and fxTWA-PLS, both to provide context for the discussion in Chapter 5 of the appropriateness of the transfer functions they generate, and to identify, and suggest a mitigation for, a consequence of the way in which WA-PLS as implemented in the *rioja* R package (specifically) applies the transfer function to fossil pollen.

Chapter 5 deals with how best to describe and understand the recorded abundance of taxa along climate gradients in a modern pollen training set, where and why abundance patterns depart from the unimodal and Gaussian model implicit in WA-PLS and fxTWA-PLS, and explores the consequences and possible mitigations.

Chapter 6 applies 'pattern matching' as developed in Chapter 2 to quantitative climate reconstructions made using fxTWA-PLS, and tests the effect of different parameters on the robustness and plausibility of identification of potential D-Os. Then it combinies the evidential support for potential D-Os in the fossil records, the uncertainty in the fossil pollen age models, and the uncertainty in the GICC05modelext date of GIs, to create plausible matches between potential D-Os and GIs.

Chapter 7 summarises and discusses the findings and suggests further work.

Appendix A: Mean binned abundances and loess curves of 138 taxa from the SMPDS

Appendix B: Bootstrapped loess curves of 138 taxa from the SMPDS

Appendix C: Reconstructions of tmin and gdd for 16 cores

Appendix D: Pattern matching filtering plots for 14 cores

1.10 References

Ackerly, D.D. (2003) 'Community assembly, niche conservatism, and adaptive evolution in changing environments', *International Journal of Plant Sciences*, 164(S3), pp. S165–S184. Available at: https://doi.org/10.1086/368401.

Adolphi, F. *et al.* (2018) 'Connecting the Greenland ice-core and U/Th timescales via cosmogenic radionuclides: testing the synchroneity of Dansgaard–Oeschger events', *Climate of the Past*, 14, pp. 1755–1781. Available at: https://doi.org/10.5194/cp-14-1755-2018.

Ahn, J. and Brook, E.J. (2007) 'Atmospheric CO2 and climate from 65 to 30 ka B.P.', *Geophysical Research Letters*, 34(10), p. L10703. Available at: https://doi.org/10.1029/2007GL029551.

Ahn, J. and Brook, E.J. (2008) 'Atmospheric CO_2 and Climate on Millennial Time Scales during the Last Glacial Period', *Science*, 322(5898), pp. 83–85. Available at: http://www.jstor.org.libezproxy.open.ac.uk/stable/20144949 (Accessed: 20 May 2017).

Ahn, J. and Brook, E.J. (2014) 'Siple Dome ice reveals two modes of millennial CO2 change during the last ice age', *Nature Communications*, 5. Available at: https://doi.org/10.1038/ncomms4723.

Alfano, M.J. *et al.* (2003) 'Comparison of climate model results with European vegetation and permafrost during oxygen isotope stage three☆', *Quaternary Research*, 59(1), pp. 97–107.

Allen, J.R.M. and Huntley, B. (2009) 'Last Interglacial palaeovegetation, palaeoenvironments and chronology: a new record from Lago Grande di Monticchio, southern Italy', *Quaternary Science Reviews*, 28(15), pp. 1521–1538. Available at: https://doi.org/10.1016/j.quascirev.2009.02.013.

Alley, R.B., Anandakrishnan, S. and Jung, P. (2001) 'Stochastic resonance in the North Atlantic', *Paleoceanography*, 16(2), pp. 190–198. Available at: https://doi.org/10.1029/2000PA000518.

Antoine, P. *et al.* (2016) 'Upper Pleistocene loess-palaeosol records from Northern France in the European context: Environmental background and dating of the Middle Palaeolithic', *Quaternary International*, 411, pp. 4–24. Available at: https://doi.org/10.1016/j.quaint.2015.11.036.

Banderas, R. *et al.* (2015) 'An interhemispheric mechanism for glacial abrupt climate change', *Climate Dynamics*, 44(9–10), pp. 2897–2908. Available at: https://doi.org/10.1007/s00382-014-2211-8.

Barbosa, S. *et al.* (2023) *Automatic characterisation of Dansgaard-Oeschger events in palaeoclimate ice records*. other. oral. Available at: https://doi.org/10.5194/egusphere-egu23-3612.

Bartlein, P.J. *et al.* (2011) 'Pollen-based continental climate reconstructions at 6 and 21 ka: a global synthesis', *Climate Dynamics*, 37(3–4), pp. 775–802. Available at: https://doi.org/10.1007/s00382-010-0904-1.

Bartlein, P.J., Prentice, I.C. and Webb, T. (1986) 'Climatic Response Surfaces from Pollen Data for Some Eastern North American Taxa', *Journal of Biogeography*, 13(1), p. 35. Available at: https://doi.org/10.2307/2844848.

Beaulieu, J.-L.D. and Reille, M. (1984) 'A long Upper Pleistocene pollen record from Les Echets, near Lyon, France', *Boreas*, 13(2), pp. 111–132. Available at: https://doi.org/10.1111/j.1502-3885.1984.tb00066.x.

Behling, H. (1998) 'Late Quaternary vegetational and climatic changes in Brazil', *Review of Palaeobotany and Palynology*, 99(2), pp. 143–156. Available at: https://doi.org/10.1016/S0034-6667(97)00044-4.

Bennett, K.D. (1996) 'Determination of the number of zones in a biostratigraphical sequence', *New Phytologist*, 132(1), pp. 155–170. Available at: https://doi.org/10.1111/j.1469-8137.1996.tb04521.x.

Bereiter, B. *et al.* (2015) 'Revision of the EPICA Dome C CO2 record from 800 to 600 kyr before present', *Geophysical Research Letters*, 42(2), pp. 542–549. Available at: https://doi.org/10.1002/2014GL061957.

Birks, H.J.B. *et al.* (2010) 'Strengths and Weaknesses of Quantitative Climate Reconstructions Based on Late-Quaternary', *The Open Ecology Journal*, 3(1). Available at: https://benthamopen.com/ABSTRACT/TOECOLJ-3-2-68 (Accessed: 17 April 2023).

Birks, H.J.B. (Harry J.B. and Birks, H.H. (1980) *Quaternary palaeoecology*. London : Edward Arnold, 1980.

Blaauw, M. (2010) 'Methods and code for "classical" age-modelling of radiocarbon sequences', *Quaternary Geochronology*, 5(5), pp. 512–518. Available at: https://doi.org/10.1016/j.quageo.2010.01.002.

Blockley, S.P.E., Bronk Ramsey, C. and Pyle, D.M. (2008) 'Improved age modelling and high-precision age estimates of late Quaternary tephras, for accurate palaeoclimate reconstruction', *Journal of Volcanology and Geothermal Research*, 177(1), pp. 251–262. Available at: https://doi.org/10.1016/j.jvolgeores.2007.10.015.

Boers, N., Ghil, M. and Rousseau, D.-D. (2018) 'Ocean circulation, ice shelf, and sea ice interactions explain Dansgaard–Oeschger cycles', *Proceedings of the National Academy of Sciences of the United States of America*, 115(47), pp. E11005–E11014. Available at: https://doi.org/10.1073/pnas.1802573115.

ter Braak, C.J.F. (1987) 'The Analysis of Vegetation-Environment Relationships by Canonical Correspondence Analysis', *Vegetatio*, 69(1/3), pp. 69–77. Available at: https://www.jstor.org/stable/20038104 (Accessed: 1 August 2019).

Bradley, R.S. (2015) *Paleoclimatology*. Third. San Diego: Academic Press. Available at: https://doi.org/10.1016/B978-0-12-386913-5.00002-8.

Brauer, A. *et al.* (2007) 'Evidence for Last Interglacial Chronology and Environmental Change from Southern Europe', *Proceedings of the National Academy of Sciences of the United States of America*, 104(2), pp. 450–455. Available at: http://www.jstor.org/stable/25426122 (Accessed: 27 April 2018).

Brewer, S. *et al.* (2008) 'The climate in Europe during the Eemian: a multi-method approach using pollen data', *Quaternary Science Reviews*, 27(25–26), pp. 2303–2315. Available at: https://doi.org/10.1016/j.quascirev.2008.08.029.

Brito-Morales, I. *et al.* (2018) 'Climate Velocity Can Inform Conservation in a Warming World', *Trends in Ecology & Evolution*, 33(6), pp. 441–457. Available at: https://doi.org/10.1016/j.tree.2018.03.009.

Broecker, W.S. (1992) 'The great ocean conveyor', in *AIP Conference Proceedings*. AIP, pp. 129–161. Available at: http://aip.scitation.org/doi/abs/10.1063/1.41925 (Accessed: 3 February 2017).

Bronk Ramsey, C. (2009) 'Bayesian Analysis of Radiocarbon Dates', *Radiocarbon*, 51(1), pp. 337–360. Available at: https://doi.org/10.1017/S0033822200033865.

Brook (2013) *Correlations Between Greenland and Antarctica*. Available at: http://ac.els-cdn.com.libezproxy.open.ac.uk/B9780444536433003228/3-s2.0-B9780444536433003228-main.pdf?_tid=21ee5bae-2f4b-11e7-9715-00000aab0f02&acdnat=1493738719_ae6b5fc67d4080975a3dffd4c6eff74d (Accessed: 2 May 2017).

Broström, A. *et al.* (2008) 'Pollen productivity estimates of key European plant taxa for quantitative reconstruction of past vegetation: a review', *Vegetation History and Archaeobotany*, 17(5), pp. 461–478. Available at: https://doi.org/10.1007/s00334-008-0148-8.

Burrows, M.T. and Schoeman, D.S. (no date) *Geographical limits to species-range shifts are suggested by climate velocity - ProQuest*. Available at: https://search-proquest-

com.idpproxy.reading.ac.uk/docview/1516066676/fulltextPDF/6E8C98508AB486APQ/1?accountid=13460 (Accessed: 7 February 2018).

Campbell, I.D. *et al.* (1999) 'Long-distance transport of pollen into the Arctic', *Nature*, 399(6731), pp. 29–30. Available at: https://doi.org/10.1038/19891.

Chevalier, M. *et al.* (2020) 'Pollen-based climate reconstruction techniques for late Quaternary studies', *Earth-Science Reviews*, 210, p. 103384. Available at: https://doi.org/10.1016/j.earscirev.2020.103384.

Clark, J.S. *et al.* (1998) 'Reid's Paradox of Rapid Plant Migration', *BioScience*, 48(1), pp. 13–24. Available at: https://doi.org/10.2307/1313224.

Clement, A.C., Cane, M.A. and Seager, R. (2001) 'An Orbitally Driven Tropical Source for Abrupt Climate Change', *Journal of Climate*, 14(11), pp. 2369–2375. Available at: https://www.jstor.org/stable/26247431 (Accessed: 22 August 2022).

Correa-Metrio, A. *et al.* (2012) 'Rapid climate change and no-analog vegetation in lowland Central America during the last 86,000 years', *Quaternary Science Reviews*, 38, pp. 63–75. Available at: https://doi.org/10.1016/j.quascirev.2012.01.025.

Corrick, E.C. *et al.* (2020) 'Synchronous timing of abrupt climate changes during the last glacial period', *Science*, 369(6506), pp. 963–969. Available at: https://doi.org/10.1126/science.aay5538.

Cruz-Silva, E. *et al.* (2022) 'A new method based on surface-sample pollen data for reconstructing palaeovegetation patterns', *Journal of Biogeography*, 49(7), pp. 1381–1396. Available at: https://doi.org/10.1111/jbi.14448.

Cuffey, K.M. *et al.* (1994) 'Calibration of the δ18O isotopic paleothermometer for central Greenland, using borehole temperatures', *Journal of Glaciology*, 40(135), pp. 341–349. Available at: https://doi.org/10.1017/S0022143000007425.

Dansgaard et al (1993) 'Evidence for general instability of past climate from a 250-kyr ice core record', *Nature* [Preprint]. Available at: http://www.nature.com.libezproxy.open.ac.uk/nature/journal/v364/n6434/pdf/364218a0.pdf (Accessed: 24 February 2017).

Davis, M.B. (2000) 'Palynology after Y2K—Understanding the Source Area of Pollen in Sediments', *Annual Review of Earth and Planetary Sciences*, 28(1), pp. 1–18. Available at: https://doi.org/10.1146/annurev.earth.28.1.1.

de Beaulieu, J.-L. and Reille, M.: (1992) 'The last climatic cycle at La Grande Pile (Vosges, France), a new pollen profile', *Quaternary Sci. Rev., 11, 431–438, 1992.* [Preprint].

Di Rita, F., Anzidei, A.P. and Magri, D. (2013) 'A Lateglacial and early Holocene pollen record from Valle di Castiglione (Rome): Vegetation dynamics and climate implications', *Quaternary International*, 288, pp. 73–80. Available at: https://doi.org/10.1016/j.quaint.2011.11.011.

Djamali, M. *et al.* (2008) 'A late Pleistocene long pollen record from Lake Urmia, Nw Iran', *Quaternary Research*, 69(3), pp. 413–420. Available at: https://doi.org/10.1016/j.yqres.2008.03.004.

Dobrowski, S.Z. *et al.* (2013) 'The climate velocity of the contiguous United States during the 20th century', *Global Change Biology*, 19(1), pp. 241–251. Available at: https://doi.org/10.1111/gcb.12026.

Dobrowski, S.Z. and Parks, S.A. (2016) 'Climate change velocity underestimates climate change exposure in mountainous regions', *Nature Communications*, 7, p. 12349. Available at: https://doi.org/10.1038/ncomms12349.

Dokken, T.M. *et al.* (2013) 'Dansgaard-Oeschger cycles: Interactions between ocean and sea ice intrinsic to the Nordic seas', *Paleoceanography*, 28(3), pp. 491–502. Available at: https://doi.org/10.1002/palo.20042.

Emiliani, C. (1955) 'Pleistocene temperatures', *Journal of Geology*, 63, pp. 538–578.

Fægri, K., Kaland, P.E. and Krzywinski, K. (1989) 'Textbook of pollen analysis.', *Textbook of pollen analysis.* [Preprint], (Ed. 4). Available at: https://www.cabdirect.org/cabdirect/abstract/19930670810?q=(Textbook+of+Pollen+Analysis) (Accessed: 3 July 2023).

Feurdean, A. (2008) *Lateglacial climate development in NW Romania--Comparative results from three quantitative pollen-based methods | Tudor Tamas - Academia.edu*, *Palaeogeography, Palaeoclimatology, Palaeoecology*. Available at: https://www.academia.edu/1117108/Lateglacial_climate_development_in_NW_Romania--Comparative_results_from_three_quantitative_pollen-based_methods?auto=download (Accessed: 9 October 2019).

Finsinger, W. *et al.* (2007) 'Modern Pollen Assemblages as Climate Indicators in Southern Europe', *Global Ecology and Biogeography*, 16(5), pp. 567–582. Available at: https://www.jstor.org/stable/30134091 (Accessed: 2 January 2021).

Fletcher, W.J. *et al.* (2010) 'Millennial-scale variability during the last glacial in vegetation records from Europe', *Quaternary Science Reviews*, 29(21), pp. 2839–2864. Available at: https://doi.org/10.1016/j.quascirev.2009.11.015.

Fletcher, W.J. and Sánchez Goñi, M.F. (2008) 'Orbital- and sub-orbital-scale climate impacts on vegetation of the western Mediterranean basin over the last 48,000 yr', *Quaternary Review* [Preprint]. Available at: https://www-cambridge-org.libezproxy.open.ac.uk/core/services/aop-cambridge-core/content/view/228F2B11A480ADE72A701FC9FCA7D220/S0033589400005640a.pdf/orbital_and_suborbitalscale_climate_impacts_on_vegetation_of_the_western_mediterranean_basin_over_the_last_48000_yr.pdf (Accessed: 11 December 2017).

Gaillard, M.-J. *et al.* (2010) 'Holocene land-cover reconstructions for studies on land cover-climate feedbacks', *Climate of the Past*, 6(4), pp. 483–499. Available at: https://doi.org/10.5194/cp-6-483-2010.

Garreta, V. *et al.* (2010) 'A method for climate and vegetation reconstruction through the inversion of a dynamic vegetation model', *Climate Dynamics*, 35(2), pp. 371–389. Available at: https://doi.org/10.1007/s00382-009-0629-1.

Genty, D. *et al.* (2003) 'Precise dating of Dansgaard–Oeschger climate oscillations in western Europe from stalagmite data', *Nature*, 421(6925), pp. 833–837. Available at: https://doi.org/10.1038/nature01391.

Genty, D. *et al.* (2005) 'Rapid climatic changes of the last 90 kyr recorded on the European continent', *Comptes Rendus Geoscience*, 337(10), pp. 970–982. Available at: https://doi.org/10.1016/j.crte.2005.04.010.

Gildor, H. and Tziperman, E. (2003) 'Sea-Ice Switches and Abrupt Climate Change', *Philosophical Transactions: Mathematical, Physical and Engineering Sciences*, 361(1810), pp. 1935–1944. Available at: https://www.jstor.org/stable/3559153 (Accessed: 22 August 2022).

Giorgino, T. (2009) 'Computing and Visualizing Dynamic Time Warping Alignments in R: The dtw Package', *Journal of Statistical Software*, 31(1), pp. 1–24. Available at: https://doi.org/10.18637/jss.v031.i07.

Golyandina, N. and Korobeynikov, A. (no date) 'Basic Singular Spectrum Analysis and forecasting with R', *Computational Statistics & Data Analysis*, 71, pp. 934–954. Available at: https://www.academia.edu/12899418/Basic_Singular_Spectrum_Analysis_and_forecasting_with_R (Accessed: 16 September 2020).

Goñi, M.F.S. *et al.* (2000) *European Climatic Response to Millennial-Scale Changes in the Atmosphere–Ocean System during the Last Glacial Period*, *Quaternary Research*. Available at: https://doi.org/10.1006/qres.2000.2176.

Guiot, J. *et al.* (1989) 'A 140,000-year continental climate reconstruction from two European pollen records', *Nature*, 338(6213), pp. 309–313. Available at: https://doi.org/10.1038/338309a0.

Guiot, J. *et al.* (2000) 'Inverse vegetation modeling by Monte Carlo sampling to reconstruct palaeoclimates under changed precipitation seasonality and CO2 conditions: application to glacial climate in Mediterranean region', *Ecological Modelling*, 127(2), pp. 119–140. Available at: https://doi.org/10.1016/S0304-3800(99)00219-7.

Harrison, S.P. *et al.* (2010) 'Ecophysiological and bioclimatic foundations for a global plant functional classification', *Journal of Vegetation Science*, 21(2), pp. 300–317. Available at: https://doi.org/10.1111/j.1654-1103.2009.01144.x.

Harrison, S.P. (2019) 'Modern pollen data for climate reconstructions, version 1 (SMPDS)', *University of Reading* [Preprint]. Available at: http://dx.doi.org/10.17864/1947.194.

Harrison, S.P. and Sánchez Goñi, M.F. (2010) 'Global patterns of vegetation response to millennial-scale variability and rapid climate change during the last glacial period', *Quaternary Science Reviews*, 29(21–22), pp. 2957–2980. Available at: https://doi.org/10.1016/j.quascirev.2010.07.016.

Hassani, H. (no date) 'A Brief Introduction to Singular Spectrum Analysis', p. 11.

Hellman, S. *et al.* (2008) 'The REVEALS model, a new tool to estimate past regional plant abundance from pollen data in large lakes: validation in southern Sweden', *Journal of Quaternary Science*, 23(1), pp. 21–42. Available at: https://doi.org/10.1002/jqs.1126.

Huber, C. *et al.* (2006) 'Isotope calibrated Greenland temperature record over Marine Isotope Stage 3 and its relation to CH4', *Earth and Planetary Science Letters*, 243(3–4), pp. 504–519. Available at: https://doi.org/10.1016/j.epsl.2006.01.002.

Huisman, J., Olff, H. and Fresco, L.F.M. (1993) 'A Hierarchical Set of Models for Species Response Analysis', *Journal of Vegetation Science*, 4(1), pp. 37–46. Available at: https://doi.org/10.2307/3235732.

Huntley, B. (2012) 'Reconstructing palaeoclimates from biological proxies: Some often overlooked sources of uncertainty', *Quaternary Science Reviews*, 31, pp. 1–16. Available at: https://doi.org/10.1016/j.quascirev.2011.11.006.

Izumi, K. and Bartlein, P.J. (2016) 'North American paleoclimate reconstructions for the Last Glacial Maximum using an inverse modeling through iterative forward modeling approach applied to pollen data', *Geophysical Research Letters*, 43(20), p. 10,965-10,972. Available at: https://doi.org/10.1002/2016GL070152.

Jackson, S.T. and Weng, C. (1999) 'Late Quaternary extinction of a tree species in eastern North America', *Proceedings of the National Academy of Sciences*, 96(24), pp. 13847–13852. Available at: https://doi.org/10.1073/pnas.96.24.13847.

Jackson, S.T. and Williams, J.W. (2004) 'MODERN ANALOGS IN QUATERNARY PALEOECOLOGY: Here Today, Gone Yesterday, Gone Tomorrow?', *Annual Review of Earth and Planetary Sciences*, 32, pp. 495–537. Available at: https://www.proquest.com/docview/220804837/abstract/B4D707EE96834FF9PQ/1 (Accessed: 1 June 2023).

Jouzel, J. *et al.* (2003) 'Magnitude of isotope/temperature scaling for interpretation of central Antarctic ice cores', *Journal of Geophysical Research: Atmospheres*, 108(D12), p. 4361. Available at: https://doi.org/10.1029/2002JD002677.

Juggins, S. and Birks, H.J.B. (2012) *Quantitative Environmental Reconstructions from Biological Data.*, *Tracking environmental change using lake sediments: data handling and numerical techniques. [Developments in*

Paleoenvironmental Research Volume 5.]. Juggins, Steve; School of Geography, Politics & Sociology, Newcastle University, Newcastle-upon-Tyne, NE1 7RU, United Kingdom, United Kingdom.: Springer, pp. 431–494.

Keogh, E.J. and Pazzani, M.J. (2001) 'Derivative Dynamic Time Warping', in *Proceedings of the 2001 SIAM International Conference on Data Mining*. *Proceedings of the 2001 SIAM International Conference on Data Mining*, Society for Industrial and Applied Mathematics, pp. 1–11. Available at: https://doi.org/10.1137/1.9781611972719.1.

Kindler, P. *et al.* (2014a) 'Temperature reconstruction from 10 to 120 kyr b2k from the NGRIP ice core', *Climate of the Past*, 10(2), pp. 887–902. Available at: https://doi.org/10.5194/cp-10-887-2014.

Kindler, P. *et al.* (2014b) 'Temperature reconstruction from 10 to 120 kyr b2k from the NGRIP ice core', *Climate of the Past*, 10(2), pp. 887–902. Available at: https://doi.org/10.5194/cp-10-887-2014.

Lacourse, T. and Gajewski, K. (2020) 'Current practices in building and reporting age-depth models', *Quaternary Research*, 96, pp. 28–38. Available at: https://doi.org/10.1017/qua.2020.47.

Laskar, J. *et al.* (2004) 'A long-term numerical solution for the insolation quantities of the Earth', *Astronomy & Astrophysics*, 428(1), pp. 261–285. Available at: https://doi.org/10.1051/0004-6361:20041335.

Lechleitner, F.A. *et al.* (2018) 'The potential of speleothems from western europe as recorders of regional climate: A critical assessment of the sisal database', *Quaternary*, 1(3). Available at: https://doi.org/10.3390/quat1030030.

Leuschner, D.C. and Sirocko, F. (2000) 'The low-latitude monsoon climate during Dansgaard–Oeschger cycles and Heinrich Events', *Quaternary Science Reviews*, 19(1–5), pp. 243–254. Available at: https://doi.org/10.1016/S0277-3791(99)00064-5.

Lin, L. *et al.* (2014) 'Probabilistic sequence alignment of stratigraphic records', *Paleoceanography*, 29(10), pp. 976–989. Available at: https://doi.org/10.1002/2014PA002713.

Lisiecki, L.E. and Lisiecki, P.A. (2002) 'Application of dynamic programming to the correlation of paleoclimate records: DYNAMIC PROGRAMMING SIGNAL CORRELATION', *Paleoceanography*, 17(4), pp. 1-1-1–12. Available at: https://doi.org/10.1029/2001PA000733.

Lisiecki, L.E. and Raymo, M.E. (2005) 'A Pliocene-Pleistocene stack of 57 globally distributed benthic δ18O records', *Paleoceanography*, 20(1), p. PA1003. Available at: https://doi.org/10.1029/2004PA001071.

Liu, M. *et al.* (2020) 'An improved statistical approach for reconstructing past climates from biotic assemblages', *Proceedings of the Royal Society A* [Preprint]. Available at: https://doi.org/10.1098/rspa.2020.0346.

Liu, M. *et al.* (2023) 'Holocene climates of the Iberian Peninsula: pollen-based reconstructions of changes in the west–east gradient of temperature and moisture', *Climate of the Past*, 19(4), pp. 803–834. Available at: https://doi.org/10.5194/cp-19-803-2023.

Loarie, S.R. *et al.* (2009) 'The velocity of climate change', *Nature; London*, 462(7276), pp. 1052–5. Available at: https://search.proquest.com/docview/204548344/abstract/EA83D4C2010346DBPQ/1 (Accessed: 18 January 2018).

Lough, J.M. and Fritts, H.C. (1987) 'An assessment of the possible effects of volcanic eruptions on North American climate using tree-ring data, 1602 to 1900 A.D.', *Climatic Change*, 10(3), pp. 219–239. Available at: https://doi.org/10.1007/BF00143903.

Lowe, J.J. (Joseph J. and Walker, M.J.C. (Mike J.C.) (2015) *Reconstructing Quaternary environments*. 3rd ed. Routledge, 2014.

Lynch-Stieglitz (2017) 'The Atlantic Meridional Overturning Circulation and Abrupt Climate Change', *Annual Review of Marine Science*, 9(1), pp. 83–104. Available at: https://doi.org/10.1146/annurev-marine-010816-060415.

Magri, D. (1999) 'Late Quaternary vegetation history at Lagaccione near Lago di Bolsena (central Italy)', *Review of Palaeobotany and Palynology*, 106(3–4), pp. 171–208. Available at: https://doi.org/10.1016/S0034-6667(99)00006-8.

Malmierca-Vallet, I. *et al.* (2023) 'Dansgaard–Oeschger events in climate models: review and baseline Marine Isotope Stage 3 (MIS3) protocol', *Climate of the Past*, 19(5), pp. 915–942. Available at: https://doi.org/10.5194/cp-19-915-2023.

Margari, V. *et al.* (2007) 'Mediterranean tephra stratigraphy revisited: Results from a long terrestrial sequence on Lesvos Island, Greece', *Journal of Volcanology and Geothermal Research*, 163(1–4), pp. 34–54. Available at: https://doi.org/10.1016/j.jvolgeores.2007.02.002.

Margari, V. *et al.* (2009) 'Character of vegetational and environmental changes in southern Europe during the last glacial period; evidence from Lesvos Island, Greece', *Quaternary Science Reviews*, 28(13–14), pp. 1317–1339. Available at: https://doi.org/10.1016/j.quascirev.2009.01.008.

Marinova, E. *et al.* (2018) 'Pollen-derived biomes in the Eastern Mediterranean–Black Sea–Caspian-Corridor', *Journal of Biogeography*, 45(2), pp. 484–499. Available at: https://doi.org/10.1111/jbi.13128.

McDermott, F. (2004) 'Palaeo-climate reconstruction from stable isotope variations in speleothems: a review', *Quaternary Science Reviews*, 23(7–8), pp. 901–918. Available at: https://doi.org/10.1016/j.quascirev.2003.06.021.

Moore, P.D. and Webb, J.A. (1991) *Pollen analysis.* 2nd ed. / P.D. Moore, J.A. Webb, M.E. Collinson. Oxford : Blackwell Scientific, 1991.

Naughton, F. *et al.* (2016) 'Climate variability across the last deglaciation in NW Iberia and its margin', *Quaternary International*, 414, pp. 9–22. Available at: https://doi.org/10.1016/j.quaint.2015.08.073.

New, M. *et al.* (2002) 'A high-resolution data set of surface climate over global land areas', *Climate Research*, 21, pp. 1–25. Available at: https://doi.org/10.3354/cr021001.

Nogués-Bravo, D. (2009) 'Predicting the past distribution of species climatic niches', *Global Ecology and Biogeography*, 18(5), pp. 521–531. Available at: https://doi.org/10.1111/j.1466-8238.2009.00476.x.

Overpeck, J.T., Webb, R.S. and Webb, T., III (1992) 'Mapping eastern North American vegetation change of the past 18 ka: No-analogs and the future', *Geology*, 20(12), pp. 1071–1074. Available at: https://doi.org/10.1130/0091-7613(1992)020<1071:MENAVC>2.3.CO;2.

Overpeck, J.T., Webb, T. and Prentice, I.C. (1985) 'Quantitative Interpretation of Fossil Pollen Spectra: Dissimilarity Coefficients and the Method of Modern Analogs', *Quaternary Research*, 23(1), pp. 87–108. Available at: https://doi.org/10.1016/0033-5894(85)90074-2.

Pachauri, R.K., Mayer, L. and Intergovernmental Panel on Climate Change (eds) (2015) *Climate change 2014: synthesis report*. Geneva, Switzerland: Intergovernmental Panel on Climate Change.

Pèrez-Obiol, R. and Julià, R. (1994) 'Climatic Change on the Iberian Peninsula Recorded in a 30,000-Yr Pollen Record from Lake Banyoles', *Quaternary Research*, 41(1), pp. 91–98. Available at: https://doi.org/10.1006/qres.1994.1010.

Petersen, S.V., Schrag, D.P. and Clark, P.U. (2013) 'A new mechanism for Dansgaard-Oeschger cycles', *Paleoceanography*, 28(1), pp. 24–30. Available at: https://doi.org/10.1029/2012PA002364.

Prentice, I C (1988) ‘Palaeoecology-and-plant-population-dynamic_1988_Trends-in-Ecology---Evolutio.pdf’.

Prentice, I.C. (1985) ‘Pollen Representation, Source Area, and Basin Size: Toward a Unified Theory of Pollen Analysis’, *Quaternary Research*, 23(1), pp. 76–86. Available at: https://doi.org/10.1016/0033-5894(85)90073-0.

Prentice, I.C. *et al.* (1996) ‘Reconstructing biomes from palaeoecological data: a general method and its application to European pollen data at 0 and 6 ka’, *Climate Dynamics*, 12, pp. 185–194.

Prentice, I.C. and Harrison, S.P. (2009) ‘Ecosystem effects of CO2 concentration: evidence from past climates’, *Clim. Past*, p. 11.

Prentice, I.C., Villegas-Diaz, R. and Harrison, S.P. (2022) ‘Accounting for atmospheric carbon dioxide variations in pollen-based reconstruction of past hydroclimates’, *Global and Planetary Change*, 211, p. 103790. Available at: https://doi.org/10.1016/j.gloplacha.2022.103790.

Punt, W. *et al.* (2007) ‘Glossary of pollen and spore terminology’, *Review of Palaeobotany and Palynology*, 143(1), pp. 1–81. Available at: https://doi.org/10.1016/j.revpalbo.2006.06.008.

R Core Team (2023) ‘R: A language and environment for statistical computing’. Vienna: R Foundation for Statistical Computing. Available at: http://www.R-project.org/.

Rahmstorf, S. (2002) ‘Ocean circulation and climate during the past 120,000 years’, *Nature*, 419(6903), pp. 207–214. Available at: https://doi.org/10.1038/nature01090.

Rasmussen, S.O. *et al.* (2014) ‘A stratigraphic framework for abrupt climatic changes during the Last Glacial period based on three synchronized Greenland ice-core records: refining and extending the INTIMATE event stratigraphy’, *Quaternary Science Reviews*, 106, pp. 14–28. Available at: https://doi.org/10.1016/j.quascirev.2014.09.007.

Rasmussen, S.O. *et al.* (2023) *Evaluating the accuracy of the Greenland Ice-Core Chronology (GICC)*. EGU23-4545. Copernicus Meetings. Available at: https://doi.org/10.5194/egusphere-egu23-4545.

Reid, C. (1899) *The Origin of the British Flora*. London: Dulau.

Reille, M. and de Beaulieu, J.-L. (1990) ‘Pollen analysis of a long upper Pleistocene continental sequence in a Velay maar (Massif Central, France)’, *Palaeogeograpy, Palaeoclimatology, Palaeoecology*, 80, pp. 35–48.

Reimer, P.J. *et al.* (2020) ‘The IntCal20 Northern Hemisphere Radiocarbon Age Calibration Curve (0–55 cal kBP)’, *Radiocarbon*, 62(4), pp. 725–757. Available at: https://doi.org/10.1017/RDC.2020.41.

Rousseau, D.-D. *et al.* (2008) ‘Long-distance pollen transport from North America to Greenland in spring’, *Journal of Geophysical Research: Biogeosciences*, 113(G2). Available at: https://doi.org/10.1029/2007JG000456.

Rousseau, D.-D. *et al.* (2020) ‘Dansgaard–Oeschger-like events of the penultimate climate cycle: the loess point of view’, *Climate of the Past*, 16(2), pp. 713–727. Available at: https://doi.org/10.5194/cp-16-713-2020.

Salas, M.R. (1983) ‘Long-distance pollen transport over the southern Tasman Sea: evidence from Macquarie Island’, *New Zealand Journal of Botany*, 21, pp. 285–292. Available at: https://www.tandfonline.com/doi/epdf/10.1080/0028825X.1983.10428559?needAccess=true&role=button (Accessed: 2 June 2023).

Sánchez Goñi, M.F. (2006) ‘Vegetation-climate relationships over the last 425,000 years in western Europe. What can pollen from marine archives tell us?’, *Quaternaire*, 17(1), pp. 3–25.

Sánchez Goñi, M.F. *et al.* (2017) 'The ACER pollen and charcoal database: a global resource to document vegetation and fire response to abrupt climate changes during the last glacial period', *Supplement to: Sanchez Goñi, MF et al. (2017): The ACER pollen and charcoal database: a global resource to document vegetation and fire response to abrupt climate changes during the last glacial period. Earth System Science Data, 9(2), 679-695, https://doi.org/10.5194/essd-9-679-2017*. Available at: https://doi.org/10.1594/PANGAEA.870867.

Sanchez Goñi, M.F. *et al.* (2017) 'The ACER pollen and charcoal database: a global resource to document vegetation and fire response to abrupt climate changes during the last glacial period', *Supplement to: Sanchez Goñi, MF et al. (2017): The ACER pollen and charcoal database: a global resource to document vegetation and fire response to abrupt climate changes during the last glacial period. Earth System Science Data, 9(2), 679-695, https://doi.org/10.5194/essd-9-679-2017*. Available at: https://doi.org/10.1594/PANGAEA.870867.

Sánchez Goñi, M.F. *et al.* (2018) 'Pollen from the Deep-Sea: A Breakthrough in the Mystery of the Ice Ages', *Frontiers in Plant Science*, 9. Available at: https://doi.org/10.3389/fpls.2018.00038.

Sanchez Goñi, M.F. and Harrison, S.P. (2010) 'Millennial-scale climate variability and vegetation changes during the Last Glacial: Concepts and terminology', *Quaternary Science Reviews*, 29(21–22), pp. 2823–2827. Available at: https://doi.org/10.1016/j.quascirev.2009.11.014.

Seager, R. and Battisti, D.S. (2007) 'Challenges to our understanding of the general circulation: Abrupt climate change', in *The global circulation of the atmosphere / edited by Tapio Schneider and Adam H. Sobel ; foreword by Edward N. Lorenz.* Princeton University Press.

Seierstad, I.K. *et al.* (2014) 'Consistently dated records from the Greenland GRIP, GISP2 and NGRIP ice cores for the past 104 ka reveal regional millennial-scale δ18O gradients with possible Heinrich event imprint', *Quaternary Science Reviews*, 106, pp. 29–46. Available at: https://doi.org/10.1016/j.quascirev.2014.10.032.

Shackleton, N.J. (1987) 'Oxygen isotopes, ice volume and sea level', *Quaternary Science Reviews*, 6(3–4), pp. 183–190. Available at: https://doi.org/10.1016/0277-3791(87)90003-5.

Shelford, V.E. (1931) 'Some Concepts of Bioecology', *Ecology*, 12(3), pp. 455–467. Available at: https://doi.org/10.2307/1928991.

Sime, L.C., Hopcroft, P.O. and Rhodes, R.H. (2019) 'Impact of abrupt sea ice loss on Greenland water isotopes during the last glacial period', *Proceedings of the National Academy of Sciences of the United States of America*, 116(10), pp. 4099–4104. Available at: https://doi.org/10.1073/pnas.1807261116.

Sinopoli, G. *et al.* (2019) 'Pollen-based temperature and precipitation changes in the Ohrid Basin (western Balkans) between 160 and 70ka', *Climate of the Past*, 15(1), pp. 53–71. Available at: https://doi.org/10.5194/cp-15-53-2019.

Smol, J.P. (John P.), Last, W.M. and Birks, H.J.B. (Harry J.B. (2001) *Tracking environmental change using lake sediments.* Dordrecht ; London : Kluwer Academic Publishers, c2001- (Developments in paleoenvironmental research. v. 3).

Steffensen, J.P. *et al.* (2008) 'High-Resolution Greenland Ice Core Data Show Abrupt Climate Change Happens in Few Years', *Science*, 321(5889), pp. 680–684. Available at: https://www.jstor.org/stable/20054642 (Accessed: 31 May 2023).

Sugita, S. (1994) 'Pollen Representation of Vegetation in Quaternary Sediments: Theory and Method in Patchy Vegetation', *Journal of Ecology*, 82(4), pp. 881–897. Available at: https://doi.org/10.2307/2261452.

Sugita, S. (2007a) 'Theory of quantitative reconstruction of vegetation I: pollen from large sites REVEALS regional vegetation composition', *The Holocene*, 17(2), pp. 229–241. Available at: https://doi.org/10.1177/0959683607075837.

Sugita, S. (2007b) 'Theory of quantitative reconstruction of vegetation II: all you need is LOVE', *The Holocene*, 17(2), pp. 243–257. Available at: https://doi.org/10.1177/0959683607075838.

Sweeney, J. *et al.* (2018) 'Statistical challenges in estimating past climate changes', *Wiley Interdisciplinary Reviews: Computational Statistics*, 10(5), p. e1437. Available at: https://doi.org/10.1002/wics.1437.

Tang, Z., Du, S. and Liu, F. (2017) 'Late Pleistocene changes in vegetation and the associated human activity at Beiyao Site, Central China', *Review of Palaeobotany and Palynology*, 244, pp. 107–112. Available at: https://doi.org/10.1016/j.revpalbo.2017.04.002.

Ter Braak, C.J.F. and Juggins, S. (1993) 'Weighted averaging partial least squares regression (WA-PLS) : an improved method for reconstructing environmental variables from species assemblages', *Hydrobiologia*, 269/270, pp. 485–502.

Trachsel, M. and Telford, R.J. (2017) 'All age–depth models are wrong, but are getting better', *The Holocene*, 27(6), pp. 860–869. Available at: https://doi.org/10.1177/0959683616675939.

Tschudy, R.H. (Robert H. and Scott, R.A. (Richard A. (1969) *Aspects of palynology*. New York ; Chichester : Wiley-Interscience, 1969.

Turner, M.G. *et al.* (2020) 'The impact of methodological decisions on climate reconstructions using WA-PLS', *Quaternary Research*, pp. 1–16. Available at: https://doi.org/10.1017/qua.2020.44.

Tzedakis, P.C., Hooghiemstra, H. and Pälike, H. (2006) 'The last 1.35 million years at Tenaghi Philippon: revised chronostratigraphy and long-term vegetation trends', *Quaternary Science Reviews*, 25(23–24), pp. 3416–3430. Available at: https://doi.org/10.1016/j.quascirev.2006.09.002.

Vautard, R. and Ghil, M. (1989) 'Singular spectrum analysis in nonlinear dynamics, with applications to paleoclimatic time series', *Physica D: Nonlinear Phenomena*, 35(3), pp. 395–424. Available at: https://doi.org/10.1016/0167-2789(89)90077-8.

Vautard, R., Yiou, P. and Ghil, M. (1992) 'Singular-spectrum analysis: A toolkit for short, noisy chaotic signals', *Physica D: Nonlinear Phenomena*, 58(1), pp. 95–126. Available at: https://doi.org/10.1016/0167-2789(92)90103-T.

Voelker, A.H.L. (2002) 'Global distribution of centennial-scale records for Marine Isotope Stage (MIS) 3: a database', *Quaternary Science Reviews*, 21(10), pp. 1185–1212. Available at: https://doi.org/10.1016/S0277-3791(01)00139-1.

Wang, Y.J. *et al.* (2001) 'A High-Resolution Absolute-Dated Late Pleistocene Monsoon Record from Hulu Cave, China', *Science*, 294(5550), pp. 2345–2348. Available at: http://www.jstor.org.libezproxy.open.ac.uk/stable/3085243 (Accessed: 31 March 2017).

Wei, D. *et al.* (2019) 'Climate changes in interior semi-arid Spain from the last interglacial to the late Holocene', *Climate of the Past Discussions*, pp. 1–31. Available at: https://doi.org/10.5194/cp-2019-16.

Williams, J.W. and Jackson, S.T. (2007) 'Novel Climates, No-Analog Communities, and Ecological Surprises', *Frontiers in Ecology and the Environment*, 5(9), pp. 475–482. Available at: https://www.jstor.org/stable/20440743 (Accessed: 4 July 2023).

Williams, J.W., Shuman, B.N. and Webb, T. (2001) 'Dissimilarity Analyses of Late-Quarternary Vegetation and Climate in Eastern North America', *Ecology*, 82(12), pp. 3346–3362. Available at: https://doi.org/10.2307/2680157.

Yeh, M. *et al.* (2018) 'Time series joins, motifs, discords and shapelets: a unifying view that exploits the matrix profile', *Data Mining and Knowledge Discovery*, 32(1), pp. 83–123. Available at: https://doi.org/10.1007/s10618-017-0519-9.

2 Identifying D-Os in pollen series

This Chapter explores whether it is possible to find the shapes of D-Os in pollen-derived time series.

One technique for matching palaeoenvironmental time series uses objective tie points; for instance, the GICC05modelext chronology (Seierstad *et al.*, 2014) matched the GISP2, GRIP and NGRIP ice core data using a rich set of tie points such as tephra and other volcanogenic signals, caused principally by Icelandic volcanic events (Seierstad *et al.*, 2014). Volcanogenic tie points are very rare between Mediterranean pollen cores from the glacial period, and none exist between them and the Greenland ice core record. Another technique uses similarity between geometric features in two time series; for instance, the LR04 benthic marine $\delta^{18}O$ stack (Lisiecki and Raymo, 2005) matched multiple series by feature, using algorithms developed in Lisiecki and Lisiecki (2002); Lin *et al.* (2014) comment that this required parameter choices which depended "on user judgment to determine whether the resulting alignment is reasonable". A recently developed generic technique of very wide application which both discovers and locates 'motifs' (recurring patterns), Matrix Profile (e.g. Yeh *et al.* (2018)), has been applied to the Greenland $\delta^{18}O$ series and was found to identify some D-Os (Barbosa *et al.*, 2023).

In this Chapter, features are used to attempt matches between the Greenland and pollen time series.

2.1 D-Os and pattern matching

The pattern which initiates a GI is distinctively asymmetrical. 'Pattern matching' is a technique used during this project. It searches in pollen records for events which are similar to these asymmetrical patterns in Greenland. The outline of the process is as follows.

A window containing the pattern of a GI onset (a D-O) in the Kindler series (a 'template') is moved along a target time series in which D-Os are expected to be present. At each step, a distance measure is calculated between the template and the target series, creating a distance curve over time. The distance value is recorded in the target series at the point which aligns with the midpoint of the rise in the template. The lowest points in the curve are those where the

target series is most like the template, and therefore most like a D-O. A window with a perfect match has a distance of zero. The process is repeated using templates for other GIs onsets. The distance curves are combined and the result used to discriminate between intervals which are likely to represent D-Os (D-O-like points, DOLPs) and those which are not. In the following sections, the detailed definition of the distinctive pattern and the evidence that it is highly consistent between GIs are presented. Pattern matching is then tested on the Kindler series and on pollen data.

2.2 Characteristics of D-Os

The important distinction in Fig 1.2 is between the Greenland Interstadials (GIs), shown as grey blocks, denoting warm calm periods, and stadials, which are cold, windy and dusty. GIs are numbered youngest to oldest, and increased precision and sampling resolution over time means there are now decimal versions such as GI 5.2 and 5.1, and subdivisions such as GI 7 a, b and c. Stadials are numbered by the older interstadial.

2.2.1 Definitions

The term “Dansgaard-Oeschger cycle” or “Dansgaard-Oeschger event” have been used to refer to both the intervals of the abrupt increase in $\delta^{18}O$ which initiates a Greenland Interstadial (GI), and more generically to a whole interstadial. Sanchez Goñi and Harrison (2010) define the initial rapid rise as the D-O event, and include it and the following slow cooling in the Greenland Interstadial. In contrast, Rasmussen *et al.* (2014), p. 15, recognise the ambiguity but define “‘event’ to refer to the entire stadial or interstadial periods (or their subperiods). However, the defining characteristic of each ‘event’ is the abrupt climatic change that occurs at its onset, and it is these major climatic signals that constitute the pinning points for the event stratigraphy." Kindler *et al.*, (2014), p. 887, adopting the same principle, define a ‘D-O event’ as "a rapid temperature increase followed by a gradual cooling back to stadial conditions". Malmierca-Vallet *et al.* (2023) also provide definitions of these and related terms.

In this thesis, the term “D-O” is used mainly to denote the signature asymmetrical pattern, starting before the abrupt rise and ending at some point early in the decline from the peak, and not the whole of an interstadial. The effect of choices of different start and end points for this D-O in pattern matching is discussed below in 2.4.3; while all the

abrupt rises at the initiation of GIs are of similar shape and duration, though of differing amplitude, the rate of decline in temperature after the peak in $\delta^{18}O_{ice}$ varies significantly.

The term "D-O-like-point" (DOLP) is used in this thesis where a searching algorithm identifies an interval in a pollen series which appears like a Greenland D-O.

2.2.2 Kindler temperature series

In this thesis the Kindler temperature series (Kindler *et al.*, 2014), rather than $\delta^{18}O_{ice}$, is most commonly used to describe Greenland climate and patterns of change, since it is specifically a climate variable. The Kindler series adjusts the NGRIP2 $\delta^{18}O$ series to give a time series in °C (Figure 2.1). It adjusts for changes in seasonal timing of precipitation and in water source, especially between stadial (low accumulation) and interstadial (high accumulation), and for $\delta^{15}N$ and gas ages in reaching the final temperature (Kindler *et al.*, 2014). The patterns of the $\delta^{18}O$ series and the Kindler temperature series are in most intervals highly similar, and the difference in GI initiation pattern and location between the two series is small (Figure 2.1), though the Kindler series exhibits greater variation in some stadials, especially in GS 2 (15 ka to 23 ka).

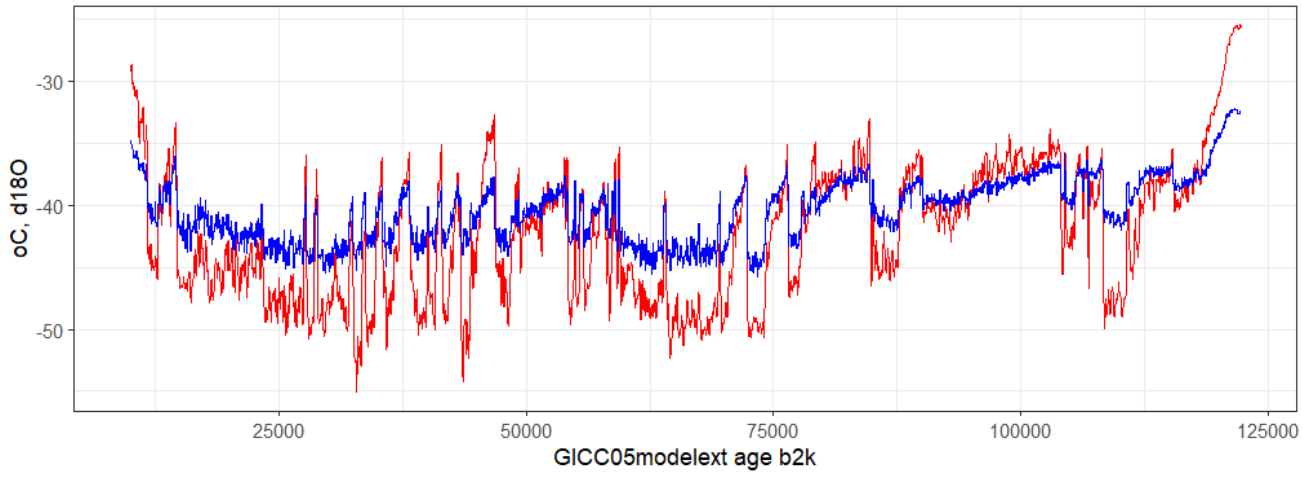

Figure 2.1 NGRIP Kindler temperatures °C (red) and $\delta^{18}O_{ice}$ ‰ (blue).

Kindler *et al.* (2014) never specify the exact meaning of their resulting temperature, but since it is based on $\delta^{18}O$, the series represents a mean annual air temperature, or more precisely a mean during the periods of precipitation during the year.

Kindler *et al.* (2014) p. 887 count the temperature rise at a D-O from the low to the high point: "The detected temperature rises at the onset of D-O events range from 5 ˚C (D-O 25) up to 16.5 ˚C (D-O 11) with an uncertainty of ±3 ˚C". These are equivalent to a substantial part of the temperature rise recorded in Greenland at the last glacial termination.

2.3 Consistency of D-O patterns in Kindler series

All the abrupt rises at the onset of GIs are of similar shape and duration, but the rate and pattern of decline after the peak in temperature varies greatly (Figure 2.2; age increases to the right). In this analysis, the Kindler series is normalised, and the intervals including the GIs are extracted and aligned on the midpoint of the rise at x = 100. They differ in absolute temperature and in amplitude despite the normalisation of the series as a whole. The long age range of ~ 2750 years also means that in some cases a younger GI is also seen in the tail, or younger interval (GI 4 also shows GI 3, for instance).

A reference dating point needs to be consistently defined in each D-O. In this project this is taken as the midpoint of the temperature rise; different D-Os can be centred on it to test for similarity. Inconsistencies with other practices and the Rasmussen dates are covered in the next section.

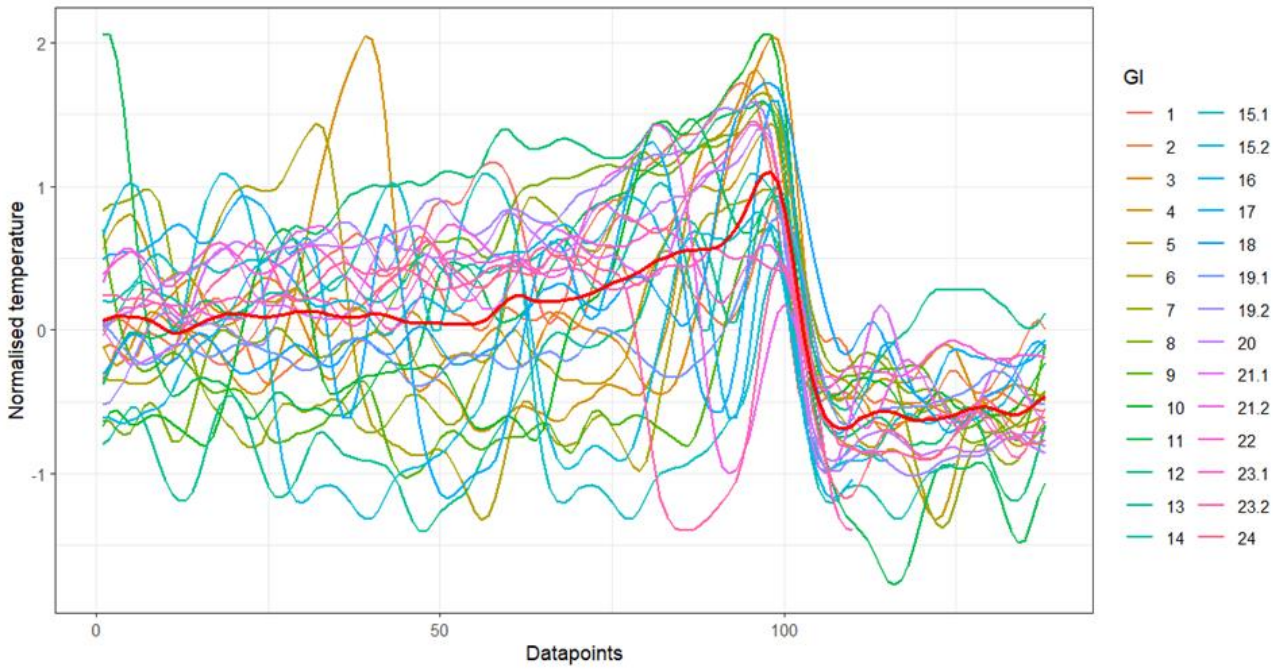

Figure 2.2: Kindler temperatures for all GIs, not individually normalised, aligned on common point (x = 100), and mean of all GIs (thick red line), taken from normalised Kindler series. X axis is data points in Kindler series, intervals ~ 20 years, time range ~2750 years).

To give a clear and consistent pattern for the initiation, to be compared with a target pollen series, these differences in scale and absolute temperature, and variability in the tail, need to be removed. An example result is presented in Figure 2.3, which shows the onset phases of multiple GIs, taken by extracting windows from the detrended Kindler series, from 15 data points before, or older than (~ 300 years), to 10 data points after, or younger than (~200 years), the Rasmussen date of the onset of each GI. The windows are then individually normalised to remove the scale and absolute temperature differences. The sensitivity to different start and end points for templates is tested in 2.4.3. The window width chosen in Figure 2.3 limits the impact of different post-peak rates of decline and duration seen in Figure 2.2.

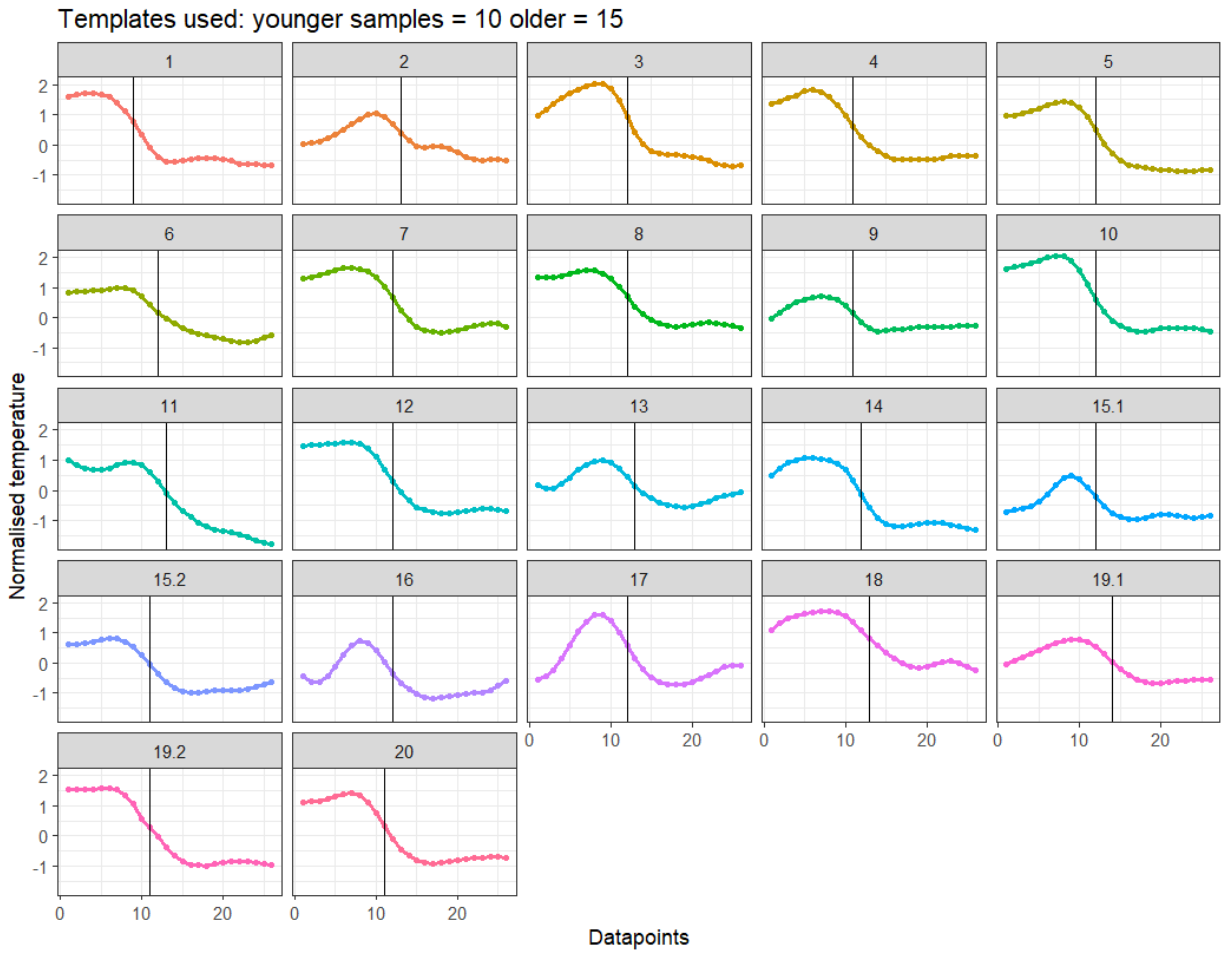

Figure 2.3 GI templates taken from normalised Kindler temperature then individually normalised; vertical lines denote midpoint of rise. Youngest on the left. Samples ~ 20 yrs apart, age range ~ 500 years. Headings are GI numbers.

The pattern of all D-Os is very similar when expressed like this, the variability being mainly in the tail. If the requirement is to identify specific D-Os in a target series by their individual patterns, a wider window than in Figure 2.3 would be needed.

2.3.1 Defining a reference dating point in a D-O

The reference point during the pattern to which we can consistently attach a date was defined above as the midpoint of the rise. Others have chosen other points. Rasmussen et al (2014), p. 23, say "The aim has been to define the event onsets at the first clear mark of a transition, e.g. at the first data point of the steep part that clearly deviates from the base-line level preceding the transition". However the midpoints of the rise in the Kindler series, shown as vertical lines in Figure 2.3, clearly do not fall consistently at the same point in the Rasmussen-dated windows (Rasmussen et al (2014) Table 2), although both use the same GICC05modelext chronology. The difference may be to do with Kindler's translation of $\delta^{18}O$ to temperature. The difference in age between 'first clear mark' and midpoint of rise is small (~ 40-100 years) compared with the uncertainties in the GICC05modelext chronology (e.g. maximum counting error 1,133 years for GI 5 at 32.6 ka) but in this thesis, the midpoint of the rise (vertical line in Figure 2.3) is the preferred reference point.

2.3.2 Similarity of GI onsets: Superposed Epoch Analysis

Superposed Epoch Analysis (SEA) (Lough and Fritts, 1987, and references therein) is a more formal way than plotting of showing that GI onsets are (a) highly similar and (b) not like other parts of the Kindler series. SEA takes a set of intervals from a series which are believed to contain a consistent pattern, aligns them on a consistent point in the pattern, and averages ('composites') them. It compares this mean shape with shapes composited from multiple sets of randomly chosen intervals from the series to find the probability that the shape has arisen by chance. SEA was applied using code modified from the sea function of the dplR package (Bunn A, Korpela M, Biondi F, Campelo F, Mérian P, Qeadan F, Zang C (2022). dplR: Dendrochronology Program Library in R. R package version 1.7.4, https://CRAN.R-project.org/package=dplR) to the onsets of GIs 1 to 20, aligned on the midpoint of the rise. In this analysis, the Kindler series is not modified by detrending or normalisation, which provides a stiffer challenge than comparing windows from the modified series shown in Figure 2.3, which removes offsets and scale differences.

The probability that these patterns arose by chance can be seen in Figure 2.4 to be very small by the low probabilities associated with each bar; thus the selected patterns are highly similar to one another and very different from other intervals in the Kindler series.

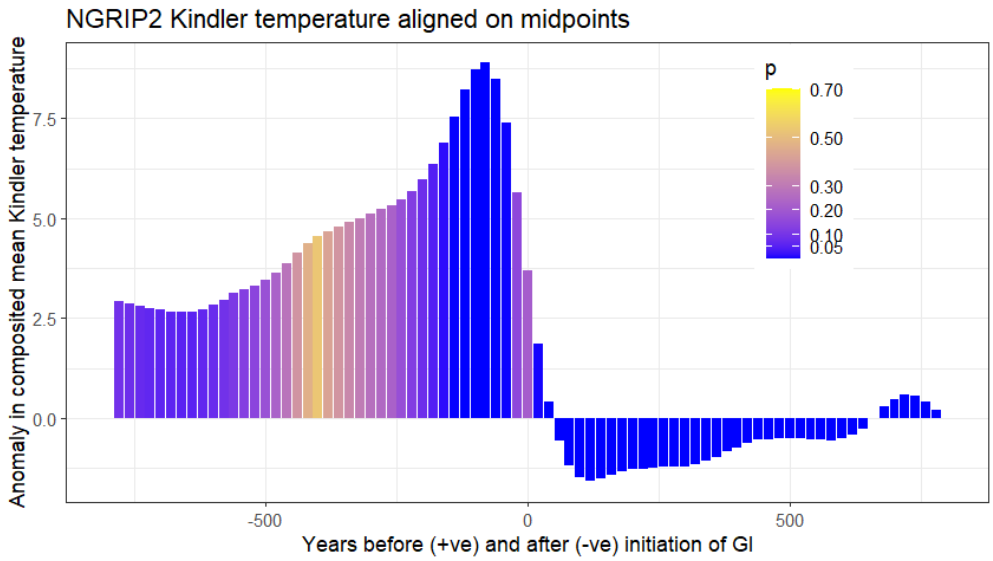

Figure 2.4 SEA: composited mean of Kindler temperatures during GI initiations and early part of GIs for GIs 1 to 20, aligned on midpoint of rise. Script: SEA CoP v2

The strong result in Figure 2.4 is not surprising, since the intervals were selected because of their clear patterns, but it gives assurance that SEA is able to provide clear evidence of the existence and uniqueness of such patterns within a series, in preparation for applying SEA to potential D-Os found in fossil pollen data.

2.4 Objective pattern matching using Euclidean distance

So far, it has been shown that GI onsets (D-Os) in the Greenland archives have highly similar and distinctive asymmetrical patterns. Although the response of vegetation and of pollen as recorded in cores to the climate changes recorded in Greenland is unlikely, for many reasons (see Chapter 1), exactly to replicate this crisp pattern, it is highly plausible that it would exhibit asymmetrical abrupt changes similar enough to be recognisable.

This section describes pattern matching in more detail. It can be applied to any time series expected to contain evidence of D-Os, and although the processes involved in making quantitative reconstructions have not been described yet and are the subjects of Chapters 3, 4, and 5, some reconstructions are used below as examples of

target time series. Chapter 6.3.5 has the reference to the R code which performs pattern matching. One of the underlying concepts was taken from https://www.r-bloggers.com/2012/01/time-series-matching/.

The choice of distance measure is first described, as it is key to the testing of template choices in subsequent sections.

2.4.1 Distance measures

A distance is calculated at each step between the template and the target series. Three distance measures were tested. The preferred measure is Euclidean distance (ED).

$$\text{ED} = \sqrt{\sum(x_i - y_i)^2} \quad (1)$$

Squared chord distance (SCD, $\sum\left(\sqrt{x_i} - \sqrt{y_i}\right)^2$) was rejected; it is structurally similar to ED but it cannot handle negative numbers, which occur in normalised data, and it suppresses large differences, which is undesirable.

Cross-correlation $\sum x_i y_i$ is similar in effect to ED but gives high values, not low, when a good match is achieved. It identifies match points little different from those found by ED, and ED was preferred as logically superior and simpler.

In the next section, a distance measure which combines Euclidean distance curves from multiple passes is used (*smmdist*); Section 2.4.5 describes how it is constructed.

Figure 2.5 shows an example of this distance curve found by applying pattern matching to a time series reconstructing GDD0 for the Lac du Bouchet core using fxTWA-PLS. The red points are potential D-Os, since they are where the series is most like the templates, and the down-spikes are very clear, suggesting that precise and obvious matches are possible in the time dimension.

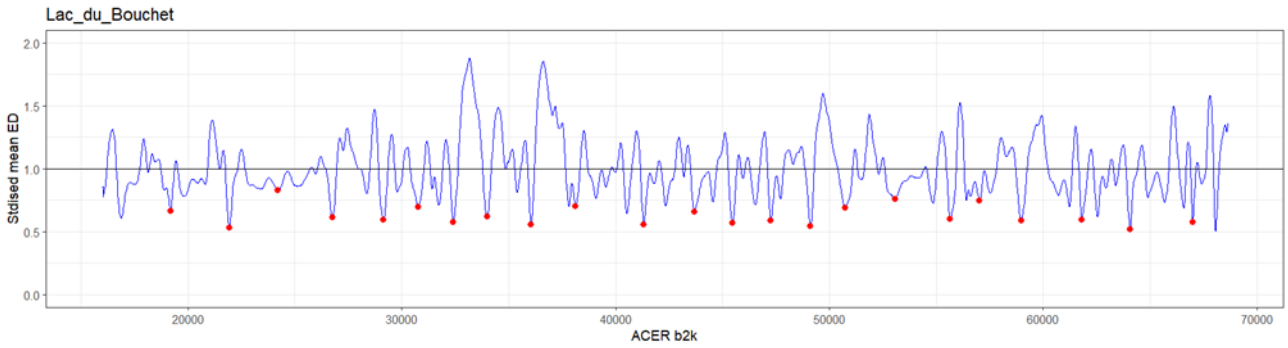

*Figure 2.5 Standardised mean of means of Euclidean distances (*smmdist*) for a reconstructed GDD0 (growing degree days > 0 ºC) time series from Lac du Bouchet. Blue line:* smmdist*. Red points: potential D-O, marking trough points where* smmdist *< 0.9 and nearest trough point is > ~ 1 ka distant, since D-Os do not occur that close together.*

2.4.2 Methodological choices in pattern matching

Several choices have to be made and tested during pattern matching, and these affect the clarity of the result significantly. These are:

- Template choices; section 2.4.3
    - How far the template window should extend before and after the midpoint.
    - How many, and which, GI template(s), to use.
- How to treat templates and target consistently, by detrending and normalising templates and target series; section 2.4.4.
- How to combine the distance measures if many templates or target series are used; section 2.4.5.
- How to accept/reject potential D-Os based on a continually varying distance curve; section 2.4.6.

2.4.3 Template widths and choices

The sharp rise is the most distinctive feature and varies only slightly between GIs. The duration and behaviour of the subsequent decline varies much more between GIs, and the more of the declining interval included in the templates, the more the impact on the distance measure. Therefore the ideal is to choose a template window width that maximises the contribution of the rise and minimises the contribution of the decline to the calculation of the distance measure. Minimising the contribution of the declining portion of the event also minimises the chances of including part of another GI in the calculation.

Three window widths are tested against the Kindler series. Firstly, a window from 10 data points younger than the Rasmussen date of the GI initiation to 15 data points older, data points being ~ 20 years apart in the Kindler series, giving a window from ~ 200 years younger to ~ 300 years older than the initiation (Figure 2.6; templates shown in Figure 2.7); this focusses on the abrupt rise.

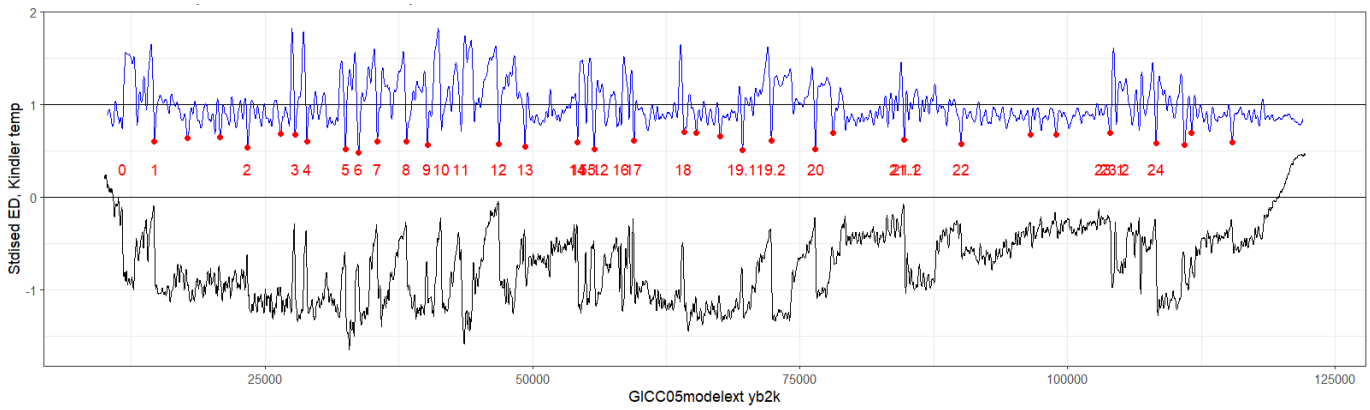

Figure 2.6 Pattern matching distance curve applied to detrended, normalised Kindler temperature series from which templates for GIs 1 to 20 were taken. Template width: 10 points younger to 15 older than GI date. Blue line: smmdist *curve. Red points are troughs where* smmdist *< 0.7; these are candidate D-Os. Red figures: GI numbers. Black line: original Kindler series, arbitrarily scaled.*

Using this window width, an ED value of ~ 0.7 is a working definition of the cutoff which defines a probable D-O in the Kindler series (red points), since this successfully identifies all the named GIs with the exception of 10 and 11, but limits to a handful other events identified as D-O-like. (In Chapter 6 the events between GIs 1 and 2 are discussed further.)

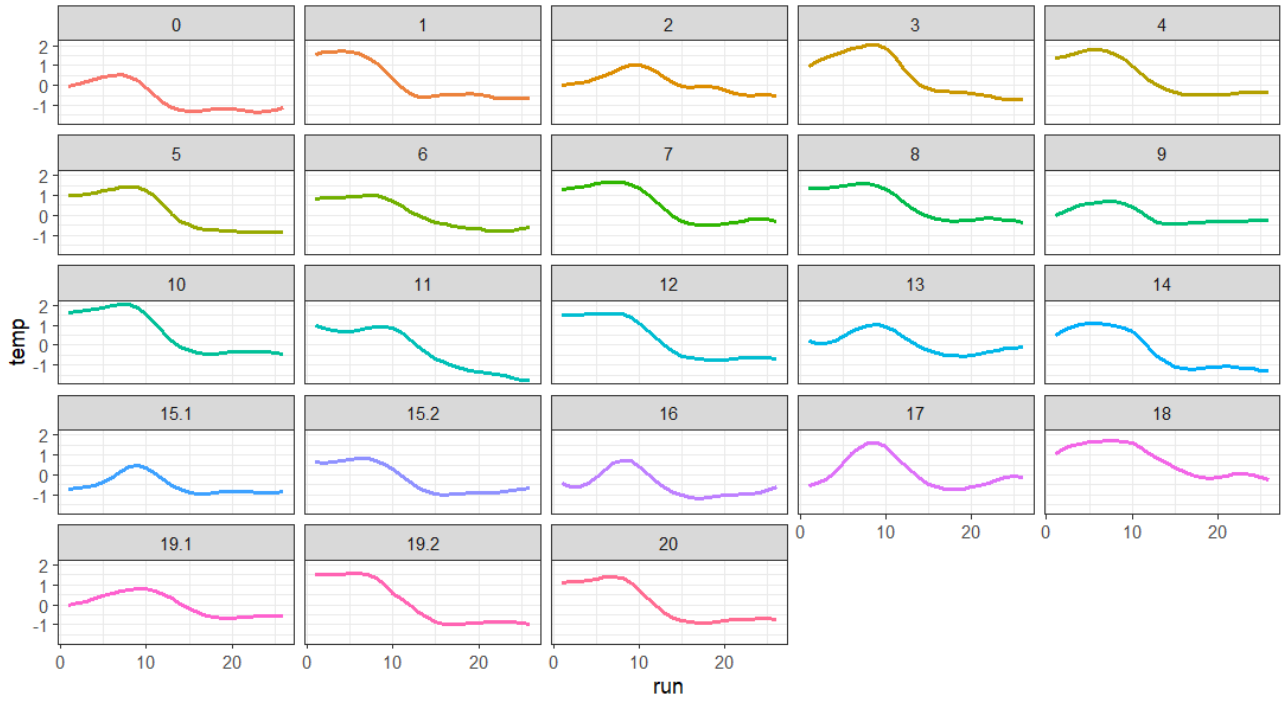

Figure 2.7 GI templates extracted from Kindler series from 10 data points younger to 15 older than the GI initiation date.

Secondly, a window including 37 datapoints both before and after the GI date, equating to ~750 years either side is tested (Figure 2.8). The discrimination is worse than in Figure 2.6, and many true GIs are missed at a cutoff of *smmdist* < 0.7; only 9 are identified as potential D-Os by red points. Relaxing this to ED < 0.75 only adds a handful of points, coloured grey. The worse performance is attributable to the less distinctive patterns now included in the templates (Figure 2.9).

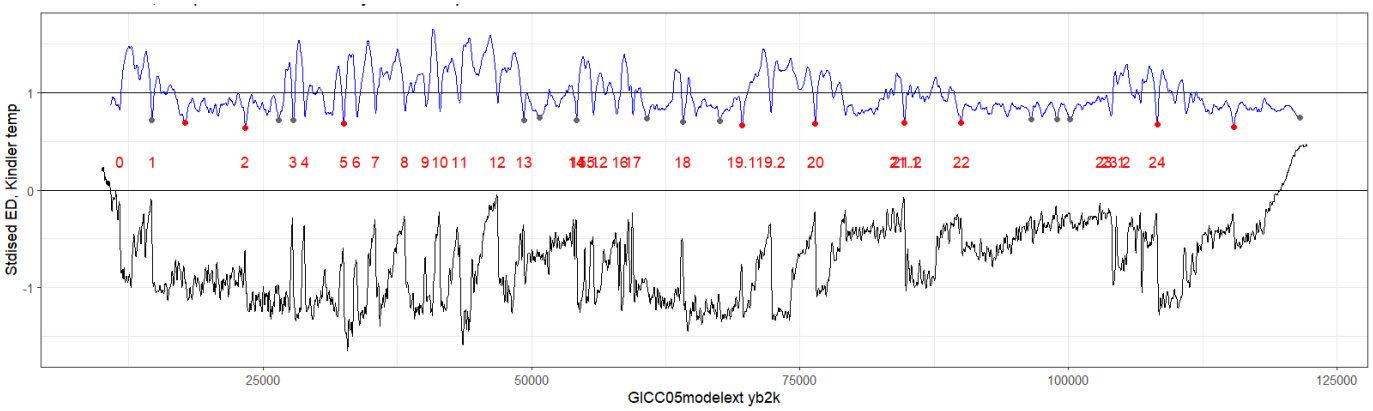

Figure 2.8 Pattern matching distance curve applied to Kindler temperature series from which templates for GIs 1 to 20 were taken. Template width: 37 points younger to 37 older than GI date. Blue line: smmdist *curve. Red points are troughs where* smmdist *< 0.7, and grey where* smmdist *< 0.75; these are candidate D-Os. Red figures: GI numbers. Black line: original Kindler series, arbitrarily scaled.*

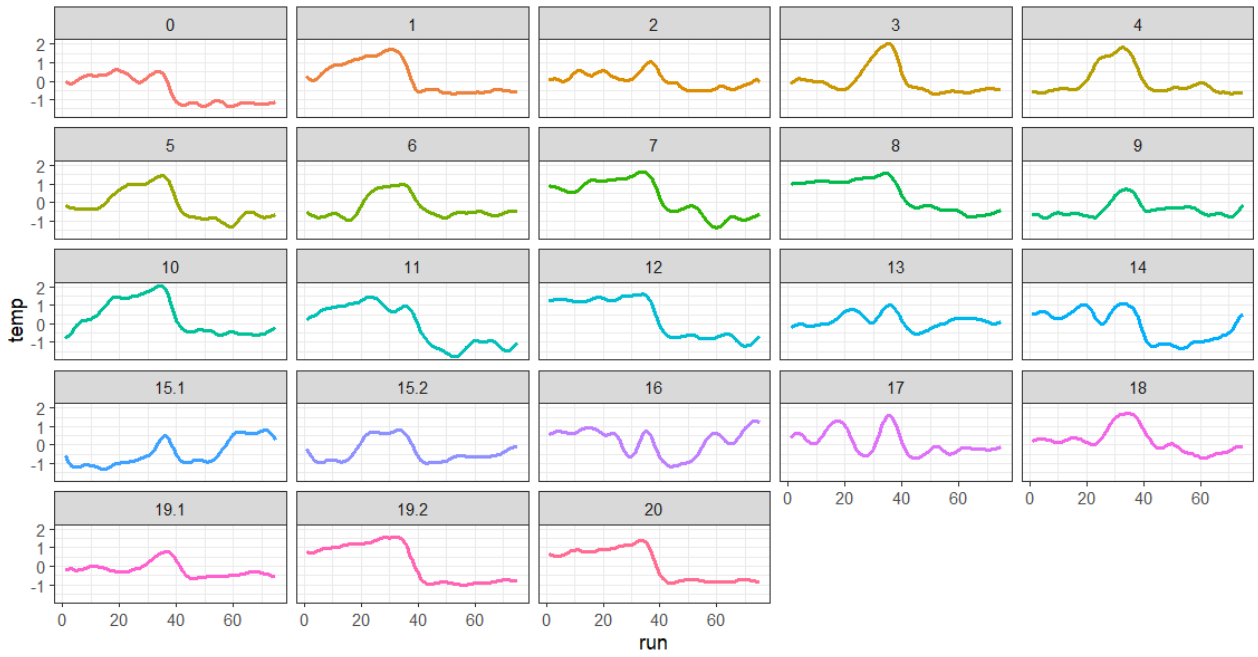

Figure 2.9 GI templates extracted from Kindler series from 37 data points younger to 37 older than the GI initiation date.

Lastly, a window is tested from 100 datapoints younger to 37 older than the GI date, equating to ~2000 years younger and ~750 years older, which usually includes a whole GI (templates in Figure 2.11). The result is of no value in identifying D-Os, because templates include long stretches which vary greatly between them, and in some case multiple GIs are included, despite truncation where appropriate (Figure 2.10).

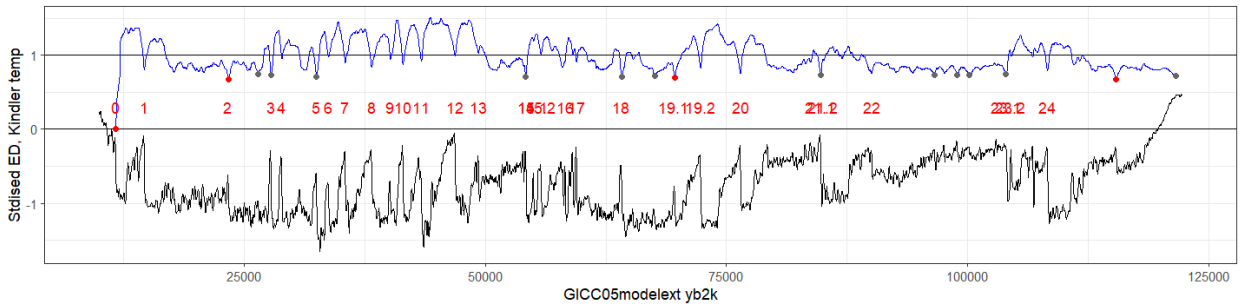

Figure 2.10 Pattern matching distance curve applied to Kindler temperature series from which templates for GIs 1 to 20 were taken. Template width: 100 data points younger to 37 older than the GI initiation date. Blue line: smmdist *curve. Red points are troughs where* smmdist *< 0.7, and grey where* smmdist *< 0.75; these are candidate D-Os. Red figures: GI numbers. Black line: original Kindler series, arbitrarily scaled.*

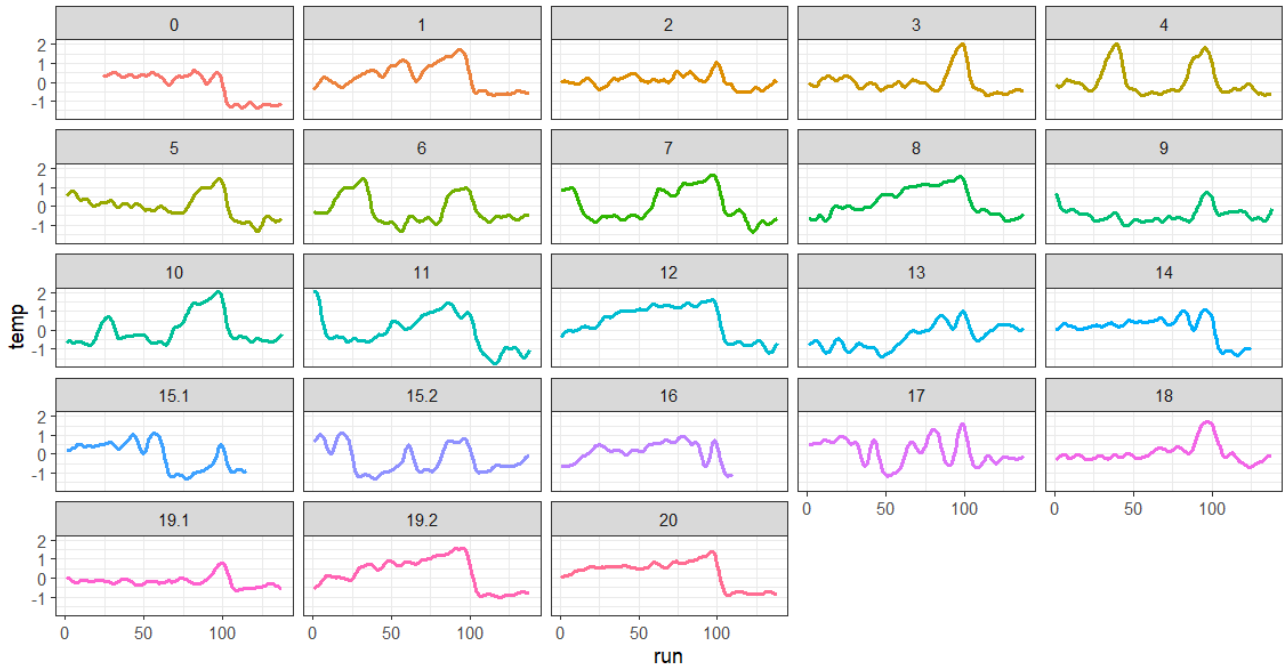

Figure 2.11 Templates extracted from Kindler series from 100 data points younger to 37 older than the GI initiation date.

This demonstrates the superiority of a narrow window focussed on the rapid rise, and a window of 10 younger to 15 older data points than the Rasmussen GI initiation date (~ 200 years and ~300 years respectively) is the chosen option.

2.4.3.1 Number of templates

The simplest case is to use a single template to determine the distance curve. Each template scores a perfect match at one point when applied to the parent Kindler series - the point from which it was extracted. However, GIs differ slightly; applying multiple GI templates may utilise the information from all the GIs in finding a match, especially in series less clear-cut than Kindler.

It might be considered preferable to compare GI templates with intervals in the target series which are of apparently similar age to the GI. However, weighting the distance curves so that GIs of age closest to the apparent pollen age attract more weight provided no clearer distance curves than the unweighted use of multiple templates, so weighting was rejected. This is further evidence that the differences between GIs are very small.

Then the choice is how many, and which, templates to use. Options include:

- a representative selection, for instance from short, medium and long GIs

- those within the apparent age range of the core
- all GIs, or all back to a certain age.

It was found that the difference in the distance curves between these choices is small, and the choice was made to include GIs 1 to 20. GI 0, the termination, is excluded as not a true D-O; GI 21 and following are excluded because they are rather different in shape from most younger GIs, and since few of the cores used in this project extend to such ages, their slightly poorer matches would weaken the distance curves of cores in which, by reason of their ages, they could not in practice be matches.

2.4.4 Consistency of treatment

2.4.4.1 Template extraction

Normalising then detrending the Kindler series before extracting the templates means that each template sits within roughly the same range. Figure 2.12 shows the normalised and detrended Kindler series.

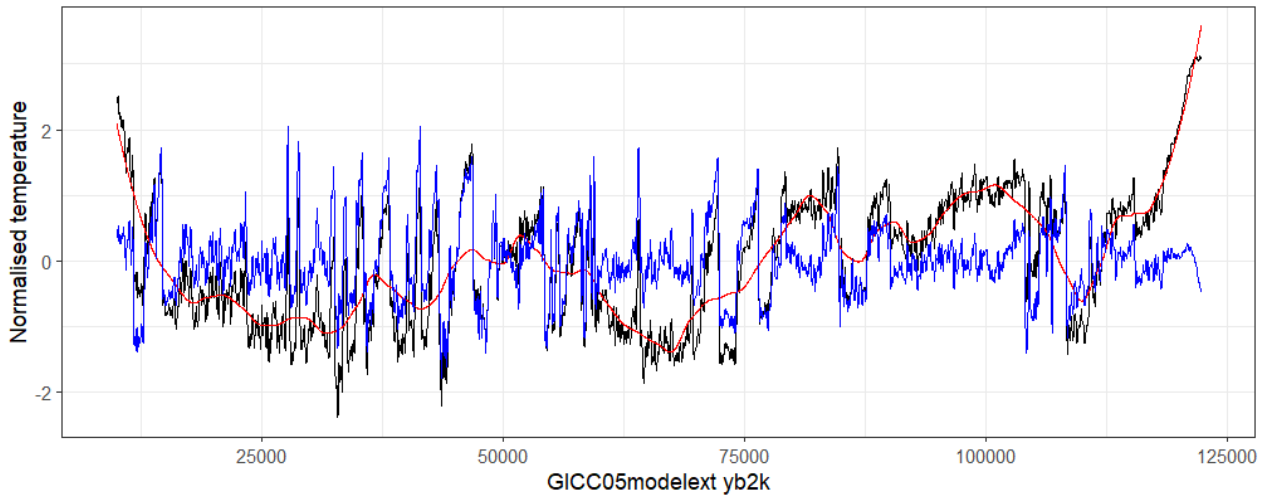

Figure 2.12 Detrending of normalised Kindler series. Black: normalised Kindler series; red: loess curve through normalised series, span = 0.1; blue: detrended curve, i.e. normalised less loess curve.

The detrending was performed by subtracting a loess curve through the normalised Kindler series with span = 0.1. Singular Spectrum Analysis (SSA) was applied to test whether loess was too crude a method (SSA and its use in analysing Kindler and pollen series is discussed in detail in 2.6.5.2). The difference between detrending using loess (span = 0.1) and using the residuals after extracting the sum of SSA longwave components was not considered

significant (Figure 2.13), especially in terms of the position and amplitude of significant changes, so loess was accepted as simpler to implement.

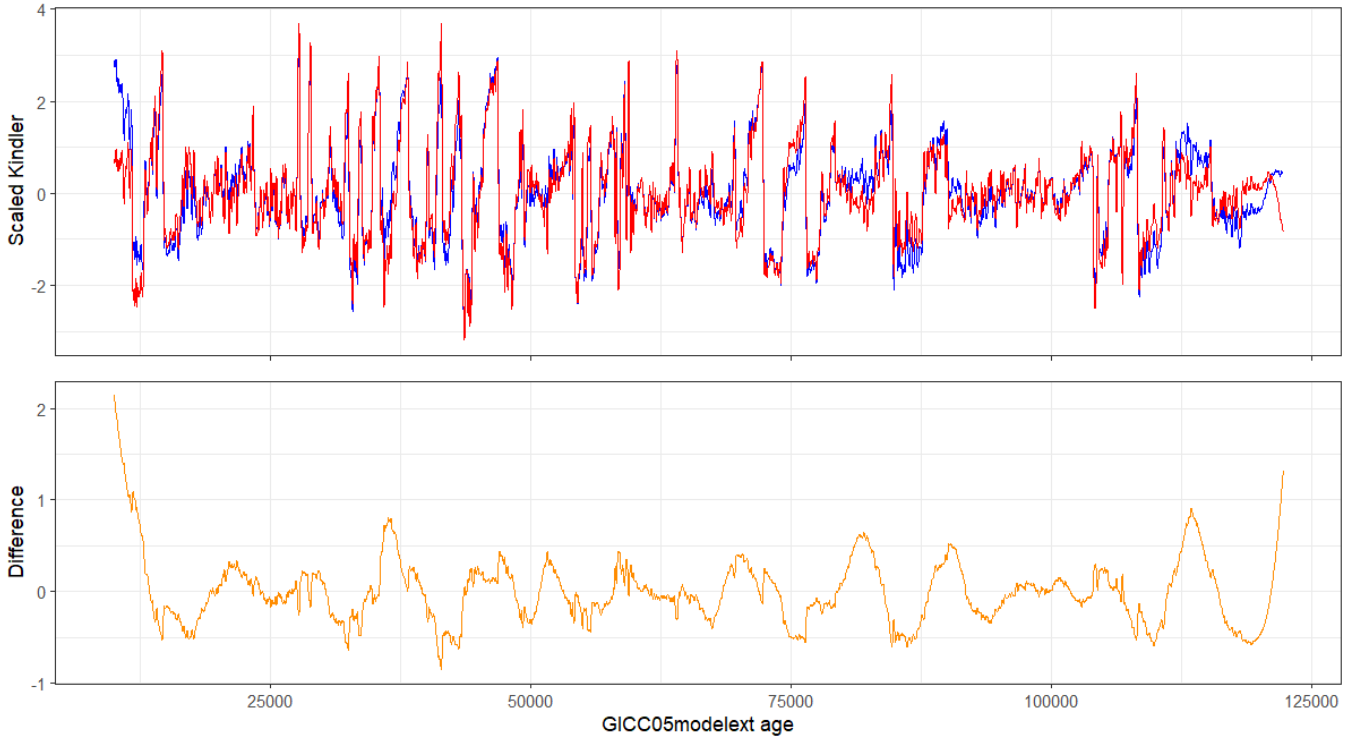

Figure 2.13 Upper panel: comparison of SSA residuals (red) and normalised and loess-detrended series for Kindler (black), both normalised. Lower panel: difference between (scaled) SSA residual and loess-based result.

Each template is then extracted as a window in the normalised and detrended Kindler series around the Rasmussen start date of the GI, the width defined by the number of Kindler data points younger and, separately, older than that point.

Each template separately is then normalised again by subtracting its mean. This ensures that all templates have a mean of zero; if this is not done, despite the previous normalisation and detrending of the complete series, templates will have slightly different means, and difference curves will partly reflect these offsets. The start and end of the temperature rise are found and a midpoint identified.

Figure 2.14 shows the resulting templates.

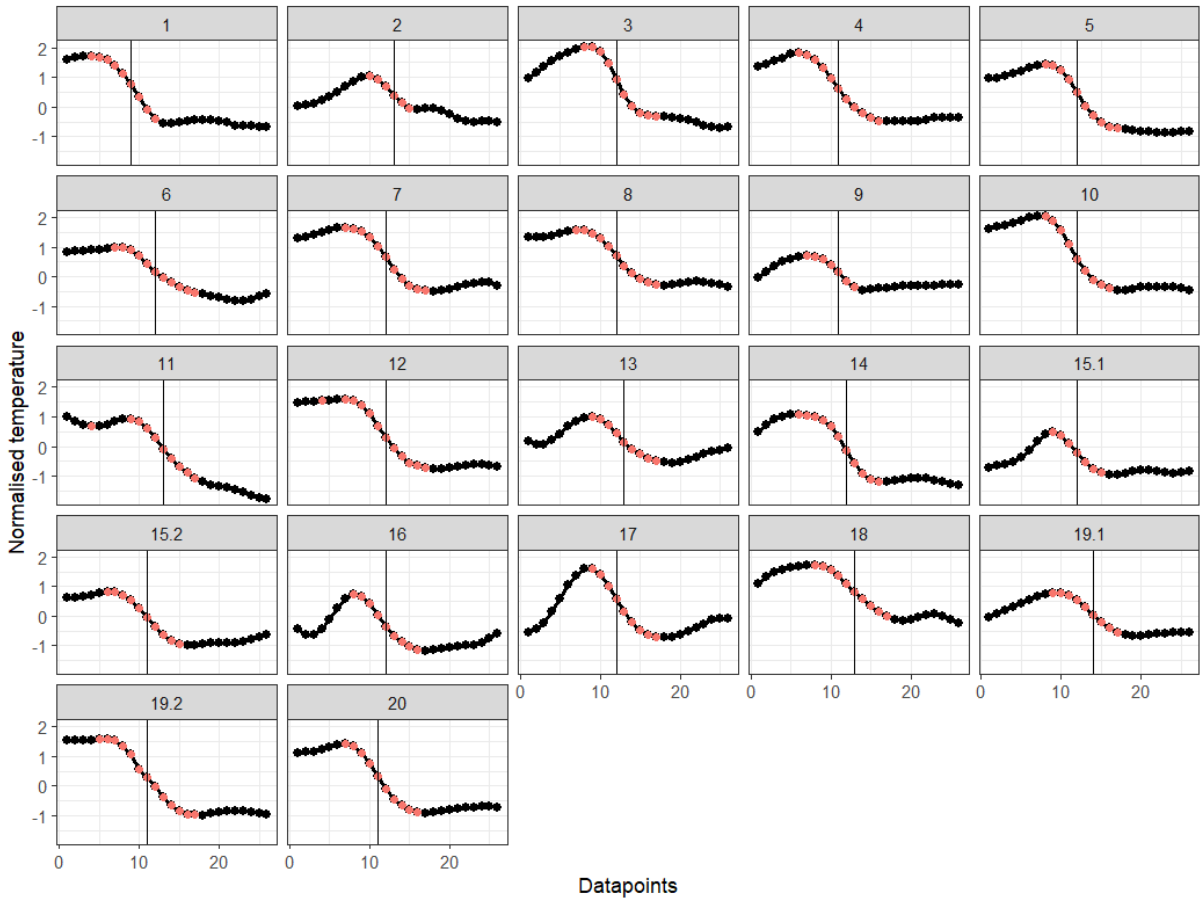

Figure 2.14 Templates extracted from Kindler series for GIs 1 to 20. Headings are GI numbers. Orange data points are the rising part of the temperature change, and the vertical line denotes the midpoint of the rise.

2.4.4.2 Treatment of the target series

To calculate a distance, the numbers of data points in the windows being compared must be the same. To achieve this the target series is linearly interpolated to the same resolution as the templates, i.e. the same as the Kindler series. All pollen series used in this project have resolutions much coarser that the ~ 20 years available in the Kindler series. Linear interpolation between core samples neither loses information nor adds spurious information: inflection points, rates of change and therefore shapes remain the same. However, in Chapter 6 the strength of the evidence for a D-O depends partly on the underlying number of original core samples which define a shape in an interpolated pollen series.

The age-interpolated pollen series is normalised and detrended in the same way as the parent Kindler series.

It can be argued that each instance of the running window in the target series should be normalised again, to be compatible with the treatment of templates. Such a second normalisation is applied to each template for the

purpose of removing residual differences in scale and absolute value, so that templates all have the same means and similar scales. The argument is that similar treatment of the running window would make matches between templates and the running window more precise: an exact match (ED = 0) might be achieved where the target series pattern is identical to the template, whereas unnormalized windows taken from a detrended normalised target series will suffer, like the templates, from small differences in absolute value. However, this is not safe where fossil pollen is concerned. Where the target series is already known to contain patterns highly similar to the templates and of similar amplitude, such as the parent Kindler series, this is safe, but is not safe where the target series may contain many different patterns of different scales. The effect of a second normalisation is to render all patterns in the target series of similar amplitude with a mean of zero, so that a pattern of originally small amplitude, possibly arising from noise, could appear identical to an originally large-amplitude pattern which marks an important change in the pollen. Both would attract the same low distance measure. Second normalisation of the running window is therefore rejected.

In this way the templates and the running window in the target series are made as far as possible consistent and without significant offsets to cause spurious differences.

2.4.5 Combining distance curves

A single template provides a single distance time series, which is easily understood. But as discussed above, and especially where the patterns in the target series are less clear-cut than in the Kindler templates, it is important to use multiple templates to maximise the chance of good matches. This leads to multiple distance curves which then need to be combined in some way to be able to discriminate D-O-like intervals.

2.4.5.1 The combination challenge

When run against the Kindler series, the distance curve for a template exhibits a perfect match (ED = 0) only against the interval from which it was extracted; see Figure 2.15 which uses the GI 5 template alone and has a perfect match at GI 5. Note that the distance curve at many other GIs shows excellent matches for GI 5, demonstrating again the similarity between onsets, but also that the method is sensitive enough to show that there are differences.

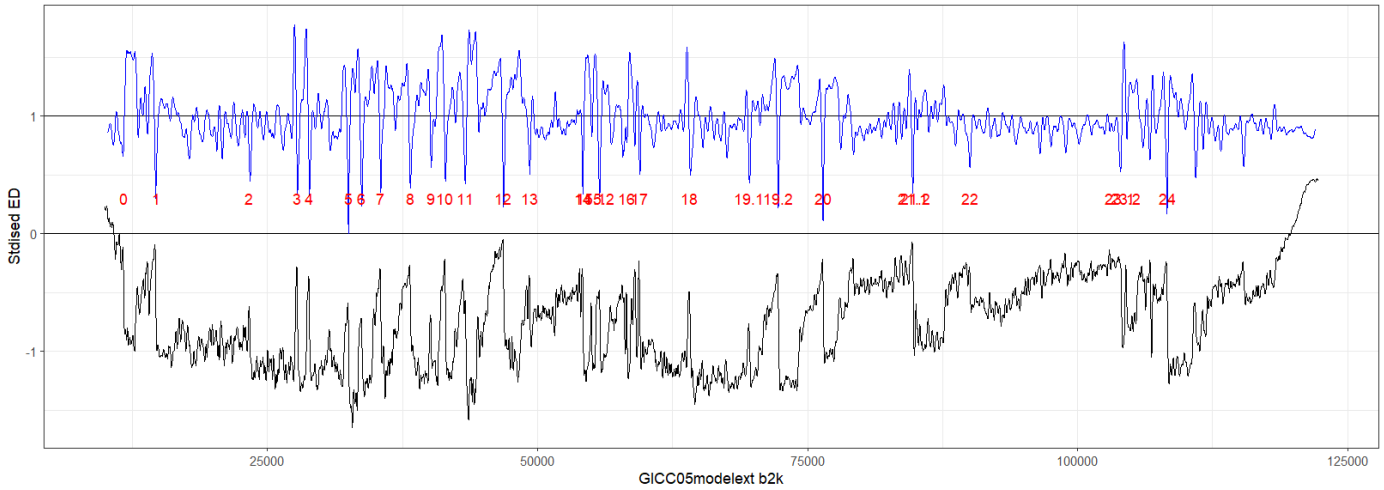

Figure 2.15 Pattern matching distance curve applied to detrended, normalised Kindler temperature series using a single template (GI 5) . Blue line: smdist *curve. Red figures: GI numbers. Black line: original Kindler series, arbitrarily scaled.*

The simplest combination is to take a mean of all the distance curves, implicitly attributing equal importance to each template. In 2.4.3 the idea of weighting template curves by the apparent nearness in age of the template to the interval in the target series was raised as a theoretical ideal, but it seems to have no practical value. Figure 2.16, a repeat of Figure 2.6, shows that a combined mean ED of multiple templates (*smmdist* – see below for definition), even in the ideal environment of being applied to the parent Kindler series, can never show ED = 0, but the similarities between templates still lead to many low-ED points at D-O-like points. In this figure low points with ED < 0.7 are labelled red, as an initial filter to identify the most probable D-Os.

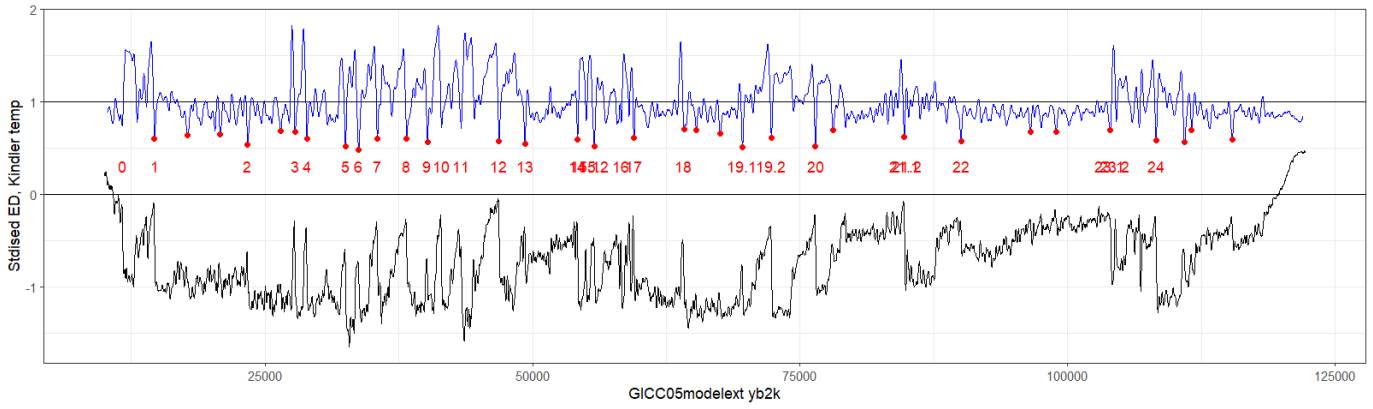

Figure 2.16 Pattern matching distance curve applied to detrended, normalised Kindler temperature series from which templates for GIs 1 to 20 were taken. Template width: 10 points before to 15 after GI date. Blue line: smmdist *curve. Red points are troughs where* smmdist *< 0.7; these are candidate D-Os. Red figures: GI numbers. Black line: original Kindler series, arbitrarily scaled.*

While pattern matching is based on shape, and by leaving the running windows unnormalized the differences in amplitude of any shapes in the target series are not lost, the method does not always distinguish perfectly between

smaller and larger scale patterns. In Figure 2.16 with a cut-off at *smmdist* = 0.7, small excursions in the Kindler series can register as good matches, for instance between GI 1 and GI 2, and between GI 22 and GI 24. These apparent inaccuracies arise because we have deliberately run multiple templates which are not identical, because the aim is to apply it to noisy fossil pollen data, and the intention is to capitalise on the slight differences between templates.

As an alternative to using the mean, it is possible to combine curves by taking the minimum of all the individual curves. This is on the grounds that each template finds its own home in the parent series perfectly, whereas a mean allows the many other less perfect matches to dilute this. This provides a compelling plot (Figure 2.17) when run against the Kindler series, with each GI picked out perfectly at *mdist* = 0, where *mdist* is the minimum of all ED curves. A related possible combination is the lower quartile of the individual curves.

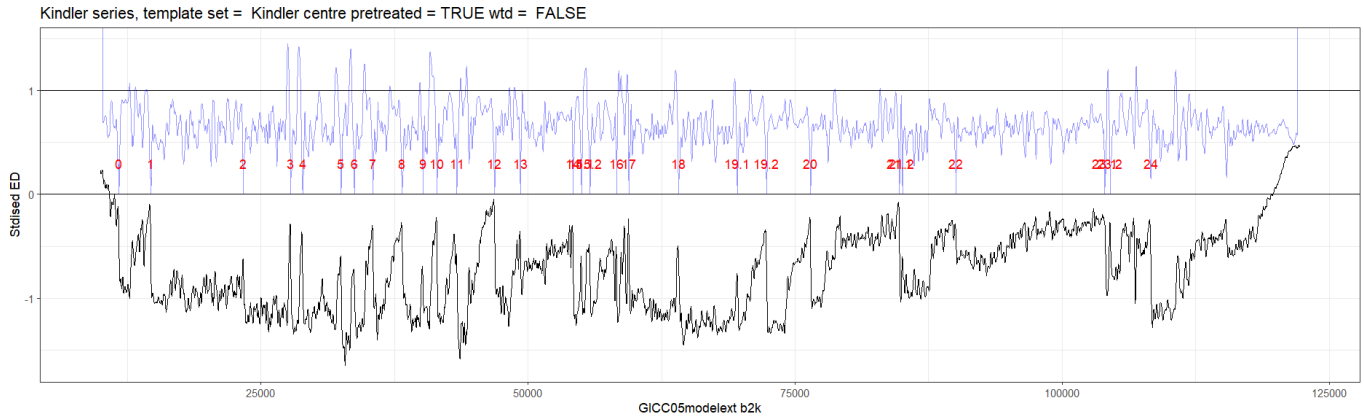

Figure 2.17 Pattern matching distance curve applied to detrended, normalised Kindler temperature series from which templates for GIs 1 to 24 were taken. Template width: 10 points before to 15 after GI date. Blue line: mdist *= minimum of all template curves. Red figures: GI numbers. Black line: original Kindler series, arbitrarily scaled.*

Both minimum and lower quartile measures perform poorly when applied to pollen-based series, since the minima are much less pronounced, owing to the less clear features in the pollen-based series, so a mean measure *smmdist* was retained.

2.4.5.2 *The consistency issue and* smmdist

To permit satisfactory combination or comparison of EDs generated by different templates or by different pollen-based series, ED must be consistently stated. The ED time series for each template is first standardised by division by the length of the template, since templates may be of different lengths, and greater length means greater sum of distance. Then it is divided by its own mean, such that the final series has a mean of 1. A value of 1 means the match

is no better than random for this series, and a perfect match has a value of zero. Points which resemble the template will fall between 1 and 0, and the nearer to 0, the better the match. This is referred to as the standardised mean of means distance (*smmdist*).

ED series can then be directly compared and combined not only across multiple templates applied to a single target series, but also across multiple target series such as different bioclimatic variables, since they may all contribute information about the position of D-Os. In this case a second process is needed, taking the mean of the individual target series *smmdist* curves. This is only reliable if the standardisation described above has been applied.

2.4.6 From distance curve to binary choice: D-O or not?

Ideally criteria are needed which, applied to the distance curve (*smmdist*), allow acceptance or rejection of potential D-Os.

The simplest option is to set a universal threshold value, so that troughs in the curve which project below this are accepted as potential D-Os (DOLPs). This may not be wholly satisfactory, even within a single series, as Figure 2.16 demonstrates by missing GIs 10 and 11. Further, a single threshold cannot be applied to all series; pollen series from different cores exhibit different levels of variability, so that their distance curves may show different ranges of trough values.

In Chapter 6, when applying pattern matching to quantitative reconstructions, additional filters are applied, for instance by testing the size of the apparent subsequent interstadial.

2.4.7 Summary of section 2.4: pattern matching

This section has described 'pattern matching', a technique designed to look in time series for patterns which resemble the distinctive asymmetrical shape of the sharp rise in temperature seen at the onset of GIs in the Greenland ice archives. This can identify intervals in the time series which may represent D-Os.

The onset phase of all GIs has a very similar but not identical pattern. Templates extract the intervals around GI initiations from the Kindler temperature series to represent instances of this asymmetric pattern. A relatively narrow template around the GI initiation provides the best discrimination. A Euclidean distance between a template and a

target pollen-derived series along which it is run defines where and how well the target series matches the template. The two series must be consistently treated by detrending and normalisation, to minimise spurious differences. Multiple templates from GI 1 to GI 20 should be used to capitalise on the slight differences between them, when applying the method to fossil pollen. The distance curves of multiple templates can best be combined by taking their mean.

This technique can be applied to any time series from a palaeoclimate archive. Below, time series are made directly from fossil pollen series, and in Chapter 6 time series are made by quantitative reconstruction of bioclimatic values from fossil pollen series. Pattern matching is applied in both cases, where suitable, to find possible D-Os.

2.5 Application of pattern matching to identify D-Os in pollen time series.

2.5.1 Selection of pollen core data

Pollen core records were selected that extend as far as possible into the last glacial (Weichselian, 11.7 ka – 123 ka), but did not have to extend into intervals younger than 20 ka. Records that only provided summary information at functional type level (e.g. herbs, temperate trees) were discarded. Only records for which dating information was available were used. Records from atypical settings, such as deltaic formations or archaeological sites, were also discarded. This selection process resulted in the list of 16 cores in Table 2-1.

Table 2-1 Pollen cores.

Lat	Long	Elevation (m)	Site code used in this thesis	Name in source	Reference	DOI for pollen counts
39.650	20.916	470	Ioannina	Ioannina	Sanchez Goñi et al. (2017)	https://doi.org/10.1594/PANGAEA.870867
44.830	3.820	1200	Lac_du_Bouchet	Lac du Bouchet - DIGI		
42.570	11.800	355	Lagaccione	Lagaccione		
40.940	15.610	656	Lago_Grande_di_Monticchio	Lago Grande di Monticchio		
42.130	2.750	173	Lake_Banyoles	Lake Banyoles		
39.050	22.270	500	Lake_Xinias	Lake Xinias		
39.103	26.321	323	Megali_Limni	Megali Limni		
39.100	-0.680	225	Navarres	Navarrés		
42.130	12.320	220	Stracciacappa	Stracciacappa		
41.900	12.760	44	Castiglione	Valle di Castiglione		
31.508	35.471	-430	Dead_Sea	Dead Sea	Miebach et al. (2019)	https://doi.org/10.1594/PANGAEA.900564
35.683	36.300	167	Ghab	Ghab-1	Bottema (2010)	https://doi.org/10.1594/PANGAEA.738784
40.433	29.533	83	Iznik	Lake Iznik	Miebach et al. (2016)	https://doi.org/10.1594/PANGAEA.858056
45.900	4.930	267	Les_Echets_redone_2	Les_Echets G	Beaulieu and Reille (1984)	https://D-OI: 10.1111/j.1502-3885.1984.tb00066.x
40.490	-1.290	985	Villarquemado	El Canizar de Villarquemado	Harrison et al. (2019)	http://dx.doi.org/10.17864/1947.219
35.533	46.117	1287	Zeribar	Lake Zeribar	Bottema, Sytze; Neotoma Dataset 4548, Lake Zeribar, Pollen Dataset - European Pollen Database	https://doi.org/10.21233/b54b-nw94

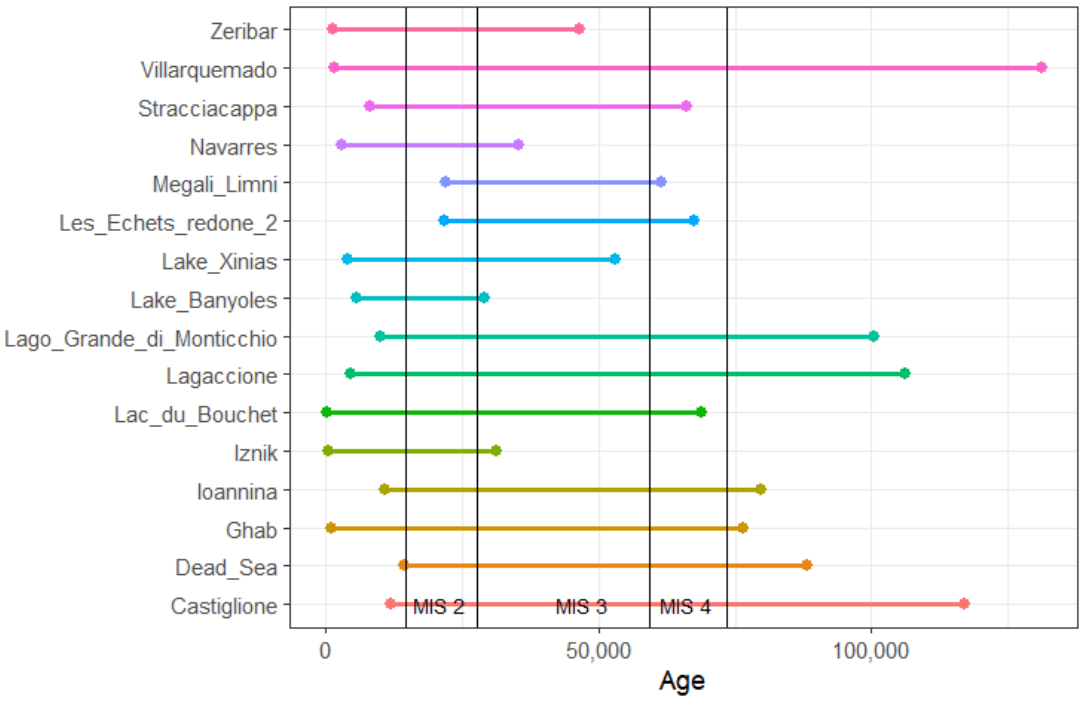

Figure 2.18 Age ranges of cores, according to age models provided with core data.

2.5.2 Testing whether sampling resolution affects the recognition of D-Os

These cores vary in chronological sampling resolution (Figure 2.19), based on the age models provided with the cores. (Lac du Bouchet in the ACER database records 505 samples, but these are points digitised from the original printed figure; the number of physical samples was 279 (Reille and de Beaulieu, 1990). Nevertheless, the true resolution is still good in the context of the set of cores). A compromise must be struck between high sampling resolution and the time required for analysis, especially with a long core, and the choice of physical sampling resolution may be made before the dating is available and may turn out to provide low temporal resolution. Sediment compaction also means that consistently spaced physical samples cover longer time intervals towards the bottom of a core.

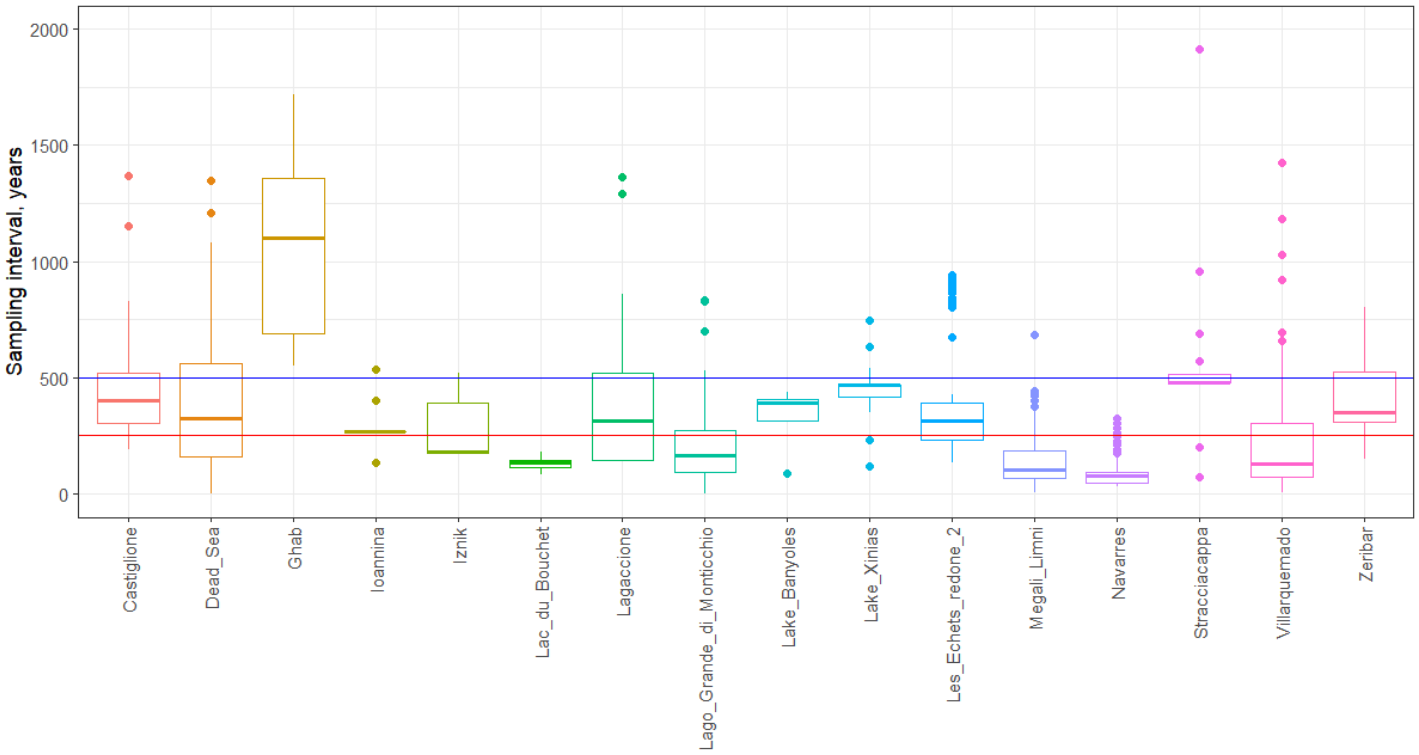

Figure 2.19 Sampling intervals of cores; horizontal lines at 250 and 500 years.

A test was performed to determine whether the sampling resolutions of these cores are too coarse to enable century-scale D-Os to be seen. For this test it was assumed that the ages attributed to samples in a core are precise GICC05modelext ages, and that the core provides data which perfectly replicate the Kindler temperatures at those ages. Figure 2.20 plots in colour the Kindler series only at the points when the core has physical samples, for a selection of cores. Only a few of the rapid warmings in the grey full Kindler series are not replicated in the coloured series overlying it; there are examples at, for instance, Lago Grande di Monticchio and Lake Xinias. This suggests that sampling resolution is not a major bar and that the great majority of D-Os are in principle capable of being represented by cores with these sampling resolutions. At Navarres, the missed GIs are the result of an hiatus.

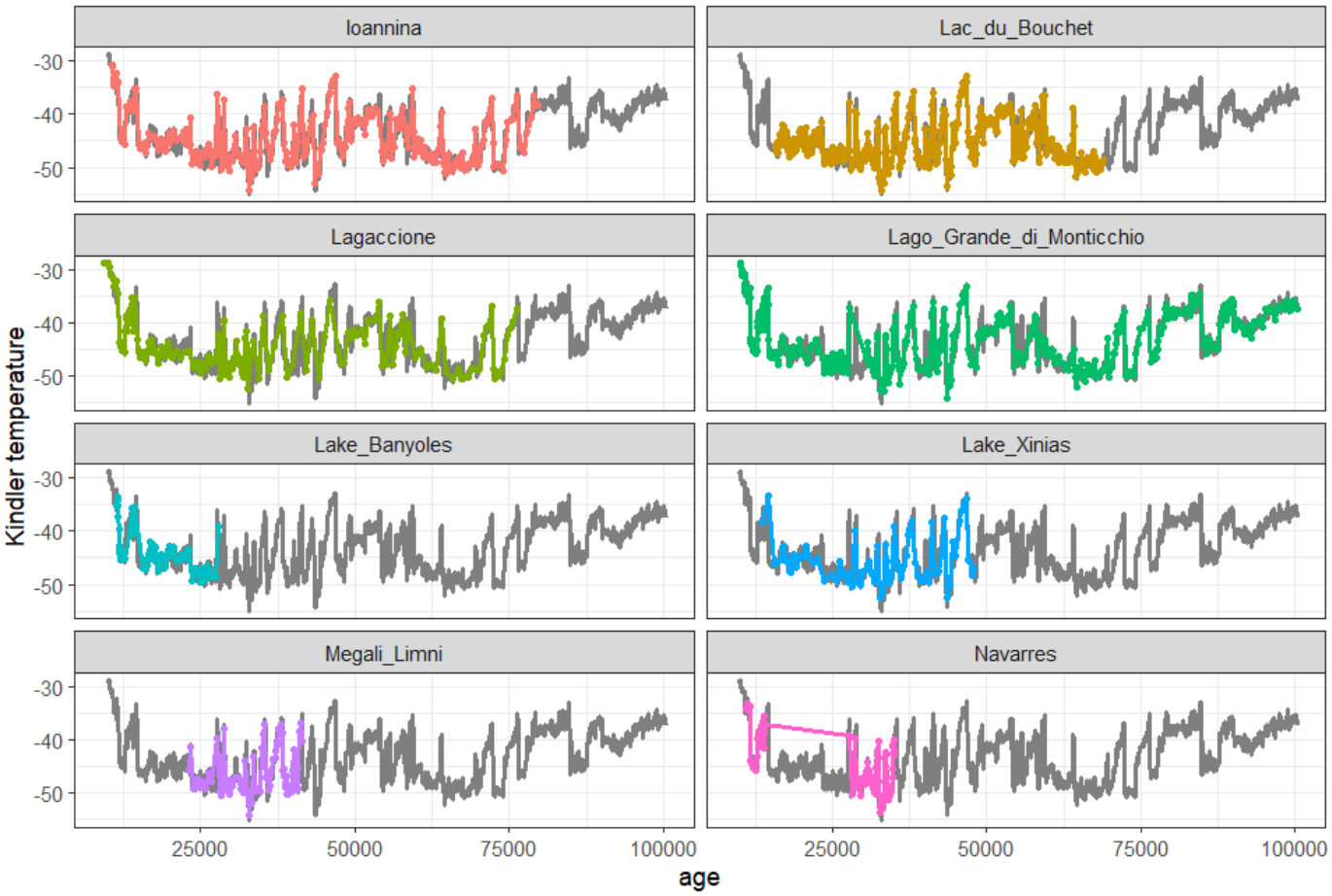

Figure 2.20 Demonstration of sampling resolution: grey line: Kindler temperature series; coloured lines: Kindler series sampled only where core has samples; ages: ACER age models for cores, GICC05modelext for Kindler.

2.6 Evidence of D-Os in fossil pollen data sets of reduced dimensions

2.6.1 Dimension reduction by PCA and DCA

Pollen data is multi-dimensional (multiple taxa) and it is therefore helpful to reduce the number of dimensions to allow patterns to emerge. Principal Components Analysis (PCA), also known as Empirical Orthogonal Functions (EOF), and Detrended Correspondence Analysis (DCA) are established dimension reduction techniques. PCA and DCA were applied to multi-taxon fossil pollen series. Both provide multiple time series ('components' or 'axes') explaining decreasing fractions of the variation. PCA assumes monotonic linear relationships, which are not common in abundance distributions, whereas DCA is designed to handle unimodal distributions of abundance along an environmental gradient, which is approximately the expected distribution of taxon abundance (see Chapters 1, 4 and 5).

PCA was calculated in R using the prcomp() function in the R stats package (R Core Team, 2023). DCA used the decorana() function in the vegan package (Oksanen et al, 2022. vegan: Community Ecology Package. R package version 2.6-4, https://CRAN.R-project.org/package=vegan.

In both PCA and DCA, the sign attributed to a component is arbitrary. This presents a problem, in that the climate change which denotes a D-O in Greenland is a temperature increase, but the direction of warming along a PCA or DCA component is not obvious, and in any case no component has been found to be interpretable as a simple aspect of climate such as temperature or moisture. This means that abrupt changes in PCAs and DCAs might be coolings, warmings, or both, or changes in another climate variable or combination of variables, whereas the templates against which they are compared are warmings; very poor matching might result.

Below, Lac du Bouchet is used as the main example, since it is commonly considered to exhibit D-O patterns e.g. Fletcher *et al.* (2010).

Table 2-2: % variation explained by PCA components at Lac du Bouchet

	Component	% variation explained	Cumulative % variation explained
PCA	1	39.4	39.4
	2	28.6	68.0
	3	13.6	81.6
	4	12.3	93.9
	5	1.4	95.3

Figure 2.21 shows the first 3 components as time series obtained by applying PCA and DCA to the pollen record from Lac du Bouchet; similar results are obtained from other cores. The locations and amplitudes of abrupt changes, which might signify D-Os, differ significantly between PCA and DCA, and also between different components in each. The intervals between abrupt changes in PCA are very short and do not appear to relate to ages which might match any D-Os; there are few sharp changes in DCA, which should represent modal distributions better than PCA, and although the first components of PCA and DCA should

represent the strongest signals, the two are very different. This strongly suggests that PCA and DCA time series do not demonstrate D-O-like patterns well. Applying PCA and DCA to other cores, none appear to show markedly asymmetrical changes.

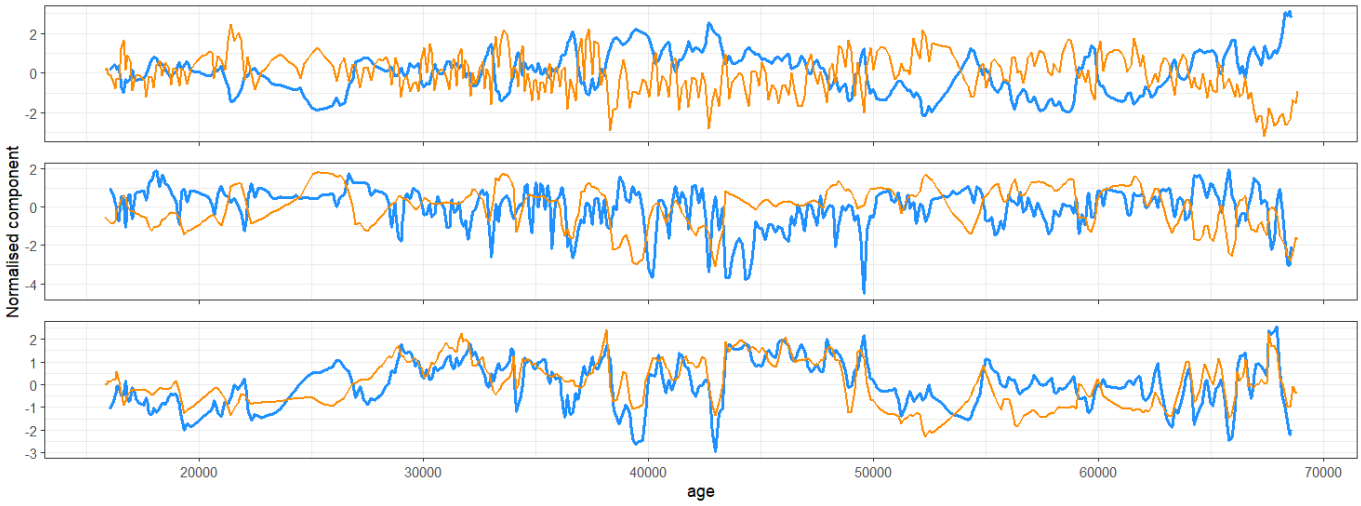

Figure 2.21 First 3 PCA (orange) and DCA (blue) components for Lac du Bouchet, all normalised for comparability. Top to bottom: First, second and third components

This view gains strength when pattern matching is applied to the components for Lac du Bouchet, giving the three distance curves shown in Figure 2.22 for PCA and in Figure 2.23 for DCA. As noted above, owing to the arbitrary sign, there is no certainty that an increase in the *y* dimension is related to a warming rather than to a cooling, if either, so both troughs and peaks are identified by points. In both PCA and especially DCA plots for this and other cores, different components identify template-similar points at different locations in the core with few coincidences.

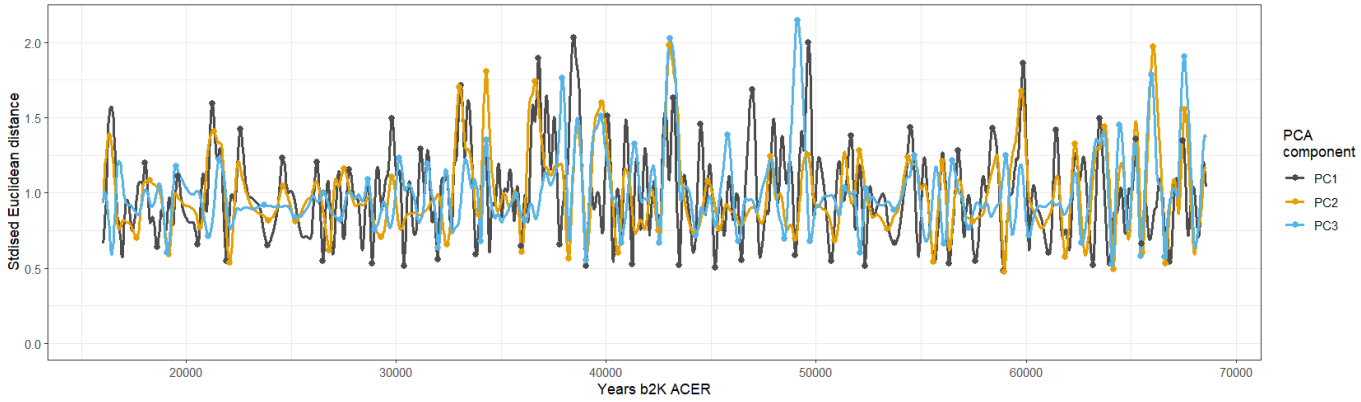

Figure 2.22 Euclidean distance curves (smmdist) for first 3 PCA components for Lac du Bouchet. Points are troughs (and peaks in case the series is inverted) in the curves. Age is from ACER age model.

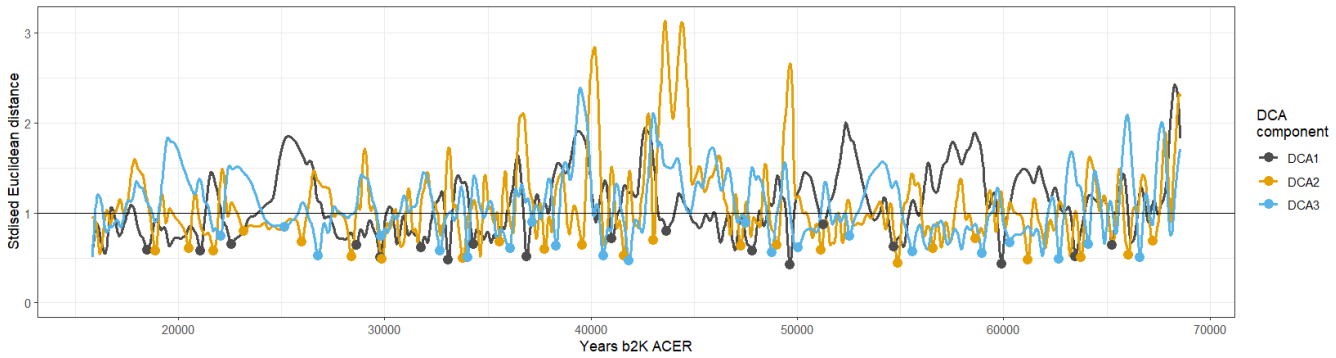

Figure 2.23 Euclidean distance curves (smmdist) for first 3 DCA components for Lac du Bouchet. Points are trough points in the curves, most similar to templates. Age is from ACER age model. Script: # Pattern hunting DCA allT v2, pbx

These time series do not tell similar stories about the location of abrupt changes. Combining these distance curves, in the expectation that each component contributes something new to the picture, results in a number of potential D-Os which far exceeds the number of GIs expected in the age range. This is interpreted to mean that we are finding genuine D-O events but also other events, presumably including rapid coolings, but that we cannot distinguish between them.

2.6.2 Squared Chord Distance (SCD)

Rapid climate change should result in rapid change of pollen composition, and this can be identified by Squared Chord Distance (SCD) (see 2.4.1 for the definition) by calculating the differences between sequential taxon abundance vectors (sample rows) in the fossil pollen. The rate of change of SCD was also calculated, as change per ka.

SCD gives a magnitude, but not a direction, of change between samples. While it integrates the effects of all influences on the pollen, and so should include a signal of climate, on the other hand it cannot distinguish between changes arising from warmings from those due to coolings or influences unrelated to temperature or even climate.

An SCD curve, and its rate of change, for Lac du Bouchet is shown in Figure 2.24. It is interpolated to the Kindler timescale for comparability with plots above. In this case the rate of change is little different from the SCD since the intervals on which the timescale has been interpolated (those in the Kindler series) are evenly spaced along the series; this will not be the case with all series, so the adjustment should always be made. It identifies many points of rapid change as upward spikes.

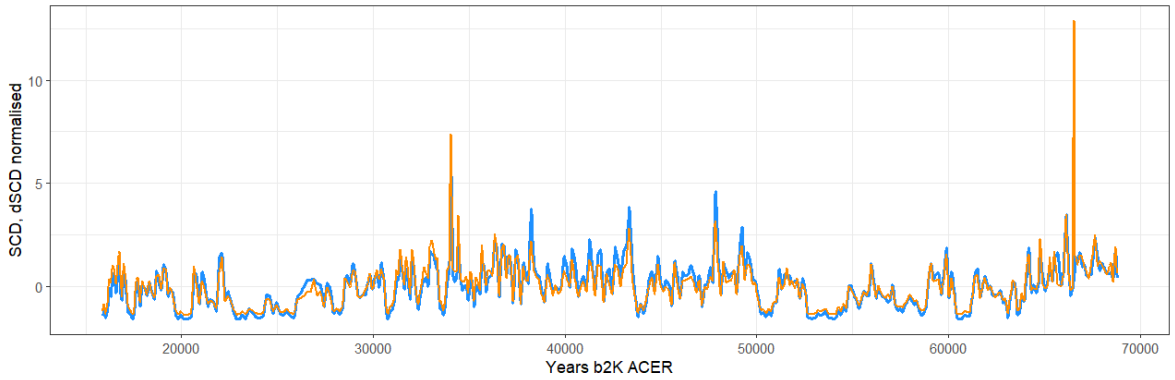

Figure 2.24 SCD (blue) and rate of change in SCD (orange), both normalised and interpolated to the Kindler timescale, for Lac du Bouchet pollen series.

The largest changes in pollen composition should indicate the sharpest changes in climate. In Figure 2.25, after removing a low amplitude long wave component using loess (span = 0.5) and normalising the residual SCD, peak changes are labelled with red points, and compared with the positions of GIs in the Kindler series. There are several apparently close coincidences, such as at GIs 4, 6, 8, 10 and 11. Conversely, GIs 2, 5, 7 and 12, which would be expected to leave a mark in the pollen, do not make a clear appearance, and an event is registered at ~18 ka which has no counterpart in the Greenland record.

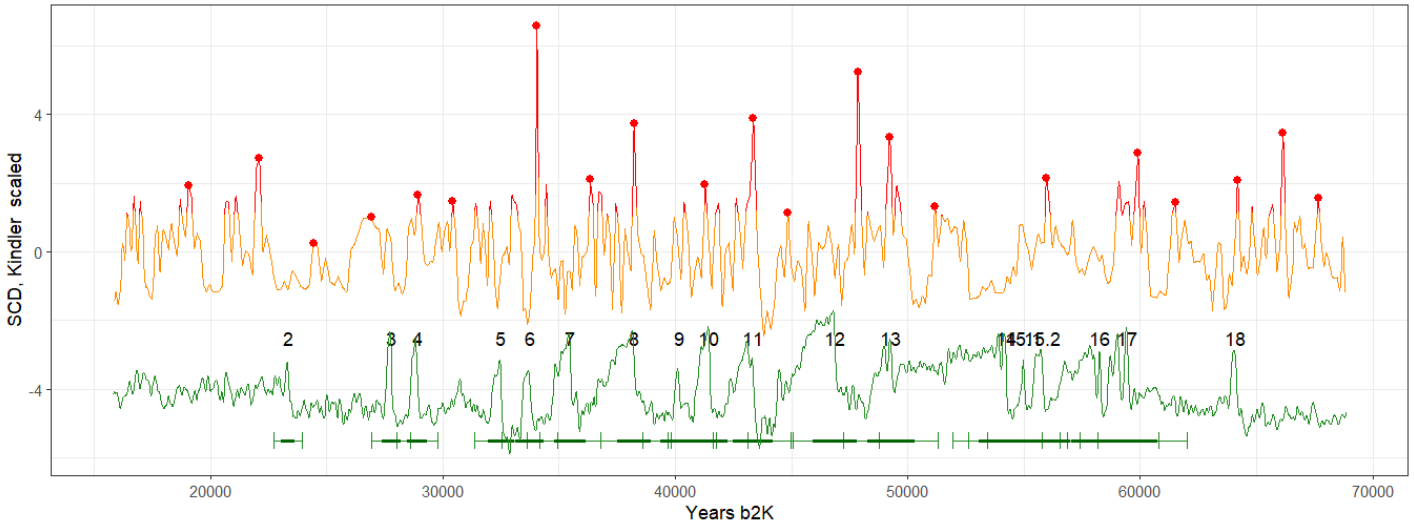

Figure 2.25 Orange line: detrended normalised SCD for Lac du Bouchet, on ACER age model scale; green line: arbitrarily scaled Kindler temperatures, on GICC05modelext chronology, with GI numbers and, below, ± 1 sigma error bar (MCE) in GI age (thick line) and ± 2 sigma error bar (thin line).

This inconclusive result is replicated in other cores. This leads to the conclusion that while SCD clearly describes substantial changes in pollen composition, and that some of these may well relate to D-Os, it cannot reliably be used to locate D-Os. The explanation may lie in the calculation of SCD, which utilises the fractional abundance of each taxon, and so attributes equal importance to all taxa. In Chapter 5 it is shown that different taxa are differently sensitive to climate; in particular, some abundant taxa are not very sensitive to some bioclimatic variables, so that substantial change in abundant taxa may be of little climatic importance. In addition, as noted above, SCD sweeps the result of all influences into one measure, so that it is possible that two or more influences, such as temperature and moisture, may mute or cancel each other out.

2.6.3 Grouping taxa

A common approach in palynology is to use a simple classification of pollen taxa to identify events. For example, the ratio of arboreal to non-arboreal pollen ('AP/NAP', e.g. Birks and Birks (1980)) has been used, with increased AP interpreted as interstadial conditions. This approach is explored by using objective ways of summarising pollen series into a small number of classes which behave similarly, and looks in time series constructed from those classes for abrupt changes.

2.6.3.1 *Hierarchical clustering*

Hierarchical clustering was selected in preference to *k*-means clustering since the choice of *k* could be considered arbitrary. In hierarchical clustering, a correlation matrix of the pollen abundance is used to identify groups of taxa which are found together. In Figure 2.26, where this is applied to the Lagaccione pollen record from 14 ka to 36.2 ka, available from the ACER database, two large groups emerge, which have clear meanings: trees and non-trees. Within trees, other lesser clusters emerge. Within non-trees, *Artemisia* and Amaranthaceae form a cluster, and others can be suggested, but generally there is less clarity.

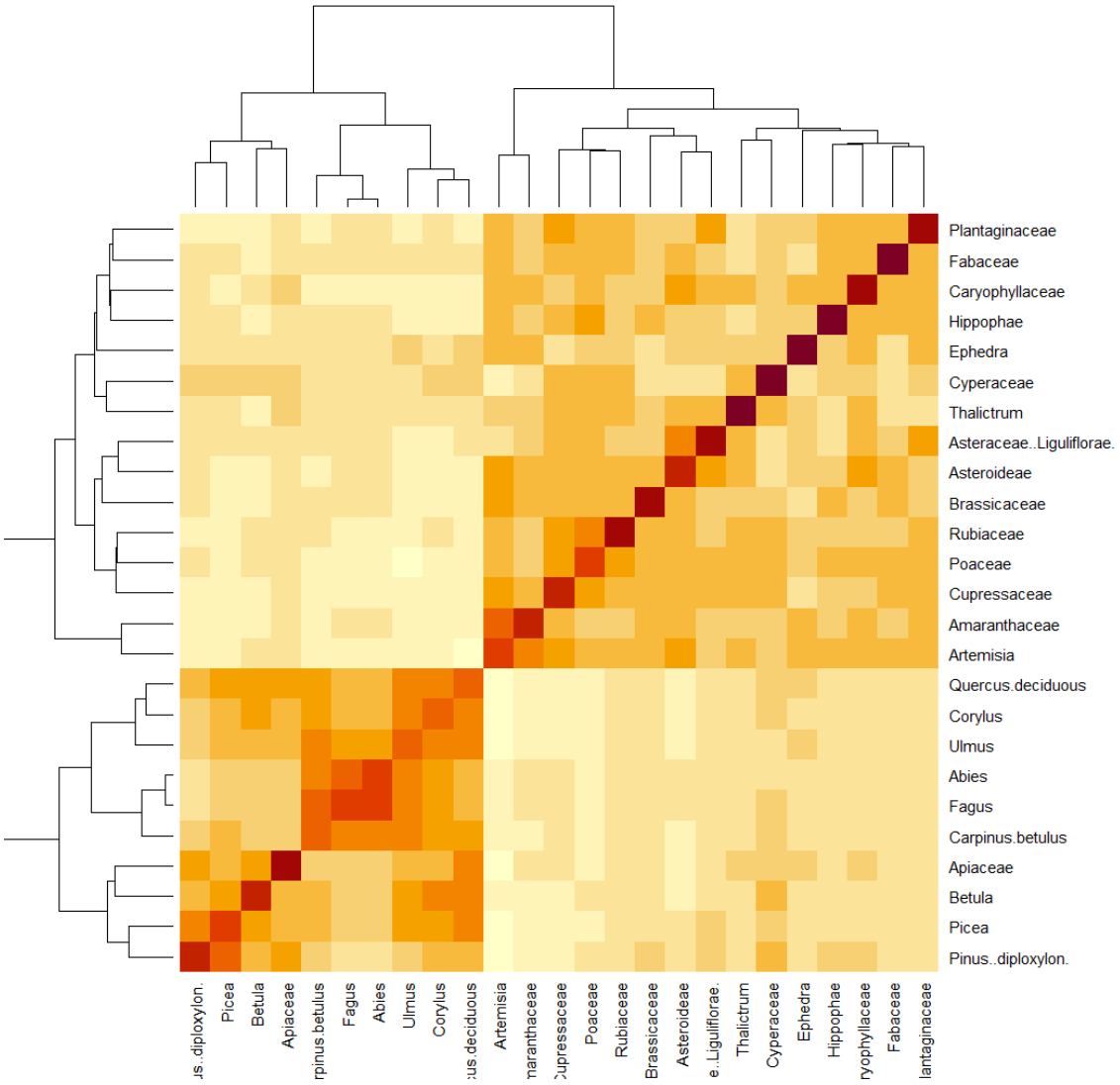

Figure 2.26 Heatmap of correlation matrix of taxon abundances for Lagaccione for 25 most abundance taxa (96% of total abundance) from 14 ka to 36.2 ka.

However, the clusters found are sensitive to the time range considered. Clustering using an extended series from 9.2 ka to 76 ka (additional data provided by Donatella Magri, pers. comm., June 2020) shows a less clear result with different groupings, and the tree group is fragmented (Figure 2.27). This arises because the relative taxon abundances differ in different intervals. Thus the groups found by hierarchical clustering are unstable.

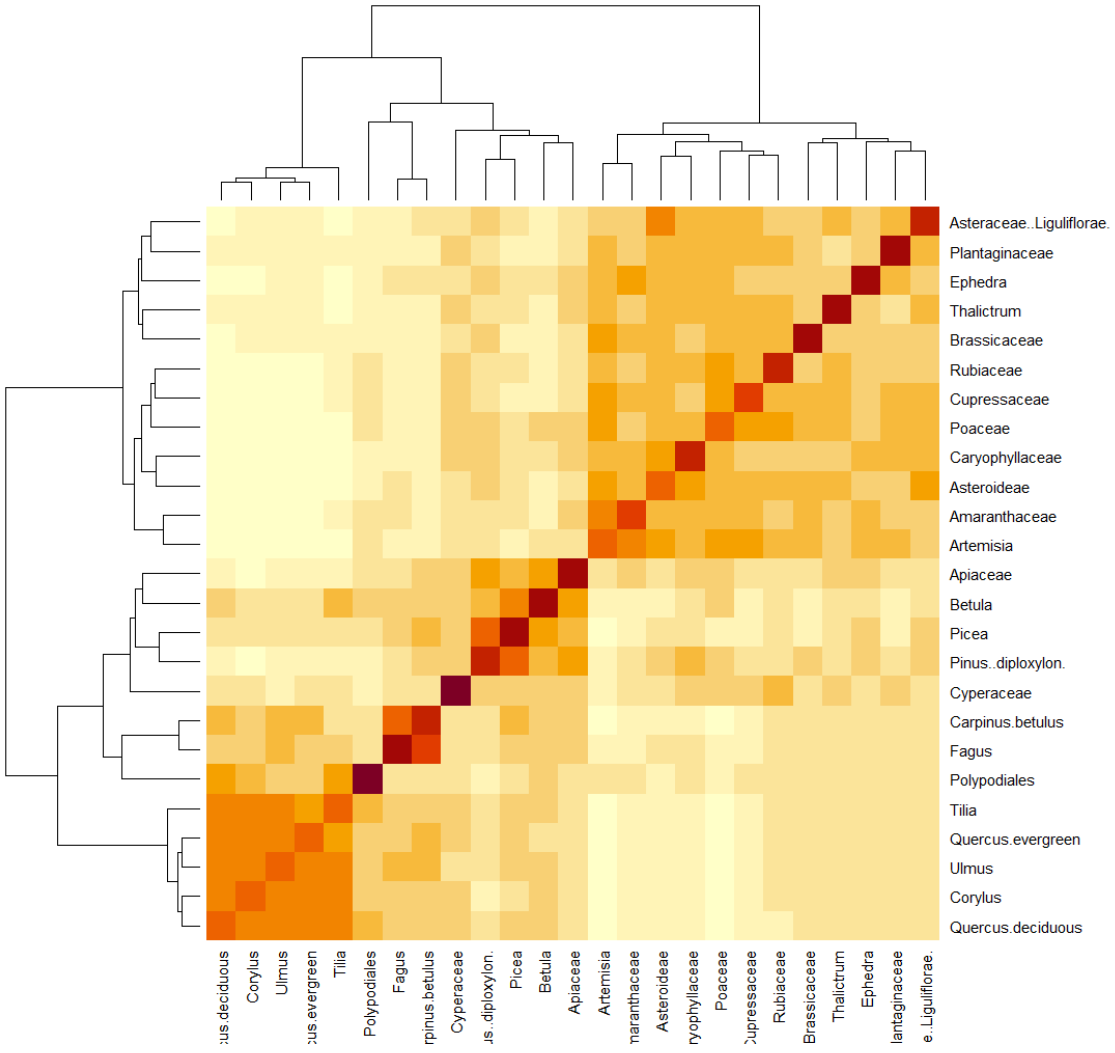

Figure 2.27 Heatmap of correlation matrix of taxon abundances for Lagaccione for 25 most abundance taxa (96% of total abundance) for age range 9.2 ka to 76.2 ka.

Similarly, different cores have different assemblages, and give different clusters in consequence. This in itself is not a problem, since each core will signify D-Os in its own way, but the sensitivity of the groups to the choice of age ranges renders clustering unreliable.

2.6.3.2 Grouping by Plant Functional Types (PFTs)

Plants may be grouped into plant functional types (PFTs), of which there are many possible definitions depending on the purpose. A PFT is a group of taxa which have similar responses to physical or biotic environmental factors, and similar expressions of multiple traits such as physical form and phenology; that is, they 'work the same way', however distant they may be phylogenetically (e.g. Harrison *et al.*, 2010), and changes in relative abundance of PFTs may therefore signal D-Os. AP and NAP form a very simple PFT classification, but here the set of PFTs provided for use with the ACER database is tested. Some taxa can belong to more than one PFT, and their allocation to a PFT therefore depends partly on context; if the other components of one of the candidate PFTs are abundant, a taxon is likely to be attributed to that PFT.

In a typical fossil core, the 10 most abundant PFTs (as defined above) cover approaching 90% of the pollen abundance. The two examples below – Lac du Bouchet and Ioannina - show that cores can display rapid switches in abundance between different PFTs, which is promising as possible evidence of D-Os, and also that different cores can be dominated by different PFTs.

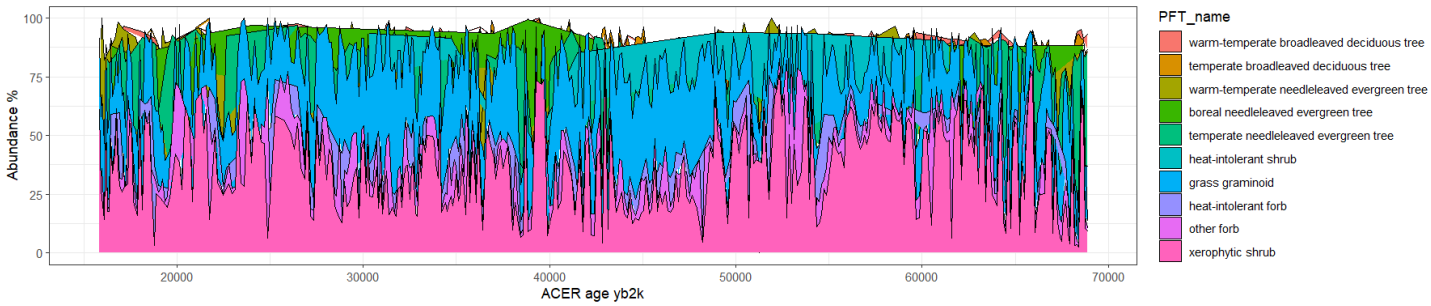

Figure 2.28 Stacked area plot of abundances of 10 most abundant PFTs covering 86% of total abundance at Lac du Bouchet over time.

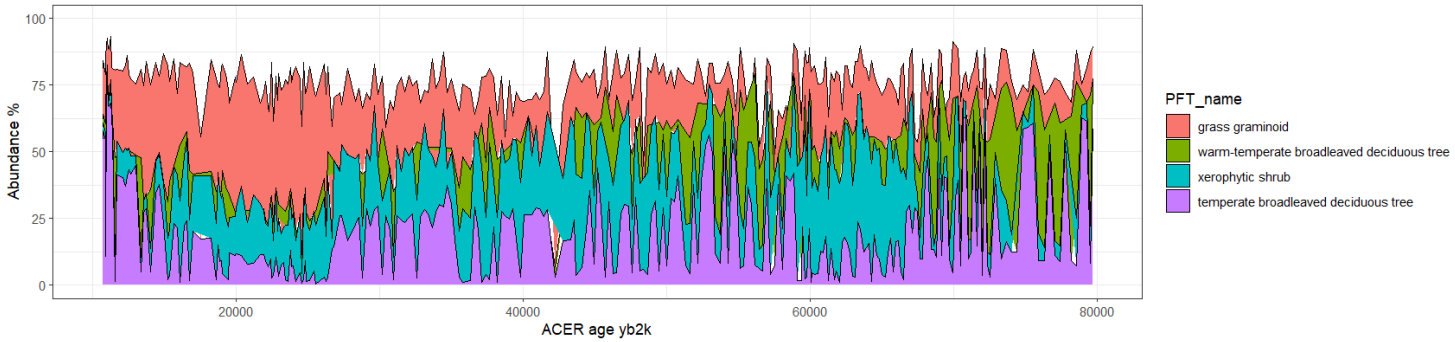

Figure 2.29: Stacked area plot of abundances of 4 major PFTs covering 75% of total abundance at Ioannina over time (NB legend colours differ from Figure 2.28).

Figure 2.28 shows that at Lac du Bouchet there are major switches between xerophytic shrubs and grass graminoids, which between them dominate the abundance.

Figure 2.29, which plots only the 4 major PFTs for clarity, show that at Ioannina at 470 m asl on the western side of Greece, temperate and warm-temperate broadleaved deciduous trees are the most abundant PFTs in the earlier part, and that the main switches are between on the one hand a combination of broadleaved deciduous trees and xerophytic shrubs and on the other grass graminoids.

This means that the dominant changes are between (usually) two significant PFTs, which ignores much information, but more importantly the number of similar-scaled rapid changes appears much greater than the expected number of D-Os in the age range. For these reasons, grouping by PFTs was not pursued.

2.6.4 Dynamic Time Warping (DTW)

DTW, a method widely used in signal processing and speech recognition, matches features in two time series by locally stretching and shrinking the time frame of one of the series to minimise the distance between them (Giorgino (2009), Keogh and Pazzani (2001)). Here one is the Kindler temperature series, and the other a time series derived from pollen. Unlike pattern matching, which extracts multiple templates and deals with them individually, DTW attempts to match the Kindler series as a whole with a pollen series as a whole. Minimising the distance between the two series is achieved by moving features of the pollen series in the time dimension to match features in the reference (Kindler) series. Since the features in the Kindler series are principally D-Os, this should align any D-O-like features in the pollen series with counterparts in

the Kindler series by adjusting the pollen series sample ages. This would permit simultaneous identification of all these D-O-like features along with their revised ages.

DTW matches series by finding the lowest cumulative distance through a distance matrix of the two series, given

- permissible 'step' patterns, that is, which moves between cells are allowed
- permissible 'window' types and widths, that is, how much deviation from the diagonal is allowed.

The dtw R package (Giorgino, 2009) was used to explore this technique.

The method recognises uncertainties in the pollen age model by defining how much the age of a sample can be changed, while the reference (Kindler) series ages remain fixed. This is achieved by constraining the permissible width of lowest-distance path within a window about the diagonal in the distance matrix; this determines the permitted change in the ages of the pollen samples. Since we need to reflect increasing age uncertainties with age, none of the standard window types available in the package are appropriate, and a parameter-driven function was implemented which provides a window which widens along the diagonal.

DTW by default stretches a shorter series to match the longer, so if one series has many more observations than the other for a given age range, DTW will match many points in the shorter vector to a single point in the longer. This cannot represent physical reality in a pollen core, so the less densely sampled pollen series is interpolated to the same timescale as the Kindler series, as is done in pattern matching.

Figure 2.30 is an example of the result. It shows the path taken through a distance matrix where the axes are the data points in the Kindler time series and those in the interpolated ACER age model for Ioannina. The matching is between the Kindler temperature series and a quantitative reconstruction of gdd at Ioannina. It uses the custom widening window reflecting increasing age uncertainty over time. The distance of the path from the 1:1 diagonal represents the amount by which the age of the Ioannina sample has been changed to achieve the match. This is an unsatisfactory result, and is repeated for other cores. If DTW were

providing good matches, the path would move in very small steps. The pronounced vertical and horizontal movements seen in practice mean that (a) several points in one series are matched with one in the other, which is physically impossible, and (b) that the age adjustment applied to sequential samples does not progress smoothly but often switches from one extreme permitted by the window to the other. This can be expressed as the change to sample ages shown in Figure 2.31.

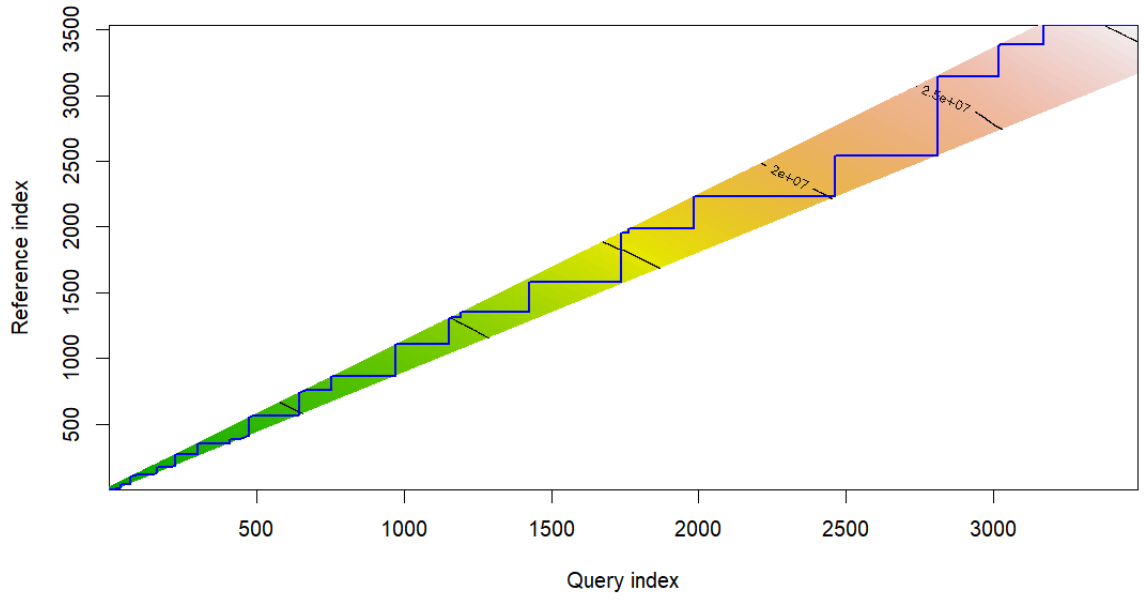

Figure 2.30 Ioannina distance matrix, with custom-built widening window and the path (blue) taken through it to minimise the cumulative distance (represented by colour). 'Reference' is the Kindler series, and 'Query' the interpolated points in the ACER age model for Ioannina, using a quantitative reconstruction of gdd as the time series to be matched.

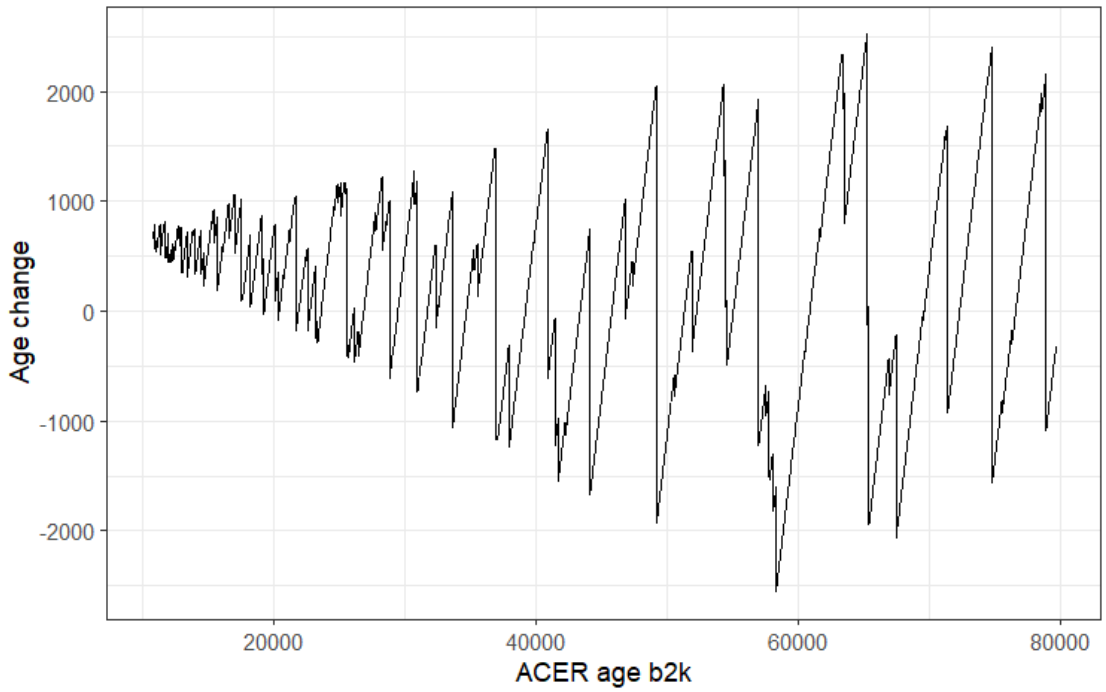

Figure 2.31 Changes in Ioannina sample ages implied by DTW run shown in Figure 2.30 above.

Despite experimentation with several parameters available in the dtw R package, DTW always performs poorly when applied to pollen core data.

There is no means of controlling the detail of how DTW matches the series, for instance by fixing certain points as already matching, or by providing dating points. This means that if DTW picks a poor match early in the sequence, the rest is nonsense. Long sequences tend to run out of control, while short sequences with a limited number of clear and already closely matching features, such as overlaps in speleothem records, or a spoken phrase and a reference sonogram, work well. DTW is known to suffer from the ease with which it can provide these 'pathological' solutions, and especially those where a point in one series is matched to many in the other (Giorgino (2009), Keogh and Pazzani (2001)). This is interpreted to mean that a high degree of initial similarity between the features of the two series is critical to success, and that the similarity between the pollen series features and those in the Kindler series is not sufficient.

2.6.5 Other methods

Ther are other methods that could be applied to quantitative reconstructions, such as those described in Chapter 5. These include Hidden Markov models and Singular Spectrum Analysis.

2.6.5.1 Hidden Markov models (HMMs)

Hidden Markov models identify underlying 'states' in a time series. Given that D-Os represent a change from a stadial to an interstadial state, the expectation was that HMMs could identify D-Os in climate-related series.

HMMs were used by Lin *et al.*, (2014) to improve the matching process used in the LR04 marine benthic $\delta^{18}O$ stack (Lisiecki and Raymo, 2005) and establish uncertainties in the match.

A Markov chain is a series of sequential steps, each of which can be characterised by one of two or more different 'states'. To determine the current state, no information is needed from further back in the chain than the previous state; it 'has no memory', or more accurately, the entire memory is enshrined in the previous state. For instance a Fibonacci series is not a Markov chain: the last two states determine the current state. A Markov model requires a transition matrix, which is the table of probabilities that one state will at the next step change to another.

A *hidden* Markov model uses 'emissions' (the observations, here the pollen data) to hypothesise the underlying unobservable Markov states (the climate states, e.g. GIs and GSs). The R package depmixS4 (Ingmar Visser, Maarten Speekenbrink (2010). depmixS4: An R Package for Hidden Markov Models. Journal of Statistical Software, 36(7), 1-21. URL https://www.jstatsoft.org/v36/i07/) was used to explore this possibility. In this package, the transition matrix is established heuristically by the software.

The user chooses the number of states to use by experimentation. The method was first applied to the Kindler temperature series as a test. Applying 4 states to the detrended, normalised Kindler Greenland temperature series, the HMM clearly distinguishes GIs, GSs, and two climate regimes which are neither GS nor GI (Figure 2.32). While HMMs give no information about the physical meaning of the states, the clear interpretation here is that 1 (blue) is GSs, 4 (red) is GIs, 3 (orange) is low-amplitude change generally occurring at transitions and intervals slightly above the mean, and 2 (green) is similar to 3 but below the mean. This means that nearly all D-Os can be identified in the Kindler series by the transitions from state 1 to state 4.

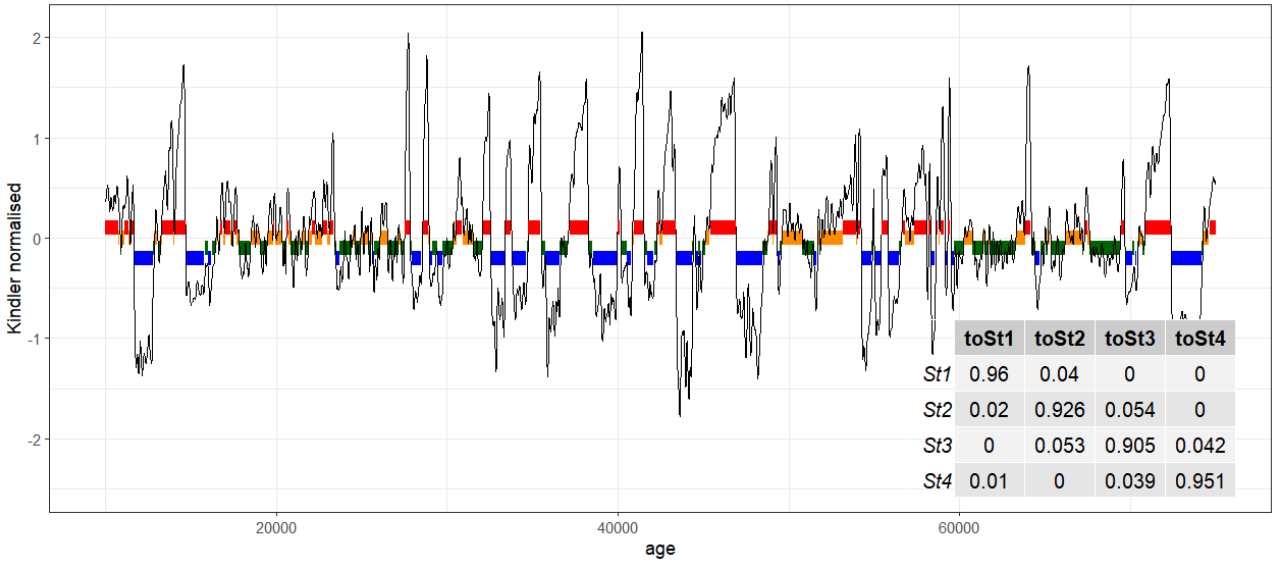

Figure 2.32 4-state HMM for Kindler temperature (normalised and detrended), with transition matrix. States: 1 = blue, 2 = green , 3 = orange, 4 = red.

Applying 2, 3 and 4 state HMMs to pollen core series, whether quantitative reconstructions or PCA, DCA or other time series, does not, however, identify rapid increases neatly. For example Figure 2.33 shows a 3 state HMM applied to a Lagaccione climate reconstruction.

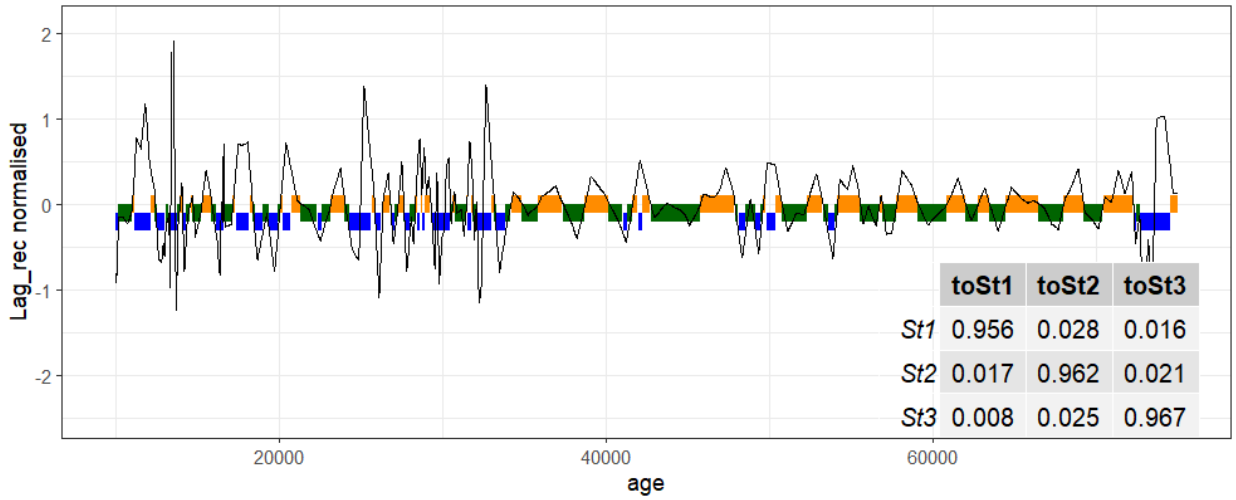

Figure 2.33 Lagaccione reconstruction mean: 3 states. Green = clear low peaks, orange = high amplitude peaks and troughs, blue = uneventful, near 0. Table is the heuristically found transition matrix. Script: Hidden Markov test2

The conclusion is that HMMs do not help to locate D-Os in pollen series. HMMs find persistent states, not sharp transitions, and in pollen series this can degenerate to dividing above from below mean intervals. The method works for the Kindler series because the persistent states are separated by sharp transitions.

2.6.5.2 Singular Spectrum Analysis (SSA)

Singular Spectrum Analysis (SSA) decomposes a time series into trends, periodic components, and a residual, which is considered noise; some choices are required in what is treated as periodic (Vautard and Ghil, 1989; Vautard, Yiou and Ghil, 1992; Hassani, no date). It is a non-parametric method, making no assumptions about underlying distributions or linearities. It is sometimes used for 'de-noising', that is, identifying noise so that it can be removed from a series. Its use was motivated by the possibility that some element of the decomposition would identify D-Os, and/or that it could de-noise the data or remove a periodic component to leave D-Os more clearly visible.

Rssa is the only R package which performs SSA (Golyandina and Korobeynikov, no date). It was applied to the Kindler series as a test.

Figure 2.34 decomposes the unmodified Kindler series into components as time series, and Figure 2.35 shows the results as trajectories in phase space. After trend (eigenvectors 1+6 in the figures), several sine/cosine pairs of eigenvectors are identifiable as approximately circular plots in phase space (Figure 2.35), denoting sinusoidal components, e.g. 2+3, 4+5, 7+8, 9+10.

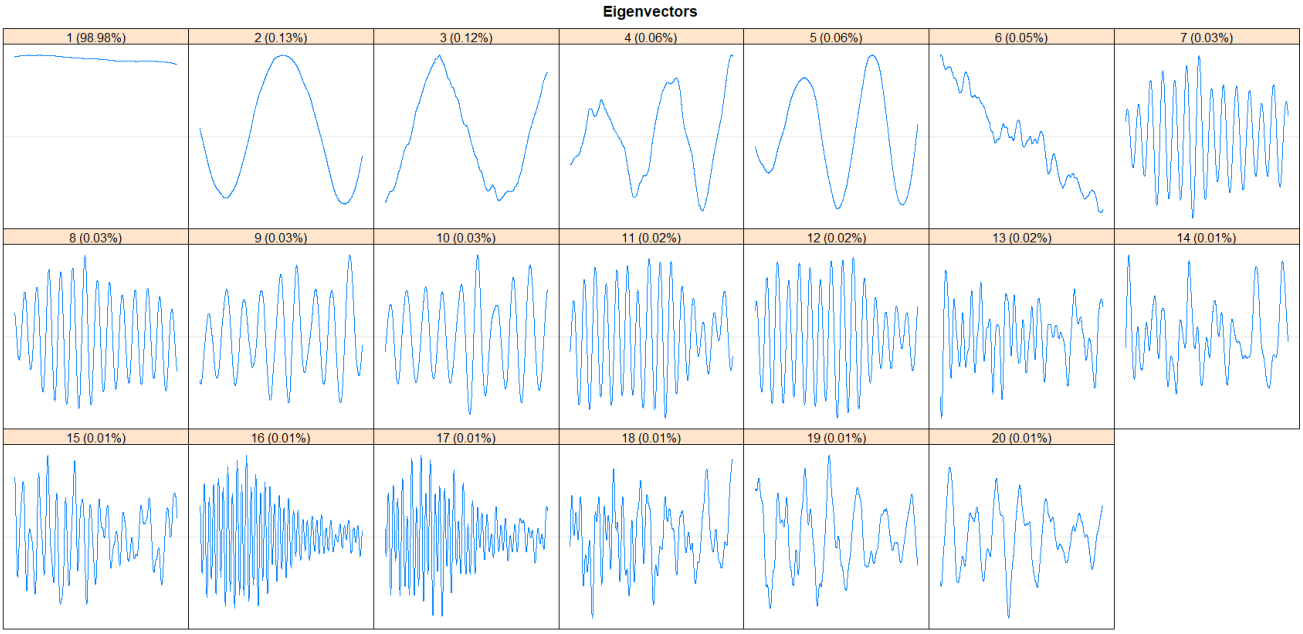

Figure 2.34 First 20 principal components of SSA applied to the Kindler temperature series, plotted as time series; headings include % variation explained.

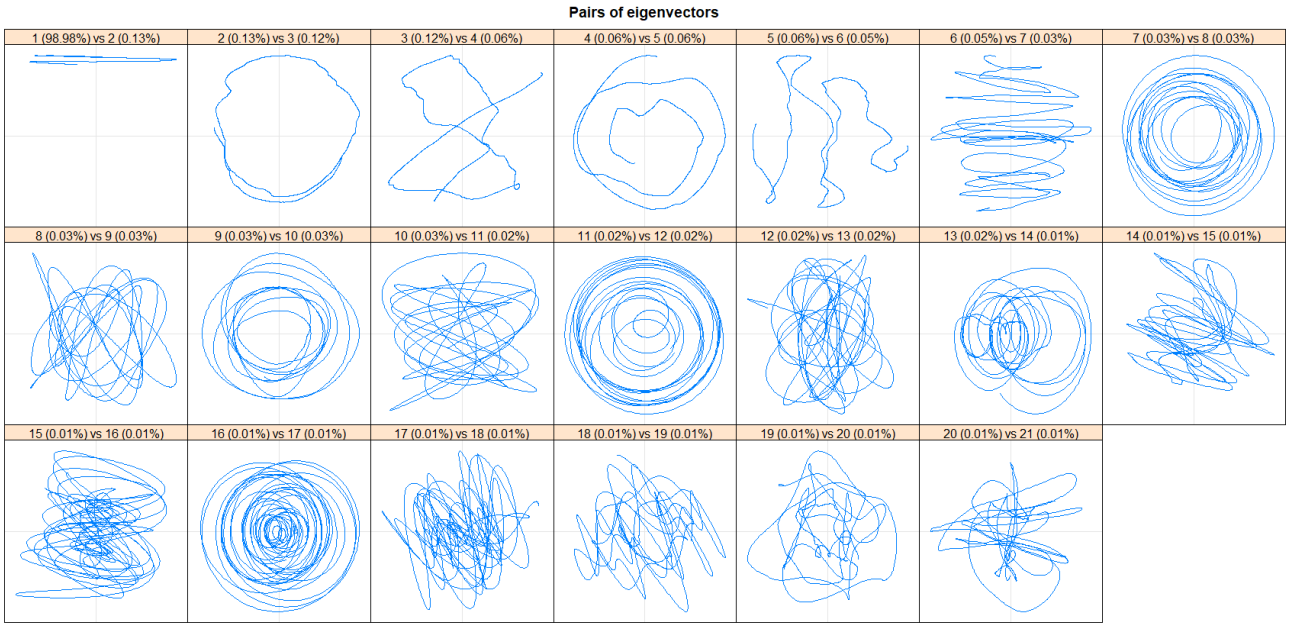

Figure 2.35 First 20 principal components of SSA applied to the Kindler temperature series, plotted in phase space

Combining selected pairs of principal components yields the reconstruction in Figure 2.36, in which it is plain that the D-Os are in the residuals.

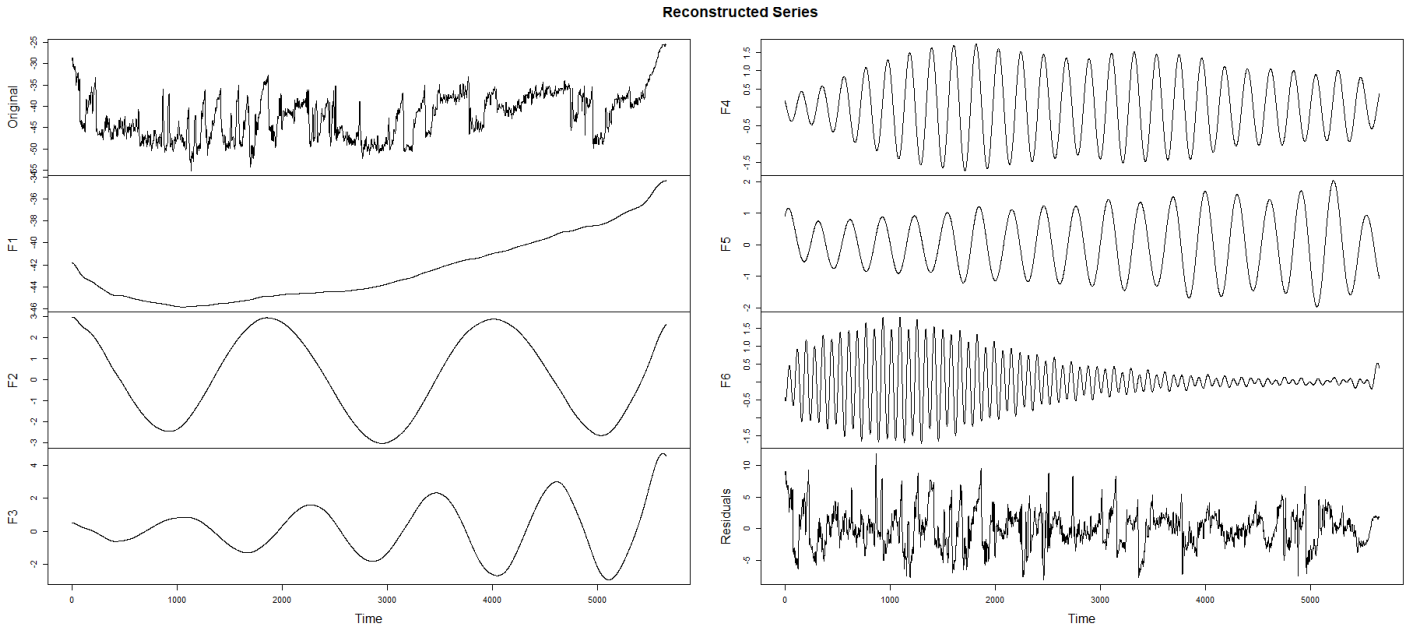

Figure 2.36 Reconstruction of components of the original series using the following combinations of principal components: F1 = (1,6), F2 = (2,3), F3 = (4,5), F4 = (7,8), F5 = (9,10), F 6 = (16,17). Residual is after these 6 series are extracted. X axis time steps are ~20 year intervals, so x = 5000 represents age = 100 ka; max age ~123ka.

The residuals can be decomposed further, finding ever smaller sinusoids, but there is never a component which isolates the D-O warmings, and there are no further significant qualitative changes in the remaining

residuals or in their range. In other words, because D-Os are neither trend nor periodic, it is not possible to separate D-O signals from noise using SSA even in the Kindler series.

SSA provides further potentially useful information. In the Kindler series, the first four components after the trend are reconstructed into two longwave periodicities (F2, F3) with ranges of ~ +/- 3 °C which can readily be recognised as obliquity and precession from their periods and phases, and from the change in amplitude of precession over time, when compared with the Laskar *et al.* (2004) insolation values for 65 °N (Figure 2.37). There is a lag from obliquity to the Greenland signal of ~ 1.9 ka and a larger lag from precession. This finding is not novel and is not explored further here. The physical meaning of three shorter low-amplitude periodicities, F4 at ~4300 years, F5 at ~6250 years and F6 at ~1670 years, is not known.

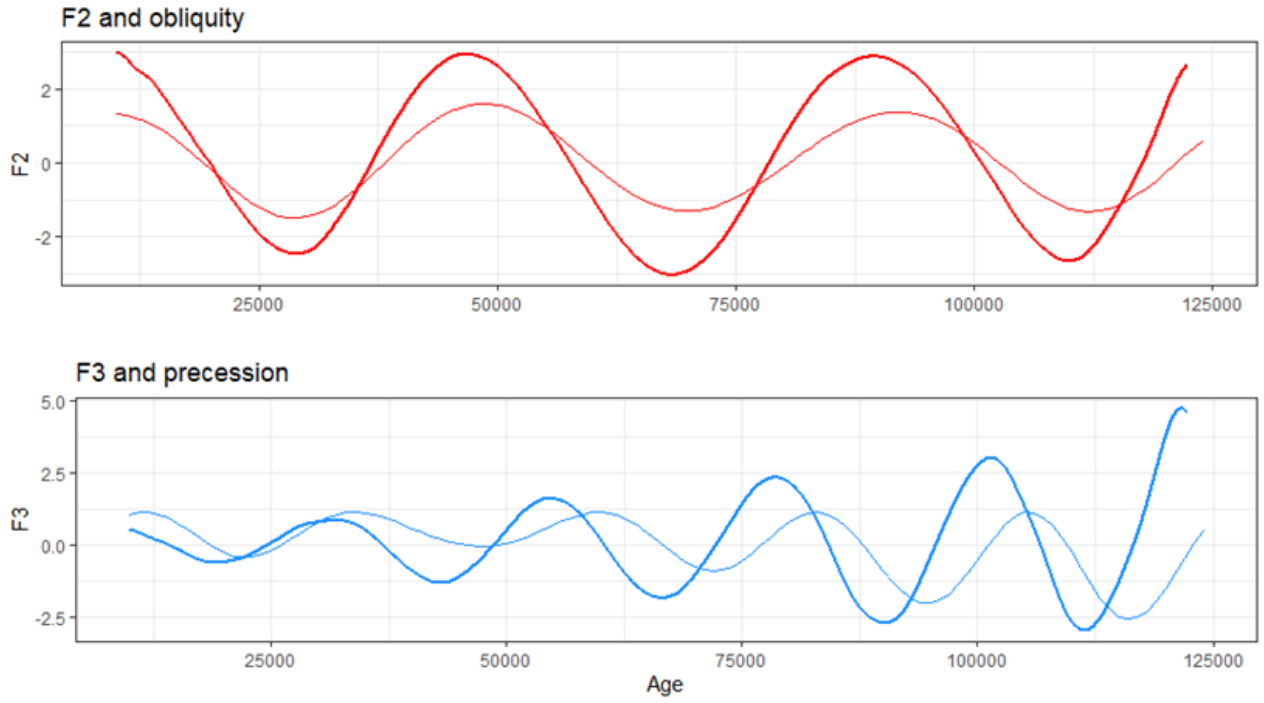

Figure 2.37 Comparison of F2 and F3 components calculated by SSA from the Greenland Kindler series (Kindler et al., 2014) (bold) with (Laskar et al., 2004) obliquity and (inverted) precession (thin), both normalised, at 65 °N summer solstice. Script: Taxon metrics\DTW\Rssa v3.R

In contrast, these Milanković periodicities are not clear in any pollen-based core series examined using SSA. Had they been present and explained a useful fraction of the variation, their extraction would have

removed a non-D-O signal from the series, leaving the D-O signal more obvious. The lack of a Milanković signal in fossil pollen series, when it is present in the Greenland record of the climate changes which must have driven changes in the pollen, is a sign of the lower signal-to-noise ratio of the pollen records, and again suggests that there is a considerable non-climatic component in the pollen signal.

Singular Spectrum Analysis is designed to identify trend and periodic components. It is cannot separate out different non-periodic or asymmetrical components. Hence it leaves D-Os in its residuals, where they remain inseparable from noise.

2.7 Summary of chapter

This Chapter investigates how to find D-O-like patterns in time series derived in some way from pollen cores. The anatomy of a Dansgaard-Oeschger event is described and defined, and the Kindler temperature series is chosen as the key Greenland series and the source of D-O patterns ('templates'). SEA shows that D-Os – the initiation phases of Greenland Interstadials – are very similar but not identical to each other, and are distinctive compared with other intervals in the Greenland data.

Pattern matching compares multiple D-O templates taken from the Kindler series with a pollen-based series, using Euclidean distance to establish the degree of similarity to the templates and to locate the points in the pollen series which are most like a D-O. Templates with a relatively narrow focus on the rising portion of the GI initiation yield the best discrimination, and a standardised mean of means of the Euclidean distances (*smmdist*) is the best way of combining distance curves from multiple passes. Pattern matching applied to the parent Kindler series successfully finds all but two GIs, suggesting good results may be obtainable when applied to pollen series.

The selection of Mediterranean terrestrial fossil pollen cores is discussed, and it is shown that their relatively low chronological sampling resolution does not preclude them from identifying D-Os.

A common theme emerges that pollen records are noisy and include non-climatic signals, and features which may represent Dansgaard-Oeschger events are much less clear than in the Greenland data.

The last section examines eight ways of summarising multi-taxon fossil pollen records to provide a limited number of time series in which D-Os may be visible, and may optionally be tested by pattern matching. These are PCA, DCA, SCD, grouping by hierarchical clustering and by PFTs, DTW, HMM, and SSA. As a test of principle, most of these are run against the Kindler series.

None perform very well. PCA and DCA show few asymmetrical intervals, and when pattern matching is run, potential D-Os are inconsistently located across different components. None of the components appear to have a simple climatic meaning and the signs of the components are arbitrary. It appears that PCAs and DCAs sweep together many non-temperature influences, making comparison with a warming potentially nonsensical.

SCD identifies abrupt changes in pollen composition, but it is not clear whether these are warmings, coolings or something else; only some coincide with expected dates of GIs, and other events are picked which are clearly not GIs. SCD in this analysis attributes equal importance to all percentage changes in abundance, so variability in highly abundant taxa which are climatically relatively insensitive, and therefore of little significance to the identification of D-Os, may dominate the result.

The groups found by hierarchical clustering and by grouping by PFTs are unstable, being sensitive to the assemblage within the age range chosen, and vary between cores. DTW requires a higher degree of initial similarity between the Greenland features and those in the pollen series than the pollen series can offer. HMMs are good at identifying persistent states but not at locating sharp changes. SSA is unable to separate non-periodic components, leaving the irregular D-O signal included in noise.

A contributor to the relatively poor performance of these methods is that few of the time series have an identifiable climatic meaning, whereas the Kindler series does. This led to the making of quantitative climate reconstructions to provide time series with clear climatic meaning in which to search for D-Os. The following three Chapters deal with the methodology of quantitative climate reconstruction, before returning in Chapter 6 to the use of pattern matching to locate D-Os in the reconstructed series.

2.8 References

Barbosa, S. *et al.* (2023) *Automatic characterisation of Dansgaard-Oeschger events in palaeoclimate ice records*. other. oral. Available at: https://doi.org/10.5194/egusphere-egu23-3612.

Birks, H.J.B. (Harry J.B. and Birks, H.H. (1980) *Quaternary palaeoecology*. London : Edward Arnold, 1980.

Fletcher, W.J. *et al.* (2010) 'Millennial-scale variability during the last glacial in vegetation records from Europe', *Quaternary Science Reviews*, 29(21), pp. 2839–2864. Available at: https://doi.org/10.1016/j.quascirev.2009.11.015.

Giorgino, T. (2009) 'Computing and Visualizing Dynamic Time Warping Alignments in R: The dtw Package', *Journal of Statistical Software*, 31(1), pp. 1–24. Available at: https://doi.org/10.18637/jss.v031.i07.

Golyandina, N. and Korobeynikov, A. (no date) 'Basic Singular Spectrum Analysis and forecasting with R', *Computational Statistics & Data Analysis*, 71, pp. 934–954. Available at: https://www.academia.edu/12899418/Basic_Singular_Spectrum_Analysis_and_forecasting_with_R (Accessed: 16 September 2020).

Harrison, S.P. *et al.* (2010) 'Ecophysiological and bioclimatic foundations for a global plant functional classification', *Journal of Vegetation Science*, 21(2), pp. 300–317. Available at: https://doi.org/10.1111/j.1654-1103.2009.01144.x.

Hassani, H. (no date) 'A Brief Introduction to Singular Spectrum Analysis', p. 11.

Keogh, E.J. and Pazzani, M.J. (2001) 'Derivative Dynamic Time Warping', in *Proceedings of the 2001 SIAM International Conference on Data Mining*. *Proceedings of the 2001 SIAM International Conference on Data Mining*, Society for Industrial and Applied Mathematics, pp. 1–11. Available at: https://doi.org/10.1137/1.9781611972719.1.

Kindler, P. *et al.* (2014) 'Temperature reconstruction from 10 to 120 kyr b2k from the NGRIP ice core', *Climate of the Past*, 10(2), pp. 887–902. Available at: https://doi.org/10.5194/cp-10-887-2014.

Laskar, J. *et al.* (2004) 'A long-term numerical solution for the insolation quantities of the Earth', *Astronomy & Astrophysics*, 428(1), pp. 261–285. Available at: https://doi.org/10.1051/0004-6361:20041335.

Lin, L. *et al.* (2014) 'Probabilistic sequence alignment of stratigraphic records', *Paleoceanography*, 29(10), pp. 976–989. Available at: https://doi.org/10.1002/2014PA002713.

Lisiecki, L.E. and Lisiecki, P.A. (2002) 'Application of dynamic programming to the correlation of paleoclimate records: DYNAMIC PROGRAMMING SIGNAL CORRELATION', *Paleoceanography*, 17(4), pp. 1-1-1–12. Available at: https://doi.org/10.1029/2001PA000733.

Lisiecki, L.E. and Raymo, M.E. (2005) 'A Pliocene-Pleistocene stack of 57 globally distributed benthic δ18O records', *Paleoceanography*, 20(1), p. PA1003. Available at: https://doi.org/10.1029/2004PA001071.

Lough, J.M. and Fritts, H.C. (1987) 'An assessment of the possible effects of volcanic eruptions on North American climate using tree-ring data, 1602 to 1900 A.D.', *Climatic Change*, 10(3), pp. 219–239. Available at: https://doi.org/10.1007/BF00143903.

Malmierca-Vallet, I. *et al.* (2023) 'Dansgaard–Oeschger events in climate models: review and baseline Marine Isotope Stage 3 (MIS3) protocol', *Climate of the Past*, 19(5), pp. 915–942. Available at: https://doi.org/10.5194/cp-19-915-2023.

R Core Team (2023) ‘R: A language and environment for statistical computing’. Vienna: R Foundation for Statistical Computing. Available at: http://www.R-project.org/.

Rasmussen, S.O. *et al.* (2014) ‘A stratigraphic framework for abrupt climatic changes during the Last Glacial period based on three synchronized Greenland ice-core records: refining and extending the INTIMATE event stratigraphy’, *Quaternary Science Reviews*, 106, pp. 14–28. Available at: https://doi.org/10.1016/j.quascirev.2014.09.007.

Reille, M. and de Beaulieu, J.-L. (1990) ‘Pollen analysis of a long upper Pleistocene continental sequence in a Velay maar (Massif Central, France)’, *Palaeogeograpy, Palaeoclimatology, Palaeoecology*, 80, pp. 35–48.

Sanchez Goñi, M.F. and Harrison, S.P. (2010) ‘Millennial-scale climate variability and vegetation changes during the Last Glacial: Concepts and terminology’, *Quaternary Science Reviews*, 29(21–22), pp. 2823–2827. Available at: https://doi.org/10.1016/j.quascirev.2009.11.014.

Seierstad, I.K. *et al.* (2014) ‘Consistently dated records from the Greenland GRIP, GISP2 and NGRIP ice cores for the past 104 ka reveal regional millennial-scale δ18O gradients with possible Heinrich event imprint’, *Quaternary Science Reviews*, 106, pp. 29–46. Available at: https://doi.org/10.1016/j.quascirev.2014.10.032.

Vautard, R. and Ghil, M. (1989) ‘Singular spectrum analysis in nonlinear dynamics, with applications to paleoclimatic time series’, *Physica D: Nonlinear Phenomena*, 35(3), pp. 395–424. Available at: https://doi.org/10.1016/0167-2789(89)90077-8.

Vautard, R., Yiou, P. and Ghil, M. (1992) ‘Singular-spectrum analysis: A toolkit for short, noisy chaotic signals’, *Physica D: Nonlinear Phenomena*, 58(1), pp. 95–126. Available at: https://doi.org/10.1016/0167-2789(92)90103-T.

Yeh, M. *et al.* (2018) ‘Time series joins, motifs, discords and shapelets: a unifying view that exploits the matrix profile’, *Data Mining and Knowledge Discovery*, 32(1), pp. 83–123. Available at: https://doi.org/10.1007/s10618-017-0519-9.

3 The impact of methodological decisions on climate reconstructions using WA-PLS

This Chapter is a paper published in Quaternary Research and is available to read online at https://doi.org/10.1017/qua.2020.44. It has been written and referenced in the style guidelines of that journal. The authors were Mark Turner, Dongyang Wei, Sandy P. Harrison and Iain Colin Prentice. All authors contributed to the concept, the analyses were performed by MT, and DW provided climate and Generalised Additive Model (GAM) data. The initial draft was written by MT and SPH, and all authors contributed to the final paper. Estimated contributions: MT 60%, SPH 25%, DW and ICP together 15%.

The motivation for the paper was to consider the selection and treatment of data in constructing training sets for quantitative climate reconstructions. The training set is the foundation of any calibration process in quantitative climate reconstruction. The main subjects were the climate space sampled by the set, and the inclusion, exclusion and amalgamation of taxa. The reconstruction method chosen was Weighted Averaging Partial Least Squares (WA-PLS).

3.1 Abstract

Most techniques for pollen-based quantitative climate reconstruction use modern assemblages as a reference data set. We examine the implication of methodological choices in the selection and treatment of the reference data set for climate reconstructions using Weighted Averaging Partial Least Squares (WA-PLS) regression and records of the last glacial period from Europe. We show that the training data set used is important because it determines the climate space sampled. The range and continuity of sampling along the climate gradient is more important than sampling density. Reconstruction uncertainties are generally reduced when more taxa are included, but combining related taxa that are poorly sampled in the data set to a higher taxonomic level provides more stable reconstructions. Excluding taxa that are climatically insensitive, or systematically overrepresented in fossil pollen assemblages because of known biases in

pollen production or transport, makes no significant difference to the reconstructions. However, the exclusion of taxa overrepresented because of preservation issues does produce an improvement. These findings are relevant not only for WA-PLS reconstructions but also for similar approaches using modern assemblage reference data. There is no universal solution to these issues, but we propose a number of checks to evaluate the robustness of pollen-based reconstructions.

3.2 INTRODUCTION

Models of the coupled climate system are used to project how changes in natural and anthropogenic forcing will affect future climates (Collins et al., 2013; Kirtman et al., 2013). The expected changes in twenty-first-century forcing and climate are larger than those experienced during the recent historic period against which these models have been calibrated. Quaternary climate states in which the changes in forcing and climate are as large as those projected for the end of the twenty-first century are therefore now routinely used as an out-of-sample test of such models (Braconnot et al., 2012; Schmidt et al., 2014; Harrison et al., 2015). This evaluation is crucially dependent on the availability of reliable quantitative reconstructions of multiple climate variables (Harrison et al., 2014). Indications of past climate can be found in many different marine and terrestrial archives, but pollen analysis provides by far the most geographically widespread source of data for terrestrial palaeoclimate reconstructions (Bartlein et al., 2011; Marsicek et al., 2018 and references therein). There are many methods to make quantitative reconstructions of climate variables from pollen data using both statistical relationships and process-based modelling. Most reconstructions of terrestrial palaeoclimate rely on statistical relationships between modern pollen abundances and modern climate. There are two basic approaches (see discussion in ter Braak and Juggins, 1993): analogue methods select the modern climate associated with the modern pollen samples whose abundance patterns are most like a given fossil sample; regression-based methods calculate a transfer coefficient for each pollen taxon and the climate variable, which is then applied to taxon abundances in fossil pollen samples to reconstruct climate through time.

Weighted averaging partial least squares (WA-PLS; ter Braak and Juggins, 1993) is the most widely used of the regression-based methods. Weighted averaging is a form of regression adapted to the fact that taxon abundances generally show unimodal, rather than monotonic, responses to climate variables. The climate estimate for any given sample is the abundance-weighted mean of the estimated optima of all the taxa present. WA-PLS refines these optima by looking for further information in the residuals between the initial regression and the modern observations and repeats this until the incremental change ceases to be statistically significant. WA-PLS is considered more robust against spatial autocorrelation than modern analogue methods—that is, it is considered to be less affected by the fact that geographically clustered sites may inherently show similar taxon composition (Telford and Birks, 2005). WA-PLS has been widely used for climate reconstructions based on biotic assemblages, including pollen, diatoms, chironomids, and foraminifera (Lotter et al., 1997; Brooks and Birks, 2001; Seppä et al., 2009). In some more recent publications WA-PLS reconstructions have been presented alongside reconstructions using other statistical methods, such as modern analogue methods (Brewer et al., 2008; Peyron et al., 2011; Sinopoli et al., 2019). A number of methodological choices have to be made in the application of WA-PLS, including the choice of a training data set and which taxa are included in the regression. Studies using WA-PLS generally rely on model performance statistics as a measure of the reliability of reconstructions. They are usually silent about how methodological decisions were reached, and the implications of specific choices for the quality of the reconstructions are rarely made explicit. However, a number of studies of quantitative reconstruction techniques (Birks and Seppä, 2004; Bjune et al., 2010; Telford and Birks, 2011; Juggins, 2013; Salonen et al., 2013; Juggins et al., 2015; Shennan et al., 2015; Jonkers and Kuč era, 2018) have examined some of these choices and suggested that they can influence the quality of the reconstructions. None of the previous studies provides a comprehensive analysis of the issues or discriminates between the quality of the statistical model and the impact on the climate reconstructions. Our goal in this paper is to increase confidence in the quantitative reconstructions of past climates that are used for model evaluation through an analysis of the implications of methodological decisions both on model performance measures under modern conditions and the resulting quantitative reconstructions of glacial climates in southern Europe. We

propose ways in which the implications of specific methodological choices can be evaluated in order to document the reliability of the resulting reconstructions.

3.3 METHODS

We test the impact of methodological choices by making climate reconstructions for selected fossil pollen records using subsets of a continental-scale modern training data set as inputs to WA-PLS (see "Modern pollen data"). In order to run these tests under climate conditions substantially different from present, we use fossil pollen records from southern Europe covering the last glacial period (see "Fossil pollen"). We examine the effects of methodological choices on WA-PLS model parameters and on the resulting climate reconstructions and their uncertainties (see "Application of WA-PLS"). Modern pollen data The modern pollen data set (Figure 3.1, Supplementary Fig. 1), which we refer to as SMPDS, was constructed by combining records from the European Modern Pollen Database (EMPD) v3.0 (Davis et al., 2013), the Eastern Mediterranean-Black Sea-Caspian Corridor Biomes (EMBSeCBIO, which we abbreviate as EMB) database (Marinova et al., 2018), additional published records (see Supplementary Table 1) from the European Pollen Database (http://www.europeanpollendatabase.net/) or taken from Pangaea (https://www.pangaea. de/), and 73 modern surface samples from northern Spain (Wei et al., 2019a). About two-thirds of the sites (4575) were derived from the EMPD v3.0 (Davis et al., 2013), and a further 1088 sites were derived from the EMBSeCBIO database (Marinova et al., 2018). Some of the sites in the EMPD also occur in the EMBSeCBIO database, and these duplicates have been removed. The final SMPDS data set consists of records from 6458 terrestrial sites (Harrison, 2019). We compare the EMPD and EMBSeCBIO subsets of the SMPDS data set to the full data set to examine the impact of the choice of training data set. The majority of the records were available as raw pollen counts; the remainder were percentages. The individual pollen records were taxonomically standardised and cleaned to remove obligate aquatics, insectivorous species, introduced species, and taxa that only occur as cultivars. The final data set expresses the counts as a percentage of the sum of all taxa remaining after this screening. There are 1558 taxa recorded in the SMPDS. Since some of these taxa are only recorded sporadically, we

amalgamated them at higher taxonomic levels to produce a data set with 249 taxa (Harrison, 2019). We confined our analyses to taxa with ten or more occurrences in the SMPDS (n = 195).

3.3.1 Modern climate data

Modern climate data were derived from the Climate Research Unit CRU CL 2.0 data set, which provides monthly mean precipitation, monthly mean temperature, and fractional sunshine hours as long-term means for 1961 to 1990 at 10 minute spatial resolution (New et al., 2002). Geographically weighted regression (GWR) (Brunsdon et al., 2002) using latitude, longitude, and elevation as predictors was performed in ArcGIS (ESRI, 2014) to obtain the climate at the location and elevation of each modern pollen site. We then calculated three bioclimatic variables: (a) mean temperature of the coldest month (MTCO), (b) growing degree days above a baseline of 0°C (GDD0), and (c) moisture index (MI), the ratio of annual precipitation to annual potential evapotranspiration. MTCO was taken directly from GWR output. Daily values of temperature, sunshine fraction, and precipitation were derived using a mean-conserving interpolation (Rymes and Myers, 2001) of the monthly data. MI was calculated from the daily temperature, precipitation, and sunshine data using modified Python code from the Simple Process-Led Algorithms for Simulating Habitats (SPLASH) model (Davis et al., 2017).

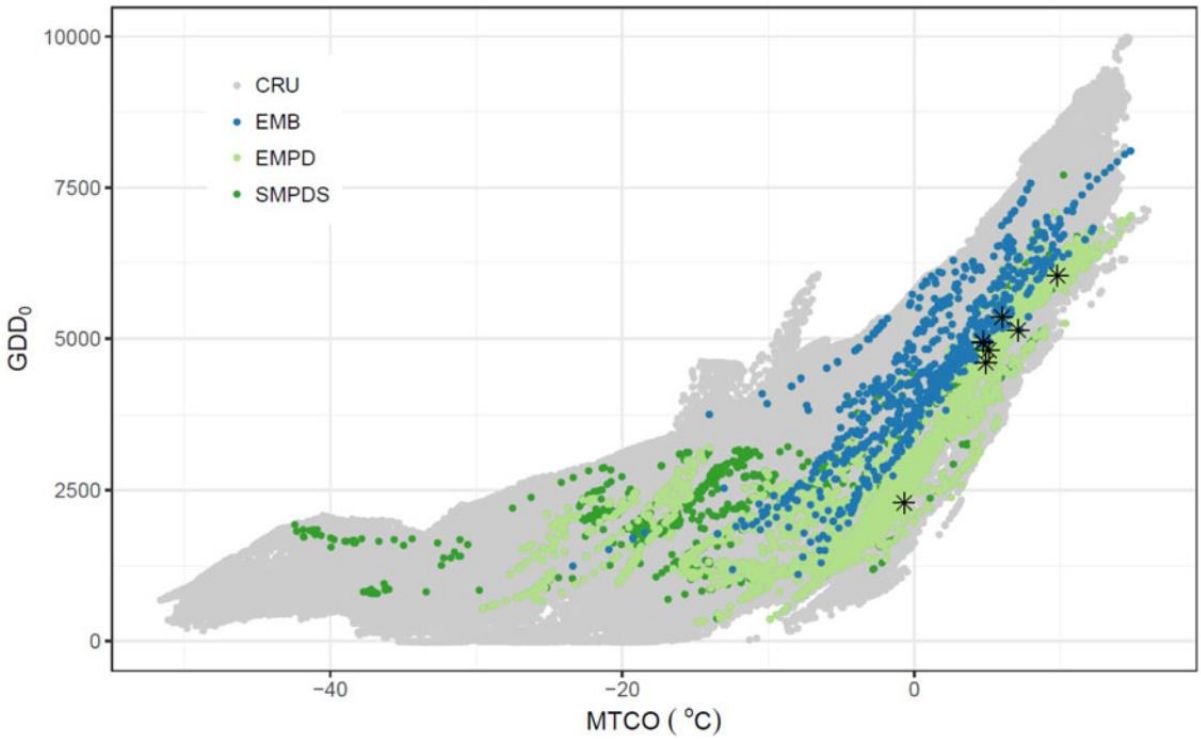

Figure 3.1 Distribution of modern pollen samples in climate space, represented by growing degree days above 0°C (GDD0) and mean temperature of the coldest month (MTCO), sampled by Eastern Mediterranean-Black Sea-Caspian Corridor Biomes (EMBSeCBIO) (labelled EMB), the European Modern Pollen Database (EMPD), and the full SMPDS data sets; SMPDS includes EMB and EMPD. The background shows the climate space for a rectangular area (latitude 29° N to 82° N, longitude 21° W to 150° E) enclosing the SMPDS data set, derived from the Climate Research Unit CRU CL 2.0 database (New et al., 2002). Stars indicate the present climate at the eight fossil sites used as examples.

These three bioclimatic variables have been shown to provide a good prediction of vegetation distribution both at global (Wang et al., 2017) and regional (Wang et al., 2013) scales because they reflect important and distinct ecophysiological controls on plant growth (Harrison et al., 2010). MTCO is a surrogate for extreme winter temperatures and influences the survival of woody plants through a wide range of low temperature–tolerance mechanisms, GDD0 is a combined measure of the length and warmth of the growing season that determines potential annual carbon accumulation, and MI is a measure of plant-available moisture (Harrison et al., 2010). Canonical correspondence analysis (CCA) applied to the SMPDS data set (Wei et al., 2019a) showed a strong correlation between species abundance and these climate variables. The modern climate data at each of the SMPDS sites (Harrison, 2020) are available online (doi: 10.5281/zenodo.3605003). Partial CCA carried out using each climate variable in turn, with the other two as covariates, shows that each variable has a highly significant effect ($p < 0.001$) that is independent of the others (Wei et al., 2019a).

3.3.2 Fossil pollen

The fossil pollen data were taken from the Abrupt climate Changes and Environmental Responses (ACER) database (Sanchez Goñi et al., 2017). The ACER database includes 93 pollen records globally covering part or all of the last glacial period (73–15 ka) with a temporal resolution better than 1000 years. Glacial-age pollen records provide a test of reconstruction techniques under climate conditions substantially different from present and therefore allow rigorous testing of the adequacy of the modern training data set. As examples, we use eight lacustrine records from southern Europe from the ACER database (Supplementary Table 2). The database provides standardised age models for all these cores, but the sampling resolution varies among cores. The Ioannina core (northwestern Greece, 39° 45’ N, 20° 51’ E) is used here as the primary example because it covers a long period (79.7–10.6 ka) and has relatively high temporal resolution (mean 237 years). However, as discussed below, the conclusions based on this core are supported by analysis of the other fossil data sets.

3.3.3 Climate space analysis

One assumption of WA-PLS is that the taxa used for reconstruction show a unimodal response to the climate variable being reconstructed. In order to test whether this assumption holds true, particularly for amalgamations to higher taxonomic levels, the climate space occupied by individual pollen taxa was represented and visualised using Generalized Additive Models (GAM) (Guisan et al., 2002) implemented with the Mixed GAM Computation Vehicle (mgcv) R package (Wood, 2017). This approach fits a response surface to the concentration of the pollen abundance in 3D climate space. Abundance is taken as the pollen percentage based on a pollen sum that includes all of the 195 taxa. Convex hulls are used to delineate the area of climate space that contains sampling points and thus avoid representing taxon abundances in climates not closely constrained by the modern pollen data. Convex hulls were fitted using the alphahull and ggplot2 packages in R (Pateiro-Lopez and Rodriguez-Casal, 2016; Wickham, 2016). We used a square root transformation of MI, as differences between MI values at the low end of the MI scale are more important than differences at the high end in their effect on vegetation (Prentice et al., 2017); taking the square root “stretches” the lower values and “compresses” the higher ones. MTCO and GDD0 were not

transformed. We do not include interactions among the climate variables since previous analyses (Wei et al., 2019a) have shown that they each have a significant and independent influence on the distribution of plant taxa and vegetation types. For visualisation purposes, we show 2D slices (MTCO and MI) through the fitted 3D response surfaces at low, medium, and high values of GDD0. Here we present a number of illustrative GAMs; Wei et al. (2019b, 2020) provide GAMs for all of the 195 pollen and pteridophyte spore taxa from the SMPDS data set.

3.3.4 Application of WA-PLS

The modern bioclimatic and pollen data were used to create pollen-climate transfer functions independently for MTCO, GDD0, and √MI using WA-PLS (ter Braak and Juggins, 1993). WA-PLS was implemented with the rioja R package (v0.9-15.1; Juggins, 2017). The performance of the calibration models was assessed through leave-one-out crossvalidation. The number of components used in each model was estimated through a randomisation t-test on the results of this cross-validation (van der Voet, 1994). We selected the significant component with the lowest root mean square error (RMSE), but only if there was a significant improvement in RMSE relative to a lower number of components—since including more components can result in over-fitting of the data so that model predictive value decreases. When making direct comparisons between different subsets of the data and SMPDS, we used the component that was considered significant for that subset (see Supplementary Table 3) rather than the same component across all sets. This choice does not affect the analysis, and for completeness we include an example comparison using the same components for all training sets in the Supplementary Information (Supplementary Figs. 2, 3, and 4). The (in)stability of transfer coefficients and the statistical uncertainty of reconstructions were assessed by bootstrapping the modern sample set with replacement 1000 times (Efron, 1979) and running WA-PLS each time to derive 1000 instances of both the taxon transfer coefficients and the reconstructed climate for each sample. The standard deviations (SDs) of the taxon transfer coefficients and the SDs of the reconstructions were then calculated from the 1000 bootstrap samples. The variability of a taxon coefficient, as measured by its SD, reflects how consistently the available modern samples including that taxon represent climate. The SD of the reconstruction calculated in this way

represents the combined effect of the taxon coefficient variability across all taxa in a fossil sample. This approach differs from the standard method for calculating uncertainties in the rioja R package (Juggins, 2017), which is based only on bootstrapping of the modern data set, because it combines the uncertainties of individual taxa from the modern pollen data set. Data analysis and plotting were performed in R v3.5.1 (R Core Team, 2018).

3.4 RESULTS

WA-PLS provides a transfer coefficient for each taxon and each bioclimatic variable. The validity of this transfer coefficient depends on the taxon being sampled across the full range of its realised niche in climate space, and this in turn is determined by the climate space sampled in the modern pollen training data set. Our initial tests therefore focus on the impact of the sampling of climate space on WA-PLS performance metrics and the resulting reconstructions (see "Impact of choice of training data set" below). One of the factors that affects the width of the realised taxon niche is taxonomic resolution, with species in general occupying a more limited niche than genera or families. The use of higher taxonomic groupings increases the number of samples available and can improve the sampling of climate space. We therefore examine the impact of using higher taxonomic groupings on the sampling of climate (see "Impact of amalgamation of pollen taxa to higher taxonomic levels" below). The choice of taxa included in the WA-PLS model will also impact the overall width of the sampled climate space, and we also address the potential impact of including or excluding taxa on model performance and the resulting reconstructions (see "Impact of number of taxa" below).

3.4.1 Impact of choice of training data set

In order to test the impact of the choice of training data set on WA-PLS performance metrics and reconstructions, we compared results from the full SMPDS data set and those obtained using either the EMB or the EMPD subsets. The EMB samples warmer seasonal climates than the EMPD (see Figure 3.1, Supplementary Fig. 5). The SMPDS samples much colder winter climates (as measured by MTCO) than either the EMB or EMPD data sets, and colder summers (as measured by GDD0) than the EMB set. These

differences in the sampled climate space are reflected in reconstructions of winter (Figure 3.2, see Supplementary Fig. 2) and summer (see Supplementary Fig. 3) temperatures, and also in moisture (as measured by MI) (see Supplementary Fig. 4).

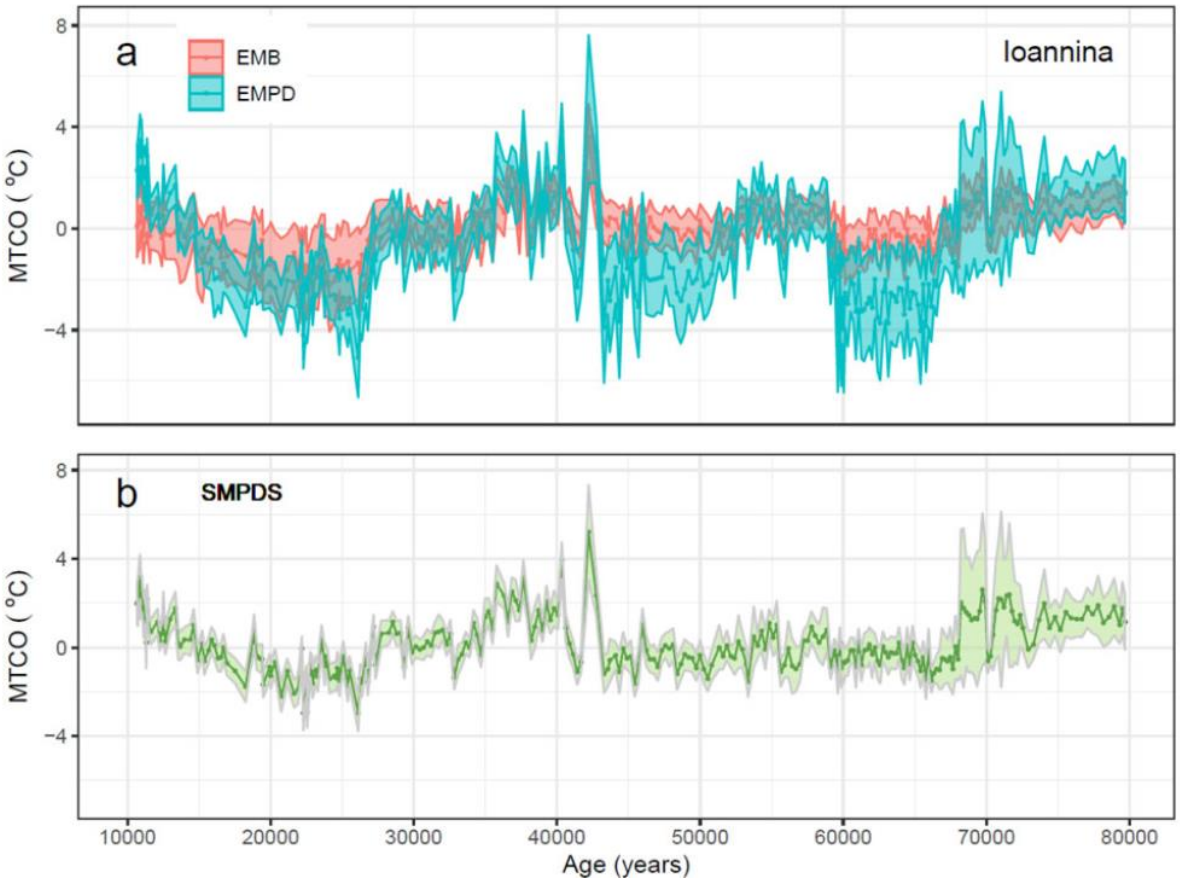

Figure 3.2 Reconstructions of mean temperature of the coldest month (MTCO) during the last glacial period (80,000 to 10,000 calendar years before 2000) using the pollen record from Lake Ioannina, (a) using the Eastern Mediterranean-Black Sea-Caspian Corridor Biomes (EMBSeCBIO) (labelled EMB) and the European Modern Pollen Database (EMPD) as training data sets, and (b) using the full SMPDS data set. The reconstruction spread (±2σ) is obtained by resampling the training set 1,000 times.

Reconstructions based on the EMB data set are generally warmer than those based on the EMPD, and there is little overlap between the spread of the reconstruction estimates in the coldest intervals of the glacial period (see Figure 3.2). The SMPDS data set produces temperature reconstructions similar to those based on the EMPD but has a considerably narrower reconstruction spread because it samples a wider climate space and contains more samples for each pollen taxon and thus a more complete sampling of the taxon's climatic range. The SDs of the coefficients are related to the number of occurrences (Figure 3.3) of the taxon in the sampled data set.

The difference in the reconstructions and their stability is not reflected in differences in the WA-PLS model performance measures (Table 3-1). Model performance is poorer for EMB-based reconstructions than for SMPDS-based reconstructions, but all of the measures of model performance (r2, RMSE, maximum bias) are better for EMPD than for the SMPDS data set because they are measures of how well the WA-PLS model replicates the sampled climate space, rather than whether the training data set encompasses a sufficiently large climate space. The standard performance measures are therefore an insufficient guide to the reliability of WA-PLS reconstructions. Comparison of observed versus predicted values (and their residuals) for the SMPDS data set show that this data set adequately reproduces modern climate (Supplementary Fig. 6).

Both the range and the continuity of the sampled climate are important. This is a consequence of the underlying assumption of WA-PLS that response curves are unimodal and extend across the full realised niche of the taxon; an abundance distribution which is truncated or has gaps cannot be expected to give reliable coefficients. This is borne out by analyses in which the density of sampling is artificially reduced. A proportion of the modern samples was progressively removed while preserving the overall range of climate space (Figure 3.4, Supplementary Figs. 7, 8, and 9), having permuted the samples to avoid artificial similarities when samples which are neighbours in the database are also geographically close. Even a 70% reduction in the number of samples does not change the reconstructed winter (see Fig. 4, Supplementary Fig. 10) or summer (Supplementary Figs. 11 and 12) temperature, providing that the range of the sampled climate is maintained (see Supplementary Figs. 7 and 8). It does, however, lead to larger uncertainties because the number of times each taxon is sampled is reduced and the taxon coefficients are therefore less stable (Supplementary Fig. 9). Again, model performance measures do not discriminate between the quality of the reconstructions made with the reduced density or the full SMPDS data set (Table 3-2).

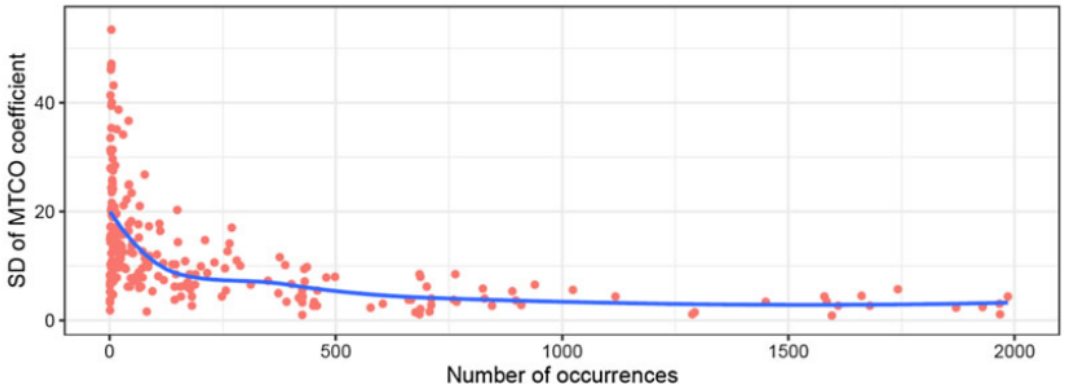

Figure 3.3 (color online) Relationship between the number of occurrences of a taxon and the standard deviation (SD) of the bootstrapped taxon coefficients. The analysis was made using the full SMPDS data set.

Tests in which samples from part of the climate range are systematically removed demonstrate the importance of continuous sampling of the climate range (Figure 3.5). Removing blocks of the MTCO gradient representing equal numbers of samples shows that discontinuities result in greater uncertainties (as measured by the bootstrapped SDs of the taxon coefficients) than those of the full SMPDS set. With one marginal exception, the uncertainties are also greater than those of a set from which the same number of samples randomly selected has been removed. Width and continuity are both important for obtaining stable taxon coefficients. Thus, it is important to ensure that the modern pollen training data set encompasses a wide range of climate space, to avoid offsets in the climate reconstructions. It is also important that the training data set samples the bioclimatic gradient as continuously as possible, in order to provide the most precise coefficients.

Table 3-1 Weighted Averaging Partial Least Squares (WA-PLS) model parameters for the reconstructions of mean temperature of the coldest month (MTCO, 0°C), growing degree days above a baseline of 0°C (GDD0, °day) and the square root of Moisture Index (√MI, unitless) using the Eastern Mediterranean-Black Sea-Caspian Corridor Biomes (EMBSeCBIO) (EMB), the European Modern Pollen Database (EMPD), and full SMPDS as training data sets, including the cross-validated r2, number of significant components ($p < 0.05$), root mean square error (RMSE), maximum bias, and number of samples. Supplementary Table 2 provides a complete list of WA-PLS model parameters for all data sets.

Variable	Data Set	r^2	No. of components	RMSE	Maximum bias	p	No. of samples
MTCO	EMB	0.417	2	3.97	19.6	0.002	1088
	EMPD	0.743	3	3.91	6.1	0.001	4675
	SMPDS	0.691	4	4.82	10.3	0.019	6458
GDD_0	EMB	0.508	2	960	1727	0.001	1088
	EMPD	0.667	3	901	1898	0.001	4675
	SMPDS	0.660	3	910	2039	0.001	6458
√MI	EMB	0.592	2	0.128	0.439	0.010	1088
	EMPD	0.602	3	0.190	0.838	0.001	4675
	SMPDS	0.598	3	0.185	0.910	0.001	6458

3.4.2 Impact of amalgamation of pollen taxa to higher taxonomic levels

Large modern pollen data sets are created by combining data collected by many palynologists, often for different types of studies, and as a result the level of taxonomic discrimination varies among sites. Many pollen taxa are recorded at a limited number of sites in such data sets, either because they are not regularly identified or because they are genuinely rare. Using taxa that are only recorded rarely, or show geographic clustering suggesting that they have not been sampled across the whole of their potential climate range, leads to unstable WA-PLS coefficients because the bioclimatic range of the taxon is unlikely to have been sampled continuously. The principle of niche conservatism indicates that higher taxa commonly have coherent environmental distributions (Ackerly, 2003; Wake et al., 2009)(Figure 3.6), and this principle provides a basis for amalgamating taxa that are only recorded at a few sites in the training data set. The coherency of the climate space occupied by the amalgamated taxon can be assessed using, for example, GAMs. Wei et al. (2019b) have tested the assumption that the taxa used here for reconstructions show a unimodal response to individual climate variables. They show that some taxa are unimodal with respect to one climate variable but are insensitive to others; the classic example is Artemisia, which appears to be insensitive to temperature but shows a clear optimum with respect to moisture. The assumption of unimodality holds true for most taxa across all climate variables; amalgamation to higher taxonomic levels does not modify this response substantially. As we show here, amalgamating rare taxa into higher taxa improves the bootstrapped SD of the transfer coefficients (Table 3-3, Supplementary Information Tables 5 and 6) by providing a more continuous sampling of bioclimatic gradients, and as a result leads to reduced uncertainties in the reconstructions.

3.4.3 Impact of number of taxa

Some taxa appear to be relatively uninformative either because they have a wide climatic tolerance or because they are rarely sampled, which raises the issue of whether such taxa should be excluded from the WA-PLS regression. However, analyses of randomly sampled taxa show that increasing the number of taxa monotonically narrows the reconstruction spread (Figure 3.7a). In our analyses, the impact of including

more taxa is steep initially and becomes discernibly more gradual above about 80 taxa, after which the mean reconstruction remains relatively stable with minimal offsets (Figure 3.7b).

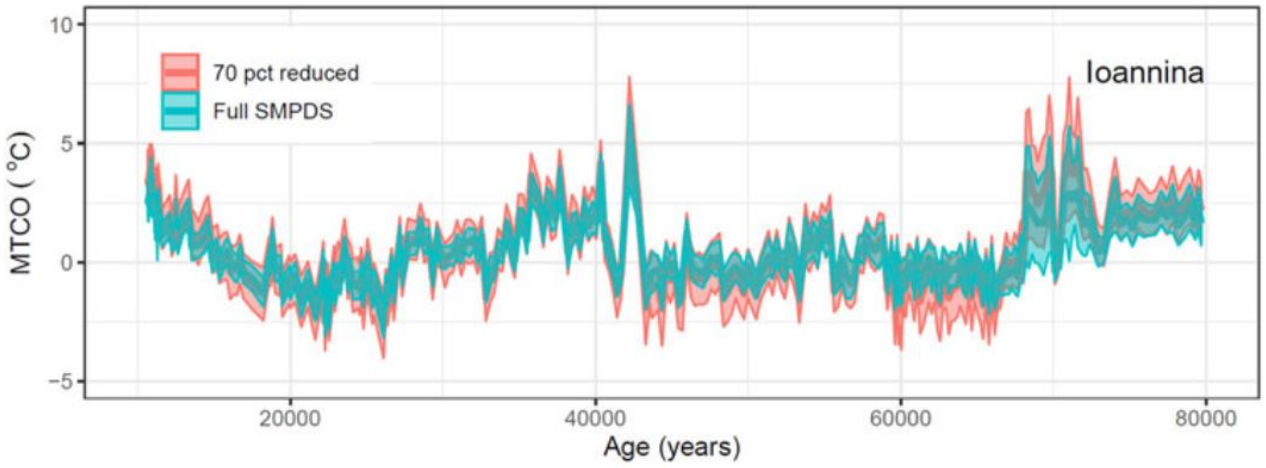

Figure 3.4 Impact of reducing the sampling density of the modern training data set on reconstructions of mean temperature of the coldest month (MTCO) during the last glacial period (80,000 to 10,000 calendar years before 2000) using the pollen record from Lake Ioannina. The plots show the impact of randomly removing 70% of the modern samples while preserving the overall range of climate space (see also Supplementary Figs. 7, 8, and 9) on the MTCO reconstructions compared to reconstructions made with the full SMPDS data set.

The abundance of pollen does not directly correspond to the abundance of a taxon in the vegetation (Prentice and Parsons, 1983; Prentice, 1985; Sugita, 2007; Hellman et al., 2008). Some taxa are systematically overrepresented in pollen assemblages (e.g., Pinus) while others are systematically under-represented (e.g., Larix). Furthermore, the comparative ease of pollen transport from closed canopy vegetation such as forest into more open landscapes that produce and disperse less pollen means that arboreal pollen is systematically overrepresented at sites in open tundra or steppe-type vegetation (e.g., Edwards et al., 2000; Bigelow et al., 2003; Marinova et al., 2018). However, the inclusion of taxa that are substantially overrepresented in modern assemblages compared to their abundance in the vegetation does not degrade model performance. Reconstructions made with the full SMPDS data set and with a data set that excludes Pinus (Supplementary Fig. 14) show little difference either in reconstructed MTCO or in reconstruction spread across multiple sites. Thus, although some studies (e.g., Sinopoli et al., 2019) have excluded such taxa, there is no general a priori reason to do so.

Table 3-2 Weighted Averaging Partial Least Squares (WA-PLS) model parameters for the reconstructions of mean temperature of the coldest month (MTCO), growing degree days above zero (GDD0) and the square root of Moisture Index (√MI) at Lake Ioannina using the full SMPDS data set and a version of this data set randomly reduced by 70% for the training data sets, including the cross-validated r2, number of significant components (p < 0.05), root mean square error (RMSE), maximum bias, and number of samples. Because the reduced sets are randomly chosen, different runs give different results; the standard deviations across 10 runs are given. The number of components is given as, for example, 2(7) meaning 7 runs allowed 2 significant components to be extracted; the balance allowed 3.

Variable	Data Set	r^2	No. of components	RMSE	Maximum bias	No. of samples
MTCO	Reduced	0.664 ± 0.022	2(6)	5.05 ± 0.07	12.7 ± 3.6	1959
	SMPDS	0.691	4	4.82	10.3	6458
GDD_0	Reduced	0.644 ± 0.010	2(7)	942 ± 17.8	2001 ± 257	1959
	SMPDS	0.660	3	910	2039	6458
√MI	Reduced	0.585 ± 0.013	2(8)	0.189 ± 0.004	0.898 ± 0.092	1959
	SMPDS	0.598	3	0.185	0.910	6458

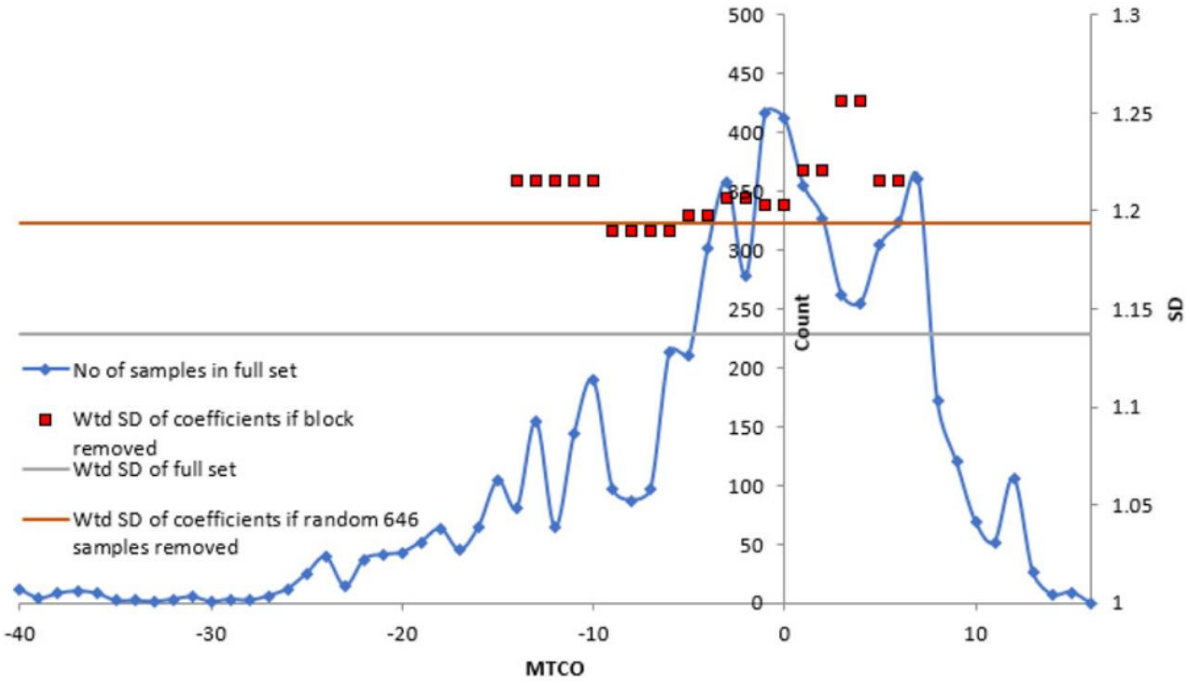

Figure 3.5 Impact of lack of continuity in sampling showing the effect on standard deviation (SD) of coefficients of the full set of taxa (n = 195), weighted by abundance, of removal of all samples in a given specified range of MTCO from the calibration data set. The red blocks (weighted [Wtd] SD of coefficients if block removed) show the impact of removing a specified number of samples (in this case 646 samples) contiguous in climate space. The low number of cold samples means that the first gap (samples 647–1293) starts at -14.6°C. The abundance-weighted SD using the full sample set (n = 6458) is indicated as a grey line for comparison, and the effect of removal of 646 randomly selected samples is indicated by a red line.

Fossil pollen assemblages almost always contain fewer taxa than the training data set. Thus, it might seem logical to base reconstructions solely on the taxa present in the fossil assemblages. However, the absence of taxa can also provide information about climate and thus can contribute usefully to the WA-PLS

reconstruction. Reconstructions of MTCO using only the taxa that are present in the fossil pollen samples at Lake Ioannina are not distinguishable from those made with the full SMPDS, either in terms of mean values or reconstruction spread (Supplementary Fig. 15b). However, at other sites, the use of only taxa present in the fossil record results in a difference in the reconstructions. At Megali Limni, for example, the reconstructions based on the fossil-taxa-only model are ca 1°C colder than those based on the full SMPDS data set (Supplementary Fig. 15a). At both Lake Ioannina and at Megali Limni, the model performance indicators show a substantial improvement using the full SMPDS data set: the r2 increases from ~0.55 to 0.7 at both sites, and the RMSE decreases from 5.80 to 4.82 at Ioannina and from 5.88 to 4.82 at Megali Limni (Supplementary Table 3). Using the full SMPDS data set is beneficial because, although taxon transfer coefficients are nearly independent of each other (and thus are little affected by the presence/ absence of other taxa), WA-PLS uses information from other taxa to refine the coefficients.

The coefficients of rare taxa are not stable (see Figure 3.3), and this can cause problems if these taxa are anomalously abundant, even at relatively low levels, in fossil samples. Changes in reconstruction spread are one indication of what is essentially a poor-analogue problem. At Lake Ioannina, for example, the increased spread in reconstructed MTCO during the interval between 73 and 68 ka (see Figure 3.2b) occurs because the abundance of Ulmus/Zelkova increases from ca 0.75% to 6–8% of the sample total. This taxon is recorded at only 31 sites in the modern data set and has a very large SD (14.7°C). Alternative methods, such as squared chord distance (Supplementary Fig. 16), confirm that this interval has poor analogues. Although little can be done about such poor-analogue situations, it is important to identify them through the use of a robust measure of reconstruction uncertainty for individual samples, such as the reconstruction spread measure used here.

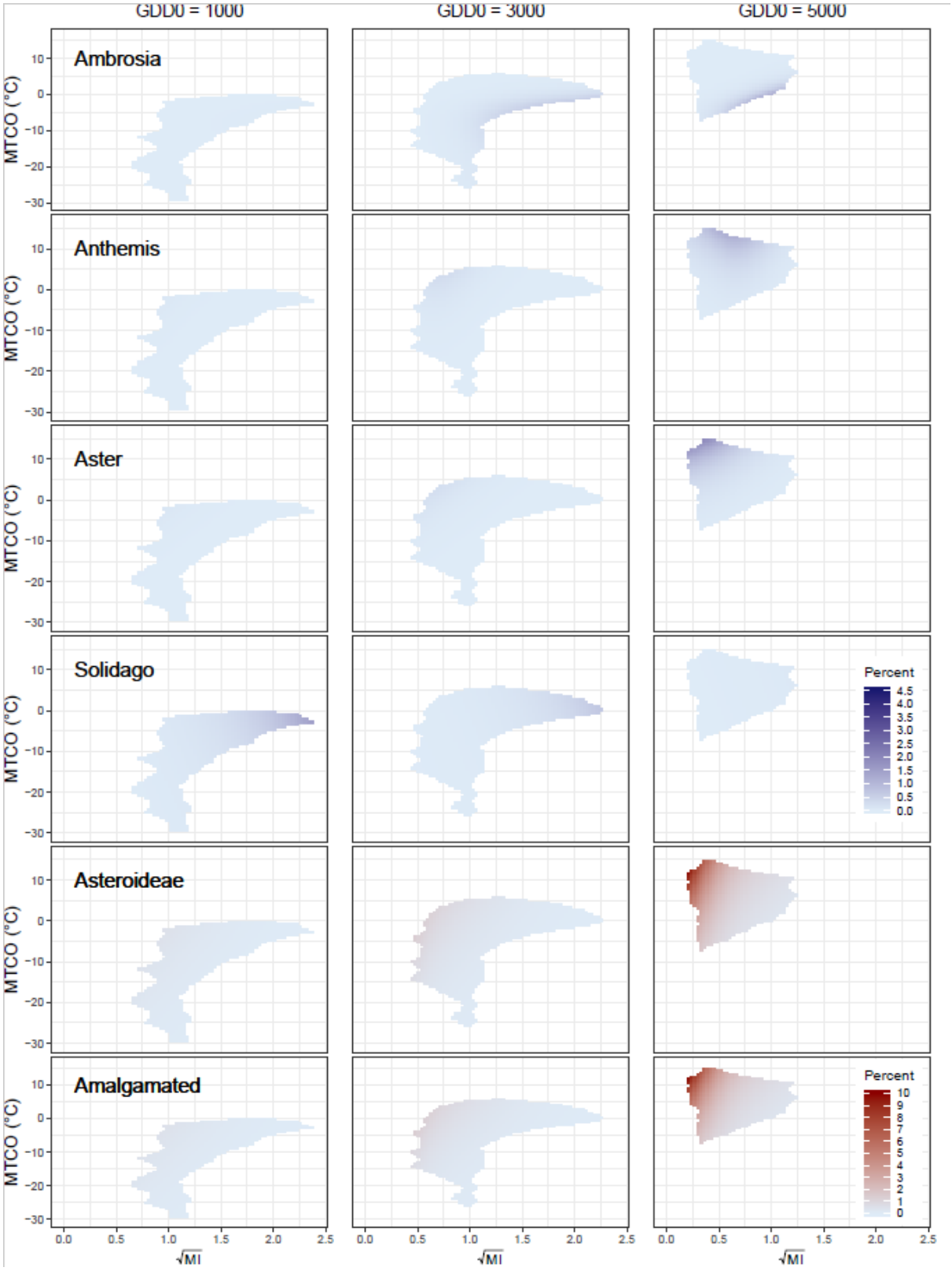

Figure 3.6 Climate space diagrams for individual taxa in the Asteroideae, based on Generalized Additive Models (GAMs). The plots are two dimensional representations of a three-dimensional space defined by mean temperature of the coldest month (MTCO, °C), growing degree days above a baseline of 0°C (GDD0, °C day), and the square root of a moisture index (MI, unitless), defined as the ratio of annual precipitation to annual potential evapotranspiration. The three columns show slices of the GAM at the points where GDD0 is 1000°C, 3000°C, and 5000°C day. The plots have been trimmed so that they only represent the sampled areas using convex hulls. The top four rows show the relative abundance on climate space of four of the most important taxa in the Asteroideae, the

fifth row shows the relative abundance of Asteroideae where this was explicitly recorded as a taxon in the original pollen counts, and the bottom panels show the relative abundance for the amalgamated taxon Asteroideae, created by summing all named component taxa together. Two scales are used, distinguished by colour: the scale for the top four panels is shown in the Solidago row, and for the bottom two the scale is shown in the Amalgamated row. Supplementary Fig. 13 shows the abundance in the same climate space at the sample level.

3.5 DISCUSSION

We have shown that the breadth and continuity of the climate space sampled by the modern training data set are important determinants of the quality of the reconstructions, although this may not be reflected in the WA-PLS model performance indicators. The number of samples in the data set does not provide a measure of the adequacy of sampling. There is a risk that training sets that rely on a very small number of samples (e.g., Xu et al., 2010; Salonen et al., 2012; Ding et al., 2017) do not sample a large enough range of climate space to encompass the true past climate if this is very different from present. However, as our comparison between reconstructions based on the EMPD and the full SMPDS shows, even large data sets may not have a sufficiently continuous sampling of climate space to provide stable coefficients and hence robust reconstructions. Furthermore, large data sets may still not encompass more extreme climates. This issue could be particularly important if the goal is to reconstruct climates very different from present-day climates, such as those of the last glacial period. Although most studies specify the training data set used, very few discuss how the training set was chosen or whether it samples an appropriate range of climate for the target reconstruction. Our analyses suggest that a minimum requirement is to plot the sampled climate space and thus to evaluate whether it is fit for purpose (

Table 3-4). From the perspective of improving existing training data sets, the focus should be on filling gaps in climate space rather than adding samples in climate space already represented.

Amalgamating pollen taxa to higher taxonomic levels can provide a way of increasing the continuity of the sampling of climate and reducing the statistical error of the reconstructions. Huntley et al. (1989) were the first to demonstrate niche conservatism in surface pollen data, showing that the abundance distribution of Fagus as recorded in surface pollen samples in North America could be predicted from the distribution of

the genus in Europe and vice versa. Subsequent studies have emphasised the degree to which lineages are conservative in terms of climate preferences (Ackerly, 2003; Wake et al., 2009). Williams and Shuman (2008) have provided counterexamples, where congeneric species occur at different parts of the moisture gradient in eastern and western North America. However, they also point out that the impact of this on reconstructions of climate decreases as the number of taxa used increases. Nevertheless, it should not be assumed that taxon amalgamation is always or automatically justified. One way of testing whether taxon distributions are unimodal and whether amalgamations to higher taxonomic levels are defensible is to construct GAMs (Wei et al., 2019b).

Table 3-3 Examples of the impact of amalgamating taxa to higher taxonomic levels on the bootstrapped standard deviation (SD) of transfer coefficients for mean temperature of the coldest month (MTCO). The mean SD of the component taxa (column 3) is weighted by abundance. Additional information on the component taxa and the transfer coefficients (climate optima) identified for the component taxa and the amalgamated taxon is given in Supplementary Tables 4 and 5.

Amalgamation level	Amalgamated taxon	Mean SD of component taxa	SD of amalgamated taxon
Family	Apiaceae	2.3	1.7
Family	Plantaginaceae	2.2	1.2
Subfamily	Asteroideae	2.5	1.3
Subfamily	Carduoideae	3.6	2.1
Subfamily	Cichoroideae	1.0	1.0
Genus	*Cistus*	2.5	1.7
Genus	*Ephedra*	4.8	3.5
Functional grouping	Deciduous Quercus	0.8	0.5
Functional grouping	Evergreen Quercus	0.7	0.4

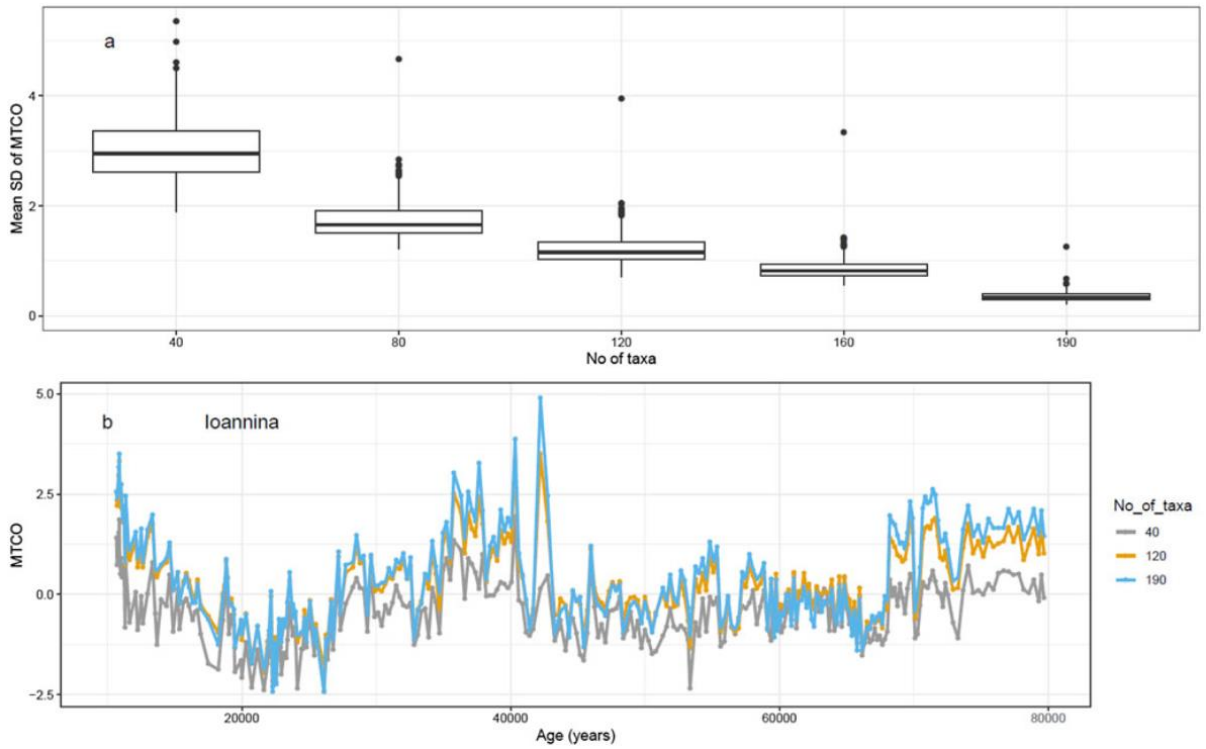

Figure 3.7 (a) Change in the standard deviation (SD) of the reconstruction of mean temperature of the coldest month (MTCO) as increasing numbers of taxa are used in the Weighted Averaging Partial Least Squares (WA-PLS) regression, taken across the whole time series, and (b) the mean reconstructions at three example points. The specified number of taxa is randomly selected without replacement 100 times, and the WA-PLS reconstruction run. The SD is taken across the 100 runs. Three WA-PLS components were used, but only results with $p < 0.05$ in a random t-test were included in the means and SDs.

The SMPDS includes sites from across the whole of the Palaearctic phytogeographic region (Wallace, 1876; Good, 1974; Kreft and Jetz, 2010; Dengler et al., 2014) in order to create a training data set that samples colder and more continental climates than would be available from a more limited region. Although the sampling of this region is incomplete, since there are large sampling gaps in Russia and northern China, the SMPDS provides samples from much colder winter climates and climates with a greater seasonal temperature range (see Figure 3.1). The expansion to the Palaearctic phytogeographic region relies on the fact that this region is characterised by taxa that have diversified in relatively recent geological time, that is, during approximately the past 20 Ma. The climate preferences of these taxa are expected to be conservative, as has been demonstrated for many plant lineages (Ackerly, 2003; Williams and Shuman, 2008; Wake et al., 2009).

Table 3-4 Checklist of issues, steps to identify them, and some potential solutions.

Issue	Potential actions
Is the sampling of climate space sufficient to reconstruct very different climates from present?	1) Plot sampled climate space and determine whether this provides information that would allow reconstruction of different (e.g., much warmer or much colder than present) climates. 2) Expand training data set to include a wider sampling of climate, as determined by the expected past climate change (i.e., colder climate for glacial samples, warmer climates for early Holocene samples), by expanding the geographical coverage of the data set.
Is the sampling of climate space continuous or are there gaps which result in ambiguous or multiple optima for individual taxa?	1) Plot sampled climate space to identify regions that are underrepresented. 2) Plot taxon distributions in climate space to identify existence of multiple optima which might indicate discontinuous sampling of the climate niche of the taxon. 3) Expand training data sets by explicit field sampling of underrepresented areas of climate space.
Is the amalgamation of taxa into higher taxonomic groupings appropriate?	1) Use Generalized Additive Models (or similar approaches) to test whether the individual taxa included within a higher taxonomic grouping occupy a similar climate niche.
How many taxa should be included in the model?	1) Do not exclude taxa a priori. 2) Exclude taxa that are not represented at a sufficient number of sites in the training data set to sample their full climate range. The definition of the minimum number of sites could be based on whether these sites cover the modern climate niche of the taxon (e.g., as shown by presence/absence data) or from modern distribution maps. 3) Use independent evidence (e.g., sedimentological evidence) to exclude taxa that reflect local non-climate signals (e.g., erosion). 4) Check that the exclusion of rarely sampled taxa or taxa reflecting anomalous local signals has no impact on the resulting reconstruction.
Do taphonomic or preservation issues have an impact on the reconstructions?	1) Check the abundance of indeterminable (e.g., corroded) grains in the samples as a measure of the quality of the assemblage and the likelihood that there are preservation issues. 2) Calculate a biodiversity index (e.g., HillsN2) to assess the degree to which samples might be affected by preservation issues.
Is the choice of model appropriate?	1) Do not rely on the standard model diagnostics to select a model. 2) Use diagnostics that demonstrate the stability of transfer coefficients and consequent reconstruction spread to calculate uncertainties on the reconstructions for individual samples.

The expansion of a training data set to increase the diversity of sampled climates is useful in principle, because it increases the range of different climates that can be reconstructed. As in the case of amalgamations to higher taxonomic levels, however, it is both possible and desirable to test (e.g., using GAMs, see

Table 3-4) whether the taxa considered retain a coherent, unimodal relationship to the climate variables of interest. There is no established rule about the choice of training data set, and the general hypothesis of climatic niche conservatism within phytogeographic regions would repay further research. However, the

common practice of using training data sets with limited geographic coverage (Xu et al., 2010; Salonen et al., 2012; Ding et al., 2017) effectively limits the range of climates that can be reconstructed. Similarly, exclusion of modern pollen samples from particular vegetation types (Sinopoli et al., 2019) prevents the reconstruction of climates characterised by these vegetation types.

We have shown that WA-PLS model performance statistics and the stability of the coefficients improve as taxa are added. Several studies have examined the impact of using a subset of important taxa, defined in terms of abundance (Birks, 1994) or predictive importance (Racca et al., 2003), on reconstructions based on weighted averaging (WA). The results have been inconclusive. Juggins et al. (2015) showed that removing uninformative taxa resulted in better performance using artificially constructed data sets but did not have a similar impact on real data sets. Jonkers and Kuč era (2018) found no impact from reducing the number of foraminifera species on WA model performance but showed that the resulting sea surface temperature reconstructions were significantly different between reduced- and full-taxa reconstructions. A similar conclusion was reached by Bjune et al. (2010) in a study contrasting climate reconstructions based on 191 vs. 321 core-top pollen samples.

The impact of including taxa that do not have a significant relationship to the climate variable being reconstructed and therefore have limited predictive power is closely tied to whether they are influenced by other climate or environmental factors, which would result in a degradation of model performance as shown by the analysis in Juggins et al. (2015). Thus, the choice of appropriate variables to reconstruct, and accounting for interactions among variables, is probably more useful than removing taxa that are thought to be uninformative.

Some studies have excluded taxa that are overrepresented in pollen assemblages, such as Pinus, on the assumption that these suppress the expression of the signal from less abundant taxa (e.g., Sinopoli et al., 2019). Our analyses suggest there is no reason to exclude such taxa on a priori grounds. However, there may be circumstances that warrant exclusion of specific taxa. Wei et al. (2019a), for example, excluded both Poaceae and Polypodiales from the taxa used to reconstruct climate at El Cañizar de Villarquemado on the

grounds that high abundances of these two taxa caused anomalous excursions in moisture reconstructions that were not seen in temperature reconstructions, and because independent sedimentological evidence supported the idea that anomalously high abundances of these two taxa in some samples represented reeds (aquatic grasses, in the case of Poaceae) or erosional inputs (in the case of Polypodiales). They showed that the removal of these taxa had no impact except on the MI reconstructions of the anomalous samples. Insofar as anomalous results can be attributed to the high abundance of specific taxa that could reflect the influence of non-climatic factors, exclusions may be warranted. It is, however, important to test the impact of these exclusions on the final reconstructions (see *Table 3-4).*

It is often tacitly assumed that better WA-PLS model performance means better reconstruction, but we have shown that WA-PLS models of equivalent performance can produce very different reconstructions (e.g., see Figure 3.2). WA-PLS model performance only reflects how well the model replicates the climate space of the modern training data set but says nothing about whether that climate space is adequate or appropriate. We conclude that model performance must be considered alongside an assessment of the representativeness of climate at the data set and taxon level (see *Table 3-4*).

This could be done, for example, by plotting the sites and taxon abundances in climate space and expanding the calibration data set to ensure that it samples a range of climates commensurate with the climate that might have been experienced at a given location. Although the RMSE of the modern calibration is generally used as a measure of reconstruction uncertainty, it is in fact a measure of the average uncertainty for a randomly selected surface sample. Thus, it provides the same estimate of uncertainty for all fossil pollen samples, regardless of whether the taxa in the fossil samples are well represented in the modern data set and have stable coefficients. It provides no information about uncertainties arising because of mismatches between the sampling of modern taxa and their representation in fossil assemblages. We have used an alternative approach that propagates the calibration errors into the downcore reconstructions by assessing the calibration error associated with the particular assemblage in an individual pollen sample. This approach provides a way of identifying specific intervals downcore where the reconstruction errors are well

constrained and differentiating these from intervals with larger uncertainties. As we show in the Lake Ioannina example (see Figure 3.2b), it is then possible to identify the specific cause of these larger uncertainties and, in particular, a way of identifying poor-analogue situations that would be overlooked using the standard approach to representing uncertainty. Thus, the bootstrapped reconstruction spread provides an alternative, and we would argue better, measure of the consistency and redundancy of the calibration set and thus indirectly the robustness of the reconstructions than the standard use of RMSE.

There will be a continuing need for quantitative estimates of past climates in order to evaluate climate model simulations, and it is important to continue to explore ways to demonstrate and, if possible, improve their robustness. While there are alternative approaches to statistical reconstruction, such as vegetation-model inversion (Guiot et al., 2000;Wu et al., 2007, 2009; Izumi and Bartlein, 2016) or data assimilation (Goosse et al., 2006; Annan and Hargreaves, 2013; Cleator et al., 2019), they do not provide a panacea—in the one case because they are heavily dependent on the specifics of the model, in the other because they require quantitative estimates as inputs. It has been suggested (Brewer et al., 2008) that more robust estimates of past climates can be obtained by using multiple statistical approaches, and this has been done in an increasing number of studies (Xu et al., 2010; Guiot and de Vernal, 2011; Peyron et al., 2011; Jonkers and Kuč era, 2018; Sinopoli et al., 2019). However, many of the sampling issues described here apply equally to all analogue- or regression-based reconstruction methods. Thus, while using several methods together may provide an indication of the robustness of a reconstruction, such robustness does not necessarily demonstrate that the reconstructions are correct. Exploring and documenting methodological decisions, as suggested here, should lead to more transparent reconstructions and perhaps greater consistency between reconstructions at different sites.

3.6 CONCLUSIONS

Care needs to be exercised in the application of statistical reconstruction techniques, such as WA-PLS, in order to ensure that the results are robust and reasonable. We have demonstrated that WA-PLS model performance metrics are not a sufficient guide to the reliability of the reconstructions: models with similar

performance metrics nevertheless provide different reconstructions of past climates. We argue that the modern pollen training data set should not only sample the full width of the climate niche of each taxon but also provide a continuous sampling of this range. The width and continuity of the sampling of climate space are more important than number of samples. Width and continuity can be improved by amalgamating taxa to higher taxonomic levels, providing the assumptions about the unimodality of these higher taxa with respect to individual climate variables are explicitly tested. We also argue that it is important for the modern training set to sample climates that encompass the full range of the climates that might be expected to have occurred in the past; for example, to sample colder and drier climates that might be found in the Mediterranean during the last glacial period. While it is difficult to know a priori how broad a sampling of climate space is necessary to ensure this for a specific site or region, ensuring that the training data set is broad enough to test explicit hypotheses about the expected climate change would be useful. These hypotheses could be based on alternative sources of palaeoclimate information, including model experiments.

Our analyses are not designed to provide a prescription for how to apply WA-PLS: we are not recommending the use of a specific modern pollen training data set or specific methods to test the usefulness of this data set. Instead, we are advocating that the robustness of statistical reconstructions should be explicitly tested and documented. We have suggested a number of straightforward checks (see Table 4) that should be made. These include: (1) testing the range and continuity of the sampling of climate gradients in the modern training data set by plotting the modern samples in climate space; (2) ensuring that the sampled climate covers a sufficient range to be able to reconstruct substantially different climates in the past, for example by ensuring that the training data set includes samples which are both much warmer/colder and wetter/drier than the modern climate of the region; (3) examining whether amalgamation to higher taxonomic levels provides a more continuous sampling of climate space by plotting the climate space of both individual taxa and the higher taxon into which they are placed; and (4) using the largest number of taxa in the reconstructions and avoiding a priori taxon exclusions. The reasons for any exclusions should be transparent and supported by independent evidence, and the impact of these

exclusions on the reconstructed climate should be tested. The proposed checks do not necessarily identify whether specific methodological choices are correct, but they do provide insights into the uncertainties associated with the reconstructions.

3.7 ACKNOWLEDGMENTS

SPH and DW acknowledge support from the European Research Council (ERC)-funded project Global Change 2.0: Unlocking the past for a clearer future (GC2.0), grant number 694481. This research is a contribution to the AXA Chair Programme in Biosphere and Climate Impacts and the Imperial College initiative on Grand Challenges in Ecosystems and the Environment (ICP). ICP also acknowledges funding from the ERC under the European Union's Horizon 2020 research and innovation programme (grant agreement No: 787203 REALM). SPH also acknowledges support from the JPI-Belmont project "PAlaeo-Constraints on Monsoon Evolution and Dynamics (PACMEDY)" through the UK Natural Environmental Research Council (NERC). The pollen data used in our analyses were taken from the ACER database. We thank members of the ACER Working Group for this compilation and the creation of standardised age models. We also thank Cajo ter Braak and an anonymous reviewer for their helpful comments on this paper.

3.8 AUTHOR CONTRIBUTIONS

All authors contributed to the conceptual development. Formal analysis, methods, and software: MT with contributions from DW on climate and GAMs. Writing—original draft: MT and SPH. Writing—editing and review: all authors.

3.9 SUPPLEMENTARY MATERIAL

The supplementary material for this article can be found at https:// doi.org/10.1017/qua.2020.44.

3.10 REFERENCES

Ackerly, D.D., 2003. Community assembly, niche conservatism, and adaptive evolution in changing environments. *International Journal of Plant Sciences* 164, S165–S184. https://doi.org/10.1086/368401.

Annan, J.D., Hargreaves, J.C., 2013. A new global reconstruction of temperature changes at the Last Glacial Maximum. *Climate of the Past* 9, 367. http://dx.doi.org/10.5194/cp-9-367-2013.

Bartlein, P.J., Harrison, S.P., Brewer, S., Connor, S., Davis, B.A.S., Gajewski, K., Guiot, J., et al., 2011. Pollen-based continental climate reconstructions at 6 and 21 ka: a global synthesis. *Climate Dynamics* 37, 775–802. https://doi.org/10.1007/s00382-010-0904-1.

Bigelow, N., Brubaker, L., Edwards, M.E., Harrison, S.P., 2003. Climate change and Arctic ecosystems: 1. Vegetation changes north of 55°N between the last glacial maximum, mid-Holocene, and present. *Journal of Geophysical Research* 108. https://doi.org/10.1029/2002JD002558.

Birks, H.J.B., 1994. The importance of pollen and diatom taxonomic precision in quantitative palaeoenvironmental reconstructions. *Review of Palaeobotany and Palynology* 83, 107–117. https://doi.org/10.1016/0034-6667(94)90062-0.

Birks, H.J.B., Seppä, H., 2004. Pollen-based reconstructions of late-Quaternary climate in Europe - Progress, problems, and pitfalls. *Acta Palaeobotanica* 44, 317–334.

Bjune, A.E., Birks, H.J.B., Peglar, S.M., Odland, A., 2010. Developing a modern pollen-climate calibration data set for Norway. *Boreas* 39, 674–688. https://doi.org/10.1111/j.1502-3885.2010.00158.x.

Braconnot, P., Harrison, S.P., Kageyama, M., Bartlein, P.J., Masson-delmotte, V., Abe-ouchi, A., Otto-bliesner, B., Zhao, Y., 2012. Evaluation of climate models using palaeoclimatic data. *Nature Climate Change;* London 2, 417–424. http://dx.doi.org/10.1038/nclimate1456

Brewer, S., Guiot, J., Sánchez-Goñi, M.F., Klotz, S., 2008. The climate in Europe during the Eemian: a multi-method approach using pollen data. *Quaternary Science Reviews* 27, 2303–2315. https://doi.org/10.1016/j.quascirev.2008.08.029.

Brooks, S.J., Birks, H.J.B., 2001. Chironomid-inferred air temperatures from Lateglacial and Holocene sites in north-west Europe: progress and problems. *Quaternary Science Reviews, European Quaternary Biostratigraphy* 20, 1723–1741. https://doi.org/10.1016/S0277-3791(01)00038-5.

Brunsdon, C., Fotheringham, A.S., Charlton, M., 2002. Geographically weighted summary statistics—a framework for localised exploratory data analysis. *Computers, Environment and Urban Systems* 26, 501–524. https://doi.org/10.1016/S0198-9715(01)00009-6.

Cleator, S.F., Harrison, S.P., Nichols, N.K., Prentice, I.C., Roulstone, I., 2019. A method for generating coherent spatially explicit maps of seasonal palaeoclimates from site-based reconstructions. arXiv:1902.04973 [physics].

Collins, M., Knutti, R., Arblaster, J., Dufresne, J.-L., Fichefet, T., Friedlingstein, P., Gao, X., Gutowski, W., Johns, T., Krinner, G, 2013. Long-term climate change: projections, commitments and irreversibility. In: *Climate Change 2013—The Physical Science Basis: Working Group I Contribution to the Fifth Assessment Report of the Intergovernmental Panel on Climate Change*. Cambridge University Press, Cambridge, pp. 1029–1136.

Davis, B.A.S., Zanon, M., Collins, P., Mauri, A., Bakker, J., Barboni, D., Barthelmes, A., et al., 2013. The European Modern Pollen Database (EMPD) project. *Vegetation History and Archaeobotany* 22, 521–530. https://doi.org/10.1007/s00334-012-0388-5.

Davis, T.W., Prentice, I.C., Stocker, B.D., Thomas, R.T., Whitley, R.J., Wang, H., Evans, B.J., Gallego-Sala, A.V., Sykes, M.T., Cramer, W., 2017. Simple process-led algorithms for simulating habitats (SPLASH v.1.0): robust indices of radiation, evapotranspiration and plant-available moisture. *Geoscientific Model Development* 10, 689–708. http://dx.doi.org/10.5194/gmd-10-689-2017.

Dengler, J., Janišová, M., Török, P., Wellstein, C., 2014. Biodiversity of Palaearctic grasslands: a synthesis. In: *Agriculture, Ecosystems & Environment*, Biodiversity of Palaearctic grasslands: processes, patterns and conservation 182, 1–14. https://doi.org/10.1016/j.agee.2013.12.015.

Ding, W., Xu, Q., Tarasov, P.E., 2017. Examining bias in pollen-based quantitative climate reconstructions induced by human impact on vegetation in China. *Climate of the Past* 13, 1285.

Edwards, M.E., Anderson, P.M., Brubaker, L.B., Ager, T.A., Andreev, A.A., Bigelow, N.H., Cwynar, L.C., et al., 2000. Pollen-Based Biomes for Beringia 18,000, 6000 and 0 14C yr BP. *Journal of Biogeography* 27, 521–554.

Efron, B., 1979. Bootstrap Methods: Another Look at the Jackknife. *The Annals of Statistics* 7, 1–26.

ESRI, 2014. ArcGIS Desktop. Environmental System Research Institute, Redlands, California.

Good, R., 1974. *The Geography of Flowering Plants*. 4th ed. Addison-Wesley-Longman.

Goosse, H., Renssen, H., Timmermann, A., Bradley, R.S., Mann, M.E., 2006. Using paleoclimate proxy-data to select optimal realisations in an ensemble of simulations of the climate of the past millennium. *Climate Dynamics* 27, 165–184. https://doi.org/10.1007/s00382-006-0128-6.

Guiot, J., de Vernal, A., 2011. Is spatial autocorrelation introducing biases in the apparent accuracy of paleoclimatic reconstructions? *Quaternary Science Reviews* 30, 1965–1972. https://doi.org/10.1016/j.quascirev.2011.04.022.

Guiot, J., Torre, F., Jolly, D., Peyron, O., Boreux, J.J., Cheddadi, R., 2000. Inverse vegetation modeling by Monte Carlo sampling to reconstruct palaeoclimates under changed precipitation seasonality and CO_2 conditions: application to glacial climate in Mediterranean region. *Ecological Modelling* 127, 119–140. https://doi.org/10.1016/S0304-3800(99)00219-7.

Guisan, A., Edwards, T.C., Hastie, T., 2002. Generalized linear and generalized additive models in studies of species distributions: setting the scene. *Ecological Modelling* 157, 89–100. https://doi.org/10.1016/S0304-3800(02)00204-1.

Harrison, S.P., 2019. Modern pollen data for climate reconstructions, version 1 (SMPDS). University of Reading. http://dx.doi.org/10.17864/1947.194.

Harrison, S.P., 2020. Climate reconstructions for the SMPDSv1 modern pollen data set. https://doi.org/10.5281/zenodo.3605003.

Harrison, S.P., Bartlein, P.J., Brewer, S., Prentice, I.C., Boyd, M., Hessler, I., Holmgren, K., Izumi, K., Willis, K., 2014. Climate model benchmarking with glacial and mid-Holocene climates. *Climate Dynamics* 43, 671–688. https://doi.org/10.1007/s00382-013-1922-6.

Harrison, S.P., Bartlein, P.J., Izumi, K., Li, G., Annan, J., Hargreaves, J., Braconnot, P., Kageyama, M., 2015. Evaluation of CMIP5 palaeo-simulations to improve climate projections. *Nature Climate Change* 5, 735–743. https://doi.org/10.1038/nclimate2649.

Harrison, S.P., Prentice, I.C., Barboni, D., Kohfeld, K.E., Ni, J., Sutra, J.-P., 2010. Ecophysiological and bioclimatic foundations for a global plant functional classification. *Journal of Vegetation Science* 21, 300–317. https://doi.org/10.1111/j.1654-1103.2009.01144.x.

Hellman, S., Gaillard, M.-J., Broström, A., Sugita, S., 2008. The REVEALS model, a new tool to estimate past regional plant abundance from pollen data in large lakes: validation in southern Sweden. *Journal of Quaternary Science* 23, 21–42. https://doi.org/10.1002/jqs.1126.

Huntley, B., Bartlein, P.J., Prentice, I.C., 1989. Climatic Control of the Distribution and Abundance of Beech (*Fagus L.*) in Europe and North America. *Journal of Biogeography* 16, 551–560. https://doi.org/10.2307/2845210.

Izumi, K., Bartlein, P.J., 2016. North American paleoclimate reconstructions for the Last Glacial Maximum using an inverse modeling through iterative forward modeling approach applied to pollen data. *Geophysical Research Letters* 43, 10,965–10,972. https://doi.org/10.1002/2016GL070152.

Jonkers, L., Kučera, M., 2018. Sensitivity to species selection indicates the effect of nuisance variables on marine microfossil transfer functions. *Climate of the Past Discussions* 1–19. https://doi.org/10.5194/cp-2018-107.

Juggins, S., 2013. Quantitative reconstructions in palaeolimnology: new paradigm or sick science? *Quaternary Science Reviews*.Juggins, S, 2017. rioja: Analysis of quaternary science data. CRAN.

Juggins, S., Simpson, G.L., Telford, R.J., 2015. Taxon selection using statistical learning techniques to improve transfer function prediction. *The Holocene* 25, 130–136. https://doi.org/10.1177/0959683614556388.

Kirtman, B., Power, S.B., Adedoyin, A.J., Boer, G.J., Bojariu, R., Camilloni, I., Doblas-Reyes, F., Fiore, A.M., Kimoto, M., and Meehl, G., 2013. Near-term Climate Change: Projections and Predictability. In: *Climate*

Change 2013—The Physical Science Basis: Working Group I Contribution to the Fifth Assessment Report of the Intergovernmental Panel on Climate Change. Cambridge University Press, Cambridge, pp. 953–1020.

Kreft, H., Jetz, W., 2010. A framework for delineating biogeographical regions based on species distributions: Global quantitative biogeographical regionalizations. *Journal of Biogeography* 37, 2029–2053. https://doi.org/10.1111/j.1365-2699.2010.02375.x.

Lotter, A.F., Birks, H.J.B., Hofmann, W., Marchetto, A., 1997. Modern diatom, cladocera, chironomid, and chrysophyte cyst assemblages as quantitative indicators for the reconstruction of past environmental conditions in the Alps. I. *Climate. Journal of Paleolimnology* 18, 395–420. https://doi.org/10.1023/A:1007982008956.

Marinova, E., Harrison, S.P., Bragg, F., Connor, S., Laet, V. de, Leroy, S.A.G., Mudie, P., et al., 2018. Pollen-derived biomes in the Eastern Mediterranean–Black Sea–Caspian-Corridor. *Journal of Biogeography* 45, 484–499. https://doi.org/10.1111/jbi.13128.

Marsicek, J., Shuman, B.N., Bartlein, P.J., Shafer, S.L., Brewer, S., 2018. Reconciling divergent trends and millennial variations in Holocene temperatures. *Nature* 554, 92–96. https://doi.org/10.1038/nature25464.

New, M., Lister, D., Hulme, M., Makin, I., 2002. A high-resolution data set of surface climate over global land areas. *Climate Research 21*, 1–25. https://doi.org/10.3354/cr021001.

Pateiro-Lopez, B., Rodriguez-Casal, A., 2016. alphahull: Generalization of the Convex Hull of a Sample of Points in the Plane. CRAN.

Peyron, O., Goring, S., Dormoy, I., Kotthoff, U., Pross, J., de Beaulieu, J.-L., Drescher-Schneider, R., Vannière, B., Magny, M., 2011. Holocene seasonality changes in the central Mediterranean region reconstructed from the pollen sequences of Lake Accesa (Italy) and Tenaghi Philippon (Greece). *The Holocene* 21, 131–146. https://doi.org/10.1177/0959683610384162.

Prentice, I.C., 1985. Pollen Representation, Source Area, and Basin Size: Toward a Unified Theory of Pollen Analysis. *Quaternary Research* 23, 76–86. https://doi.org/10.1016/0033-5894(85)90073-0.

Prentice, I.C., Cleator, S.F., Huang, Y.H., Harrison, S.P., Roulstone, I., 2017. Reconstructing ice-age palaeoclimates: Quantifying low-CO_2 effects on plants. *Global and Planetary Change* 149, 166–176. https://doi.org/10.1016/j.gloplacha.2016.12.012.

Prentice, I.C., Parsons, R.W., 1983. Maximum Likelihood Linear Calibration of Pollen Spectra in Terms of Forest Composition. *Biometrics* 39, 1051–1057. https://doi.org/10.2307/2531338.

R Core Team, 2018. *R: A language and environment for statistical computing*. R Foundation for Statistical Computing, Vienna.

Racca, J.M.J., Wild, M., Birks, H.J.B., Prairie, Y.T., 2003. Separating wheat from chaff: Diatom taxon selection using an artificial neural network pruning algorithm. *Journal of Paleolimnology* 29, 123–133.

Rymes, M.D., Myers, D.R., 2001. Mean preserving algorithm for smoothly interpolating averaged data. *Solar Energy* 71, 225–231. https://doi.org/10.1016/S0038-092X(01)00052-4.

Salonen, J.S., Ilvonen, L., Seppä, H., Holmström, L., Telford, R.J., Gaidamavičius, A., Stančikaitė, M., Subetto, D., 2012. Comparing different calibration methods (WA/WA-PLS regression and Bayesian modelling) and different-sized calibration sets in pollen-based quantitative climate reconstruction. *The Holocene* 22, 413–424. https://doi.org/10.1177/0959683611425548.

Salonen, J.S., Seppä, H., Birks, H.J.B., 2013. The effect of calibration data set selection on quantitative palaeoclimatic reconstructions. *The Holocene* 23, 1650–1654. https://doi.org/10.1177/0959683613496295.

Sanchez Goñi, M.F., Desprat, S., Daniau, A.-L., Bassinot, F.C., Polanco-Martínez, J.M., Harrison, S.P., Allen, J.R.M., et al., 2017. The ACER pollen and charcoal database: a global resource to document vegetation and fire response to abrupt climate changes during the last glacial period. https://doi.org/10.1594/PANGAEA.870867. Supplement to: Sanchez Goñi, M.F., Desprat, S., Daniau, A.-L., Bassinot, F.C., Polanco-Martínez, J.M., Harrison, S.P., Allen, J.R.M., et al., 2017. The ACER pollen and charcoal database: a global resource to document vegetation and fire response to abrupt climate changes

during the last glacial period. *Earth System Science Data*, 9, 679–695, https://doi.org/10.5194/essd-9-679-2017.

Schmidt, G.A., Annan, J.D., Bartlein, P.J., Cook, B.I., Guilyardi, E., Hargreaves, J.C., Harrison, S.P., et al., 2014. Using palaeo-climate comparisons to constrain future projections in CMIP5. *Climate of the Past* 10, 221–250. https://doi.org/10.5194/cp-10-221-2014.

Seppä, H., Bjune, A.E., Telford, R.J., Birks, H.J.B., Veski, S., 2009. Last nine-thousand years of temperature variability in Northern Europe. *Climate of the Past* 13.

Shennan, I., Long, A.J., Horton, B.P., 2015. *Handbook of Sea-Level Research*. American Geophysical Union, Washington, United Kingdom.

Sinopoli, G., Peyron, O., Masi, A., Holtvoeth, J., Francke, A., Wagner, B., Sadori, L., 2019. Pollen-based temperature and precipitation changes in the Ohrid Basin (western Balkans) between 160 and 70ka. *Climate of the Past* 15, 53–71. https://doi.org/10.5194/cp-15-53-2019.

Sugita, S., 2007. Theory of quantitative reconstruction of vegetation I: pollen from large sites REVEALS regional vegetation composition. *The Holocene* 17, 229–241. https://doi.org/10.1177/0959683607075837.

Telford, R.J., Birks, H.J.B., 2005. The secret assumption of transfer functions: problems with spatial autocorrelation in evaluating model performance. *Quaternary Science Reviews* 24, 2173–2179. https://doi.org/10.1016/j.quascirev.2005.05.001.

Telford, R.J., Birks, H.J.B., 2011. A novel method for assessing the statistical significance of quantitative reconstructions inferred from biotic assemblages. *Quaternary Science Reviews* 30, 1272–1278. https://doi.org/10.1016/j.quascirev.2011.03.002.

ter Braak, C.J.F., Juggins, S., 1993. Weighted averaging partial least squares regression (WA-PLS): an improved method for reconstructing environmental variables from species assemblages. *Hydrobiologia* 269/270, 485–502.

van der Voet, H., 1994. Comparing the predictive accuracy of models using a simple randomization test. *Chemometrics and Intelligent Laboratory Systems* 25, 313–323. https://doi.org/10.1016/0169-7439(94)85050-X.

Wake, D.B., Hadly, E.A., Ackerly, D.D., 2009. Biogeography, Changing Climates, and Niche Evolution. *Proceedings of the National Academy of Sciences of the United States of America* 106, 19631–19636.

Wallace, A.R., 1876. *The geographical distribution of animals.* Harper and Brothers, New York.

Wang, H., Prentice, I.C., Keenan, T.F., Davis, T.W., Wright, I.J., Cornwell, W.K., Evans, B.J., Peng, C., 2017. Towards a universal model for carbon dioxide uptake by plants. *Nature Plants* 3, 734. https://doi.org/10.1038/s41477-017-0006-8.

Wang, H., Prentice, I.C., Ni, J., 2013. Data-based modelling and environmental sensitivity of vegetation in China. *Biogeosciences* 10, 5817. http://dx.doi.org/10.5194/bg-10-5817-2013.

Wei, D., González-Sampériz, P., Gil-Romera, G., Harrison, S.P., Prentice, I.C., 2019a. Climate changes in interior semi-arid Spain from the last interglacial to the late Holocene. *Climate of the Past* Discussions 1–31. https://doi.org/10.5194/cp-2019-16.

Wei, D., Harrison, S., Prentice, I.C., 2019b. *The climate space of European pollen taxa.* University of Reading.

Wei, D., Prentice, I.C., Harrison, S., 2020. *The climatic space of European pollen taxa.* Ecology/Ecological Archives (in press).

Wickham, H., 2016. ggplot2: Create Elegant Data Visualisations Using the Grammar of Graphics. CRAN.

Williams, J.W., Shuman, B., 2008. Obtaining accurate and precise environmental reconstructions from the modern analog technique and North American surface pollen dataset. *Quaternary Science Reviews* 27, 669–687. https://doi.org/10.1016/j.quascirev.2008.01.004.

Wood, S, 2017. mgcv: Mixed GAM Computation Vehicle with Automatic Smoothness Estimation.

Wu, H., Guiot, J., Brewer, S., Guo, Z., 2007. Climatic changes in Eurasia and Africa at the last glacial maximum and mid-Holocene: reconstruction from pollen data using inverse vegetation modelling. *Climate Dynamics* 29, 211–229. https://doi.org/10.1007/s00382-007-0231-3.

Wu, H., Guiot, J., Peng, C., Guo, Z., 2009. New coupled model used inversely for reconstructing past terrestrial carbon storage from pollen data: validation of model using modern data. *Global Change Biology* 15, 82–96. https://doi.org/10.1111/j.1365-2486.2008.01712.x.

Xu, Q., Xiao, J., Li, Y., Tian, F., Nakagawa, T., 2010. Pollen-Based Quantitative Reconstruction of Holocene Climate Changes in the Daihai Lake Area, Inner Mongolia, China. *Journal of Climate* 23, 2856–2858,2861–2868.

3.11 Supplementary Information: The impact of methodological decisions on climate reconstructions using WA-PLS

Mark G. Turner, Dongyang Wei, I. Colin Prentice and Sandy P. Harrison

This supplementary contains the following figures and tables:

SI Figure 1. Locations of samples in the EMBSeCBIO (Eastern Mediterranean-Black Sea-Caspian corridor BIOmes) database (EMB), the European Modern Pollen Database v3.0 (EMPD) and the additional sites in the SMPDS. Stars indicate location of example fossil cores.
SI Figure 2. Reconstructions of mean temperature of the coldest month (MTCO, ° C) during the last glacial period (80,000 to 10,000 calendar years before 2000) using the pollen records from 8 example cores, using the EMBSeCBIO (Eastern Mediterranean-Black Sea-Caspian corridor BIOmes) database (EMB), the European Modern Pollen Database v3.0 (EMPD), and the full SMPDS data set as training data sets. The reconstruction spread (±2σ) is obtained by resampling the training set 1,000 times.
SI Figure 3. Reconstructions of growing degree days above 0 ° C (GDD0, °days) during the last glacial period (80,000 to 10,000 calendar years before 2000) using the pollen records from 8 example cores, EMBSeCBIO (Eastern Mediterranean-Black Sea-Caspian corridor BIOmes) database (EMB), the European Modern Pollen Database v3.0 (EMPD), and the full SMPDS data set as training data sets. The reconstruction spread (±2σ) is obtained by resampling the training set 1,000 times.
SI Figure 4. Reconstructions of the square root of Moisture Index (sqrt(MI) during the last glacial period (80,000 to 10,000 calendar years before 2000) using the pollen records from 8 example cores, using the EMBSECBIO (Eastern Mediterranean-Black Sea-Caspian corridor BIOmes) database (EMB), the European Modern Pollen Database v3.0 (EMPD)), and the full SMPDS data set as training data sets. The reconstruction spread (±2σ) is obtained by resampling the training set 1,000 times. The reconstruction shown here does not account for the direct impact of CO_2 on plant growth and thus will underestimate the actual value of (sqrt(MI)) during the glacial period (Wei et al, 2019a).
SI Figure 5. Comparison of reconstructions of mean temperature of the coldest month (MTCO, ° C) for downcore samples from Ioannina usingthe EMBSeCBIO (Eastern Mediterranean-Black Sea-Caspian corridor BIOmes) database (EMB) and the European Modern Pollen Database v3.0 (EMPD).
SI Figure 6. WA-PLS predictions for mean temperature of coldest month (MTCO, ° C), growing degree days above a baseline of 0 °C (GDD0, °C days) and the square root of Moisture Index (sqrt(MI)), compared with observations of modern climate for the 6 458 SMPDS sample sites. The righthand plots show the residuals against the predicted values. Red stars indicate the modern position on the climatic gradient of the 8 fossil sites used as examples.
SI Figure 7. Distribution of modern pollen samples in climate space, represented by growing degree days above 0ºC (GDD_0, °C days) and mean temperature of the coldest month (MTCO, °C), sampled by the full SMPDS (SMPDS) data set and after randomly reducing the data set by 70% (Red7).
SI Figure 8. Histogram comparing of the distribution of samples along the mean temperature of the coldest month (MTCO, °C) and growing degree days above 0 ºC (GDD_0, °C days) gradients using the full SMPDS set (Full SMPDS) and a set randomly removing 70% of the samples (Red7*).*
SI Figure 9. Change in mean standard deviation (reconstruction spread) of (a) mean temperature of the coldest month (MTCO, °C), (b) growing degree days above 0 ºC (GDD0, °C days), and (c) square root of Moisture index (sqrt(MI), unitless) as the percentage of samples randomly removed increases. 10 runs were made for each reduction, each comprising 100 bootstrapped reconstructions.
SI Figure 10. Impact of reducing the sampling density of the modern training data set on reconstructions of temperature of the coldest month (MTCO, °C) during the last glacial period (100,000 to 10,000 calendar years before 2000) using the pollen record from Lago Grande di Monticchio. The plots show the impact of removing 70% of the modern samples randomly while preserving the overall range of climate space on the MTCO reconstructions, compared to reconstructions made with the full SMPDS data set.
SI Figure 11. Impact of reducing the sampling density of the modern training data set on reconstructions of growing degree days above a baseline of 0° C (GDD_0, ° days) during the last glacial period (80,000 to 10,000 calendar years before 2000) using the pollen record from Lake Ioannina. The plots show the impact of removing 70% of the modern samples randomly while preserving the overall range of climate space on the GDD_0 reconstructions, compared to reconstructions made with the full SMPDS data set.

SI Figure 12. Impact of reducing the sampling density of the modern training data set on reconstructions of growing degree days above a baseline of 0° C (GDD_0, ° days) during the last glacial period (100,000 to 10,000 calendar years before 2000) using the pollen record from Lago Grande di Monticchio. The plots show the impact of removing 70% of the modern samples randomly while preserving the overall range of climate space on the GDD_0 reconstructions, compared to reconstructions made with the full SMPDS data set.

SI Figure 13. Abundance in climate space of Asteroideae and its main subtaxa at the sample level, complementing GAMs in Figure 5. "GDD <2000" includes all samples in that range, etc. Scale applies to all plots.

SI Figure 14. Reconstructed mean temperature of the coldest month (MTCO, °C) at 8 sites in Europe, comparing regression using the full SMPDS set and after removing *Pinus*.

SI Figure 15. Reconstructed mean temperature of the coldest month (MTCO, °C) using the full SMPDS set compared to regressions based on only taxa found in the fossil set at (a) Megali Limni and (b) Ioannina. See SI Table 3.

SI Figure 16. Squared chord distances of the 10 nearest analogues in the SMPDS to the fossil samples at Ioannina. The lowest dot, or end of line, represents the nearest analogue.

SI Table 1. In addition to data from the EMPD and the EMBSeCBIO databases, the SMPDS modern training data set includes sites from the following publications.

SI Table 2. Details of the 8 sites from the Abrupt climate Changes and Environmental Responses (ACER) database (Sanchez Goñi et al., 2017) used as examples in this study.

SI Table 3. WA-PLS model parameters for all the data sets used in this study for reconstructions of mean temperature of the coldest month (MTCO, 0° C), growing degree days above a baseline of 0° C (GDD0, °day) and the square root of Moisture Index (√MI, unitless) Cross-validated r^2, number of components with $p < 0.05$, root mean square error (RMSE), maximum bias, p tested by random t-test, and sample set size. Best components are identified by bold p value.

SI Table 4. WA-PLS model parameters for reconstructed mean temperature of the coldest month (MTCO, 0° C) comparing regression using the full SMPDS set with regression based only taxa found in the fossil set from (a) at Megali Limni (b) at Ioannina (see SI Figure 15). Cross-validated r^2, number of components with $p < 0.05$, root mean square error (RMSE), maximum bias, and taxon set size.

SI Table 5. Amalgamated taxa as in Table 3, for MTCO, GDD0 and square root (MI), showing number of occurrences, total abundance, abundance-weighted SD of coefficients (optima) of component taxa, SD of coefficient of amalgamated taxon, and coefficient of amalgamated taxon. SDs are obtained by bootstrapping the sample set 1000 times.

SI Table 6. Component taxon data for amalgamated taxa in SI Table 5, for MTCO, GDD and square root (MI), showing number of occurrences, total abundance, SD of coefficients (optima) of component taxa, and coefficient of component taxa. SDs are obtained by bootstrapping the sample set 1000 times.

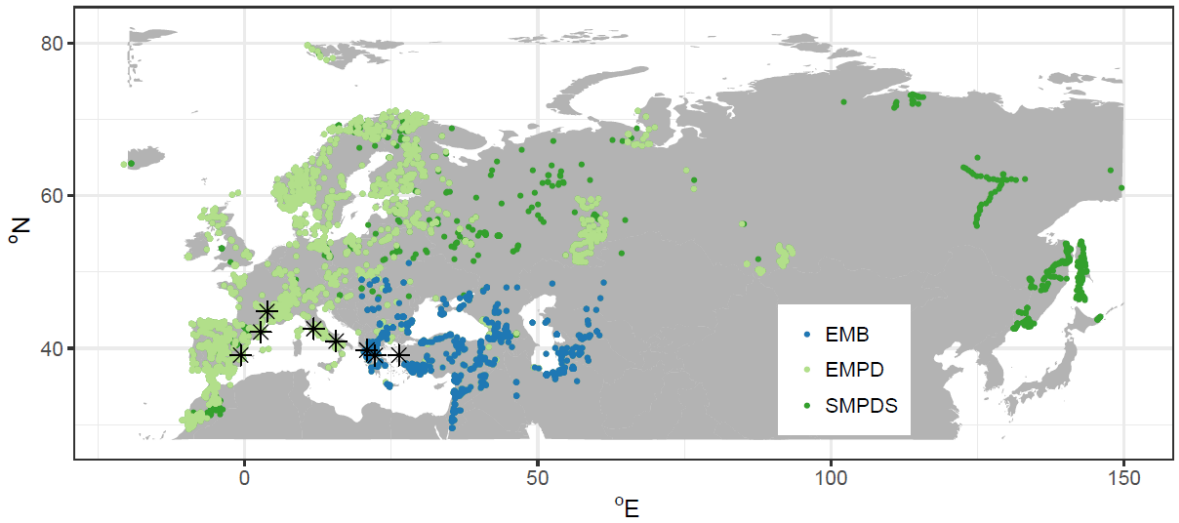

SI Figure 1. Locations of samples in the EMBSeCBIO (Eastern Mediterranean-Black Sea-Caspian corridor BIOmes) database (EMB), the European Modern Pollen Database v3.0 (EMPD) and the additional sites in the SMPDS. Stars indicate location of example fossil cores.

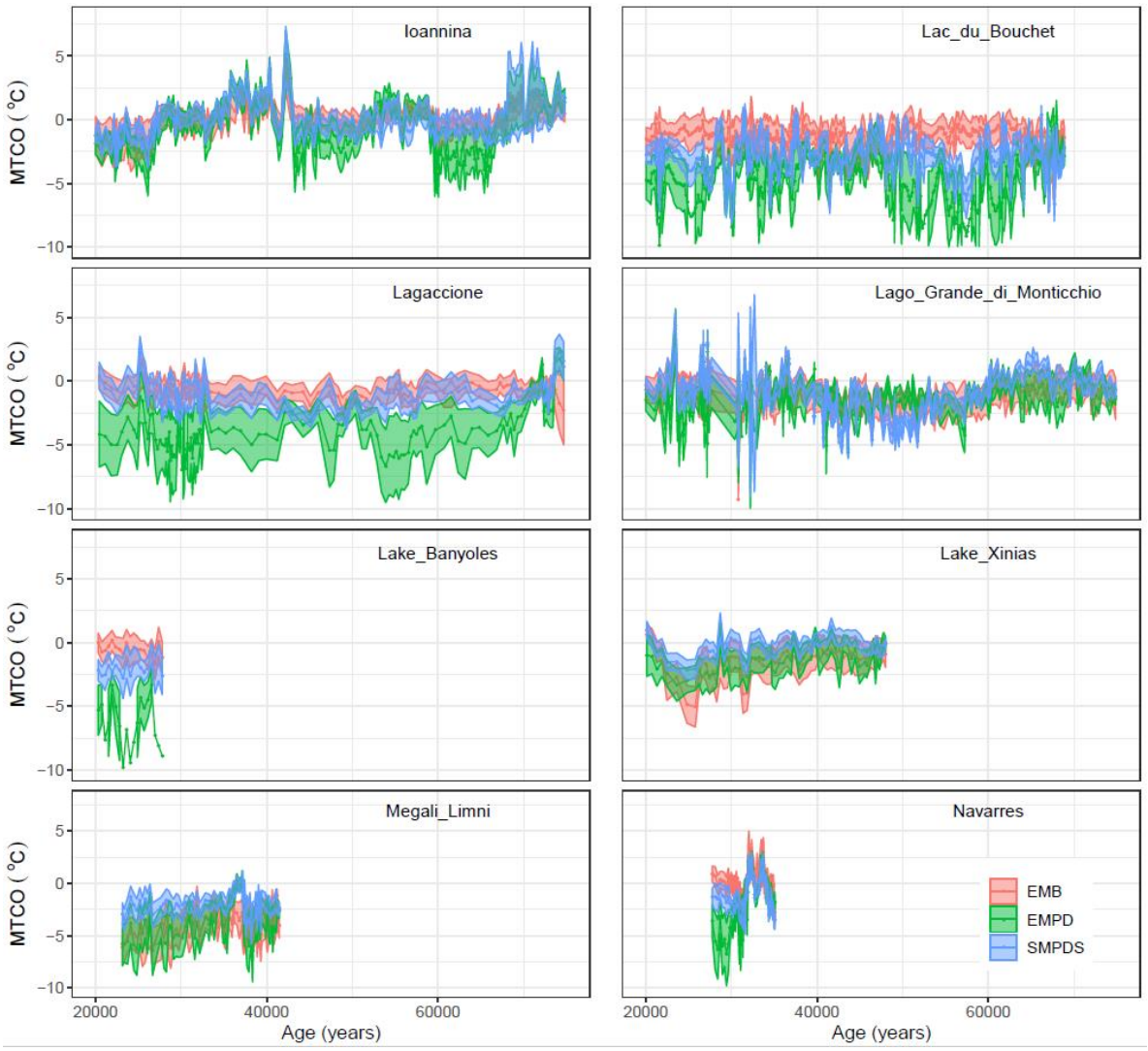

SI Figure 2. Reconstructions of mean temperature of the coldest month (MTCO, ° C) during the last glacial period (80,000 to 10,000 calendar years before 2000) using the pollen records from eight example cores, using the EMBSeCBIO (Eastern Mediterranean-Black Sea-Caspian corridor BIOmes) database (EMB), the European Modern Pollen Database v3.0 (EMPD), and the full SMPDS data set as training data sets. The reconstruction spread (±2σ) is obtained by resampling the training set 1,000 times.

SI Figure 3. Reconstructions of growing degree days above 0 ° C (GDD0, °days) during the last glacial period (80,000 to 10,000 calendar years before 2000) using the pollen records from eight example cores, EMBSeCBIO (Eastern Mediterranean-Black Sea-Caspian corridor BIOmes) database (EMB), the European Modern Pollen Database v3.0 (EMPD), and the full SMPDS data set as training data sets. The reconstruction spread (±2σ) is obtained by resampling the training set 1,000 times.

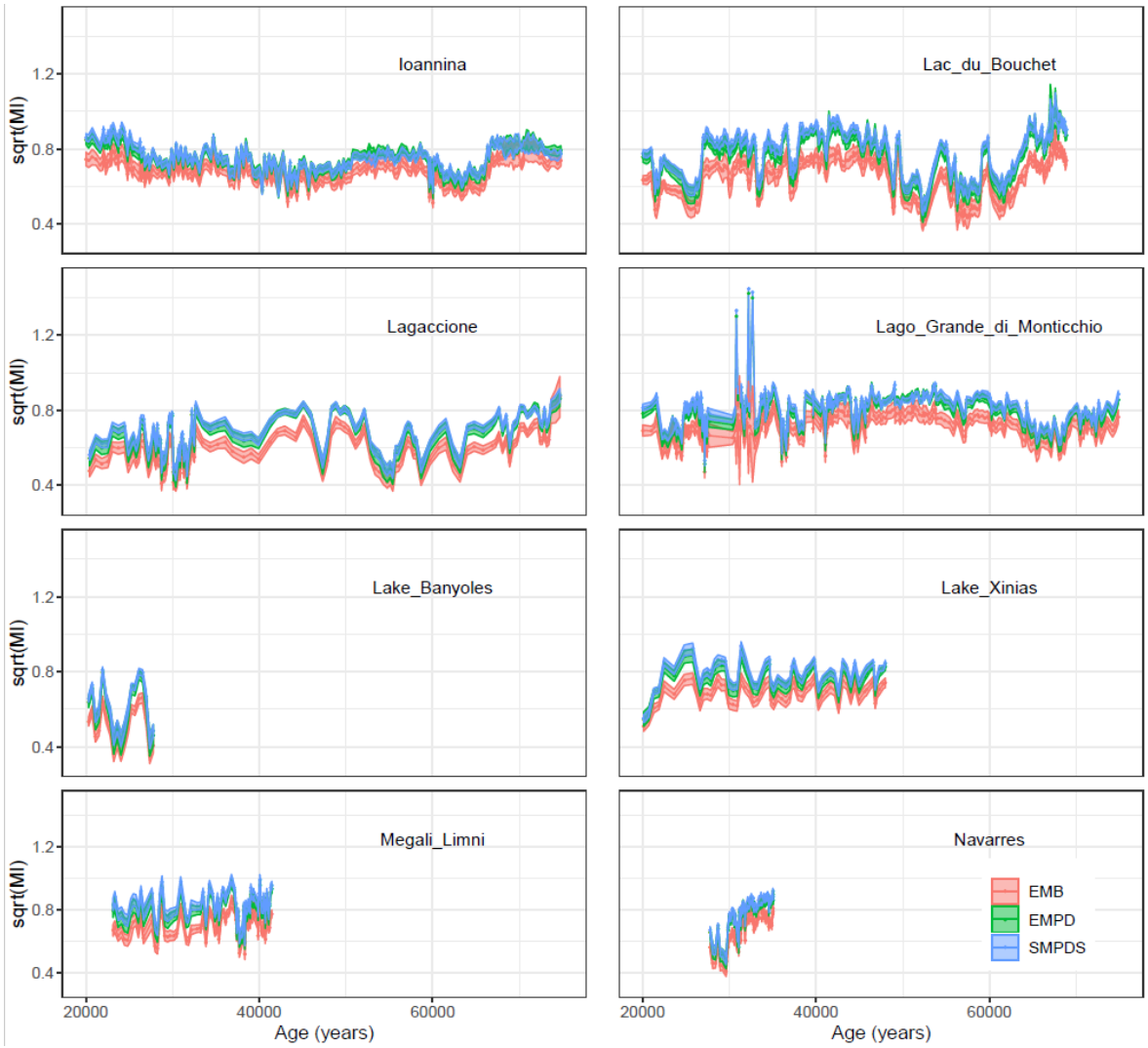

SI Figure 4. Reconstructions of the square root of Moisture Index (sqrt(MI)) during the last glacial period (80,000 to 10,000 calendar years before 2000) using the pollen records from eight example cores, using the EMBSECBIO (Eastern Mediterranean-Black Sea-Caspian corridor BIOmes) database (EMB), the European Modern Pollen Database v3.0 (EMPD), and the full SMPDS data set as training data sets. The reconstruction spread (±2σ) is obtained by resampling the training set 1,000 times. The reconstruction shown here does not account for the direct impact of CO_2 on plant growth and thus will underestimate the actual value of (sqrt(MI)) during the glacial period (Wei et al., 2019a).

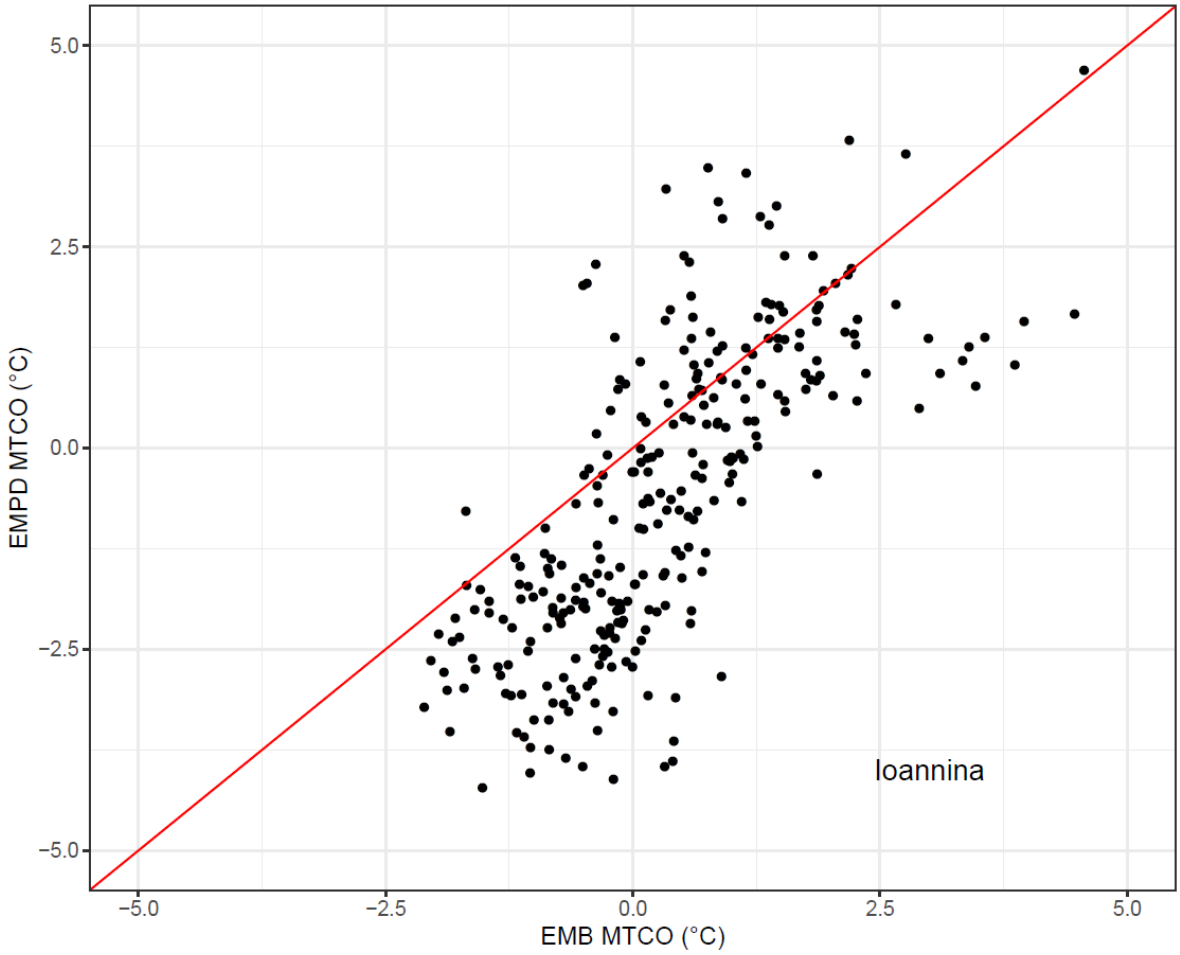

SI Figure 5. Comparison of reconstructions of mean temperature of the coldest month (MTCO, ° C) for downcore samples from Ioannina using the EMBSeCBIO (Eastern Mediterranean-Black Sea-Caspian corridor BIOmes) database (EMB) and the European Modern Pollen Database v3.0 (EMPD).

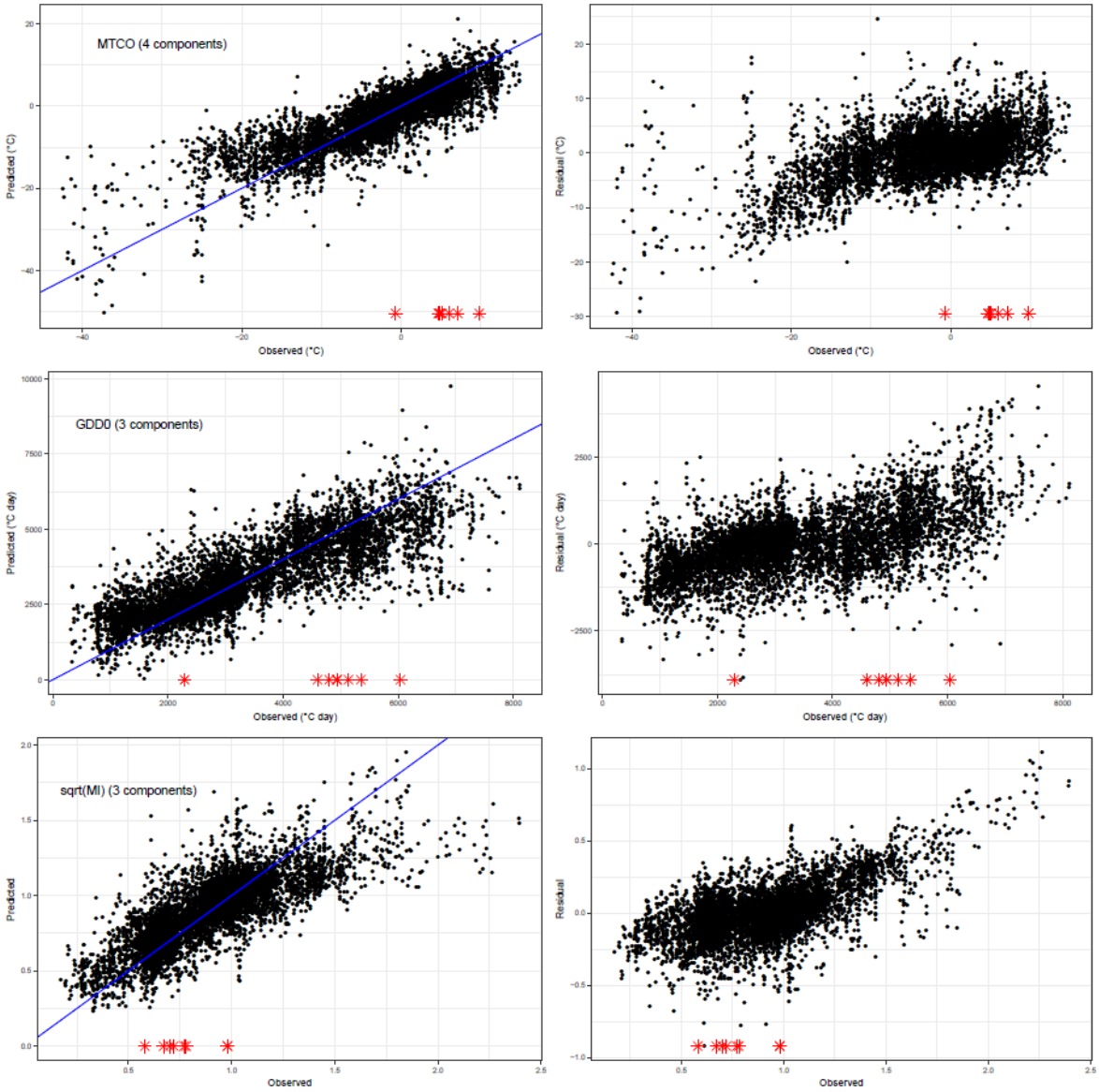

SI Figure 6. WA-PLS reconstructions for mean temperature of coldest month (MTCO, ° C), growing degree days above a baseline of 0 °C (GDD0, °C days) and the square root of Moisture Index (sqrt(MI)), compared with observations of modern climate for the 6458 SMPDS sample sites. The right-hand plots show the residuals against the predicted values. Red stars indicate the modern position on the climatic gradient of the eight fossil sites used as examples.

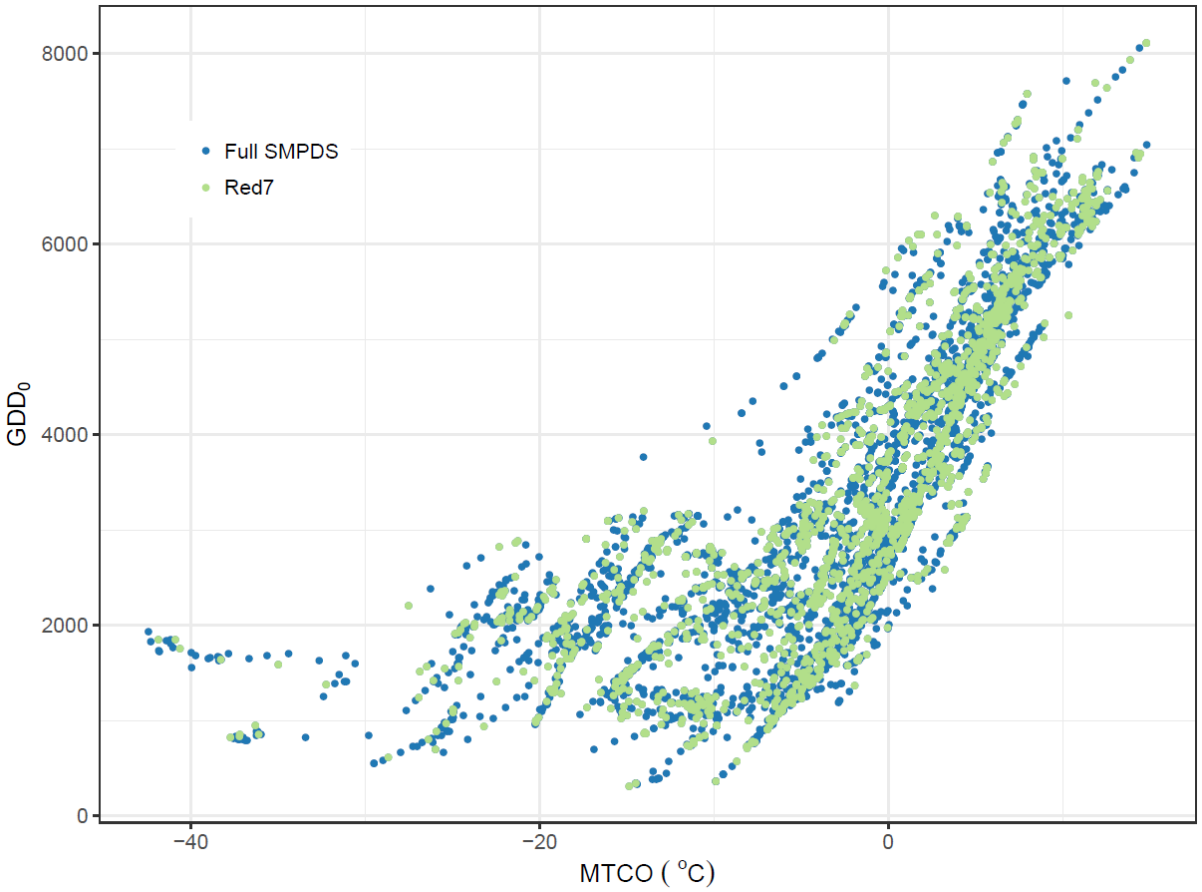

SI Figure 7. Distribution of modern pollen samples in climate space, represented by growing degree days above 0°C (GDD_0, °C days) and mean temperature of the coldest month (MTCO, °C), sampled by the full SMPDS (SMPDS) data set and after randomly reducing the data set by 70% (Red7).

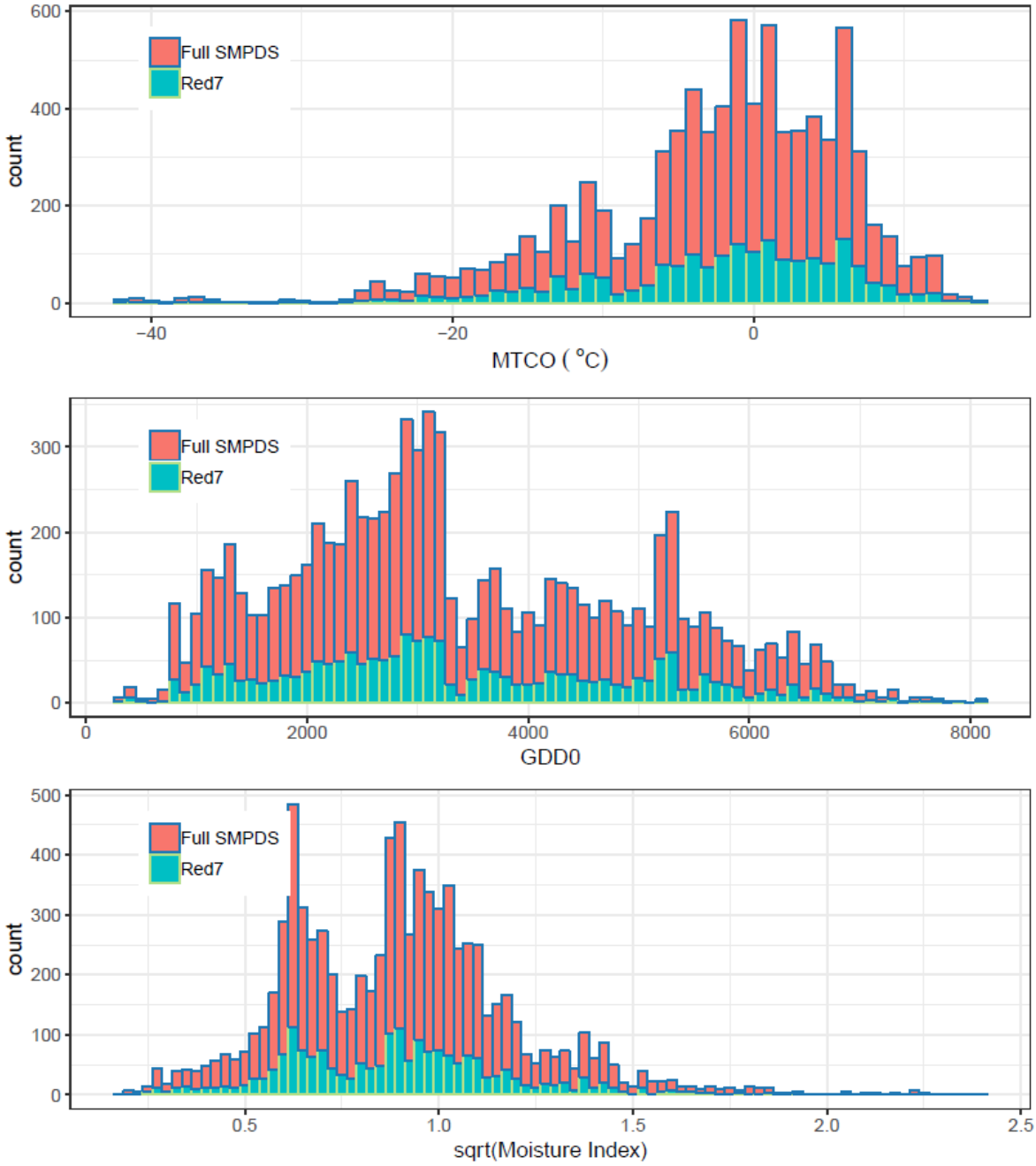

SI

Figure 8. Histograms comparing the distribution of samples along the mean temperature of the coldest month (MTCO, °C), growing degree days above 0°C (GDD_0, °C days), and square root of Moisture Index (sqrt(Moisture Index) gradients using the full SMPDS set (Full SMPDS) and a set randomly removing 70% of the samples (Red7*)*.

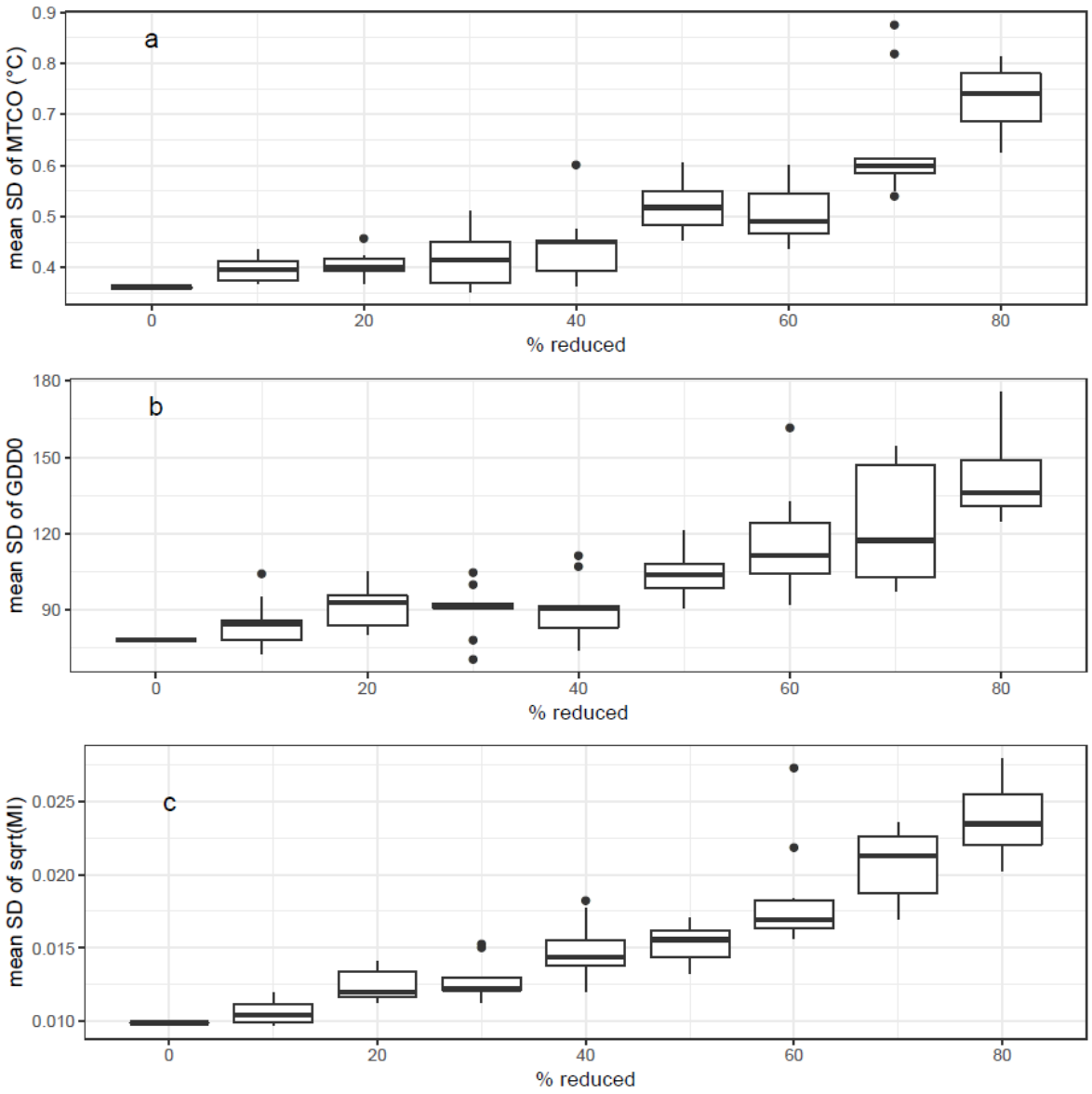

SI Figure 9. Change in mean standard deviation (reconstruction spread) of (a) mean temperature of the coldest month (MTCO, °C), (b) growing degree days above 0 ºC (GDD0, ºC days), and (c) square root of Moisture index (sqrt(MI), unitless) as the percentage of samples randomly removed increases. 10 runs were made for each reduction, each comprising 100 bootstrapped reconstructions.

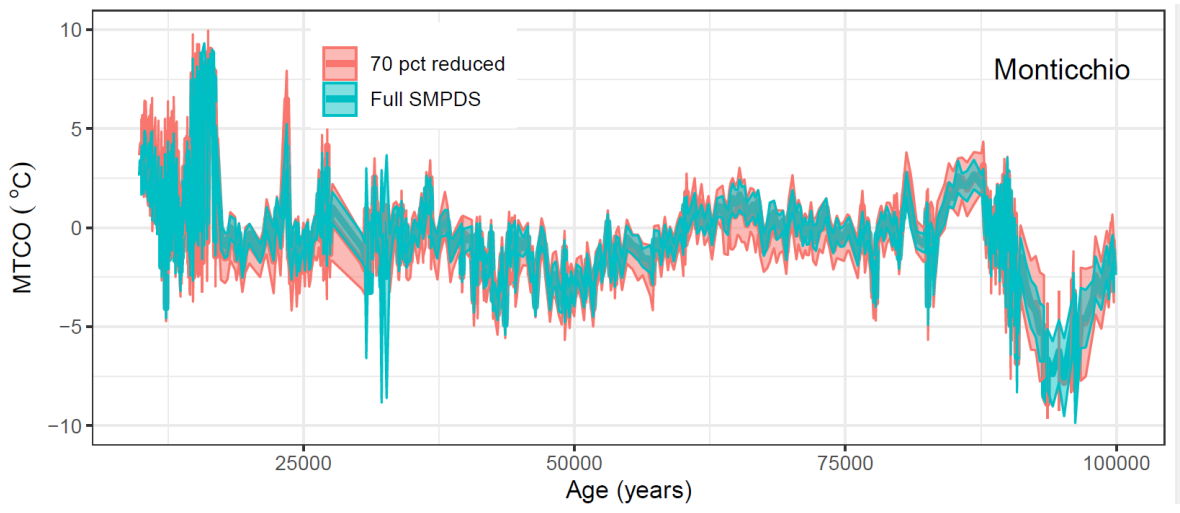

SI Figure 10. Impact of reducing the sampling density of the modern training data set on reconstructions of temperature of the coldest month (MTCO, °C) during the last glacial period (100,000 to 10,000 calendar years before 2000) using the pollen record from Lago Grande di Monticchio. The plots show the impact of removing 70% of the modern samples randomly while preserving the overall range of climate space on the MTCO reconstructions, compared to reconstructions made with the full SMPDS data set.

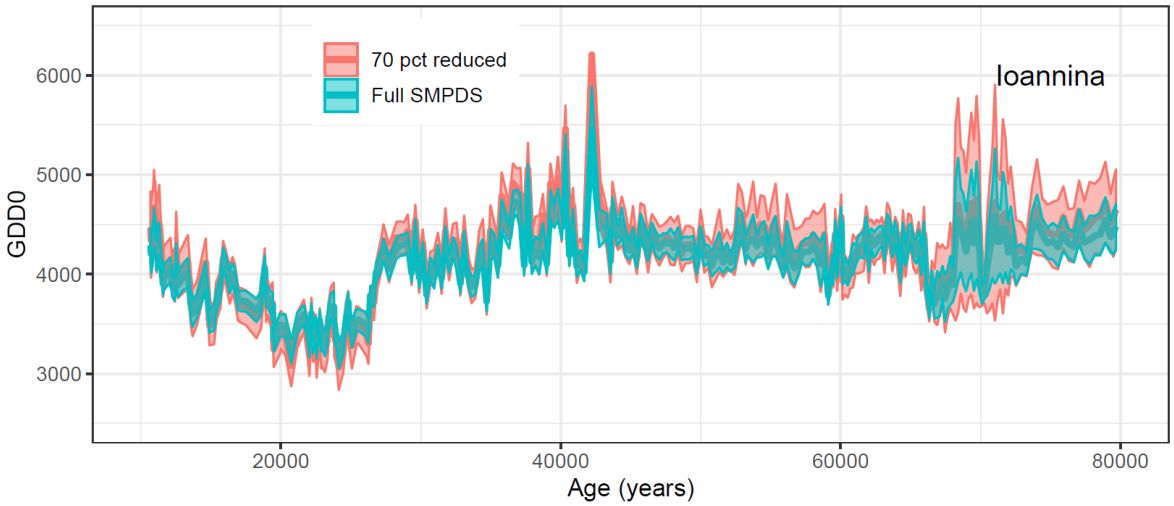

SI Figure 11. Impact of reducing the sampling density of the modern training data set on reconstructions of growing degree days above a baseline of 0° C (GDD_0, ° days) during the last glacial period (80,000 to 10,000 calendar years before 2000) using the pollen record from Lake Ioannina. The plots show the impact of removing 70% of the modern samples randomly while preserving the overall range of climate space on the GDD_0 reconstructions, compared to reconstructions made with the full SMPDS data set.

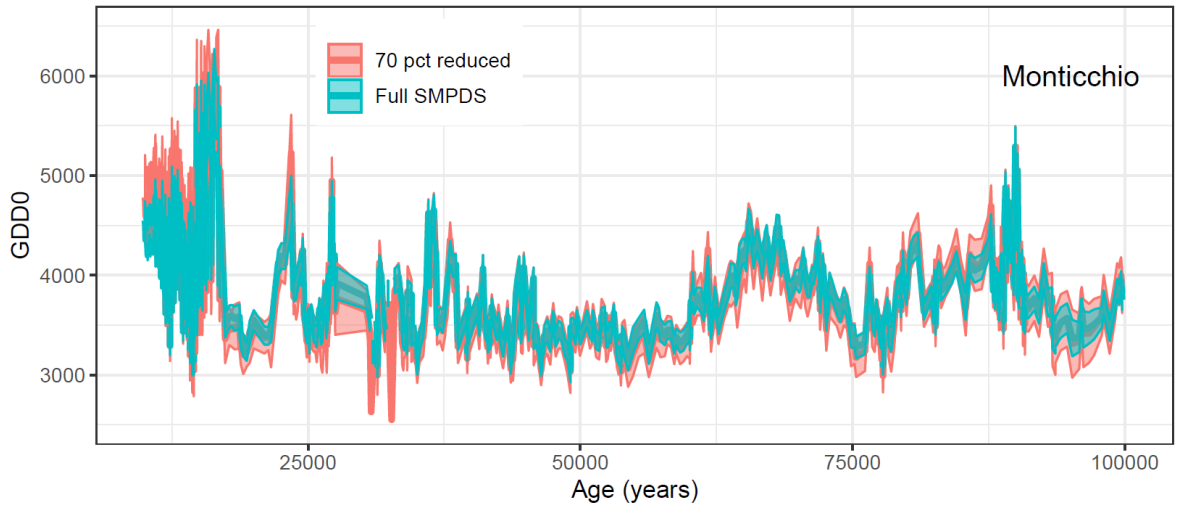

SI Figure 12. Impact of reducing the sampling density of the modern training data set on reconstructions of growing degree days above a baseline of 0° C (GDD_0, ° days) during the last glacial period (100,000 to 10,000 calendar years before 2000) using the pollen record from Lago Grande di Monticchio. The plots show the impact of removing 70% of the modern samples randomly while preserving the overall range of climate space on the GDD_0 reconstructions, compared to reconstructions made with the full SMPDS data set.

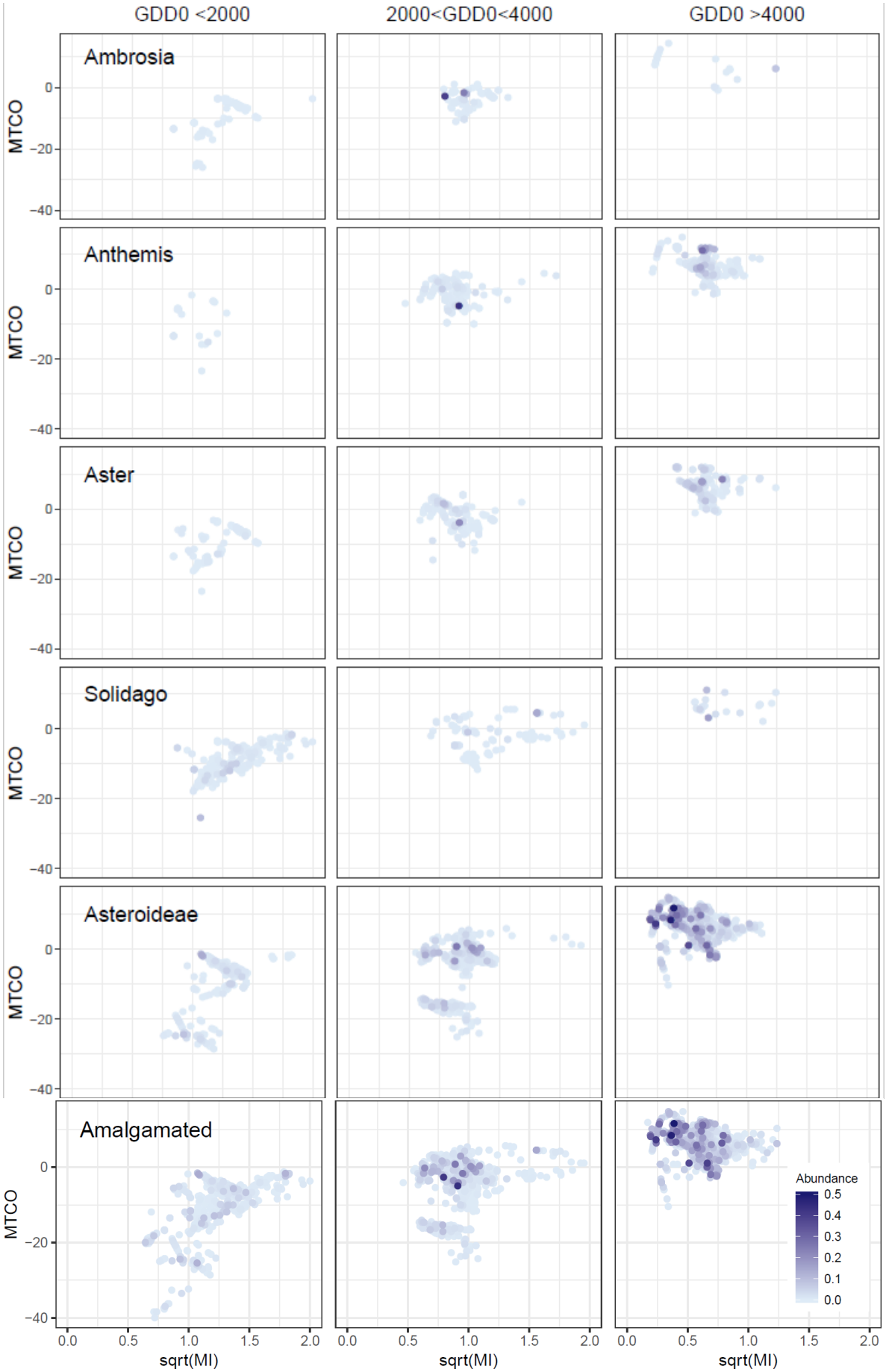
GDD0 <2000
2000<GDD0<4000
GDD0 >4000
Ambrosia
Anthemis
Aster
Solidago
Asteroideae
Amalgamated
MTCO
0
−20
−40
0.0
0.5
1.0
1.5
2.0
sqrt(MI)
Abundance
0.5
0.4
0.3
0.2
0.1
0.0

SI Figure 13. Abundance in climate space of Asteroideae and its main subtaxa at the sample level, complementing GAMs in Figure 6. "GDD <2000" includes all samples in that range, etc. Scale applies to all plots.

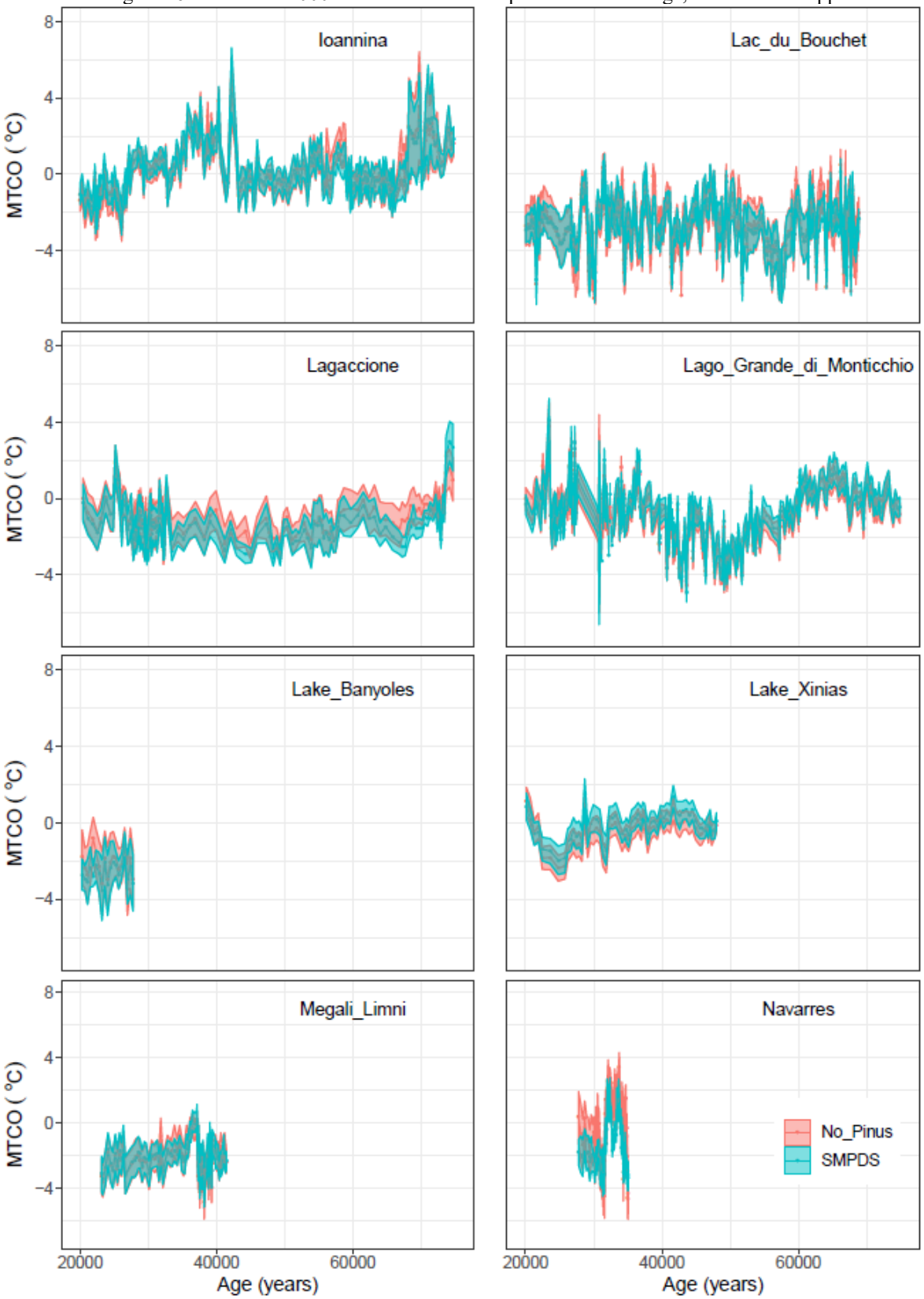

SI Figure 14. Reconstructed mean temperature of the coldest month (MTCO, °C) at eight sites in Europe, comparing regression using the full SMPDS set and after removing *Pinus*.

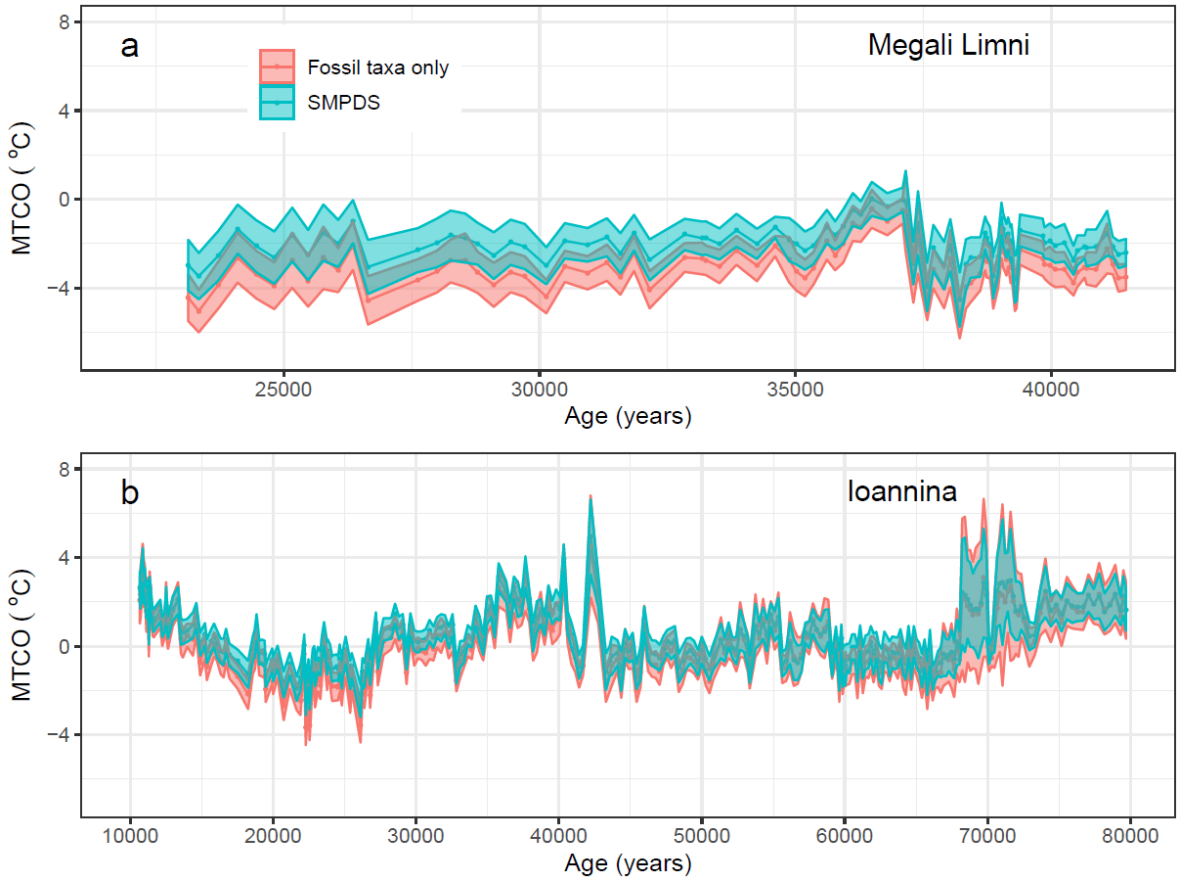

SI Figure 15. Reconstructed mean temperature of the coldest month (MTCO, °C) using the full SMPDS set compared to regressions based on only taxa found in the fossil set at (a) Megali Limni and (b) Ioannina. See SI Table 3.

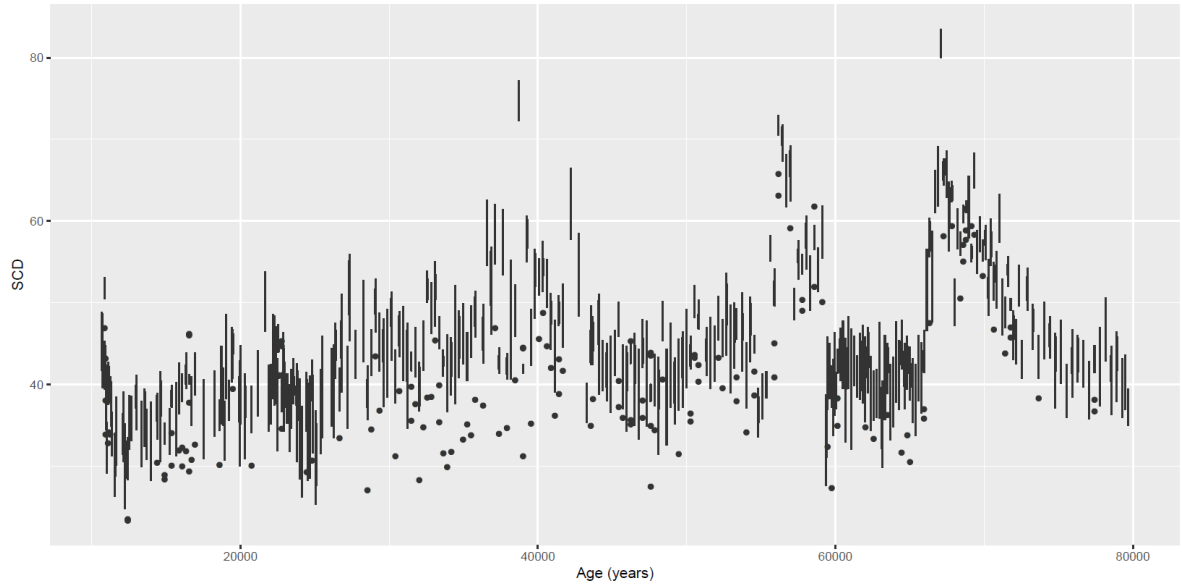

SI Figure 16. Squared chord distances of the 10 nearest analogues in the SMPDS to the fossil samples at Ioannina. The lowest dot, or end of line, represents the nearest analogue.

SI Table 1. In addition to data from the EMPD and the EMBSeCBIO databases, the SMPDS modern training data set includes sites from the following publications:

Bell, B.A. and Fletcher, W. J.: Modern surface pollen assemblages from the Middle and High Atlas, Morocco: Insights into pollen representation and transport, Grana, 55, 286-301, https://doi.org/10.1080/00173134.2015.1108996, 2016.
de Klerk, P., Haberl, A., Kaffke, A., Krebs, M., Matchutadze, I., Minke, M., Schulz, J., and Joosten, H.: Vegetation history and environmental development since ca 6000 cal yr BP in and around Ispani 2 (Kolkheti lowlands, Georgia), Quaternary Sci. Rev., 28, 890-910, https://doi.org/10.1016/j.quascirev.2008.12.005, 2009.
Grüger, E. and Jerz, H.: Untersuchung einer Doline auf dem Zugspitzplatt: Ein palynologischer Beitrag zur holozänen Gletschergeschichte im Wettersteingebirge, E&G Quaternary Sci. J., 59, 66-75, https://doi.org/10.3285/eg.59.1-2.06, 2010.
Matthias, I., Semmler, M. S. S., and Giesecke, T.: Pollen diversity captures landscape structure and diversity, J. Ecol., 103, 880-890, https://doi.org/10.1111/1365-2745.12404, 2015.
Müller, S., Tarasov, P., Andreev, A. A., Tutken, T., Gartz, S., and Diekmann, B.: Late Quaternary vegetation and environments in the Verkhoyansk Mountains region (NE Asia) reconstructed from a 50-kyr fossil pollen record from Lake Billyakh, Quat. Sci. Rev., 29, 2071-2086, https://doi.org/10.1016/j.quascirev.2010.04.024, 2010.
Niemeyer, B., Klemm, J., Pestryakova, L. A., and Herzschuh, U.: Relative pollen productivity estimates for common taxa of the northern Siberian Arctic, Rev. Palaeobot. Palyno., 221, 71-82, https://doi.org/10.1016/j.revpalbo.2015.06.008, 2015.
Novenko, E., Mazei, N., and Kusilman, M.: Tree pollen representation in surface pollen assemblages from different vegetation zones of European Russia, Ecological Questions, 26, 61–65, http://doi.org/10.12775/EQ.2017.018, 2017.
Saadi, F. and Bernard, J.: Rapport entre la pluie pollinique actuelle, le climat et la vegetation dans les steppes à Artemisia et les milieu limitrophes au Maroc, Palaeoecol. Africa, 22, 67-86, 1991.
Tarasov, P. E., Nakagawa, T., Demske, D., Österle, H., Igarashi, Y., Kitagawa, J., Mokhova, L., Bazarova, V., Okuda, M., Gotanda, K., Miyoshi, N., Fujiki, T., Takemura, K., Yonenobu, H., and Fleck, A.: Progress in the reconstruction of Quaternary climate dynamics in the Northwest Pacific: A new modern analogue reference dataset and its application to the 430-kyr pollen record from Lake Biwa, Earth-sci. Rev, 108, 64-79, https://doi.org/10.1016/j.earscirev.2011.06.002, 2011.
Werner, K., Tarasov, P. E., Andreev, A. A., Müller, S., Kienast, F., Zech, M., Zech, W., and Diekmann, B.: A 12.5-kyr history of vegetation dynamics and mire development with evidence of Younger Dryas larch presence in the Verkhoyansk Mountains, East Siberia, Russia, Boreas, 39, 56-68, https://doi.org/10.1111/j.1502-3885.2009.00116.x, 2010.

SI Table 2. Details of the 8 sites from the Abrupt climate Changes and Environmental Responses (ACER) database (Sanchez Goñi et al., 2017) used as examples in this study.

Site	Lat	Long	References
Lagaccione	42.57	11.8	Magri, D (1999): Late Quaternary vegetation history at Lagaccione near Lago di Bolsena (central Italy). Review of Palaeobotany and Palynology, 106(3-4), 171-208, doi:10.1016/S0034-6667(99)00006-8
			Magri, D (2008): Two long micro-charcoal records from central Italy. In: Charcoals from the Past: Cultural and Palaeoenvironmental Implications Proceedings of the Third International Meeting of Anthracology, Cavallino - Lecce (Italy), June 28th - July 1st 2004 BAR International Series 1807
Lake_Banyoles	42.13	2.75	Pérez-Obiol, R P; Julia, R (1994): Climatic change on the Iberian Peninsula recorded in a 30,000-year pollen record from Lake Banyoles. Quaternary Research, 41(1), 91-98, doi:10.1006/qres.1994.1010

Site	Lat	Long	References
Lake_Xinias	39.05	22.27	Bottema, S (1979): Pollen analytical investigations in Thessaly (Greece). Palaeohistoria, 21, 19-40, http://rjh.ub.rug.nl/Palaeohistoria/article/view/24996/22455
Megali_Limni	39.1025	26.3208	Margari, V; Gibbard, P L; Bryant, C L; Tzedakis, PC (2009): Character of vegetational and environmental changes in southern Europe during the last glacial period; evidence from Lesvos Island, Greece. Quaternary Science Reviews, 28(13-14), 1317-1339, doi:10.1016/j.quascirev.2009.01.008
			Margari, V; Pyle, D M; Bryant, C; Gibbard, P L (2007): Mediterranean tephra stratigraphy revisited: Results from a long terrestrial sequence on Lesvos Island, Greece. Journal of Volcanology and Geothermal Research, 163(1-4), 34-54, doi:10.1016/j.jvolgeores.2007.02.002
Lago_Grande_di_Monticchio	40.94	15.61	Allen, J R M; Huntley, B (2000): Weichselian palynological records from southern Europe: correlation and chronology. Quaternary International, 73-74, 111-125, doi:10.1016/S1040-6182(00)00068-9
			Allen, J R M; Brandt, U; Brauer, A; Huntley, B; Keller, J; Kraml, M; Mackensen, A; Mingram, J; Negendank, J F W; Nowaczyk, N R; Watts, W A; Wulf, S; Zolitschka, B; Hubberten, H-W; Oberhänsli, H (1999): Rapid environmental changes in southern Europe during the last glacial period. Nature, 400(6746), 740-743, doi:10.1038/23432
			Allen, J R M; Watts, W A; Huntley, Brian (2000): Weichselian palynostratigraphy, palaeovegetation and palaeoenvironment; the record from Lago Grande di Monticchio, southern Italy. Quaternary International, 73-74, 91-110, doi:10.1016/S1040-6182(00)00067-7
			Brauer, A; Allen, J R M; Mingram, J; Dulski, P; Wulf, S; Huntley, B (2007): Evidence for last interglacial chronology and environmental change from Southern Europe. Proceedings of the National Academy of Sciences, 104(2), 450-455, doi:10.1073/pnas.0603321104
			Huntley, B; Watts, W A; Allen, J R M; Zolitschka, B (1999): Palaeoclimate, chronology and vegetation history of the Weichselian Lateglacial: comparative analysis of data from three cores at Lago Grande di Monticchio, southern Italy. Quaternary Science Reviews, 18(7), 945-960, doi:10.1016/S0277-3791(99)00007-4
Navarres	39.1	-0.68	Carrión, J S; van Geel, B (1999): Fine-resolution Upper Weichselian and Holocene palynological record from Navarrés (Valencia, Spain) and a discussion about factors of Mediterranean forest succession. Review of Palaeobotany and Palynology, 106, 209-236, doi:10.1016/S0034-6667(99)00009-3
Lac_du_Bouchet	44.83	3.82	Reille, M; de Beaulieu, J-L (1990): Pollen analysis of a long upper Pleistocene continental sequence in a Velay maar (Massif Central, France). Palaeogeography, Palaeoclimatology, Palaeoecology, 80(1), 35-48, doi:10.1016/0031-0182(90)90032-3

Site	Lat	Long	References
Ioannina	39.75	20.85	Tzedakis, P C; Frogley, M R; Lawson, I T; Preece, R C; Cacho, I; de Abreu, L (2004): Ecological thresholds and patterns of millennial-scale climate variability: The response of vegetation in Greece during the last glacial period. Geology, 32(2), 109, doi:10.1130/G20118.1
			Tzedakis, P C; Lawson, I T; Frogley, M R; Hewitt, G M; Preece, R C (2002): Buffered tree population changes in a Quaternary refugium: evolutionary emplications. Science, 297(5589), 2044-2047, doi:10.1126/science.1073083

SI Table 3. WA-PLS model parameters for all the data sets used in this study for reconstructions of mean temperature of the coldest month (MTCO, 0° C), growing degree days above a baseline of 0° C (GDD0, °day) and the square root of Moisture Index (√MI, unitless). Cross-validated r^2, number of components, root mean square error (RMSE), maximum bias, *p* tested by random *t*-test, and sample set size. Best components are identified by bold *p* value.

Variable	**Data Set**	r^2	**No of components**	**RMSE**	**Max. bias**	***p***	**No of samples**
MTCO	EMB	0.377	1	4.08	20.6	0.001	1 088
	EMB	0.417	2	3.97	19.6	**0.002**	
	EMB	0.418	3	4.02	18.6	0.534	
	EMPD	0.690	1	4.30	8.4	0.001	4 675
	EMPD	0.731	2	4.01	5.7	0.001	
	EMPD	0.743	3	3.91	6.1	**0.001**	
	EMPD	0.743	4	3.92	5.9	0.500	
	70% reduced	0.618	1	5.27	17.8	0.001	1930
	70% reduced	0.655	2	5.06	16.3	**0.001**	
	70% reduced	0.661	3	5.09	17.2	0.133	
	Megali Limni fossil assemblage (67 taxa)	0.471	1	6.31	33.2	0.001	6 458
		0.528	2	5.96	32.7	0.001	
		0.539	3	5.89	32.3	0.001	
		0.541	4	5.88	32.4	**0.030**	
	Ioannina fossil assemblage (78 taxa)	0.477	1	6.28	33.4	0.001	
		0.539	2	5.89	32.9	0.001	
		0.552	3	5.80	32.2	**0.001**	
	SMPDS	0.624	1	5.31	14.2	0.001	6 458
	SMPDS	0.671	2	4.97	8.8	0.001	
	SMPDS	0.687	3	4.85	8.5	0.001	
	SMPDS	0.691	4	4.82	10.3	**0.019**	
GDD0	EMB	0.475	1	992	1843	0.001	1 088
	EMB	0.508	2	960	1727	**0.001**	
	EMB	0.502	3	969	1690	0.889	
	EMPD	0.616	1	968	2567	0.001	4675
	EMPD	0.654	2	917	1960	0.001	
	EMPD	0.667	3	901	1898	**0.001**	
	70% reduced	0.603	1	974	2110	0.001	1878
	70% reduced	0.644	2	931	1948	**0.001**	
	70% reduced	0.649	3	941	1793	0.334	
	SMPDS	0.600	1	987	2419	0.001	6458
	SMPDS	0.646	2	929	2155	0.001	
	SMPDS	0.660	3	910	2039	**0.001**	
√MI	EMB	0.574	1	0.130	0.449	0.001	1 088
	EMB	0.592	2	0.128	0.439	**0.010**	
	EMB	0.587	3	0.129	0.423	0.700	
	EMPD	0.546	1	0.203	0.978	0.001	4 675
	EMPD	0.595	2	0.191	0.851	0.001	
	EMPD	0.602	3	0.190	0.838	**0.001**	
	70% reduced	0.542	1	0.194	1.069	0.001	1933
	70% reduced	0.591	2	0.185	0.972	**0.001**	
	70% reduced	0.595	3	0.187	0.930	0.362	
	SMPDS	0.532	1	0.198	1.057	0.001	6 458
	SMPDS	0.589	2	0.187	0.940	0.001	
	SMPDS	0.598	3	0.185	0.910	**0.001**	

	SMPDS	0.600	4	0.185	0.911	0.130	

SI Table 4. WA-PLS model parameters for reconstructed mean temperature of the coldest month (MTCO, 0° C) comparing regression using the full SMPDS set with regression based only taxa found in the fossil set from (a) at Megali Limni (b) at Ioannina (see SI Figure 15). Cross-validated r^2, number of components with $p < 0.05$, root mean square error (RMSE), maximum bias, and taxon set size.

Set	*r*2	No of components	RMSE	Maximum bias	*p*	No of taxa
SMPDS set	0.691	4	4.82	10.3	0.019	195
Megali Limni fossil only	0.541	4	5.88	32.4	0.030	67
Ioannina fossil only	0.552	3	5.80	32.2	0.001	78

SI Table 5. Amalgamated taxa as in Table 3, for MTCO, GDD0 and square root (MI), showing number of occurrences, total abundance, abundance-weighted SD of coefficients (optima) of component taxa, SD of coefficient of amalgamated taxon, and coefficient of amalgamated taxon. SDs are obtained by bootstrapping the sample set 1000 times.

Amalgamated taxon	Occurrences	Total abundance	Abundance-weighted SD of subtaxon coefficients MTCO	SD of amalgamated taxon coefficients MTCO	Coefficient of amalgamated taxon MTCO	Abundance-weighted SD of subtaxon coefficients GDD	SD of amalgamated taxon coefficients GDD	Coefficient of amalgamated taxon GDD	Abundance-weighted SD of subtaxon coefficients sqrt(MI)	SD of amalgamated taxon coefficients sqrt(MI)	Coefficient of amalgamated taxon sqrt(MI)
Apiaceae	5485	9617	2.4	1.7	-8.4	498	231	1667	0.07	0.04	0.90
Asteroideae	6171	8053	2.5	1.3	12.6	601	305	7135	0.09	0.05	0.40
Carduoideae	2363	1620	3.7	2.1	1.1	1033	659	3598	0.16	0.11	0.69
Cichorioideae	3260	8877	1.0	1.0	6.6	207	220	5906	0.04	0.04	0.48
Cistus	956	1756	2.7	1.7	10.9	674	418	6797	0.07	0.06	0.42
Ephedra	813	913	5.0	3.5	3.2	1012	652	6562	0.16	0.16	0.05
Plantaginaceae	5565	8012	2.2	1.2	13.0	592	366	5901	0.08	0.05	0.65
Quercus deciduous	4920	34212	0.8	0.5	3.4	213	109	4728	0.04	0.02	0.75
Quercus evergreen	2378	24196	0.7	0.4	6.3	206	119	5435	0.03	0.02	0.55

SI Table 6. Component taxon data for amalgamated taxa in SI Table 4, for MTCO, GDD and square root (MI), showing number of occurrences, total abundance, SD of coefficients (optima) of component taxa, and coefficient of component taxa. SDs are obtained by bootstrapping the sample set 1000 times.

Amalgamated taxon	Component taxon	Occurrences	Total abundance	SD MTCO	Coefficient MTCO	SD GDD	Coefficient GDD	SD sqrt(MI)	Coefficient sqrt(MI)
Apiaceae		5485	9617						
	Aegopodium	2	2	5.5	-8.8	1350	6034	0.16	-0.31
	Aegopodium.podagraria	2	0	8.4	-27.5	532	-4630	0.96	1.37
	Ammi.type	1	0	1.7	-33.4	358	644	0.04	1.00
	Angelica	4	6	12.2	4.7	4170	8807	0.85	-0.60
	Angelica.archangelica	1	0	6.6	69.4	445	-1014	0.21	3.65
	Angelica.type	84	17	4.0	6.4	473	538	0.22	2.44
	Anisosciadium.type	6	1	14.1	-3.4	3307	7855	0.34	-0.07
	Anthriscus	2	0	6.6	-52.6	420	-3992	0.20	1.30
	Anthriscus.sylvestris	24	22	11.3	-21.0	1121	1394	0.44	0.41
	Anthriscus.sylvestris.type	66	10	3.7	8.5	625	-769	0.12	1.93
	Anthriscus.type	6	1	9.9	-21.2	1477	163	0.55	0.23
	Apiaceae	3084	3618	1.3	0.9	336	3174	0.05	0.99
	Apium.Berula	13	2	3.6	15.8	875	7791	0.18	-0.63
	Apium.type	4	0	9.4	14.9	1095	4251	0.60	0.39
	Astrantia	3	1	4.7	7.4	1806	-1663	0.35	1.46
	Astrantia.type	34	3	13.4	-24.6	2212	-771	0.20	1.22
	Athamanta.cretensis	11	35	8.0	-24.9	4804	-4044	1.22	2.27
	Berula.erecta.type	1	0	1.3	22.2	201	7315	0.04	-0.24
	Bunium.type	45	29	4.2	11.9	1380	9439	0.14	-0.17
	Bupleurum	14	4	8.4	-3.6	3036	-2433	0.47	2.02
	Bupleurum.type	150	159	5.9	-50.4	675	-673	0.23	0.89
	Carum.carvi	10	2	5.4	14.8	839	-563	0.16	1.97
	Chaerophyllum	5	2	12.1	-15.3	4271	-5583	0.60	2.44
	Chaerophyllum.hirsutum.type	101	35	2.9	-8.2	626	-3610	0.13	2.45
	Chaerophyllum.type	10	7	23.6	-36.9	3675	557	0.11	0.75
	Conopodium	3	1	18.8	64.7	1518	8932	0.50	2.64
	Conopodium.majus	1	0	2.9	16.6	584	6549	0.32	-1.27
	Daucaceae	2	0	1.3	-9.7	287	1974	0.11	0.29
	Daucus.carota	38	3	6.2	-0.2	1633	-2029	0.30	2.32
	Daucus.carota.type	2	0	11.2	24.4	3948	6312	0.25	1.13
	Daucus.type	50	12	6.5	-5.3	789	4420	0.24	0.20
	Echinophora	5	3	5.9	6.6	1371	5850	0.14	1.02
	Echinophora.type	2	0	4.3	29.3	1279	11793	0.10	-0.91
	Eryngium	265	282	4.1	8.5	1246	5736	0.09	1.01
	Eryngium.ilicifolium	37	63	3.2	26.7	745	9613	0.12	-0.24
	Eryngium.type	138	152	8.6	22.1	1858	8491	0.20	0.22
	Falcaria.type	402	2790	2.7	-12.0	294	1284	0.06	0.93
	Ferula.type	12	2	9.3	12.8	2719	6711	0.23	0.24
	Heracleum	76	42	3.9	-2.3	1118	-806	0.24	1.79
	Heracleum.laciniatum.type	1	0	5.5	29.8	881	-804	0.35	5.64
	Heracleum.sphondylium	25	8	10.0	-68.8	1015	621	0.16	1.02
	Heracleum.type	13	2	18.5	-37.7	2793	-669	0.22	0.16
	Laserpitium.latifolium.type	4	0	9.6	8.4	1155	-565	0.30	1.77
	Laserpitium.prutenicum	2	1	7.3	-5.3	3745	-563	0.61	2.22
	Ligusticum.mutellina	62	16	2.1	-15.8	897	-5266	0.23	2.78
	Malabaila	13	3	4.3	-5.6	2140	2956	0.23	0.20
	Meum	9	6	5.6	0.2	868	-5242	0.15	2.19
	Meum.athamanticum	1	0	1.4	-6.4	257	-6191	0.06	3.03
	Neogaya.simplex.type	2	0	13.6	1.4	815	-831	0.92	2.67
	Oenanthe	2	0	4.5	-20.3	1122	4598	1.10	-1.04

Amalgamated taxon	Component taxon	Occurrences	Total abundance	SD MTCO	Coefficient MTCO	SD GDD	Coefficient GDD	SD sqrt(MI)	Coefficient sqrt(MI)
	Oenanthe.type	2	0	1.4	-3.9	860	2952	0.04	0.55
	Orlaya	5	1	4.4	-0.9	1137	3712	0.25	-0.19
	Orlaya.grandiflora	2	0	3.7	-8.7	552	-3666	0.11	2.53
	Pastinaca.type	4	1	15.2	-13.8	2252	4523	0.19	0.40
	Peucedanum	16	4	6.6	-9.1	1422	-3051	0.28	1.68
	Peucedanum.ostruthium	1	0	2.2	-24.8	440	-7019	0.09	3.35
	Peucedanum.type	128	65	7.7	0.8	2022	3274	0.32	1.15
	Pimpinella	5	0	12.4	-23.9	1657	578	0.36	0.57
	Pimpinella.major.type	34	3	6.0	-8.8	1542	-3474	0.31	2.49
	Pimpinella.type	274	2078	1.9	-6.8	571	943	0.05	1.10
	Pleurospermum.austriacum	3	0	9.2	-17.0	5555	4430	1.09	1.18
	Sanicula	13	5	13.7	-1.0	1490	-362	0.14	1.48
	Sanicula.europaea	2	0	2.2	-18.6	544	-5902	0.10	2.93
	Sanicula.type	38	52	2.5	3.2	748	4451	0.13	0.23
	Scandix	5	4	7.0	-11.3	1561	839	0.39	0.47
	Seseli.type	9	2	17.9	-29.6	3585	-7763	0.68	3.33
	Smyrnium.type	4	0	22.2	-28.9	3935	-1219	0.28	1.19
	Torilis	3	4	21.2	2.1	5431	4126	0.41	0.53
	Torilis.arvensis	5	1	9.5	-8.5	2254	-3331	1.48	3.52
	Torilis.type	31	7	2.4	6.7	628	5517	0.09	-0.31
	Turgenia.type	51	44	5.4	3.8	1510	4051	0.19	0.34
Asteroideae		6171	8053						
	Achillea	29	14	9.3	-17.4	1132	2589	0.26	0.46
	Achillea.Aster	24	22	3.8	8.8	1171	2945	0.20	-0.01
	Achillea.Aster.type	13	10	5.8	-2.2	1083	-5355	0.13	0.92
	Achillea.type	341	230	3.5	-5.4	1440	-693	0.38	1.85
	Adenostyles.type	2	1	2.3	-6.6	1430	-4210	0.41	2.90
	Ambrosia	156	118	5.3	-3.3	874	4456	0.11	0.65
	Ambrosia.artemisiifolia.type	52	14	2.5	-8.1	344	3142	0.09	0.67
	Ambrosia.type	78	34	9.6	14.3	1920	8737	0.33	0.99
	Ambrosia.Xanthium	7	1	4.7	-79.1	556	-6281	0.12	0.98
	Antennaria	1	0	1.9	13.2	337	-613	0.05	0.64
	Antennaria.type	7	7	25.1	39.2	8377	11119	0.78	0.13
	Anthemis	25	61	9.8	35.7	2403	11515	0.20	0.10
	Anthemis.type	785	697	4.7	12.1	978	7425	0.10	0.32
	Arnica.montana	47	12	2.1	-6.4	617	-1737	0.15	1.88
	Aster	39	18	9.5	-19.8	1175	-721	0.23	0.63
	Aster.bellidiastrum	1	0	2.2	-24.8	440	-7019	0.09	3.35
	Aster.type	827	1016	1.3	16.5	368	8932	0.06	0.04
	Asteroideae	2020	4543	1.1	11.7	307	6537	0.05	0.46
	Bellis	13	8	26.2	-13.8	4528	2585	0.52	0.57
	Bellis.type	20	36	3.1	16.2	541	5010	0.06	1.09
	Bidens	5	4	16.0	-6.0	3363	-2707	0.69	1.90
	Bidens.type	60	37	4.1	14.7	1403	5280	0.17	0.54
	Calendula	11	1	5.1	1.7	859	2929	0.46	0.94
	Calendula.type	2	1	3.3	68.3	679	19527	0.09	-0.03
	Chrysanthemum.alpinum	1	0	2.2	-24.8	440	-7019	0.09	3.35
	Doronicum	2	0	10.7	25.4	1689	12070	0.47	-0.45
	Erigeron	56	9	3.1	-17.4	1132	-4120	0.32	2.34
	Eupatorium	1	0	2.0	23.1	465	6590	0.06	1.42
	Eupatorium.type	1	1	1.4	31.7	159	2332	0.04	2.24
	Evax	1	0	4.1	17.1	1329	9679	0.11	0.72
	Filago.type	74	48	3.2	14.8	1577	12170	0.10	-0.24
	Gnaphalium	13	1	10.9	-7.9	794	-3178	0.57	2.77
	Gnaphalium.type	29	3	6.4	-24.3	1125	-7796	0.31	3.26
	Helianthus	23	11	4.0	41.6	934	13380	0.32	1.50

	Helianthus.type	1	0	1.3	16.6	229	6595	0.04	-0.06
	Homogyne	39	3	5.1	-13.9	1216	-5609	0.29	2.80
Amalgamated taxon	**Component taxon**	**Occurrences**	**Total abundance**	**SD MTCO**	**Coefficient MTCO**	**SD GDD**	**Coefficient GDD**	**SD sqrt(MI)**	**Coefficient sqrt(MI)**
	Homogyne.alpina	7	2	3.6	-12.7	1014	-34	0.20	0.50
	Inula	1	0	2.1	12.1	282	-68	0.05	1.68
	Inula.type	4	1	14.5	15.6	2385	8943	0.69	0.19
	Matricaria.type	263	300	2.6	2.8	1024	5477	0.10	0.31
	Petasites	6	1	15.8	0.6	3087	4559	0.76	0.38
	Petasites.type	3	0	15.1	-11.6	4643	-2114	0.58	1.48
	Senecio	67	18	2.6	-11.4	814	-3489	0.18	2.43
	Senecio.type	186	148	16.5	-15.3	2531	2210	0.16	0.49
	Solidago	82	65	12.3	-19.4	838	-2421	0.17	1.83
	Solidago.type	323	214	5.1	7.3	1374	2779	0.26	1.44
	Solidago.virgaurea.type	20	46	2.4	31.3	637	4056	0.18	3.85
	Tussilago.farfara	2	0	15.5	22.8	8037	9311	0.80	1.18
	Tussilago.type	6	0	8.2	-34.9	1283	-1334	0.20	1.13
	Xanthium	290	179	4.5	6.0	1098	6333	0.10	0.46
	Xanthium.spinosum	1	0	4.2	10.1	470	2474	0.17	0.72
	Xanthium.spinosum.type	7	1	29.2	-21.1	1556	-688	0.42	0.38
	Xanthium.strumarium	1	0	7.3	30.9	1610	9551	0.16	-1.14
	Xanthium.type	96	113	4.2	1.0	771	4393	0.11	0.72
Carduoideae		2363	1620						
	Arctium	7	1	17.1	-12.1	4369	4593	0.85	0.15
	Arctium.Jurinea	18	8	5.5	4.4	2057	5039	0.21	0.10
	Arctium.type	4	2	15.7	13.8	5636	6330	0.97	0.24
	Carduoideae	20	20	3.8	-3.6	1177	1800	0.18	0.71
	Carduus	72	11	3.1	-11.0	980	-4964	0.16	2.69
	Carduus.type	120	68	3.4	7.8	955	7405	0.17	-0.08
	Carlina	26	4	5.9	-3.3	1525	-4790	0.44	2.76
	Carlina.type	6	2	8.3	22.1	2727	7926	0.18	0.52
	Carthamus	20	5	5.7	7.1	2225	5748	0.20	0.46
	Centaurea	262	507	2.8	7.3	1357	3199	0.21	1.00
	Centaurea.collina	1	0	1.4	-9.4	364	-8785	0.06	2.87
	Centaurea.collina.type	1	0	2.8	29.6	467	3137	0.07	1.13
	Centaurea.cyanus	221	59	2.1	-8.7	446	2896	0.09	0.53
	Centaurea.cyanus.type	227	123	1.9	3.7	428	4449	0.07	0.45
	Centaurea.depressa.type	4	3	4.1	-0.3	3194	3563	0.31	0.31
	Centaurea.diffusa	1	0	2.0	-4.0	966	6100	0.14	0.06
	Centaurea.jacea	11	5	10.4	2.7	1390	4175	0.29	1.24
	Centaurea.jacea.type	113	73	2.4	-10.1	818	557	0.10	0.75
	Centaurea.montana	18	2	6.2	7.5	1272	-2008	0.28	2.26
	Centaurea.montana.type	4	1	19.9	-94.7	3401	-6312	0.72	-0.05
	Centaurea.nigra	10	4	11.0	-11.3	3758	-7100	0.83	2.61
	Centaurea.nigra.type	141	51	3.6	7.2	754	5713	0.14	0.54
	Centaurea.rhenana.type	1	0	3.9	12.7	337	4457	0.06	0.94
	Centaurea.scabiosa	12	4	4.4	5.4	1633	4103	0.41	1.21
	Centaurea.scabiosa.type	17	4	4.4	-11.5	1150	-113	0.37	1.00
	Centaurea.solstitialis	2	0	3.9	38.9	962	11509	0.19	1.06
	Centaurea.solstitialis.type	257	231	1.8	1.5	605	4805	0.09	0.36
	Centaurea.type	17	21	3.2	40.2	1769	15153	0.20	-1.78
	Cirsium	124	35	4.9	-17.0	595	-388	0.17	1.28
	Cirsium.Carduus	74	26	5.7	-8.6	1026	3136	0.11	0.70
	Cirsium.Carduus.type	1	1	1.2	-9.9	243	3385	0.04	0.24
	Cirsium.Gundelia	41	23	5.5	-0.7	1558	4738	0.14	-0.15
	Cirsium.type	355	266	6.4	2.9	983	5214	0.12	0.62
	Cousinia	14	15	4.8	-11.6	1450	-1782	0.20	1.02
	Echinops	32	8	4.6	10.4	1342	6631	0.18	0.14

	Echinops.ritro	1	0	2.2	-11.1	569	5594	0.10	0.07
	Jurinea.type	5	2	6.8	3.1	633	5200	0.46	0.73
	Onopordum.type	8	2	9.1	-3.5	2896	1557	0.38	0.58
	Saussurea	27	8	6.3	-8.9	869	-2562	0.31	2.05
Amalgamated taxon	**Component taxon**	**Occurrences**	**Total abundance**	**SD MTCO**	**Coefficient MTCO**	**SD GDD**	**Coefficient GDD**	**SD sqrt(MI)**	**Coefficient sqrt(MI)**
	Saussurea.alpina	9	2	8.9	-13.5	1180	-4305	0.28	1.83
	Saussurea.type	48	17	17.0	-69.8	1186	-3222	0.14	-0.25
	Serratula	4	1	10.5	-17.7	3775	-7910	0.92	2.22
	Serratula.type	7	3	7.7	24.8	2667	9202	0.37	1.07
Cichorioideae		3260	8877						
	Cichorioideae	2950	8331	0.7	7.5	179	5508	0.03	0.60
	Cichorium	16	34	9.9	-36.7	1077	-2633	0.19	1.34
	Cichorium.intybus.type	31	20	4.9	-13.1	1503	-8329	0.21	2.72
	Cichorium.type	59	125	4.4	-42.2	809	166	0.08	0.54
	Crepis	2	1	6.1	13.8	1740	5225	0.40	0.75
	Crepis.aurea	1	0	2.2	-24.8	440	-7019	0.09	3.35
	Crepis.type	1	0	1.3	27.9	207	6693	0.04	0.00
	Hieracium.type	2	1	2.2	27.4	809	6610	0.20	0.96
	Lactuca	16	4	8.1	-1.5	2418	2312	0.29	0.78
	Lactuca.sativa.type	1	0	1.2	20.8	234	1826	0.04	1.47
	Lactuca.type	4	0	2.7	19.6	214	4939	0.04	0.22
	Leontodon.helveticus	1	0	2.2	-24.8	440	-7019	0.09	3.35
	Leontodon.type	20	27	10.6	-8.0	872	-2965	0.71	2.92
	Scorzonera.humilis.type	15	15	6.3	5.6	874	3216	0.14	0.85
	Scorzonera.type	6	9	6.4	-7.9	2111	2515	0.54	0.01
	Sonchus.type	10	1	6.3	-8.4	684	3623	0.07	0.48
	Taraxacum	36	10	8.6	-40.2	1564	-3322	0.26	1.24
	Taraxacum.type	89	299	3.8	-4.0	331	4349	0.22	0.36
Cistus		956	1756						
	Cistus	202	666	2.7	15.5	640	7353	0.06	0.54
	Cistus.albidus.type	12	6	12.8	37.0	2172	13274	0.39	0.28
	Cistus.incanus.type	10	2	8.8	46.6	2078	16839	0.40	-0.18
	Cistus.ladanifer	222	432	1.1	2.2	345	4943	0.04	0.47
	Cistus.ladanifer.type	14	18	6.1	18.4	857	9717	0.22	-0.11
	Cistus.monspeliensis	5	4	16.7	75.0	4049	24041	0.47	-1.20
	Cistus.monspeliensis.type	3	10	25.1	37.6	4726	12791	0.73	0.27
	Cistus.populifolius.type	67	164	3.4	5.2	937	4235	0.08	0.70
	Cistus.salvifolius	46	28	11.8	32.5	2645	11182	0.16	0.27
	Cistus.salviifolius.type	7	9	13.3	50.8	2506	15361	0.36	0.06
	Cistus.type	320	340	1.6	5.3	504	5077	0.05	0.55
	Cistus.villosus.type	48	78	5.2	18.6	1201	7446	0.12	0.41
Ephedra		813	913						
	Ephedra	79	69	19.5	7.8	2701	9331	0.24	-0.49
	Ephedra.alata.type	6	18	11.2	-23.5	948	4555	0.54	-0.90
	Ephedra.distachya	198	309	4.3	-4.0	1078	6798	0.19	-0.27
	Ephedra.distachya.type	118	62	7.5	-7.1	971	6214	0.21	-0.56
	Ephedra.fragilis	68	60	3.3	4.5	1355	4166	0.26	0.92
	Ephedra.fragilis.type	326	392	2.5	8.8	617	6251	0.09	0.42
	Ephedra.major	1	0	1.5	23.3	308	2685	0.05	1.37
	Ephedra.type	17	3	5.2	-12.6	1503	-509	0.19	1.13
Plantaginaceae		5565	8012						
	Globularia	21	1	11.4	-5.2	1853	-3773	0.39	2.52
	Gratiola.officinalis	2	0	1.5	17.8	407	4505	0.06	0.30
	Hippuris.vulgaris	10	7	12.0	13.3	1177	2428	0.99	2.72
	Plantaginaceae	73	61	3.9	-14.1	1898	2514	0.22	0.41
	Plantago	1156	2049	1.4	19.2	525	7305	0.09	0.51
	Plantago.afra.type	1	0	1.7	23.9	465	10737	0.06	0.88

	Plantago.albicans	38	37	8.6	2.2	1695	4828	0.10	0.06
	Plantago.alpina	39	105	3.7	-20.4	831	-8347	0.15	2.82
	Plantago.alpina.type	160	241	1.6	-17.8	559	-5527	0.15	2.63
	Plantago.coronopus	243	546	3.7	18.7	832	8327	0.09	0.34
	Plantago.coronopus.type	348	527	1.9	13.9	465	8662	0.09	0.13
	Plantago.cylindrica.type	11	2	6.7	-15.0	2992	-1592	0.45	0.48
Amalgamated taxon	**Component taxon**	**Occurrences**	**Total abundance**	**SD MTCO**	**Coefficient MTCO**	**SD GDD**	**Coefficient GDD**	**SD sqrt(MI)**	**Coefficient sqrt(MI)**
	Plantago.lanceolata	1407	1655	1.8	3.2	421	1961	0.07	1.46
	Plantago.lanceolata.Plantago.major.type	3	3	9.1	-16.6	1894	445	0.40	-0.19
	Plantago.lanceolata.type	1110	2082	1.7	6.2	471	5577	0.04	0.45
	Plantago.lusitanica	4	3	36.6	41.3	11290	13788	0.80	-0.84
	Plantago.major	244	73	2.2	-6.8	772	-421	0.14	1.19
	Plantago.major.type	93	69	11.2	-20.7	2258	1649	0.12	0.54
	Plantago.maritima	25	20	7.3	17.3	1557	6365	0.44	1.69
	Plantago.maritima.Plantago.alpina.type	1	0	2.2	-9.8	355	-9180	0.05	1.27
	Plantago.maritima.type	134	87	6.9	-12.6	1858	5797	0.12	0.21
	Plantago.media	116	40	3.0	13.4	397	129	0.09	1.71
	Plantago.media.type	43	28	2.4	10.0	672	5667	0.29	0.86
	Plantago.montana.type	42	14	3.6	15.7	891	-612	0.20	1.82
	Plantago.ovata.type	25	26	4.8	4.5	1915	8798	0.19	-0.11
	Plantago.psyllium.type	71	81	3.4	22.8	760	8542	0.11	0.30
	Plantago.tenuiflora.type	9	4	6.0	-4.1	1760	6250	0.25	-0.83
	Plantago.type	136	250	4.0	1.4	1069	2752	0.12	1.13
Quercus deciduous		4920	34212						
	Quercus	2695	16051	0.7	3.7	132	4613	0.03	0.80
	Quercus.cerris	1	1	3.0	18.5	371	2924	0.07	-0.16
	Quercus.cerris.type	747	6277	0.6	1.3	161	4944	0.02	0.62
	Quercus.deciduous	992	8818	0.6	3.3	253	4385	0.03	0.82
	Quercus.infectoria.type	1	1	1.4	17.9	316	9965	0.06	-0.79
	Quercus.petraea	2	27	3.8	1.0	1167	6584	0.22	0.40
	Quercus.robur	75	1077	3.1	16.1	1106	6405	0.15	0.46
	Quercus.robur.Quercus.petraea	4	1	4.0	-5.6	1213	1722	0.13	0.65
	Quercus.robur.type	403	1959	1.6	9.5	356	3948	0.07	1.03
Quercus evergreen		2378	24196						
	Quercus.coccifera	307	4057	0.9	9.5	278	6268	0.02	0.56
	Quercus.coccifera.Quercus.ilex	36	174	4.8	8.5	1192	5024	0.12	0.53
	Quercus.coccifera.type	89	801	2.4	6.3	594	5487	0.17	0.12
	Quercus.evergreen	1050	12664	0.3	4.6	106	4949	0.02	0.60
	Quercus.ilex	126	184	3.0	23.1	1005	7902	0.11	0.04
	Quercus.ilex.type	514	4553	0.7	4.2	211	4525	0.02	0.64
	Quercus.rotundifolia.type	2	61	0.4	8.5	91	6895	0.02	0.20
	Quercus.suber	165	1331	1.1	14.2	333	7369	0.03	0.55
	Quercus.suber.type	89	370	2.8	23.7	611	9716	0.08	0.14

4 Examination of some algorithms in WA-PLS and fxTWA-PLS

Since D-Os could not be reliably identified directly from pollen series (Chapter 2) an alternative approach using pollen-derived quantitative reconstruction of climate variables was explored. The reconstructions were made using fxTWA-PLS, a variant of WA-PLS. In this chapter, the algorithms in WA-PLS and fxTWA-PLS and their implications for the reliability of these reconstructions are examined.

This Chapter describes the algorithms in WA-PLS (Ter Braak and Juggins, 1993) and fxTWA-PLS version 1 (Liu *et al.*, 2020), both to give context for later Chapters, and because scrutiny reveals a problem with the reconstruction process in WA-PLS as implemented in the R package *rioja* (Juggins, 2017) , which has potentially significant implications for the robustness of reconstructions.

In this Chapter 'MTCO' and 'Tmin' are used synonymously to indicate the mean temperature of the coldest month; Tmin here does not indicate the lowest winter temperature. 'gdd' is synonymous with 'GDD0' (growing degree days over 0 ^{o}C), and 'rtmi' is the square root of MI, Moisture Index, the ratio of actual to potential evapotranspiration.

4.1 WA-PLS

WA-PLS was developed in Ter Braak and Juggins (1993). Juggins later provided WAPLS functions in the *rioja* R package (Juggins, 2017), though the algorithms can be shown not to be identical with those in Ter Braak and Juggins (1993) - see Table 4-1. WA-PLS performs weighted averaging and inverse regression. WA-PLS, used in Chapter 3, Turner *et al.* (2020), was improved in fxTWA-PLS (Liu *et al.*, 2020, 2023), the 2020 version of which is used in this project.

In the 'calibration' process, WA-PLS provides a transfer function for each taxon, which is intended to represent the central location of the abundance distribution of the taxon along an environmental gradient. Statistical tests are available to test how well it performs in replicating the observed climate in the training

set. The ‘reconstruction’, or ‘prediction’, process then applies the transfer function to fossil abundances to reconstruct past climate.

The internal processes of averaging, regression and de-shrinking and their effects are discussed in this Chapter and further in Chapter 5, which focusses on the distribution of taxon abundance along a climate gradient, and compares this with the climate preferences as found by fxTWA-PLS, as far as they can be known.

4.1.1 Calibration

Below, ‘WA-PLS’ refers to the algorithms described in Ter Braak and Juggins (*1993*), and ‘WAPLS*rioja*’ to the WA-PLS-related functions implemented in *rioja* (Juggins, 2017).

Figure 4.1 outlines the calibration process. The weighted averaging element multiplies the environmental vector by the abundances, and finds a weighted mean environmental value for each taxon. This is the first estimate of the ‘optimum’ or taxon preference. These first-estimate optima are then taken as good, and multiplied by the abundances again to give a taxon-weighted environment. Summing the sample rows of the taxon-weighted environment provides a trial reconstruction vector which, in a perfect world, would replicate the original environmental vector. The observed and reconstructed vectors are then regressed to establish the fit.

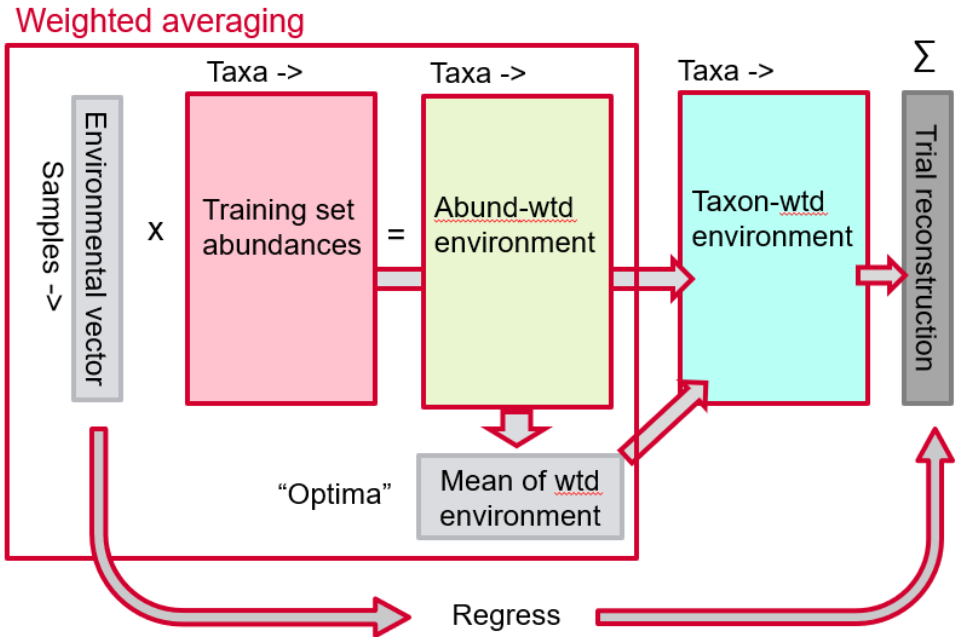

Figure 4.1 WA-PLS calibration: the weighted averaging and regression process.

An example of the regression is shown in Figure 4.2, using the SMPDS v1 training set. A line of best fit through the trial reconstruction lies at an angle to the 1:1 line which would represent a good fit with the observed environment. The difference in slope arises because the double averaging has reduced, or shrunk, the range of the values in the reconstruction, and is a well-understood issue (e.g. Ter Braak and Juggins, 1993; Simpson, 2013). This is corrected by 'de-shrinking', by twisting the reconstruction vector to the 1:1 line, that is, multiplying by the slope coefficient of the inverse regression. This leaves a cloud of points aligned along the 1:1 line as the current best estimate of the reconstructed environmental vector. The dispersion of the points about the line shows that the training set abundances do not perfectly reflect this climate variable and must be influenced by other factors, including noise.

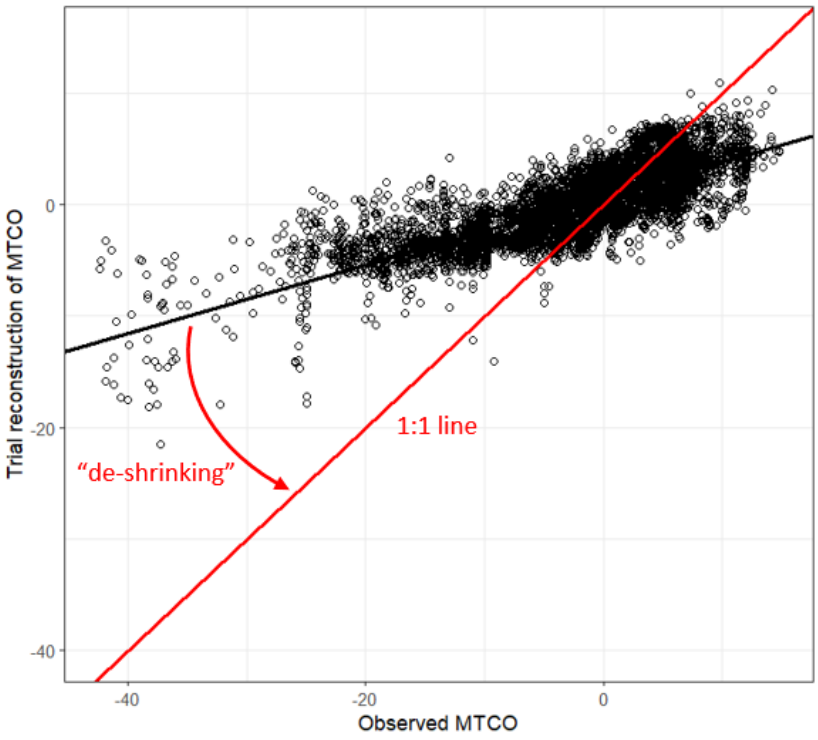

Figure 4.2 An example of the result of WA-PLS regression, and the de-shrinking requirement using SMPDS v1 and component 1 for MTCO in °C (temperature of coldest month).

Table 4-1 shows the calibration algorithm more formally, using the terminology of Ter Braak and Juggins (1993), notes where the *rioja* function WAPLS() (Juggins, S, 2017) differs, and includes notes resulting from reverse engineering the *rioja* WAPLS() function and the C code called by it.

Table 4-1 WA-PLS calibration algorithms in ter Braak and Juggins and in rioja *WAPLS() function.*

ter Braak and Juggins (1993)	WAPLS*rioja* (Juggins)
Step 0. Centre the environmental variable by subtracting the weighted mean, i.e. $x_i = x_i - \sum_i y_{i+} x_i / y_{++}$ This simplifies the formulae.	Same
Step 1. Take the centred environmental variable (x_i) as initial site scores (r_i) . Do Steps 2 to 7 for each component :	Same
Step 2. Calculate new species scores (u^*_k) by weighted averaging of the site scores, i.e. $u^*_k = \sum_i y_{ik} r_i / y_{+k}$	Same
Step 3. Calculate new site scores (r_i) by weighted averaging of the species scores, i.e. new $r_i = \sum_k y_{ik} u^*_k / y_{i+}$	Same

***Step 4**. For the first axis go to Step 5. For second and higher components, make the new site scores (r_i) uncorrelated with the previous components by orthogonalization (Ter Braak, 1987: Table 5.2b)*	Never performed (no explanation). If performed, has very small effect.
***Step 5**. Standardize the new site scores (r_i) (Ter Braak (1987 : Table 5.2c).* ***Step 6**. Take the standardized scores as the new component.*	Not performed. Has no effect on 'prediction' if performed, since it is exactly counteracted by regression.
Step 7. Regress the environmental variable (x_i) on the components obtained so far using weights (y_{i+}/y_{++}) in the regression and take the fitted values as current estimates ($xhat_i$). *This is multiple linear regression for 2nd and later components.* Go to Step 2 with the residuals of the regression as the new site scores (r_i).	Same. Purpose is 2-fold: (i) obtain residuals for use in next component as new r_i in Step 2 (ii) obtain intercept and slope coefficient(s) a_0, a_1, …, a_c for Prediction Step 2 below. *Notes:* x_i is the ***observed***, not centred, environment, and "components so far" means r_i for each component c. $xhat_i$ is not used. Weights are unimportant if sample abundance sums are equal e.g. all samples sum to 1.

The 'partial least squares' process (PLS) is based on the expectation that the residuals of the inverse regression after de-shrinking contain further information, so they are taken as the environmental vector input to a second round of weighted averaging and regression. This search for additional information in the residuals is iterated, finding a series of 'components' whose values are cumulated. Statistical tests of the skill of the different components in replicating the observed climate, using leave-one-out cross validation and random *t*-testing, then determine the number of components (the result of iterations) to be used. There are examples of the results in Chapter 3, Turner *et al.* (2020).

4.1.2 Reconstruction ('prediction')

For each component, the WA-PLS calibration process provides a transfer function for each taxon enshrining the climate preference of that taxon. The highest component which is still statistically valid is selected based on the cross-validation and random *t*-tests. Ter Braak and Juggins (1993) does not specify how the calibration result should be applied to data from which a reconstruction is to be made, and an issue arises with the method applied in WAPLS*rioja*.

4.2 De-shrinking and reconstruction in WAPLS*rioja*

Two interacting issues are covered in the following sections: how de-shrinking is applied, and how this impacts reconstructions where the relative abundances of taxa in the fossil core are very different from those in the training set.

The de-shrinking factor is found in the calibration process from the slope of the inverse regression of the observed environmental vector against the reconstructed vector, which has been averaged twice. In the reconstruction process, WAPLS*rioja* applies this factor not, as consistency would require, to the twice-averaged new trial reconstruction of the fossil climate but to the once-averaged taxon optimum. It then multiplies these 'de-shrunk' optima by the sample abundances of the related taxa to reconstructed a climate value for each sample.

This can make some optima nonsensical, for instance by placing them outside the range of climate observed in the training set of the individual taxon, or even outside the entire observed range of the training set. Whether or not the observed ranges in the training set represent the true climatic ranges of the taxa is not relevant; the point is that WAPLS*rioja* is capable of placing optima outside the ranges it is given. Figure 4.3 show the 91 taxa out of 195 in the SMPDS for which WAPLS*rioja* provides Component 3 de-shrunk optima which fall outside the observed Tmin (temperature of coldest month) range for the individual taxa; similar results are seen for gdd and rtmi. Many of these are low-abundance or rarely sampled taxa in the SMPDS, but this does not mean that their optima are of no importance, since some occur in much higher abundances in fossil cores, and some of the 91 taxa are abundant even in the SMPDS. While these 91 optima are obviously problematical by virtue of falling outside the observed ranges, the same process is likely to have displaced the optima of other taxa which fall within their observed ranges.

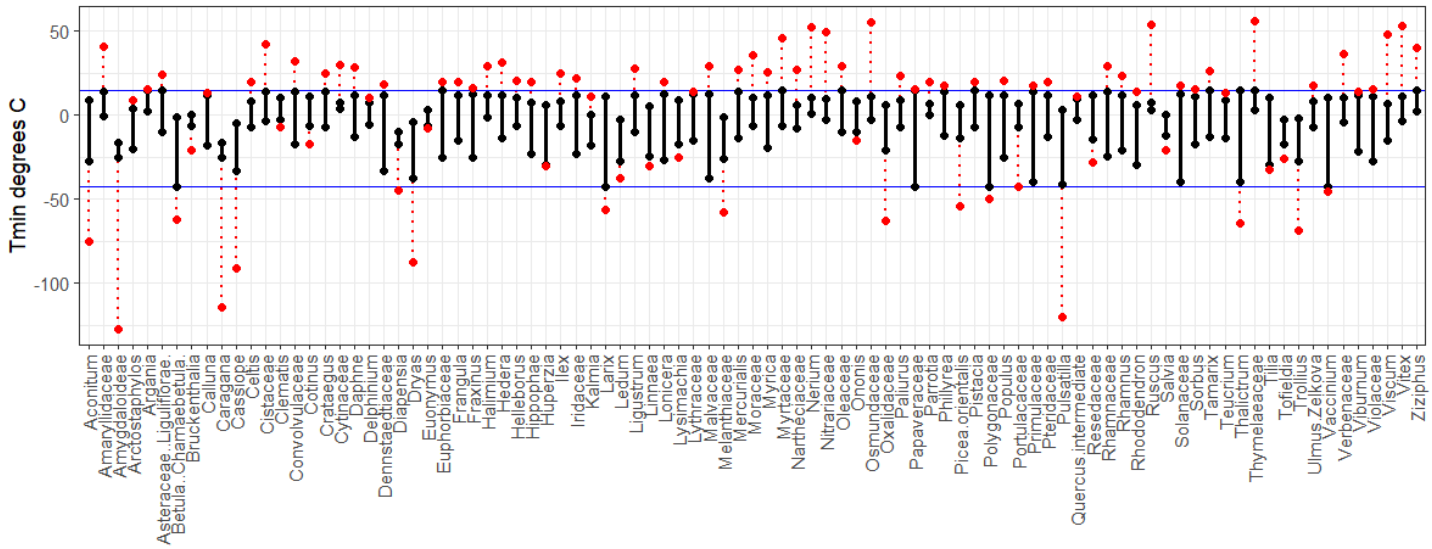

*Figure 4.3 Observed ranges for Tmin (temperature of coldest month) in SMPDS (black lines and points) and ranges of Component 3 optima provided by WAPLS*rioja *(red dotted lines and points). Blue lines: maximum and minimum observed Tmin in SMPDS.*

It could be argued that these 'optima' are just a stage in the calculation and that no physical meaning should be attached to them, but 4.2.6 below shows that it matters greatly when the taxon abundances in a fossil data set are very different from those in the training set, and explains why the issue is not immediately obvious at the calibration stage. WA-PLS will no doubt remain in use, so that a method of avoiding this error is a useful option.

4.2.1 An alternative reconstruction algorithm

This proposal tackles differences in reconstruction algorithms, not whether the underlying unmodified, first-estimate optima found by WAPLS*rioja* are good estimates of the climate preferences of the taxa. That subject is examined in Chapter 5.

WA-PLS*rioja* de-shrinks not the trial reconstruction but the first-estimate optima, or taxon coefficients. The proposed alternative leaves the taxon coefficients unmodified, and applies the de-shrinking to the estimate of the trial reconstruction of the environmental variable instead, as the method by which it was determined dictates. It results in good predictions of the training set and good statistical results, but potentially very different reconstructions when applied to fossil pollen.

The key point is that shrinking and its correction are determined by the effect on the vector of *sample* reconstructions, the combined result of two averaging processes. It does *not* describe the effect on the *taxon* coefficients, which have only suffered one averaging. It is not obvious how the shrinking can be partitioned between the two steps, and the once-averaged taxon coefficients remain shrunk to some degree.

4.2.2 WAPLS*rioja* regression coefficients and taxon coefficients

WAPLS*rioja* applies the entire de-shrinking factor to the once-averaged coefficients, then adds the intercept to yield scalar transfer coefficients. When multiplied by the taxon abundances in the training set, these give sample reconstructions with a 1:1 regression line with the observed. Since the entire de-shrinking is allocated to the coefficients, this necessarily widens the range of the coefficients, which is one cause of the out-of-range optima identified above. The process is more formally described as follows.

There are i samples (or sites), k taxa and n PLS components are extracted.

$y_{i,k}$ is the abundance in sample i of taxon k.

p is the intercept, represents the centring offset applied to the observed environmental variable for simplicity of calculation, and does not change with n.

$s_{n,m}$ are the slope coefficient(s) found by inverse regression of the observed environmental vector on the site scores for the nth component. There are as many slope coefficients m as the number of the current component (i.e. $m = n$) (Table 4-2). Note that $s_{x,m}$ for the current component may not be the same as $s_{x\text{-}1,m}$ or for previous component(s), because further explanatory variables have been added.

Table 4-2 WA-PLS slope coefficient notation

Slope coefficient notation		m			
	n	1	2	3	4
PLS1	1	$S_{1,1}$			
PLS2	2	$S_{2,1}$	$S_{2,2}$		
PLS3	3	$S_{3,1}$	$S_{3,2}$	$S_{3,3}$	
PLS4	4	$S_{4,1}$	$S_{4,2}$	$S_{4,3}$	$S_{4,4}$

$u_{k,n}$ is the initial coefficient found for taxon k for component n without de-shrinking. It is the centred weighted average of the taxon abundances multiplied by the preceding site/sample environmental scores (u_k* in Ter Braak and Juggins (1993) notation denotes the vector of $u_{k,n}$ for all k taxa).

The coefficient for taxon k for the nth component in WAPLS*rioja* is given by

$$c_{k,n} = p + u_{k,1}s_{n,1} + u_{k,2}s_{n,2} + \cdots + u_{k,n}s_{n,m} \qquad \textit{Equation 4-1}$$

It is these coefficients that are perceived to lack physical realism.

Prediction for sample i for component n is then

$$\sum_1^k y_{i,k}c_{k,n}/\sum y_{i,k} \qquad \textit{Equation 4-2}$$

In calculating the next component, these modified coefficients are ignored. Each component is independent, with the same process repeated. The residuals from the last component are taken as the environmental vector, new *uk** coefficients are found, and an inverse regression of the observed against the current sample estimates is performed. The slope-adjusted transfer coefficient for the new component is added to the previous transfer coefficient.

4.2.3 Alternative method

Instead of taking taxon optima to which the de-shrinking factor has been applied, and applying them to pollen samples, it is logical instead to preserve the unmodified once-averaged coefficient, calculated as by WAPLS*rioja* in Step 2 of Table 4-1, and apply some de-shrinking factor *f* to the trial reconstructed environmental vector as follows:

$$(uk^*. y_{ik}) f$$ *Equation 4-3*

In the case of Component 1 this is identical to the rioja WAPLS*rioja* method, which is $(uk^*. f) y_{ik..}$.

The issue is how to obtain *f* for higher components. In WAPLS*rioja* for components > 1 there is no single value for *f,* and the de-shrinking adjustment is a composite of the slopes applied in each component (Table 4-2).

The alternative uses inverse regression of the observed against the trial reconstruction to adjust the trial reconstruction, and adds the intercept to the result. The slope provides a single de-shrinking adjustment *f* at any component. The regression may be simple linear regression on the cumulative reconstruction, or multiple linear regression on incremental reconstructions. The two processes are compared in Table 4-3.

*Table 4-3 WAPLS*rioja *and alternative 'prediction' algorithms*

ter Braak and Juggins (1993)	Rioja WAPLS () and WA() functions	Alternative method
From WA description, which has only one "component": Estimate the x-values of the sites by weighted averaging of the species optima, $x_i^* = \sum_k y_{ik} u^*_k / y_{i+}$	r_i is the equivalent of x_i^* in WA.	Estimated x-values for samples/site at each component are available as r_i in Step 3 in Table 4-1. **Step A0**: sum r_i for each component c to obtain the cumulative trial reconstruction, $x_{i,c}^* = \sum_c r_{i,c}$.
The final prediction formula […] is thus $xhat_o = a_o + a_1 x^*_0$ $= a_o + a_1 \sum_k y_{0k} u^*_k / y_{0+}$ $= \sum_k y_{0k} \hat{u}_k / y_{0+}$ where a_o and a_1 are the coefficients of the deshrinking regression and $\hat{u}_k = a_o + a_1 u^*_k$.	**Step 1**: For c^{th} component, find transfer coefficient $\hat{u}_{k,c}$ by applying regression coefficients from Step 7 above: $\hat{u}_{k,c} = a_o + a_1 u^*_{k,1} + a_2 u^*_{k,2} + \ldots + a_c u^*_{k,c}$ **Step 2**: Estimate x-values by applying transfer coefficients $\hat{u}_{k,c}$ to the abundances. $xhat_{i,c} = \sum_k y_{i,k} \hat{u}_{k,c} / y_{i+}$	**Step A1**: Regress the observed environmental variable on the trial reconstruction (= sample/site scores) $x_i^*_c$ for each component, (otherwise as Step 7), to obtain a_o, a_c **Step A2:** Estimate x-values by applying slope and intercept to x_i^* for each component: $xhat_{i,c} = a_o + a_1 x_i^*_{,c}$. For 1st component the result is identical to rioja WAPLS() result.

4.2.4 Comparison of the methods

Figure 4.4 compares the reconstructions of the training set by the alternative method with that by WAPLS*rioja* for Tmin, the mean temperature of the coldest month, for Component 3. The gross patterns are almost identical, which is to be expected. At the sample level, there are no differences at Component 1; differences are expected at higher components, and are seen in the lower two panels of Figure 4.4, where > 95% of the differences are within 2.5 °C and the mode of the differences is near zero. Such a difference will also be found in reconstructions from fossil cores.

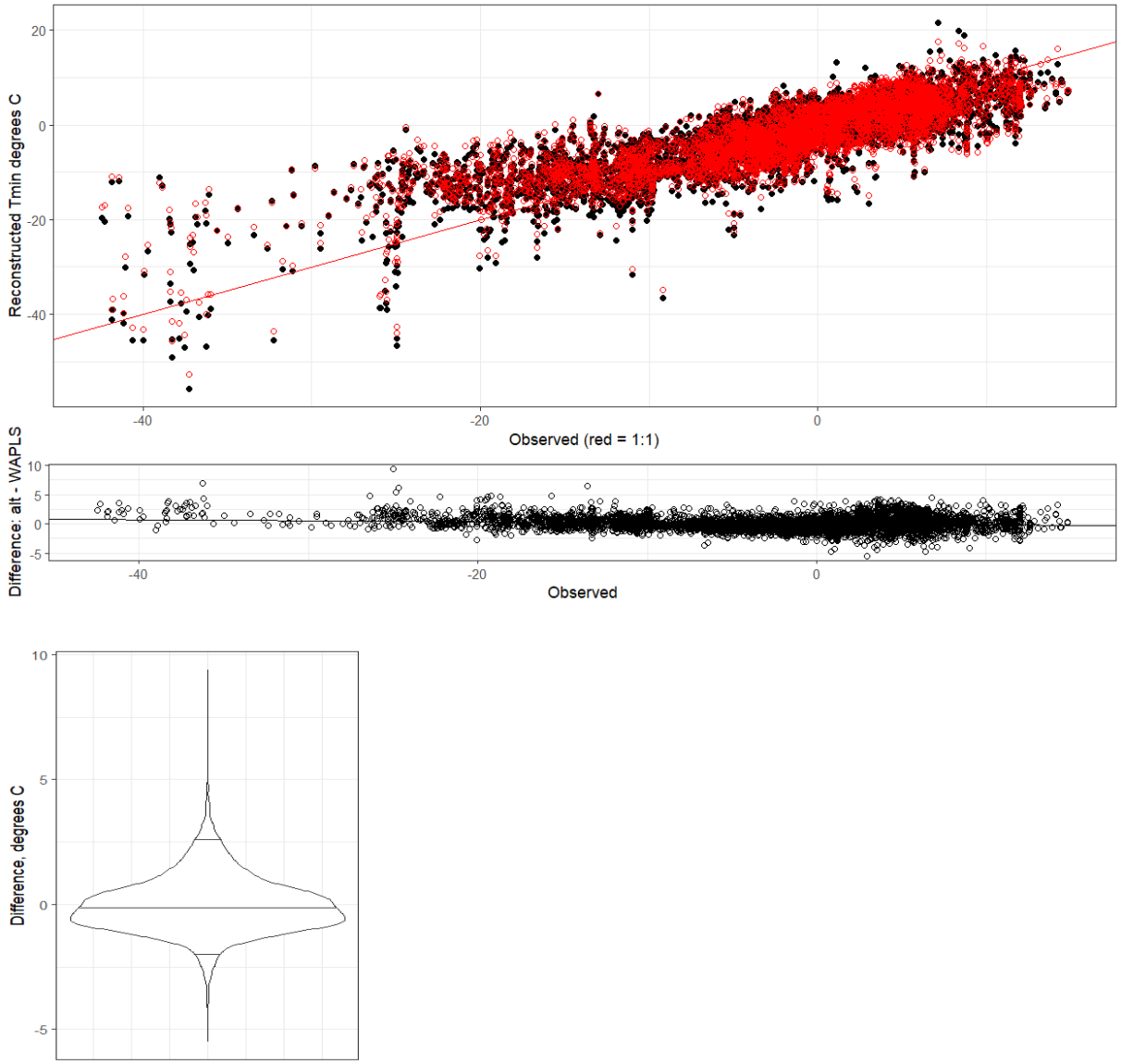

*Figure 4.4 Top panel: alternative (red open circles) v WAPLS*rioja *(black points) "prediction" of training set for Tmin (temperature of the coldest month) for Comp 3 in °C. Red line = 1:1 slope. Middle panel: difference between them. Lower panel: differences between them as violin plot, with quantiles shown as horizontal lines at 0.025, 0.5 and 0.975*

The results of cross-validation and random *t*-testing, taking Tmin as an example, are shown in Table 4-4 (WAPLS*rioja*), Table 4-5 (Alternative, simple linear regression) and Table 4-6 (Alternative, multiple linear regression); similar results are obtained for gdd and rtmi. The cross-validation code used in producing Table 4-4 is native *rioja*. The first cross-validation of the alternative (Table 4-5) uses code in fxTWA-PLS v1 modified for the alternative reconstruction method, and applies simple linear regression on the cumulative component; the second version (Table 4-6) applies multiple linear regression on incremental reconstructions. The random *t*-test code is taken directly from fxTWA-PLS, and can be shown to give the same result as WAPLS*rioja* when run on WAPLS*rioja* data.

*Table 4-4 WAPLS*rioja *cross-validation and random t-test results reconstructing Tmin (temperature of the coldest month)*

Component	RMSE	R2	Avg.Bias	Max.Bias	delta.RMSE	*p*
Comp01	5.31	0.624	0.00349	14.24	-38.71	0.001
Comp02	4.97	0.671	-0.00248	8.841	-6.39	0.001
Comp03	4.84	0.687	-0.00056	8.491	-2.44	0.001
Comp04	4.82	0.690	-0.00487	10.259	-0.55	0.025

Table 4-5 Alternative leave-one-out cross-validation and random t test result for Tmin (temperature of the coldest month), simple linear regression

Component	RMSEP	R2	Avg.Bias	Max.Bias	delta.RMSEP	*p*
Comp01	5.31	0.624	-0.00348	32.70	-38.71	0.001
Comp02	5.00	0.668	0.00073	31.77	-5.93	0.001
Comp03	4.95	0.674	-0.00141	31.17	-0.96	0.001
Comp04	4.94	0.674	0.00160	31.31	-0.05	0.347

Table 4-6 Alternative leave-one-out cross-validation and random t test result for Tmin (temperature of the coldest month), multiple linear regression on incremental reconstructions.

Component	RMSEP	R2	Avg.Bias	Max.Bias	delta.RMSEP	*p*
Comp01	5.31	0.624	-0.00348	32.70	-38.71	0.001
Comp02	5.00	0.668	0.00072	31.73	-5.92	0.001
Comp03	4.95	0.674	-0.00145	30.97	-0.88	0.001
Comp04	4.95	0.674	0.00162	31.03	0.04	0.57

The alternative replicates the training set as successfully as WAPLS*rioja*, which was to be expected. For the first component, as expected, the results are the same, with the exception of maximum bias. Thereafter the

alternative is highly similar to WAPLS*rioja*. In each case, component 3 is preferred on the basis of the statistical tests. There is little difference between multiple and simple linear regression in the alternative method, and such differences as there are may well be within the variability generated by the random *t*-test.

Large differences, however, emerge between WAPLS*rioja* and alternative method reconstructions when applied to fossil pollen. Using Lac du Bouchet and Tmin as an example (Figure 4.5), unmodified coefficients are substantially different from double-shrunk WAPLS*rioja* transfer coefficients, as intended, and the relative abundance of taxa is also very different between the SMPDS training set and fossil cores.

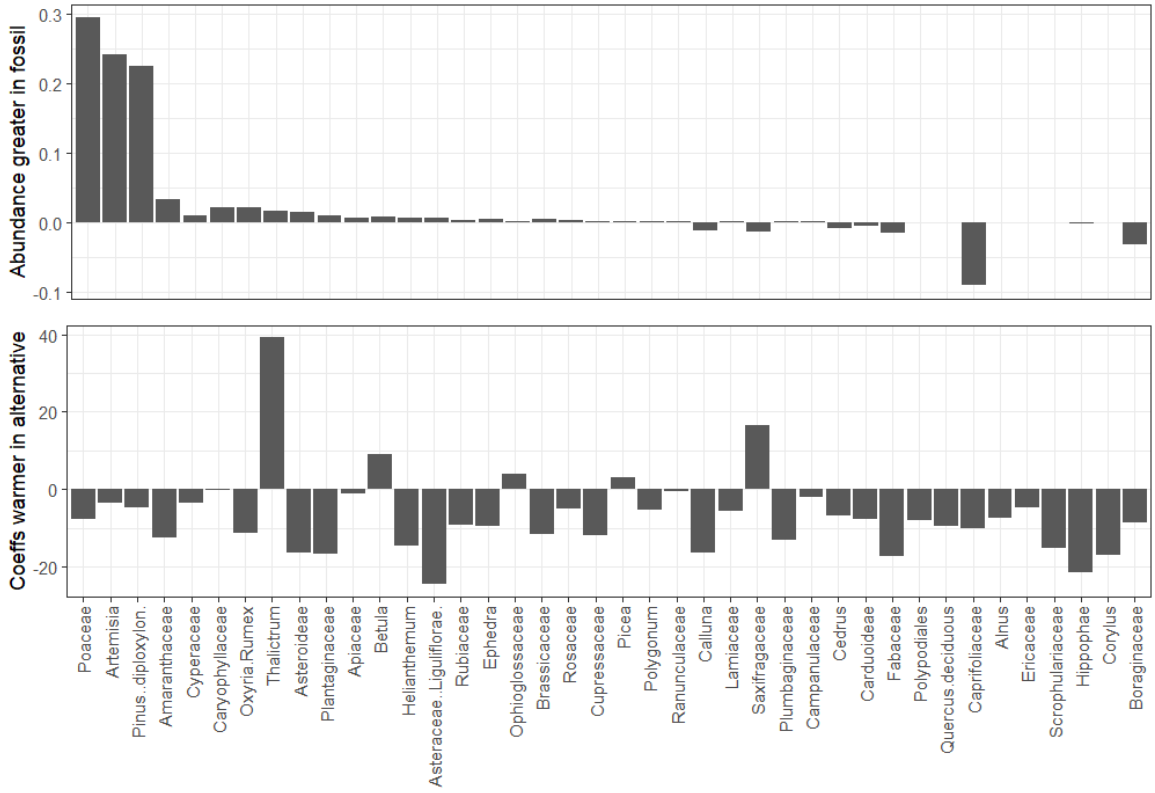

*Figure 4.5 Upper panel: differences in mean fractional abundances in SMPDS and in Lac du Bouchet core. Lower panel: differences in °C between unmodified ("alternative") and WAPLS*rioja *transfer coefficients for Tmin (temperature of the coldest month) for Comp 3, for the 40 most abundant taxa at Lac du Bouchet.*

Figure 4.6 shows that while there are many similarities between the WAPLS*rioja* and alternative reconstructions of Tmin, including ages and directions of changes, which are important to the search for D-Os, there are also significant differences in some intervals, most obviously around 25 ka where a 2 °C difference arises (red line). How does this difference arise and does it appear justified?

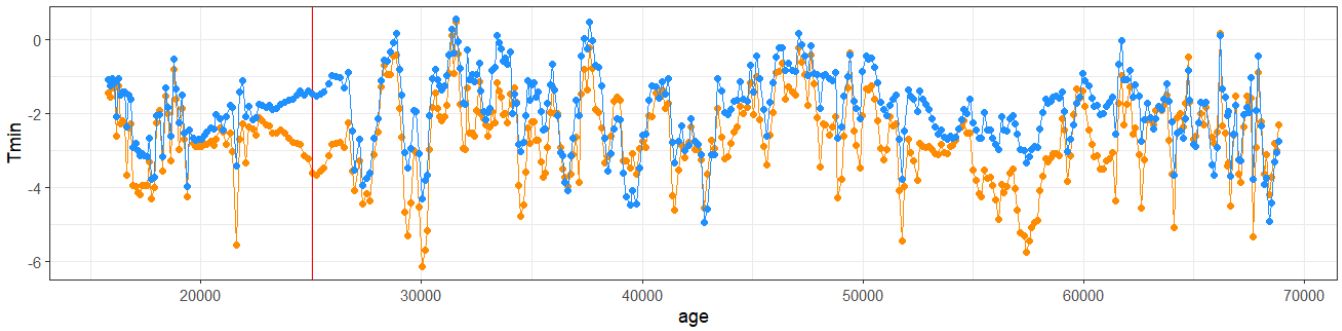

Figure 4.6 WAPLSrioja Tmin (temperature of the coldest month) Component 3 for Lac du Bouchet reconstruction (orange); blue = reconstructed by alternative. Red vertical line at 25.05 ka.

The contribution of different taxa to this difference is not easy to compare directly because of the application of the intercept in the alternative. In the 25.05 ka sample the end values are constructed as in Table 4-7; this analysis of taxon contribution is not available within WAPLS*rioja*, but can be obtained by preserving taxon-level data at Steps 2 and 3 in Table 4-1.

*Table 4-7 Different contributions of taxa to Tmin at 25.05 ka under WAPLS*rioja *and alternative methods*

		Contribution to reconstruction, °C	
Taxon	**Abundance %**	**Alternative**	**WAPLS*rioja***
Amaranthaceae	9.49	0.4562	0.7123
Artemisia	45.47	-2.6611	-2.3319
Brassicaceae	2.5	0.1017	0.1606
Caryophyllaceae	6.01	-0.436	-0.5611
Lamiaceae	1.29	-0.0112	-0.0257
Oxyria/Rumex	4.67	0.0487	0.2605
Pinus diploxylon	0.4	-0.0334	-0.0144
Poaceae	26.97	-0.5541	0.2223
Thalictrum	3.2	-1.5031	-2.0428
Sum	100		
Intercept		3.103	
Reconstructed Tmin, °C		***-1.49***	***-3.62***

As an example, *Thalictrum* pulls the final temperature down much less in the alternative. *Thalictrum* represents 3.2% of the 25.05 ka sample abundance, but 0.07% of the SMPDS abundance. It attracts an out-of-range -64 °C WAPLS*rioja* optimum, and an alternative unshrunk optimum of -21.3 °C. While *Thalictrum* may be very thinly evidenced in the SMPDS and its optimum therefore suspect, a visual comparison with its

abundance on the Tmin gradient in SMPDS suggests that -21.3 °C is a not unreasonable value (Figure 4.7) and that -64 °C is unacceptable. (Chapter 5 focusses on abundance distributions).

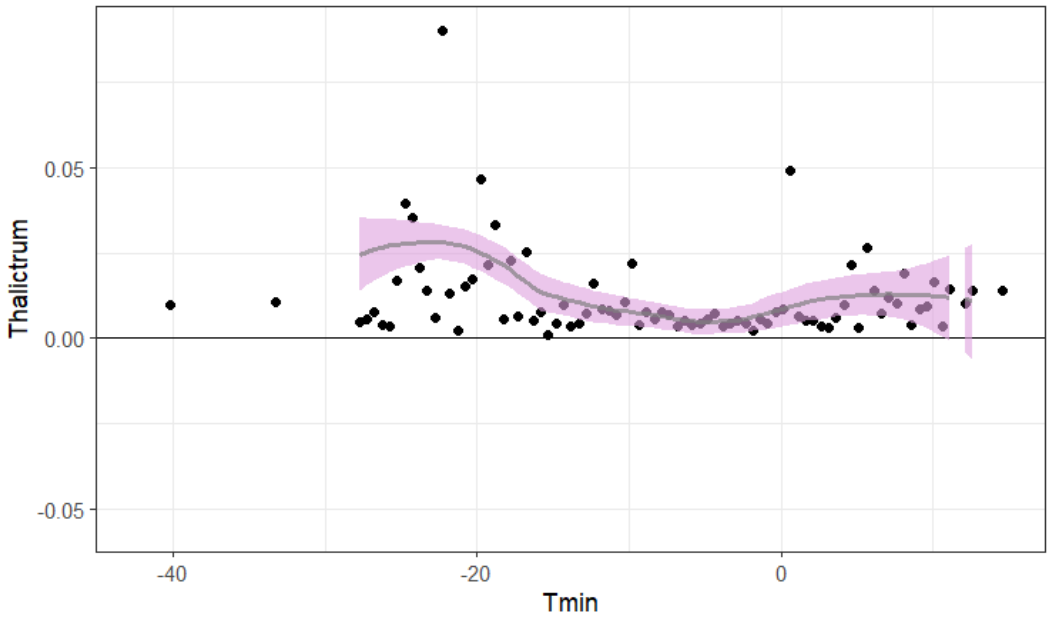

Figure 4.7 SMPDS fractional abundance of Thalictrum *on Tmin (temperature of the coldest month) gradient: points are mean fractional abundance in each 0.5 °C bin; line is loess curve (span = 0.5) with ± 2 SD ribbon*

This appears indicative of an improvement in fossil reconstructions using the alternative, and the coefficients applied appear more plausible, though there is no reconstruction made using other materials against which to test them; this unfalsifiability is a persistent issue with reconstructions made from fossil cores.

4.2.5 Conclusion on the alternative reconstruction method

The new method is a more logical alternative to the WAPLS*rioja* method. It uses the same principle as WA-PLS that replication of the observed is the touchstone. It avoids a fossil site reconstruction being strongly influenced by optima which are physically impossible.

The alternative deals with only one aspect of three which must be considered relating to the reliability of optima.

- The extreme nature of some double-shrunk WAPLS*rioja* optima and their impact on reconstructions; this is avoided by the alternative method, or by the use of fxTWA-PLS which correctly applies the de-shrinking factor to the trial reconstruction.
- How coefficients move with higher components; this is intrinsic to the operation of WAPLS*rioja* and fxTWA-PLS, and does not always provide plausible optima. This is dealt with in Chapter 5, is not related to the de-shrinking issue and is not solved by the use of the alternative or fxTWA-PLS.
- Whether transfer functions as calculated by WAPLS*rioja* and fxTWA-PLS properly represent the climate preferences of the taxa. This is also dealt with in Chapter 5.

4.2.6 Taxon abundance imbalance between training set and fossil set

The de-shrinking issue identified above becomes important because of the dissimilarity of taxon abundances between training set and fossil set (Figure 4.5). Put at its most extreme, the optima are only strictly true for the set of relative abundances of the taxa in the training set. If a fossil sample has a very different balance of taxon abundances from that in the training set, which is common as will be seen in Chapter 5 and is exampled in Figure 4.5, taxa with weakly-based or improbable optima can significantly influence the reconstruction.

This problem is not obvious during calibration. The calibration process and its statistical tests only say how well the calibration succeeds in replicating the training set. Calibration attempts to make the reconstructed value for each training set sample as close to the observed environment as possible. In each sample, high-abundance taxa influence the reconstruction far more than low-abundance taxa. Taxa which do not form an important fraction of the samples they inhabit have little influence on the reconstructions of those samples. The optima of taxa with persistently low abundances or rare occurrences may therefore be unrepresentative of their true preferences.

These effects are natural and intended results of the calibration process: more frequently occurring and more abundant taxa provide better evidence of climate. The consequence when training set and fossil set differ widely in abundances, however, has not been debated.

The de-shrinking problem is not obvious when reconstructing the training set, because the effect of abnormal optima is exactly counteracted by the de-shrinking factor derived from the regression, which is weighted by the balance of taxon abundance in the training set. The overall result is arithmetically correct, and the optima never need to be looked at either in the calibration or the reconstruction. It is only when the optima are examined - as when identifying the contributions of different taxa to a sample reconstruction - that the problem becomes visible.

Many studies apparently successfully apply WA-PLS to (for instance) aquatic and marine biotic abundances and their relationship to water chemistry and temperature. This is interpreted to mean that in these cases the ranges of species abundances and of environmental variables are similar enough between the training sets and the sets to be reconstructed for the problem not to become obvious or important.

The consequence is that apparently minor taxa whose influence in the calibration process is negligible can have significant impact on reconstructions. This places more importance on the robustness of their optima, a question dealt with above in 4.2.1, and a key subject in Chapter 5.

4.3 Frequency weighted tolerance adjusted WA-PLS (fxTWA-PLS)

In future Chapters fxTWA-PLS, not WA-PLS, is used to make reconstructions. This section describes the differences between them, one of which is that fxTWA-PLS correctly applies the slope coefficient to the trial reconstruction, avoiding the optimum-de-shrinking problem in WA-PLS; another is that there is no simple expression of the taxon climate preferences it finds, which presents a difficulty when trying in Chapter 5 to test its transfer functions against abundance distributions.

Investigation of the WA-PLS processes and assumptions and their consequences were part of the motivation for the development of 'frequency weighted tolerance adjusted WA-PLS' (fxTWA-PLS) (Liu *et al.*, 2020), but the principal motivation was the observation that the training set reconstruction was still compressed in range after de-shrinking. fxTWA-PLS makes two adjustments.

Firstly, an implicit assumption in WA-PLS is that all taxa have equally wide tolerances, i.e. that the width of the unimodal distribution is the same for all taxa for a given climate gradient (Ter Braak and Juggins, 1993). This is demonstrably not the case (see Chapter 5), so fxTWA-PLS weights different taxa based on the widths of their dispersions ('tolerance weighting').

Secondly, as Turner *et al.* (2020) point out, if training sets do not sample the climate gradient evenly, this can result in a poor reading of the climate and poor transfer functions. In Turner *et al.* (2020) the proposed mitigation is to ensure as far as possible that a training set samples the climate gradients continuously and comprehensively. fxTWA-PLS recognises that in reality, training sets will not achieve sampling perfection, and weights the importance of different parts of the gradient by a factor inversely related to the frequency with which the training set samples that part ('frequency adjustment'). While fxTWA-PLS can mitigate the effect of uneven sampling, a training set which samples the climate gradient well remains a prerequisite, as demonstrated under WA-PLS in Chapter 3, Turner *et al.* (2020).

The transfer function in fxTWA-PLS is not a scalar. As shown below at Step 2 in Table 4-8, during calibration the initial trial reconstruction is made combining the initial optima and the tolerance factor; since this vector is standardised then regressed and then multiplied by the regression slope and the intercept added, the final effective optima are not available to the user, and a way has not been found of deconvolving the final reconstruction to obtain them (Mengmeng Liu, pers. comm., July 2021, April 2023). The fxTWA-PLS package provides so-called 'optima' in Step 6, but these are a memo item, not used in the reconstruction, and Liu recommends paying no attention to them (pers. comm., July 2023).

Table 4-8 fxTWA-PLS summary algorithms

fxTWA-PLS summary algorithms, R pseudocode
y = training set abundance matrix x = observed environmental vector for training set t = taxon tolerance vector (dispersion of abundance of each taxon) fx = frequency vector (no. of training set samples in each bin) %*% is the matrix multiplication operator t() is the matrix transposition function in R
Calibration for a single component:
Step 1: Calculate vector of initial taxon optima

u <- t(y) %*% x / colSums(y)
Step 2: Calculate vector of trial site scores, adjusting for tolerance r <- (y %*% (u / t ^ 2)) / (y %*% (1 / t ^ 2))
Step 3: Standardise z = mean(r) s <- sqrt(sum((r - z)^2)/ sum(y)) r <- (r- z) / s
Step 4: Regress observed against trial score, weighting for frequency of sampling lm <- MASS::rlm(x ~ r, weights = 1 / fx ^ 2)
Step 5: Record regression coefficients and obtain fit alpha<- lm[["coefficients"]] fit<- lm$fitted
Step 6: Record partial optima: standardise u, apply intercept and slope u_sd <- (u - z) / s optimum <- alpha[intercept] + u_sd * alpha[slope]
Reconstruction ('prediction') for a fossil core for a single component:
Requires from calibration: u, t, z, s, alpha y = fossil abundance matrix
Step 1: Calculate trial site scores, adjusting for tolerance r <- (y %*% (u / t ^ 2)) / (y %*% (1 / t ^ 2))
Step 2: Standardize r <- (r- z) / s
Step 3: Reconstruct fossil climate vector fit <-alpha[intercept] + alpha[slope] * r

Before considering transfer functions in more detail, note that the calibration shows that despite the improvements over WA-PLS, fxTWA-PLS cannot replicate the observed environmental vector precisely, as illustrated for gdd in Figure 4.8. The distribution lies satisfactorily on the 1:1 line, but there remains dispersion about the line and some extreme reconstructed values fall outside the observed range (313, 8112) degree days, or are even physically impossible (gdd < 0). This indicates two things:

- The abundance of pollen is not wholly controlled by this bioclimatic variable, which is not surprising; other factors are involved, which are assumed to be other bioclimatic variables, non-climatic variables, and noise.
- fxTWA-PLS is capable of providing suspect results, which may only be obvious at the extremes of a climate gradient.

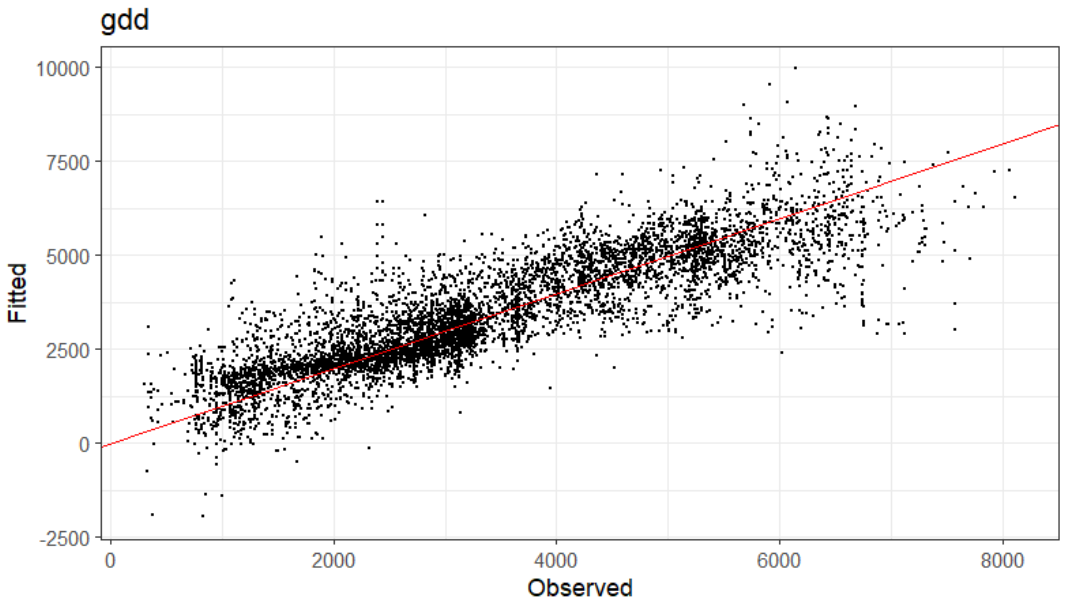

Figure 4.8 fxTWA-PLS calibration Step 4: fitted (trial reconstructed) gdd (growing degree days > 0 °C) plotted against observed gdd in SMPDS, Component 4. Red line is 1:1

4.4 (Un)availability of effective optima

Chapter 5 examines how abundance distributions exhibit the climate preferences of taxa, and seeks to compare this with the transfer functions found by WA-PLS and fxTWA-PLS; a simple example of such a comparison was given in Figure 4.7.

The 'effective optima' are those scalars which, multiplied by the taxon abundance and summed by sample, would give the reconstructed environmental vector. However, the transfer functions provided by WA-PLS and fxTWA-PLS are not expressed as scalars, except in the case of WAPLS*rioja*, which uses the de-shrunk optimum, with its attendant problems. In the case of the alternative method and fxTWA-PLS, the intercept added at the last stage of reconstruction makes it impossible to determine a scalar optimum for each taxon, and in the case of fxTWA-PLS the frequency and tolerance adjustments add further complexity. In both cases, the situation is made more complex by progressive change through the higher components.

Simpler alternatives have to substitute for the unknowable true effective optima. The simplest is the unmodified 'optimum' for Component 1, although by definition this has already suffered an indeterminable degree of shrinking.

4.5 Chapter summary

This Chapter is the first in a series designed to evaluate the robustness of quantitative reconstructions which can provide time series of variables with specific climatic meanings, which could in turn be used to identify D-Os.

The algorithms in WA-PLS are analysed and the differences between WA-PLS and fxTWA-PLS are described. The most important problem is that large differences in relative abundance between the taxa which (a) dominate the training set (b) dominate a fossil sample can result in the fossil sample reconstruction becoming dependent on weakly evidenced optima. This is compounded when WAPLS*rioja* inappropriately applies a de-shrinking factor directly to taxon optima. A method of avoiding this issue by an alternative WA-PLS reconstruction algorithm is described and evaluated.

No scalar value is available from the fxTWA-PLS transfer function to represent the position of the taxon climate preference on the climate gradient. When Chapter 5 attempts to compare pollen abundance distributions with the implicit preference, first-estimate optima which do not include all the elements used in the reconstruction have to substitute.

4.6 References

Juggins, S (2017) 'rioja: Analysis of quaternary science data'. CRAN. Available at: http://cran.r-project.org/package=rioja.

Liu, M. *et al.* (2020) 'An improved statistical approach for reconstructing past climates from biotic assemblages', *Proceedings of the Royal Society A* [Preprint]. Available at: https://doi.org/10.1098/rspa.2020.0346.

Liu, M. *et al.* (2023) 'Holocene climates of the Iberian Peninsula: pollen-based reconstructions of changes in the west–east gradient of temperature and moisture', *Climate of the Past*, 19(4), pp. 803–834. Available at: https://doi.org/10.5194/cp-19-803-2023.

Simpson, G. (2013) 'Monotonic deshrinking in weighted averaging models', *From the Bottom of the Heap* [Preprint]. Available at: https://www.fromthebottomoftheheap.net/2013/01/05/monotonic-deshrinking-in-weighted-averaging-models/ (Accessed: 30 July 2018).

Ter Braak, C.J.F. and Juggins, S. (1993) 'Weighted averaging partial least squares regression (WA-PLS) : an improved method for reconstructing environmental variables from species assemblages', *Hydrobiologia*, 269/270, pp. 485–502.

Turner, M.G. *et al.* (2020) 'The impact of methodological decisions on climate reconstructions using WA-PLS', *Quaternary Research*, pp. 1–16. Available at: https://doi.org/10.1017/qua.2020.44.

5 The representation of abundance and its application in the WA-PLS family

The reliability of WA-PLS and fxTWA-PLS reconstructions depends on their ability to utilise abundance distributions in a training set. There are two questions here. The first is how well the taxa in the training set represent the climate, a question mostly relating to the number and distribution of samples of a taxon and its abundance. The second is how the distribution of abundance exhibits climate preference and how this accords with how WA-PLS and fxTWA-PLS operate. This Chapter explores how best to describe the abundance of taxa along climate gradients in a modern pollen training set, and by applying this to the SMPDS, examines whether these abundance distributions provide reliable representations of climate preferences. Then it focusses on where and why abundances depart from the unimodal and Gaussian model implicit in WA-PLS and fxTWA-PLS, and what the consequences and mitigations are.

5.1 Gradient analysis and response patterns

The distribution of abundance of a taxon along an environmental gradient demonstrates the environment preference of the taxon. There is a substantial literature on gradient analysis and ordination, that is, methods of organising and describing distributions of abundance, or present/absence, of one or more taxa, along environmental gradients (Gauch, Whittaker and Wentworth, 1977; Ter Braak and Prentice, 1988; Oksanen and Minchin, 2002; Jansen and Oksanen, 2013).

Ter Braak and Prentice (1988) describe three families of gradient analysis methods where an environmental variable is already known; firstly, linear response models, which are statistically simple but are of limited practical use since few biotic responses are linear; secondly, those which use a unimodal, Gaussian-like response model; and lastly, those based on weighted averaging, which they describe as heuristic.

Hill (1973) introduced reciprocal averaging (RA), also known as correspondence analysis (CA), which implicitly assumes a linear response. Starting with a vector of arbitrary values, by iteratively averaging taxon (column) scores and sample (row) scores it converges on a stable vector, to which the abundances appear to respond. This vector then must be interpreted in some physical sense; this is termed indirect gradient

analysis. ter Braak (1986) developed this further into Canonical Correspondence Analysis (CCA) by adding regression techniques. Two further ordination techniques, Principal Components Analysis (PCA), which assumes linear responses, and Detrended Correspondence Analysis (DCA), which assumes a unimodal response and is a development of RA (ter Braak, 1986), were described and applied in Chapter 2 to summarise pollen abundance matrices.

fxTWA-PLS is the current end-point development of weighted averaging, CCA, and partial least squares. It retains the implicit assumption that the distribution is unimodal and Gaussian or approximately so (Ter Braak and Juggins, 1993).

The typical shape of abundance along the environmental gradient is often assumed to be approximately unimodal and symmetrical and approximately Gaussian (Shelford, 1931; Gauch, Whittaker and Wentworth, 1977; Braak and Looman, 1986). This model has convenient mathematical properties. However, abundance distributions often depart from this symmetrical pattern, and response models other than symmetrical unimodal have been fitted to ecological data. Huisman, Olff and Fresco (1993) describe five response models (no trend/null response, two types of sigmoidal monotonic change, symmetrical unimodal, and skewed unimodal). Oksanen and Minchin (2002) found that the responses of less than half of the taxa studied in a Tasmanian plant dataset could be fitted by a Gaussian model, and skewness was often present. Bjune *et al.* (2010), applying the same models to Norwegian pollen abundance-climate relationships, found that only a minority of abundance patterns could be characterised as symmetrical unimodal. Jansen and Oksanen (2013) added two further bimodal models based on analysis of a large set of data relating plant abundances to soil pH.

In this Chapter, since the WA-PLS family consider a single bioclimatic gradient at a time, the interest lies mostly in the response curve of individual taxa (a 1-D approach). This approach is a potential weakness, since plants respond to multiple climatic and other variables. Although in principle the ideas can be extended to multiple dimensions, this is not pursued here.

The climate variables considered here are growing degree days above 0 °C (gdd), mean temperature of the coldest month (MTCO, or synonymously in this project Tmin or tmin) and the square root (rtmi) of Moisture Index, which is the ratio of actual evapotranspiration to potential evapotranspiration.

5.2 Substitute for true optima

Chapter 4 showed that no scalar value is available which represents the position of the environmental 'optimum' underlying the transfer function provided by WA-PLS or fxTWA-PLS. The simplest substitute for this unknowable true optimum found by WA-PLS and fxTWA-PLS is the mean climate in which the taxon is found, weighted by abundance (abundance-weighted mean, '*awm*'). The algorithm finding this is described in Table 4-1 at Step 2 for WA-PLS: 'Calculate new species scores (u^*_k)', for the first component', and Table 4-8 at Step 1 for fxTWA-PLS. The mean climate value must be added back; using the variables in the fxTWA-PLS calibration, *awm = u[,1] + meanx*. In Chapter 4 it was noted that the range of these values has been shrunk to an undeterminable degree.

5.3 Distilling abundance along a gradient

5.3.1 Scatterplots

The simplest representation of the abundance of a taxon in a training set is a scatterplot. Figure 5.1 shows these for *Picea*, an example of a frequently occurring taxon in the SMPDS v1 modern pollen training set. The abundance distribution of this taxon is assumed to represent its climate preferences well since it occurs in nearly half of the samples in the SMPDS, which in Chapter 3 was seen to sample a wide climate space. These scatterplots can be compared with the overall sampling density of the gradients by SMPDS in the histograms in the lower panels. *Picea* is a single genus, which limits the risk that the distribution conflates genera with potentially different behaviours.

This figure demonstrates some important features of real abundance distributions.

- The picture is more complex than a symmetrical unimodal curve.

- Even in an apparently preferred region of the gradient, there are many instances of low abundance; conversely, there are few regions where the taxon is not found, and there can be instances of high abundance well away from the preferred regions.
- Nevertheless, abundances can show climate preferences: taking the position of the abundance-weighted means, *Picea* prefers cooler gdd and wetter soil than the average taxon (shown in the lower panel histograms).
- One of the distributions (Tmin) appears bimodal.

Scatterplots do not allow us to summarise abundance distributions by drawing a line through, or an envelope round, the points.

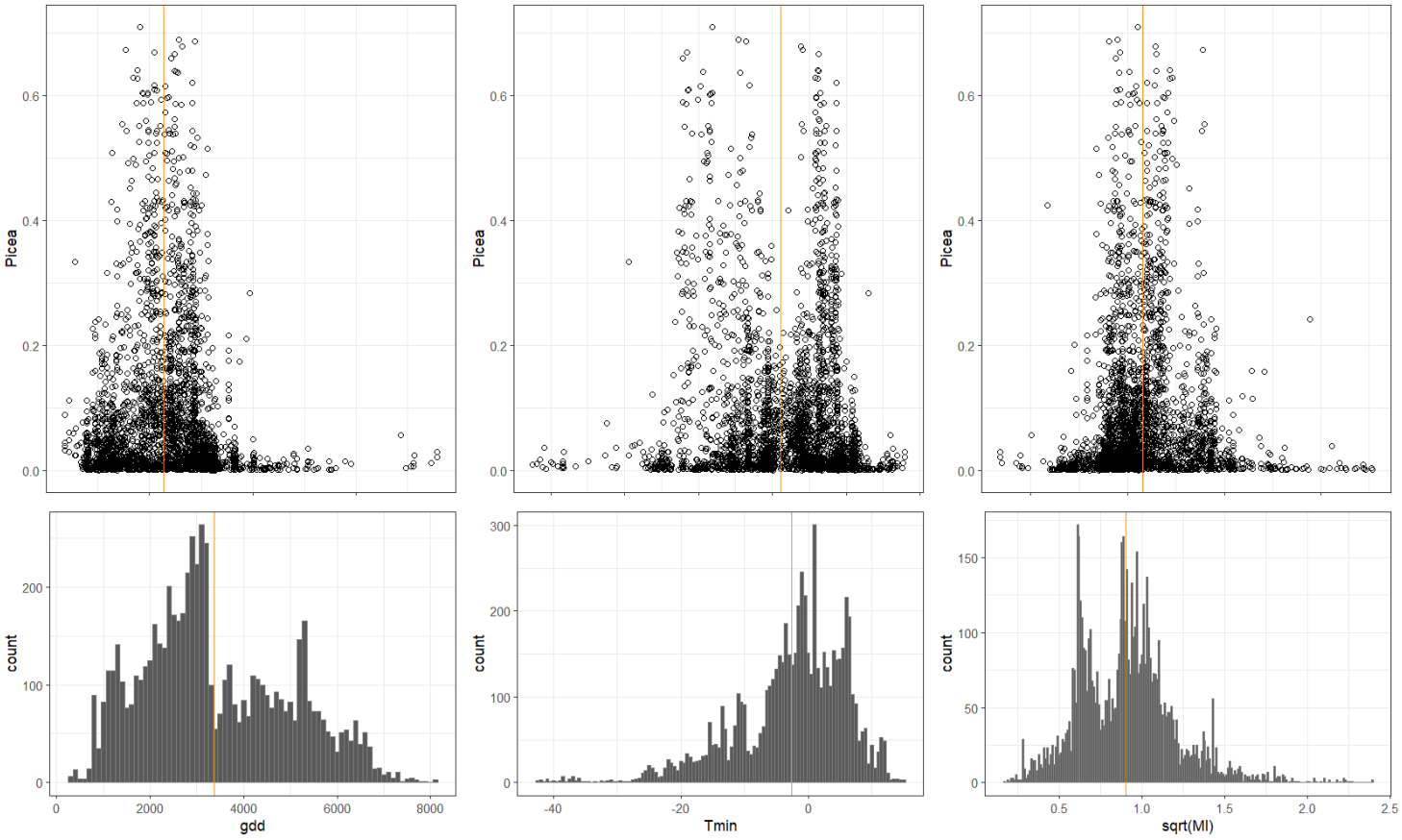

Figure 5.1 Upper panels: Abundance of Picea *as fraction of total pollen count in a sample for each SMPDS sample including* Picea*, against modern climate at that point; gdd = growing degree days above 0 °C, Tmin = mean temperature of the coldest month (MTCO) in °C; sqrt(MI) = square root of Moisture Index, which is actual evapotranspiration / potential evapotranspiration. Orange vertical line: mean climate, weighted by abundance (*awm*). Lower panels: histograms of counts of samples in SMPDS (n = 6458) showing how densely the gradients are sampled at different points. Orange vertical line: mean climate, weighted by observations.*

5.3.2 Shapes versus means

The orange vertical line in Figure 5.1 upper panels is the mean climate in which the taxon is found, weighted by abundance (abundance-weighted mean, '*awm*') for Component 1.

Neither WA-PLS nor fxTWA-PLS test the shape of the distribution, despite their ultimate reliance on the unimodality and symmetry of the shape. Departure from this shape, for instance by skewness or multimodality, may result in a misleading or meaningless optimum. To understand whether a taxon's shape is problematical, its abundance distribution must be described in a way which identifies such departures.

5.3.3 Simple 1-D case

The aim is to develop a smooth curve which represents the abundance along the gradient. It must not be too stiff, since this may disguise multiple peaks in response, and can introduce cliffs at the edge of the observed range, where a few high values occur near the ends of the gradient. It must be sufficiently stiff that it usefully exhibits modes and does not overfit. There is no useful statistical test of the ideal degree of smoothing.

There are many smoothing techniques available, such as moving averages using different weighting systems (e.g. kernel smoothing), polynomial curve fitting, and local regressions methods such as loess. These are partially controllable by specifying the width and shape of the weighting or the span or the style of the regression. If the gradient is treated as a continuous variable, none of these techniques perform well when applied directly to the abundances. This is illustrated in Figure 5.2. A loess curve with span = 0.3 and a Generalised Additive Model (GAM) curve are fitted to the data, and neither appears to represent well either the visual pattern, the abundance-weighted mean, or the pattern of occurrences along the gradient shown in the histogram. As with many smoothing mechanisms, the ends of the series lack data and can show instability. This poor ability to summarise abundance arises because neighbouring samples record very different abundances.

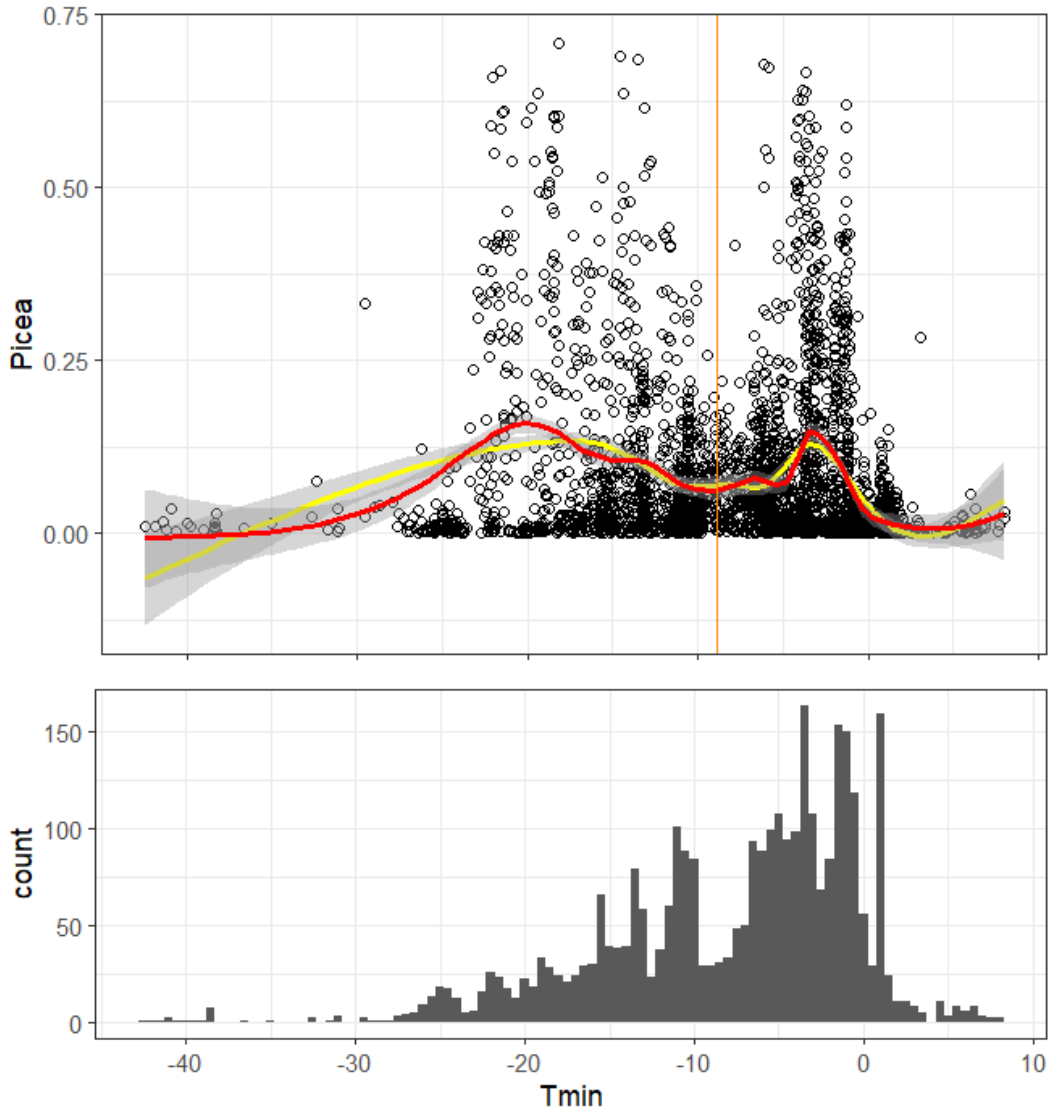

Figure 5.2 Upper panel: Picea *fractional abundance along Tmin gradient, with attempted summarisation by loess, span = 0.3 (red curve) and GAM (yellow curve). Orange vertical line: abundance-weighted mean Tmin. Lower panel: occurrence of* Picea *samples along gradient (binwidth 0.5 °C).*

5.3.4 Binning

This is mitigated by summarising abundance into bins along the gradient.

Figure 5.3 shows that summing the abundances in the bin is greatly influenced by the number of occurrences in the bin, which in turn is greatly influenced by how the SMPDS as a whole samples the climate gradient (Figure 5.1). Therefore a histogram or pdf of the summed abundances does not meet the need to describe the climate preference.

A mean of the abundances in each bin, on the other hand, demonstrates a taxon's average preference for that small part of the gradient, and this is the best basis on which to construct a curve. The mean

abundance of the taxon in each bin is calculated by reference to the number of all samples found in the bin, which is here denoted *fxab*. The example in Figure 5.3 is *fxab*.

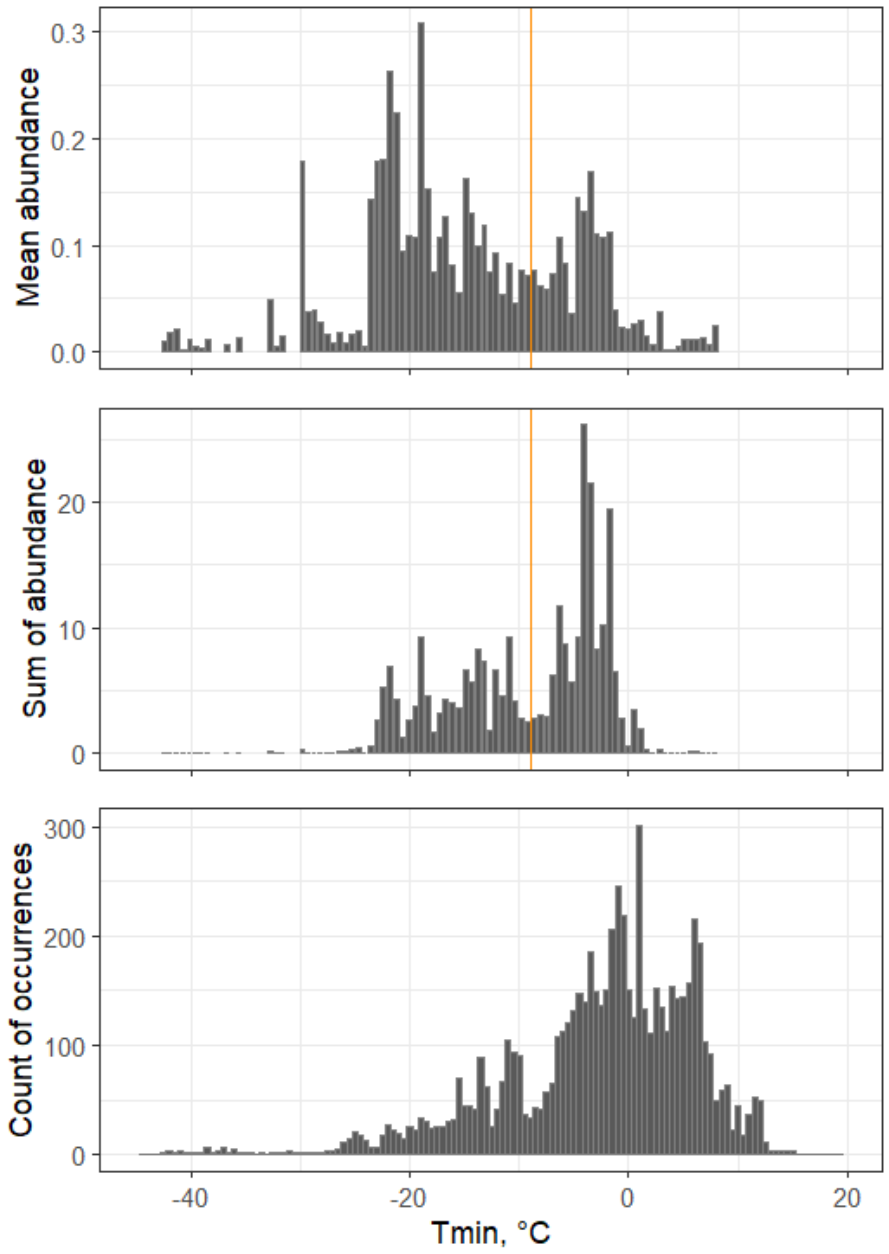

Figure 5.3 From the bottom: simple histogram of counts of occurrences of Picea in SMPDS, binned at 0.5 °C intervals; sums of fractional abundances in bins; means of fractional abundances in bins. Orange vertical line: abundance-weighted mean Tmin.

A measure other than mean might be considered applicable, for instance the top quartile, or the maximum (see the discussion in Chapter 2, where distance measures are combined). The argument is that if high abundances are present in a bin, then the climate is self-evidently suitable for the taxon, and low abundances may be the consequence of other factors and are of lesser importance. Figure 5.4 shows that in practice, for this taxon (and the condition is replicated in many others) the mean and the upper and

lower quartiles travel in company. It was concluded that there was no advantage in using anything but the mean.

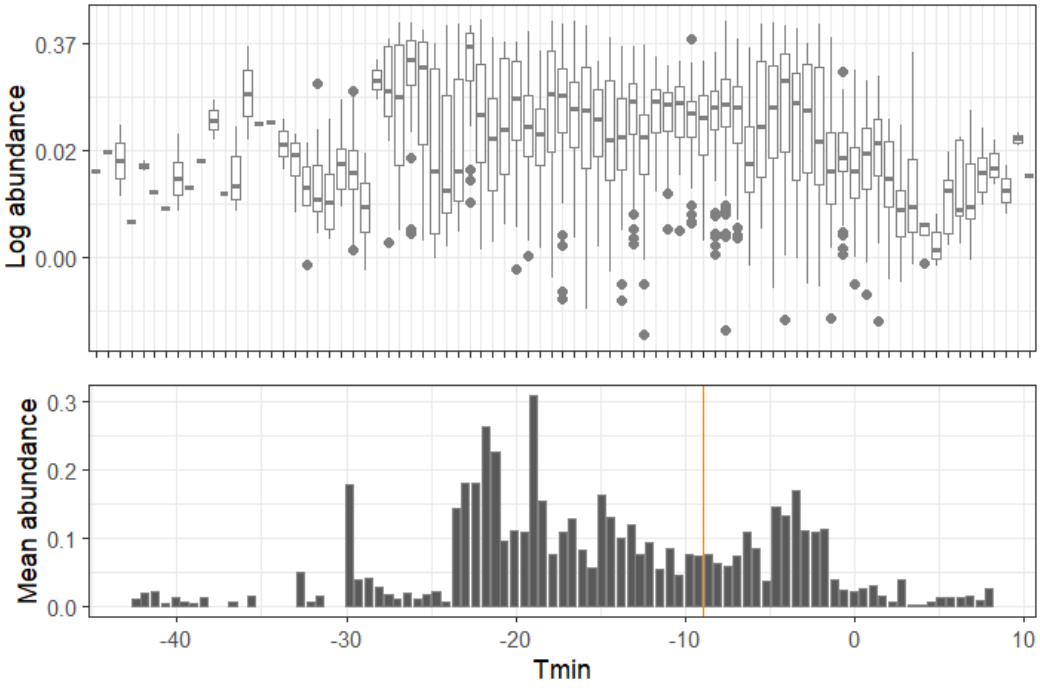

*Figure 5.4 Distribution of abundances of Picea in each bin: lower panel: mean binned abundance (*fxab*); upper panel, boxplots of distribution, on log scale. X axes not precisely aligned.*

It is already clear that the abundance-weighted mean climate (orange vertical line) at -9 °C, identified by fxTWA-PLS, may not usefully represent the preferred climate of *Picea*, which is widely tolerant and is commonest around ~-20 °C and ~-4 °C.

The absolute values of *fxab* vary with the total abundance of the taxon in the SMPDS training set, and for consistency between taxa they can be expressed as a fractional abundance, *fxabf*, which is *fxab* divided by the sum of *fxab* for that taxon, so that the sum of *fxabf* for each taxon is 1.

5.3.5 Smoothing

Having chosen fractional mean binned abundances as the basis of the curve, there are then two smoothing considerations: bin widths, and the smoothing method and its stiffness.

Dividing a gradient into ~ 100 bins strikes a sensible balance between computational run time and sensitivity. Large bins e.g. n < 50 tend to fail to show modes well; small bins e.g. n > 300 result in

neighbouring bin means which vary greatly, and merely move the smoothing load to the smoothing method.

The bin widths used in fxTWA-PLS v1 are adopted here, for ease and for consistency when comparing with fxTWA-PLS products:

- For gdd, 50 degree days
- For Tmin, 0.5 ^{o}C
- For rtmi, 0.01 (dimensionless units).

Many smoothing methods are available. Loess gives a smooth curve and provides a standard error of the fit, though near the ends of the gradient, where data become sparse, the s.e. expands and the polynomial becomes unreliable. GAMs are highly similar to loess for degree 2 polynomial with spans in the ranges evaluated, and loess is preferred as simpler to implement. All smoothing methods produce similar results if smoothing parameters are chosen carefully, but rolling means and kernel smoothing remain locally rough, unless parameters are set so wide that modal behaviour becomes invisible.

No statistical test is available which optimises the balance between closeness of fit and ability to demonstrate modal behaviour since the latter is not quantifiable, and the choice is made by judgement. The span parameter can be chosen by minimising a value, for instance the sum of squares of the residuals, but this will follow the points very closely and will overfit (typical suggested span = 0.04). Figure 5.5 shows loess curves using three spans, 0.3, 0.5 and 0.75, for 9 abundant taxa taken as examples. The span significantly affects the visibility of modes; in general, span = 0.3 yields too flexible and 0.75 too stiff a curve, and span = 0.5 tends to demonstrate the modal behaviour adequately. In the plots in section 5.4 more than one span is shown to give a more comprehensive picture.

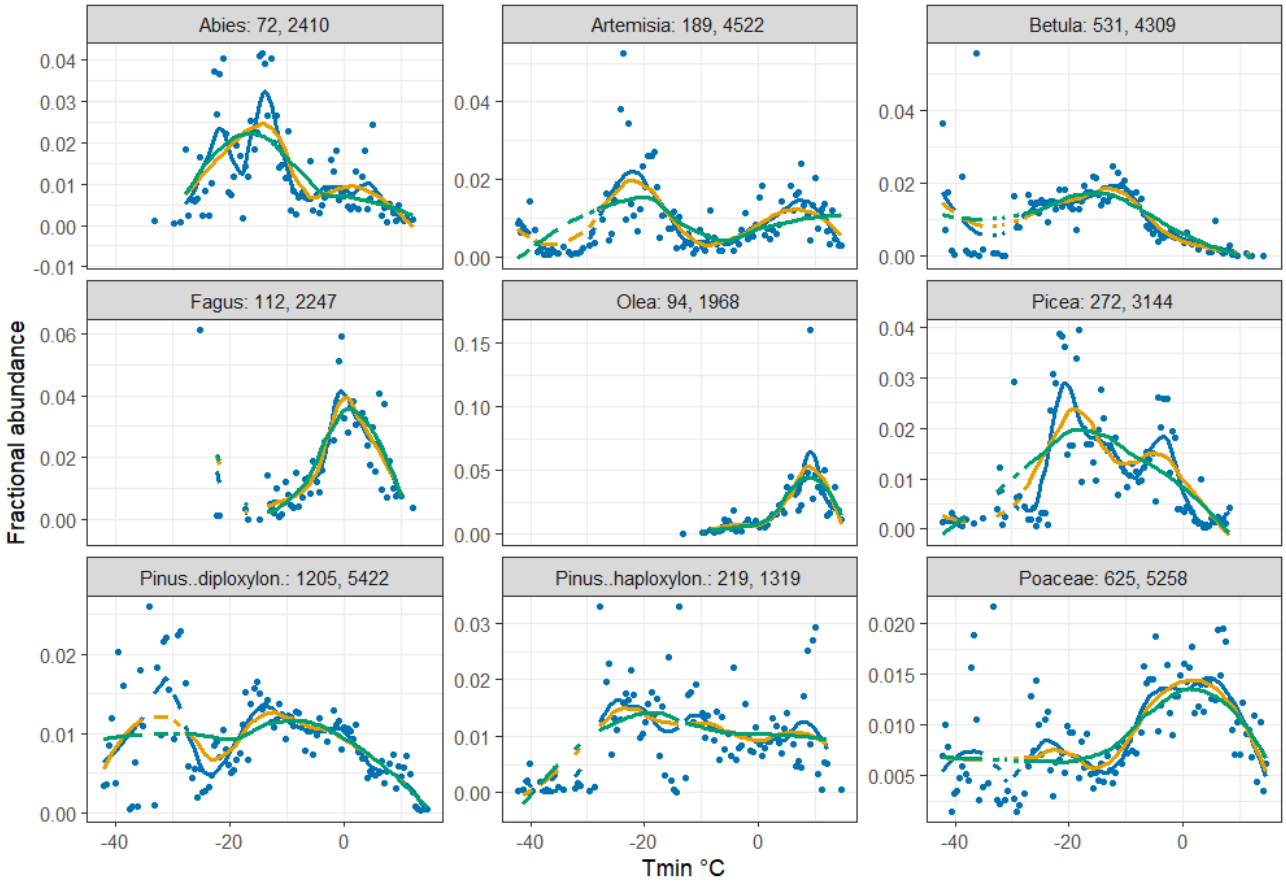

Figure 5.5 Response curves of 9 abundant taxa in the SMPDS by abundance to Tmin (MTCO, temperature of the coldest month), using different loess spans. No weighting is applied. Numbers in headings are respectively the sum of fractional abundances of the taxon and the number of occurrences of the taxon in SMPDS (number of SMPDS samples = sum of fractional abundances = 6458). Points: fxabf *(fractional mean binned abundance). Blue line: loess curve, span = 0.3; orange line: loess curve, span = 0.5; green line: loess curve, span = 0.75.*

5.3.6 Sampling frequency

Chapter 3 (Turner et al 2020) showed that adequate sampling of climate space is important in providing robust taxon abundance distributions, and the distribution of taxon samples along the modern pollen climate gradient depends partly on how densely each part of the gradient is sampled by the training set.

The mean binned value *fxab* does not consider sampling density, attributing equal importance to each bin however many samples it contains, and the use of *fxab* without adjusting for frequency is consistent with the WA stages of both WA-PLS and fxTWA-PLS. fxTWA-PLS responds to possible uneven sampling by applying a frequency adjustment late in the process.

The robustness of the mean abundance of each bin is a function of the number of samples in the bin (frequency) and how well each bin mean fits with its neighbours. One possible response is to weight the loess curve by the frequency, which is determined by counting the samples of each taxon in each bin of the

climate gradient. This evidences the frequency with which the given taxon samples the climate, rather than how the whole SMPDS samples the climate. This weighting has limited impact (Figure 5.6) since the regressions are local. The differences between curves which are unweighted, weighted by the reciprocal of the square root of frequency and weighted by the reciprocal of frequency are small. On the basis that frequency varies greatly across bins, the square root option is preferred.

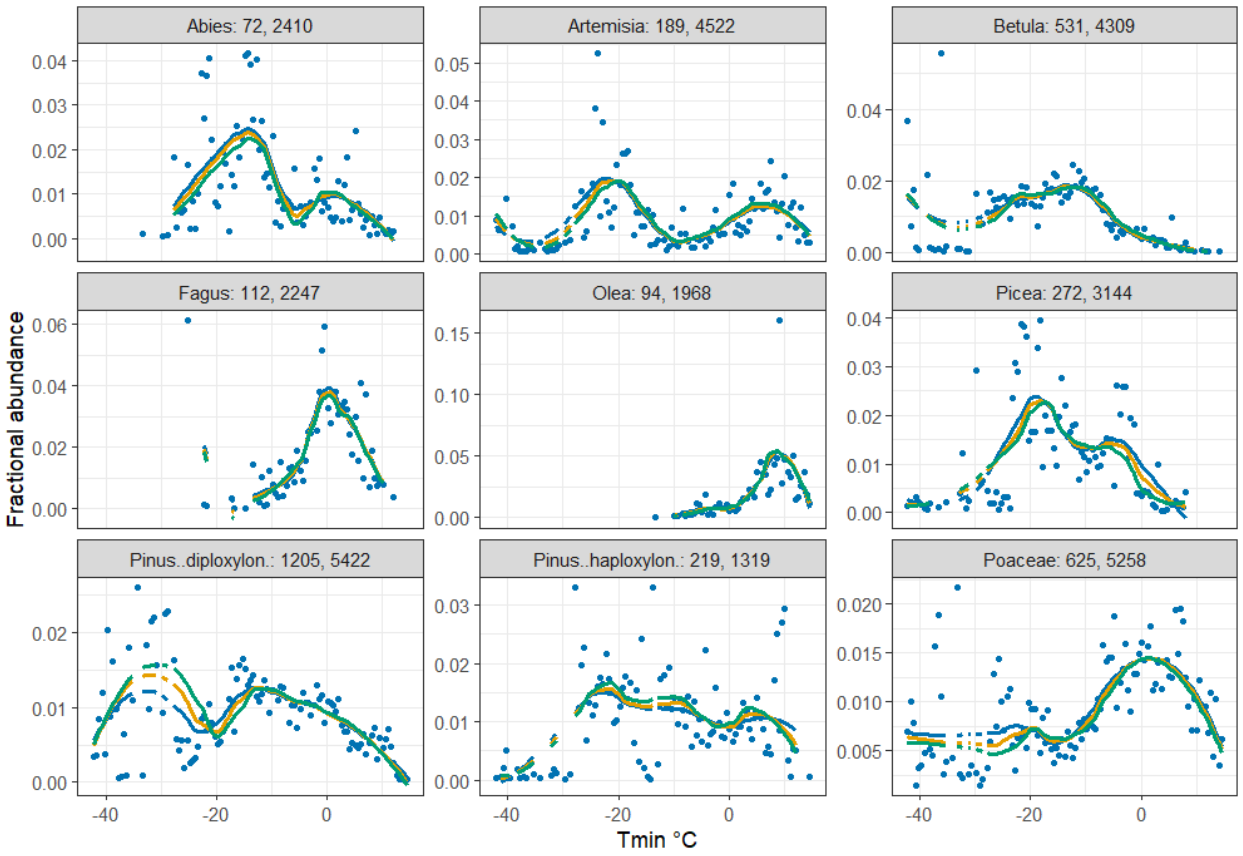

Figure 5.6 Response curves of 9 abundant taxa in the SMPDS by abundance to Tmin (MTCO), using different loess weightings: span = 0.5 in all cases. Numbers in headings are respectively the sum of fractional abundances of the taxon and the number of occurrences of the taxon in SMPDS (number of SMPDS samples = sum of fractional abundances = 6458). Points: fxabf *(mean binned fractional abundance). Blue line: loess curve, no weighting; orange line: loess curve, weighted by square root of frequency; green line: loess curve, weighted by frequency.*

The confidence intervals of the weighted loess curve are tested in Figure 5.7, and are found to be narrow.

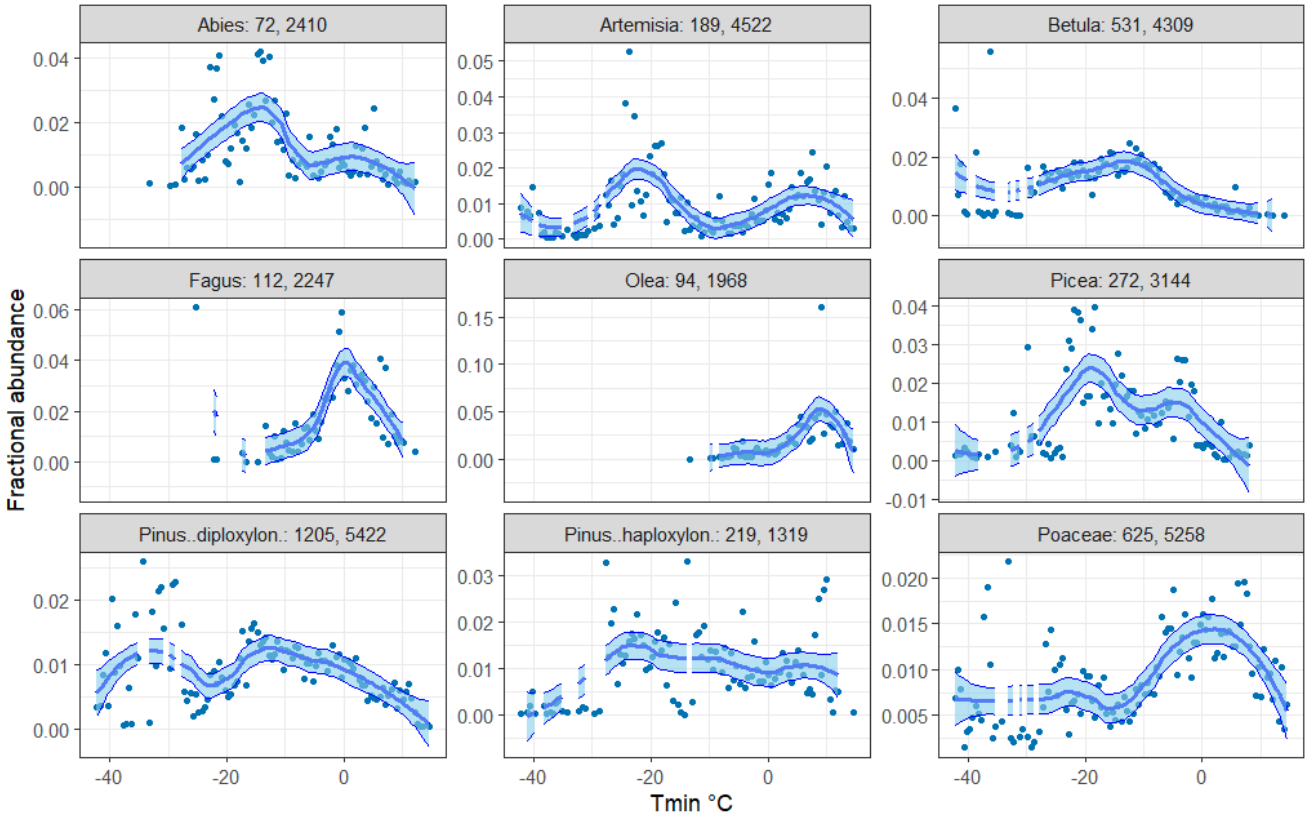

Figure 5.7 Response curves of 9 abundant taxa in the SMPDS by abundance to Tmin (MTCO), using loess weighting = 1/square root of frequency, and span = 0.5. Numbers in headings are respectively the sum of fractional abundances of the taxon and the number of occurrences of the taxon in SMPDS (number of SMPDS samples = sum of fractional abundances = 6458). Points: fxabf *(mean binned fractional abundance). Blue line: loess curve; ribbon = ± 2 SD provided by loess calculation.*

5.4 Results of applying loess curves to abundant taxa

Figure 5.8 shows the response of the 24 taxa with the greatest total abundances in the SMPDS training set, using *fxabf*, to Tmin (or MTCO), Figure 5.9 to gdd and Figure 5.10 to rtmi. These taxa represent 83% of the total abundance across the 195 taxa in the SMPDS v1 training set. The loess curves, using three different spans, are compared with the *awm* selected by fxTWA-PLS. The plots for the 138 taxa in the SMPDS (out of the total of 195 taxa) with summed fractional abundances in excess of 0.5 (an arbitrary cut-off) are given in Appendix A.

Several different response behaviours emerge:-

- Approximately unimodal responses (e.g. for Tmin: *Betula, Castanea, Fagus*), some nearly symmetrical and some more skewed

    - The locations of obvious modes reflect the known range preferences of the taxa: e.g. *Abies* and *Betula* are cold-temperate trees, *Fagus* is a temperate tree and *Olea* is a warm-temperate tree.
- Ramps, or highly skewed distributions: the response reaches its high point at or near the edge of the gradient (e.g. for Tmin: Amaranthaceae, Asteroideae, Cichorioideae)
    - Were the gradient only narrowly sampled, these might represent truncation of the realised niche (see Turner *et al.*, 2020), but the sampled gradient has a wide range, making this unlikely.
- Multimodal response, where different loess spans may give different pictures (e.g. for Tmin: *Abies*, *Quercus* deciduous). This shades into…
- … unclear preferences or insensitivity, ranging from wide tolerance (e.g. for Tmin: Cyperaceae) to no clear preference: e.g. Apiaceae, Ericaceae, *Salix.*

These align broadly with the HOF models of Huisman, Olff and Fresco (1993) and Jansen and Oksanen (2013) (symmetrical unimodal, skewed unimodal, two types of sigmoidal monotonic change, bimodal, and no trend/null response). However, the eHOF R package (Jansen and Oksanen, 2013) assigns all taxa in the SMPDS for all three bioclimatic variables to model Type I, which is 'no trend/null response', whether applied to the mean binned abundances (*fxab)*, the fractional mean binned abundances (*fxabf*), or the points defining the weighted loess curve (span = 0.5). In all cases a GAM is preferred. This is interpreted to mean that the patterns in the SMPDS data may be too complex for this package to handle, and supports our use of loess, which under these conditions is effectively indistinguishable from GAM.

The locations of the abundance-weighted means (*awm*) reflect the differences in response.

- Symmetrical unimodal responses place the *awm* close to the mode, e.g. Tmin: *Fagus, Quercus* evergreen, Polemoniaceae.

- Skewed unimodal responses and their extreme expression, ramp responses, attract *awms* which lie nearer the centre of their distributions than where the highest preference is expressed; e.g. for Tmin: Amaranthaceae, Asteroideae, Cichorioideae, Cupressaceae, *Carpinus betulus*.
- Bimodal responses place the *awm* between the modes, e.g. for Tmin: *Artemisia, Picea*.
- Insensitivity, and curves which are neither unimodal nor ramp but a more complex or indeterminate shape, result in *awms* which tend to miss the mode, if any, and end up in the middle of the distribution. e.g. for Tmin: *Alnus,* Cyperaceae*, Calluna*, Ericaceae.

Loess curves with spans of 0.3 (blue), 0.5 (orange) and 0.75 (grey) are shown in these figures. In most cases the qualitative differences between them are not great and the same pattern (unimodal, ramp, multimodal, or inconclusive) is seen in each. In some cases, however, such as *Picea, Quercus* deciduous and Poaceae, span = 0.3 and 0.5 show bimodality when span = 0.75 does not. This suggests that the lower-value spans more usefully exhibit important behaviours at the scales of the gradients under study, and typically span = 0.5 is used going forward.

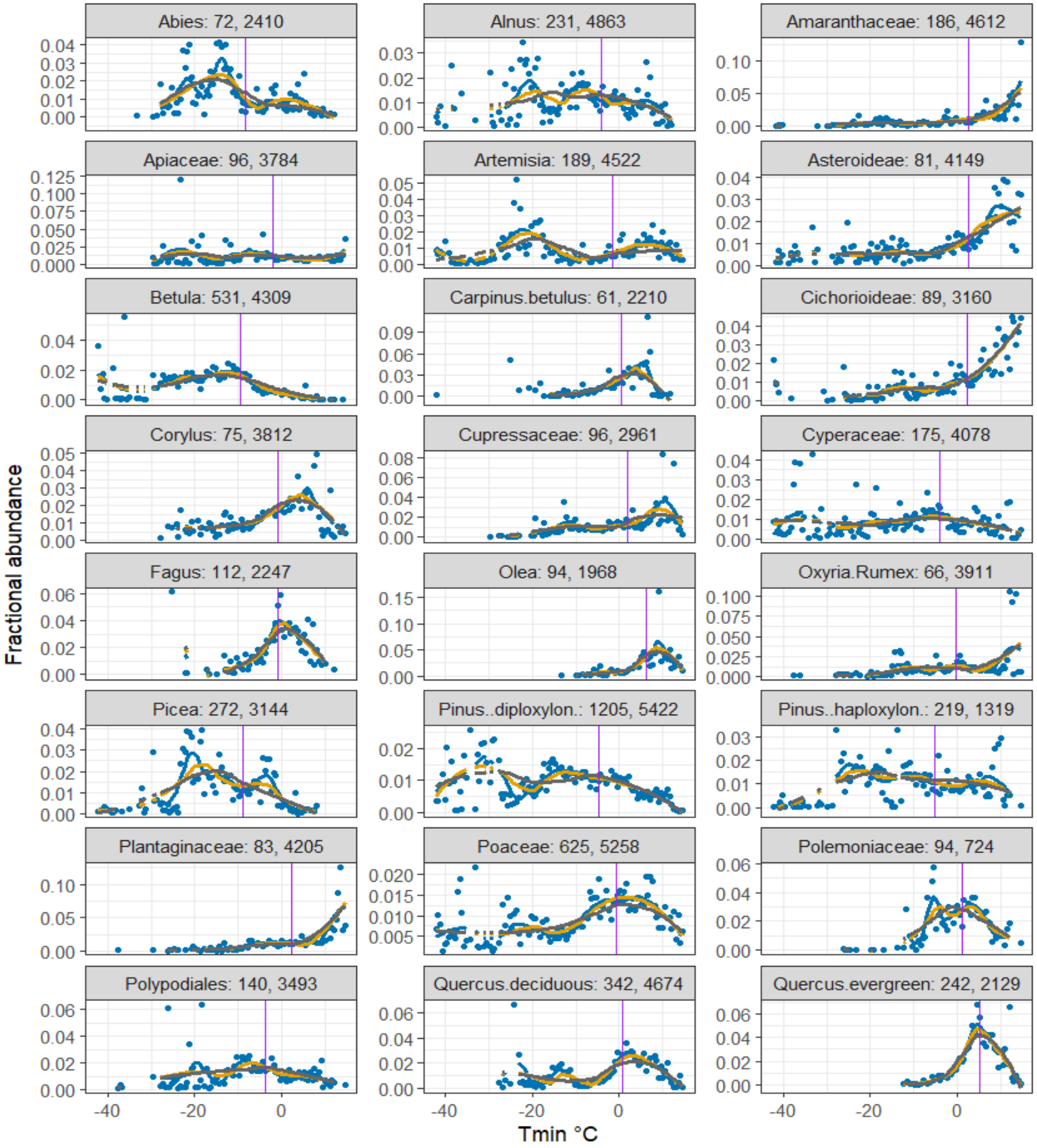

Figure 5.8 Response curves of top 24 taxa in the SMPDS by abundance to Tmin (MTCO). Numbers in taxon headings are respectively the sum of fractional abundances of the taxon and the number of occurrences of the taxon in SMPDS (number of SMPDS samples and sum of fractional abundances = 6458). Points: fxabf *(mean fractional binned abundance). Blue lines: loess curve, span = 0.3; orange lines; loess curve, span 0.5; grey lines: loess curve, span = 0.75. Vertical line: fxTWA-PLS abundance-weighted mean for component 1 (*awm*).*

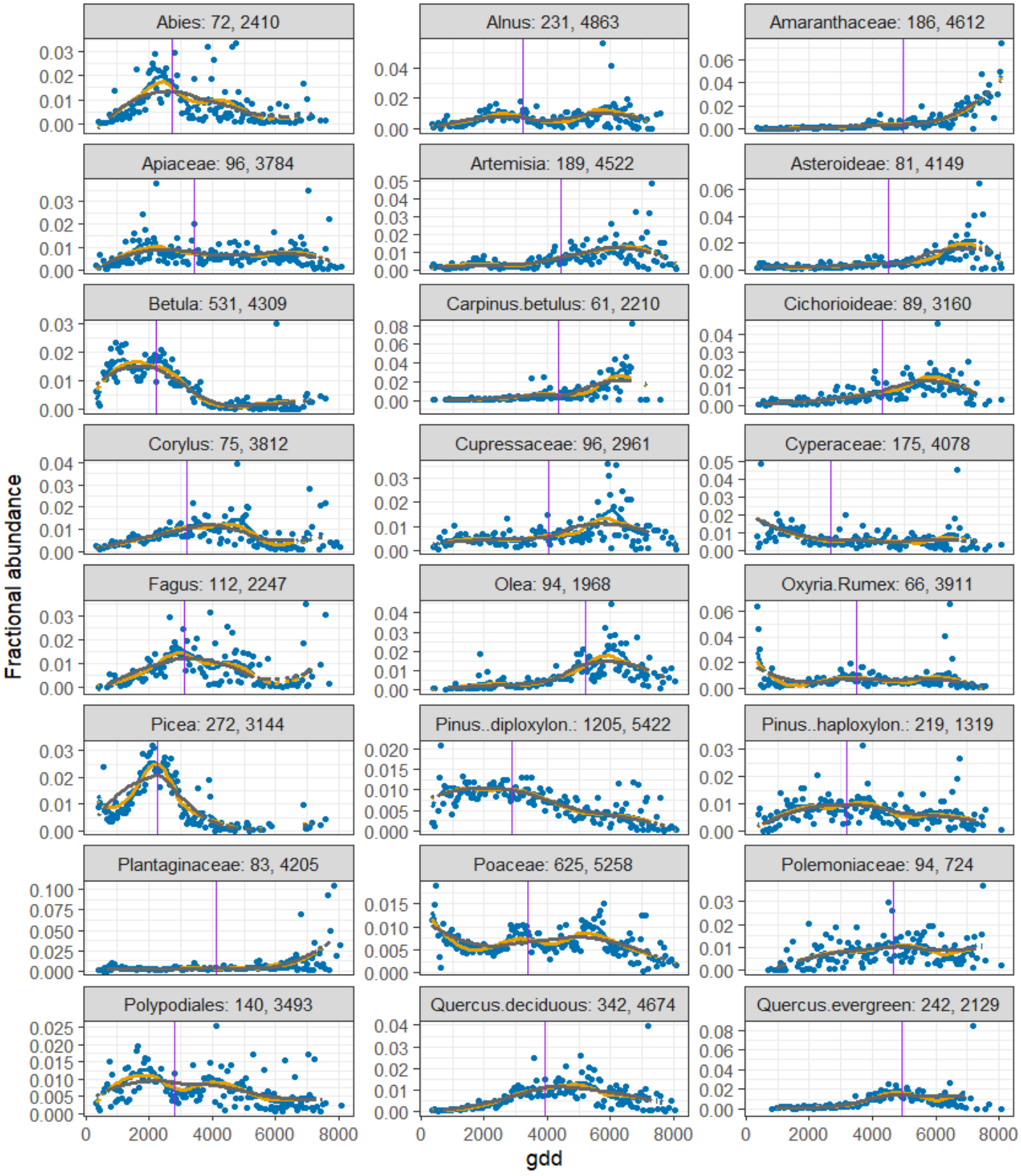

Figure 5.9 Response curves of top 24 taxa in the SMPDS by abundance to gdd. Numbers in taxon headings are respectively the sum of fractional abundances of the taxon and the number of occurrences of the taxon in SMPDS (number of SMPDS samples and sum of fractional abundances = 6458). Points: fxabf *(mean fractional binned abundance). Blue lines: loess curve, span = 0.3; orange lines; loess curve, span 0.5; grey lines: loess curve, span = 0.75. . Vertical line: fxTWA-PLS abundance-weighted mean for component 1 (*awm*).*

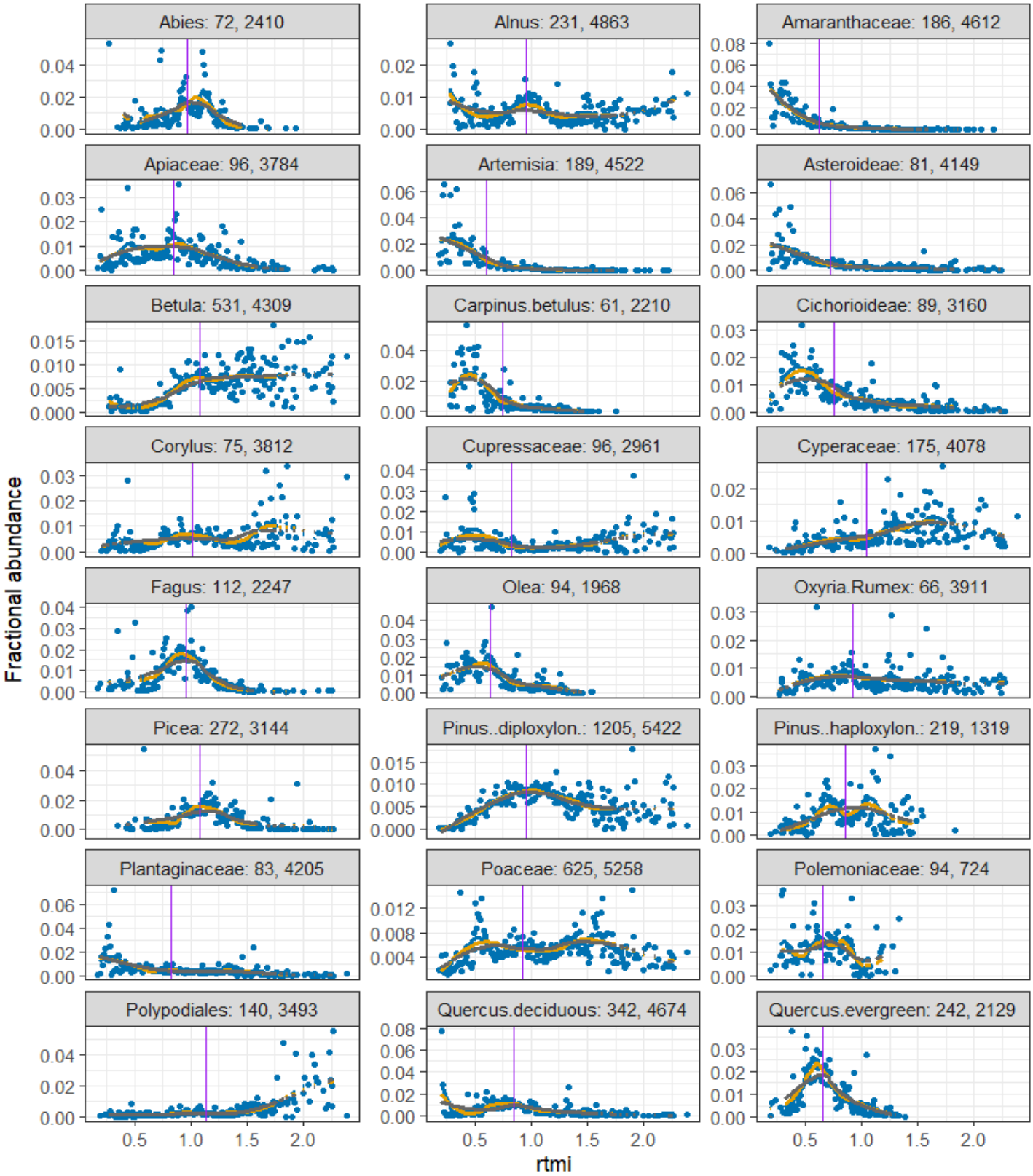

Figure 5.10 Response curves of top 24 taxa in the SMPDS by abundance to sqrt(Moisture Index). Numbers in taxon headings are respectively the sum of fractional abundances of the taxon and the number of occurrences of the taxon in SMPDS (number of SMPDS samples and sum of fractional abundances = 6458). Points: fxabf *(mean fractional binned abundance). Blue lines: loess curve, span = 0.3; orange lines; loess curve, span 0.5; grey lines: loess curve, span = 0.75. Vertical line: fxTWA-PLS abundance-weighted mean for component 1 (*awm*).*

In Figure 5.11, Figure 5.12 and Figure 5.13, the robustness of the curves of these 24 abundant taxa to differences in the training set is tested, by bootstrapping the SMPDS sample set 500 times with replacement, each time recalculating the binned mean abundances and the loess curves. The narrow ± 2 SD blue ribbons show the curves are stable. Span = 0.5 was chosen as the most useful in showing behaviour, but other spans yield the same picture of stability. There appears little difference in the robustness of the curves between different bioclimatic variables, though perhaps Tmin shows wider uncertainties. All variables show instability at the edges of the gradient.

Bootstrapped curves for all 138 taxa with summed abundances > 0.1 in the SMPDS are given in Appendix B.

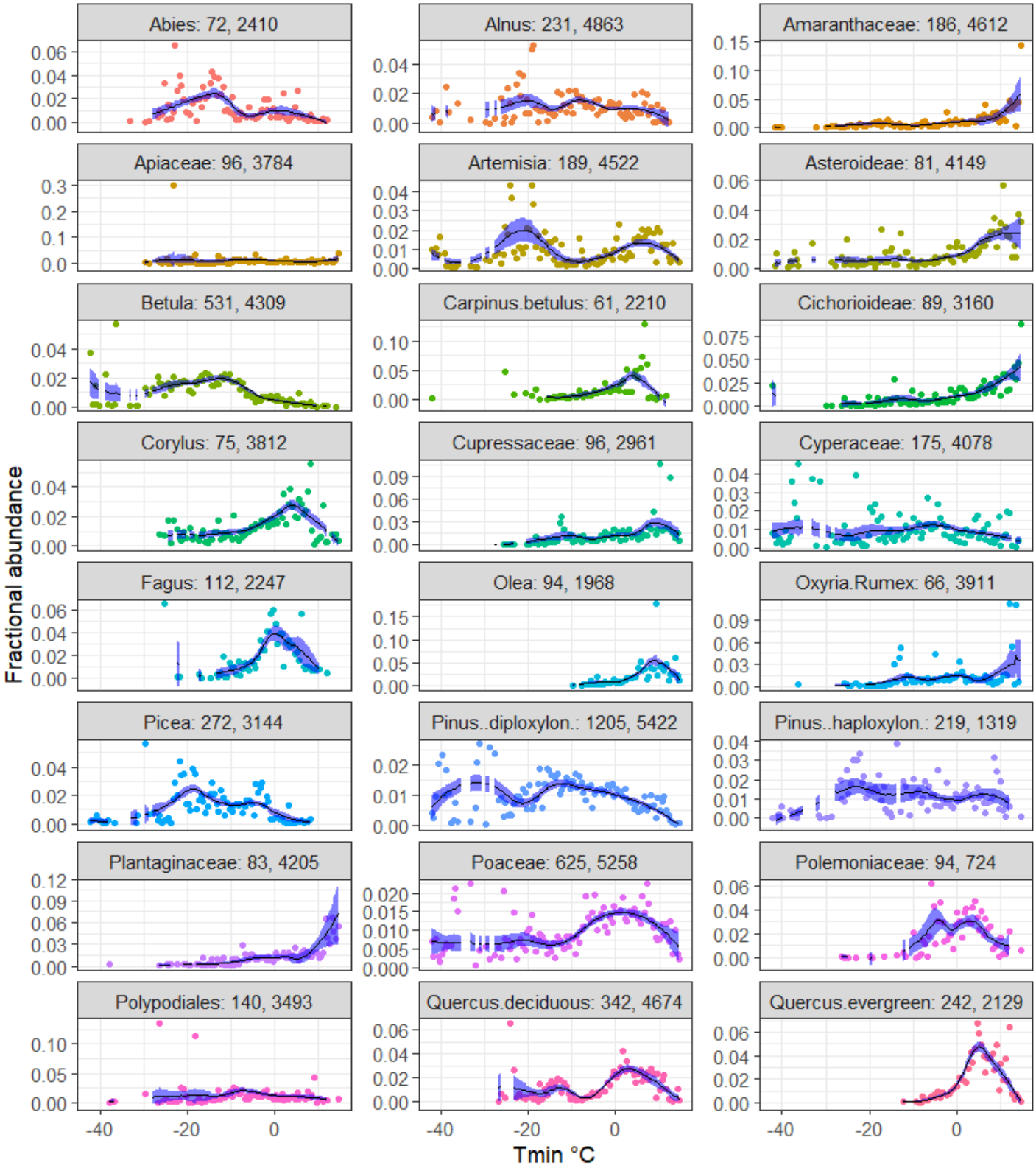

Figure 5.11 Bootstrapped response curves of top 24 taxa in the SMPDS by abundance to Tmin (MTCO, temperature of coldest month). Numbers in taxon headings are respectively the sum of fractional abundances of the taxon and the number of occurrences of the taxon in SMPDS (number of SMPDS samples = sum of fractional abundances = 6458). Points: fxabf *(mean fractional binned abundance of SMPDS set). Black line: loess curve, span = 0.5, weighting 1/square root of frequency. Blue ribbon: mean ± 2 SD of loess curve resulting from bootstrapping.*

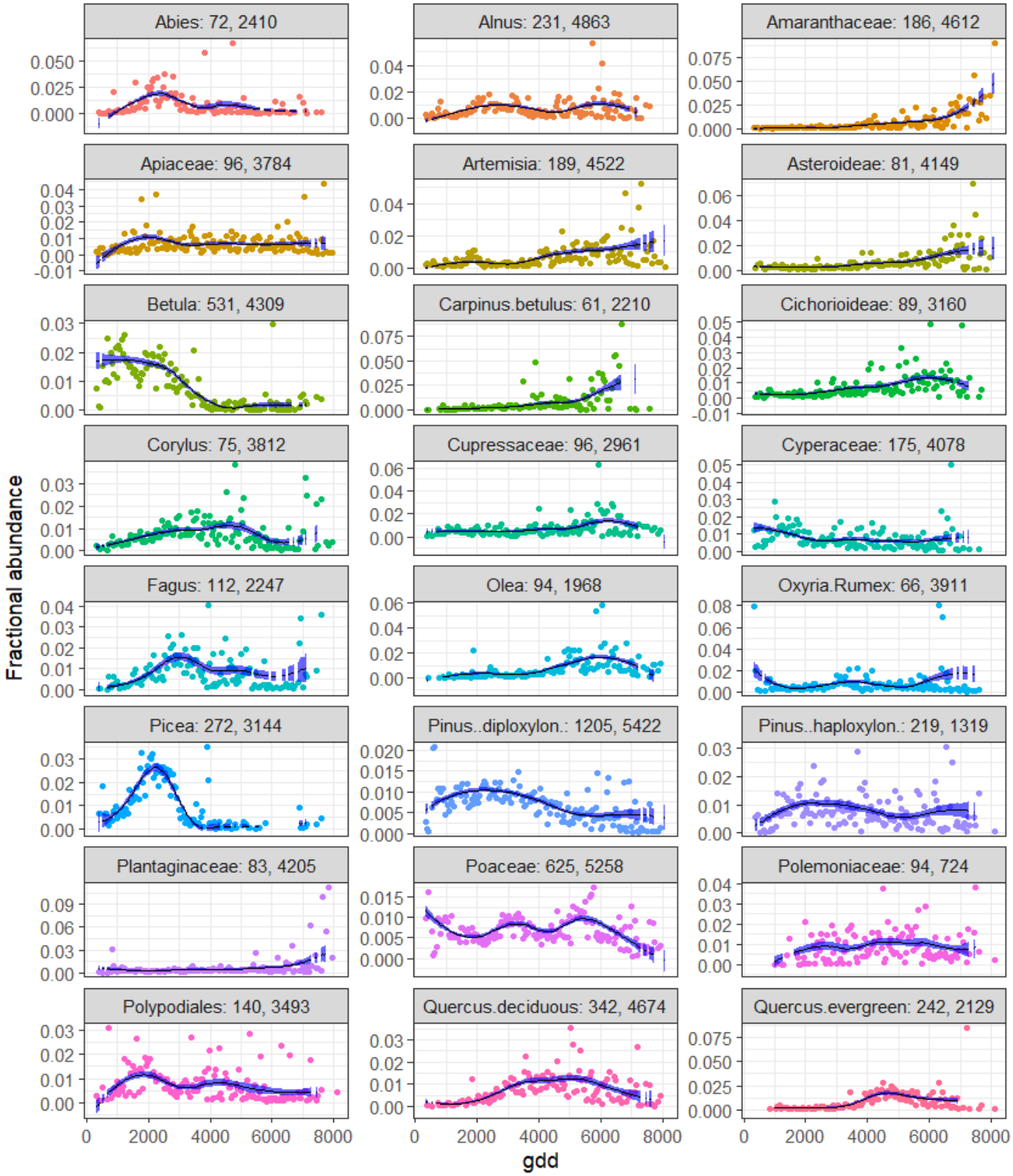

Figure 5.12 Bootstrapped response curves of top 24 taxa in the SMPDS by abundance to gdd (growing degree days > 0 °C). Numbers in taxon headings are respectively the sum of fractional abundances of the taxon and the number of occurrences of the taxon in SMPDS (number of SMPDS samples = sum of fractional abundances = 6458). Points: fxabf *(mean fractional binned abundance of SMPDS set). Black line: loess curve, span = 0.5, weighting 1/square root of frequency. Blue ribbon: mean ± 2 SD of loess curve resulting from bootstrapping.*

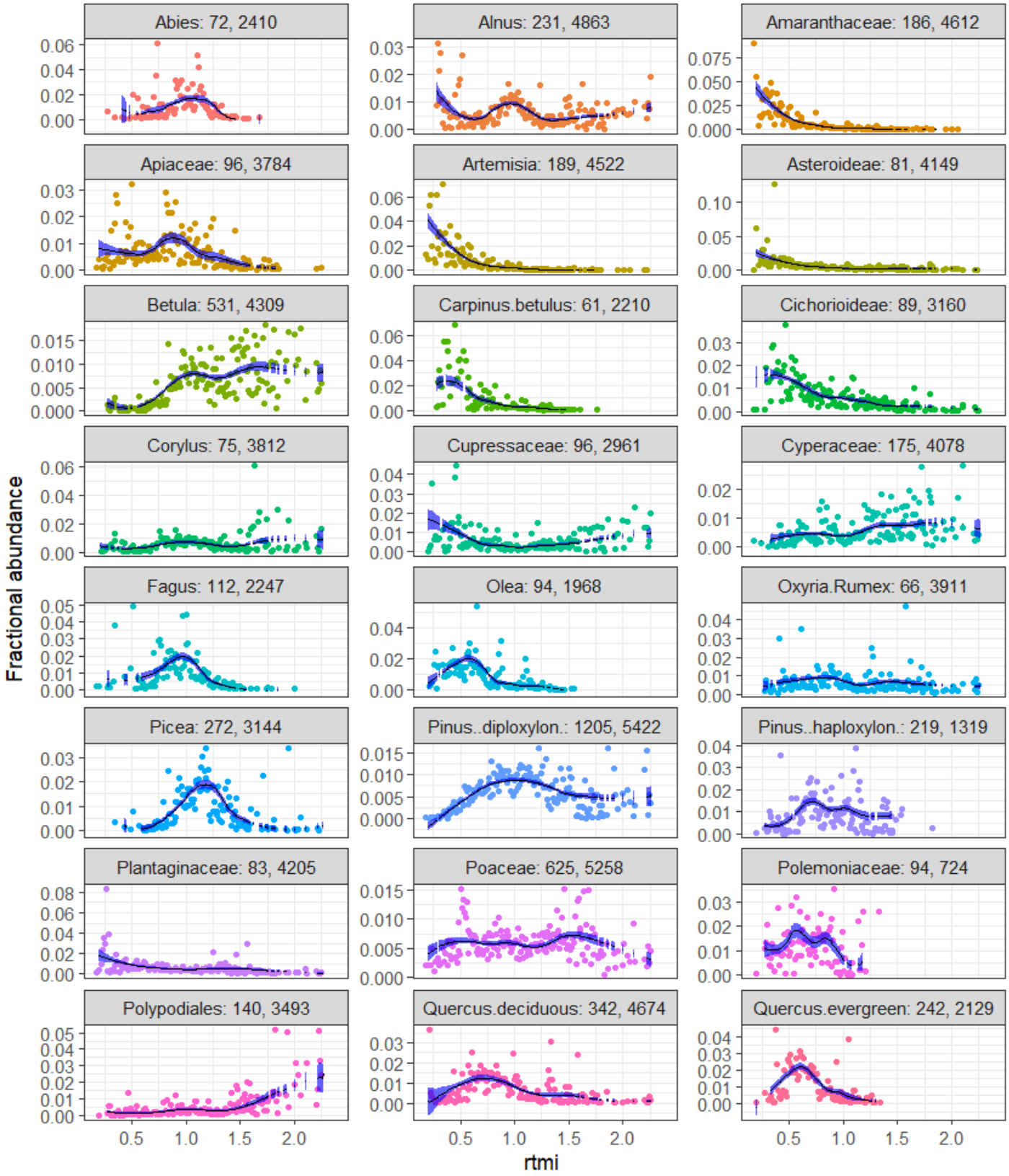

Figure 5.13 Bootstrapped response curves of top 24 taxa in the SMPDS by abundance to rtmi (square root of Moisture Index). Numbers in taxon headings are respectively the sum of fractional abundances of the taxon and the number of occurrences of the taxon in SMPDS (number of SMPDS samples = sum of fractional abundances = 6458). Points: fxabf *(mean fractional binned abundance of SMPDS set). Black line: loess curve, span = 0.5, weighting 1/square root of frequency. Blue ribbon: mean ± 2 SD of loess curve resulting from bootstrapping.*

5.5 Do abundance distributions represent climate well?

Unimodality and symmetry of the abundance distribution is far from universal in the SPMDS (Figure 5.8 to Figure 5.13). This is not a function of restricted sampling, at least for taxa with more than sparse representation, since SMPDS samples a wide climate space relatively comprehensively (Chapter 3; Turner *et al.*, 2020).

A pervasive issue is that the fewer the occurrences and the lower the abundances of a taxon in the training set, the less capable it is of representing the climate gradient. Often such taxa do not exhibit clear patterns, and show wide uncertainties in their bootstrapped curves (Appendix B). Secondly, even where occurrences and abundances appear adequate, caution is needed since pollen does not respond only to a single bioclimatic variable, and there are many sources of noise.

A multimodal curve is potentially suspect. Whether a taxon appears multimodal can depend on the degree of smoothing (Figure 5.8 to Figure 5.10). The amplitude of the modes varies between the obvious and the unconvincing, where, while technically multimodal, the taxon shows low variability along the gradient. At least in theory, bimodality may be a genuine representation of the realised niche of a taxon, if it is outcompeted in its preferred range by others, though there are no clear examples of this in the SMPDS.

Most of the taxa in the SMPDS v1 do not represent the pollen of a single species. Some are deliberate amalgamations of relatively infrequently found taxa into higher taxonomic groups, after checking the similarity of their climate preferences using 2.5D GAMs (see Turner *et al.*, 2020). But some taxa perforce represent multiple plant species because their pollen is indistinguishable, or not in practice distinguished. These may conflate plants with different climate preferences, and this may result in peaks in abundance at different points along the climate gradient. There are multiple examples of multimodality or possible multimodality in the SMPDS, e.g. *Abies* Tmin response (n = 2410 or 37% of samples in SMPDS) at span = 0.3 is trimodal and possibly bimodal at span = 0.5, but at span = 0.75 looks simply unimodal. *Alnus* (n = 4863 or 75% of samples in SMPDS) has a very variable response to Tmin and multimodality at span = 0.3 is not convincing. In no case can a specific cause be identified.

Some taxa have no significant preference respecting a given bioclimatic variable, and these appear insensitive by showing no clear abundance pattern. This may be indistinguishable from the effects of low abundance and infrequent and/or patchy occurrence, which cannot reliably sample the gradient. Both may result in apparent multimodality. There are potential examples of this among the less abundant taxa (see Appendix A). Considering gdd, apparent multimodality/insensitivity in e.g. Boraginaceae, Papaveraceae, *Platanus, Thalictrum*, and *Mercurialis* may result from patchy sampling.

Some distributions may be actively misleading, where an apparent preference for one variable can be shown to be largely driven by another. This can be demonstrated for *Artemisia*, a very abundant taxon in many fossil samples (see section 5.6). It consistently requires dry conditions (Figure 5.10) but occurs in environments with widely varying temperatures. It appears to respond positively to gdd in Figure 5.9, giving a ramp distribution.

It is not immediately obvious that there is an issue. The abundance of *Artemisia* responds mainly to low moisture, which is associated with low latitude, which in turn is associated with high gdd. Figure 5.14 shows that *Artemisia* in every latitude band strongly prefers the dry end of the available moisture gradient, and is largely absent from wetter latitudes, but in any latitude band it does not respond to gdd within the range available (Figure 5.15) and can be considered almost indifferent to gdd. Its apparent preference for high gdd arises because places with high gdd tend to have low plant available moisture. This undermines the use of its transfer function in reconstructing gdd.

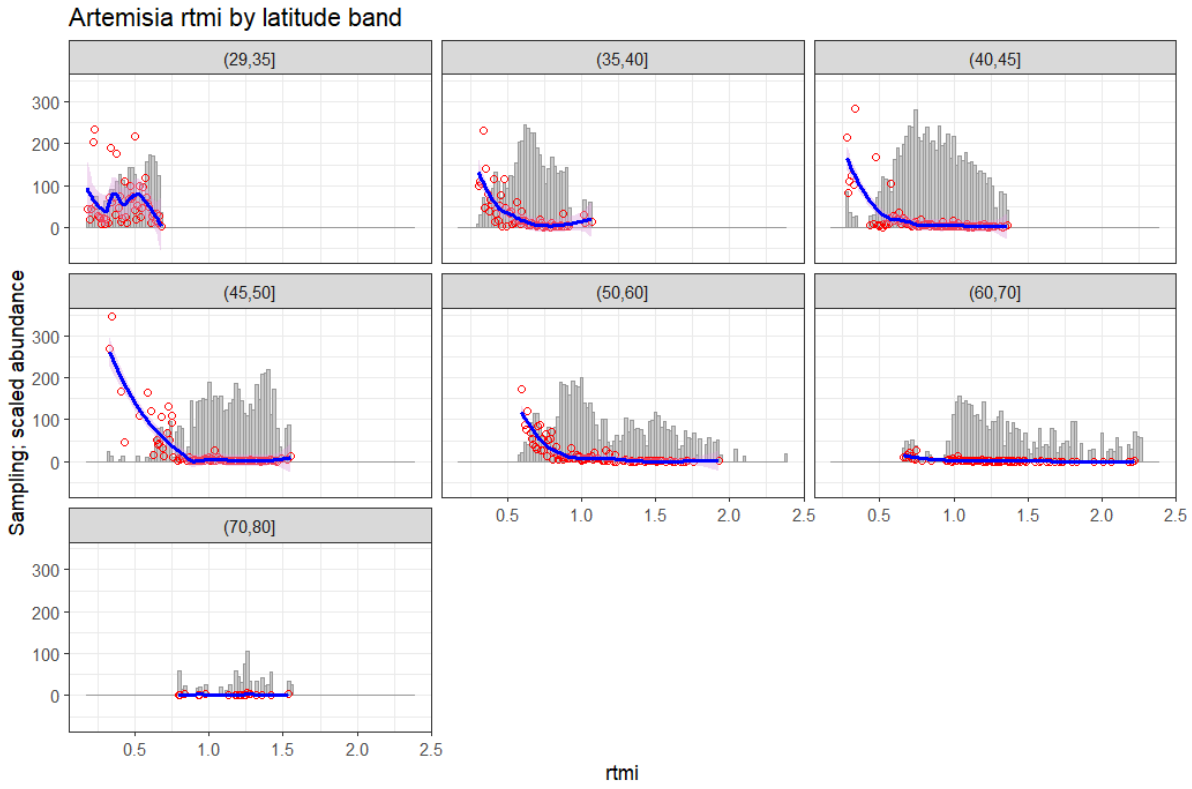

Figure 5.14 Red open circles: scaled Artemisia *mean binned abundance on the rtmi (square root of Moisture Index) gradient by latitude band in degrees N, with blue loess curves span = 0.5, plotted against background (grey histogram) of SMPDS samples in the latitude band.*

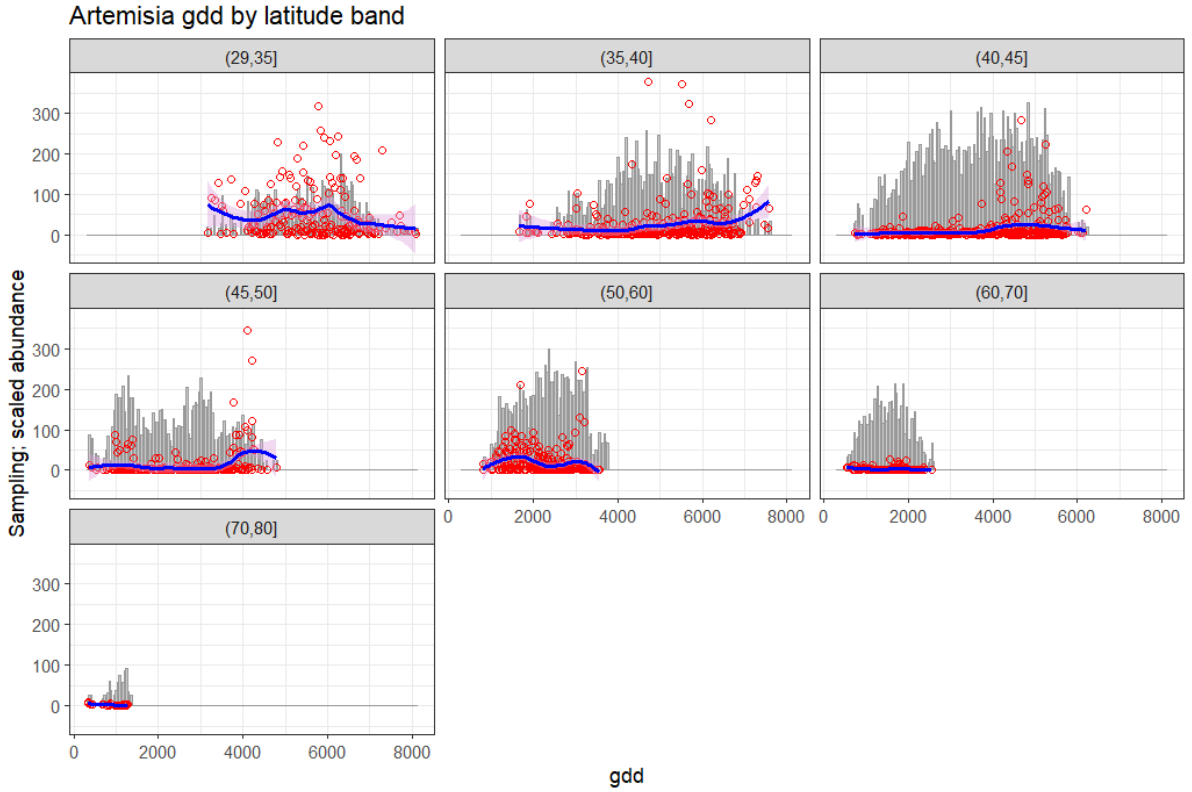

Figure 5.15 (Scaled) Artemisia *mean binned abundance on the gdd gradient by latitude band in degrees N (red points), with blue loess curves span = 0.5, plotted against background (grey histogram) of SMPDS samples in the latitude band.*

5.5.1 Summary: reading the climate

Some circumstances have been identified in which the abundance distribution may be an unreliable representation of the response to climate. These are taxa

- with multimodal or unclear abundance distributions;
- with low number of occurrences or abundances;
- which are insensitive to a specific climate gradient or whose abundance distribution along that climate gradient reflects correlations between this variable and some other aspect of climate.

5.6 Do abundance distributions support fxTWA-PLS transfer functions?

Statistical techniques which assume a unimodal distribution will not provide a good reconstruction for taxa which (a) show a climate preference distant from the mean, (b) show no clear pattern or a multimodal pattern, and (c) have a broad tolerance range.

5.6.1 Skewness and tolerance

There are many instances of skewed unimodal distributions in the SMPDS. WA-PLS and fxTWA-PLS find abundance-weighted *mean* environmental values for each taxon, but the *mode* represents the most-preferred environment. In a unimodal symmetrical distribution, the mean is also the mode, but skewness moves the mode away from the mean, so the abundance-weighted mean no longer represents the most preferred environment. However distant from unimodal and symmetrical the abundance distribution may be, however wide its dispersion and however insensitive the taxon, WA-PLS and fxTWA-PLS always provide a transfer function, which is then applied to all instances of the taxon during reconstruction.

WA-PLS makes no distinction between taxa whose distributions offer strong evidence of narrow preferences and those with very wide or unclear preferences. fxTWA-PLS adjusts for one aspect of this, the dispersion (tolerance), but still assumes symmetry. The tolerance adjustment weights the abundance-weighted mean of each taxon inversely as the square of its dispersion of its abundance along the climate gradient when constructing the trial environmental vector ($1/t^2$ is applied in Step 2 in Table 4.8; Liu *et al.* (2020) derived $1/t^2$ algebraically). A large *t,* reflecting a wide dispersion, reduces the contribution of the taxon. Some of these weightings are large, as can be seen in Figure 5.16. *awm* does not include any tolerance adjustment.

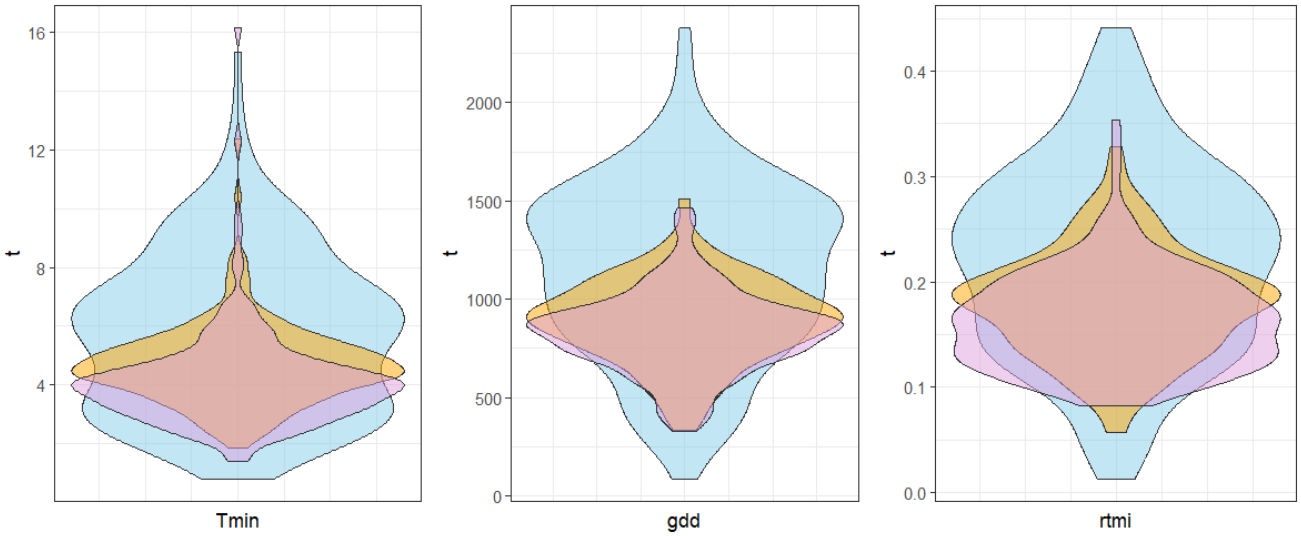

Figure 5.16 Spread of tolerance factor t *for all taxa in SMPDS with respect to Tmin (temperature of the coldest month in °C), gdd (growing degree days > 0 °C), and rtmi (square root of Moisture Index), provided by fxTWA-PLS for Components 1 (blue), 2 (orange) and 3 (purple).*

Since skewed and multimodal distributions are common in Figure 5.8, Figure 5.9, Figure 5.10, and Appendix A, the degree of displacement of the mode must be considered in evaluating the robustness of the fxTWA-PLS transfer function for a taxon. But before this, the impact of higher components on the transfer function must be considered.

5.6.2 Components higher than 1

The abundance weighted mean for Component 1 has been used to substitute for the unknowable true optima found by WA-PLS and fxTWA-PLS. Since the PLS elements of both methods make progressive changes to the unknowable true optimum embodied in the transfer function, it is important to examine how PLS develops this series of components, and whether this adversely impacts the calculation of the transfer function.

5.6.2.1 How components change

Transfer functions are cumulative as components are added. Here WA-PLS is used to illustrate the processes since its de-shrunk optima are available, and tolerance and frequency adjustments do not complicate the picture. For some taxa, there is little change between initial (Component 1) and final (e.g. Component 4), while for others there is large change.

There are two parts to the mechanism by which reconstructions are progressively changed in WA-PLS: firstly the incremental change as components are added in the abundance weighted taxon mean, or unmodified optimum, and secondly, the application of the slope coefficient for that component, obtained in the inverse regression for the purpose of de-shrinking the reconstructed environmental vector. The first element also occurs in fxTWA-PLS, but fxTWA-PLS handles the de-shrinking differently and (correctly) applies the coefficient to the trial reconstruction. In both cases the end reconstruction, which changes across components, includes the effects of both the change in the abundance-weighted mean and the de-shrinking slope. In WAPLS*rioja* the application of the slope coefficient to the abundance-weighted mean amplifies the movement and is the primary cause of out-of-range coefficients discussed in Chapter 4.

5.6.2.2 Incremental change in abundance-weighted means

The magnitudes of the transfer function increments in WAPLS calibration are determined as follows. The new environmental vector for a component > 1 is the residuals of the previous regression. For a given taxon, the increment in the optimum for components > 1 starts as the vector of the products of the residuals and the taxon abundances. The mean of this vector becomes the increment.

If the vector elements (the individual sample scores) are evenly distributed about zero, a weighted mean of zero results and there will be no change in the coefficient. A large increment requires that the elements are unbalanced about zero. This arises when the *abundances* are unevenly distributed about the zero residual, for instance when samples with abundances which are large in the context of the given taxon are found at some distance from zero, and are not balanced by similar moment on the other side. Samples near zero are of little relevance. In theory change could be caused or contributed to by *residuals* which are centred well away from zero, but in practice this is rare.

This imbalance tends to be a feature of weakly represented taxa, in that they are of low abundance and/or low occurrence and/or their distribution is not unimodal. The reconstructed value of each sample, and therefore the residual, is dominated by the high-abundance taxa in the sample. Common and highly abundant taxa tend to have small coefficient increments. This effect is a natural and not necessarily undesirable consequence of WA-PLS.

Figure 5.17, using the residuals from the first regression, shows that where samples are evenly balanced about zero, the weighted mean environmental preference of a taxon is very similar to the mean of the environments of the samples in which it is found, so the coefficient increment for Component 2 is small. Some of the example taxa are common, some very thinly evidenced, but because the product of the total sample abundances and the environment are equal on either side of zero, the new mean is approximately zero. The new mean is aligned with the centre of the histogram of the environmental vector (the previous regression residuals), restricted to the samples in which the taxon appears.

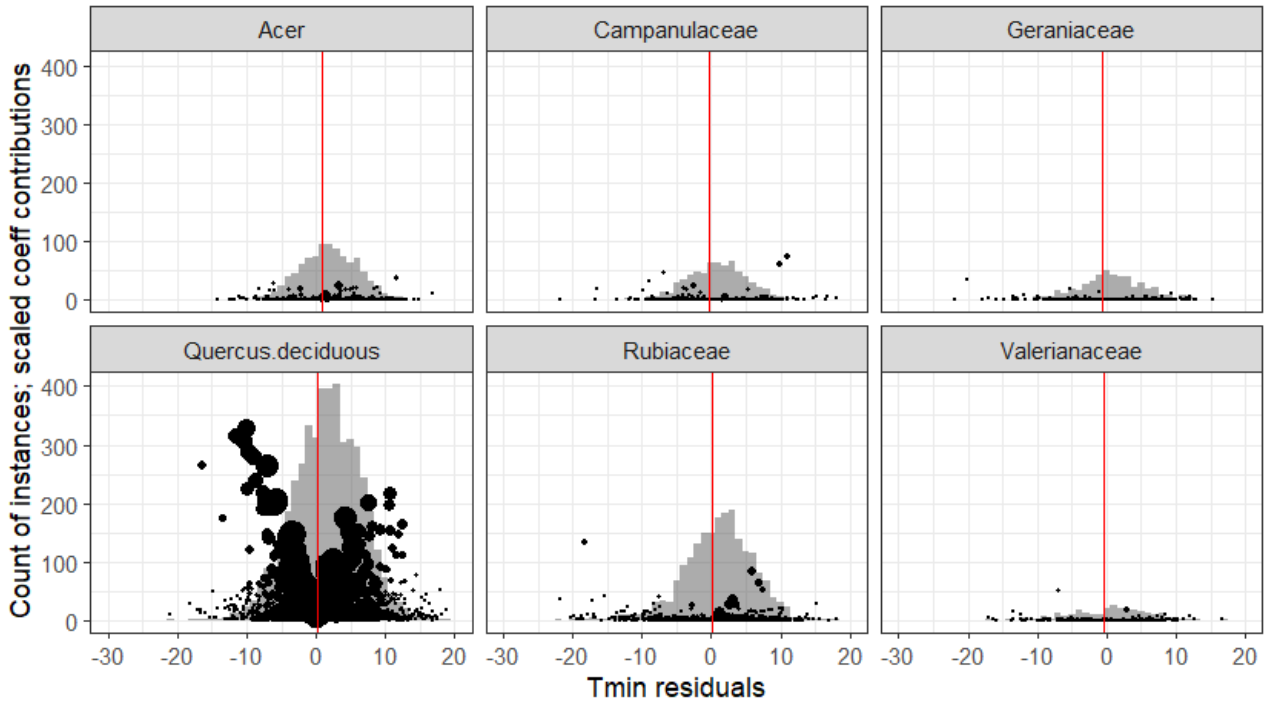

Figure 5.17 6 examples of taxa where the Component 2 Tmin increment is effectively zero in WA-PLSrioja. Histogram is residuals from previous regression, i.e. environmental vector for this component, for the samples which include this taxon; points are absolute values of product of abundance and environment i.e. elements contributing to coefficient increment; size of points is proportional to abundance; red line is resulting coefficient increment; movement is distance of red line from zero.

Figure 5.18 by contrast shows unbalanced distributions, where a small number of samples with high abundance exert great leverage (*Thalictrum*, Polygonaceae, Saxifragaceae). Here, the new weighted mean is not aligned with the histogram denoting the environment of the samples in which it appears. In other words, the taxon does not exactly share the typical preferences of the taxa with which it shares samples, so change is justified. This is a feature of low-abundance taxa; high-abundance taxa of necessity control the preferences shown by the histogram.

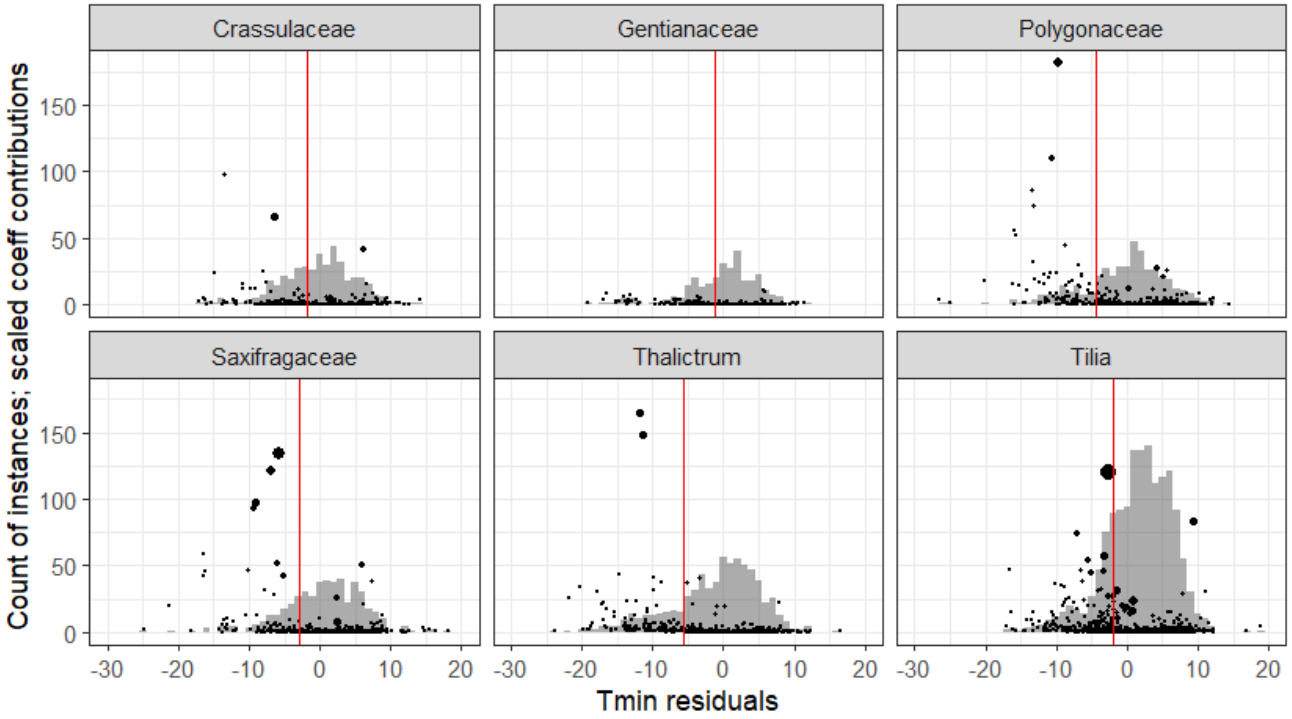

Figure 5.18 6 examples of taxa where Component 2 Tmin increment becomes colder. Histogram is residuals from previous regression, i.e. environmental vector for this component, for the samples which include this taxon; points are absolute values of product of abundance and environment i.e. elements contributing to coefficient increment; size of points is proportional to abundance; red line is resulting coefficient increment; movement is distance of red line from zero.

This example shows coefficients moving towards cold, but there are many examples resulting in warmer Tmin, and of similar behaviour in gdd and rtmi.

The conclusion is that the movement of the optima with higher components is logical, but that low-abundance taxa may suffer large changes in their transfer functions which undermine their utility.

5.6.2.3 Multiplication by the de-shrinking slope coefficient

The double-averaging in WA leads to the need for 'de-shrinking' by applying the slope coefficient to the reconstructed environmental vector (Chapter 4), and its application to the optima, rather than the trial environmental vector, is an error of principle in WAPLS*rioja*. The great amplification of the incremental change by applying the slope coefficient is a problem when the resulting coefficients are applied to taxa with very different fossil abundances to those in the modern, such that their weight is far greater.

The effect is seen in the example of *Thalictrum* in Table 5-1. Each new component taxon coefficient is found by summing the increments so far, and the related slope coefficient is then found by multiple linear regression of the reconstructed against the observed environmental vectors. Since the slope coefficients

change with each new component, finding the increments is most simply done by reverse engineering the final slope as in Table 5-1. In this example, the slope-adjusted cumulative on the right is the WAPLS*rioja* transfer coefficient of -63.9 °C for Component 3, and the Component 2 unmodified increment for Thalictrum (-5.6°C) is seen in Figure 5.18. The Component 3 value is lower than both the coldest observed *Thalictrum* sample and the coldest observed SMPDS sample, and is therefore not a transfer function which can be safely applied to reconstruct climate from fossil pollen.

The cumulative unmodified Component 3 optimum for Tmin for *Thalictrum* (-21.3 °C; Table 5-1) matches well with the apparent mode of its mean binned abundance in Appendix A. The application of the regression slope is shown in Table 5-1 to be the main driver of the physically impossible final Component 3 optimum.

Table 5-1 Thalictrum WA-PLS optima increments for Tmin °C (temperature of the coldest month)

	Unmodified optimum °C		Slope	Slope-adjusted °C	
Thalictrum	Increment	Cumulative	Slope	Increment	Cumulative
Comp 1	-12.4	-12.4	1.8	-22.7	-22.7
Comp 2	-5.6	-18.1	3.3	-18.6	-41.3
Comp 3	-3.2	-21.3	7.0	-22.6	-63.9

This illustrates again that WA-PLS transfer functions are strictly true only in the context of the relative taxon abundances in the training set. *Thalictrum* in the training set occurs 693 times with a fractional abundance total of 4.4 out of 6458, and mean of 0.0007. Arithmetically, the reconstructed environmental vector owes almost nothing to the influence of *Thalictrum*, and its coefficients are for practical purposes irrelevant to a replication of the SMPDS environment. At the detail level, however, WA-PLS, finding that *Thalictrum* does not share the climate preferences of the other taxa in the samples it shares, compensates for its tiny

abundances by a high coefficient. While the calculation is logically correct under the principles of WA-PLS, the problem is that (a) the result is physically impossible and (b) *Thalictrum* is a significant player in some fossil cores/samples.

Because fxTWA-PLS applies the de-shrinking correctly to the trial reconstruction, not the optimum, this issue is a feature of WA-PLS but not of fxTWA-PLS.

5.6.3 Mean versus mode

Modes as indicators of climate preference have so far been illustrated graphically. This section quantifies the gap between mean and mode as a measure of how far a distribution is from (approximately) Gaussian.

Figure 5.19 illustrates how apparent modes exist in the gdd loess curves of the 24 most abundant taxa in the SMPDS (blue points for most obvious, and red points for lesser modes) and how far they can be from the abundance weighted means (vertical line). Modes are defined here as points greater than their neighbours on either side within a window 20% of the length of gradient centred at that point. This means ramp responses such as Amaranthaceae do not attract modes at their high points because there is no subsequent decline.

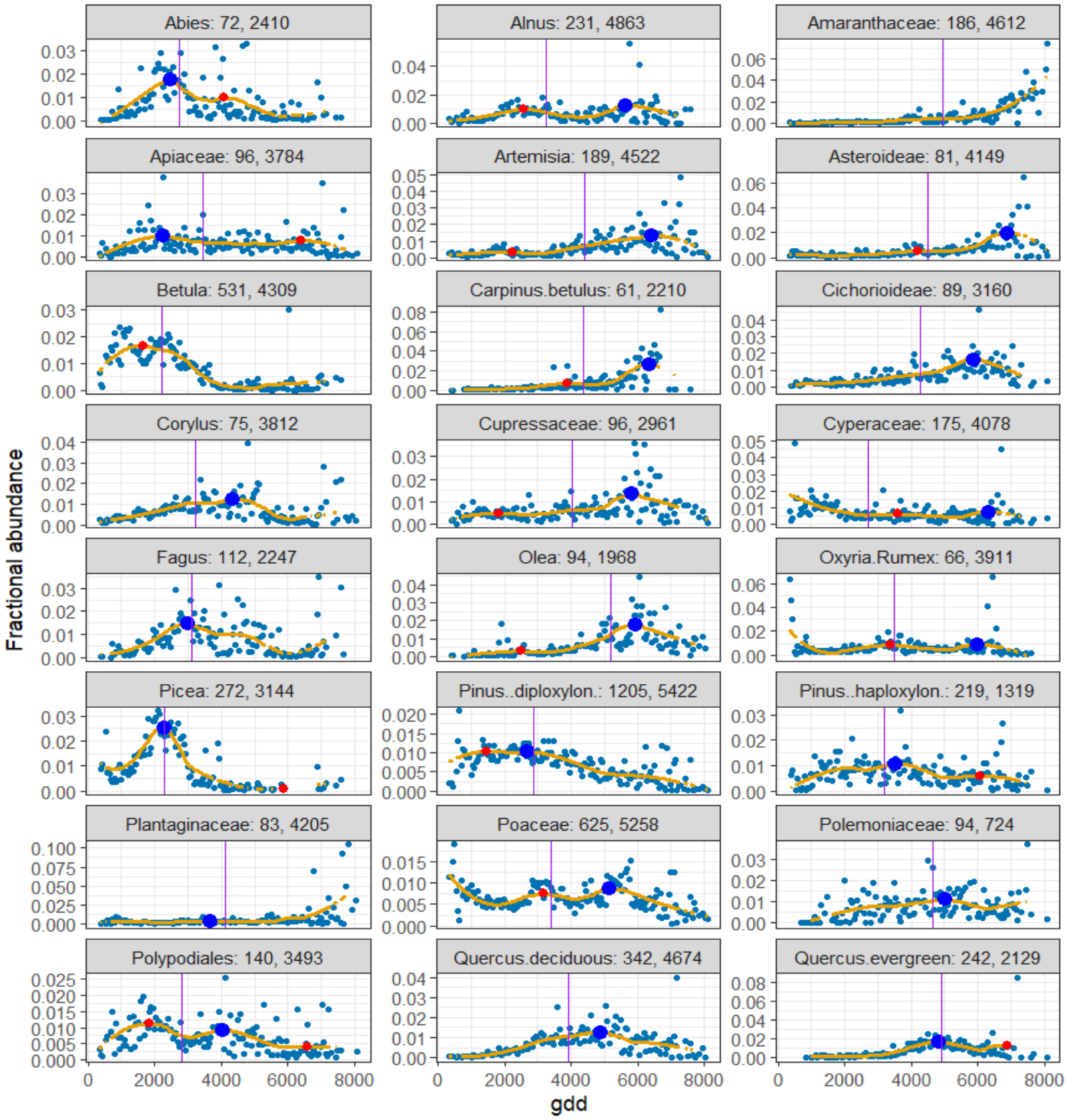

Figure 5.19 Response curves of top 24 taxa in the SMPDS by abundance to gdd. Numbers in taxon headings are respectively the sum of fractional abundances of the taxon and the number of occurrences of the taxon in SMPDS (number of SMPDS samples = sum of fractional abundances = 6458). Blue points: fxabf *(mean fractional binned abundance of SMPDS set). Orange line: loess curve, span = 0.5, weighting 1/square root of frequency. Red points: apparent modes; blue large points: 'best' mode (largest > 1800). Vertical line: fxTWA-PLS abundance-weighted mean for component 1 (*awm*).*

In the majority of these 24 taxa, mean and mode are sufficiently far apart to cast doubt on whether WA-PLS and fxTWA-PLS will find a good transfer value. The exceptions are *Abies*, *Betula, Fagus, Picea, Pinus* diploxylon and haploxylon (though both are broadly tolerant), and *Quercus* evergreen. *Corylus, Olea,* and

Quercus deciduous have broad unimodal tolerance but the mean misses the mode. Few others qualify. There is a bimodal class where the abundance weighted mean is offset from the modes (*Alnus*, *Artemisia, Asteroideae,* Poaceae), and a ramp class where the maximum abundance is at the warm end, sometimes with no mode found, and the mean is unrepresentative (Amaranthaceae, *Carpinus betulus*, Cichorioideae, Cupressaceae, Plantaginaceae); in Figure 5.11 the warm ends of these ramps can be seen to have wide uncertainties. The preferences of Apiaceae, Cyperaceae, *Oxyria/Rumex,* and Polemoniaceae are not clear.

The class of response for a given taxon varies between bioclimatic variables (for instance, *Quercus* deciduous shows a bimodal response to Tmin), but the same classes of response are found in each variable.

The distances between the abundance-weighted mean and the apparent mode, expressed numerically in Table 5-2, are therefore a potential index of the reliability of the transfer function.

Table 5-2 Most obvious mode, abundance-weighted mean found by fxTWA-PLS, and the difference between them for gdd (growing degree days > 0 °C).

Taxon	mode	mean	diff
Abies	2488	2741	253
Alnus	5638	3241	-2397
Apiaceae	2238	3432	1194
Artemisia	6438	4413	-2024
Asteroideae	6888	4503	-2385
Carpinus betulus	6338	4348	-1990
Cichorioideae	5888	4292	-1596
Corylus	4338	3210	-1128
Cupressaceae	5838	4028	-1809
Cyperaceae	6338	2693	-3645
Fagus	2988	3110	122
Olea	5938	5193	-745
Oxyria/Rumex	5988	3504	-2484
Picea	2288	2279	-9
Pinus diploxylon	2688	2876	188
Pinus haploxylon	3538	3187	-351
Plantaginaceae	3688	4106	418
Poaceae	5138	3378	-1760
Polemoniaceae	5038	4650	-388
Polypodiales	1838	2818	980
Quercus deciduous	4888	3932	-956
Quercus evergreen	4838	4929	91

5.6.4 Should outliers be removed?

Arguably, where a taxon has very high fractional abundances which fall outside the envelope of the remaining samples, these samples should be removed from the calibration, in accordance with typical statistical practice. For example, two *Thalictrum* samples have fraction abundance > 0.2 in Figure 5.18; the mean abundance of *Thalictrum* is 0.0007. In another case, Figure 5.20 plots the abundance of the far more abundant *Artemisia* in a 2D climate space of gdd and rtmi against a background of the density of SMPDS sampling of the climate space. The purple points denote fractional abundances in excess of 0.75, one reaching 0.96.

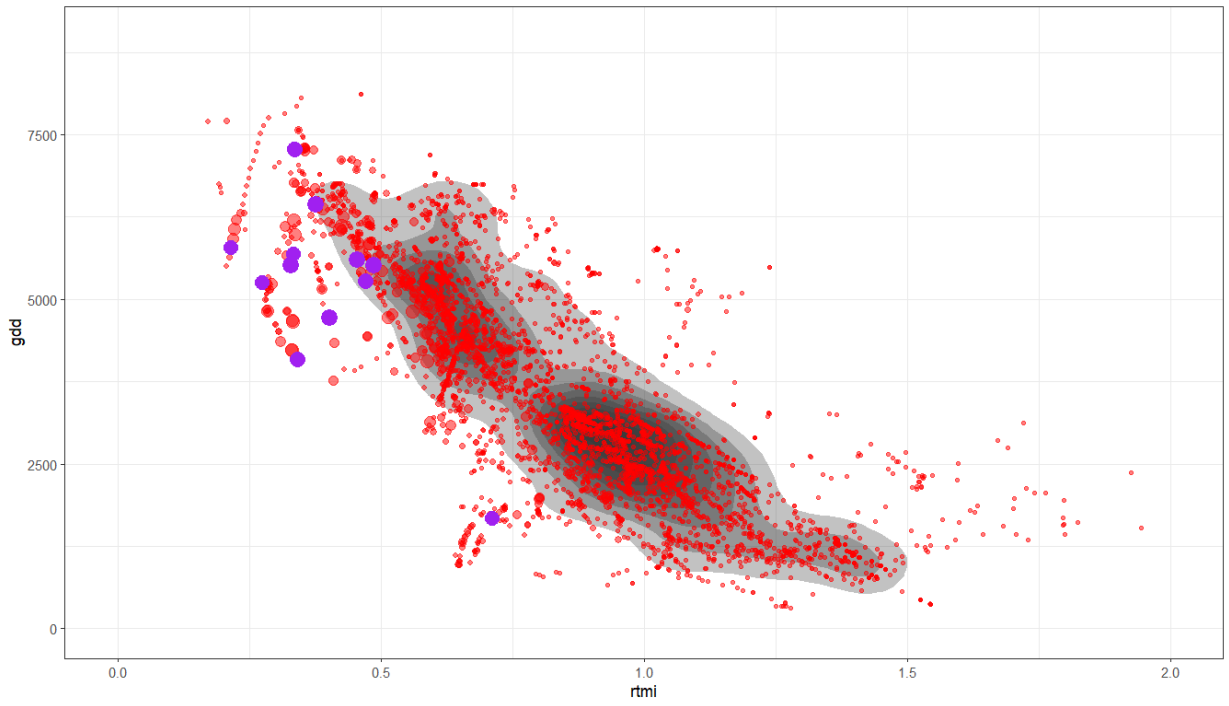

Figure 5.20 Abundance of Artemisia (red points, size ~ abundance) in a 2D rtmi/gdd climate space. Background contours are density of SMPDS samples in the climate space. Purple points: fractional abundance> 0.75.

However, in the case of *Artemisia*, the effect of removing samples with fractional abundance > 0.75 is shown in Figure 5.21 to be minor. This is because the bins in which they occur contain tens of other samples with more typical abundances. In the case of *Thalictrum* the components still run away (but less quickly) to impossible negative values. The removal of high-abundance samples was therefore not pursued.

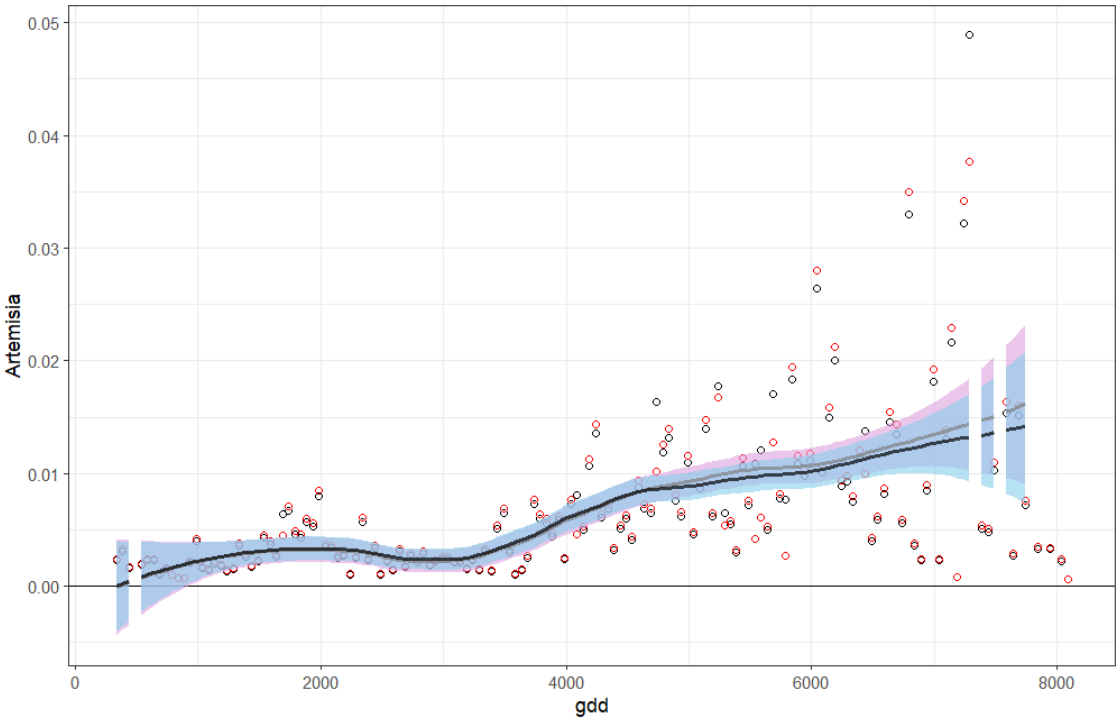

*Figure 5.21 Fractional mean binned abundances (*fxabf*) of Artemisia along gdd gradient. Black open points: all* Artemisia *samples; grey line and pink ribbon mean: loess span = 0.5 curve, and bootstrapped ±2 SD limits. Red open points:* Artemisia *samples excluding samples with fractional abundance > 0.75; black line and blue ribbon: mean loess span = 0.5 curve, and bootstrapped ±2 SD limits.*

5.7 Applying learnings to reconstructions

5.7.1 Inclusion/exclusion of taxa in calibration

Turner *et al.* (2020) concluded that all available taxa should be used in calibration unless there is good reason not to. Since WA-PLS combines information from all taxa in the calibration set to refine the trial and final reconstructions, it was argued that some information, however little, is lost to the remaining taxa if any taxon is removed from the calibration. The removal of insensitive, or very broadly tolerant, taxa from the WA-PLS calibration set was tested in Turner et al (2020) using the example of *Pinus* diploxylon and the difference in the reconstructions was found in that case to be unimportant. However, this project has identified good reasons to consider excluding or down-weighting some taxa.

Since some low abundance/low occurrence taxa are of significant abundance in the fossil record, it is not possible simply to exclude them, otherwise the reconstruction will be based on a very small set of taxa.

It might appear attractive to create core-specific calibrations, including only those taxa which occur in the core; but then different transfer functions are then being applied to different cores, which cannot be justified.

The SMPDS set already excludes such plants as obligate aquatics, carnivorous plants, introduced species, and cultivars, on the grounds that they do not represent the naturally occurring response to climate (see Chapter 1 for this and a counter-argument), and includes only taxa with occurrences > 10; the calibration excludes taxa with sum of abundance in the set < 0.1.

5.7.2 Identifying potentially unreliable taxa important in fossil record

The taxa which are most abundant in the fossil cores are often not those most abundant in the modern. The smaller the presence of a taxon in the training set, the less reliably fxTWA-PLS transfer functions may reflect its true climate preference. Where taxa are abundant in the fossil record but not in the modern, reconstructions may be undermined. Figure 5.23 and Figure 5.24 compare abundances in the SMPDS (Figure 5.22)with those in the fossil record, combining abundances from a set of 11 circum-Mediterranean fossil cores (the selection of fossil cores is discussed in Chapter 6). Taxa falling above the red 1:1 line are more abundant in the fossil than the SMPDS set, and some of the differences are very large; this is the class of taxa with the greatest risk of providing poor optima, followed by highly abundant taxa falling below the line.

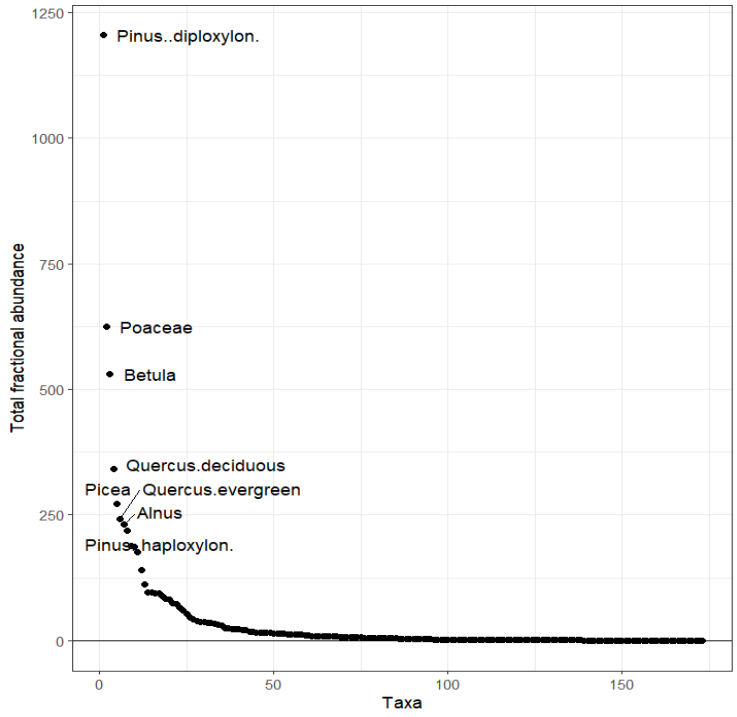

Figure 5.22 Summed fractional abundances of taxa in the SMPDS in descending order. Top few taxa labelled.

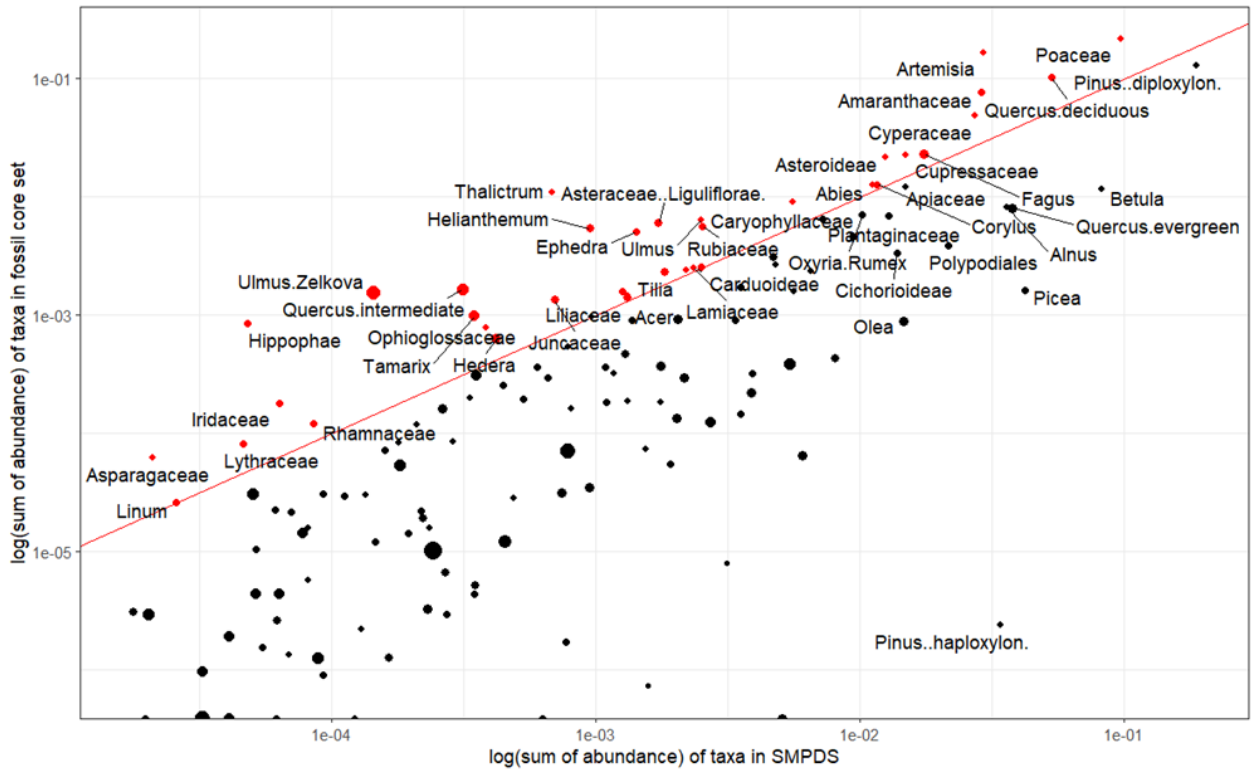

Figure 5.23 Log/log plot of summed fractional abundance (as fraction of total abundance in the set) of SMPDS and a set of fossil cores (Villarquemado, Lac_du_Bouchet, Les_Echets_redone_2, Lagaccione, Stracciacappa, Castiglione, Lago_Grande_di_Monticchio, Ioannina, Lake_Xinias, Megali_Limni, Dead_Sea). Taxa where fossil abundance is greater than in SMPDS are highlighted in red and labelled. Point size proportional to $1/t^2$ for Tmin (temperature of the coldest month). Red line: 1:1.

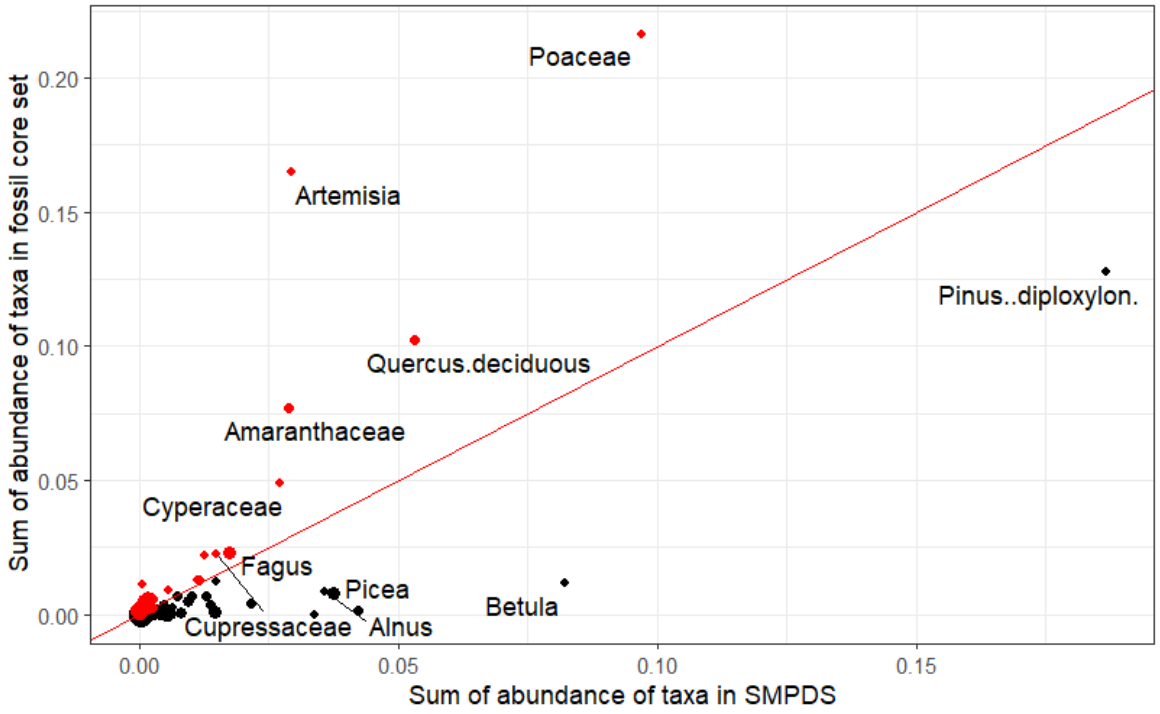

Figure 5.24 Summed fractional abundance (as fraction of total abundance in the set) of SMPDS and a set of fossil cores (Villarquemado, Lac_du_Bouchet, Les_Echets_redone_2, Lagaccione, Stracciacappa, Castiglione, Lago_Grande_di_Monticchio, Ioannina, Lake_Xinias, Megali_Limni, Dead_Sea). Taxa where fossil abundance is greater than in SMPDS highlighted in red and labelled. Point size proportional to $1/t^2$ for Tmin (temperature of the coldest month). Red line: 1:1.

The fossil set combines cores which themselves differ widely in the abundances of their dominant taxa, so these Figures present a composite picture. Both at the core level and at the sample level within cores, reconstructions are often based on a small set of potentially unreliable taxa, and this set varies between cores. Figure 5.25 uses the spread of abundances to illustrate in more detail how some taxa have very much greater presence in the fossil set than in the SMPDS.

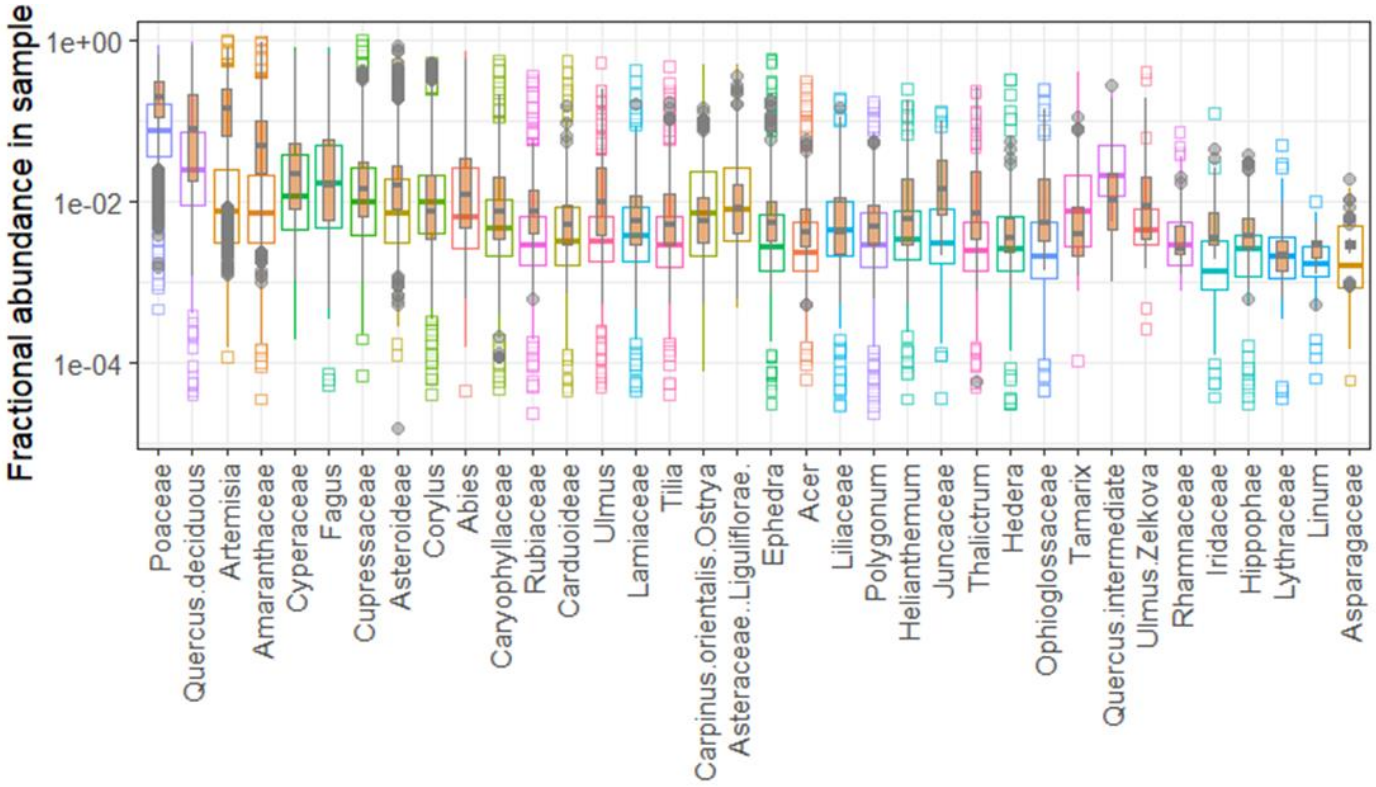

Figure 5.25 Differences in distributions on log scale of fractional abundances in samples between SMPDS (coloured, unfilled) and fossil set (dark grey with orange fill) for taxa with high abundance in SMPDS.

This discrepancy between modern and glacial pollen assemblages encompasses both abundance differences and a relatively restricted repertoire of taxa in the glacial cores. It is not surprising that glacial climates and low CO_2 led to assemblages different from the modern, often dominated by plants of low stature and wide tolerance, though it is also possible that lacustrine cores register, or preserve, pollen rather differently from the majority of the modern pollen samples, of which ~ 9% are lacustrine core tops and the majority are surface samples.

5.7.3 Tolerance

Nearly all the taxa abundant in the fossil but less so in the modern have wider tolerances (larger t) than the average of the SMPDS, and this is supported by their loess curves in Figure 5.8 to Figure 5.10. This suggests that applying a single effective optimum to all instances of these taxa in the fossil cores introduces falsely high precision. The tolerance t and tolerance weighting applied by fxTWA-PLS ($1/t^2$) is shown in Table 5-3 for the taxa with the highest abundance in SMPDS (excluding *Pinus* haploxylon, which does not appear in

the fossil records), which make up 69% of the SMPDS abundance and 83% of the abundance in the fossil set. The narrower tolerances of *Quercus* evergreen and *Fagus* mean their transfer functions reflect narrower and more justifiably precise climate preferences; this is strongly supported by their loess curves. But neither are significant in the fossil set.

Table 5-3 Top 14 by SMPDS abundances. Fossil abundances greater than SMPDS abundances in bold red. t *greater than the SMPDS mean and* $1/t^2$ *less than the SMPDS mean in bold.*

Taxon	SMPDS abundance as fraction of total	Fossil set abundance as fraction of total	*t* for Tmin, °C C	*t* for g gdd	*t* for rtmi	$1/t^2$ for Tmin	$1/t^2$ for gdd	$1/t^2$ for rtmi
Pinus diploxylon	0.187	0.128	**8.07**	**1278**	**0.243**	**0.0154**	**6.12E-07**	**16.90**
Poaceae	0.097	**0.216**	**7.34**	**1526**	**0.298**	**0.0186**	**4.29E-07**	**11.22**
Betula	0.082	0.012	**7.48**	831	**0.246**	**0.0179**	**1.45E-06**	**16.51**
Quercus deciduous	0.053	**0.102**	5.42	**1186**	0.210	**0.0340**	**7.11E-07**	**22.59**
Picea	0.042	0.002	**6.95**	608	0.154	**0.0207**	2.70E-06	**42.40**
Quercus evergreen	0.038	0.008	3.11	887	0.122	0.1033	**1.27E-06**	**67.10**
Alnus	0.036	0.008	**7.49**	**1287**	**0.245**	**0.0178**	**6.04E-07**	**16.61**
Artemisia	0.029	**0.165**	**9.64**	**1625**	**0.239**	**0.0108**	**3.79E-07**	**17.43**
Amaranthaceae	0.029	**0.077**	**6.80**	**1508**	0.217	**0.0216**	**4.40E-07**	**21.17**
Cyperaceae	0.027	**0.049**	**8.64**	**1491**	**0.327**	**0.0134**	**4.50E-07**	**9.37**
Polypodiales	0.022	0.004	**6.26**	**1340**	**0.389**	**0.0255**	**5.57E-07**	**6.60**
Fagus	0.017	**0.023**	3.10	838	0.137	0.1042	**1.43E-06**	**53.12**
Apiaceae	0.015	0.012	**7.36**	**1509**	0.217	**0.0185**	**4.39E-07**	**21.23**
Cupressaceae	0.015	**0.022**	**7.09**	**1814**	**0.384**	**0.0199**	**3.04E-07**	**6.79**
Sum of abundance	**0.688**	**0.828**						
Mean of set			**6.77**	**1266**	**0.245**	**0.0315**	**8.41E-07**	**23.50**
Overall SMPDS mean			**5.69**	**1133**	**0.219**	**0.0833**	**2.48E-06**	**95.99**

5.7.4 Taxon characteristics and possible treatment

The different characteristics of taxon abundance distributions, how they are identified, their significance, and possible responses to them are tabulated in Table 5-4. These possible changes to the calibration can be tested by (a) random *t*-test of the leave-one-out cross-validation and (b) changes in the reconstructions. A number of thresholds are proposed, which can be set by experimentation. Taxa which appear actively misleading include *Artemisia* for gdd (see 5.5.2).

Table 5-4 Characteristics of taxon abundance distributions, identification, effects, and possible responses. Grey boxes: condition not affected by characteristic.

Characteristics of taxon abundance distribution (more than one may apply)	**How identified**	**Assumed quality of climate read**	**Shape suitability for WA**	**Applicability of transfer function**	**Possible responses**
Symmetrical unimodal	Count of modes = 1, mean-mode distance low	Good	Excellent		Include in calibration
Skewed unimodal	Count of modes = 1, mean-mode distance high	Good	Depends on mean-mode		Exclude from calibration if mean-mode > threshold; or downweight in reconstruction ~ mean-mode
Wide tolerance	Tolerance large	Good		Over precise	fxTWA-PLS already weights by tolerance. Consider exclusion of highly abundant widely tolerant taxa
Multimodal	Count of modes > 1 and modes similar, mean-mode distance	Suspect	Poor		Exclude from calibration if mean-mode > threshold; or select most obvious mode; or downweight in reconstruction ~ mean-mode
Unclear/uninformative	Inspection, low variation	Suspect	Poor	Over precise	Unless significant in fossil, exclude from calibration
Low abundance/occurrence	Count of occurrences, sum of abundances, bootstrap SD	Suspect			Set thresholds: occurrences > 10, sum(abundance) > 0.1 already set.
Misleading	Inspection and analysis	Ignore			Exclude from calibration

5.7.5 Results of exclusion of taxa from a training set

The principle that some taxa provide little, or confusing, information about climate preferences was tested by performing a fxTWA-PLS gdd calibration excluding the taxa with the 4 greatest tolerances, and/or with absolute mean-mode distances > 2300 for gdd, plus *Artemisia* as misleading (not representing gdd) (Table 5-5). These were arbitrary cut-offs. This excluded set represents 33% of the total abundance in the SMPDS.

Table 5-5 Taxa to exclude from test calibration

Taxon	Tolerance *t*	abs(mean-mode) gdd
Pinus diploxylon	1278	188
Amaranthaceae	1508	-
Cyperaceae	1491	3645
Alnus	1287	2397
Asteroideae	-	2385
Oxyria/Rumex	-	2484
Artemisia	1625	2024

Table 5-6 shows that despite removing a third of the volume of evidence, the cross-validation and random *t*-test results are very similar to the full SMPDS set.

Table 5-6 Random t-test results for full and reduced SMPDS taxon set for gdd.

Full set	Component	R2	Avg.Bias	Max.Bias	Min.Bias	RMSEP	delta.RMSEP	p
	1	0.67039	121.26	4510.63	0.15	987.19	-36.74	0.001
	2	0.71568	91.13	5083.84	0.12	900.2	-8.81	0.001
	3	0.73048	64.93	5900.69	0.02	859.86	-4.48	0.001
	4	0.73197	72.44	6138.2	0.01	857.79	-0.24	0.013
Reduced set	1	0.67074	140.41	4455.68	0.19	977.09	-37.39	0.001
	2	0.71288	103.04	4968.16	0.63	889.14	-9.00	0.001
	3	0.72334	94.07	5718.96	0.50	861.92	-3.06	0.001
	4	0.72162	122.34	6666.16	0.28	877.41	1.80	0.001

Figure 5.26 shows minimal difference in the observed versus reconstructed (fitted) regression plots for the different taxon sets.

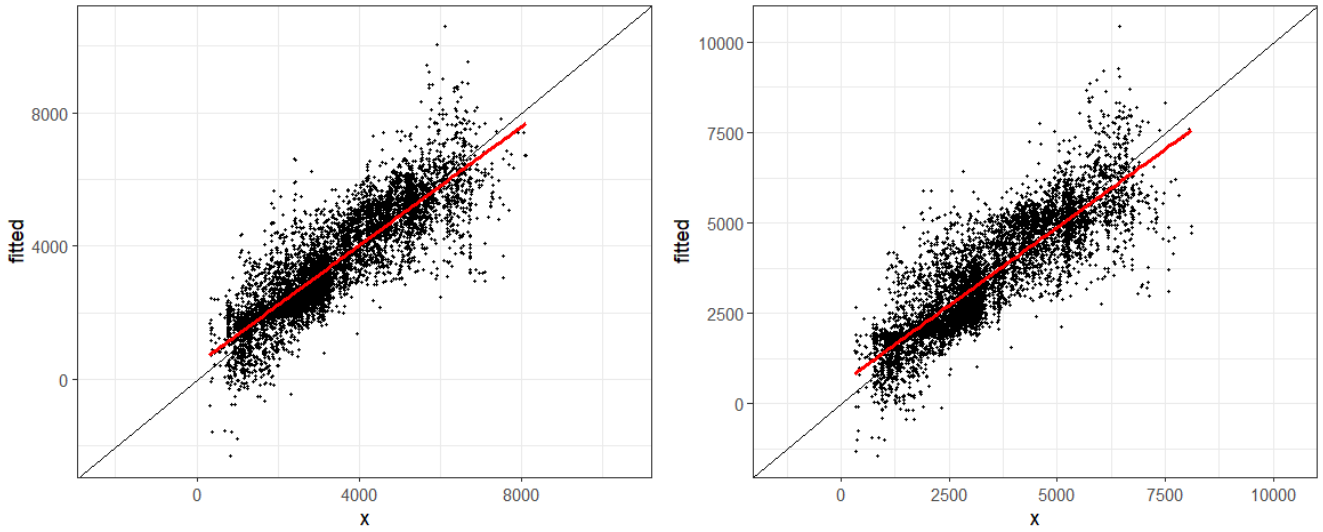

Figure 5.26 Left panel: fitted versus observed calibration result for gdd using full SMPDS set, Component 4. Right panel: using reduced set.

The interpretation is that these 7 taxa add little to the precision of the reconstruction of the training set, since either set appears to reconstruct the training set equally well.

The reduced set calibration was used to reconstruct gdd at Lac du Bouchet (Figure 5.27). While there are many similarities to the full set reconstruction, especially in the location of sharp changes, which are important in the search for evidence of D-Os, the restricted set yields an obviously different and cooler result with less amplitude of change (the loss of *Artemisia* is largely responsible for the cooling).

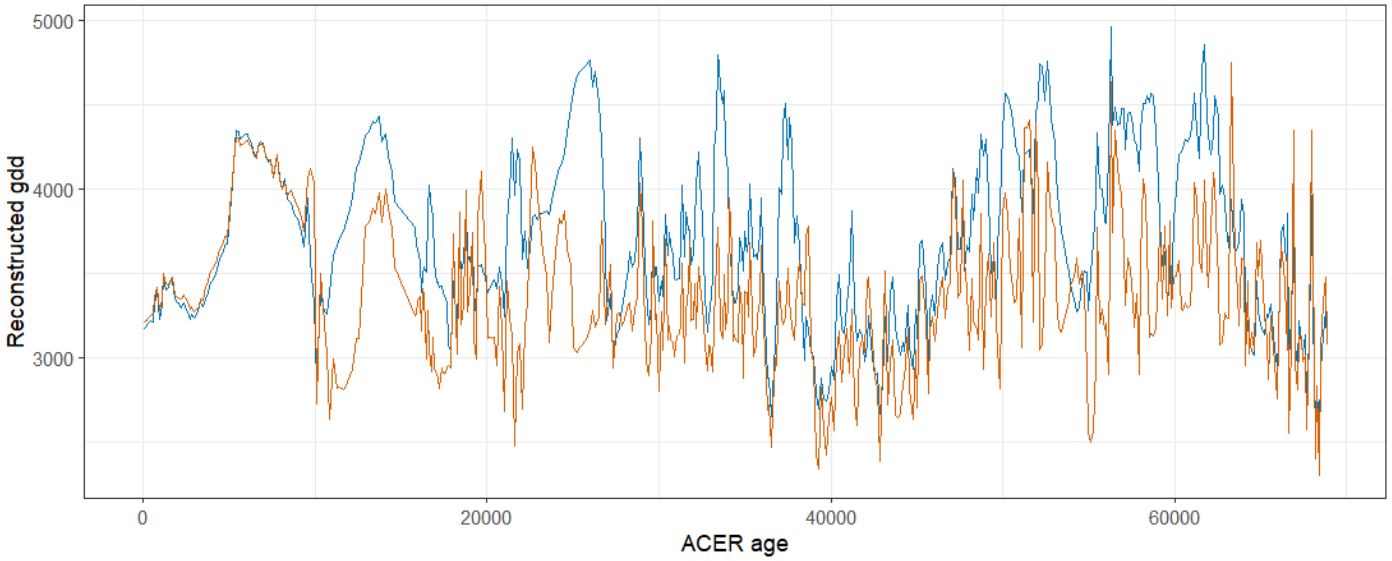

Figure 5.27 Reconstruction of gdd at Lac du Bouchet. Blue: using full SMPDS set of taxa (Component 4); orange: using restricted set (Component 3).

The taxa excluded in this demonstration are chosen based on arbitrary limits of tolerance and mean-mode distance. More experimentation would be needed to establish the impact of adjusting these thresholds, and the demonstration includes no test of the thresholds for the low abundance/low occurrence class, or of multimodal taxa. At some point the clarity of the reconstruction will start to suffer as taxa are removed or down-weighted.

This is another demonstration of the point made by Turner *et al* (2020) that indistinguishable calibration results do not lead to indistinguishable reconstructions from fossil cores, and conversely calibration results may not allow us to identify superior training sets. There is no available independent climatic evidence to show which reconstruction of the glacial climate is better, so we are thrown back on the plausibility of the argument that some classes of taxa are unlikely to help fxTWA-PLS reconstruct climate.

5.7.6 Exclusion of taxa from fossil core reconstructions

Legitimate exclusions of taxa from a fossil core when making a reconstruction include those where there is evidence to suggest that the taxon does not (or does not consistently) represent climate conditions, as for Polypodiales and Poaceae at Villarquemado (Wei *et al.*, 2019), where in some intervals sedimentary evidence suggests they reflect lacustrine conditions. Inspection of the reconstructions and the sedimentology is needed to identify such cases.

5.8 Chapter summary

Two questions are addressed: (a) how well the abundance distributions of taxa demonstrate their genuine climate preferences (b) how well WA-PLS and fxTWA-PLS can interpret abundance distributions. To do this, abundance distributions are first summarised as frequency-weighted loess curves through fractional mean binned abundances. The behaviours, or shapes, of the taxa in the SMPDS training set are categorised, and reasons are explored for shapes which do not fit the symmetrical unimodal ideal which WA-PLS and fxTWA-PLS assume, and/or which show that these taxa do not provide good evidence for climate preferences. Characteristics which may denote a poor reading of climate, or shapes not ideally suited to WA-PLS and fxTWA-PLS, include: skewness and multimodality, where the mode, which best demonstrates a climate preference, does not accord with the mean; broad tolerances, which do not closely define a preference; insensitivity or unclear preferences; and low occurrences and abundances. One abundant taxon, *Artemisia*, can be shown to be misleading, in that its response is not principally to gdd. The taxa which stand the highest risk of providing unreliable transfer functions are identified, partly by their greater abundance in the fossil cores than in the SMPDS training set.

Treatments of taxa with these problematical characteristics are suggested. It is shown that by removing 7 such taxa, representing a third of the SMPDS abundance, from the training set, the calibration is almost unaffected, but fossil reconstructions are noticeably different. Without external evidence to help distinguish between the reconstructions, both options are taken forward to Chapter 6.

Bjune, A.E. *et al.* (2010) 'Developing a modern pollen-climate calibration data set for Norway: Modern pollen-climate calibration data set for Norway', *Boreas*, 39(4), pp. 674–688. Available at: https://doi.org/10.1111/j.1502-3885.2010.00158.x.

Braak, C.J.F. and Looman, C.W.N. (1986) 'Weighted averaging, logistic regression and the Gaussian response model', *Vegetatio*, 65(1), pp. 3–11. Available at: https://doi.org/10.1007/BF00032121.

ter Braak, C.J.F. (1986) 'Canonical Correspondence Analysis: A New Eigenvector Technique for Multivariate Direct Gradient Analysis', *Ecology*, 67(5), pp. 1167–1179. Available at: https://doi.org/10.2307/1938672.

Gauch, H.G., Whittaker, R.H. and Wentworth, T.R. (1977) 'A Comparative Study of Reciprocal Averaging and Other Ordination Techniques', *Journal of Ecology*, 65(1), pp. 157–174. Available at: https://doi.org/10.2307/2259071.

Hill, M.O. (1973) 'Diversity and Evenness: A Unifying Notation and Its Consequences', *Ecology*, 54(2), pp. 427–432. Available at: https://doi.org/10.2307/1934352.

Huisman, J., Olff, H. and Fresco, L.F.M. (1993) 'A Hierarchical Set of Models for Species Response Analysis', *Journal of Vegetation Science*, 4(1), pp. 37–46. Available at: https://doi.org/10.2307/3235732.

Jansen, F. and Oksanen, J. (2013) 'How to model species responses along ecological gradients – Huisman–Olff–Fresco models revisited', *Journal of Vegetation Science*, 24(6), pp. 1108–1117. Available at: https://doi.org/10.1111/jvs.12050.

Liu, M. *et al.* (2020) 'An improved statistical approach for reconstructing past climates from biotic assemblages', *Proceedings of the Royal Society A* [Preprint]. Available at: https://doi.org/10.1098/rspa.2020.0346.

Oksanen, J. and Minchin, P.R. (2002) 'Continuum theory revisited: what shape are species responses along ecological gradients?', *Ecological Modelling*, 157(2), pp. 119–129. Available at: https://doi.org/10.1016/S0304-3800(02)00190-4.

Shelford, V.E. (1931) 'Some Concepts of Bioecology', *Ecology*, 12(3), pp. 455–467. Available at: https://doi.org/10.2307/1928991.

Ter Braak, C.J.F. and Juggins, S. (1993) 'Weighted averaging partial least squares regression (WA-PLS) : an improved method for reconstructing environmental variables from species assemblages', *Hydrobiologia*, 269/270, pp. 485–502.

Ter Braak, C.J.F. and Prentice, I.C. (1988) 'A Theory of Gradient Analysis', in M. Begon et al. (eds) *Advances in Ecological Research*. Academic Press, pp. 271–317. Available at: https://doi.org/10.1016/S0065-2504(08)60183-X.

Turner, M.G. *et al.* (2020) 'The impact of methodological decisions on climate reconstructions using WA-PLS', *Quaternary Research*, pp. 1–16. Available at: https://doi.org/10.1017/qua.2020.44.

Wei, D. *et al.* (2019) 'Climate changes in interior semi-arid Spain from the last interglacial to the late Holocene', *Climate of the Past Discussions*, pp. 1–31. Available at: https://doi.org/10.5194/cp-2019-16.

6 Identifying DOs in quantitative climate reconstructions

In this Chapter, fxTWA-PLS is applied to 16 terrestrial pollen records from the circum-Mediterranean region covering parts of the last glacial period to make quantitative climate reconstructions. These are tested for robustness using internal evidence and comparison against modern conditions. Pattern matching then locates D-O-like points ('DOLPs') in the reconstructions. The sensitivity of the identification of DOLPs to a number of pattern matching parameters is explored. To compare the apparent ages of the DOLPs identified with the ages of events in Greenland, a new set of Bayesian age models, updating the ^{14}C calibration to IntCal20 (Reimer *et al.*, 2020), is developed, and potential matches, and series of matches, between GIs and DOLPs are proposed.

This Chapter has three parts, each with methods and results sections. First the reconstruction methods and results are covered, followed by the pattern matching methods and results, and finally pattern matching is integrated with age modelling to evaluate whether DOLPs represent real D-Os and whether they can be assigned to specific GIs.

6.1 Methods: reconstructions

6.1.1 Bioclimatic variables

Reconstructions are made of mean temperature of the coldest month (MTCO or synonymously Tmin), and growing degree days (GDD0, or gdd), for 16 cores from the Mediterranean region (Chapter 2.4).

6.1.2 Treatment of suspect materials

Calibrations are made using two versions of the training set. Chapter 5 identified that equally good reconstructions of the training set climate can be made using either the full set of SMDPS taxa or a restricted set excluding taxa with very wide tolerances, highly skewed abundance distributions, or which fail to represent a response to the bioclimatic variable considered. The restricted set excludes *Artemisia*, Amaranthaceae, *Pinus* diploxylon, Cyperaceae, *Alnus*, Asteroideae, and *Oxyria/Rumex*. Successful replication of the training set is a necessary but not sufficient condition for the robust reconstruction of

climate from fossil pollen, and the close similarity of the calibrations does not allow us to discount either set.

In the Villarquemado record, Polypodiaceae and Poaceae are excluded from the fossil taxa following Wei *et al.* (2019), as not representing climatic but lacustrine conditions (Chapters 2 and 5).

6.1.3 Component selection

The performance of each fxTWA-PLS calibration model was assessed through leave-one-out cross-validation using the cv.w function of fxT, and the highest statistically reliable component was selected through a randomisation *t*-test on the results of this cross-validation using the rand.t.test.w function of fxTWA-PLS (Ter Braak and Juggins, 1993; Liu et al., 2020). Table 6-1 shows results up to Component 6 for the SMPDS full set. For GDD0/gdd Component 4 was selected as the highest statistically significant component, and for MTCO/Tmin Component 3.

Table 6-1 Results of random t-test on leave-one-out cross-validation of fxTWA-PLS calibration for SMPDS full set. b0 , b1, b0.se, b .se are the intercept, slope, standard error of the intercept, and standard error of the slope of the regression, respectively. Selected components are in bold.

	Compo-nent	R^2	Avg.Bias	Max.Bias	Min.Bias	RMSEP	delta. RMSEP	p	b0	b1	b0.se	b1.se
gdd	1	0.67039	121.26	4510.63	0.15	987.19	-36.74	0.001	532.16	0.88	28.53	0.01
	2	0.71568	91.13	5083.84	0.12	900.20	-8.81	0.001	445.32	0.90	26.13	0.01
	3	0.73048	64.93	5900.69	0.02	859.86	-4.48	0.001	456.14	0.88	24.88	0.01
	4	**0.73197**	**72.44**	**6138.20**	**0.01**	**857.79**	**-0.24**	**0.013**	**461.25**	**0.88**	**24.80**	**0.01**
	5	0.73194	73.82	6228.87	0.13	857.35	-0.05	0.290	466.22	0.88	24.78	0.01
	6	0.72897	73.85	6610.72	0.09	861.83	0.52	0.984	475.75	0.88	24.88	0.01
Tmin	1	0.67770	-2.8805	30.6405	0.0001	6.2554	-27.7814	0.001	-3.0783	0.9228	0.0715	0.0079
	2	0.73697	-1.9641	38.7902	0.0019	5.1352	-17.9076	0.001	-2.2148	0.9022	0.0606	0.0067
	3	**0.74142**	**-1.8085**	**43.2219**	**0.0012**	**5.0939**	**-0.8038**	**0.005**	**-2.0100**	**0.9214**	**0.0612**	**0.0068**
	4	0.74179	-2.0138	55.2912	0.0025	5.0498	-0.8658	0.082	-2.3086	0.8849	0.0587	0.0065
	5	0.73132	-1.3113	81.6816	0.0002	5.2789	4.5355	1.000	-1.3806	0.9729	0.0663	0.0073
	6	0.71801	-1.2574	94.1278	0.0001	5.4314	2.8904	1.000	-1.3281	0.9724	0.0685	0.0076

Table 6-2 shows results up to Component 4 for the restricted taxon set. Component 4 was selected as the last statistically significant component for GDD0/gdd and MTCO/Tmin. Part of this table is shown in Chapter 5.

Table 6-2 Results of random t-test on leave-one-out cross-validation of fxTWA-PLS calibration for first 4 components of restricted set. b0 , b1, b0.se, b .se are the intercept, slope, standard error of the intercept, and standard error of the slope of the regression, respectively. Selected components are in bold.

	Compo-nent	R2	Avg.Bias	Max.Bias	Min.Bias	RMSEP	delta.RMSEP	p	b0	b1	b0.se	b1.se
gdd	1	0.67074	140.41	4455.68	0.19	977.09	-37.39	0.001	605.9	0.86	27.98	0.01
	2	0.71288	103.04	4968.16	0.63	889.14	-9	0.001	553.72	0.87	25.47	0.01
	3	0.72334	94.07	5718.96	0.5	861.92	-3.06	0.001	576.58	0.86	24.55	0.01
	4	**0.72162**	**122.34**	**6666.16**	**0.28**	**877.41**	**1.8**	**0.001**	**552.81**	**0.87**	**25.1**	**0.01**
Tmin	1	0.71976	-1.7648	29.7667	0.0000	5.2365	-39.5450	0.001	-2.0283	0.8972	0.0629	0.0070
	2	0.75333	-1.3049	30.5895	0.0004	4.5626	-12.8689	0.001	-1.7368	0.8314	0.0535	0.0059
	3	0.73944	-1.1522	29.6493	0.0006	4.8230	5.7082	0.001	-1.4269	0.8928	0.0596	0.0066
	4	**0.75875**	**-1.2940**	**32.3841**	**0.0007**	**4.6380**	**-3.8372**	**0.001**	**-1.5726**	**0.8913**	**0.0565**	**0.0063**

6.1.4 Testing the reliability of reconstructions

A form of sample-by-sample uncertainty in the reconstructions is yielded by resampling the modern pollen training set with replacement 100 times and making a reconstruction for each resampling ('bootstrapping') (Chapter 3, Turner *et al.* (2020). Bootstrapping demonstrates the (in)stability in the climate information available in the training set arising from infrequently sampled taxa and/or those which appear in a wide range of climates.

The emphasis in pattern matching is on the robustness of the gdd reconstruction, since it is the main comparator with the Kindler series on the grounds that it is the nearest in climatic meaning (Chapter 2). Nevertheless both gdd and tmin are considered; issues affecting the reconstruction of one variable may inform the robustness of the other.

Hill's N2 (Hill, 1973) is a sample-by-sample measure of diversity in the fossil assemblage. Values below 2 are usually taken to indicate an assemblage too lacking in diversity to yield reliable measures of the environment. Hill's N2 is calculated using the Hill.N2 function in *rioja* (Juggins, S, 2017).

The level of indeterminate grains in the pollen analysis is checked.

Common sense checks are made of the range of each reconstruction, its consistency over time and between sites, and the frequency and amplitude of changes.

The reconstructions are compared with modern climate at the site, obtained by Geographically Weighted Regression using the same algorithms as those used to determine modern climate at the SMPDS sites (Chapter 1.8), using both CRU CL 2.0 (New *et al.*, 2002) at 10' resolution and, to test the impact of higher spatial resolution, WorldClim at 30" resolution (Fick and Hijmans, 2017). To give a more complete picture than top of core, the whole of the available Holocene reconstruction is considered. A further qualitative check, for the cores whose age range includes it, is made on the registration of the last glacial termination, since it is expected to be the most significant climate change experienced at these sites; good registration of the termination bodes well for locating D-Os.

The reconstructions are compared with the climatic interpretations in the literature on the cores. With one exception, Lago Grande di Monticchio, these are qualitative.

No other palaeoclimatic indicators are available from the same cores against which to test the reconstructions. While speleothems showing well-dated changes in climate that match Greenland events are to be found in the region, no sites were close enough to the pollen core sites for direct comparisons to be made, and consideration of speleothem-based climate across wider areas was prevented by the lack of pinning points between the speleothem and pollen core age models.

6.2 Results and discussion: reconstructions

6.2.1 Reliability of reconstructions

The set of reconstructions for both bioclimatic variables, using the full SMPDS set, including the results of bootstrapping, for all 16 selected cores are shown in Appendix C.

To ensure that a sharp rise is reliably evidenced, the upper 2σ bounds of the bootstrapped uncertainty at the beginnings of sharp rises should be well below the lower bounds at the peaks of the rises. Appendix C shows that most intervals in most cores satisfy this condition and should permit the identification of rapid warming events by pattern matching. But the width of the uncertainties differs between cores and along core, and at Iznik the reconstruction in the interval older than ~ 20 ka, which should include 4 GIs, fails this test, and similarly the pre-hiatus section of the Castiglione core. Neither is taken forward to pattern matching.

Some short intervals in some cores are suspect; these have wide bootstrapped uncertainties, unusual excursions, low Hill's N2, or a high fraction of indeterminate grains. We do not reject the core as a whole; when we come to the final evaluation of DOLPs, and such an interval determines the shape identified as a DOLP, we consider the evidence specifically and may reject the DOLP.

A few intervals have bootstrapped uncertainties wide enough to undermine pattern matching. These can usually be attributed to high abundance in the fossil samples of taxa poorly represented in the SMPDS which may have attracted poorly-evidenced optima (Chapter 5). For example, the uncertainty in Ioannina Tmin and gdd widens greatly between 73 and 68 ka "because the abundance of *Ulmus/Zelkova* increases from ca 0.75% to 6–8% of the sample total. This taxon is recorded at only 31 sites in the modern data set" (Turner *et al.*, 2020).

Unusual excursions in the reconstructions can also sometimes similarly be attributed to taxon abundances which are high compared to the SMPDS. Examples are the peak in reconstructed Tmin and gdd at Lake Xinias ~ 19 ka, which is driven by the dominance of Amaranthaceae, peaking at 91% of the pollen sum,

whereas in the SMPDS, this family represents 2.8% of the total abundance; and at Lago Grande di Monticchio, sharp excursions in all three variables at ~ 31 ka are attributable to 4 samples where *Equisetum*, which otherwise does not exceed 5% of the pollen sum in the 16 out of 542 core samples in which it is present, exceeds 50%; it forms only 0.1% of the abundance in the SMPDS.

Hill's N2 measures taxon diversity to establish how reliable a measure of the environment each sample provides. Appendix C shows vertical red lines at samples with Hill's N.2 < 2; these are scarce, and represent no general threat to the identification of DOLPs. They rarely coincide with wide uncertainties (an exception is the earliest Monticchio excursion), which is interpreted to mean that the main driver of bootstrapped uncertainties is high abundance of taxa poorly represented in the SMPDS, not a dearth of taxa.

6.2.2 Full versus restricted set calibration

A set of comparisons of the gdd reconstruction made using the restricted taxon set with that using the full set is shown in Figure 6.1; an example for one site was shown in Figure 5.28. The degree of difference between the two reconstructions varies greatly between cores and by age; at one extreme, they are very similar at Castiglione and Ioannina, but at the other, Iznik (already discounted above) and Zeribar diverge. The purpose is to identify sharp rises, so the offsets seen for instance in the Dead Sea and Ghab comparisons are not in themselves a problem, because the sharp rises are mostly in the same locations; but this is tested specifically in pattern matching. The match with modern climate is tested below.

The two sets yields very similar reconstructions during the termination and Holocene (~ 15 ka onwards), but the restricted set makes generally cooler reconstructions in the glacial (earlier than ~ 15 ka). Partly because of this, Lagaccione, Stracciacappa and Ghab appear to record the termination (~ 15k to 11.7 ka) better with the restricted set. The interpretation is that this reflects the substantial changes in taxon assemblages as the cores pass through the termination; both the full modern assemblage and the restricted set are good training sets for post-termination pollen cores, evidenced by highly similar calibrations and very similar Holocene reconstructions, but the difference in relative abundances drives the divergence in the glacial.

Based on this evidence, and in the absence of external evidence to support either set, we have no means of judging which is better, other than theoretical considerations – see Chapter 5. So in pattern matching (6.3) gdd based on the restricted set is included as one of the base reconstructions from which to derive DOLPs.

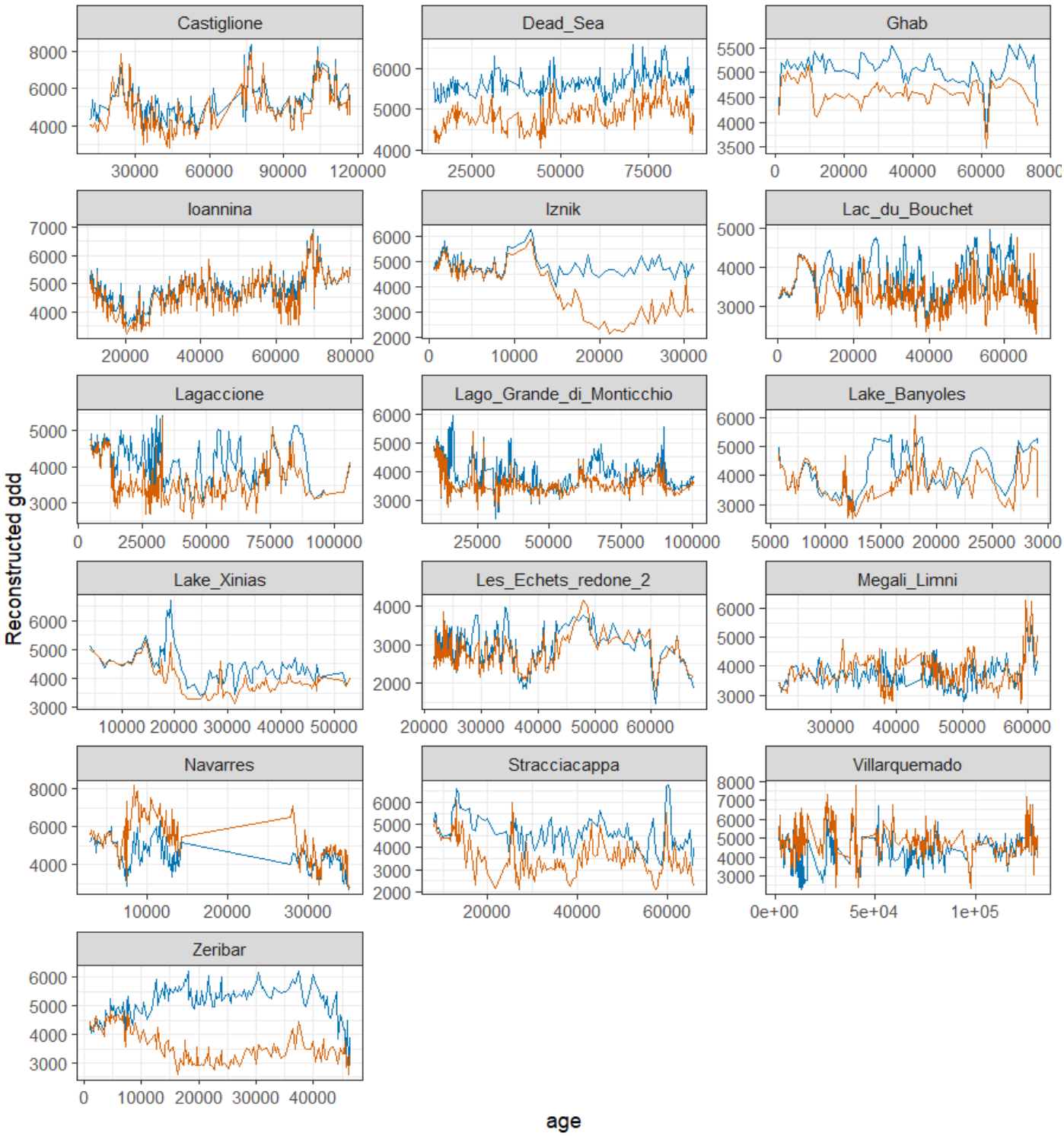

Figure 6.1 Comparison between gdd (growing degree days > 0 °C) reconstructed using the full set of 195 SMDS taxa (blue line) and using the restricted set (orange line) for the 16 selected cores.

Castiglione post-hiatus has a variable but often high fraction of indeterminate grains (Figure 6.2), which throws doubt on its ability to demonstrate D-Os well. Other cores have much lower fractions which do not impact pattern matching. This is taken into consideration when evaluating DOLPs below.

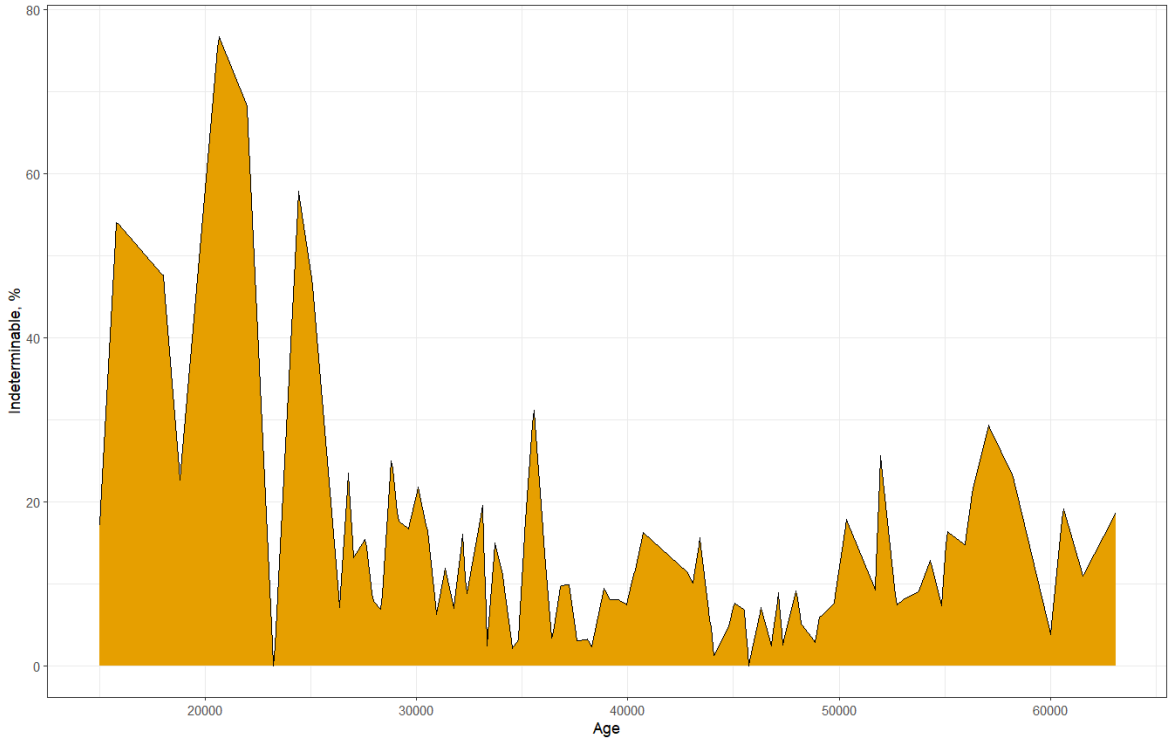

Figure 6.2 Castiglione fraction of indeterminate pollen grains, up to hiatus. Script: Castiglione indeterminates

6.2.3 Modern climate comparison

In Figure 6.3 and Figure 6.4, the Holocene portions of reconstructions for Tmin and gdd made using the full SMPDS set are tested against modern climate at the site, and appear broadly consistent with modern values, with no consistent offset. The modern climate differs very little between the 10' resolution CRU set and the 30" WorldClim set. Above it was noted that the restricted set yields very similar Holocene reconstructions.

Among the few inconsistencies are cool reconstructions for Dead Sea and Ghab, and a warm gdd (but not Tmin) reconstruction at Lac du Bouchet. A possible contribution to these differences is the nature of the catchments. The Dead Sea/Jordan catchment includes mountainous areas over 1000 m asl, so the climates

represented in its pollen are likely to be in general cooler than that at the lake site well below sea level. Similarly Ghab lies in a valley ~1000 m below the immediately surrounding terrain. Conversely, Lac du Bouchet lies at 1200 m asl at the top of a south-west facing slope in the Massif Central and may receive lowland pollen on upslope winds, a known feature of highland lakes (Liu *et al.*, 2020, and references therein), and may register pollen from climates warmer than its elevation suggests. Such offsets do not in themselves undermine the ability of the sites to register D-Os.

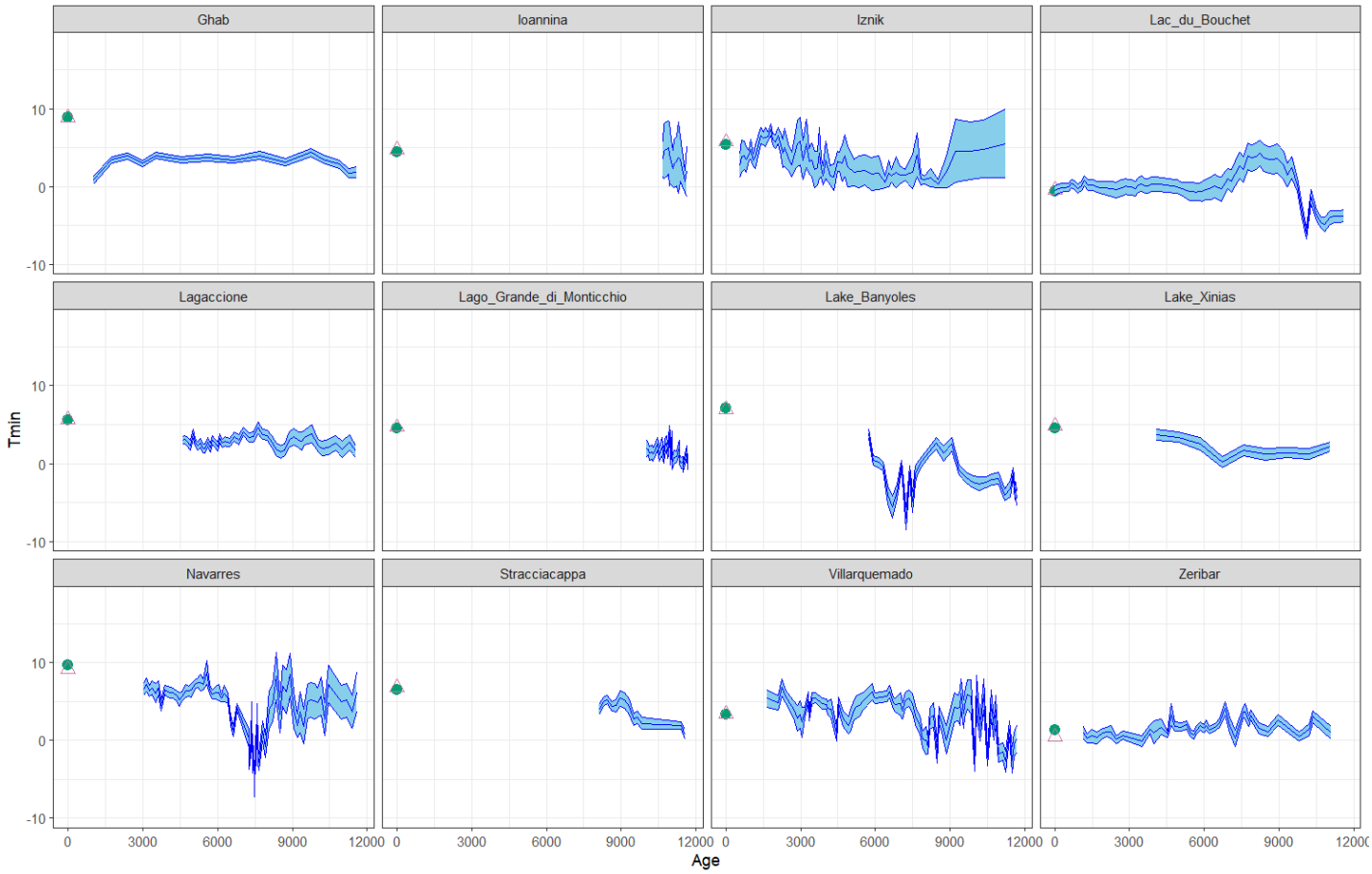

Figure 6.3 Bootstrapped (x 100) full SMPDS set reconstructions (ribbon width is ± 2 SD) for Tmin (temperature of the coldest month in °C) for the Holocene intervals (11.7 ka onwards) of the selected set of 16 cores (4 have no Holocene presence). Green points: CRU CL 2.0 modern climate at the site; pink open triangles: WorldClim modern climate at the site.

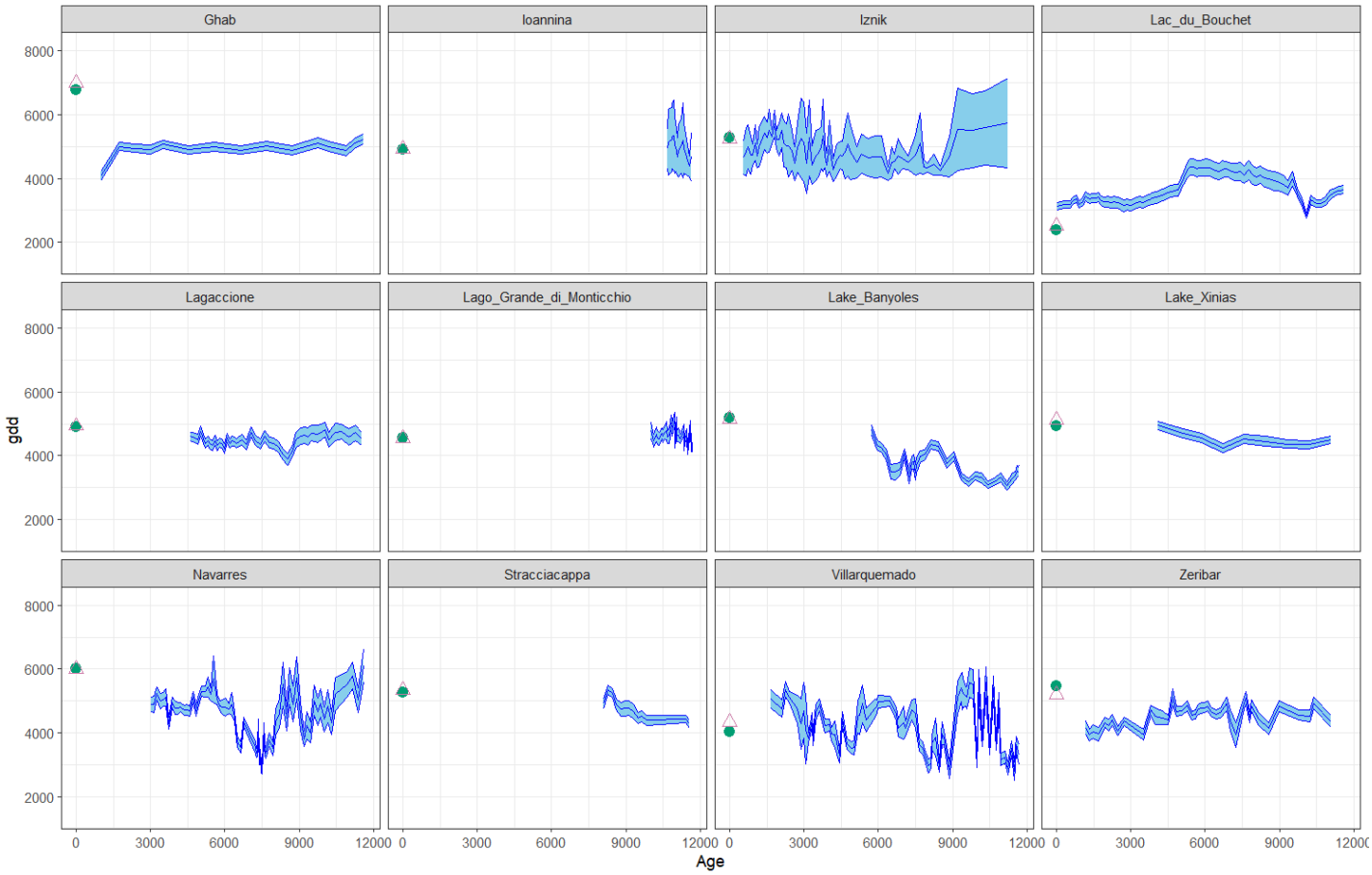

Figure 6.4 Bootstrapped (x 100) full SMPDS set reconstructions (ribbon width is ± 2 SD) for gdd (growing degree days > 0 °C) for the Holocene intervals of the selected set of 16 cores (4 have no Holocene presence). Green points: CRU CL 2.0 modern climate at the site; pink open triangles: WorldClim modern climate at the site.

In the plots in Appendix C, Lac du Bouchet, Lagaccione, Stracciacappa, and Ghab exhibit clear last glacial terminations, Navarres and Villarquemado less clearly; Zeribar may show a small offset. The situation is unclear at Banyoles and Xinias, and the Lago Grande di Monticchio termination is compromised by low N2. The restricted set reconstructions for gdd, as noted in 6.2.1, may record the termination better than the full set reconstructions, and since both sets record similar values in the youngest intervals, the restricted set reconstructions also match the modern climate well, again providing no evidence to distinguish between the two calibrations.

6.2.4 Literature comparison

The only record in the 16 core set for which quantitative, rather than qualitative, reconstructions exist is Lago Grande di Monticchio. Allen *et al.* (1999) and Allen and Huntley (2000), provide quantitative

reconstructions using response surfaces and “7816 surface samples obtained from sites scattered throughout the temperate and boreal latitudes of the northern hemisphere”, and using climate “interpolated from the IIASA database” (Allen and Huntley, 2000). They reconstructed MTCO, GDD5 (growing degree days above 5 °C) and alpha (ratio of actual to potential evapotranspiration). Their reconstructions and those made here using fxTWA-PLS show few resemblances (Figure 6.5). The response surface reconstructions tend to hop between certain values so that many sudden changes occur, and MTCO and GDD5 are both cooler on average than those made by fxTWA-PLS, which reconstructs GDD0, accounting for some of the offset. The step changes in the response surface reconstructions make it difficult to compare usefully with the fxTWA-PLS reconstructions.

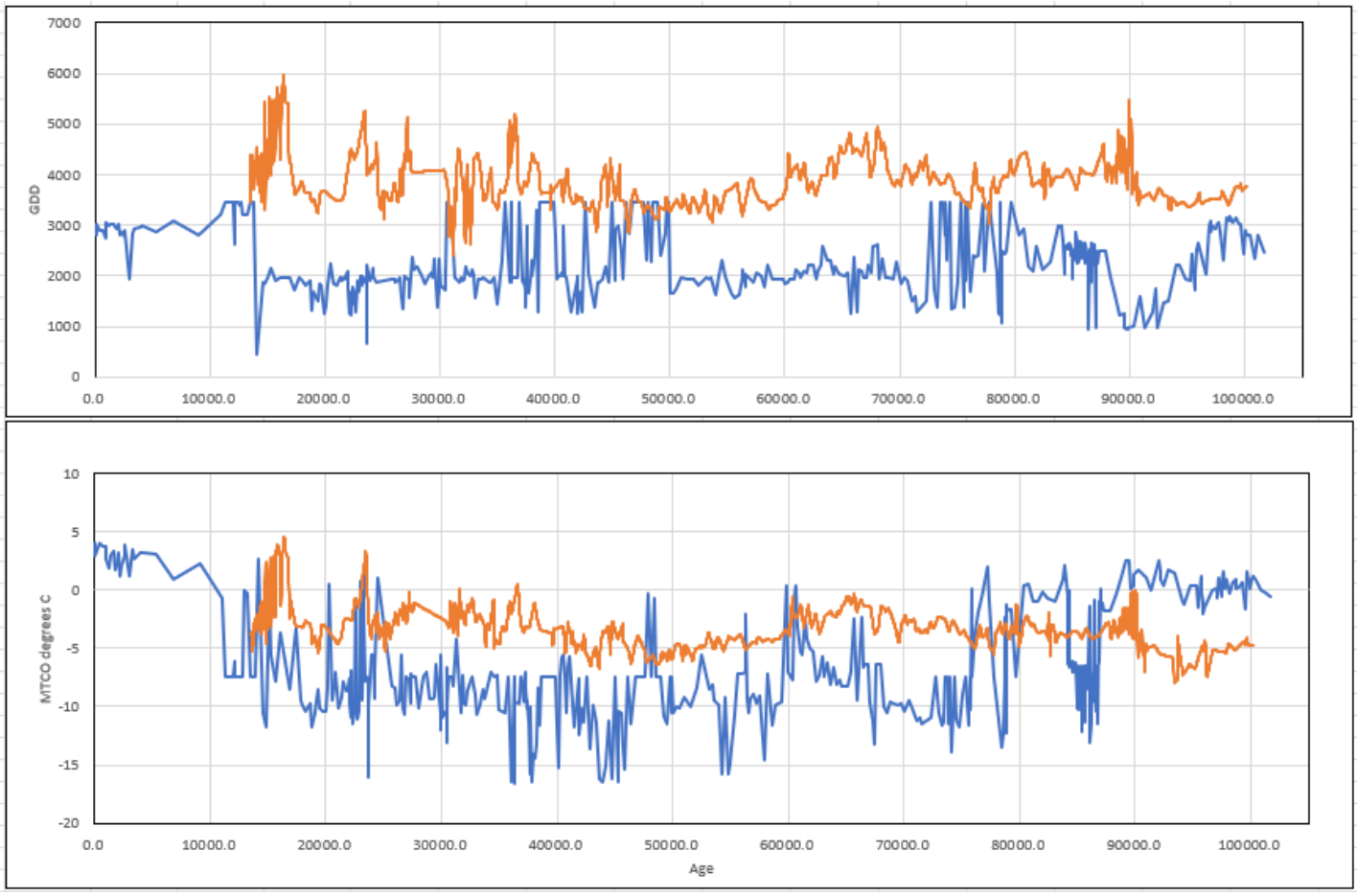

Figure 6.5 Comparison of (Allen et al., 1999; Allen and Huntley, 2000) response surface reconstructions with those made using fxTWA-PLS full SMPDS for GDD (GDD0 for fxTWA-PLS, GDD5 for A&H). Blue: Allen reconstructions. Orange: fxTWA-PLS reconstructions.

Parnell *et al.* (2016) applied BClim to the Monticchio record reconstructing the same bioclimatic values as Allen and Huntley (Figure 6.6). Some gross similarities are visible for both bioclimatic variables between the BClim and the fxTWA-PLS bootstrapped reconstructions: the instability at ~ 30 k, the feature at ~ 90 ka and the general shape between ~ 40 ka and ~ 70 ka. Closer comparison is not possible since the Parnell plots have such wide uncertainties and no mean is plotted. There is little visible similarity between the Allen and Huntley and the Parnell reconstructions.

The conclusion is that the previous reconstructions do not provide useful comparisons with fxTWA-PLS reconstructions.

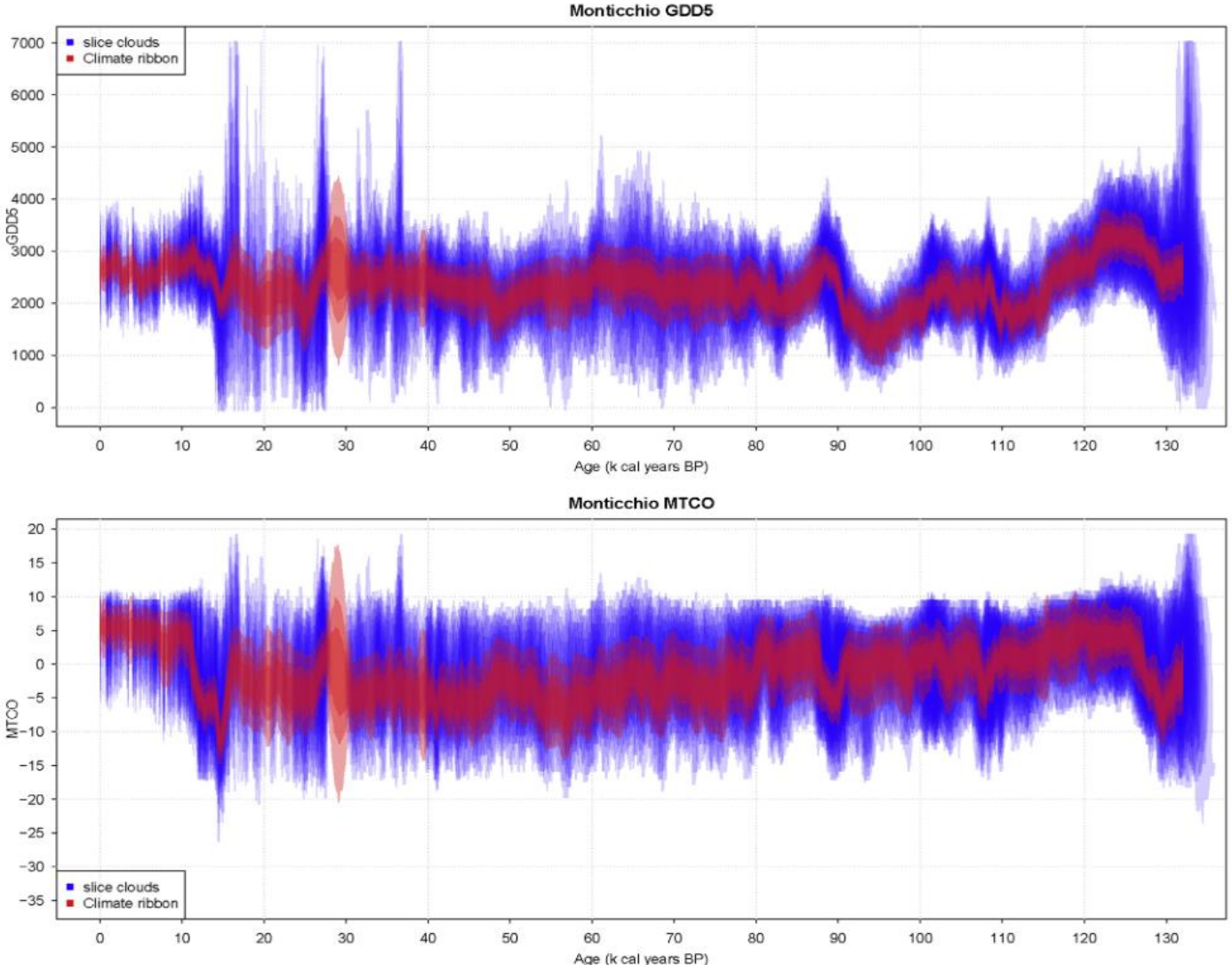

Figure 6.6 Part of Fig 3 from (Parnell et al. *(2016): Monticchio BClim reconstructions of GDD5 and MTCO. "The blue areas represent the 95% credible regions of the slice clouds whilst the red ribbons represent the 95% confidence intervals for each time grid point on a centennial time grid. Darker regions indicate the 75% and 50% regions."*

6.3 Methods: pattern matching

6.3.1 Choice of base reconstructions for pattern matching

Pattern matching (Chapter 2) takes templates from the Kindler et al. (2014) series, which are initially compared with GDD0 made using the full SMPDS taxon set (a 'base reconstruction'), with which it is most directly comparable because the Kindler temperature is likely to be weighted towards that during the season of highest snowfall, which was summer. Two other 'base reconstructions' were tested: MTCO using the full SMPDS taxon set reconstruction, since it might add information not contained in the GDD0 comparison, and GDD0 reconstructions made with the restricted taxon set.

Base reconstructions locate DOLPs. These locations can then be applied to other bioclimatic variables to test how well those other variables also exhibit DOLPs. For instance, the locations of DOLPS found by GDD0 can be applied to MTCO.

Samples younger than 13.5 ka were excluded to prevent the identification of the last termination as a D-O-like event.

6.3.2 Template and other pattern matching parameters

Template settings that were determined in Chapter 2 to be optimal are applied here, specifically:-

before = 10; *after* = 15	Template width younger and older than GI date, no. of datapoints (~20 yrs apart)
safe = 200	Minimum years between DOLPs: avoids 2 DOLPs in 1 template
meas = "smmdist"	The Euclidean distance: smmdist is standardised mean of mean distances
lspan = 0.1	Span used in loess detrending of Kindler series when extracting templates

Application of the pattern matching technique to the original Kindler temperature series showed that known D-Os were identified most reliably when the ED threshold was < ~0.7 (Chapter 2) and a default value of 0.75 was chosen for pattern matching using fossil cores, adjusted for individual cores.

To avoid identifying DOLPs which are patently too close together, the minimum age between recognised Euclidean distance troughs is 1000 years.

A DOLP is followed by a potential interstadial, a warm interval defined here as starting at the DOLP, the midpoint of the rapid rise in the bioclimatic value (Chapter 2), and ending when the reconstructed value returns to the value at the DOLP. Starting from the mid-point is a more conservative approach than starting from the first sign of a rise, the definition used by Rasmussen *et al.* (2014).

The shape traced by the bioclimatic variable during a warm interval is tested, to support the claim of the DOLP to be a real D-O. The shapes are characterised by the rise in the climatic variable after the DOLP, the area-under-the-curve of the subsequent warm interval, and the duration of the warm period. Small values reduce the probability that this is an interstadial and that the DOLP is a genuine D-O event.

rfilt = 0.75	minimum rise above DOLP (excursion; varies by bioclimatic variable)
afilt = 5	minimum area-under-curve (varies by bioclimatic variable)
tail = 100	limit to no of data points permitted in 'warm' interval (~ 2000 yrs)

Area-under-the-curve is the sum of the excess of the reconstructed values for each data point over the DOLP value during the warm interval.

To further characterise the strength of the evidence for the DOLP, the number of original physical samples which determine the shape identified as a warm interval is found, and their mean Hill's N2 is calculated.

samfilt = 3	Filters DOLPs based on sample counts
N2filt = 2	Removes warm intervals with mean N2 values < = N2filt

Figure 6.7 shows that to identify a DOLP, the underlying number of physical samples in the fossil record, from which the 20 year interval datapoints were interpolated, can never be less than four. Of these, at least two fall in the template-width window, defining the base and peak of the rise. At least one younger and one older physical sample are needed to define the low start and declining tail, and these may fall outside the

template-width window. The DOLP is the midpoint of rise, which except by accident is not a physical sample.

To define a warm interval, once the DOLP is established, a minimum of three physical samples are needed: the base and peak of the rise, and the younger sample. Of these, only the peak will necessarily fall inside the warm interval, and the base will fall before it. The count of defining physical samples for a warm interval is therefore those in the warm interval plus 2. In most cases there is more than one physical sample in the warm period. 'Rise' in Figure 6.7 is the rise from DOLP to peak tested by *rfilt* above, and the red area is the area-under-the-curve tested in *afilt*.

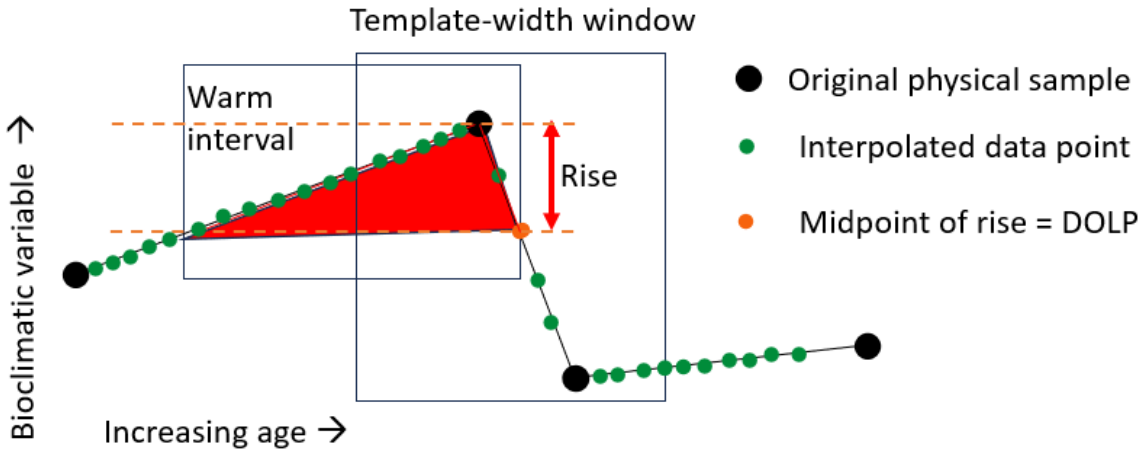

Figure 6.7 Cartoon showing the minimum number of physical samples defining a DOLP and a warm interval in a quantitative reconstruction. Orange point is DOLP at midpoint of rise, which except by accident is not a physical sample. The template-width window is the window which has identified the DOLP (interpolated points are in reality denser than shown, with 26 in the normal template-width window).

6.3.3 Core specific adjustments

The temporal resolution of the pollen cores is variable (Figure 2.19), and the amplitude of change in the reconstructed variables differs widely between cores (Appendix C). Applying the same filters to all cores finds too few rapid warming events in some and too many in others, compared with the number of Greenland D-Os to be expected during the respective interval. Therefore the ED thresholds and other parameters for these cores were adjusted, such that the number of identified points was ≤ the expected number. There is no practical alternative to setting the parameters by inspection for each core.

6.3.4 SEA tests

The plausibility of chosen sets of rapid warming events (DOLPs) was tested by Superposed Epoch Analysis (SEA) (Chapter 2).

6.3.5 Code availability

R code to provide template extraction, pattern matching and the evaluation of DOLPs is available at https://github.com/MarkGrenTurner/pattern_matching.

6.4 Results: pattern matching

The pattern matching technique works well in locating D-Os in the parent Greenland Kindler series (Chapter 2), so any weaknesses in identification of DOLPs are not principally algorithmic but relate to the data.

6.4.1 Impact of filter settings

Figure 6.8 shows by example how settings are applied and affect the identification of DOLPs, using the gdd reconstruction made using the full SMPDS set from Castiglione, including the pre-hiatus interval. After rejecting several trough points in the ED curve as being insufficiently like the templates, using the ED = 0.75 threshold, five more are rejected as the rise to the subsequent gdd peak is small; no further DOLPS are rejected on the grounds of area-under-the-curve, sample count or N2. The importance of the area and rise filters is seen where the ED curve identifies a small-scale event as a potential DOLP at ~ 100 ka which has minimal rise and area. The method is proof against some perturbations: Castiglione has a hiatus between 63 ka and 73 ka, which has not been removed prior to this analysis, and a potential DOLP is identified at 73 ka which is clearly artificial; the rise test removes it. The final result, with these filter settings, is that 18 DOLPs are accepted, compared with a potential 28 GIs in the Greenland series, though some GIs cannot registered because of the hiatus.

The bottom panel addresses the matching of DOLPs with Greenland events simplistically, without considering age uncertainties either in the core age model, which here is the ACER CLAM model, or the GICC05modelext chronology. It compares the location of DOLPs on the ACER age model chronology as red

lines with the GI initiation dates on the GICC05modelext chronology (Rasmussen *et al.*, 2014; Seierstad *et al.*, 2014), and shows rejected DOLPs as grey lines. Qualitatively it is clear that many DOLPs are highly plausibly real D-Os, but often it is not clear which D-O matches which DOLP; and before 73 ka the bootstrapped reconstruction uncertainties are too great to offer reliable DOLPs.

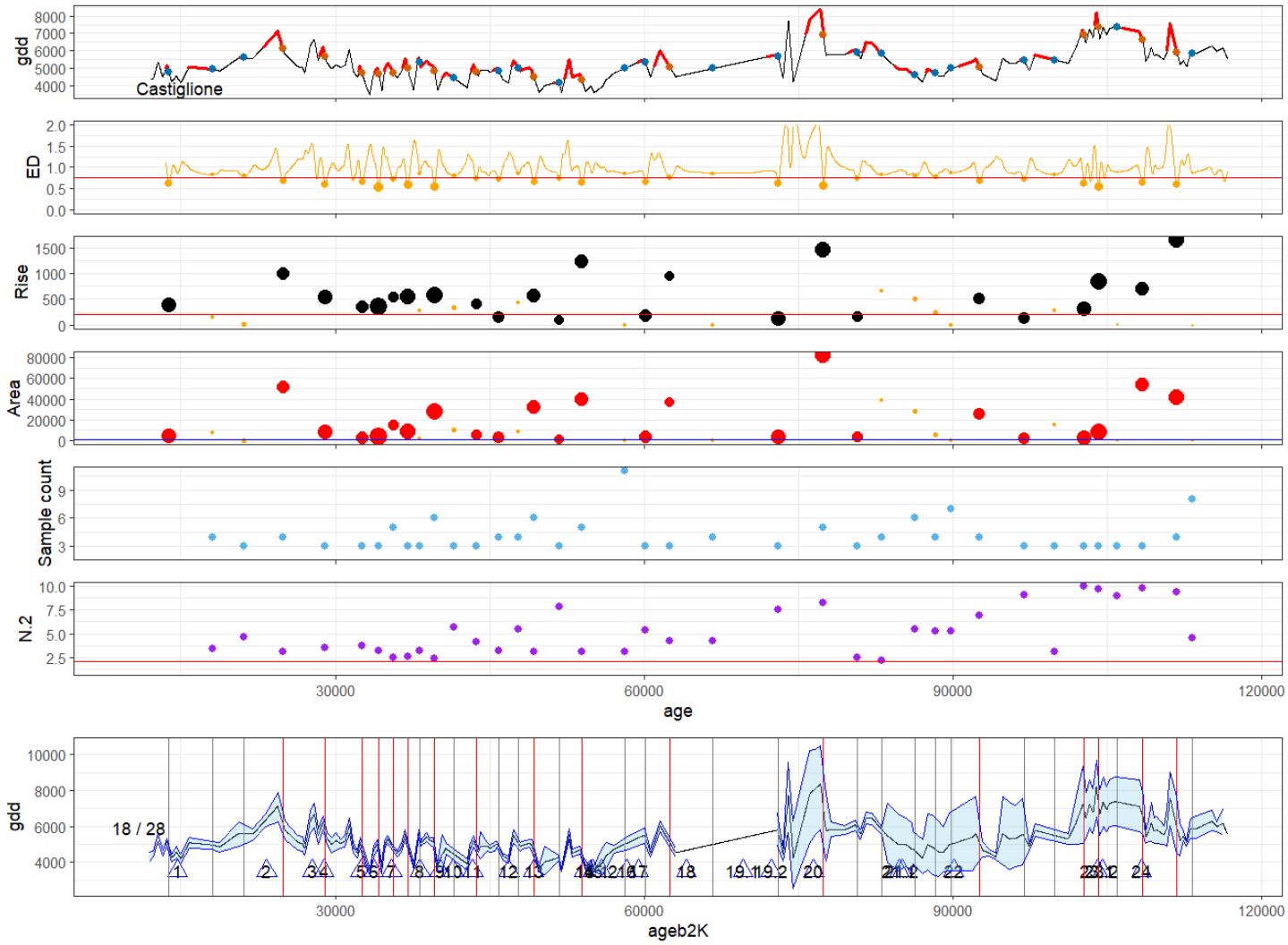

*Figure 6.8 Pattern matching filtering process applied to gdd (growing degree days > 0 °C) reconstruction at Castiglione. Top panel: gdd reconstruction; red points = finally accepted DOLPs; blue points = rejected DOLPs; red segments of reconstruction = warm intervals following all potential DOLPs. Second panel: ED curve with troughs falling below threshold (ED = 0.75) shown as points, size inverse to ED. Third panel: increase in gdd from DOLP value to peak as black points, size inverse to ED; orange points = DOLPs already rejected on grounds of ED; red line: threshold for rise (*rfilta*) = 200 degree days. Fourth panel: area-under-the-curve traced by warm interval; orange points = DOLPs already rejected on ground of ED; blue line: threshold for area (*afilta*) = 1000. Fifth panel: count of physical samples defining the shape of the warm interval. Sixth panel: mean Hill's N.2 for warm interval; red line = threshold for N.2 = 2 (*n2filt*). Bottom panel: repeat of gdd reconstruction with blue points indicating physical samples, with ±2 SD uncertainty added; red vertical lines mark finally accepted DOLPs, grey vertical lines mark rejected DOLPs; numbers are number of finally accepted DOLPs / number of GIs in apparent age range; numbers in triangles are GI numbers; GI dates on GICC05modelext scale. In all other panels, age is ACER age model.*

Inspection of Figure 6.9, which replicates the post-hiatus part of the lower panel in Figure 8.8, suggests

- Reconstruction uncertainty is not damaging to pattern matching (until the hiatus ~ 63 ka)
- if GI 2 is a genuine match for the nearby DOLP, the core age model may be inaccurate
- these settings have failed to pick up GI 3 but have picked up GI 4
- in the GI 5 to 9 interval, too many DOLPs are found and it is not clear which DOLP is which GI
- beyond that, matches are too unclear to assign to a specific GI, and GIs 14 to 17 do not appear to be registered (if the age models are sufficiently aligned to make this comparison).

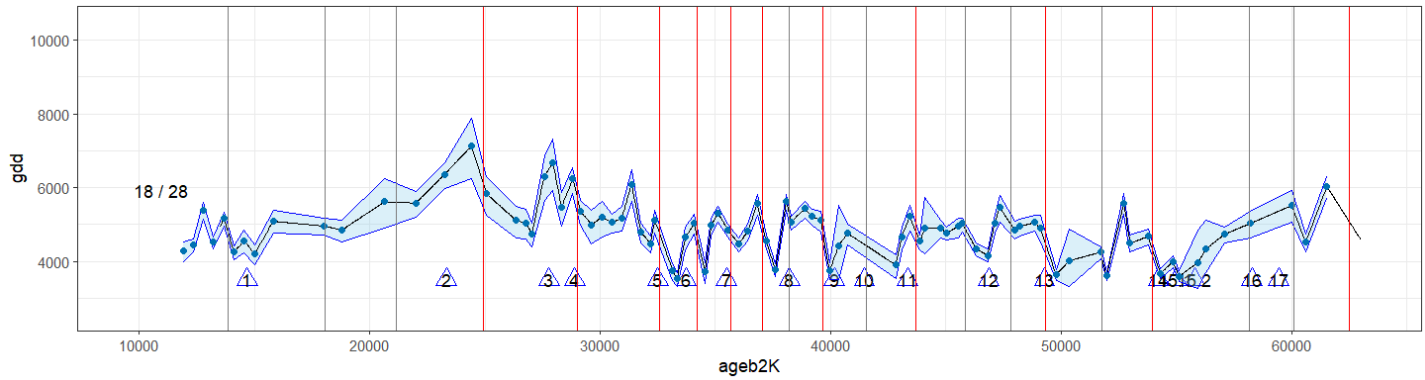

Figure 6.9 As lower panel in Figure 6.8, up to 63 ka, with ±2 SD uncertainty added.

The filter settings included in Table 6-3 appear to the best compromise for this core.

6.4.2 Pattern matching based on gdd reconstructions

Iznik and the pre-hiatus interval of Castiglione have been rejected on the grounds of wide bootstrapped uncertainty, and Villarquemado is now rejected because sharp rises in gdd cannot reliably be separated from changes caused by the multiple hiatus it contains. The plots showing pattern matching filtering for the 14 surviving cores made using the full SMPDS set reconstruction of gdd as the base reconstruction are in Appendix D. Table 6-3 summarises the filters used and the DOLPs found compared with the expected GIs in the age range of the cores, though this does not (yet) imply that the accepted DOLPs are all true D-Os.

Table 6-3 Settings applied to 14 cores, the age ranges of the cores, the number of GIs in those ranges, and the number of DOLPs accepted.

Core	ED threshold	Rise (*rfilta*)	Area (*afilta*)	Min. age	Max. age	Potential GIs in range	DOLPs accepted
Castiglione	0.75	200	1000	11,912	116,903	28	18
Dead_Sea	0.80	150	1000	14,244	88,031	24	13
Ghab	0.85	100	1000	1,000	76,335	21	6
Ioannina	0.75	300	1500	10,679	79,677	22	22
Lac_du_Bouchet	0.75	250	1000	30	68,869	19	18
Lagaccione	0.75	200	1000	4,600	106,174	27	17
Lago_Grande_di_Monticchio	0.75	200	1000	10,034	100,417	25	16
Lake_Banyoles	0.85	200	1000	5,742	29,092	3	3
Lake_Xinias	0.75	200	1000	4,098	53,048	13	3
Les_Echets_redone_2	0.75	200	1000	21,720	67,520	18	11
Megali_Limni	0.75	200	1000	22,000	61,500	17	13
Navarres	0.75	200	1000	3,018	35,210	6	4
Stracciacappa	0.80	200	1000	8,106	66,013	19	9
Zeribar	0.75	200	1000	1,157	46,386	11	7

6.4.3 Plausibility of selected D-O-like points (DOLPs)

Application of SEA to the gdd reconstruction using the full SMPDS taxon set shows that the DOLPs identified exhibit the pattern characteristic of D-O events. Navarres, Lake Banyoles, Lake Xinias, Ghab, and Zeribar provide too few DOLPs to perform SEA; Castiglione excludes the pre-hiatus interval.

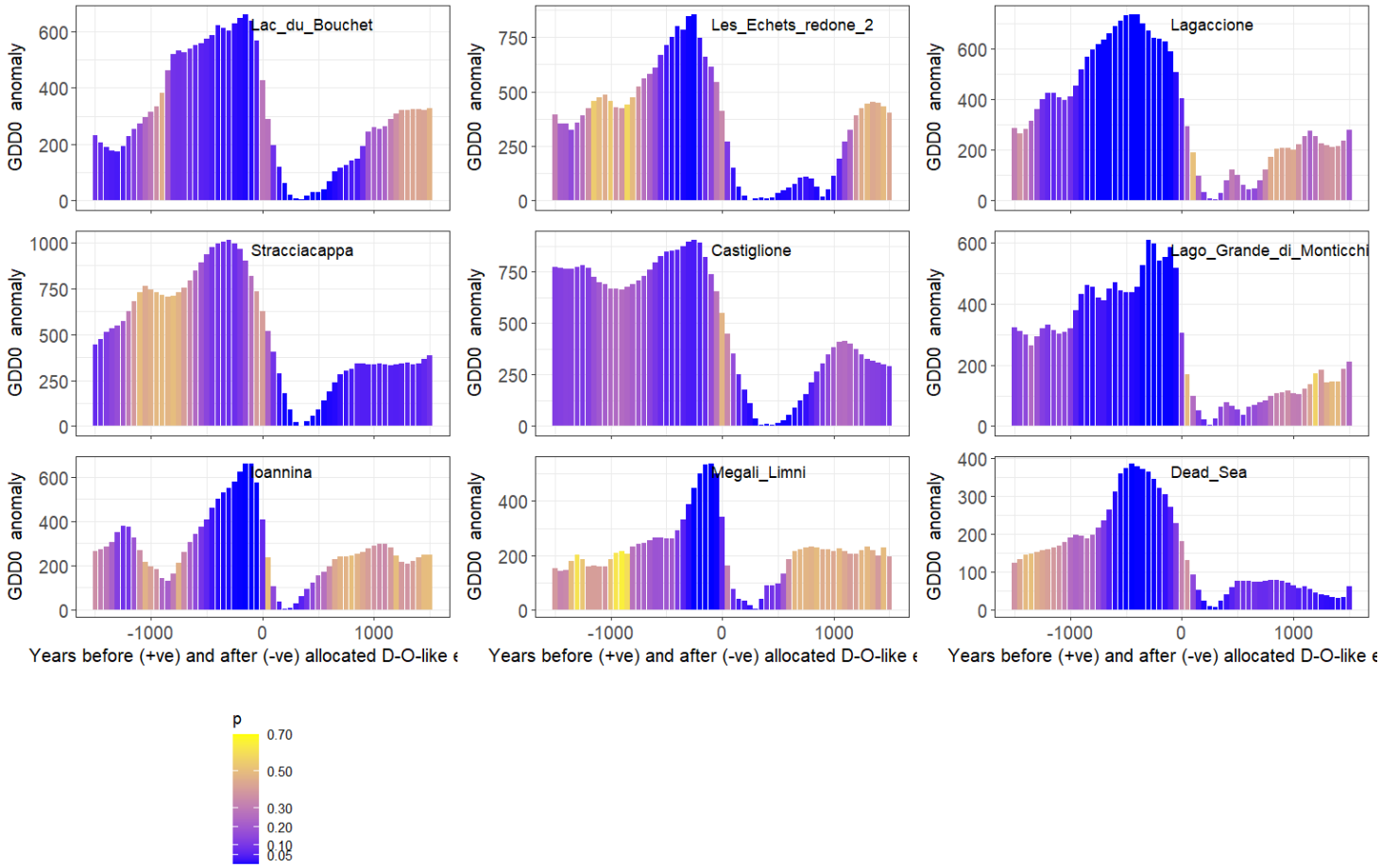

Figure 6.10 Superposed Epoch Analysis of potential warm intervals identified in the GDD0 (growing degree days > 0 ^{0}C) reconstructions made with full SMPDS. The centre-points of the rises (DOLPs) are aligned on year 0. The p *value scale indicates the probability that this mean bin value arose by chance, and applies to all panels.*

Applying SEA to the tmin (MTCO) reconstruction using the DOLP locations identified from gdd reconstructions (Figure 6.11), the SEA pattern is very similar but with sometimes higher *p*-values than for gdd, which suggests that gdd is, as proposed, the better match with Greenland events.

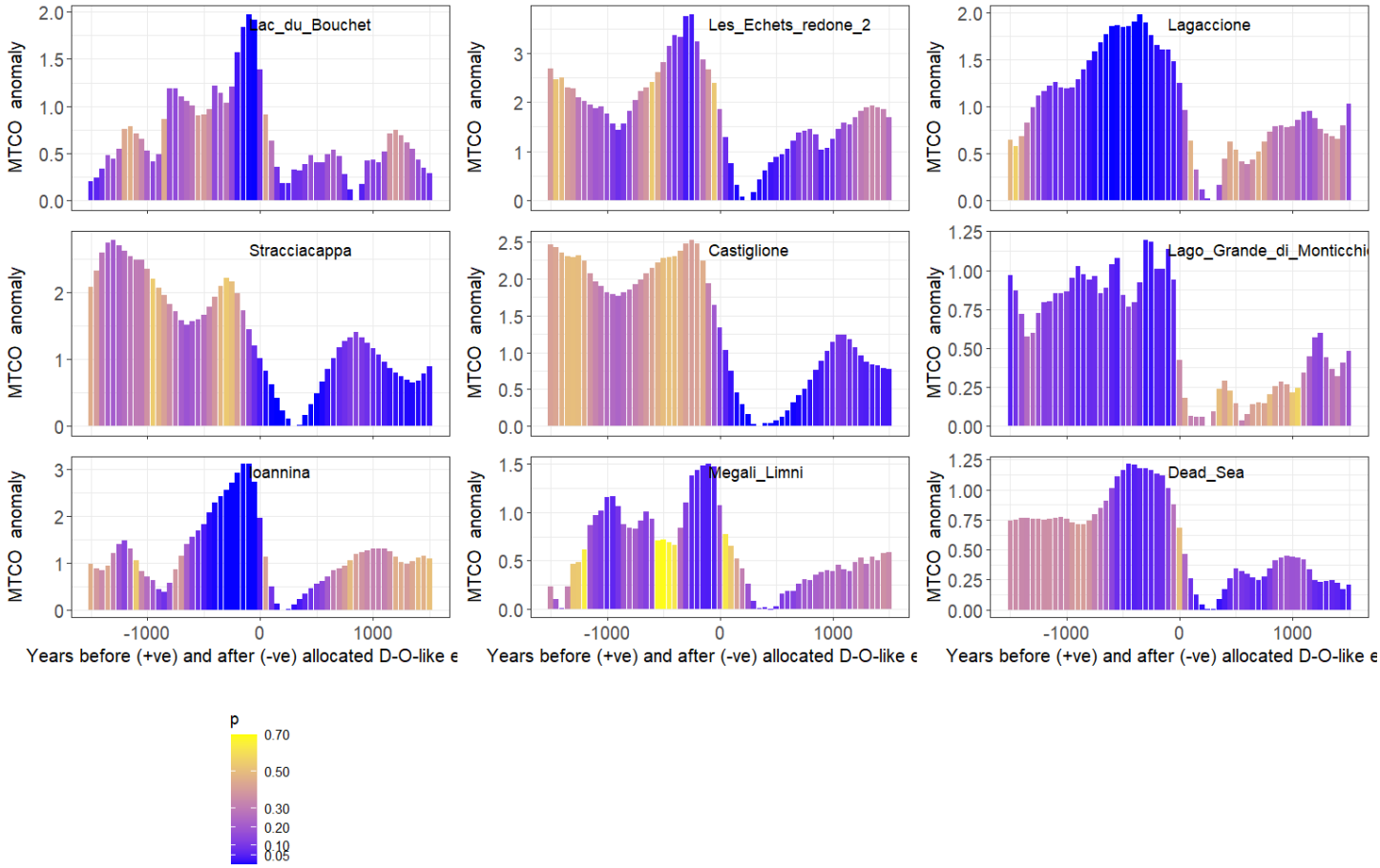

Figure 6.11 Superposed Epoch Analysis of potential warm intervals identified in the MTCO (tmin, temperature of the coldest month) reconstructions made with full SMPDS, using DOLP locations found using gdd as base reconstruction. The centre-points of the rises (DOLP) are aligned on year 0. The p *value scale indicates the probability that this mean bin value arose by chance, and applies to all panels.*

6.4.4 Base reconstructions other than full set gdd

Figure 6.12 compares DOLPs identified using (a) gdd, as above, and (b) tmin as base reconstructions, both using the full SMPDS taxon set. These bases find many DOLPS which are coeval, or nearly so, between them, especially if all potential DOLPs (rejected as well as accepted) are considered since the binary nature of the filtering process means that some DOLPs are only marginally rejected, but always there are DOLPS unique to each. While differences can be expected between the gdd and tmin patterns owing to changing seasonality due to Milanković cycles, the strong coincidences between the two strengthens support for both the reconstruction method and pattern matching. It is notable that some cores exhibit much less variability than others (for instance Ghab and Lake Xinias), making it less likely that DOLPs can be identified.

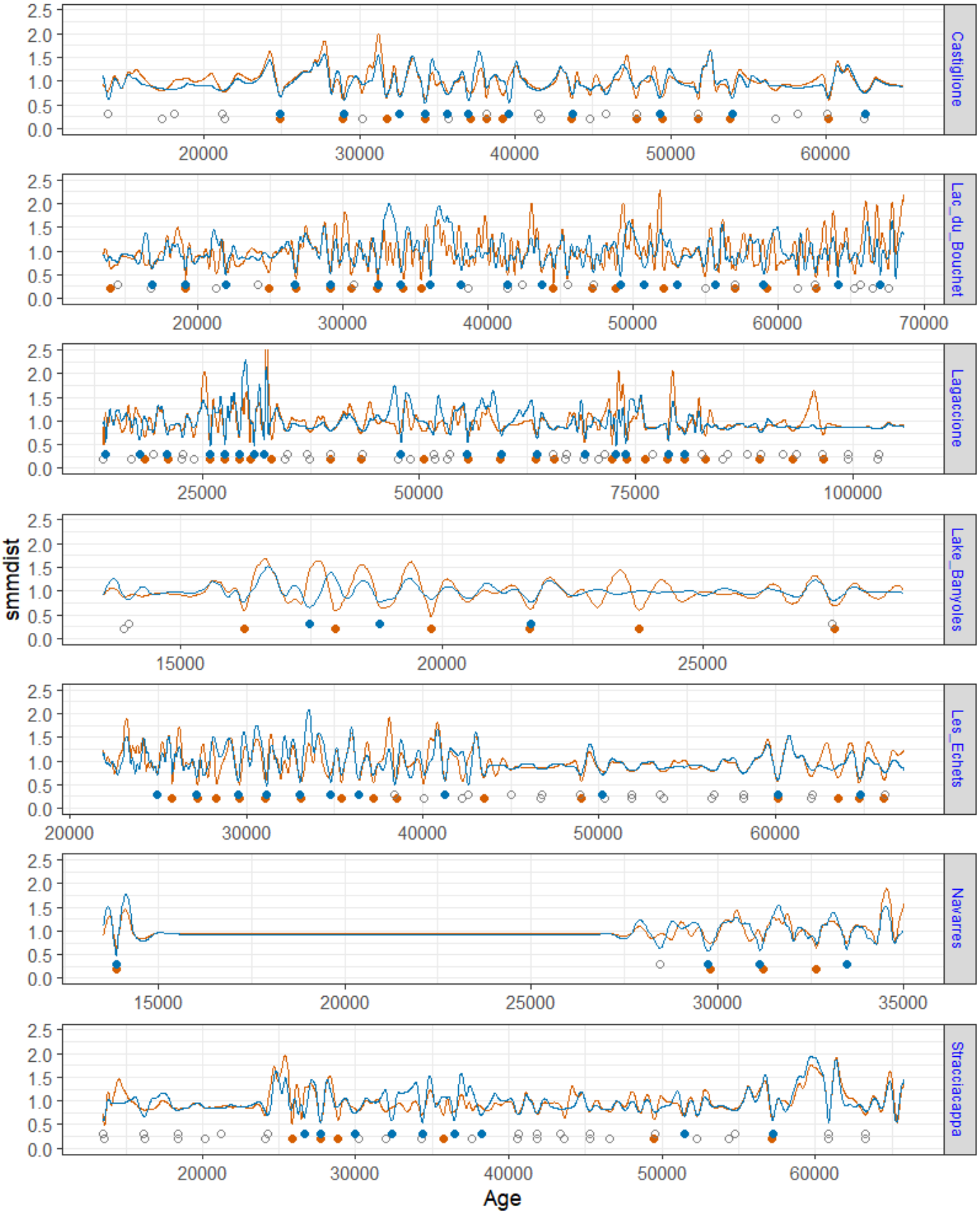
smmdist
Age
Castiglione
Lac_du_Bouchet
Lagaccione
Lake_Banyoles
Les_Echets
Navarres
Stracciacappa

*Figure 6.12 EDs (*smmdist, *standardised mean of mean distance) and DOLPs using full SMPDS set for 14 cores. Blue: using gdd (growing degree days > 0 °C) as base reconstruction; blue line =* smmdist*, blue points are final accepted DOLPs and open points on same line rejected DOLPs. Orange: using tmin (temperature of coldest month, °C) as base reconstruction; orange line =* smmdist*, orange points are final accepted DOLPs and open points on same line rejected DOLPs. Age is ACER or original given age.*

Both Figure 6.11 and Figure 6.13 show composited warm intervals in tmin. In the first, the intervals are located using gdd as the base reconstruction, in the second, using tmin. The tmin-based SEA gives a rather clearer picture with lower *p*-values in the peak area, but the difference between the two is at most sites small. The interpretation is that the differences in the patterns exhibited by gdd and tmin reconstructions are not significant.

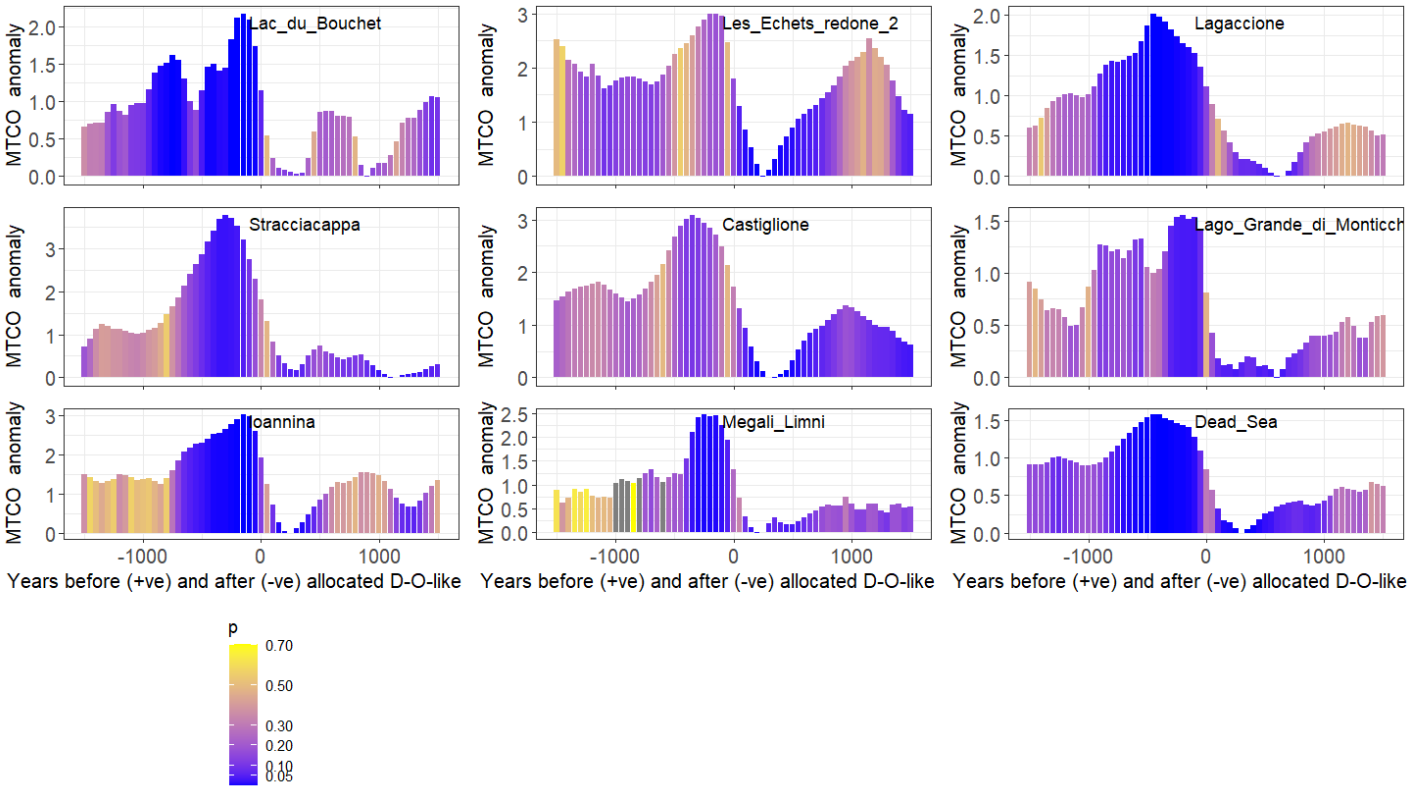

Figure 6.13 Superposed Epoch Analysis of potential warm intervals identified in the MTCO (tmin, temperature of the coldest month) reconstructions made with full SMPDS, using DOLP locations found using MTCO as base reconstruction. The centre-points of the rises (DOLP) are aligned on year 0. The p *value scale indicates the probability that this mean bin value arose by chance, and applies to all panels.*

6.4.5 Restricted set gdd reconstructions

Pattern matching applied to gdd reconstructions made using (a) the full and (b) the restricted sets (Figure 6.14) generally identifies the same DOLPs, though the degree of coincidence varies between cores. There is some evidence that the amplitude of the *smmdist* curve is increased with the restricted set, with lower trough points, signifying improved resolution of sharp rises. Given that the restricted set pattern matching used the same filters as the full set reconstructions for convenience, and that these could be tuned to the

specific reconstruction, this supports a view that, certainly for most cores, both sets provide plausible and similar DOLPs. Again this provides no grounds for preferring either set.

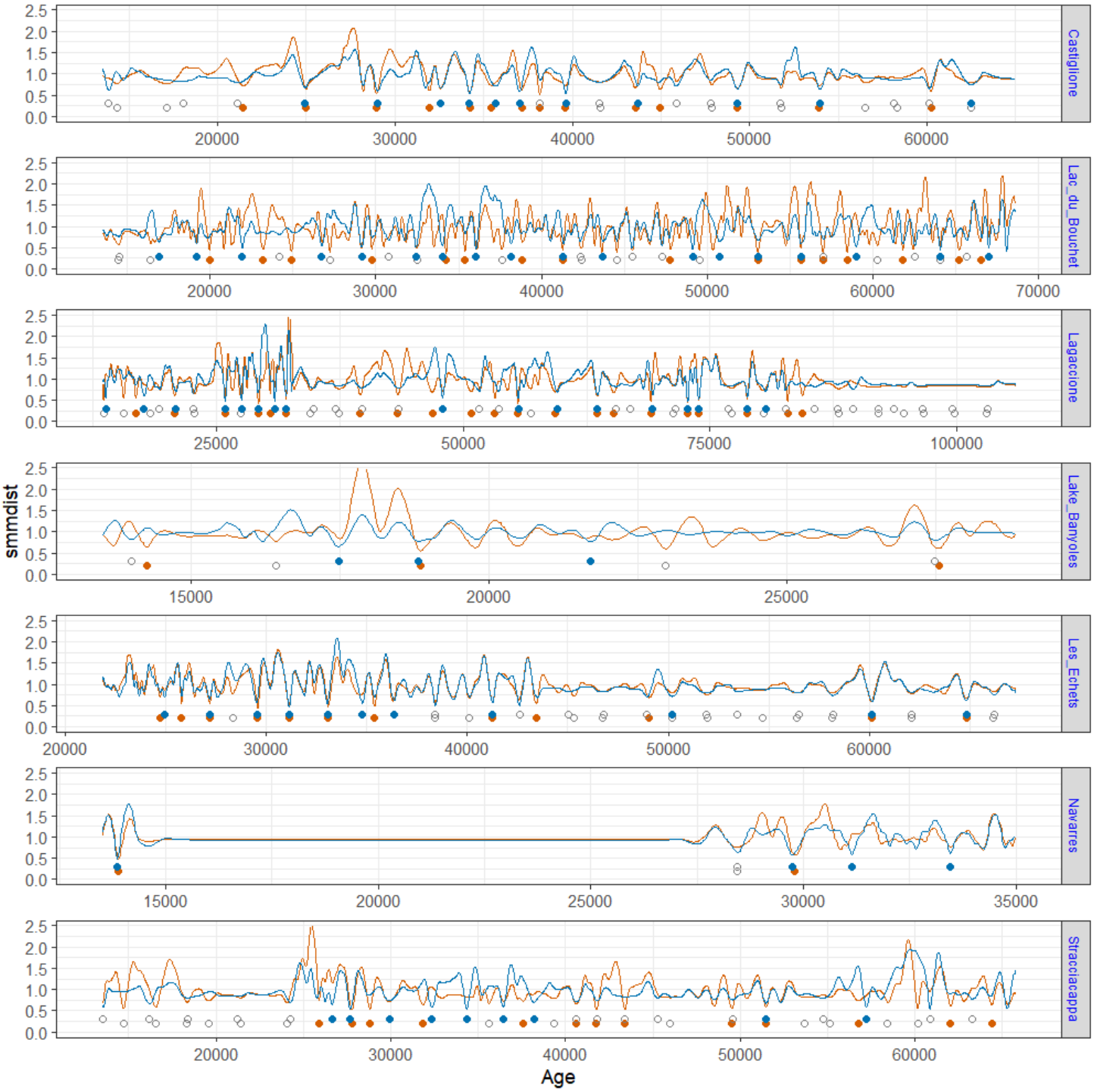

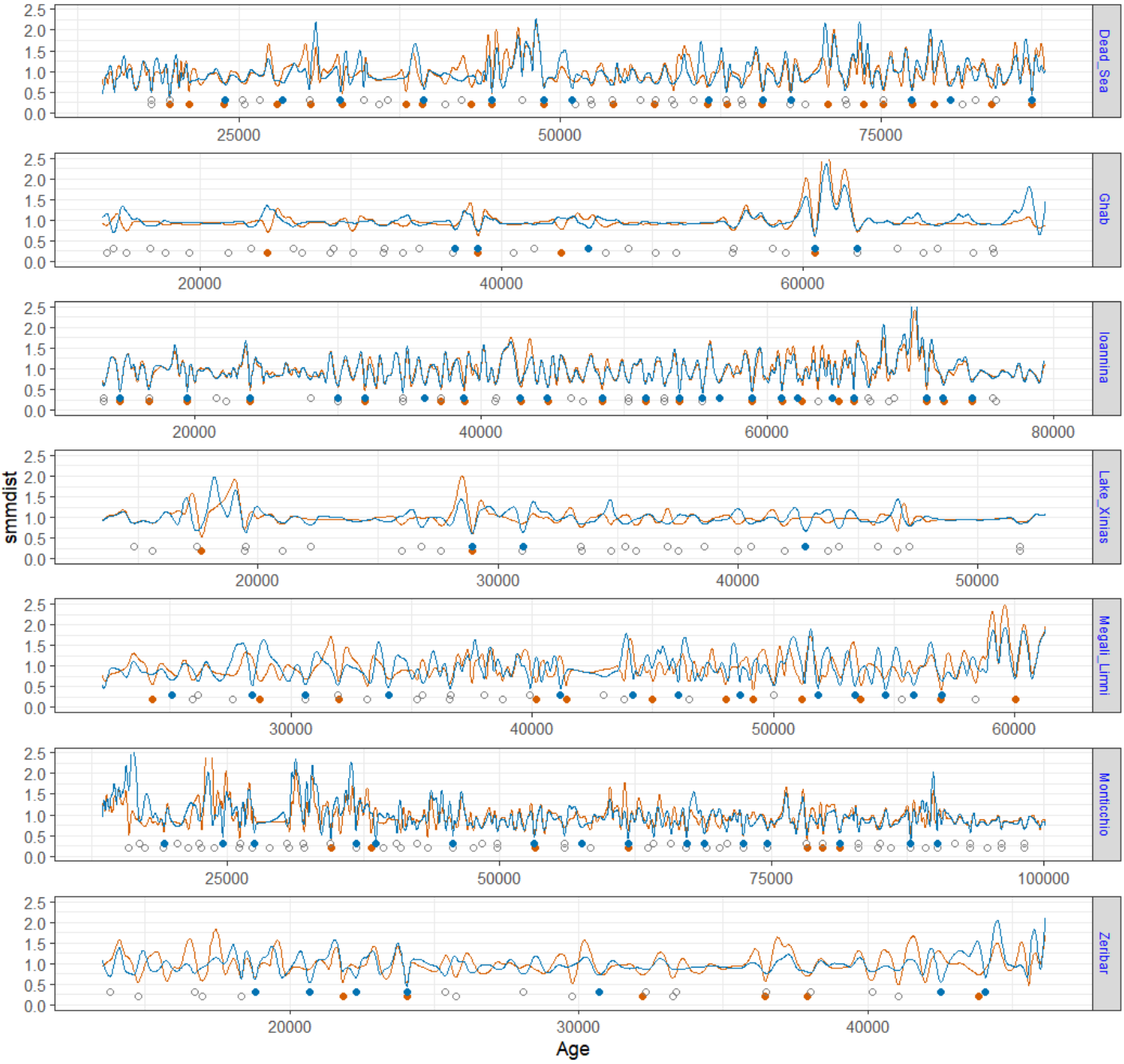

Figure 6.14 Blue line: smmdist *using gdd (growing degree days > 0 °C) reconstruction for Lac du Bouchet using full SMPDS set as base reconstruction; blue points are final accepted DOLPs and open points on same line rejected DOLPs. Orange line:* smmdist *using restricted taxon set gdd as base reconstruction; orange points are final accepted DOLPs and open points on same line rejected DOLPs. Core age is ACER or original age.*

6.5 Age comparisons

The probability that a DOLP represents a real D-O depends not only the robustness of the reconstruction

locally and the strength of the evidence that the shape is D-O-like, but also its closeness in age to a

plausibly matching Greenland event. This requires consideration of the core age models, their uncertainties, and the uncertainties in the GICC05modelext chronology.

6.5.1 Age-depth modelling

Age-depth models were developed by the original palynologists for all 14 remaining cores. The models differ in methodology. To harmonise chronologies between cores, the ACER database project (Sánchez Goñi et al., 2017) built consistently treated models, updating the radiocarbon age calibration to IntCal13; 11 of the 14 cores are taken from the ACER database, and all except Lago Grande di Monticchio, which retains its original well-based model (Allen *et al.*, 1999, and references therein), have CLAM models (Blaauw, 2010) for the majority of their age ranges, in addition to their original models. In this project, for consistency, a new set of age models was developed, updating to IntCal20, for all but Lago Grande di Monticchio.

Uncertainties in the form of maximum counting errors ('MCE') are given for the GICC05modelext chronology back to 60.2 ka, but none for the interval older than that; MCE is considered to be roughly equivalent to 2 SD (Andersen *et al.*, 2006).

6.5.2 Matching DOLPS and GIs

Potential matches between DOLPs and GIs can be proposed using the overlaps between the age uncertainties of both, but a match cannot be considered in isolation. Where a DOLP or GI is a potential match for more than one partner, which is common, the assignment of it to a specific partner excludes all other matches. This leads to the concept of a limited number of valid series of matches which must monotonically increase in both age and depth, and whose uniqueness may depend on as few as one initial match.

6.6 Methods: age comparison

6.6.1 Consistent updated age-depth models

ageR is used to develop a consistent set of age models for 13 of the 14 cores (Villegas-Diaz, Roberto, Cruz-Silva, Esmeralda, Harrison, Sandy P., 2021. ageR: Supervised Age Models. doi:10.5281/zenodo.4636715).

This is a wrapper for *rbacon* (Blaauw M, Christen J, Aquino Lopez M (2022). rbacon: Age-Depth Modelling using Bayesian Statistics. R package version 2.5.8, https://CRAN.R-project.org/package=rbacon). IntCal20 is used as the radiocarbon age calibration (Reimer *et al.*, 2020).

Dating points are taken from the ACER database for 11 cores and from Neotoma for the remainder. Some dating points are 'events'. These are changes in the pollen assemblage which are deemed to reflect climatic events, for instance D-O 8 or 12, or the onset of MIS 3, and are given the dates of these events in the Greenland record on the GICC05modelext chronology. These were ignored in constructing the new age models to avoid circularity, the purpose being to locate such events by other means. Points ignored by the ACER modelling were also ignored. Hiatus were set where they exist.

ageR runs an *rbacon* age model for every combination of (a) a set of values for sedimentation times, in years cm^{-1} ('accumulation rate') and (b) a set of values for thicknesses of slices which are treated as having constant accumulation, in cm ('thickness'). These values are set by the user. Each age model or 'scenario' is ranked in descending order of success, defined as lowest "abc" i.e. lowest area between curves of prior and posterior accumulation rates. However the process can yield implausible results, and the user must judge which model is most satisfactory. The criteria are:

- The prior distribution of accumulation rates (which assumes a gamma distribution) should be very similar to the posterior; the area between the two is "abc".
- The log of objective plot should be trendless and narrow.
- The age-depth plot should make sense compared with the dating points and their uncertainties.

Table 6-4 lists the parameters of the models selected as most plausible for the 14 cores. The original Monticchio age model is well-based, but the dating points used are not available and the dating points published with ACER do not accord with it, so no *rbacon* model was built.

Table 6-4 Accumulation rates and thicknesses for preferred rbacon *age models.*

Core	Accumulation rate (years cm^{-1})	Thickness (cm)
Ioannina	10	40
Lac_du_Bouchet	38	15
Lagaccione	20	50
Lago_Grande_di_Monticchio	Original model only	
Lake_Banyoles	05	50
Lake_Xinias	20	24
Megali_Limni	38	13
Navarres	66	2
Stracciacappa	50	14
Castiglione	53	50
Les_Echets_redone_2	30	50
Dead_Sea	07	100
Ghab	57	10
Zeribar	10	25

Each age model, other than the original, specifies the uncertainty in the age. Each core except Lago Grande di Monticchio has at least two, often three, age-depth models available, each created by a different methodology. The principal models use here are those developed using *ageR*, but ACER models are also plotted for information and to illustrate the degree of variability even in well-founded models, and differences are discussed where necessary.

6.6.2 Uncertainty overlaps

To identify possible matches of DOLPs with GIs, for each core, each DOLP accepted at the end of pattern matching is dated using the age model(s) above, including uncertainties, and compared with the ages and uncertainties associated with GIs. The repertoire of DOLPs is that provided using the full set gdd reconstruction as the base reconstruction.

A possible match is identified when the 2 SD uncertainties of the DOLP and the MCE of a GI overlap, so a given DOLP may be a possible match for more than one GI, and a given GI for more than one DOLP. The youngest DOLPs and GIs have the narrowest uncertainties. Starting at the young end, if a given DOLP is then assigned to a given GI, the next oldest assignment must be of an older DOLP to an older GI.

The results integrate pattern matching results with age modelling, and in coming to views on the realism of proposed DOLPs consider all the evidence collected so far on the reliability of the underlying data. This includes bootstrap uncertainties, unusual excursions, Hill's N2, the level of indeterminates, the filtering tests in pattern matching, the variability of the reconstruction (complacency), and the presence of hiatus. The process may be iterative, in that initially rejected DOLPs may be reviewed in the light of age uncertainty overlaps, or accepted DOLPS rejected on the grounds of age.

6.7 Results: age comparisons

6.7.1 Potential matches: example

Figure 6.15 illustrates, for Lagaccione, the process by which potential matches can be identified and evaluated.

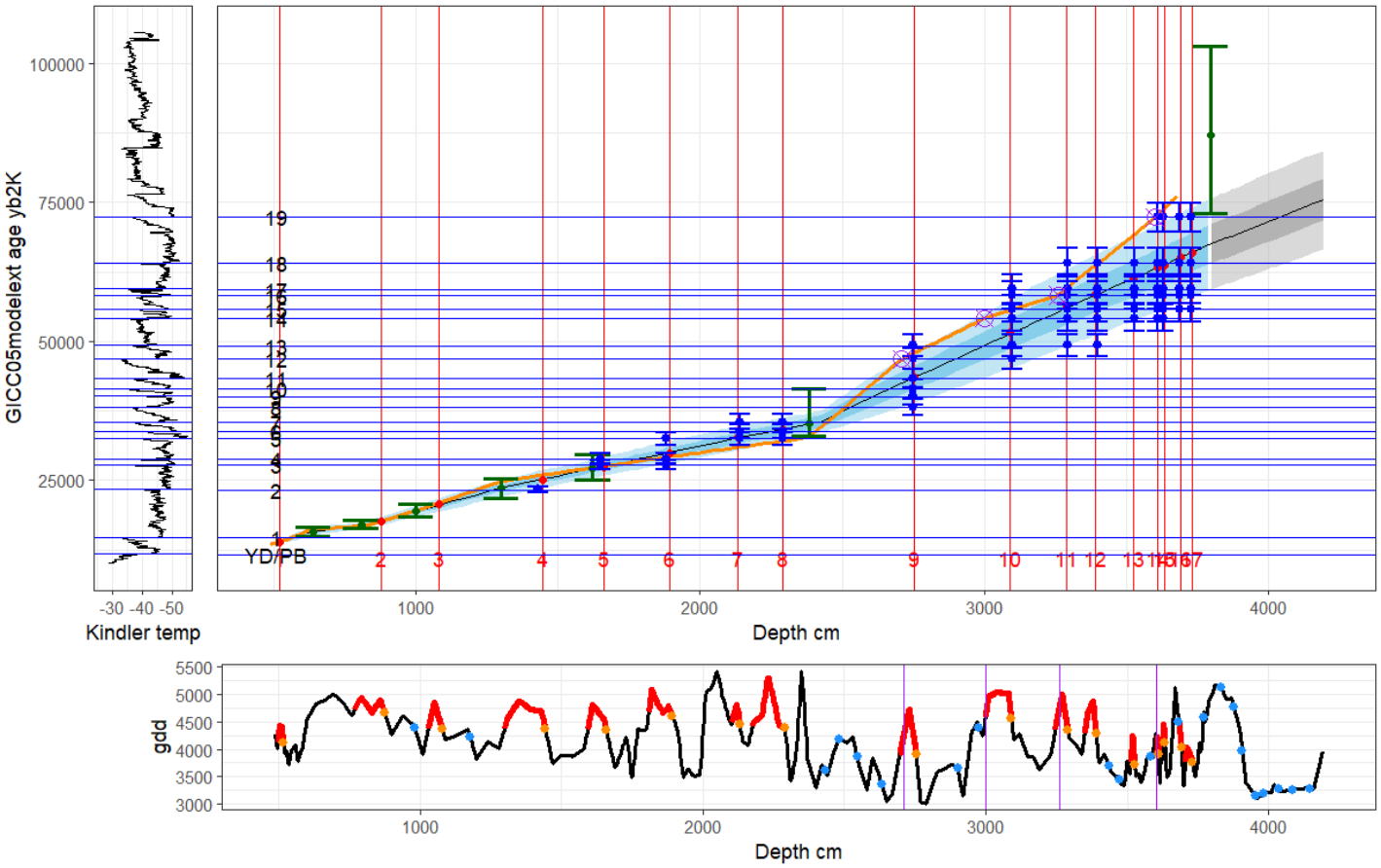

Figure 6.15 Potential matches between DOLPs, using gdd reconstruction and the full SMPDS set, and GIs for Lagaccione. Main panel: age model; vertical red lines mark accepted DOLPs, with sequential identifying numbers; blue horizontal lines are GICC05modelext ages of GIs (less 50 years), red points are intersections of DOLP and rbacon age model median; blue ribbon: central line is rbacon

age model median value, with 75% (darker) and (lighter) 95% uncertainties; green points and error bars are core dating points with uncertainties; blue points and error bars are ages and MCEs of those GIs which overlap with uncertainty of DOLP age. Orange curve: ACER age model. Purple circles with cross: 'events' determining ACER age model. Lower panel: gdd reconstruction for Lagaccione using full SMPDS taxon set, with accepted DOLPs marked by orange points; red segments of reconstruction are warm intervals; blue points are rejected DOLPs; vertical purple lines: 'event' locations in ACER age model. Vertical panel: Kindler Greenland temperature in °C on GICC05modelext scale, aligned with main panel.

The age model up to DOLP 8 (red number) is constrained by several radiometric dates with narrow uncertainties, so potential matches in this interval can be evaluated with some confidence. By inspection, DOLP 1 can be accepted as matching GI 1, but DOLPs 2 and 3 are rejected as matching no possible GI. DOLP 4 matches GI 2, which has no other matches. DOLP 5 could be GI 3 or 4, and DOLP 6 could be GI 3, 4 or 5; GIs 3 and 4 have no other potential matches, so probably DOLP 5 matches GI 3 and DOLP 6 matches GI 4. DOLPs 7 and 8 could each match any of GIs 5, 6 and 7. After that, DOLP 9 cannot match GI 7, so there are 2 DOLPs to fit 3 GIs. Given the error bar on the dating point after DOLP 8, any monotonic combination is acceptable. Reviewing the rejected DOLPs immediately older than DOLP 8 (Appendix D) shows these are rightly rejected, so it appears GI 7 is not recorded.

The conclusions from the review up to this point are that

- Some accepted DOLPs are very probably real D-Os, but conversely some are clearly not.
- Not all GIs are registered as DOLPs.
- Age uncertainties can make it hard to assign a DOLP to a specific GI even when the DOLP is highly plausibly a D-O.

After DOLP 8, the situation is more challenging because the median *rbacon* and ACER (orange line) age models now diverge, because the ACER model depends on 'event' dates, deliberately ignored by *rbacon.* These dates are shown as purple crosses in circles in the main panel of Figure 6.15 and their positions by vertical purple lines in the lower panel, and are listed in Table 6-5, where their dates are taken from the GICC05modelext chronology. These 'events' are assigned to specific D-Os and attract the Greenland dates in the ACER dating information table. This way of identifying D-Os is independent of pattern matching, yet both methods have identified highly similar intervals as D-O like, in this case DOLPS 9, 10, 11, and 14/15. This is independent support for the skill of pattern matching.

Table 6-5 'Event' based dating points at Lagaccione using GICC05modelext chronology

Depth (cm)	Age	SD of age	Event
2710	46,810	956	D-O 12
3000	54,170	1150	D-O 14
3260	58,230	1256	D-O 16
3602	72,280	1478	D-O 19

The *rbacon* model ignores the 'events', to avoid circularity; the interval after DOLP 8 is a straight-line extrapolation, and *rbacon* disregards the Vico tephra date of 87 000 ± 7 000 years cal BP at 3798 cm depth with all tested settings, so its slope is less than that of the ACER model. Even were the slope similar, similarly wide uncertainties would still exist, so this older interval is a demonstration of the issues when wide uncertainties are involved.

Because of this divergence, the assignments of DOLPs to GIs in Table 6-5 differ from those likely to be deduced from the *rbacon* model in Figure 6.15; DOLP 9 could match any GI from 8 to 12, DOLP 11 could match any GI from 12 to 17, and so forth. More generally, the interval from DOLP 9 on contains 9 DOLPs, 4 of which are supported by independent opinion based on pollen assemblage changes, and 11 candidate GIs ranging from 8 to 19, so some GIs are not registered as accepted DOLPs. Taking the matches closest to the median rbacon model, DOLP 10 matches with GI 11, 11 with 13, 12 with 15, 13 with 16, 14 with 17, and 15 and/or 16 with 19.

The review of this older interval reinforces the view that many DOLPS are real D-Os, that not all GIs are registered as DOLPs, and that wide uncertainties can make it impossible to assign DOLPs to specific GIs.

6.7.2 Potential matches: 12 cores

The plots for 12 further cores are given below, with commentary on them. At the end of the section, Table 6-6 summarises the conclusions.

Lake Banyoles identifies 3 DOLPs but yields no points where the uncertainties in the DOLP age model date overlap with the GI uncertainties, and is not shown.

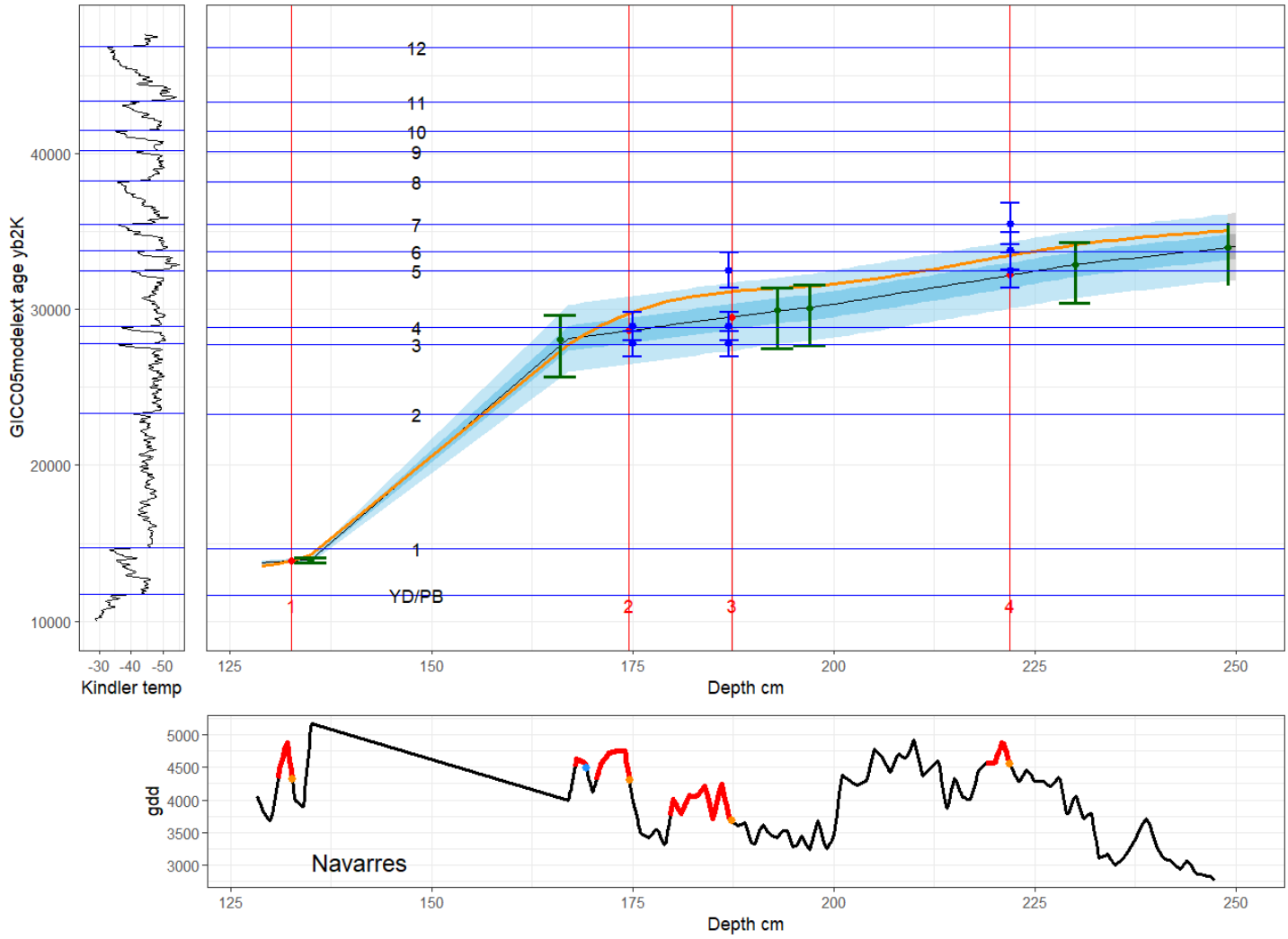

Figure 6.16 Potential matches for Navarres between DOLPs using gdd reconstruction and the full SMPDS set, and GIs. Main panel: age model; vertical red lines mark accepted DOLP, with sequential identifying numbers; blue horizontal lines are GICC05modelext ages of GIs (less 50 years), red points are intersections of DOLP and rbacon age model median; blue ribbon: central line is rbacon age model median value, with 75% (darker) and (lighter) 95% uncertainties; green points and error bars are core dating points with uncertainties; blue points and error bars are ages and MCEs of those GIs which overlap with uncertainty of DOLP age. Grey ribbon: model extrapolation beyond last effective dating point. Orange curve: ACER age model. Lower panel: gdd reconstruction for Lagaccione using full SMPDS taxon set, with accepted DOLPs marked by orange points; red segments of reconstruction are warm intervals; blue points are rejected DOLPs. Vertical panel: Kindler Greenland temperature in ºC on GICC05modelext scale, aligned with main panel.

Commentary on Navarres: all 4 DOLPS match with GIs: DOLP 1 matches GI 1, 2 matches 3, 3 matches 4, and 4 matches 5. GI 2 is missed in the hiatus from 135 to 160 cm. (The short red interval younger than the blue rejected DOLP at 163 cm is an error.)

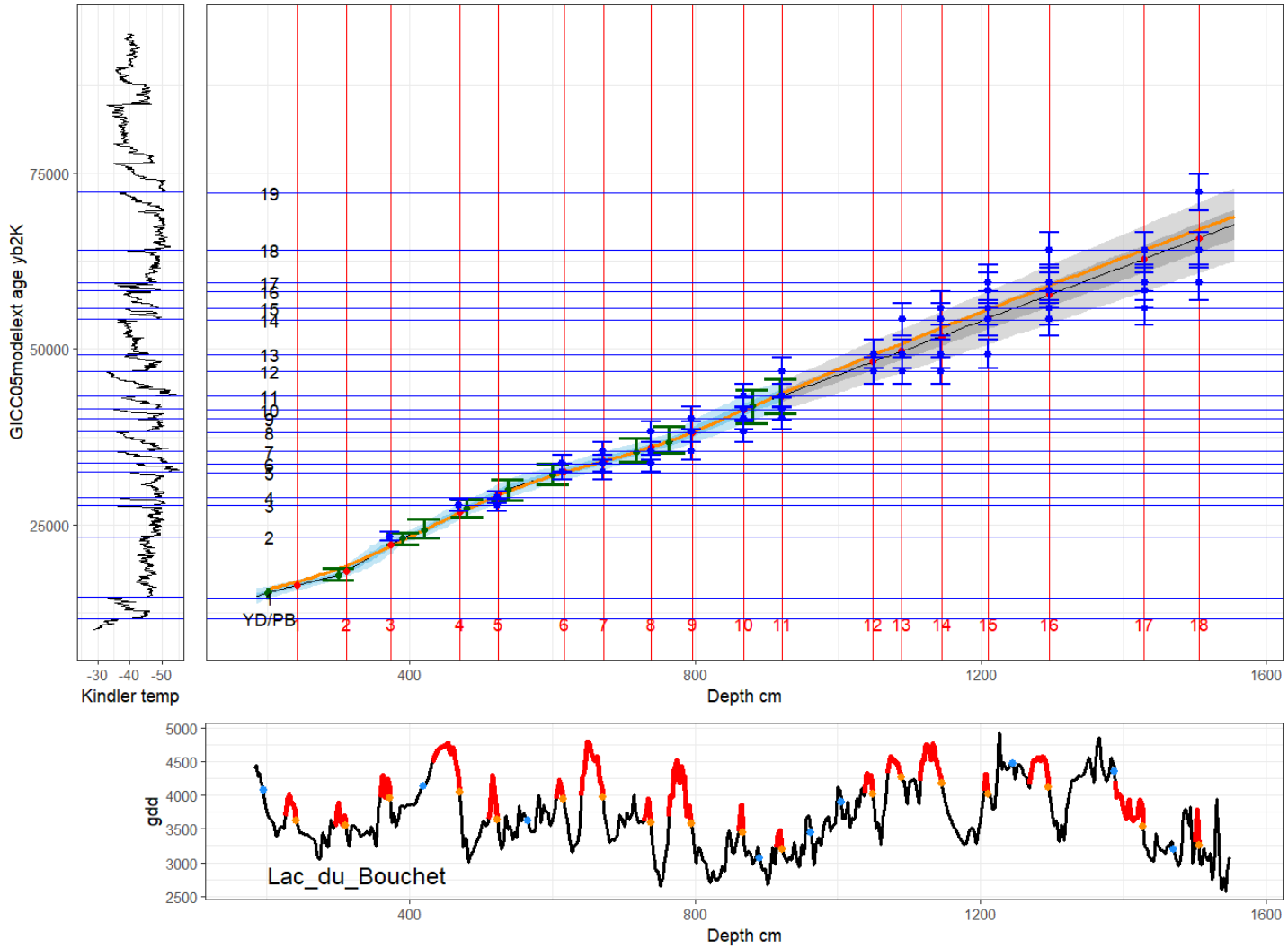

Figure 6.17 Lac du Bouchet; otherwise as caption for Figure 6.16.

Commentary for Lac du Bouchet: this core is unusually well furnished with dating points and exhibits high variability. DOLP1 is probably GI 1; DOLP 2 is rejected (but see below 6.7.3); DOLP 3 matches GI 2; DOLPs 4 and 5 match GIs 3 and 4. DOLP 6, given the neighbouring dating point, is probably GI 5 and DOLP 9 is most probably GI 8, leaving DOLPs 7 and 8 to match GIs 6 and 7. DOLP 10 could be GI 9 or 10 and DOLP 11 could be any unassigned GI from 10 to 12. To this point, all but possibly one GI is registered, and all but one DOLP matches a GI, a remarkably strong performance. Thereafter the age model is extrapolation, but the numbers of DOLPs and of GIs are the same, and the evidence of the younger interval suggests all the DOLPs are GIs.

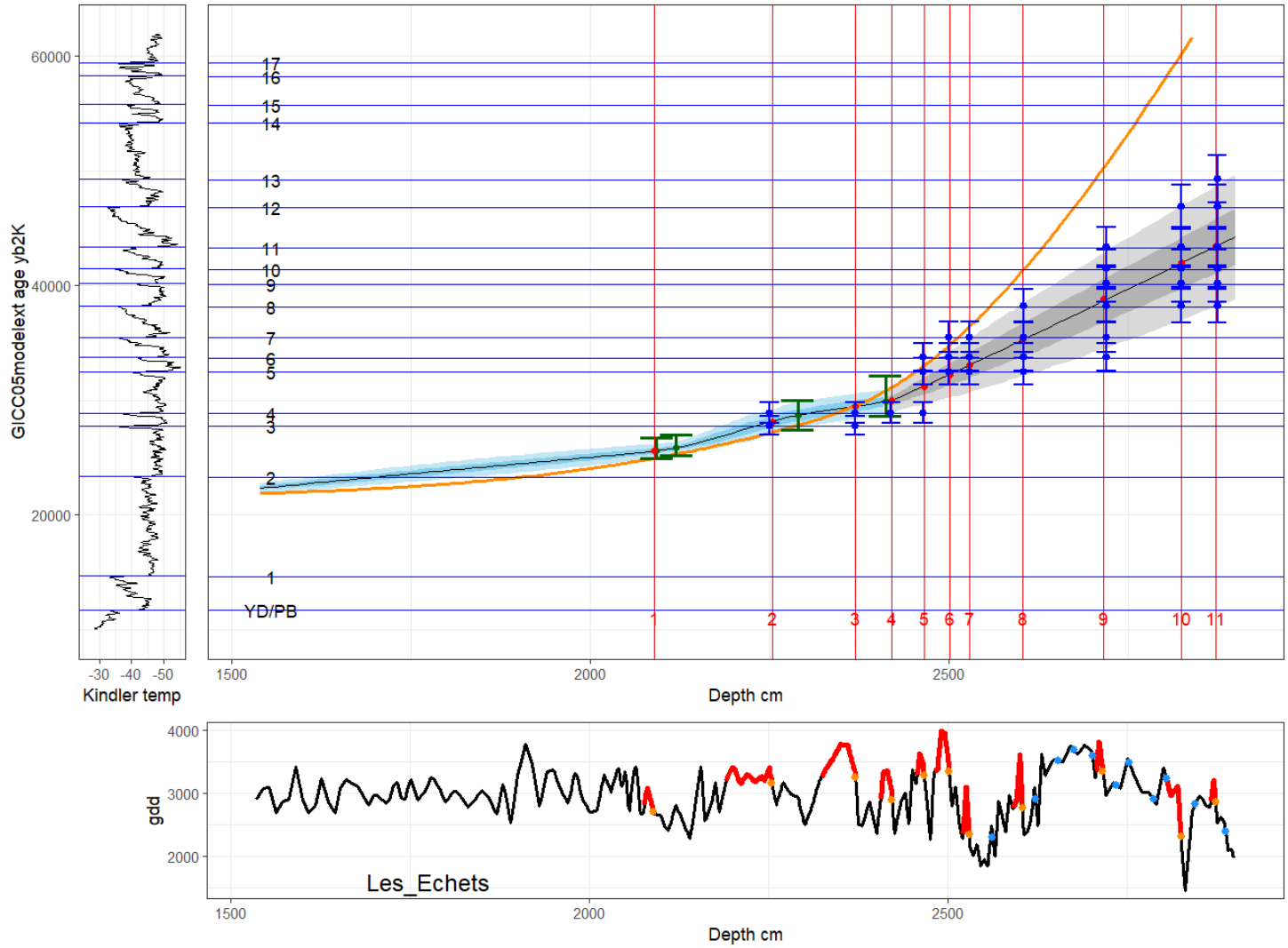

Figure 6.18 Les Echets: otherwise as caption for Figure 6.16.

Commentary for Les Echets: DOLP 1 is rejected. Review of the spike at ~1850 cm (Appendix D) shows it is not D-O-like at all, so it is not GI 2. DOLPs 2 and 3 are GIs 3 and 4. Widening uncertainties and reliance on extrapolation in the older interval render matches unclear, but since 8 DOLPs are available in an interval containing 9 GIs (assuming the *rbacon* model), these accepted DOLPS are very probably D-Os, and the rejected DOLPs are rightly rejected.

Note: the portion of the ACER age model older than DOLP 4 is based on 'events' (2975 cm is matched with GI 20, and 3095 cm with GI 21). The Les Echets pollen values in ACER are not consistent with the original hard copy pollen diagrams in Beaulieu and Reille (1984) from which it was digitised; the interval in the plot

above was re-digitised by hand for this project. These ‘events’ do not occur in this interval and their similarity to D-Os and the robustness of the ACER age model cannot be evaluated.

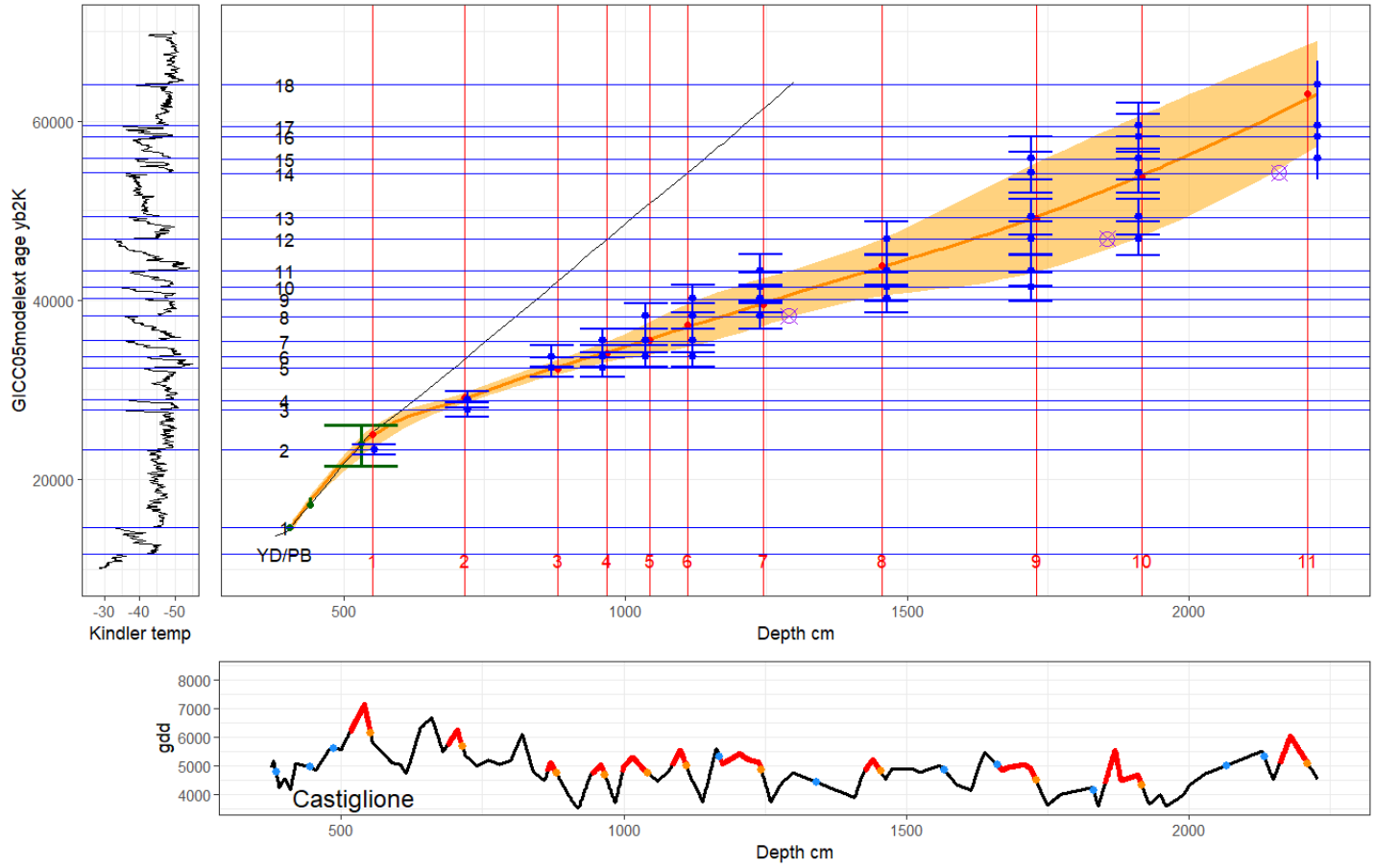

Figure 6.19 Castiglione: otherwise as caption for Figure 6.16.

Commentary for Castiglione: The pre-hiatus interval of Castiglione has already been discounted, and the remaining interval is suspect on the ground of high indeterminates (Figure 6.2), which are greatest in the 20-30 ka interval. The ACER model ignores all ^{14}C dates after DOLP 1 (reason not known), and the black line is the median of the mostly extrapolated *rbacon* model making the same assumption. The ACER dating points identify pollen changes shown by purple circles with crosses as 'events', which are close to but not identical with identified DOLPs.

Other than assigning DOLP 1 to GI 2, it is not safe to assign any DOLPS at Castiglione to GIs, or claim them as genuine D-Os, on the grounds of high indeterminates and lack of dating points.

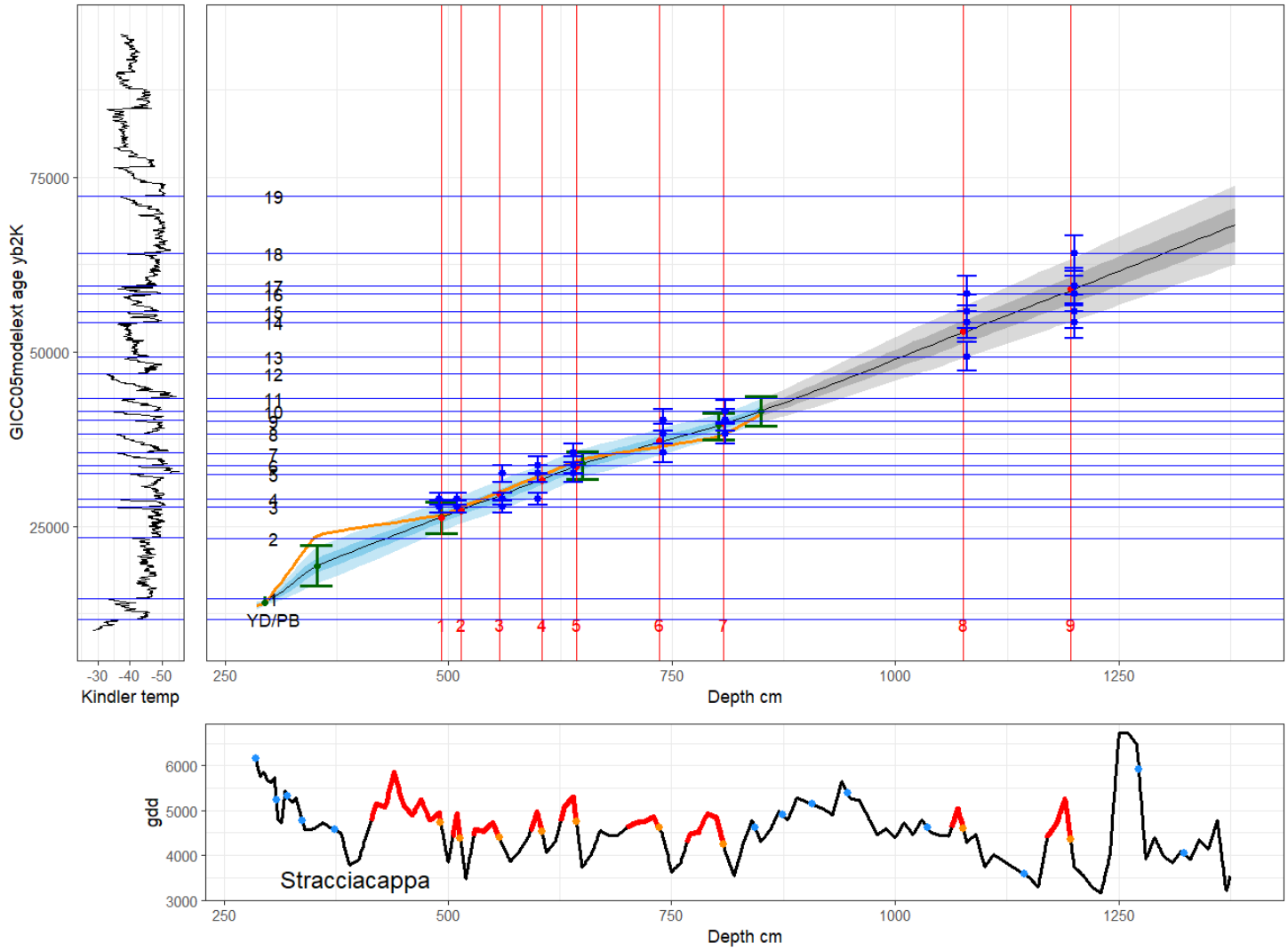

Figure 6.20 Stracciacappa: otherwise as caption for Figure 6.16.

Commentary for Stracciacappa: DOLP 1 and 2 are probably GI 3 and 4: DOLP 3 may be rejected; DOLPs 4 and 5 match some of GIs 5-7; DOLP 6 or 7 is GI 8; pre-DOLP 8 the age model is extrapolation, and DOLPs 8 and 9 can match a range of GIs. Potential DOLPS between 7 and 8 were rejected owing to poor EDs, so are unlikely to represent the GIs in this interval.

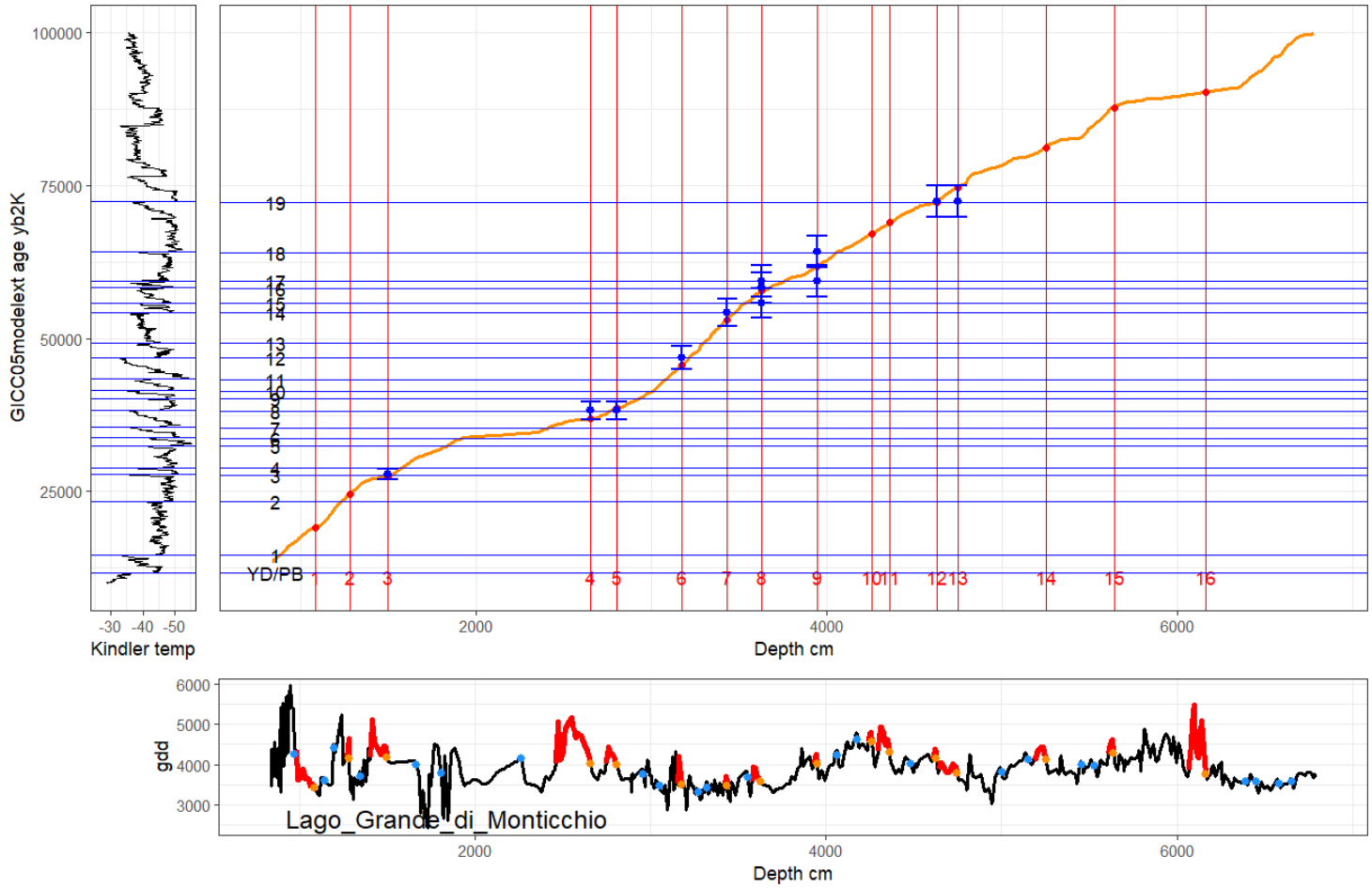

Figure 6.21 Lago Grande di Monticchio: no rbacon *model exists and the original age model (orange line) has no uncertainties. Otherwise as caption for Figure 6.16.*

Commentary for Lago Grande di Monticchio: the age model provided by Allan and Huntley to the ACER database is strongly based on multiple tephra dates and on varves, but no uncertainties are given, so only the overlap between the single-line model and the GI age uncertainty is evaluated. The very earliest part of the record is vitiated by low N2 (Appendix C) so no opinion is offered on the spike coinciding with GI 1. DOLP 1 can be rejected, DOLP 2 including possibly the succeeding spike is GI 2, and DOLP 3 is GI 3 or 4 or an amalgam; none of the rejections between DOLPs 3 and 4 appear marginal; DOLP 4 is probably GI 8, or possibly DOLP 4 and 5 combine GIs 7 and 8. The interval from DOLP 5 onwards shows low variability, and consistently with this, the DOLP selection criteria (Appendix C) show that the rejected DOLPs in this interval exhibit good shapes, as evidenced by their good EDs, and that their rejection is due to low rises and area-under-the-curve. With the current filters, larger-amplitude GIs (8, 12, 14) stand out well but lesser ones are

lost, but since the areas and rises of many potential DOLPs are so similar, tiny changes in the filters yield considerable changes. DOLPs 6 and 7 appear to match GIs 12 and 14. GI 19, however, does not emerge clearly.

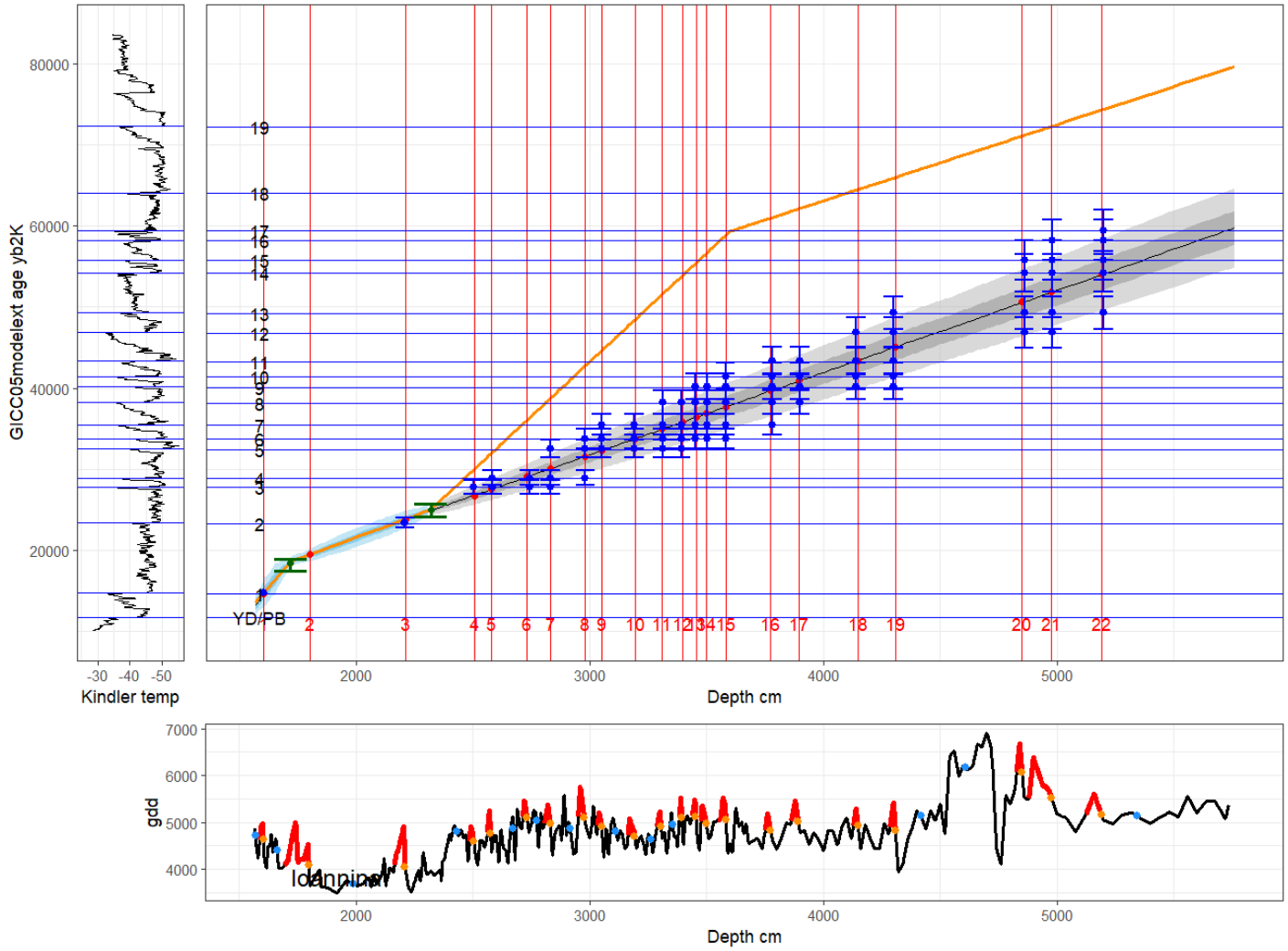

Figure 6.22 Ioannina: otherwise as caption for Figure 6.16.

Commentary for Ioannina: DOLP 1 is probably GI 1; DOLP 2 is rejected; DOLP 3 is GI 2, and DOLPS 4 and 5 are probably GIs 3 and 4. *rbacon* age model is extrapolation beyond 2318 cm, and ACER age model is based on an 'event' at 3600 cm identified as MIS3/4 boundary = GI 17; 3600 cm is the location of DOLP 15, so its assignment to GI 17 is very plausible but unprovable, so neither model provides robust dates in this interval. But the number of DOLPs and the number of GIs in this interval are similar, supporting the view that the great majority of the DOLPs are real D-Os.

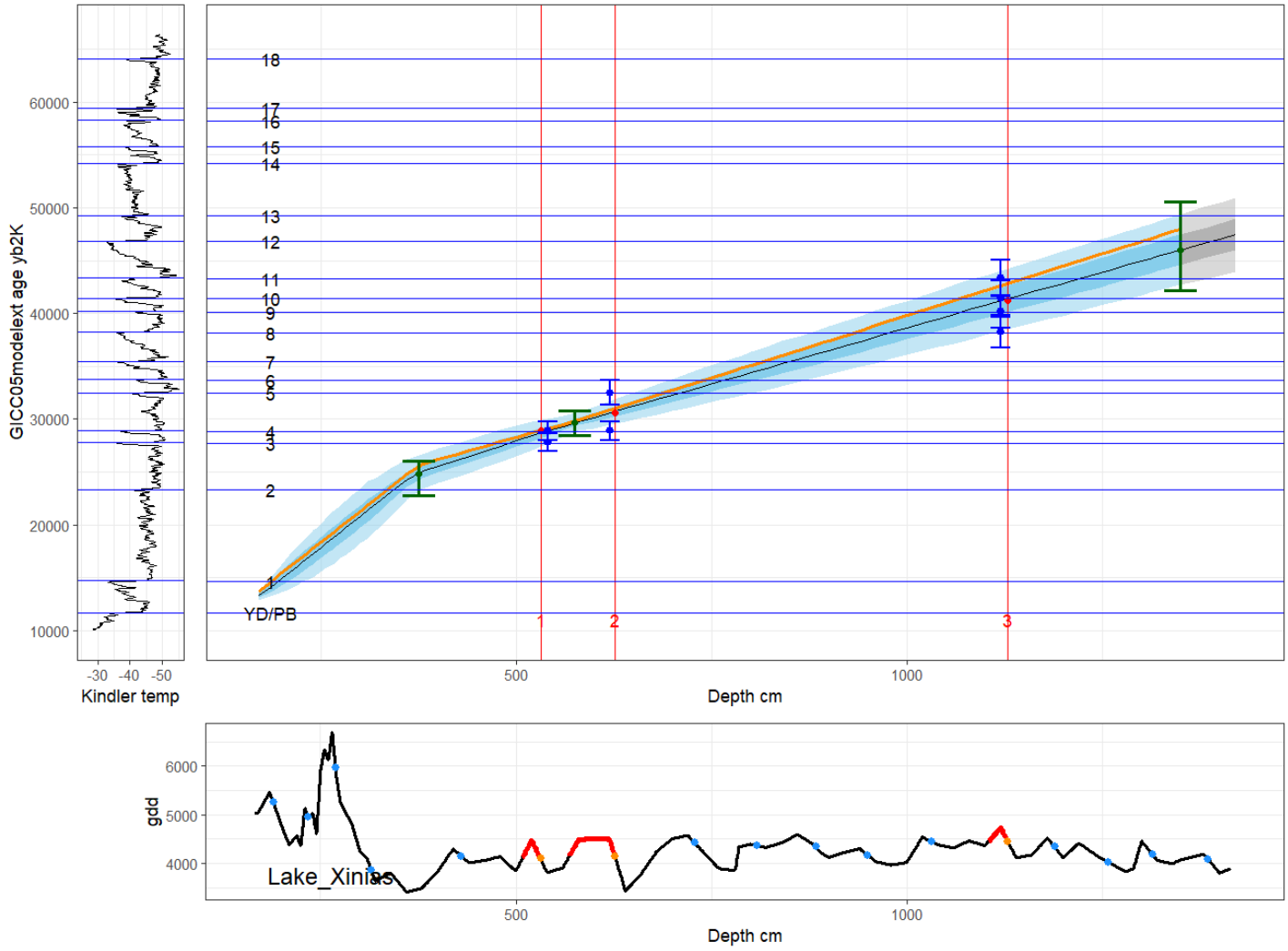

Figure 6.23 Lake Xinias: otherwise as caption for Figure 6.16.

Commentary for Lake Xinias: Lake Xinias exhibits low sampling resolution and low variability, which hampers the identification of DOLPs. The prominent spike ~ 250 cm is caused by the dominance of Amaranthaceae, peaking at 91% of the pollen sum, and should be ignored, though it is still present in a muted form in the restricted set reconstruction which eliminates Amaranthaceae (Figure 6.1). The earliest part of the core (not shown since the termination is excluded from pattern matching) is well dated, supporting the rejection of all potential DOLPs before DOLP 1. DOLPs 1 could be GI 3 or 4, and DOLP 2 could be 4 (if not already assigned to DOLP 1) or 5. A review of the rejected DOLPs between DOLPs 2 and 3 suggest they were rightly rejected on multiple grounds. DOLP 3 could be any of GIs 8 to 11, though the ^{14}C date at 1350 cm is at the limit of ^{14}C.

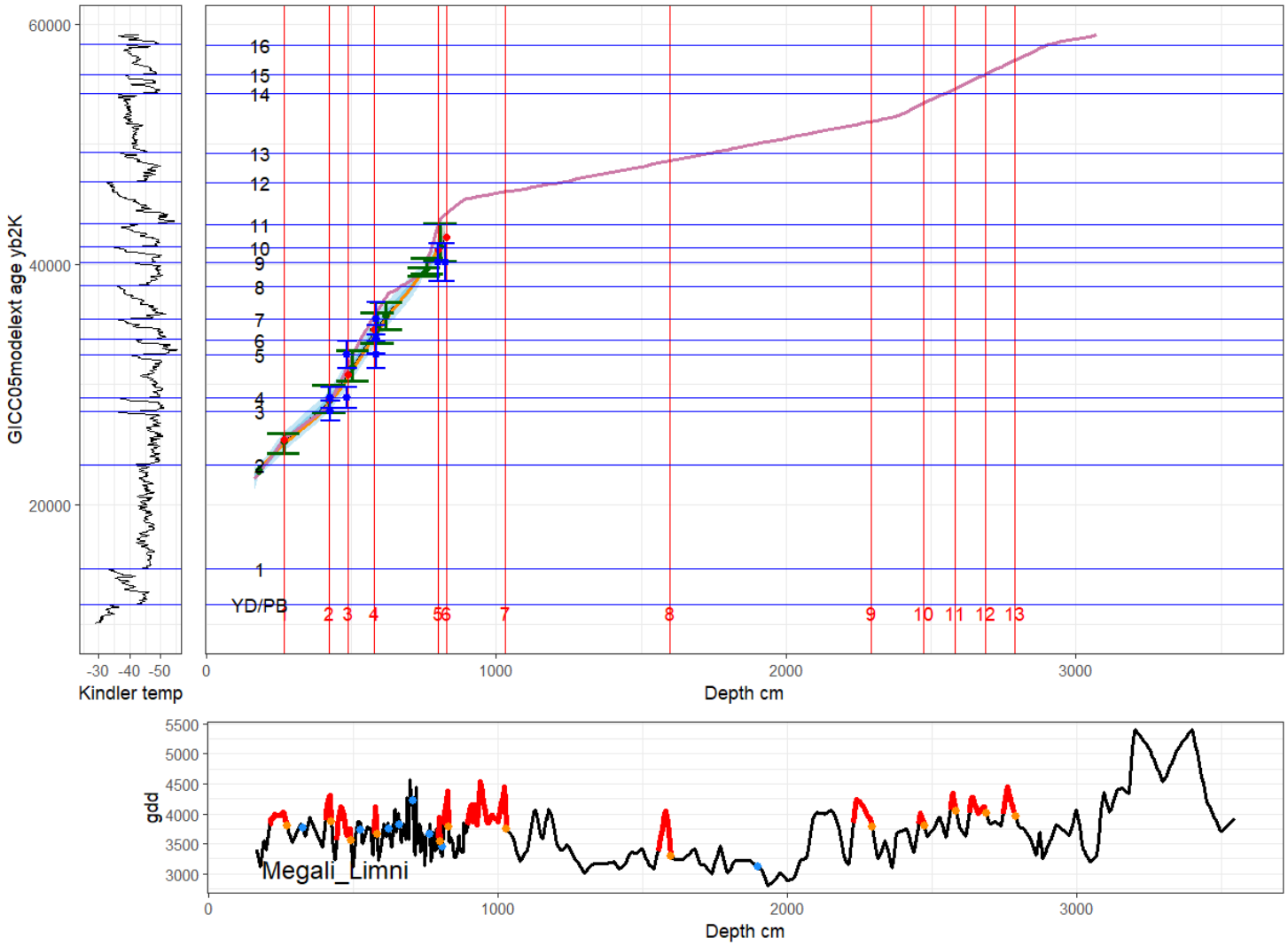

Figure 6.24 Megali Limni full core length: purple line: original age model; otherwise as caption for Figure 6.16.

Commentary on Megali Limni: the younger interval is well dated, anchored by the Y-5 tephra at 752 cm; see Figure 6.25. The older interval, shown in Figure 6.24, contains highly plausible DOLPs, but no attempt is made to assign them to GIs given the absence of dating information.

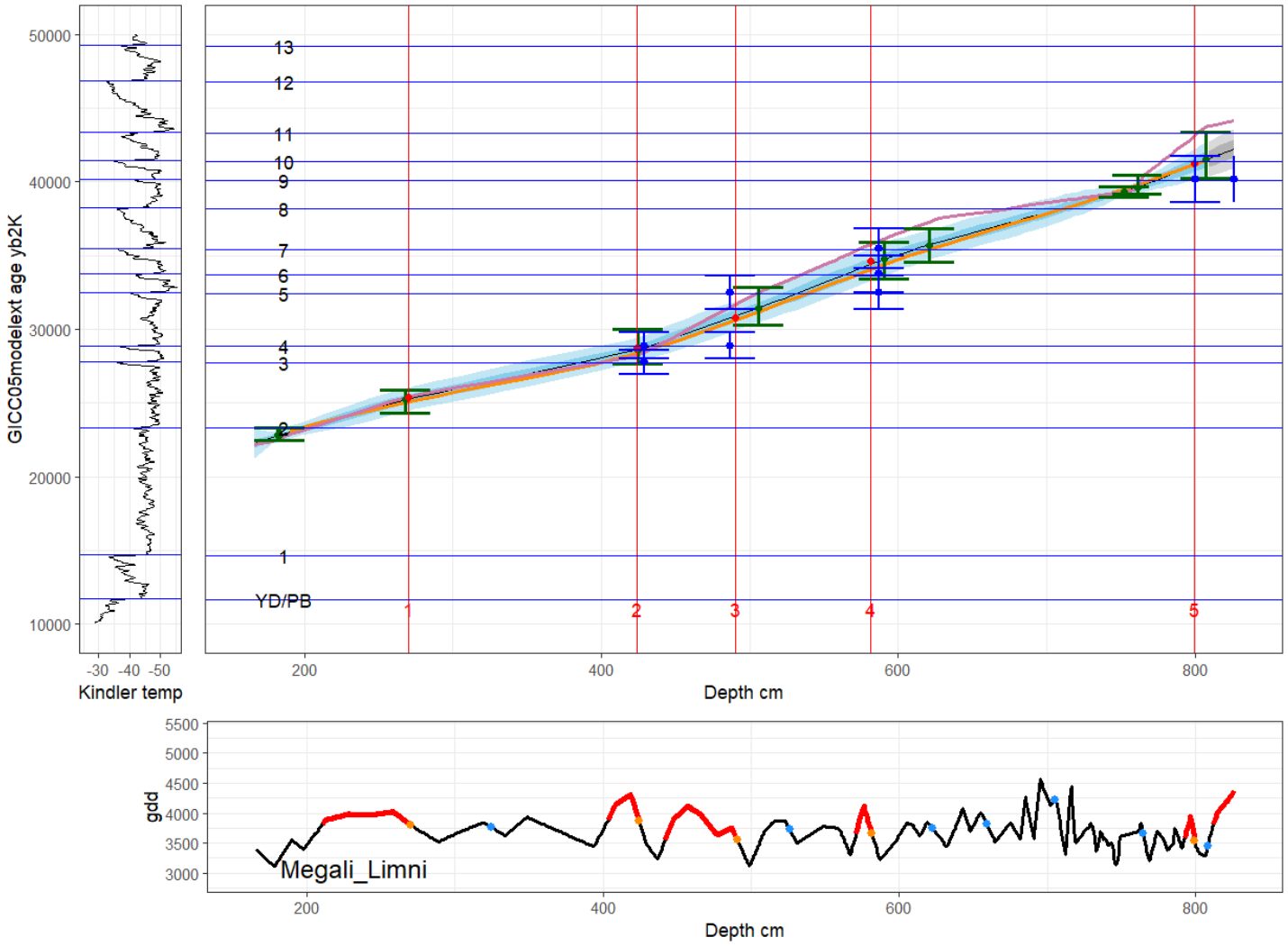

Figure 6.25 Megali Limni, well dated section only: purple line: original age model; otherwise as caption for Figure 6.16. Script: Trial id GIs v4 ML

Commentary on Megali Limni well-dated interval: DOLP 1 is improbable; DOLP 2 is GI 3, and DOLP 3 may be GI 4 or a composite of GI 4 and 5; the rejected DOLP between 3 and 4 may be GI 5; DOLP 4 may be any of GI 5 to 7, and DOLP 5, given the dating precision available, is most probably GI 9.

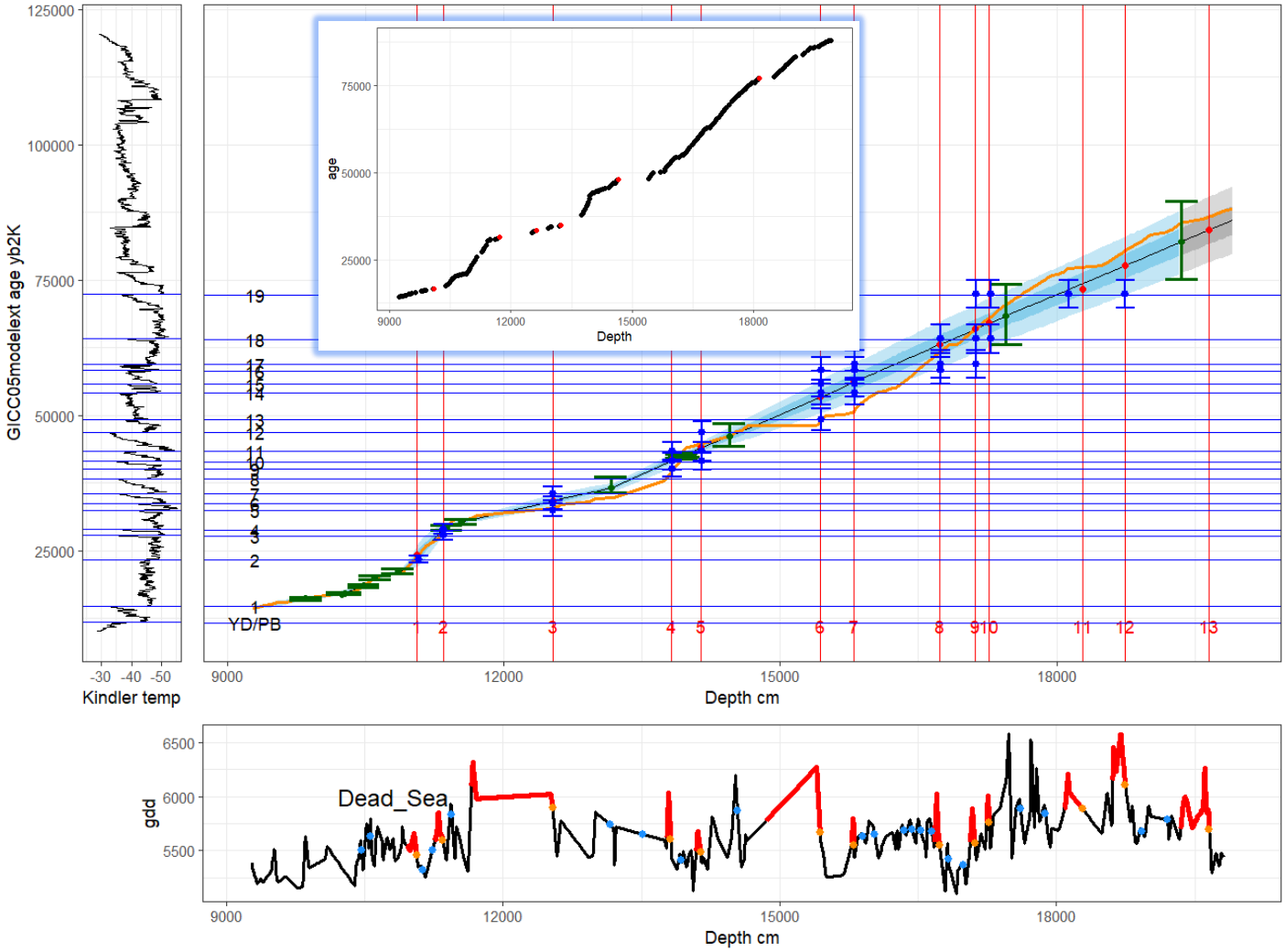

Figure 6.26 Dead Sea: Orange line is original, not ACER, model; otherwise as caption for Figure 6.16. Inset: locations of starts of hiatus marked by red points.

Commentary on Dead Sea: there are multiple hiatus (inset: red points are starts of hiatus), suggesting DOLPs 3 and 6 should be rejected. DOLP 1 is probably GI 2, DOLP 2 (and rejected older neighbour?) are GIs 3 and 4. The rejected DOLP between DOLP 5 and DOLP 6 (rejected only marginally by the ED filter but no others) is probably GI 12, given the neighbouring dating point. So DOLP 4 could be GI 9 or 10, and DOLP 5 GI 10 or 11. Beyond this, only valid series can be hypothesised, but the number of DOLPs is roughly equal to the number of available GIs.

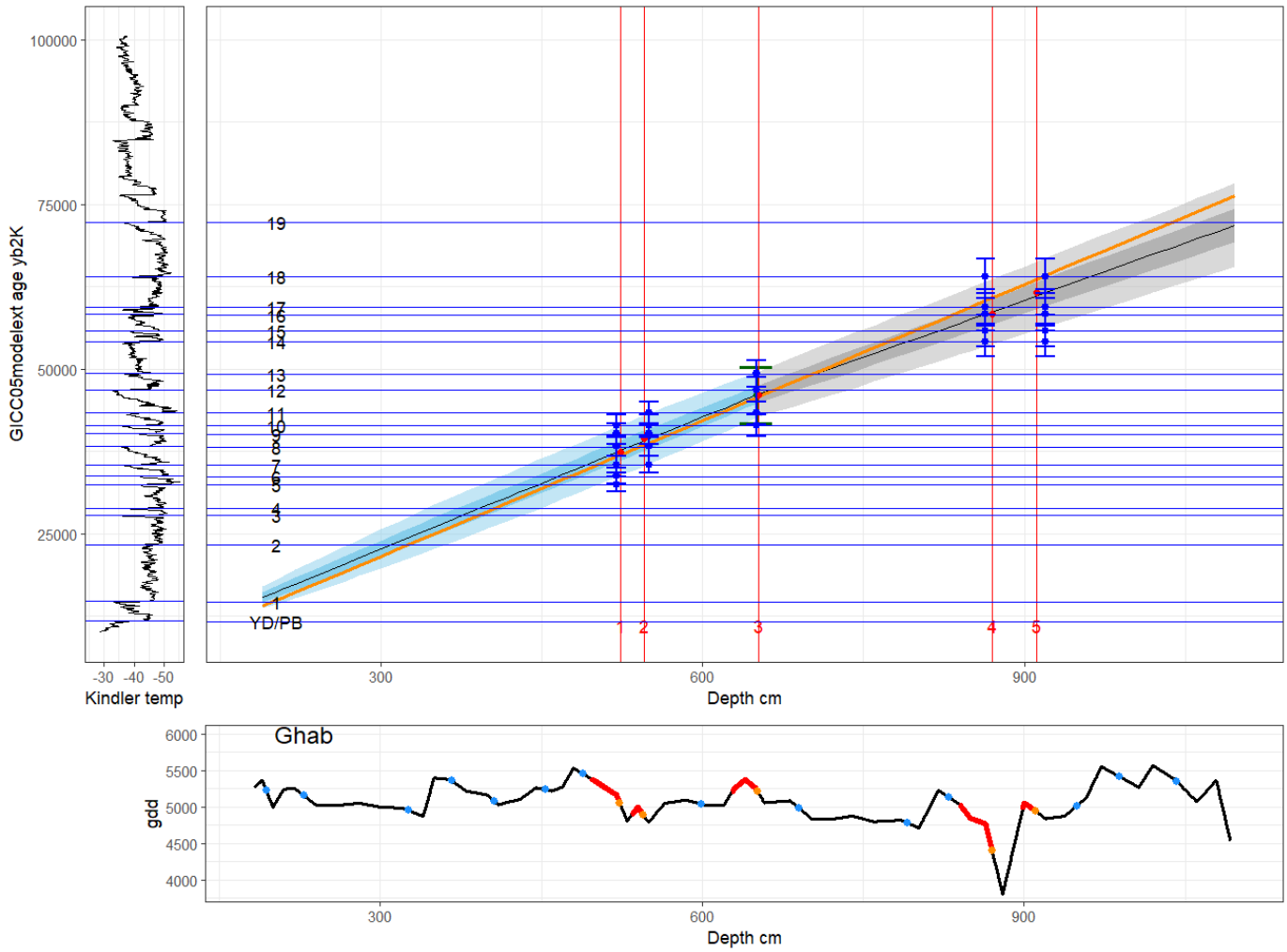

Figure 6.27 Ghab: otherwise as caption for Figure 6.16.

Commentary on Ghab: there is only one dating point (at DOLP 3), and sampling resolution and variability are low. It appears unsafe to assign any DOLPs to GIs, and it is not clear that DOLPs are real D-Os.

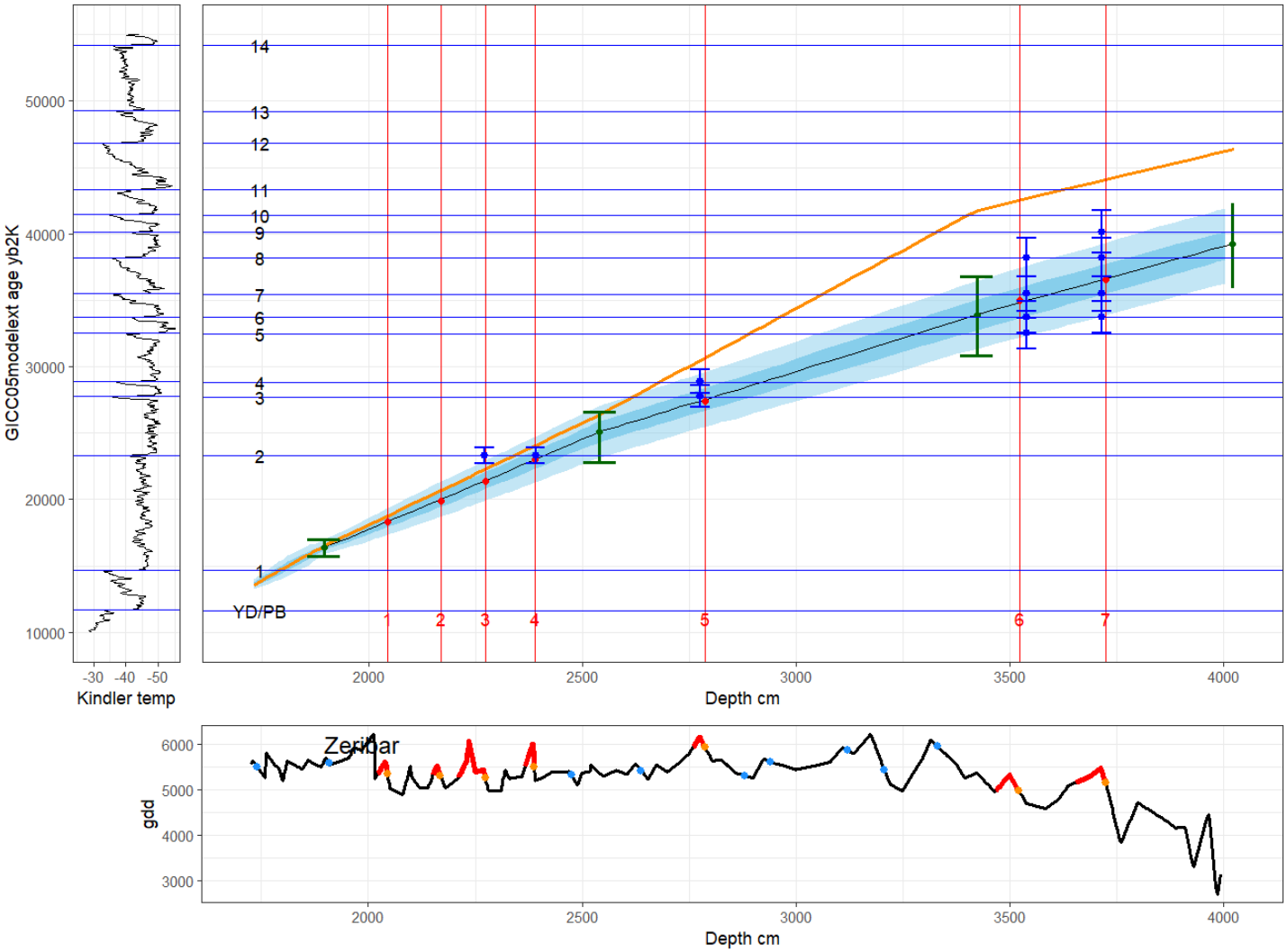

Figure 6.28 Zeribar: otherwise as caption for Figure 6.16.

Commentary on Zeribar: DOLPS 1, 2 and 3 are rejected; DOLP 4 is probably GI 2, DOLP 5 is GI 3 or 4 or an amalgam; DOLP 6 could be any of GIs 5 to 8 and DOLP 7 could be any (unassigned) GI from 6 to 9. The rejected DOLPs in the low-variability interval between DOLP 5 and 6 appear rightly rejected (Appendix D).

Table 6-6 summarises the DOLPs found and the GIs to which they are most probably assigned. Where no specific assignment is possible, the count of available DOLPS and available GIs is given.

Table 6-6 Matches between DOLP numbers and GI numbers; 'X' denotes rejected DOLP; 'rej' denotes previously rejected DOLP now accepted; beyond the point where specific assignments are made, counts of available DOLPs and available GIs are given. 'GIs missed' are not registered in the core. Source: DOLPS v GIs.xlsx

Lagaccione	DOLP	1	2	3	4	5	6	7	8	Count 9	
	GI	1	X	X	2	3	4	5	6	Count 11	
	GI missed								7		
Navarres	DOLP	1	2	3	4						
	GI	1	3	4	5						
	GI missed			2 hiatus							
Lac du Bouchet	DOLP	1	2	3	4	5	6	7	8	9	Count 9
	GI	1	X	2	3	4	5	6	7	8	Count 10
	GI missed										
Les Echets	DOLP	1	2	3	Count 8						
	GI	X	3	4	Count 9						
	GI missed	1 prior; 2									
Castiglione	DOLP	1			Count 10	Indeterminates, poor age model					
	GI	2			Count ?						
	GI missed	1									
Stracciacappa	DOLP	1	2	3	4	5			Count 4		
	GI	3	4	X	5	6			Count 6		
	GI missed										
Lago Grande di Monticchio	DOLP	1	2	3	4	5	6	7	Count 6		
	GI	X	2	3	8	?	12	14	Count 5		
	GI missed	1		4, 5, 6, 7, 9, 10, 11					Low variability		
Ioannina	DOLP	1	2	3	4	5			Count 14		
	GI	1	X	2	3	4			Count 14		
	GI missed										
Lake Xinias	DOLP	1	2		Count 1						
	GI	3	4		Count 4						
	GI missed	1, 2									
Megali Limni	DOLP	1	2	3	rej	4	5				
(well dated only)	GI	X	3	4	5	5-7	9				
	GI missed	2									
Dead Sea	DOLP	1	2	3	4	5	rej	6	Count 7		
	GI	2	3	X	9	10	12	X	Count 6		
	GI missed	1, 4, 5, 6, 7, 8, 11									
Ghab	DOLP	1	2	3	4	5					
	GI	None clear									
	GI missed										
Zeribar	DOLP	1	2	3	4	5			Count 2		
	GI	X	X	X	2	3/4			Count 4		
	GI missed										

In summary, in the range in which DOLPs could be directly assigned, and excluding Ghab where no matches were proposed, 48 out of 61 DOLPs were assigned with high plausibility to specific GIs; these included 2 previously rejected DOLPs. Of the 13 DOLPs rejected, 9 fell in the interval between GI 1 and 2 (see section below). Most cores rejected one DOLP or none, and missed one GI or none, but Monticchio owing to low variability and the Dead Sea owing to multiple hiatus missed several. In the range where DOLPS could not

be specifically assigned owing to age uncertainties, a total of 64 DOLPs had plausible matches within a set of 69 GIs. In the younger intervals where DOLPs have been assigned to GIs, the age uncertainties in both the GIs and the DOLPs appear sufficiently small to justify these assignments.

6.7.3 Events between GI 1 and GI 2

Between GI 1 and GI 2, five out of the 13 cores (Lac du Bouchet, Lago Grande di Monticchio, Ioannina, Lagaccione and Megali Limni) show one or more DOLPs, and four more (Castiglione (though compromised by indeterminates), Stracciacappa, Dead Sea and Zeribar) show one or more previously rejected DOLPS; all are rejected during the age comparison process as matching no possible GI. Les Echets does not include this interval, Lake Xinias has an unreliable interval here, and Ghab has inadequate resolution to make a judgement. This consistency hints at the existence of a warming event or events in the Mediterranean area, but it is not necessary to propose previously unknown events. Pattern matching registers two excursions in the Kindler series in this interval, seen in Figure 2.6 and commented on there, and marked with red triangles in Figure 6.29. These are not recognised GIs, which are located using $\delta^{18}O_{ice}$ and dust flux, neither of which register as strong a change as the Kindler temperature series. While they may not be GIs, the probable identification in Mediterranean cores of small-scale D-O-shaped events already identified in the Kindler series adds confidence that Mediterranean cores exhibit similar patterns to those in Greenland.

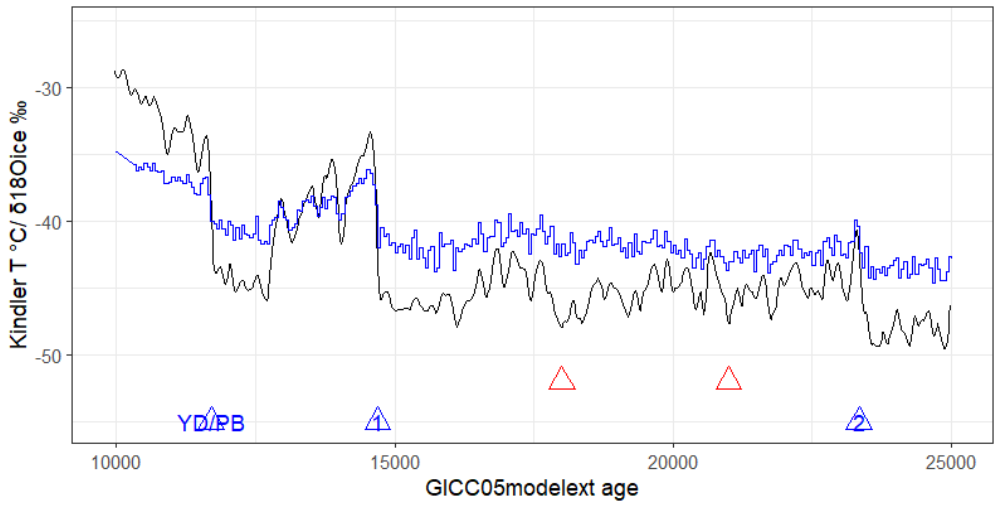

Figure 6.29 Kindler series (black line) and NGRIP $\delta^{18}O_{ice}$ ‰ (blue line) with YD and GIs 1 and 2 (blue triangles). Red triangles mark small excursions picked up by pattern matching applied to the Kindler series.

6.7.4 Age comparison section summary

Evidence from bootstrapping, unusual excursions, Hill's N2, the level of indeterminates, the filtering tests in pattern matching, the complacency of the reconstruction, and the presence of hiatus is used as a decision support system to propose the final matches of DOLPs with GIs through age comparison. Different cores provide different levels of confidence in the matches. In the younger intervals, specific assignment of DOLPs to GIs, or rejection of DOLPs, is usually possible, depending on the robustness of the core age model, and pattern matching can resolve assignments which date overlaps alone cannot. The confidence gained from these younger intervals that many DOLPs are real D-Os carries over to older intervals, where age uncertainties are usually too wide to allow specific assignments, but the number of DOLPs identified is the same or fewer than the count of real GIs in the age range considered, and series of matches can be proposed. The filter settings may be too conservative, but varying these locally rather than for a whole core is special pleading.

6.8 Chapter summary

Pattern matching seeks to identify D-O-like events in quantitative reconstructions made using fxTWA-PLS by comparing them with templates of D-O initiations extracted from the Kindler temperature series. The intervals it identifies as D-O-like highly plausibly reflect true D-Os, with low rates of false positives and false negatives. Though the method is not perfectly reliable and is dependent on the characteristics of the core, in the younger intervals it is often possibly to assign a D-O-like event to a specific GI with high plausibility. In the absence of other methods, such as high-precision age-depth models, pattern matching may serve to locate GIs.

References

Allen, J.R.M. *et al.* (1999) 'Rapid environmental changes in southern Europe during the last glacial period', *Nature*, 400(6746), pp. 740–743. Available at: https://doi.org/10.1038/23432.

Allen, J.R.M. and Huntley, B. (2000) 'Weichselian palynological records from southern Europe: correlation and chronology', *Quaternary International*, 73–74, pp. 111–125. Available at: https://doi.org/10.1016/S1040-6182(00)00068-9.

Andersen, K.K. *et al.* (2006) 'The Greenland Ice Core Chronology 2005, 15–42ka. Part 1: constructing the time scale', *Quaternary Science Reviews*, 25(23), pp. 3246–3257. Available at: https://doi.org/10.1016/j.quascirev.2006.08.002.

Beaulieu, J.-L.D. and Reille, M. (1984) 'A long Upper Pleistocene pollen record from Les Echets, near Lyon, France', *Boreas*, 13(2), pp. 111–132. Available at: https://doi.org/10.1111/j.1502-3885.1984.tb00066.x.

Fick, S.E. and Hijmans, R.J. (2017) 'WorldClim 2: new 1-km spatial resolution climate surfaces for global land areas', *International Journal of Climatology*, 37(12), pp. 4302–4315. Available at: https://doi.org/10.1002/joc.5086.

Hill, M.O. (1973) 'Diversity and Evenness: A Unifying Notation and Its Consequences', *Ecology*, 54(2), pp. 427–432. Available at: https://doi.org/10.2307/1934352.

Juggins, S (2017) 'rioja: Analysis of quaternary science data'. CRAN. Available at: http://cran.r-project.org/package=rioja.

Kindler, P. *et al.* (2014) 'Temperature reconstruction from 10 to 120 kyr b2k from the NGRIP ice core', *Climate of the Past*, 10(2), pp. 887–902. Available at: https://doi.org/10.5194/cp-10-887-2014.

Liu, M. *et al.* (2020) 'An improved statistical approach for reconstructing past climates from biotic assemblages', *Proceedings of the Royal Society A* [Preprint]. Available at: https://doi.org/10.1098/rspa.2020.0346.

New, M. *et al.* (2002) 'A high-resolution data set of surface climate over global land areas', *Climate Research*, 21, pp. 1–25. Available at: https://doi.org/10.3354/cr021001.

Parnell, A.C. *et al.* (2016) 'Joint palaeoclimate reconstruction from pollen data via forward models and climate histories', *Quaternary Science Reviews*, 151, pp. 111–126. Available at: https://doi.org/10.1016/j.quascirev.2016.09.007.

Rasmussen, S.O. *et al.* (2014) 'A stratigraphic framework for abrupt climatic changes during the Last Glacial period based on three synchronized Greenland ice-core records: refining and extending the INTIMATE event stratigraphy', *Quaternary Science Reviews*, 106, pp. 14–28. Available at: https://doi.org/10.1016/j.quascirev.2014.09.007.

Reimer, P.J. *et al.* (2020) 'The IntCal20 Northern Hemisphere Radiocarbon Age Calibration Curve (0–55 cal kBP)', *Radiocarbon*, 62(4), pp. 725–757. Available at: https://doi.org/10.1017/RDC.2020.41.

Seierstad, I.K. *et al.* (2014) 'Consistently dated records from the Greenland GRIP, GISP2 and NGRIP ice cores for the past 104 ka reveal regional millennial-scale δ18O gradients with possible Heinrich event imprint', *Quaternary Science Reviews*, 106, pp. 29–46. Available at: https://doi.org/10.1016/j.quascirev.2014.10.032.

Turner, M.G. *et al.* (2020) 'The impact of methodological decisions on climate reconstructions using WA-PLS', *Quaternary Research*, pp. 1–16. Available at: https://doi.org/10.1017/qua.2020.44.

Wei, D. *et al.* (2019) 'Climate changes in interior semi-arid Spain from the last interglacial to the late Holocene', *Climate of the Past Discussions*, pp. 1–31. Available at: https://doi.org/10.5194/cp-2019-16.

7 Conclusions and Future Work

The aim of this thesis is to examine ways of locating the responses in circum-Mediterranean terrestrial pollen records to D-O (Dansgaard-Oeschger) events during the last glacial period.

This Chapter is broken into four areas:

- Modern pollen and climate, training sets, and how pollen abundance reflects climate.
- WA-PLS and fxTWA-PLS, and how they translate a training set and a fossil record into a quantitative climate reconstruction.
- Ways of finding D-O-like events in pollen records and in quantitative reconstructions.
- Possible future work.

7.1 Pollen, climate, and training sets

Pollen reflects climate, and can be used to make good quantitative reconstructions, but the relationship is not perfect. This is seen in the cloud of points in the inverse regression in WA-PLS (e.g. Figure 4.4), in the bootstrapped uncertainties in reconstructions (Appendix C), and in the dispersion of binned means of abundance along a climate gradient (e.g. Figure 5.8). There are many possible reasons for these imperfections, including the influence of other climate variables, non-climatic variables, and noise. These imperfections do not usually obscure the fundamental relationship, but this depends on how well the taxon samples the climate space; low occurrences and low abundances make for unstable sampling, as illustrated by the bootstrapping of loess curves in Chapter 5 and Appendix B.

Statistical climate reconstruction methods need a training set from which to deduce the pollen/climate relationship. There have been few debates about the requirements of a training set compared with the rich literature on the statistical merits of different reconstruction methods (e.g. Birks *et al.*, 2010; Bartlein *et al.*, 2011; Sweeney *et al.*, 2018; Chevalier *et al.*, 2020), and the training set used in a reconstruction is often not described well or at all. Yet as Turner *et al* (2020)(Chapter 3) demonstrate, the set chosen controls the climate space sampled and therefore limits the climate that can be reconstructed. The climatic range

sampled by a training set should therefore be wide, should include the expected reconstructed climate, and should sample the climate space as continuously as possible, to avoid abundance distributions more influenced by patchy sampling than true climate preferences.

From as far back as Shelford (1931) it has often been assumed that biotic responses to environmental variables are typically unimodal and symmetrical, or approximately Gaussian, and the weighted averaging method is founded on this assumption (Ter Braak and Juggins, 1993, and references therein). Chapter 5 shows that in practice other classes of response are commonly found in pollen, including skewed, multimodal, and those showing no clear preference. Even where modes are clear, the width of dispersion may vary. These non-Gaussian responses are well known in the literature (e.g. Bio, Alkemade and Barendregt, 1998; Oksanen and Minchin, 2002). While some non-Gaussian distributions, especially of low-frequency, low-abundance taxa, may stem from deficiencies in the training set sampling of the climate, others clearly reflect genuine responses to the bioclimatic variable in question, which can include indifference. These become important in considering how well WA-PLS and fxTWA-PLS are able to utilise the information provided by non-Gaussian responses.

In summary, some taxa are more robust and/or more precise guides than others to the modern climate they typically experience. The difference may arise from sampling issues, which can be mitigated by more comprehensive training sets, or from genuine wide tolerance or insensitivity.

7.2 WA-PLS and fxTWA-PLS

Quantitative climate reconstructions were made using WA-PLS and fxTWA-PLS, which extract transfer functions from a training set (calibration) and apply them to fossil pollen to reconstruct a climate variable (reconstruction or 'prediction'). fxTWA-PLS improves on WA-PLS by considering the frequency with which a taxon samples each part of the environmental gradient, and the taxon's tolerance. In neither case is the transfer function expressed as a scalar value per taxon, which makes understanding and testing the transfer function against abundance curves describing climate preferences a challenge (Chapters 4 and 5). The

transfer function includes both a taxon-related element and sample-related elements, the regression and intercept, which cannot be decomposed to a taxon level.

In the case of WA-PLS as implemented in the *rioja* R package (Juggins, S, 2017), a shorthand method of arriving at the final reconstruction leads to a problem which is not initially obvious and has not been discussed (Chapter 4; fxTWA-PLS is free of this problem). When applied to a sample set other than the training set, the WAPLS*rioja* reconstruction is based on optima which can take patently impossible values. Chapter 4 proposes an alternative procedure, applying the regression coefficients to the abundance-weighted 'optima', which results in an indistinguishable calibration but a very different reconstruction of a fossil core.

This leads to an important general point. In Chapters 3, 4 and 5, different training sets or treatments yield highly similar calibrations but different reconstructions. In the first case subsets of the SMPDS training set are used, in the second the corrected WAPLS*rioja* reconstruction method mentioned above, and in the last high-abundance but suspect taxa are excluded from the full SMPDS. This shows that the statistical tests of the calibration only describe the internal consistency of the training set, and say nothing of its applicability to a fossil, or any other, set. Any sufficiently internally consistent training set can provide a good calibration, regardless of the climate envelope it encompasses, so calibrations cannot usefully distinguish between training sets. Furthermore, the transfer functions are strictly true only for the training set, and differentials in the abundances of taxa between the training and target sets lead to reconstructions dependent on weakly evidenced taxa.

The weighted averaging process in WA-PLS and fxTWA-PLS finds an abundance-weighted mean as the basis of the transfer function. In an (approximately) Gaussian response, the mean is also (approximately) the mode, but in all distributions the mode, rather than the mean, better represents the climate preference of the taxon, and many taxon responses, including some abundant in both to the training and fossil sets, differ from (approximately) Gaussian. Their modally expressed preferences can diverge significantly from the mean, leading to the suspicion that WA will find an inappropriate transfer function. A mode-based

'optimum' would be logically preferable, but in the series of papers in which Cajo ter Braak and others developed the thinking behind what became WA-PLS I find no discussion of response shapes other than (approximately) unimodal and symmetrical.

Before considering mitigations for these characteristics, note that the tolerance of taxa (the width of the abundance distribution) varies, and while WA-PLS assumes all taxa have equal tolerance, fxTWA-PLS down-weights widely tolerant taxa. Combined with a frequency adjustment to account for uneven sampling along the climate gradient, this reduces the remaining compression in the final calibration. All instances of the taxon in the target series attract the same transfer function. When a taxon's preference is narrowly defined (for instance, *Fagus* exhibits a narrow peak in GDD0) this is valuable. When a taxon is very widely tolerant or insensitive (e.g. *Pinus* diploxylon or Poaceae), and especially when the abundance in the target series is large, the transfer function is misleadingly precise and the down-weighting tolerance adjustment does not fully account for this.

In Chapter 5, some tests are proposed based on these considerations to identify taxa which could be damaging to a calibration (repeated as Table 7.1). The effect of excluding Pinus diploxylon, Amaranthaceae, Cyperaceae, Alnus, Asteroideae, Oxyria/Rumex, and Artemisia, being those taxa with the widest tolerances and the largest differences between mean and mode, is that the calibration was highly similar to that generated from the full SMPDS set, but an example reconstruction was substantially different. There is no independent test of which calibration better reconstructs glacial climate.

Table 7-1 Characteristics of taxon abundance distributions, identification, effects, and possible responses. Grey boxes: condition not affected by characteristic (copy of Table 5-4).

Characteristics of taxon abundance distribution (more than one may apply)	**How identified**	**Assumed quality of climate read**	**Shape suitability for WA**	**Applicability of transfer function**	**Possible responses**
Symmetrical unimodal	Count of modes = 1, mean-mode distance low	Good	Excellent		Include in calibration
Skewed unimodal	Count of modes = 1, mean-mode distance high	Good	Depends on mean-mode		Exclude from calibration if mean-mode > threshold; or downweight in reconstruction ~ mean-mode
Wide tolerance	Tolerance large	Good		Over precise	fxTWA-PLS already weights by tolerance. Consider exclusion of highly abundant widely tolerant taxa
Multimodal	Count of modes > 1 and modes similar, mean-mode distance	Suspect	Poor		Exclude from calibration if mean-mode > threshold; or select most obvious mode; or downweight in reconstruction ~ mean-mode
Unclear/uninformative	Inspection, low variation	Suspect	Poor	Over precise	Unless significant in fossil, exclude from calibration
Low abundance/occurrence	Count of occurrences, sum of abundances, bootstrap SD	Suspect			Set thresholds: occurrences > 10, sum(abundance) > 0.1 already set.
Misleading	Inspection and analysis	Ignore			Exclude from calibration

Whether a calibration should include all available taxa or a subset, and if so on what criteria, is discussed by e.g. Juggins, Simpson and Telford (2015) and Sinopoli *et al.* (2019), but no consensus exists. Turner *et al.* (2020) (Chapter 3) concluded that 'uninformative' taxa should be included unless there were good reasons not to, but the evidence above shows that exclusion may be valuable.

7.3 Reconstructions from fossil cores

Comparisons of the youngest intervals of the reconstructions, including the Holocene where available, with modern climate at the sites show good consistency. This suggests that despite the possible pitfalls associated with climate representation and reconstruction methodology, successful quantitative reconstructions can be made. Reconstructions made with the restricted set described above tend to be very similar to full set reconstructions in the Holocene but diverge and become colder in the glacial. This is a function of the substantial changes in taxon assemblages as the cores pass through the termination; the interpretation is that both are good training sets post-termination, but the full modern set may be less good for the glacial. Only Monticchio has previous quantitative reconstructions, neither of which can usefully be compared with the new reconstructions.

We can now come to an initial view of the robustness of the fxTWA-PLS reconstruction method. While there are factors which, if not considered and mitigated, would undermine the reconstructions, the similarity of Holocene reconstructions under different treatments to each other and to modern climate strongly suggest that the method is capable of providing good reconstructions, certainly for the Holocene. Because typical glacial pollen assemblages differ significantly from the modern, and the transfer functions are only strictly true of the modern relative abundances, glacial quantitative reconstructions may be less robust than those for the Holocene. But below it will be seen that glacial reconstructions are nevertheless sufficiently good that D-Os can be convincingly identified in them.

7.4 Locating D-O-like responses

7.4.1 Direct use of pollen records

It proves difficult to identify D-O-like events by looking directly in the fossil pollen records, rather than in quantitative reconstructions of climate. Dimension reduction techniques (PCA, DCA) and sample-to-sample change described by SCD do not show D-O-like changes clearly or in the numbers expected, and the axes of PCA and DCA have no clear climatic meaning and have arbitrary signs. This failure is not easy to explain, since the responses later convincingly found by pattern matching in quantitative reconstructions must exist in the raw pollen data. In the case of SCD, all changes are swept together and all changes are positive, so temperature rises are not separately identifiable. In all three cases, some highly abundant taxa in the fossil record are relatively insensitive to climate, so changes in their abundances which have little climatic significance may dominate the result.

Creating time series by grouping taxa together by hierarchical clustering proved unstable because highly dependent on the time range chosen, and pre-defined functional groups found many more sharp changes than the expected D-Os. Three further statistical methods, Dynamic Time Warping (DTW), Singular Spectrum Analysis (SSA) and. Hidden Markov Models, were applied but none reliably identified D-O events.

None of the series created directly from pollen had a clear climatic meaning, which is believed to be part of the difficulty. None of the methods deconvolved the multi-dimensional nature of the climate signal contained in the pollen record adequately to be comparable with a Greenland temperature signal.

7.4.2 Pattern and age matching

The circum-Mediterranean glacial cores which provide the fossil pollen used in this project vary in sampling resolution and in the variability over time of the pollen abundances; low variability (complacency) hampers the identification of D-O-like shapes. The sampling resolution of most cores is on the order of 200-500 years, which is shown to be adequate to define the shape of most D-Os (Figure 2.20), and though there are intervals in some cores when there are too few physical samples to identify a D-O well, the presence of hiatus is a more common cause (e.g. Dead Sea and Villarquemado).

'Pattern matching' finds shapes in a target series which resemble the distinctive asymmetrical rise in temperature at a D-O, the initiation of a Greenland Interstadial. Focussing narrowly on a window ~ 300 years before the temperature rise to ~ 200 years after, the shape of which is very consistent between GIs, avoids dilution of the asymmetrical pattern by the much more variable declining part of the GI (Chapter 2). In a Euclidean distance (ED) calculated between templates of these patterns for GIs 1 to 20 and the target series, the down-spikes locate the intervals most like a D-O, and these are mostly very clear. When tested on the Kindler series from which the templates were extracted, all GIs but two were identified, but also a few other events which are not recognised GIs. In the first case, this signifies that GI initiations are all very similar but not identical, and combining many GIs means that relatively unusual ones may not be picked. In the second, some small-scale D-O-like events exist in the Kindler temperature series which are less pronounced in the $\delta^{18}O_{ice}$ series.

While its shape, denoted by ED, is the first line of evidence that an interval in a pollen-based series is D-O-like, other attributes add to the evidence:

- size: small-scale and brief excursions are less likely to be GIs

- the strength of support for the shape in the core reconstruction
    - Number of physical samples defining the shape
    - Whether low Hill's N2, abnormal excursions, wide bootstrapped uncertainties or hiatus affect these samples.

This second category rarely disqualifies an interval, but making the check is important.

Applying an ED cutoff taken from the test against Kindler, only minor parameter variations between cores are required to select sets of potential D-O-like points (DOLPs) which are equal to or lower in number than the expected GIs in the cores' age ranges.

So far, the age of the event has not been considered, only its similarity to a D-O, and the final step is to consider the closeness, or otherwise, of a DOLP in age to a Greenland D-O. Pollen core age models are based on rather sparse dating points and tend to have widening uncertainties just when D-Os become more frequent, so identifying pollen core intervals as D-Os by age model date alone is not robust. New age-depth models for the pollen cores were created, updating the ^{14}C calibration to IntCal20, and ignoring dating points which assumed that features of the pollen reflected specific D-O events, to avoid circularity. In Chapter 6, the locations and characteristics of DOLPs found by pattern matching are combined with the overlaps in the age uncertainties in the core age models and the GICC05modelext chronology to propose the final matches of DOLPs with GIs.

The result is that pattern matching applied to quantitative reconstruction, while not perfect, locates many D-O responses with highly plausibility, generates few false positives and few false negatives, and in younger intervals allows assignments to specific GIs.

More specifically, across 12 cores which yielded good evidence, 48 out of 61 DOLPs were assigned with high plausibility to specific GIs. Of the 13 which were not assigned, 9 fell in the interval between GI 1 and 2, an interval in which pattern matching finds in the Kindler series two D-O-like events not officially recognised as D-Os because of their small scale, so it may be these which are found. Most cores rejected one DOLP or

none, and missed one GI or none. In the older range (> ~ 40 ka) where DOLPS could not be specifically assigned, a total of 64 DOLPs had plausible matches within a set of 69 GIs. The imperfections in the pattern and age matching method stem from core-related causes such as complacency and hiatus which compromise the registration of D-Os, wide age model uncertainties, and, though probably of lesser importance, imprecise reconstructions leading to less sharp changes. Of these, only the last can be mitigated by improved techniques.

7.5 What would make reconstructions better?

Higher sampling resolution of cores shares top place with access to data from other climate-sensitive materials in the same cores, to provide an independent check of the pollen-based reconstructions. Current practice favours the extraction of other materials and data alongside pollen (e.g. Pini, Ravazzi and Reimer, 2010; Camuera *et al.*, 2018). More comprehensive sampling of cold dry climates, for instance from Russia, in the training set would strengthen the evidence of glacial-like climates.

7.6 Possible future work

7.6.1 Improvements to reconstruction methods

While fxTWA-PLS assumes that the patterns of taxon abundances along environmental gradients are approximately Gaussian, many taxon responses do not resemble this, so it may misread the climate preference. A formal evaluation of classes of response could be created, for instance starting from HOF models (Huisman, Olff and Fresco, 1993; Oksanen and Minchin, 2002; Jansen and Oksanen, 2013), building towards a mechanism for accepting/rejecting taxa based on shape, and/or treating non-Gaussian responses differently, during fxTWA-PLS calibration. However, separate treatments of mode, tolerance and sensitivity by class may prove too simplistic, and continuous treatment of these characteristics may be preferable. Since the mode and not the mean represents the preferred environment of biota, a calibration which establishes a mode, or more strictly a modal class, could be made, at least when the response is not approximately symmetrical and unimodal. Several choices need to be made in establishing a modal class,

such as bin widths, curve stiffness, and rules for selection of a principal mode where the distribution is multimodal or unclear, and many combinations of these would need to be tested. The output should include a measure of taxon tolerance, reflecting the peakiness of the mode. This should be propagated to the sample level in the reconstruction to provide an uncertainty in the climate value.

A possible alternative to reconstruction using fxTWA-PLS, and which respects the importance of the mode, is to create an abundance-weighted sum of the individual taxon abundance curves for each fossil sample, thus reconstructing the climate for the sample as a curve along a climate gradient. The expected benefit is that the combined curve for a climate dimension is a unimodal probability density, the mode of which is the best estimate of the climate, and the probabilistic nature of the result provides uncertainties. The method might be capable of extension to encompass 2 or 3 dimensions of climate simultaneously.

7.6.2 Regional climate regime

Reliably identified and dated D-Os from multiple cores could be used to assemble a regional picture of the climate regime, relate this to changes in climate dynamics, and examine the hypothesis that an east-west moisture dipole existed during the glacial. If the aim is to describe the climate of all, or specific, GIs/GSs, only some events can be used, and they may not be registered in all the available cores. Alternatively, cold and warm intervals can be treated as two classes. This does not require that all D-O-like events are firmly assigned to GIs, but the definition of a cold interval, which is much harder to specify than a warm interval, requires close attention.

The concept of a moisture dipole arises because the West and the East of the region may differ climatically, beyond simple continentality. Moisture in modern Mediterranean climate has a well-documented relation with the position of the eddy-driven jet (the North Atlantic Oscillation), which at the LGM was much further south than today: it ran almost West-East over Iberia (e.g. Li and Born, 2019), and the oceanic polar front was off Iberia in stadials (Eynaud *et al.*, 2009; Marchal, Waelbroeck and Verdière, 2016). Rapid meridional movement of the jet stream during significant temperature changes such as D-Os is both climate-dynamically necessary (e.g. Corrick *et al.*, 2020) and is documented for the end of GS 1 (Lane *et al.*, 2013).

Rohling *et al.* (2013) show that the water source of precipitation in the Mediterranean tends to be the Atlantic in the West and the Mediterranean itself in the East. García-Alix *et al.* (2021) noted millennial-scale changes between the two sources in Iberia back to 35 ka. The literature consistently supports the view that interstadials were wetter than stadials (Nebout *et al.*, 2002; Stockhecke *et al.*, 2016; Budsky *et al.*, 2019). All these conclusions are based on relatively small areas, so a regional picture assembled from multiple consistently treated cores is desirable.

Tentative results were presented at the EGU (Turner and Harrison, 2022), though this suggested that stadials in the west could be wetter than interstadials. Now that it is clear that many D-Os are identifiable in pollen reconstructions and some can be matched with specific GIs it could be possible to pursue this project.

7.6.3 Data-model comparisons

In this project no attempt has been made at data-model comparison. The benefit of such comparison would be that models which successfully replicate robust quantitative reconstructions may make the processes underlying D-Os clearer and improve understanding of climate dynamics during rapid temperature changes. To date, general circulation climate models (GCMs) have not been able to replicate D-Os reliably, and the suspicion is that the models are too stable, a dangerous position under current warming. But the conditions tested have differed between models; protocols are being developed to ensure consistency (Malmierca-Vallet *et al.*, 2023) which will allow the outputs of multiple models to be directly comparable.

7.6.4 Matrix Profile

Recently Matrix Profile, a generic statistical pattern matching approach which does not require prior specification of a pattern, has been applied with partial success to the identification of D-Os in the Greenland $\delta^{18}O_{ice}$ series (Barbosa *et al.*, 2023). The window used to identify patterns was rather wide, and experience from pattern matching suggests that a narrower window which could focus on the rapid rise would be more successful. This method deserves exploration.

7.7 References

Ackerly, D.D. (2003) 'Community assembly, niche conservatism, and adaptive evolution in changing environments', *International Journal of Plant Sciences*, 164(S3), pp. S165–S184. Available at: https://doi.org/10.1086/368401.

Barbosa, S. *et al.* (2023) *Automatic characterisation of Dansgaard-Oeschger events in palaeoclimate ice records*. other. oral. Available at: https://doi.org/10.5194/egusphere-egu23-3612.

Bartlein, P.J. *et al.* (2011) 'Pollen-based continental climate reconstructions at 6 and 21 ka: a global synthesis', *Climate Dynamics*, 37(3–4), pp. 775–802. Available at: https://doi.org/10.1007/s00382-010-0904-1.

Bio, A. m. f., Alkemade, R. and Barendregt, A. (1998) 'Determining alternative models for vegetation response analysis: a non-parametric approach', *Journal of Vegetation Science*, 9(1), pp. 5–16. Available at: https://doi.org/10.2307/3237218.

Birks, H.J.B. *et al.* (2010) 'Strengths and Weaknesses of Quantitative Climate Reconstructions Based on Late-Quaternary', *The Open Ecology Journal*, 3(1). Available at: https://benthamopen.com/ABSTRACT/TOECOLJ-3-2-68 (Accessed: 17 April 2023).

Budsky, A. *et al.* (2019) 'Western Mediterranean Climate Response to Dansgaard/Oeschger Events: New Insights From Speleothem Records', *Geophysical Research Letters*, 46(15), pp. 9042–9053. Available at: https://doi.org/10.1029/2019GL084009.

Camuera, J. *et al.* (2018) 'Orbital-scale environmental and climatic changes recorded in a new ~200,000-year-long multiproxy sedimentary record from Padul, southern Iberian Peninsula', *Quaternary Science Reviews*, 198, pp. 91–114. Available at: https://doi.org/10.1016/j.quascirev.2018.08.014.

Chevalier, M. *et al.* (2020) 'Pollen-based climate reconstruction techniques for late Quaternary studies', *Earth-Science Reviews*, 210, p. 103384. Available at: https://doi.org/10.1016/j.earscirev.2020.103384.

Corrick, E.C. *et al.* (2020) 'Synchronous timing of abrupt climate changes during the last glacial period', *Science*, 369(6506), pp. 963–969. Available at: https://doi.org/10.1126/science.aay5538.

Currant, A. and Jacobi, R. (2001) 'A formal mammalian biostratigraphy for the Late Pleistocene of Britain', *Quaternary Science Reviews*, 20(16), pp. 1707–1716. Available at: https://doi.org/10.1016/S0277-3791(01)00035-X.

Eynaud, F. *et al.* (2009) 'Position of the Polar Front along the western Iberian margin during key cold episodes of the last 45 ka', *Geochemistry, Geophysics, Geosystems*, 10(7). Available at: https://doi.org/10.1029/2009GC002398.

García-Alix, A. *et al.* (2021) 'Paleohydrological dynamics in the Western Mediterranean during the last glacial cycle', *Global and Planetary Change*, 202, p. 103527. Available at: https://doi.org/10.1016/j.gloplacha.2021.103527.

Huisman, J., Olff, H. and Fresco, L.F.M. (1993) 'A Hierarchical Set of Models for Species Response Analysis', *Journal of Vegetation Science*, 4(1), pp. 37–46. Available at: https://doi.org/10.2307/3235732.

Jansen, F. and Oksanen, J. (2013) 'How to model species responses along ecological gradients – Huisman–Olff–Fresco models revisited', *Journal of Vegetation Science*, 24(6), pp. 1108–1117. Available at: https://doi.org/10.1111/jvs.12050.

Juggins, S (2017) 'rioja: Analysis of quaternary science data'. CRAN. Available at: http://cran.r-project.org/package=rioja.

Juggins, S., Simpson, G.L. and Telford, R.J. (2015) 'Taxon selection using statistical learning techniques to improve transfer function prediction', *The Holocene*, 25(1), pp. 130–136. Available at: https://doi.org/10.1177/0959683614556388.

Kindler, P. *et al.* (2014) 'Temperature reconstruction from 10 to 120 kyr b2k from the NGRIP ice core', *Climate of the Past*, 10(2), pp. 887–902. Available at: https://doi.org/10.5194/cp-10-887-2014.

Lane, C.S. *et al.* (2013) 'Volcanic ash reveals time-transgressive abrupt climate change during the Younger Dryas', *Geology*, 41(12), pp. 1251–1254. Available at: https://doi.org/10.1130/G34867.1.

Li, C. and Born, A. (2019) 'Coupled atmosphere-ice-ocean dynamics in Dansgaard-Oeschger events', *Quaternary Science Reviews*, 203, pp. 1–20. Available at: https://doi.org/10.1016/j.quascirev.2018.10.031.

Liu, M. *et al.* (2020) 'An improved statistical approach for reconstructing past climates from biotic assemblages', *Proceedings of the Royal Society A* [Preprint]. Available at: https://doi.org/10.1098/rspa.2020.0346.

Malmierca-Vallet, I. *et al.* (2023) 'Dansgaard–Oeschger events in climate models: review and baseline Marine Isotope Stage 3 (MIS3) protocol', *Climate of the Past*, 19(5), pp. 915–942. Available at: https://doi.org/10.5194/cp-19-915-2023.

Marchal, O., Waelbroeck, C. and Verdière, A.C. de (2016) 'On the Movements of the North Atlantic Subpolar Front in the Preinstrumental Past', *Journal of Climate*, 29(4), pp. 1545–1571. Available at: https://doi.org/10.1175/JCLI-D-15-0509.1.

Nebout, N.C. *et al.* (2002) 'Enhanced aridity and atmospheric high-pressure stability over the western Mediterranean during the North Atlantic cold events of the past 50 ky', *Geology*, 30(10), pp. 863–866.

Oksanen, J. and Minchin, P.R. (2002) 'Continuum theory revisited: what shape are species responses along ecological gradients?', *Ecological Modelling*, 157(2), pp. 119–129. Available at: https://doi.org/10.1016/S0304-3800(02)00190-4.

Pini, R., Ravazzi, C. and Reimer, P.J. (2010) 'The vegetation and climate history of the last glacial cycle in a new pollen record from Lake Fimon (southern Alpine foreland, N-Italy)', *Quaternary Science Reviews*, 29(23–24), pp. 3115–3137. Available at: https://doi.org/10.1016/j.quascirev.2010.06.040.

Rasmussen, S.O. *et al.* (2014) 'A stratigraphic framework for abrupt climatic changes during the Last Glacial period based on three synchronized Greenland ice-core records: refining and extending the INTIMATE event stratigraphy', *Quaternary Science Reviews*, 106, pp. 14–28. Available at: https://doi.org/10.1016/j.quascirev.2014.09.007.

Rohling, E.J. *et al.* (2013) 'Paleoclimate Variability in the Mediterranean and Red Sea Regions during the Last 500,000 Years: Implications for Hominin Migrations', *Current Anthropology*, 54(S8), pp. S183–S201. Available at: https://doi.org/10.1086/673882.

Sánchez Goñi, M.F. *et al.* (2009) 'Contrasting intrainterstadial climatic evolution between high and middle North Atlantic latitudes: A close-up of Greenland Interstadials 8 and 12', *Geochemistry, Geophysics, Geosystems*, 10(4). Available at: https://doi.org/10.1029/2008GC002369.

Shelford, V.E. (1931) 'Some Concepts of Bioecology', *Ecology*, 12(3), pp. 455–467. Available at: https://doi.org/10.2307/1928991.

Sinopoli, G. *et al.* (2019) 'Pollen-based temperature and precipitation changes in the Ohrid Basin (western Balkans) between 160 and 70ka', *Climate of the Past*, 15(1), pp. 53–71. Available at: https://doi.org/10.5194/cp-15-53-2019.

Stockhecke, M. *et al.* (2016) 'Millennial to orbital-scale variations of drought intensity in the Eastern Mediterranean', *Quaternary Science Reviews*, 133, pp. 77–95. Available at: https://doi.org/10.1016/j.quascirev.2015.12.016.

Sweeney, J. *et al.* (2018) 'Statistical challenges in estimating past climate changes', *Wiley Interdisciplinary Reviews: Computational Statistics*, 10(5), p. e1437. Available at: https://doi.org/10.1002/wics.1437.

systematicinvestor (2012) 'Time Series Matching | R-bloggers', 13 January. Available at: https://www.r-bloggers.com/2012/01/time-series-matching/ (Accessed: 23 September 2023).

Ter Braak, C.J.F. and Juggins, S. (1993) 'Weighted averaging partial least squares regression (WA-PLS) : an improved method for reconstructing environmental variables from species assemblages', *Hydrobiologia*, 269/270, pp. 485–502.

Turner, M. and Harrison, S.P. (2022) *Mediterranean climates during Dansgaard-Oechger cycles in the last glacial period*. EGU22-4968. Copernicus Meetings. Available at: https://doi.org/10.5194/egusphere-egu22-4968.

Turner, M.G. *et al.* (2020) 'The impact of methodological decisions on climate reconstructions using WA-PLS', *Quaternary Research*, pp. 1–16. Available at: https://doi.org/10.1017/qua.2020.44.

Wei, D. *et al.* (2019) 'Climate changes in interior semi-arid Spain from the last interglacial to the late Holocene', *Climate of the Past Discussions*, pp. 1–31. Available at: https://doi.org/10.5194/cp-2019-16.

Appendix A: Mean binned abundances, loess curves and fxt optima of SMPDSv1 taxa with summed fractional abundance > 0.1 (n = 138)

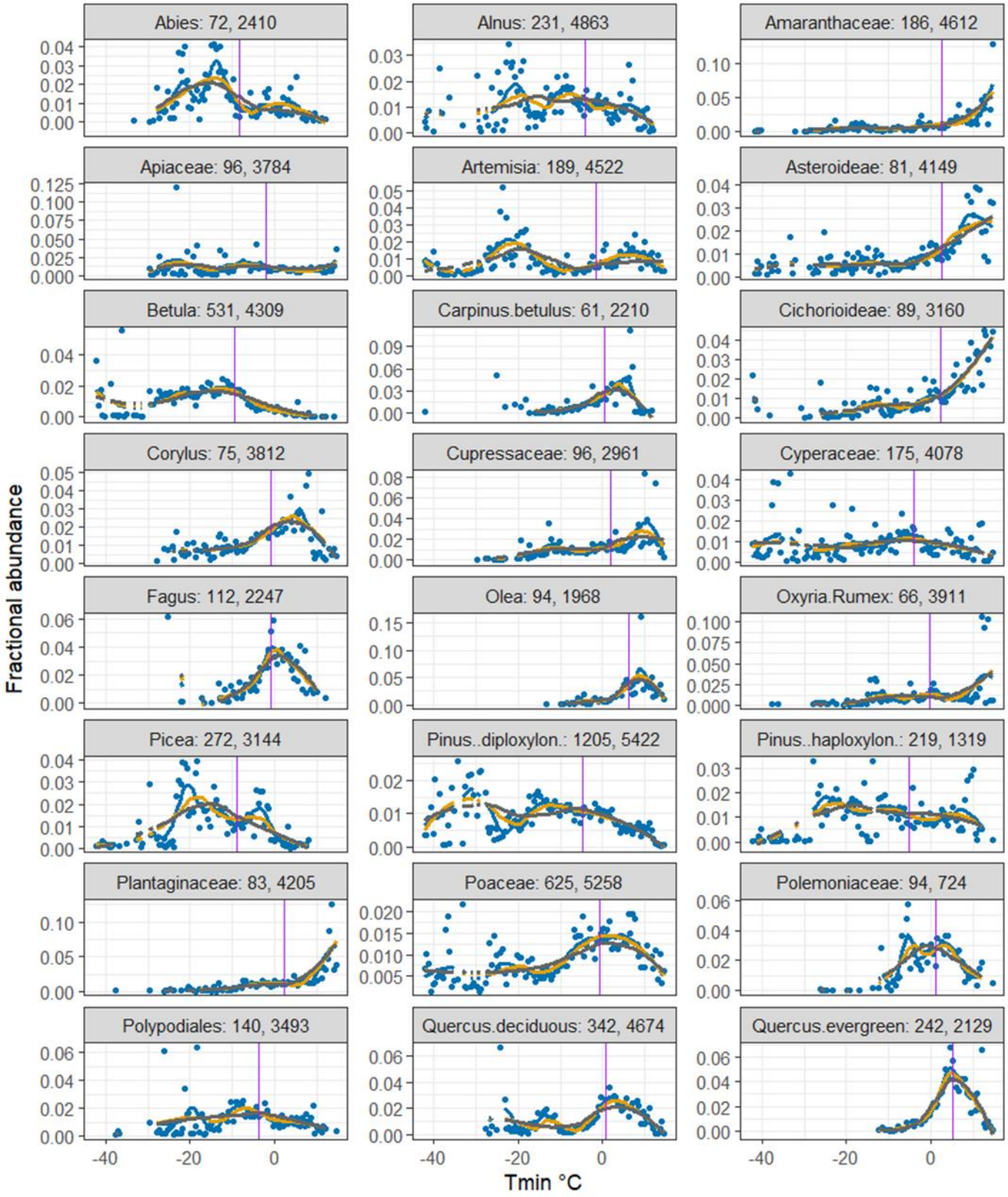
Abies: 72, 2410
Alnus: 231, 4863
Amaranthaceae: 186, 4612
Apiaceae: 96, 3784
Artemisia: 189, 4522
Asteroideae: 81, 4149
Betula: 531, 4309
Carpinus.betulus: 61, 2210
Cichorioideae: 89, 3160
Corylus: 75, 3812
Cupressaceae: 96, 2961
Cyperaceae: 175, 4078
Fagus: 112, 2247
Olea: 94, 1968
Oxyria.Rumex: 66, 3911
Picea: 272, 3144
Pinus..diploxylon.: 1205, 5422
Pinus..haploxylon.: 219, 1319
Plantaginaceae: 83, 4205
Poaceae: 625, 5258
Polemoniaceae: 94, 724
Polypodiales: 140, 3493
Quercus.deciduous: 342, 4674
Quercus.evergreen: 242, 2129
Fractional abundance
Tmin °C

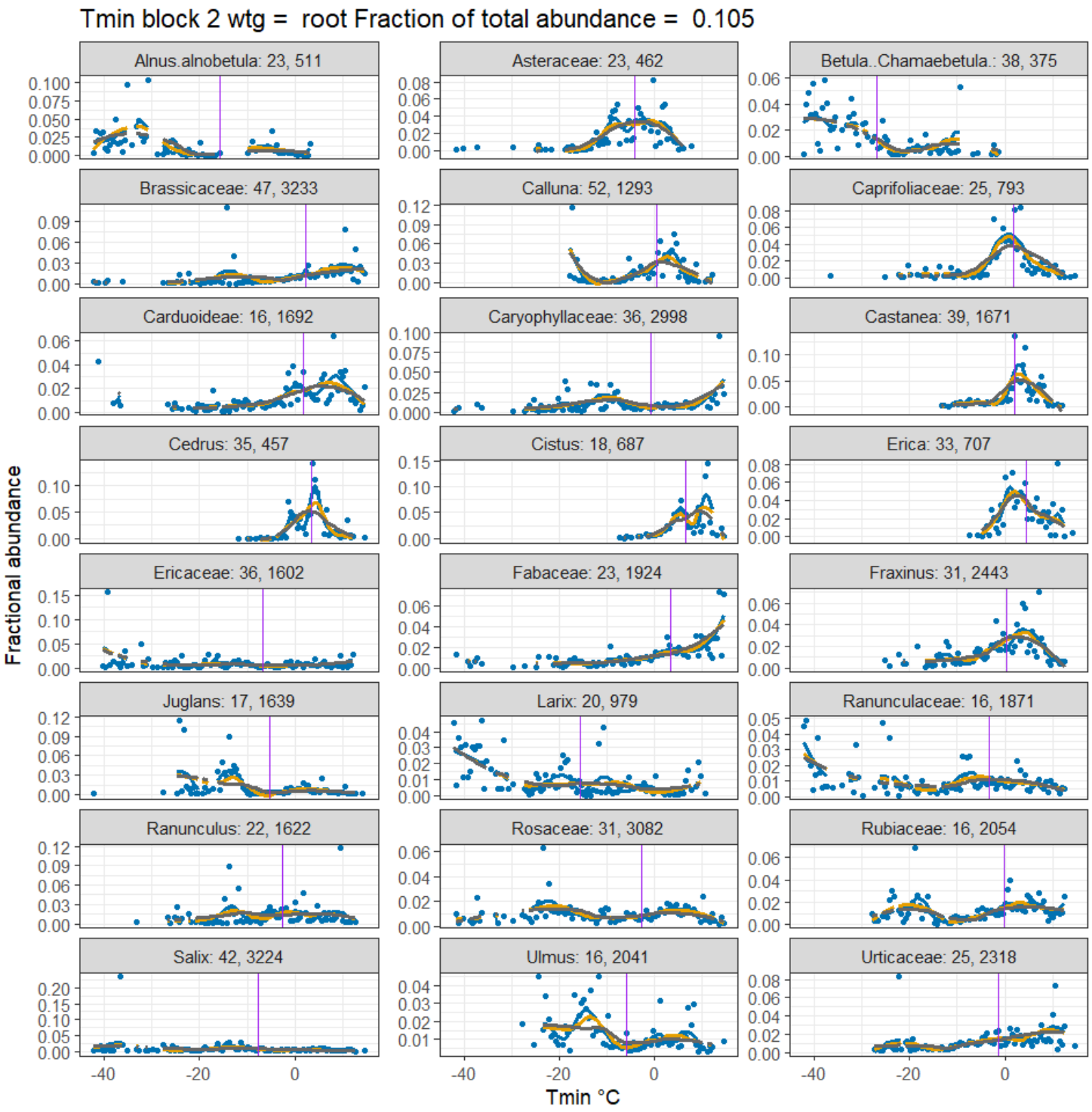
Tmin block 2 wtg = root Fraction of total abundance = 0.105
Alnus.alnobetula: 23, 511
Asteraceae: 23, 462
Betula..Chamaebetula.: 38, 375
Brassicaceae: 47, 3233
Calluna: 52, 1293
Caprifoliaceae: 25, 793
Carduoideae: 16, 1692
Caryophyllaceae: 36, 2998
Castanea: 39, 1671
Cedrus: 35, 457
Cistus: 18, 687
Erica: 33, 707
Ericaceae: 36, 1602
Fabaceae: 23, 1924
Fraxinus: 31, 2443
Juglans: 17, 1639
Larix: 20, 979
Ranunculaceae: 16, 1871
Ranunculus: 22, 1622
Rosaceae: 31, 3082
Rubiaceae: 16, 2054
Salix: 42, 3224
Ulmus: 16, 2041
Urticaceae: 25, 2318
Fractional abundance
Tmin °C

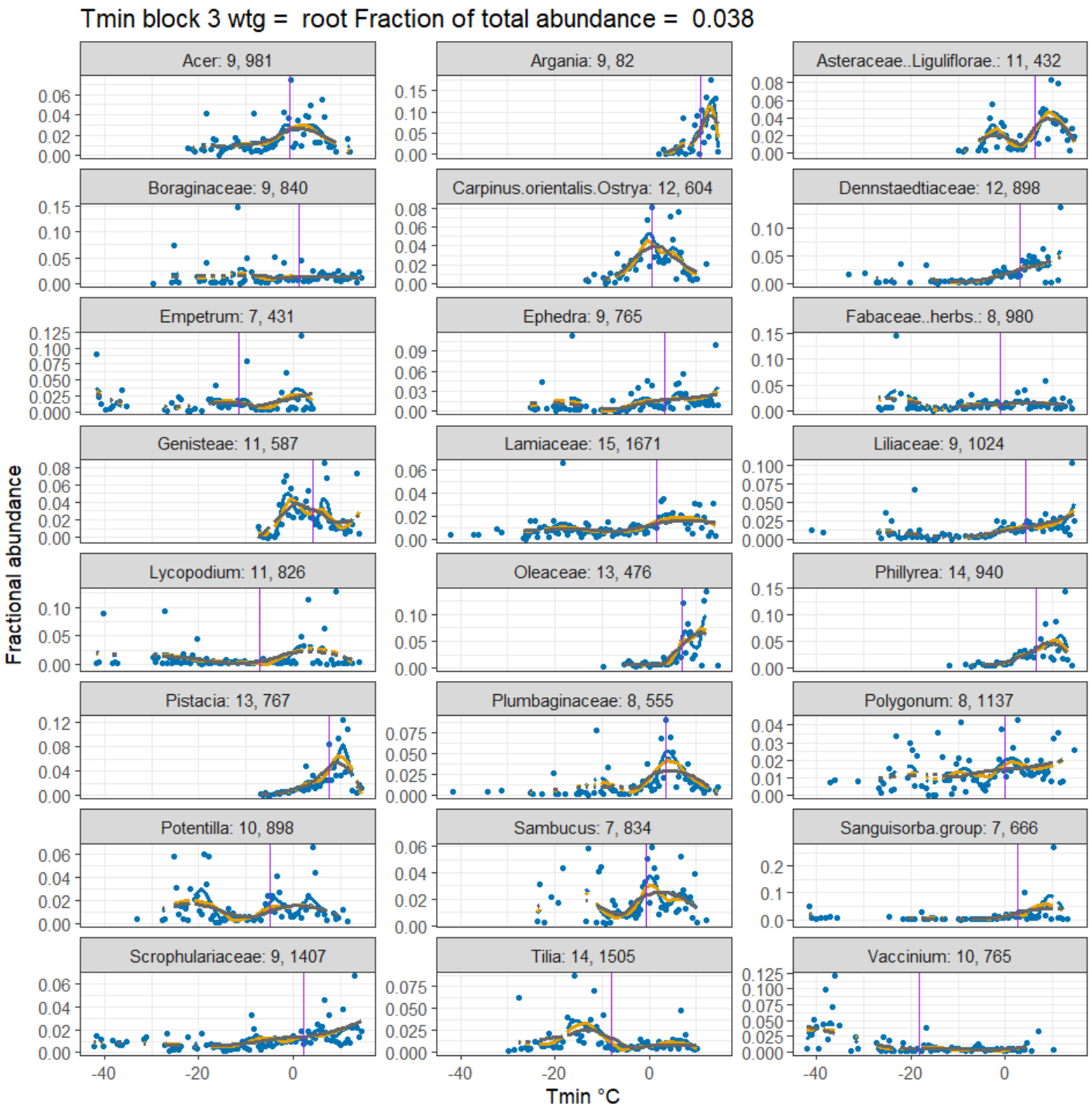
Tmin block 3 wtg = root Fraction of total abundance = 0.038
Acer: 9, 981
Argania: 9, 82
Asteraceae..Liguliflorae.: 11, 432
Boraginaceae: 9, 840
Carpinus.orientalis.Ostrya: 12, 604
Dennstaedtiaceae: 12, 898
Empetrum: 7, 431
Ephedra: 9, 765
Fabaceae..herbs.: 8, 980
Genisteae: 11, 587
Lamiaceae: 15, 1671
Liliaceae: 9, 1024
Lycopodium: 11, 826
Oleaceae: 13, 476
Phillyrea: 14, 940
Pistacia: 13, 767
Plumbaginaceae: 8, 555
Polygonum: 8, 1137
Potentilla: 10, 898
Sambucus: 7, 834
Sanguisorba.group: 7, 666
Scrophulariaceae: 9, 1407
Tilia: 14, 1505
Vaccinium: 10, 765
Fractional abundance
Tmin °C

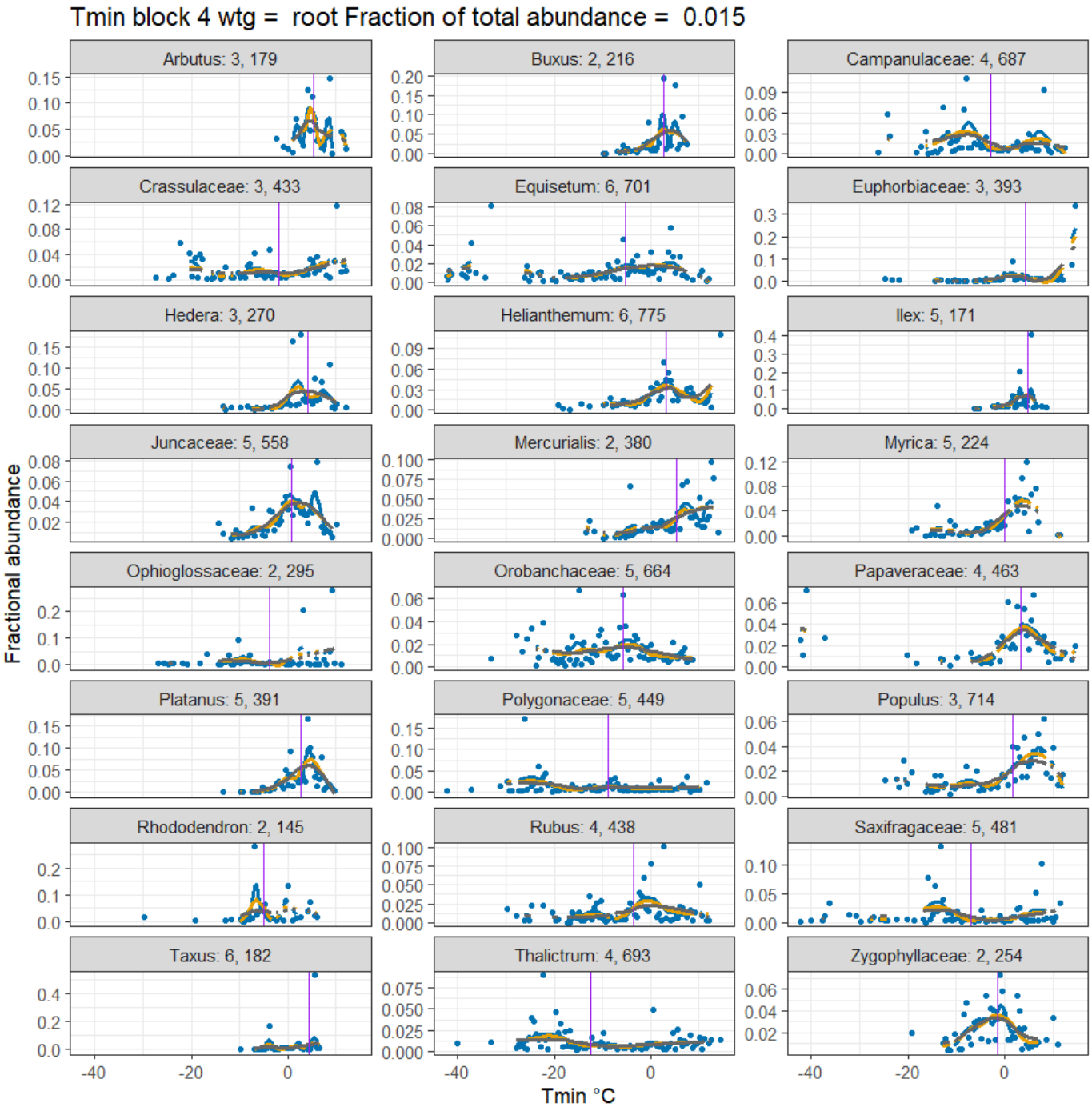
Tmin block 4 wtg = root Fraction of total abundance = 0.015
Arbutus: 3, 179
Buxus: 2, 216
Campanulaceae: 4, 687
Crassulaceae: 3, 433
Equisetum: 6, 701
Euphorbiaceae: 3, 393
Hedera: 3, 270
Helianthemum: 6, 775
Ilex: 5, 171
Juncaceae: 5, 558
Mercurialis: 2, 380
Myrica: 5, 224
Ophioglossaceae: 2, 295
Orobanchaceae: 5, 664
Papaveraceae: 4, 463
Platanus: 5, 391
Polygonaceae: 5, 449
Populus: 3, 714
Rhododendron: 2, 145
Rubus: 4, 438
Saxifragaceae: 5, 481
Taxus: 6, 182
Thalictrum: 4, 693
Zygophyllaceae: 2, 254
Fractional abundance
Tmin °C

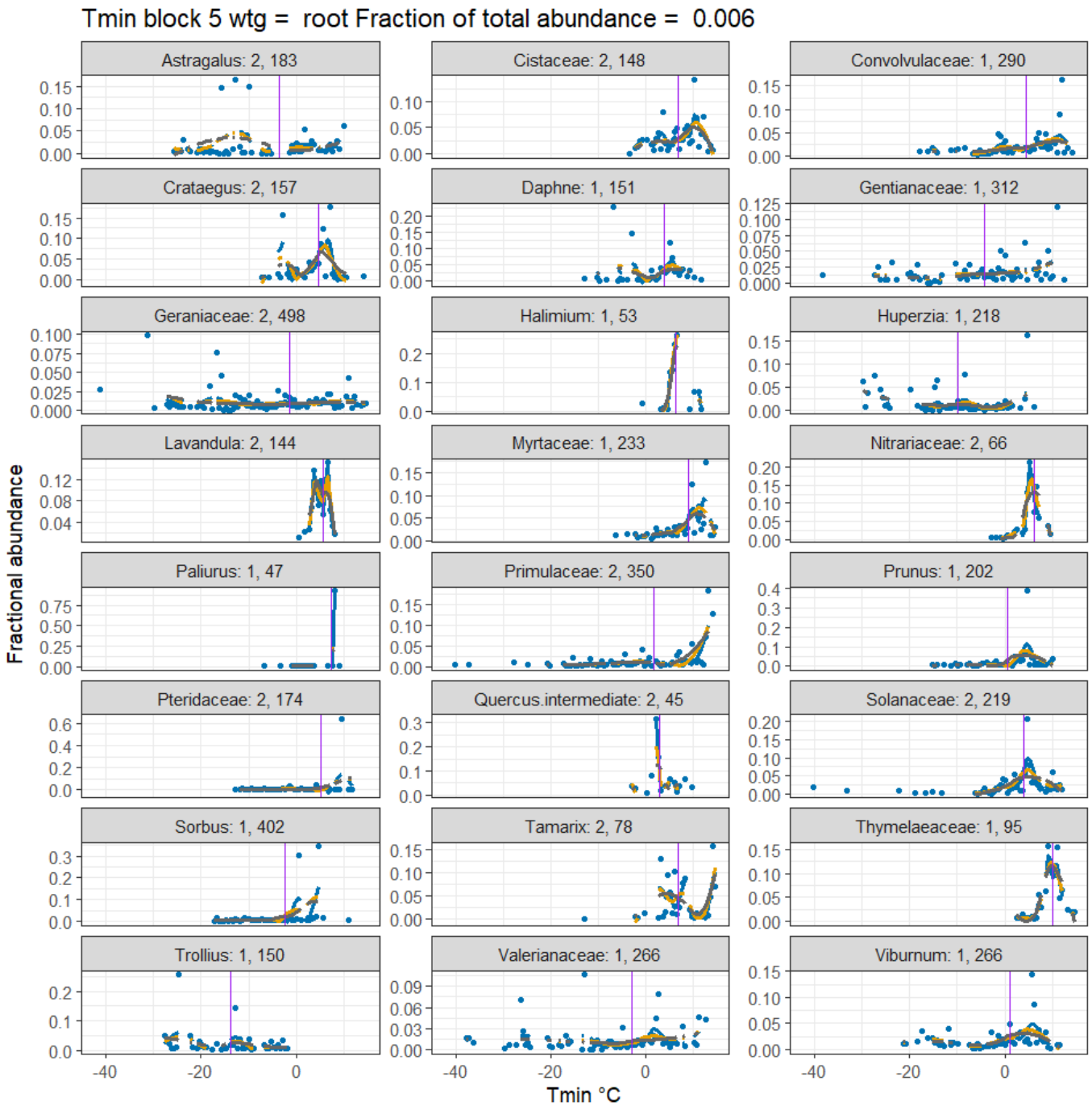
Tmin block 5 wtg = root Fraction of total abundance = 0.006
Astragalus: 2, 183
Cistaceae: 2, 148
Convolvulaceae: 1, 290
Crataegus: 2, 157
Daphne: 1, 151
Gentianaceae: 1, 312
Geraniaceae: 2, 498
Halimium: 1, 53
Huperzia: 1, 218
Lavandula: 2, 144
Myrtaceae: 1, 233
Nitrariaceae: 2, 66
Paliurus: 1, 47
Primulaceae: 2, 350
Prunus: 1, 202
Pteridaceae: 2, 174
Quercus.intermediate: 2, 45
Solanaceae: 2, 219
Sorbus: 1, 402
Tamarix: 2, 78
Thymelaeaceae: 1, 95
Trollius: 1, 150
Valerianaceae: 1, 266
Viburnum: 1, 266
Fractional abundance
Tmin °C


Tmin block 6 wtg = root Fraction of total abundance = 0.002
Aconitum: 1, 110
Aesculus: 1, 70
Caragana: 1, 20
Celastraceae: 1, 114
Ceratonia: 1, 36
Cornus: 1, 190
Frangula: 1, 189
Hypericaceae: 1, 253
Lonicera: 1, 119
Onagraceae: 1, 256
Oxalidaceae: 1, 73
Picea.orientalis: 1, 65
Rhamnaceae: 1, 76
Rhamnus: 1, 176
Rhus: 1, 69
Ulmus.Zelkova: 1, 31
Violaceae: 1, 149
Viscum: 1, 74
Fractional abundance
Tmin °C

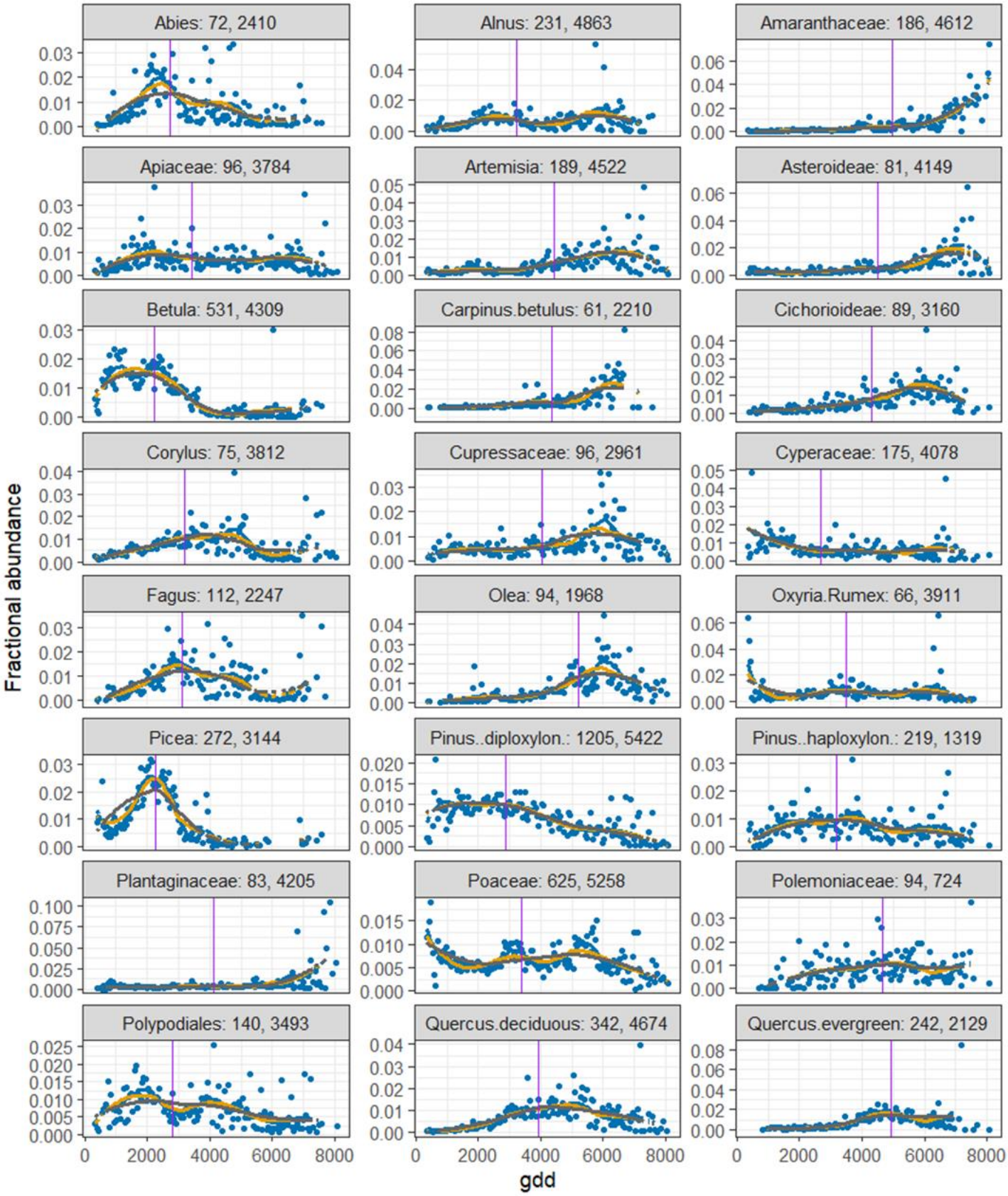
Abies: 72, 2410
Alnus: 231, 4863
Amaranthaceae: 186, 4612
Apiaceae: 96, 3784
Artemisia: 189, 4522
Asteroideae: 81, 4149
Betula: 531, 4309
Carpinus.betulus: 61, 2210
Cichorioideae: 89, 3160
Corylus: 75, 3812
Cupressaceae: 96, 2961
Cyperaceae: 175, 4078
Fagus: 112, 2247
Olea: 94, 1968
Oxyria.Rumex: 66, 3911
Picea: 272, 3144
Pinus..diploxylon.: 1205, 5422
Pinus..haploxylon.: 219, 1319
Plantaginaceae: 83, 4205
Poaceae: 625, 5258
Polemoniaceae: 94, 724
Polypodiales: 140, 3493
Quercus.deciduous: 342, 4674
Quercus.evergreen: 242, 2129
Fractional abundance
gdd
0
2000
4000
6000
8000

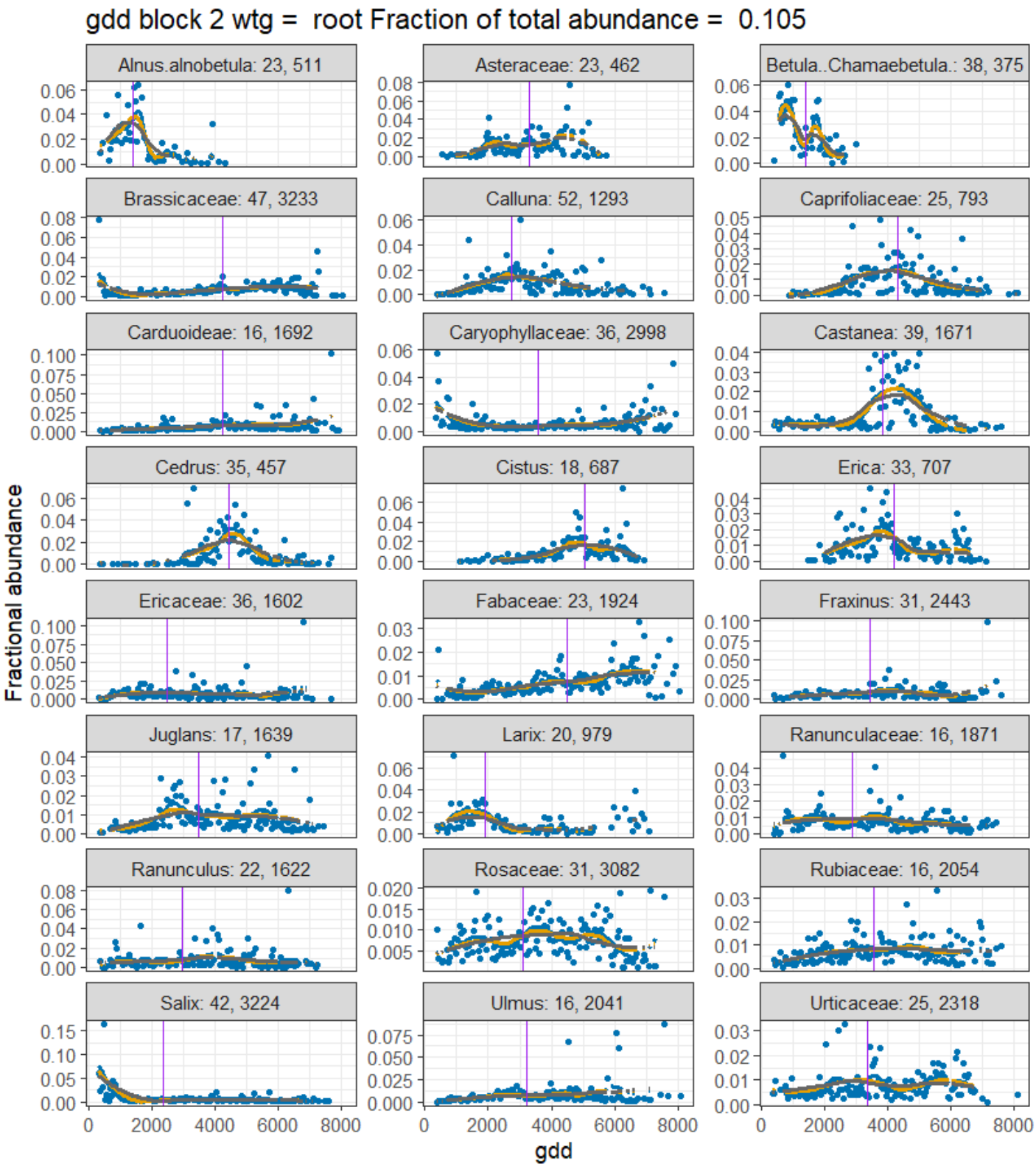
gdd block 2 wtg = root Fraction of total abundance = 0.105
Alnus.alnobetula: 23, 511
Asteraceae: 23, 462
Betula..Chamaebetula.: 38, 375
Brassicaceae: 47, 3233
Calluna: 52, 1293
Caprifoliaceae: 25, 793
Carduoideae: 16, 1692
Caryophyllaceae: 36, 2998
Castanea: 39, 1671
Cedrus: 35, 457
Cistus: 18, 687
Erica: 33, 707
Ericaceae: 36, 1602
Fabaceae: 23, 1924
Fraxinus: 31, 2443
Juglans: 17, 1639
Larix: 20, 979
Ranunculaceae: 16, 1871
Ranunculus: 22, 1622
Rosaceae: 31, 3082
Rubiaceae: 16, 2054
Salix: 42, 3224
Ulmus: 16, 2041
Urticaceae: 25, 2318
Fractional abundance
gdd

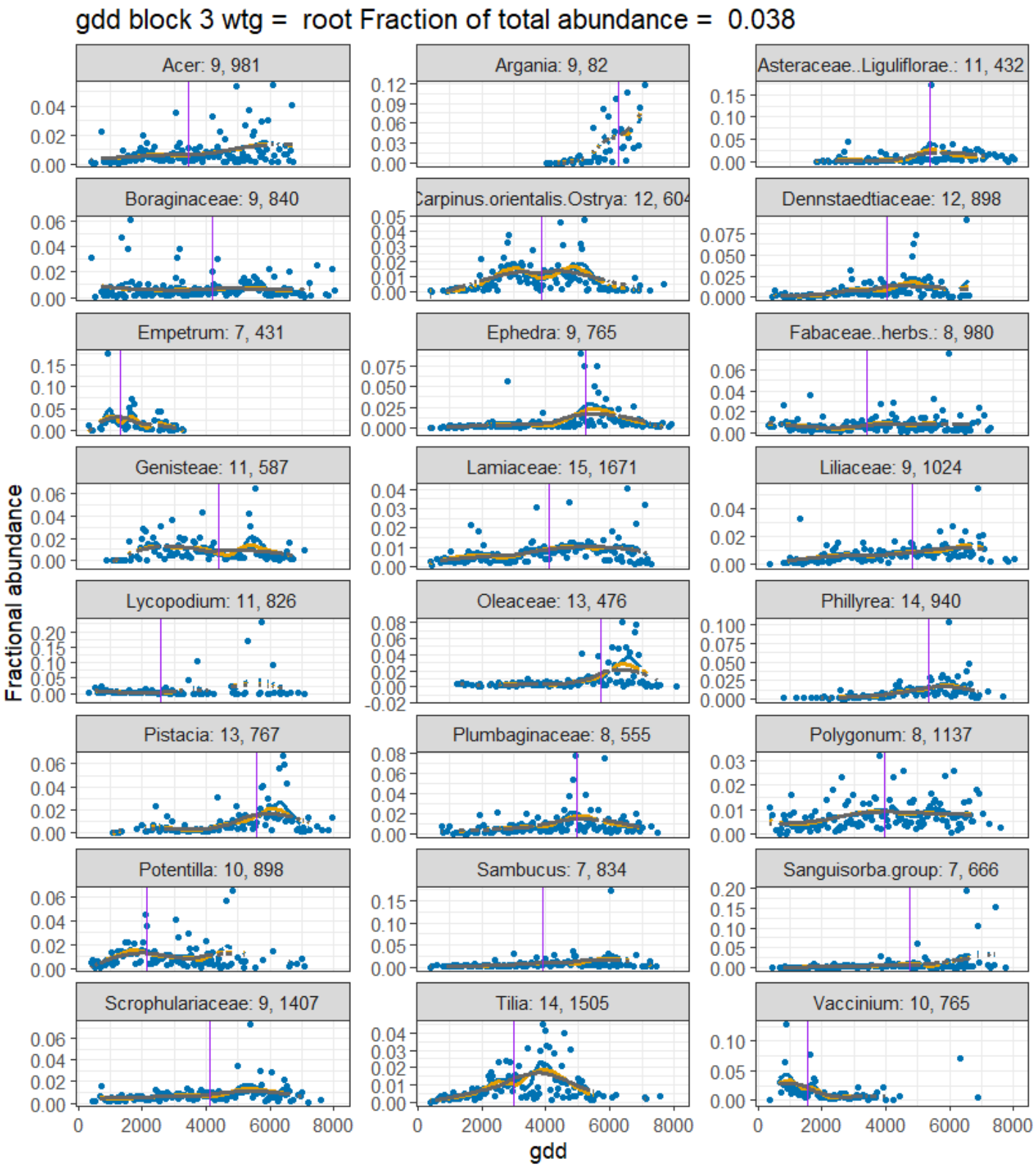
gdd block 3 wtg = root Fraction of total abundance = 0.038
Acer: 9, 981
Argania: 9, 82
Asteraceae..Liguliflorae.: 11, 432
Boraginaceae: 9, 840
Carpinus.orientalis.Ostrya: 12, 604
Dennstaedtiaceae: 12, 898
Empetrum: 7, 431
Ephedra: 9, 765
Fabaceae..herbs.: 8, 980
Genisteae: 11, 587
Lamiaceae: 15, 1671
Liliaceae: 9, 1024
Lycopodium: 11, 826
Oleaceae: 13, 476
Phillyrea: 14, 940
Pistacia: 13, 767
Plumbaginaceae: 8, 555
Polygonum: 8, 1137
Potentilla: 10, 898
Sambucus: 7, 834
Sanguisorba.group: 7, 666
Scrophulariaceae: 9, 1407
Tilia: 14, 1505
Vaccinium: 10, 765
Fractional abundance
gdd

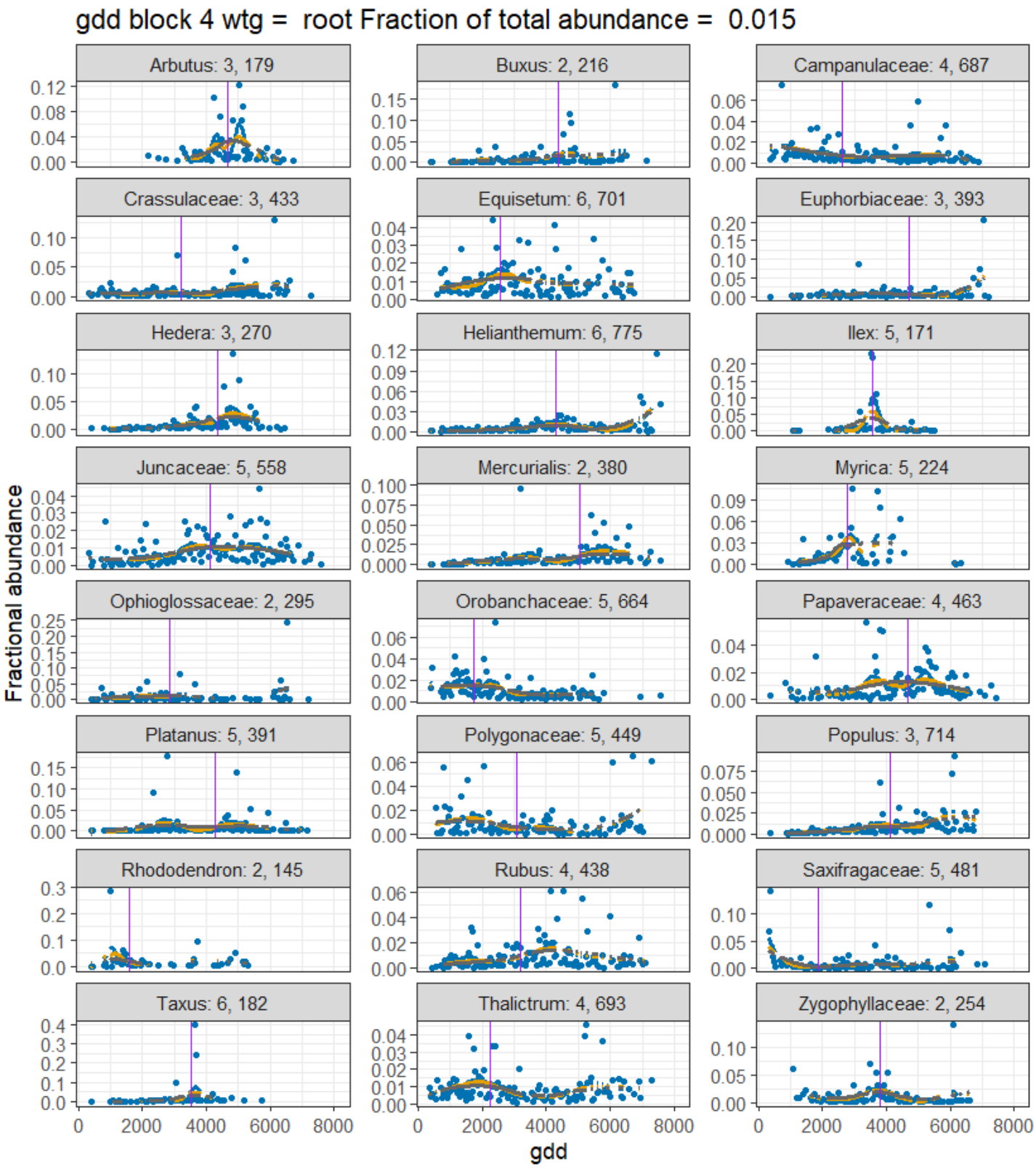
gdd block 4 wtg = root Fraction of total abundance = 0.015
Arbutus: 3, 179
Buxus: 2, 216
Campanulaceae: 4, 687
Crassulaceae: 3, 433
Equisetum: 6, 701
Euphorbiaceae: 3, 393
Hedera: 3, 270
Helianthemum: 6, 775
Ilex: 5, 171
Juncaceae: 5, 558
Mercurialis: 2, 380
Myrica: 5, 224
Ophioglossaceae: 2, 295
Orobanchaceae: 5, 664
Papaveraceae: 4, 463
Platanus: 5, 391
Polygonaceae: 5, 449
Populus: 3, 714
Rhododendron: 2, 145
Rubus: 4, 438
Saxifragaceae: 5, 481
Taxus: 6, 182
Thalictrum: 4, 693
Zygophyllaceae: 2, 254
Fractional abundance
gdd


gdd block 5 wtg = root Fraction of total abundance = 0.006
Astragalus: 2, 183
Cistaceae: 2, 148
Convolvulaceae: 1, 290
Crataegus: 2, 157
Daphne: 1, 151
Gentianaceae: 1, 312
Geraniaceae: 2, 498
Halimium: 1, 53
Huperzia: 1, 218
Lavandula: 2, 144
Myrtaceae: 1, 233
Nitrariaceae: 2, 66
Paliurus: 1, 47
Primulaceae: 2, 350
Prunus: 1, 202
Pteridaceae: 2, 174
Quercus.intermediate: 2, 45
Solanaceae: 2, 219
Sorbus: 1, 402
Tamarix: 2, 78
Thymelaeaceae: 1, 95
Trollius: 1, 150
Valerianaceae: 1, 266
Viburnum: 1, 266
Fractional abundance
gdd


gdd block 6 wtg = root Fraction of total abundance = 0.002
Aconitum: 1, 110
Aesculus: 1, 70
Caragana: 1, 20
Celastraceae: 1, 114
Ceratonia: 1, 36
Cornus: 1, 190
Frangula: 1, 189
Hypericaceae: 1, 253
Lonicera: 1, 119
Onagraceae: 1, 256
Oxalidaceae: 1, 73
Picea.orientalis: 1, 65
Rhamnaceae: 1, 76
Rhamnus: 1, 176
Rhus: 1, 69
Ulmus.Zelkova: 1, 31
Violaceae: 1, 149
Viscum: 1, 74
Fractional abundance
gdd

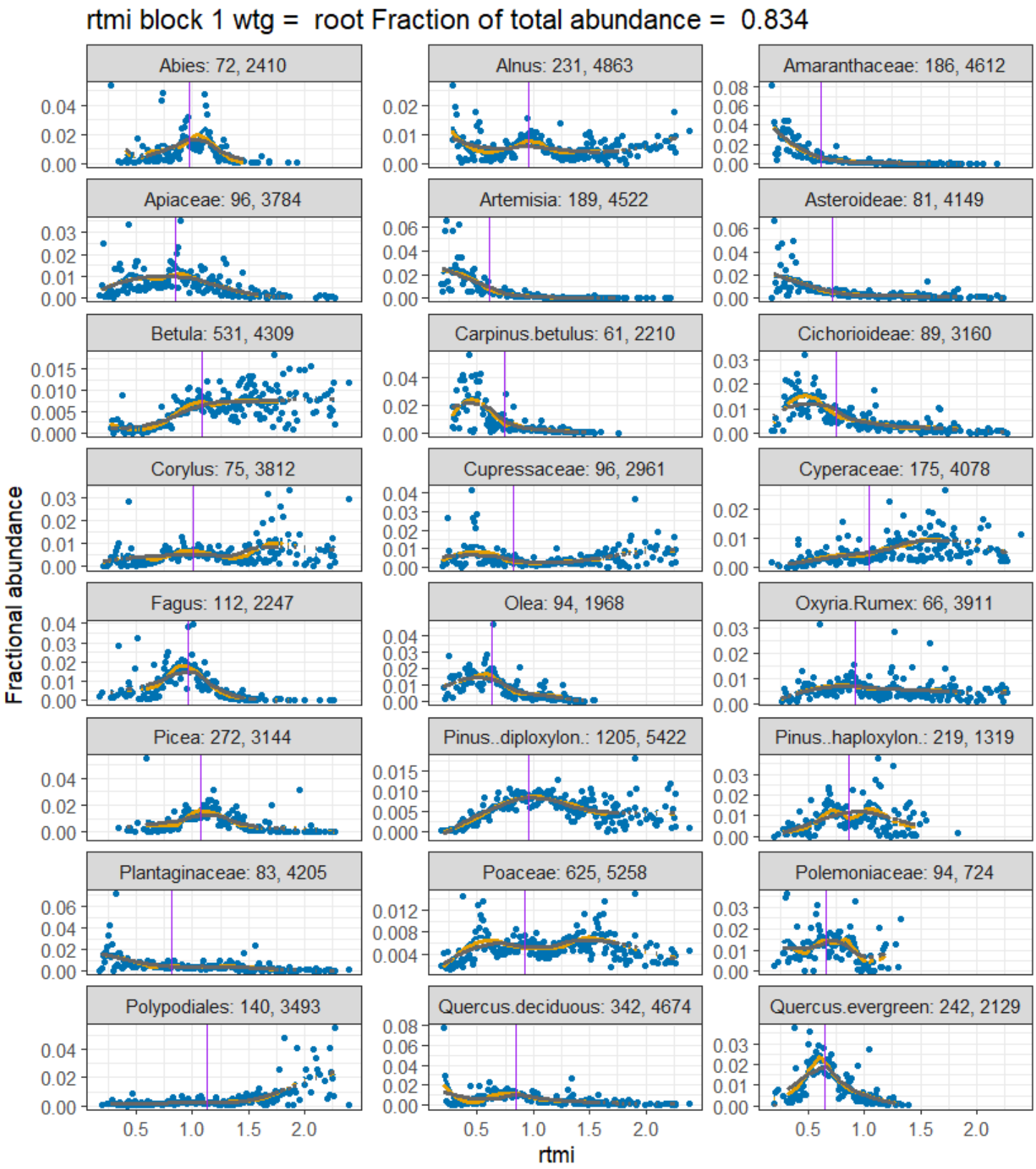
rtmi block 1 wtg = root Fraction of total abundance = 0.834
Abies: 72, 2410
Alnus: 231, 4863
Amaranthaceae: 186, 4612
Apiaceae: 96, 3784
Artemisia: 189, 4522
Asteroideae: 81, 4149
Betula: 531, 4309
Carpinus.betulus: 61, 2210
Cichorioideae: 89, 3160
Corylus: 75, 3812
Cupressaceae: 96, 2961
Cyperaceae: 175, 4078
Fagus: 112, 2247
Olea: 94, 1968
Oxyria.Rumex: 66, 3911
Picea: 272, 3144
Pinus..diploxylon.: 1205, 5422
Pinus..haploxylon.: 219, 1319
Plantaginaceae: 83, 4205
Poaceae: 625, 5258
Polemoniaceae: 94, 724
Polypodiales: 140, 3493
Quercus.deciduous: 342, 4674
Quercus.evergreen: 242, 2129
Fractional abundance
rtmi

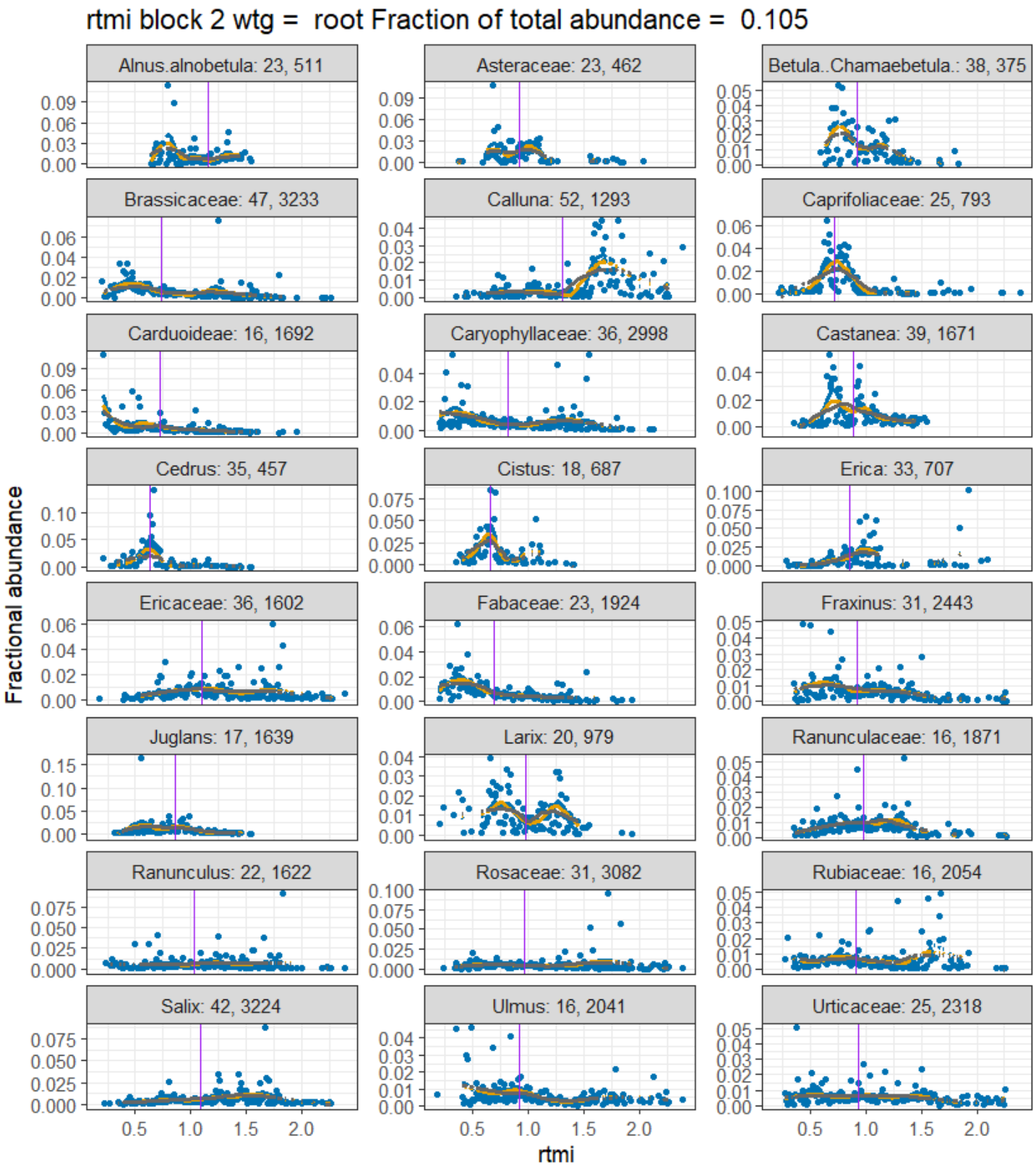
rtmi block 2 wtg = root Fraction of total abundance = 0.105
Alnus.alnobetula: 23, 511
Asteraceae: 23, 462
Betula..Chamaebetula.: 38, 375
Brassicaceae: 47, 3233
Calluna: 52, 1293
Caprifoliaceae: 25, 793
Carduoideae: 16, 1692
Caryophyllaceae: 36, 2998
Castanea: 39, 1671
Cedrus: 35, 457
Cistus: 18, 687
Erica: 33, 707
Ericaceae: 36, 1602
Fabaceae: 23, 1924
Fraxinus: 31, 2443
Juglans: 17, 1639
Larix: 20, 979
Ranunculaceae: 16, 1871
Ranunculus: 22, 1622
Rosaceae: 31, 3082
Rubiaceae: 16, 2054
Salix: 42, 3224
Ulmus: 16, 2041
Urticaceae: 25, 2318
Fractional abundance
rtmi

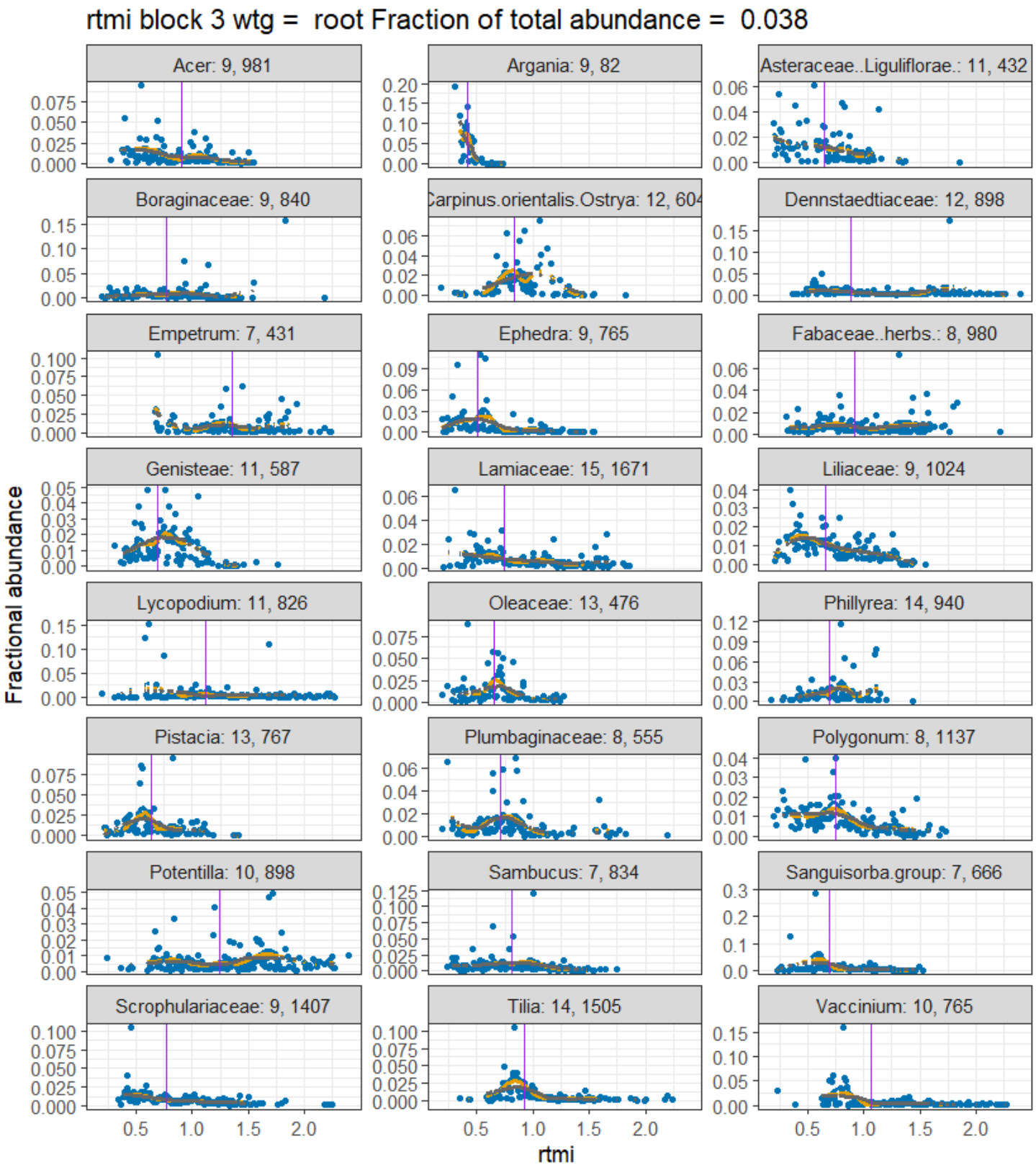
rtmi block 3 wtg = root Fraction of total abundance = 0.038
Acer: 9, 981
Argania: 9, 82
Asteraceae..Liguliflorae.: 11, 432
Boraginaceae: 9, 840
Carpinus.orientalis.Ostrya: 12, 604
Dennstaedtiaceae: 12, 898
Empetrum: 7, 431
Ephedra: 9, 765
Fabaceae..herbs.: 8, 980
Genisteae: 11, 587
Lamiaceae: 15, 1671
Liliaceae: 9, 1024
Lycopodium: 11, 826
Oleaceae: 13, 476
Phillyrea: 14, 940
Pistacia: 13, 767
Plumbaginaceae: 8, 555
Polygonum: 8, 1137
Potentilla: 10, 898
Sambucus: 7, 834
Sanguisorba.group: 7, 666
Scrophulariaceae: 9, 1407
Tilia: 14, 1505
Vaccinium: 10, 765
Fractional abundance
rtmi


rtmi block 4 wtg = root Fraction of total abundance = 0.015
Arbutus: 3, 179
Buxus: 2, 216
Campanulaceae: 4, 687
Crassulaceae: 3, 433
Equisetum: 6, 701
Euphorbiaceae: 3, 393
Hedera: 3, 270
Helianthemum: 6, 775
Ilex: 5, 171
Juncaceae: 5, 558
Mercurialis: 2, 380
Myrica: 5, 224
Ophioglossaceae: 2, 295
Orobanchaceae: 5, 664
Papaveraceae: 4, 463
Platanus: 5, 391
Polygonaceae: 5, 449
Populus: 3, 714
Rhododendron: 2, 145
Rubus: 4, 438
Saxifragaceae: 5, 481
Taxus: 6, 182
Thalictrum: 4, 693
Zygophyllaceae: 2, 254
Fractional abundance
rtmi

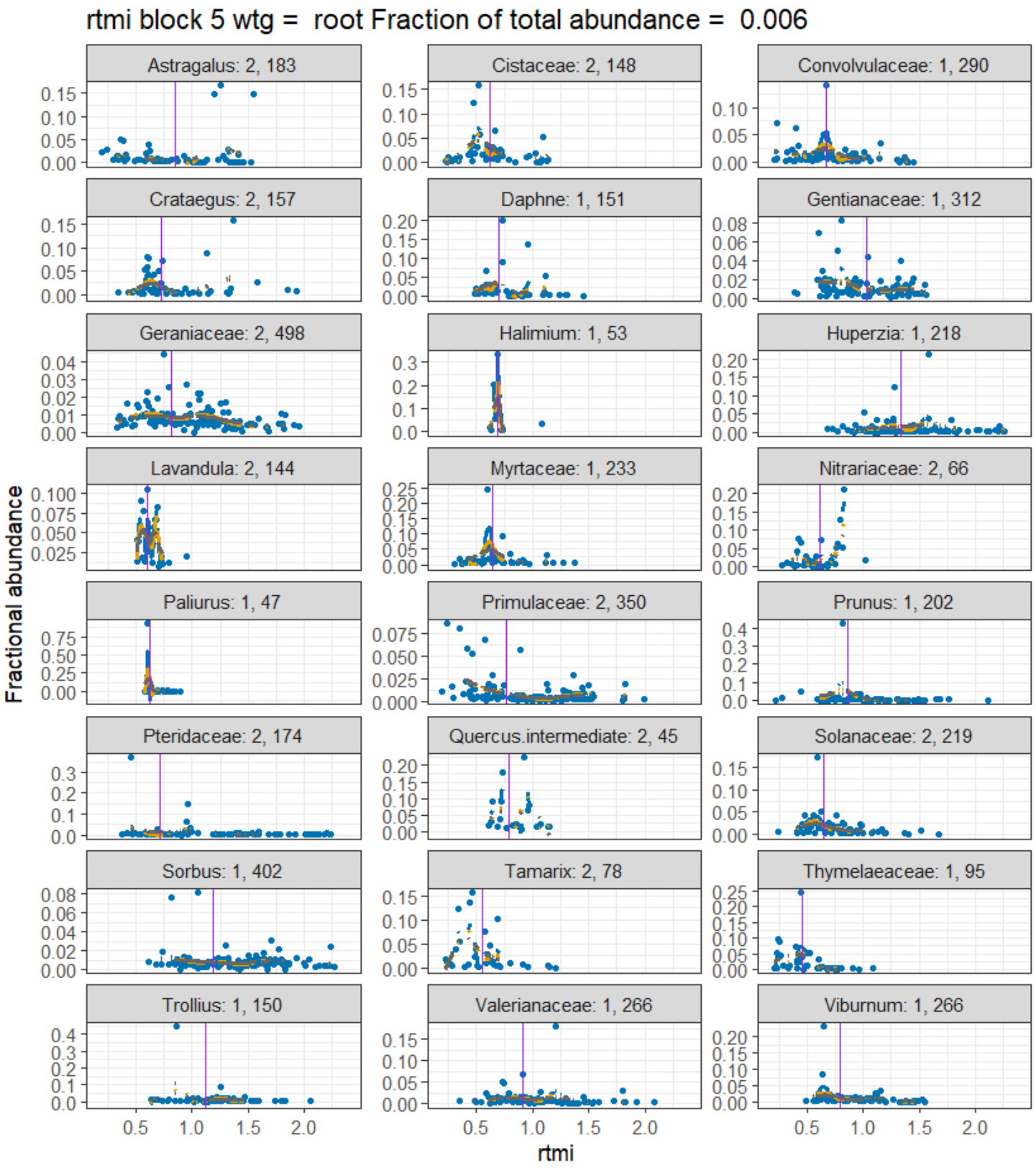
rtmi block 5 wtg = root Fraction of total abundance = 0.006
Astragalus: 2, 183
Cistaceae: 2, 148
Convolvulaceae: 1, 290
Crataegus: 2, 157
Daphne: 1, 151
Gentianaceae: 1, 312
Geraniaceae: 2, 498
Halimium: 1, 53
Huperzia: 1, 218
Lavandula: 2, 144
Myrtaceae: 1, 233
Nitrariaceae: 2, 66
Paliurus: 1, 47
Primulaceae: 2, 350
Prunus: 1, 202
Pteridaceae: 2, 174
Quercus.intermediate: 2, 45
Solanaceae: 2, 219
Sorbus: 1, 402
Tamarix: 2, 78
Thymelaeaceae: 1, 95
Trollius: 1, 150
Valerianaceae: 1, 266
Viburnum: 1, 266
Fractional abundance
rtmi

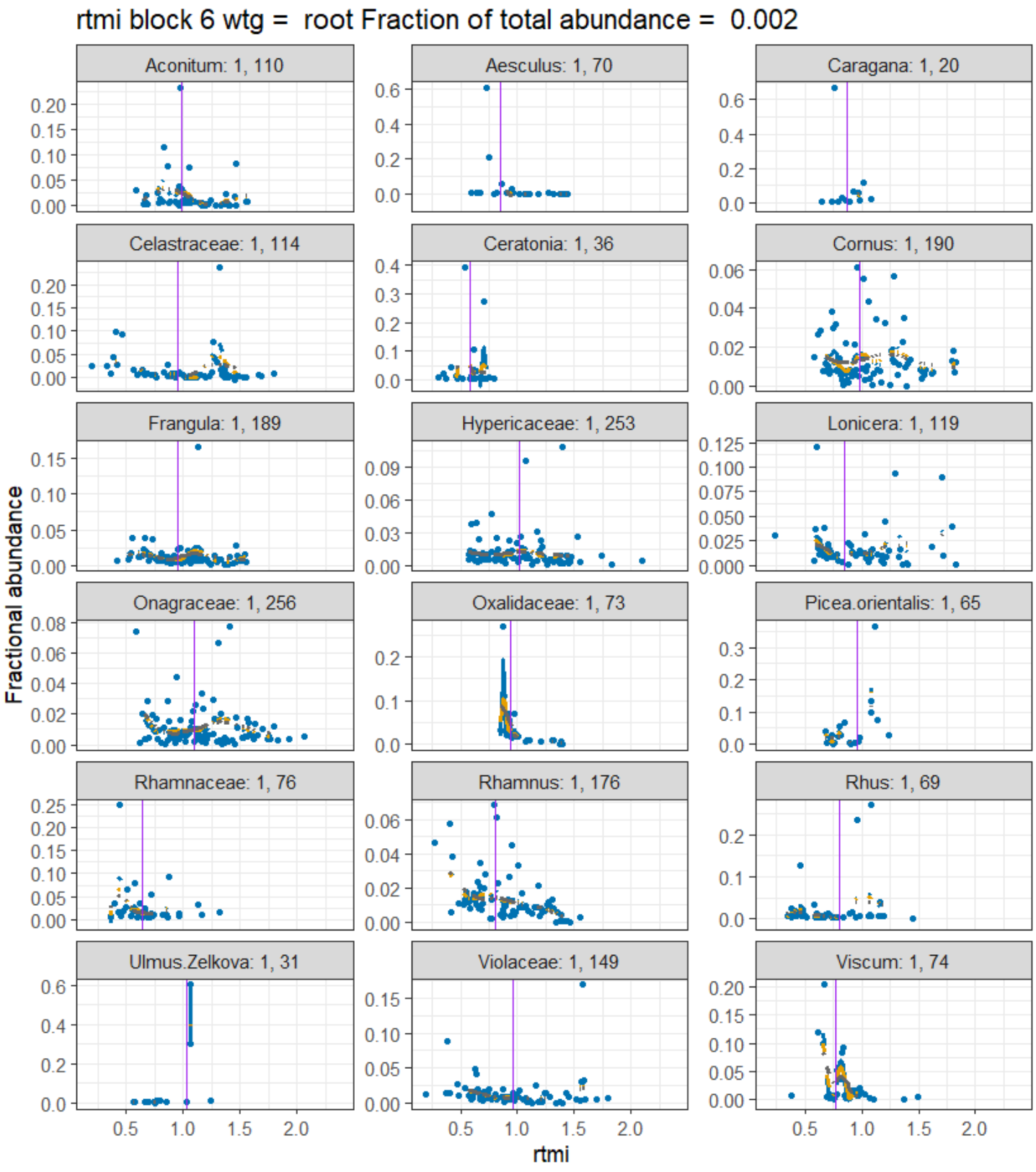

Response curves taxa in the SMPDS, in blocks of 24 in descending order of abundance, to Tmin (MTCO), gdd, and rtmi. Numbers in taxon headings are respectively the sum of fractional abundances of the taxon and the number of occurrences of the taxon in SMPDS (number of SMPDS samples = sum of fractional abundances = 6458). Points: fxabf *(fractional mean binned abundance). Blue lines: loess curve, span = 0.3; orange lines; loess curve, span 0.5; grey lines: loess curve, span = 0.75. Vertical line: fxTWA-PLS abundance-weighted mean for component 1.*

Appendix B: Bootstrapped loess curves and fxt optima of SMPDSv1 taxa with summed fractional abundance > 0.1 (n = 138)

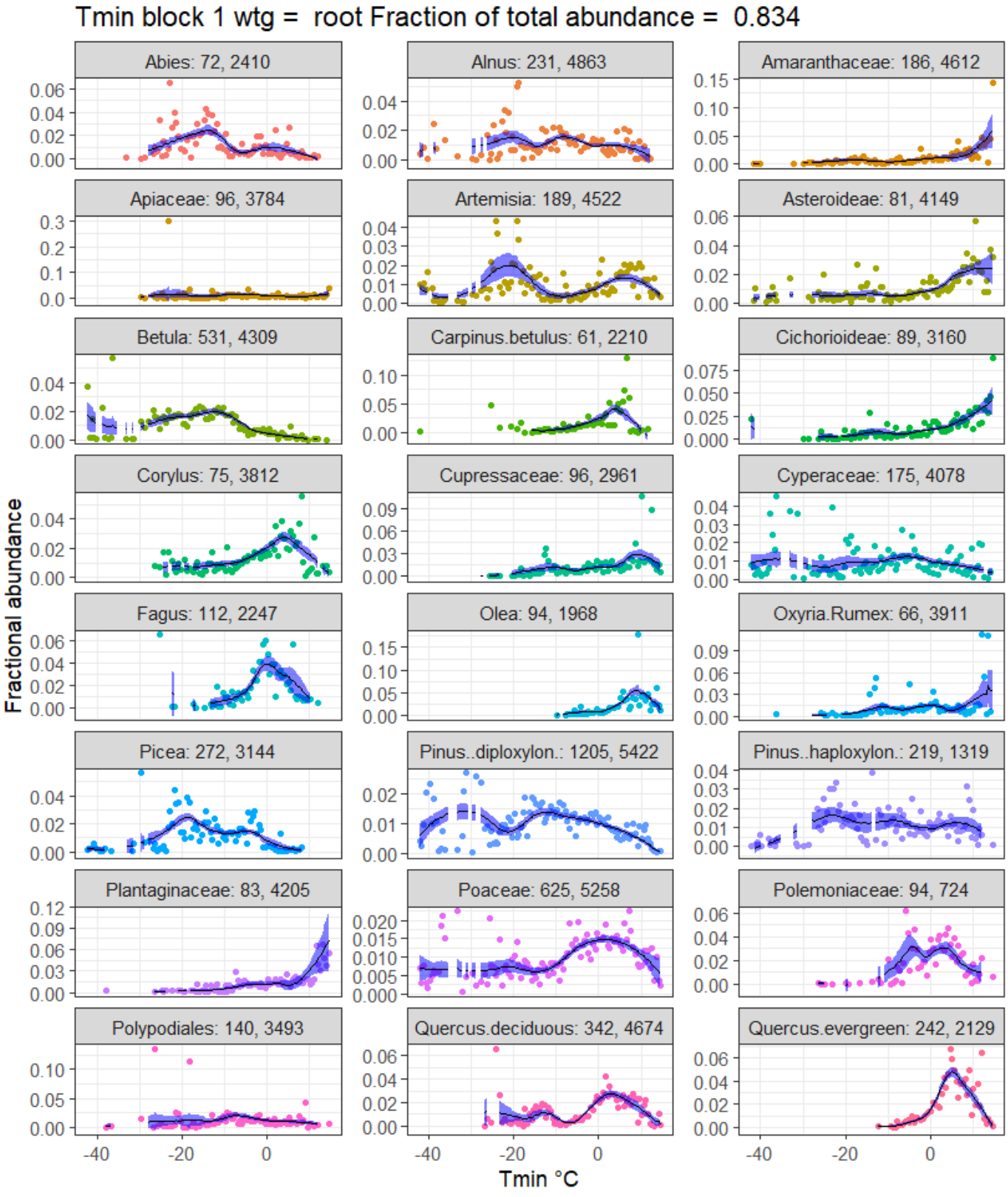

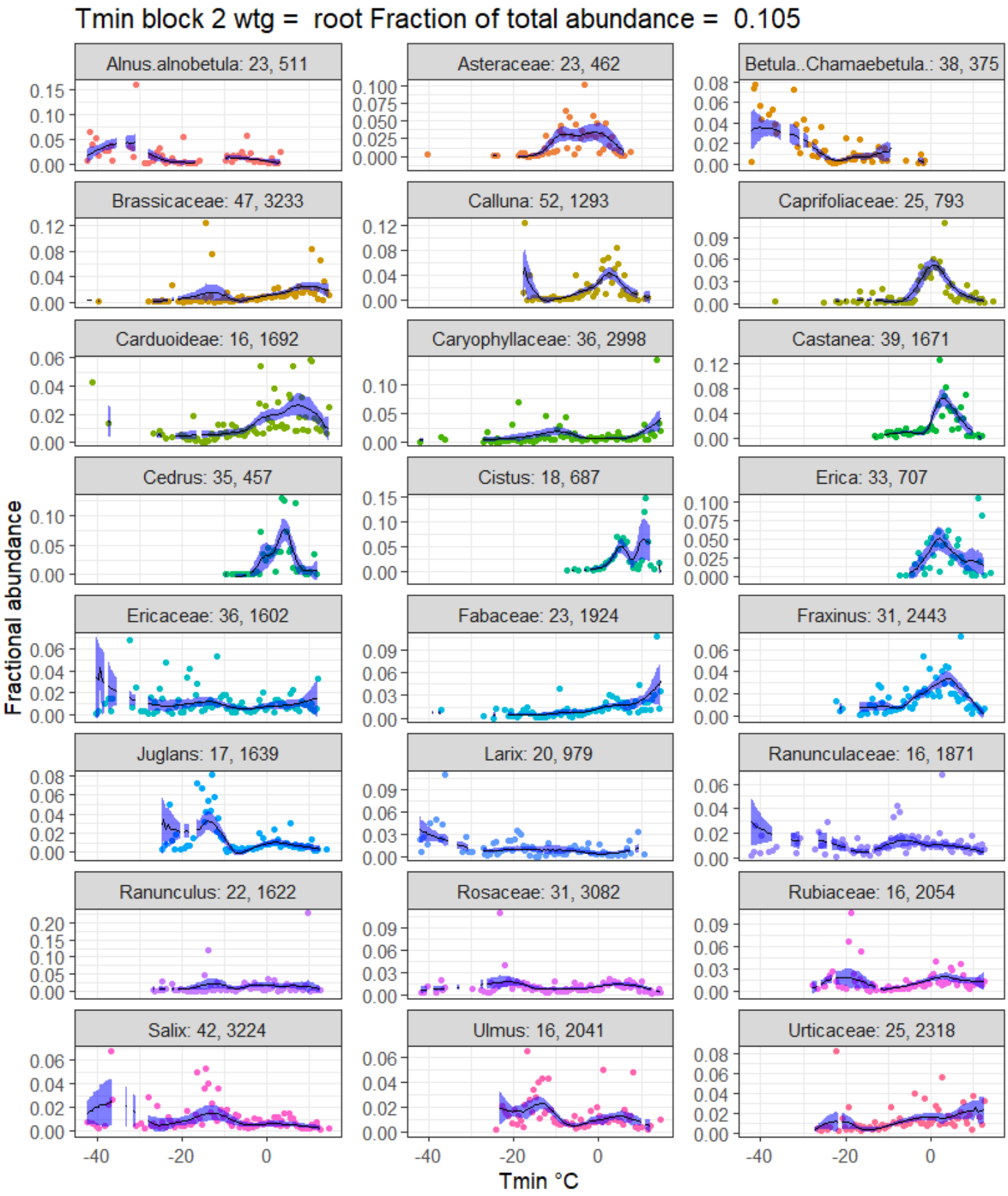
Tmin block 2 wtg = root Fraction of total abundance = 0.105
Alnus.alnobetula: 23, 511
Asteraceae: 23, 462
Betula..Chamaebetula.: 38, 375
Brassicaceae: 47, 3233
Calluna: 52, 1293
Caprifoliaceae: 25, 793
Carduoideae: 16, 1692
Caryophyllaceae: 36, 2998
Castanea: 39, 1671
Cedrus: 35, 457
Cistus: 18, 687
Erica: 33, 707
Ericaceae: 36, 1602
Fabaceae: 23, 1924
Fraxinus: 31, 2443
Juglans: 17, 1639
Larix: 20, 979
Ranunculaceae: 16, 1871
Ranunculus: 22, 1622
Rosaceae: 31, 3082
Rubiaceae: 16, 2054
Salix: 42, 3224
Ulmus: 16, 2041
Urticaceae: 25, 2318
Fractional abundance
Tmin °C

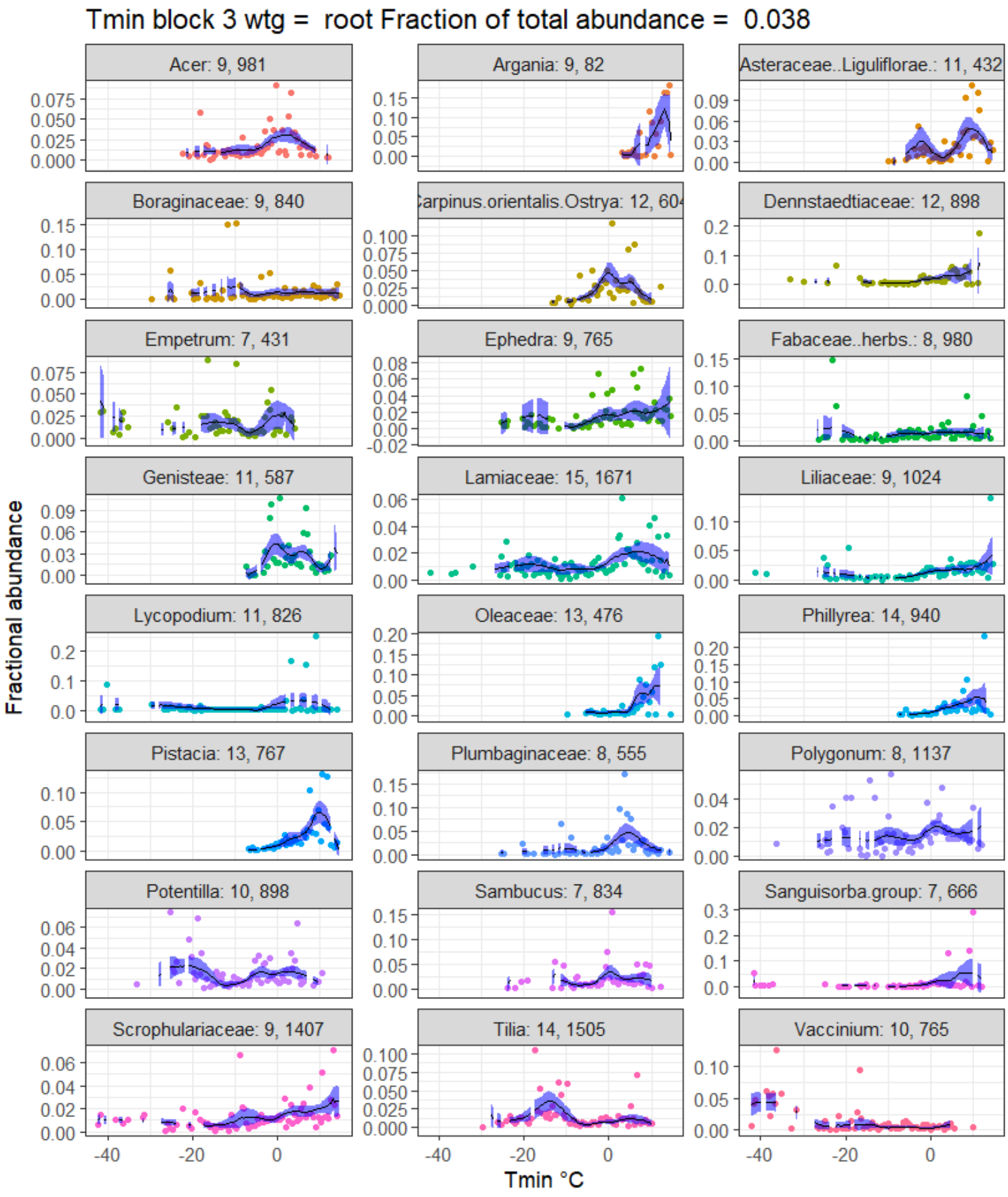
Tmin block 3 wtg = root Fraction of total abundance = 0.038
Acer: 9, 981
Argania: 9, 82
Asteraceae..Liguliflorae.: 11, 432
Boraginaceae: 9, 840
Carpinus.orientalis.Ostrya: 12, 604
Dennstaedtiaceae: 12, 898
Empetrum: 7, 431
Ephedra: 9, 765
Fabaceae..herbs.: 8, 980
Genisteae: 11, 587
Lamiaceae: 15, 1671
Liliaceae: 9, 1024
Lycopodium: 11, 826
Oleaceae: 13, 476
Phillyrea: 14, 940
Pistacia: 13, 767
Plumbaginaceae: 8, 555
Polygonum: 8, 1137
Potentilla: 10, 898
Sambucus: 7, 834
Sanguisorba.group: 7, 666
Scrophulariaceae: 9, 1407
Tilia: 14, 1505
Vaccinium: 10, 765
Fractional abundance
Tmin °C

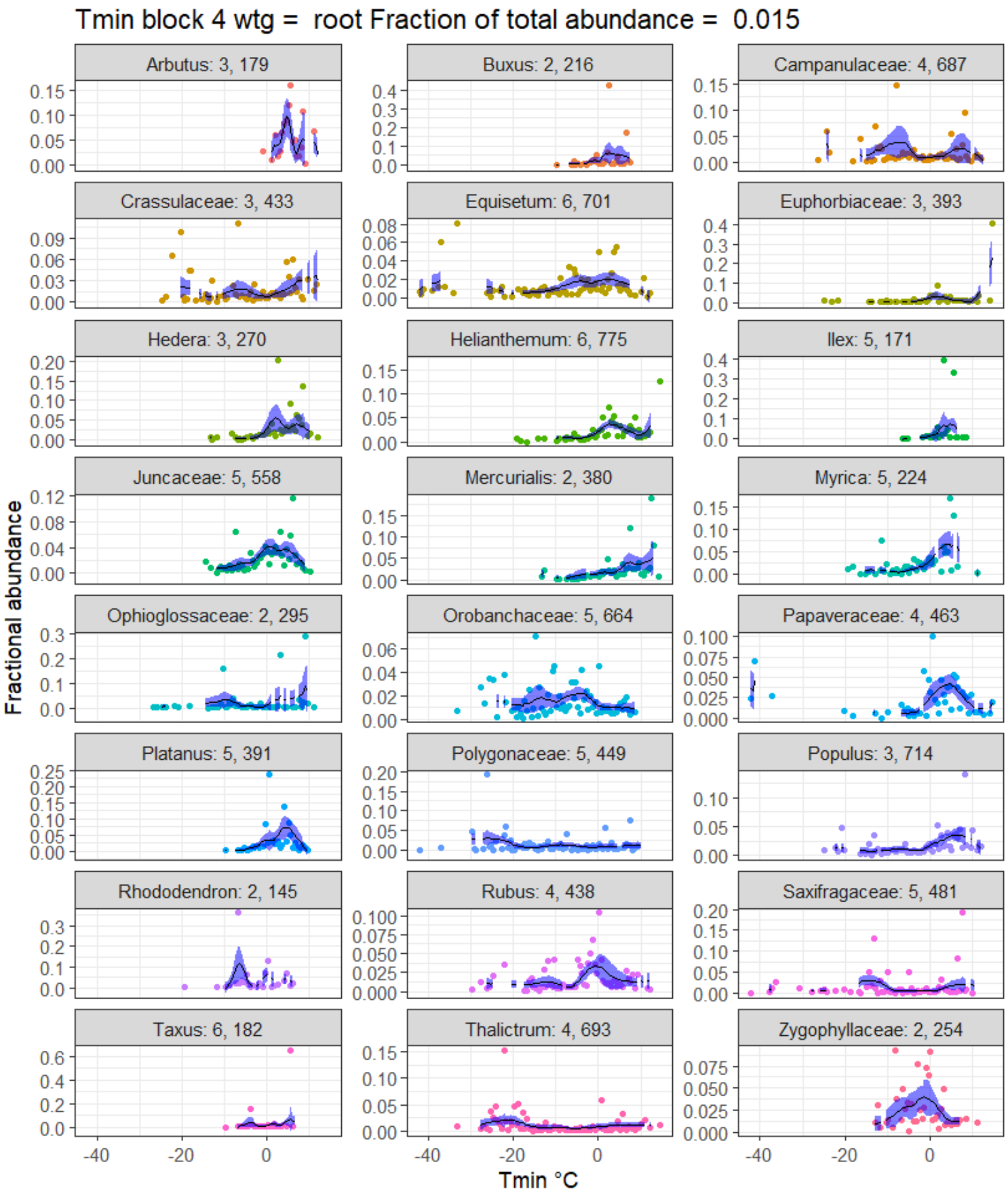
Tmin block 4 wtg = root Fraction of total abundance = 0.015
Arbutus: 3, 179
Buxus: 2, 216
Campanulaceae: 4, 687
Crassulaceae: 3, 433
Equisetum: 6, 701
Euphorbiaceae: 3, 393
Hedera: 3, 270
Helianthemum: 6, 775
Ilex: 5, 171
Juncaceae: 5, 558
Mercurialis: 2, 380
Myrica: 5, 224
Ophioglossaceae: 2, 295
Orobanchaceae: 5, 664
Papaveraceae: 4, 463
Platanus: 5, 391
Polygonaceae: 5, 449
Populus: 3, 714
Rhododendron: 2, 145
Rubus: 4, 438
Saxifragaceae: 5, 481
Taxus: 6, 182
Thalictrum: 4, 693
Zygophyllaceae: 2, 254
Fractional abundance
Tmin °C

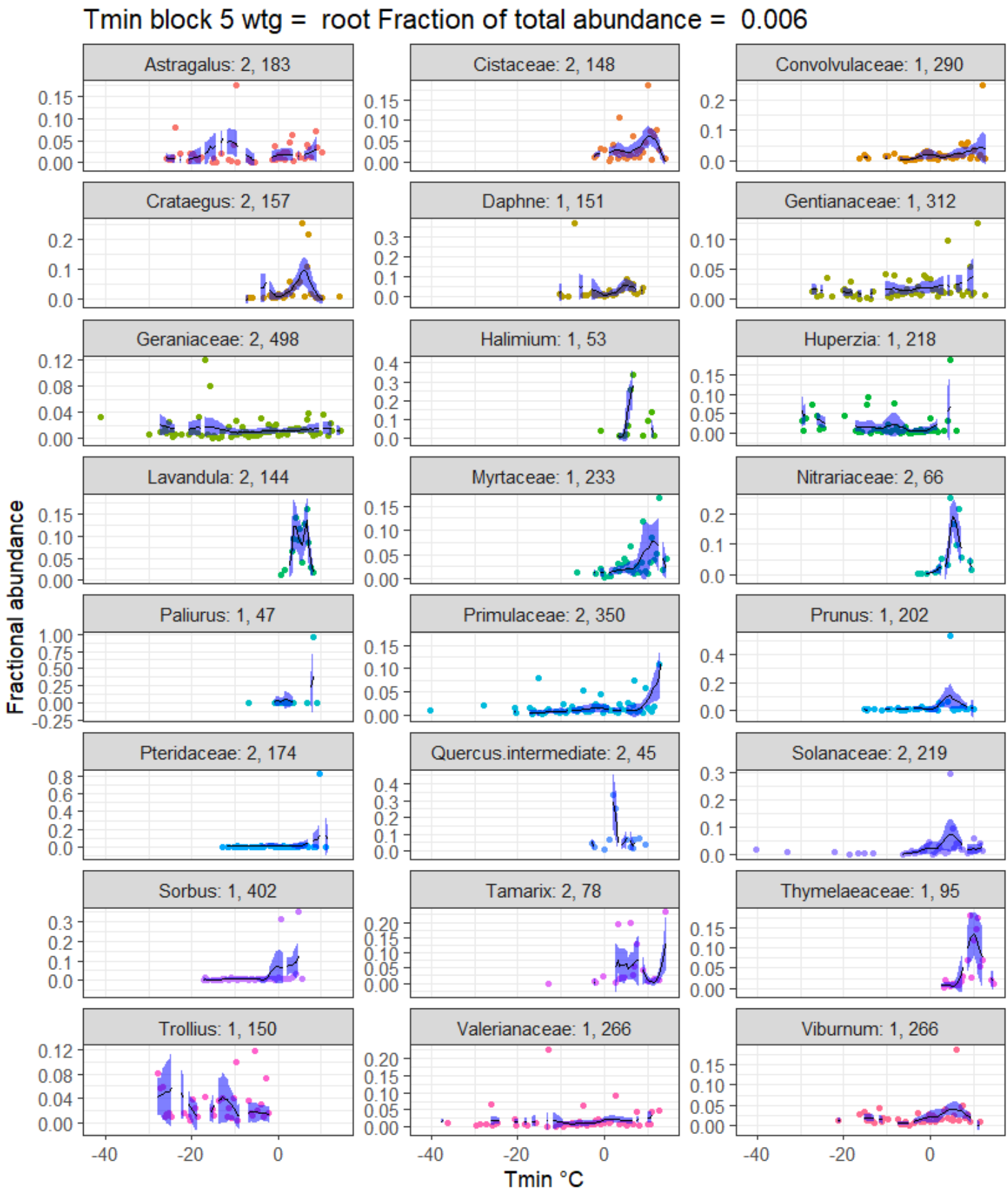
Tmin block 5 wtg = root Fraction of total abundance = 0.006
Astragalus: 2, 183
Cistaceae: 2, 148
Convolvulaceae: 1, 290
Crataegus: 2, 157
Daphne: 1, 151
Gentianaceae: 1, 312
Geraniaceae: 2, 498
Halimium: 1, 53
Huperzia: 1, 218
Lavandula: 2, 144
Myrtaceae: 1, 233
Nitrariaceae: 2, 66
Paliurus: 1, 47
Primulaceae: 2, 350
Prunus: 1, 202
Pteridaceae: 2, 174
Quercus.intermediate: 2, 45
Solanaceae: 2, 219
Sorbus: 1, 402
Tamarix: 2, 78
Thymelaeaceae: 1, 95
Trollius: 1, 150
Valerianaceae: 1, 266
Viburnum: 1, 266
Fractional abundance
Tmin °C

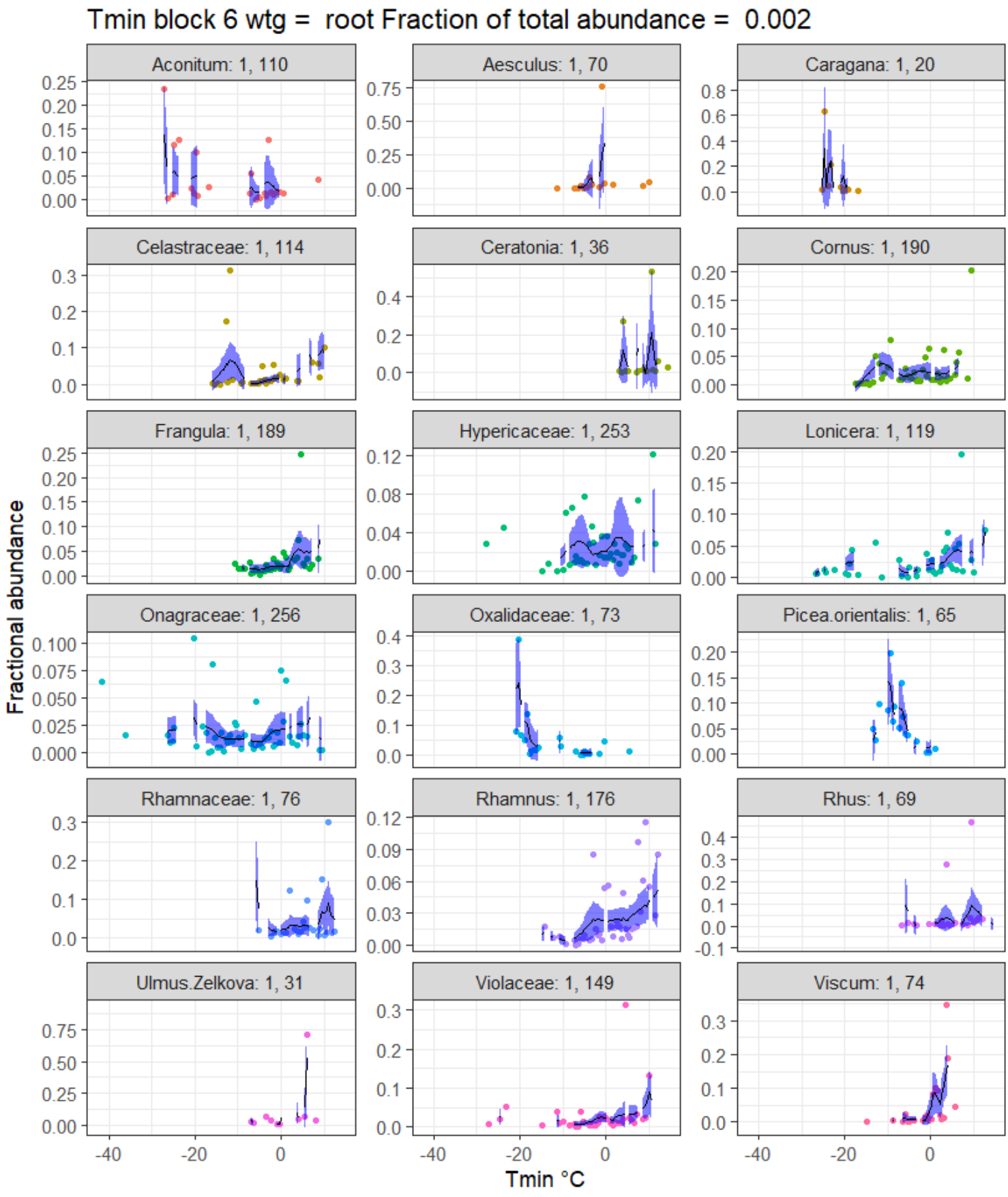
Tmin block 6 wtg = root Fraction of total abundance = 0.002
Aconitum: 1, 110
Aesculus: 1, 70
Caragana: 1, 20
Celastraceae: 1, 114
Ceratonia: 1, 36
Cornus: 1, 190
Frangula: 1, 189
Hypericaceae: 1, 253
Lonicera: 1, 119
Onagraceae: 1, 256
Oxalidaceae: 1, 73
Picea.orientalis: 1, 65
Rhamnaceae: 1, 76
Rhamnus: 1, 176
Rhus: 1, 69
Ulmus.Zelkova: 1, 31
Violaceae: 1, 149
Viscum: 1, 74
Fractional abundance
Tmin °C

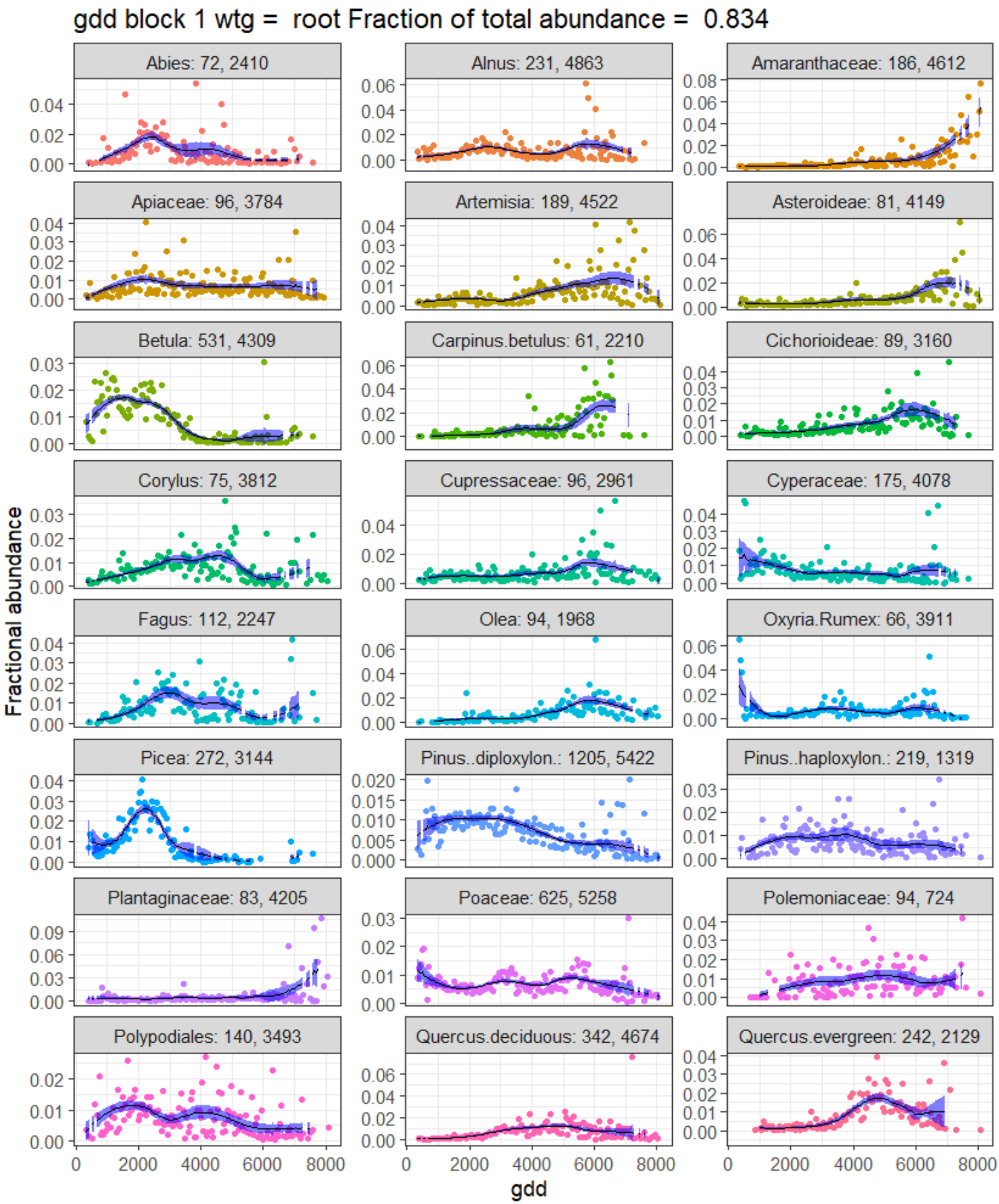
gdd block 1 wtg = root Fraction of total abundance = 0.834
Abies: 72, 2410
Alnus: 231, 4863
Amaranthaceae: 186, 4612
Apiaceae: 96, 3784
Artemisia: 189, 4522
Asteroideae: 81, 4149
Betula: 531, 4309
Carpinus.betulus: 61, 2210
Cichorioideae: 89, 3160
Corylus: 75, 3812
Cupressaceae: 96, 2961
Cyperaceae: 175, 4078
Fagus: 112, 2247
Olea: 94, 1968
Oxyria.Rumex: 66, 3911
Picea: 272, 3144
Pinus..diploxylon.: 1205, 5422
Pinus..haploxylon.: 219, 1319
Plantaginaceae: 83, 4205
Poaceae: 625, 5258
Polemoniaceae: 94, 724
Polypodiales: 140, 3493
Quercus.deciduous: 342, 4674
Quercus.evergreen: 242, 2129
Fractional abundance
gdd

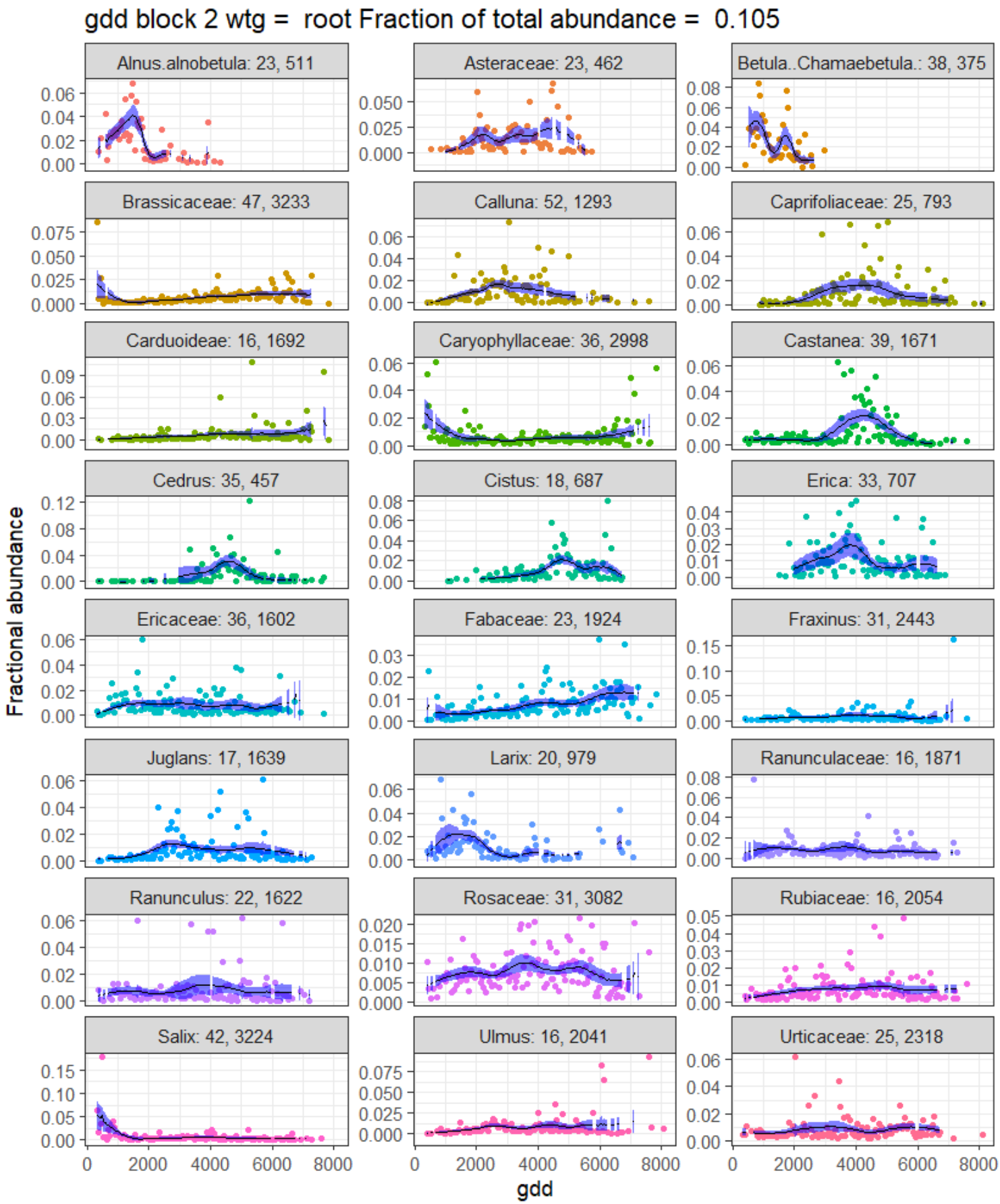
gdd block 2 wtg = root Fraction of total abundance = 0.105
Alnus.alnobetula: 23, 511
Asteraceae: 23, 462
Betula..Chamaebetula.: 38, 375
Brassicaceae: 47, 3233
Calluna: 52, 1293
Caprifoliaceae: 25, 793
Carduoideae: 16, 1692
Caryophyllaceae: 36, 2998
Castanea: 39, 1671
Cedrus: 35, 457
Cistus: 18, 687
Erica: 33, 707
Ericaceae: 36, 1602
Fabaceae: 23, 1924
Fraxinus: 31, 2443
Juglans: 17, 1639
Larix: 20, 979
Ranunculaceae: 16, 1871
Ranunculus: 22, 1622
Rosaceae: 31, 3082
Rubiaceae: 16, 2054
Salix: 42, 3224
Ulmus: 16, 2041
Urticaceae: 25, 2318
Fractional abundance
gdd

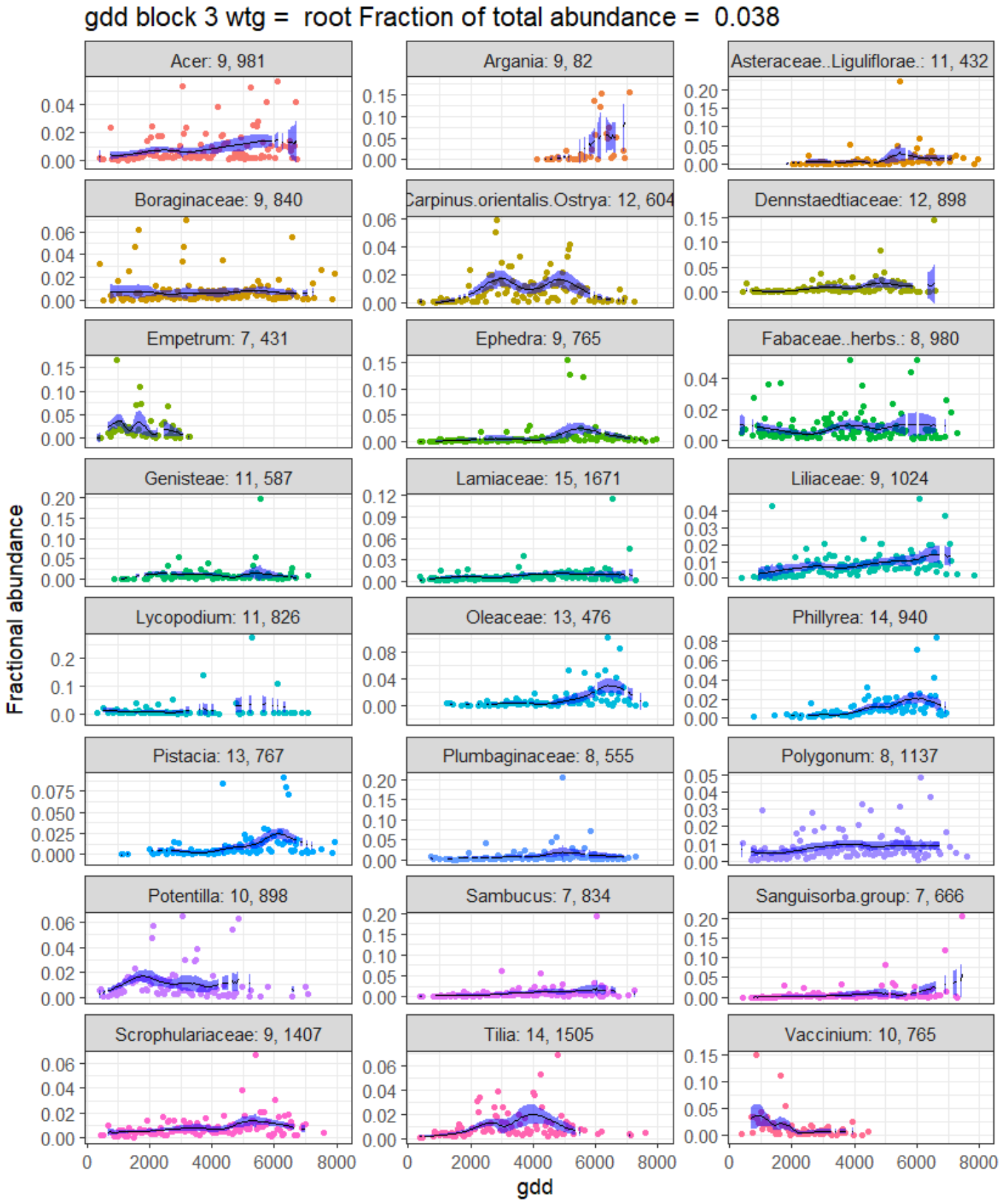
gdd block 3 wtg = root Fraction of total abundance = 0.038
Acer: 9, 981
Argania: 9, 82
Asteraceae..Liguliflorae.: 11, 432
Boraginaceae: 9, 840
Carpinus.orientalis.Ostrya: 12, 604
Dennstaedtiaceae: 12, 898
Empetrum: 7, 431
Ephedra: 9, 765
Fabaceae..herbs.: 8, 980
Genisteae: 11, 587
Lamiaceae: 15, 1671
Liliaceae: 9, 1024
Lycopodium: 11, 826
Oleaceae: 13, 476
Phillyrea: 14, 940
Pistacia: 13, 767
Plumbaginaceae: 8, 555
Polygonum: 8, 1137
Potentilla: 10, 898
Sambucus: 7, 834
Sanguisorba.group: 7, 666
Scrophulariaceae: 9, 1407
Tilia: 14, 1505
Vaccinium: 10, 765
Fractional abundance
gdd

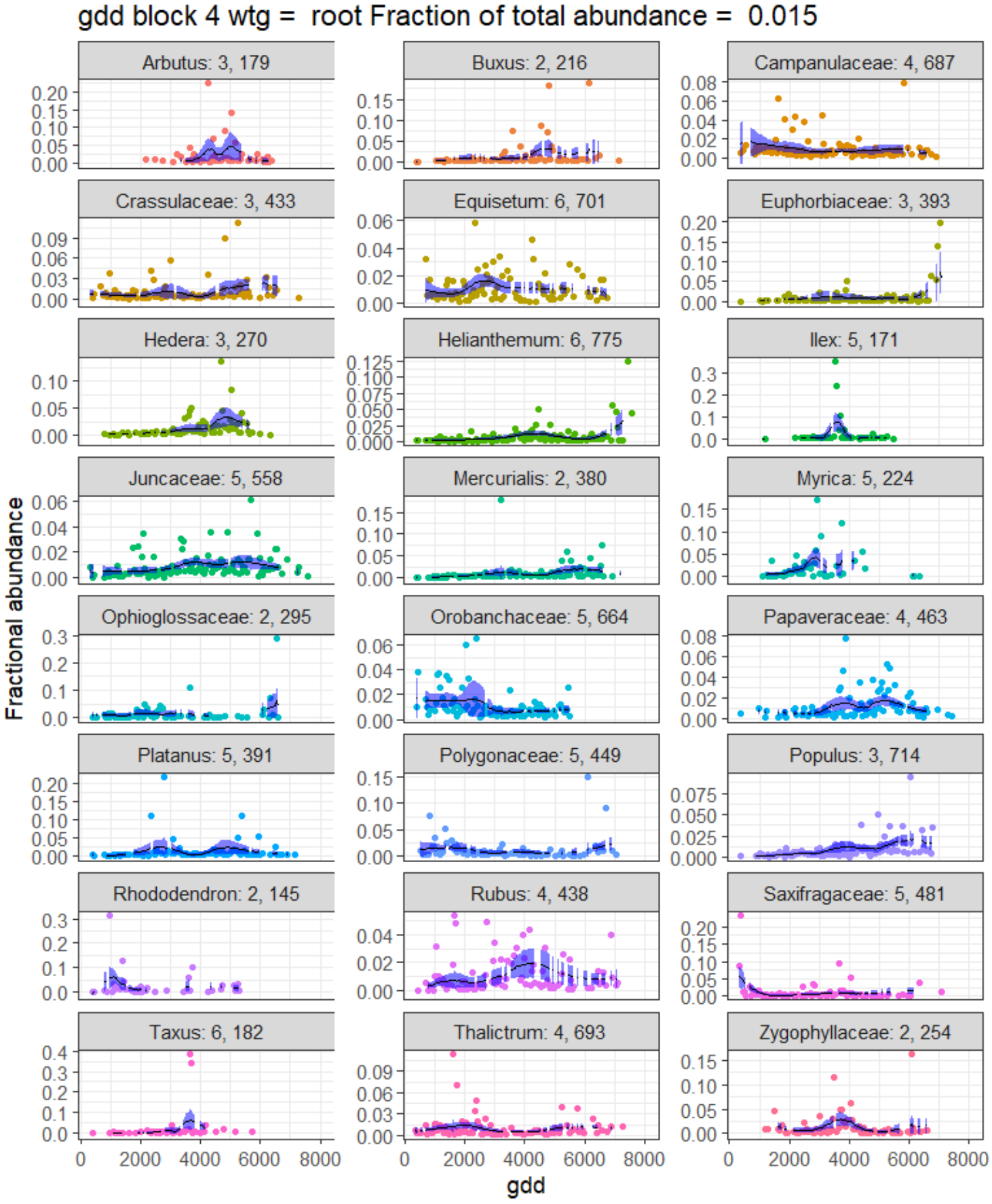
gdd block 4 wtg = root Fraction of total abundance = 0.015
Arbutus: 3, 179
Buxus: 2, 216
Campanulaceae: 4, 687
Crassulaceae: 3, 433
Equisetum: 6, 701
Euphorbiaceae: 3, 393
Hedera: 3, 270
Helianthemum: 6, 775
Ilex: 5, 171
Juncaceae: 5, 558
Mercurialis: 2, 380
Myrica: 5, 224
Ophioglossaceae: 2, 295
Orobanchaceae: 5, 664
Papaveraceae: 4, 463
Platanus: 5, 391
Polygonaceae: 5, 449
Populus: 3, 714
Rhododendron: 2, 145
Rubus: 4, 438
Saxifragaceae: 5, 481
Taxus: 6, 182
Thalictrum: 4, 693
Zygophyllaceae: 2, 254
Fractional abundance
gdd

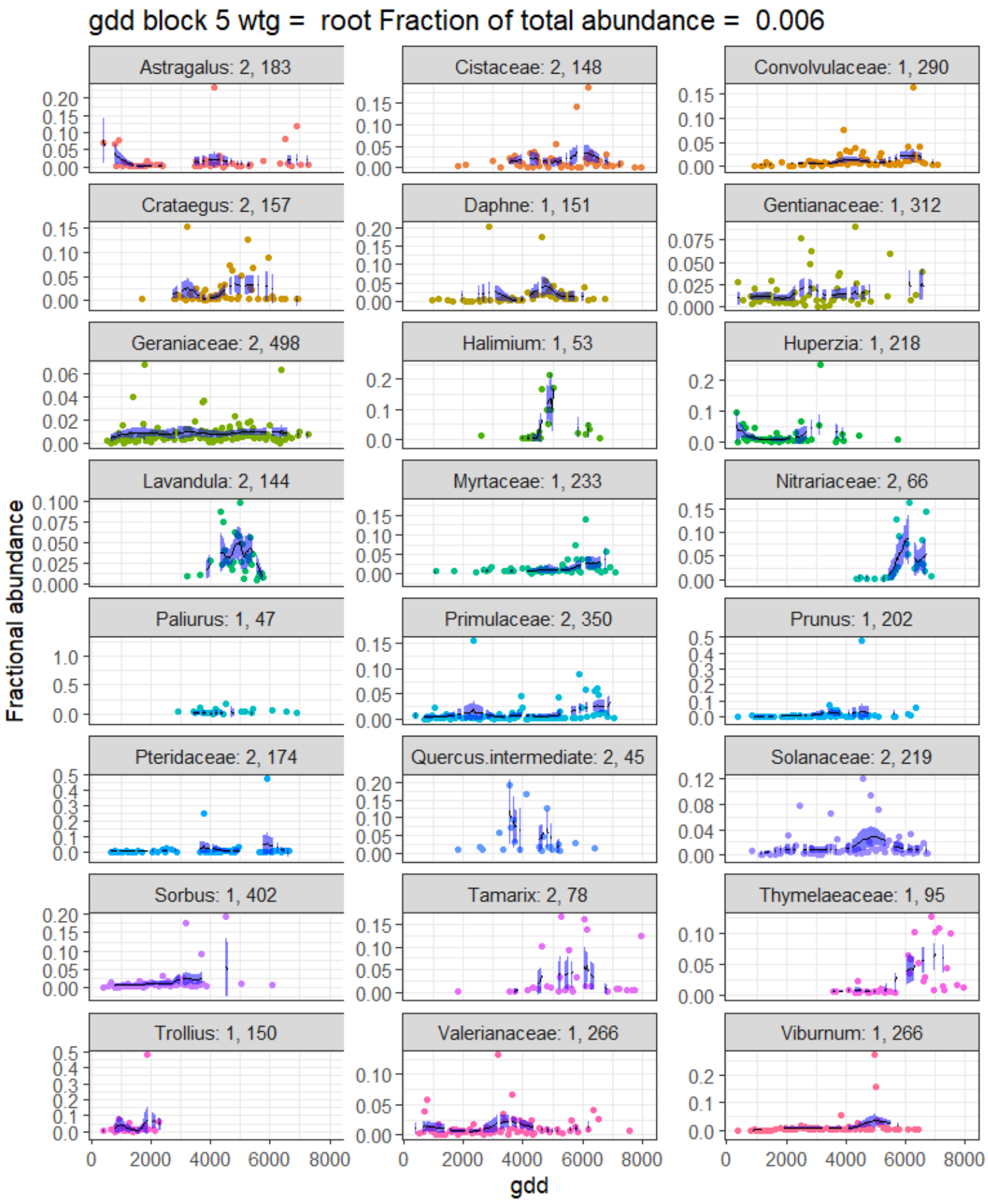
gdd block 5 wtg = root Fraction of total abundance = 0.006
Astragalus: 2, 183
Cistaceae: 2, 148
Convolvulaceae: 1, 290
Crataegus: 2, 157
Daphne: 1, 151
Gentianaceae: 1, 312
Geraniaceae: 2, 498
Halimium: 1, 53
Huperzia: 1, 218
Lavandula: 2, 144
Myrtaceae: 1, 233
Nitrariaceae: 2, 66
Paliurus: 1, 47
Primulaceae: 2, 350
Prunus: 1, 202
Pteridaceae: 2, 174
Quercus.intermediate: 2, 45
Solanaceae: 2, 219
Sorbus: 1, 402
Tamarix: 2, 78
Thymelaeaceae: 1, 95
Trollius: 1, 150
Valerianaceae: 1, 266
Viburnum: 1, 266
Fractional abundance
gdd

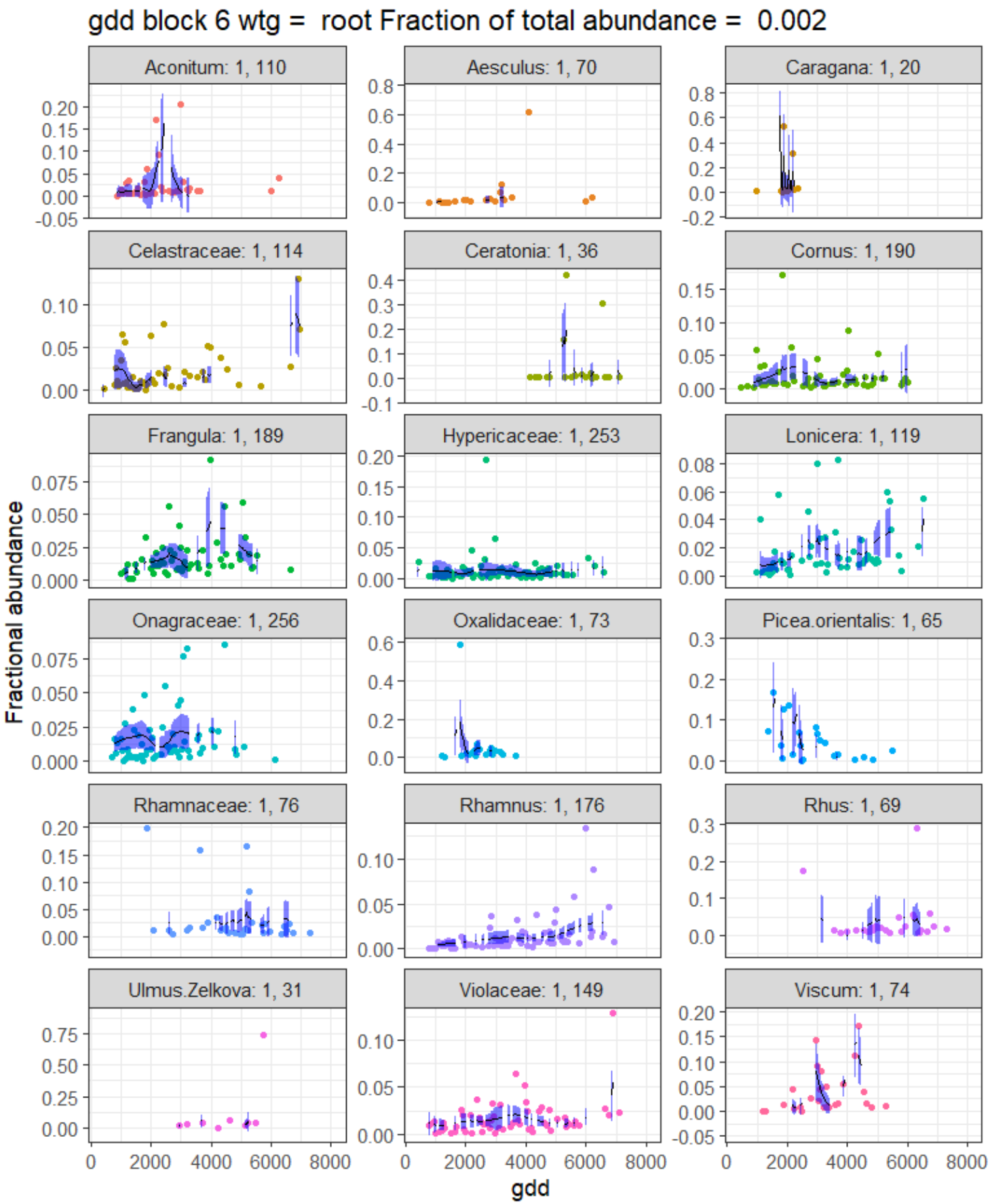
gdd block 6 wtg = root Fraction of total abundance = 0.002
Aconitum: 1, 110
Aesculus: 1, 70
Caragana: 1, 20
Celastraceae: 1, 114
Ceratonia: 1, 36
Cornus: 1, 190
Frangula: 1, 189
Hypericaceae: 1, 253
Lonicera: 1, 119
Onagraceae: 1, 256
Oxalidaceae: 1, 73
Picea.orientalis: 1, 65
Rhamnaceae: 1, 76
Rhamnus: 1, 176
Rhus: 1, 69
Ulmus.Zelkova: 1, 31
Violaceae: 1, 149
Viscum: 1, 74
Fractional abundance
gdd

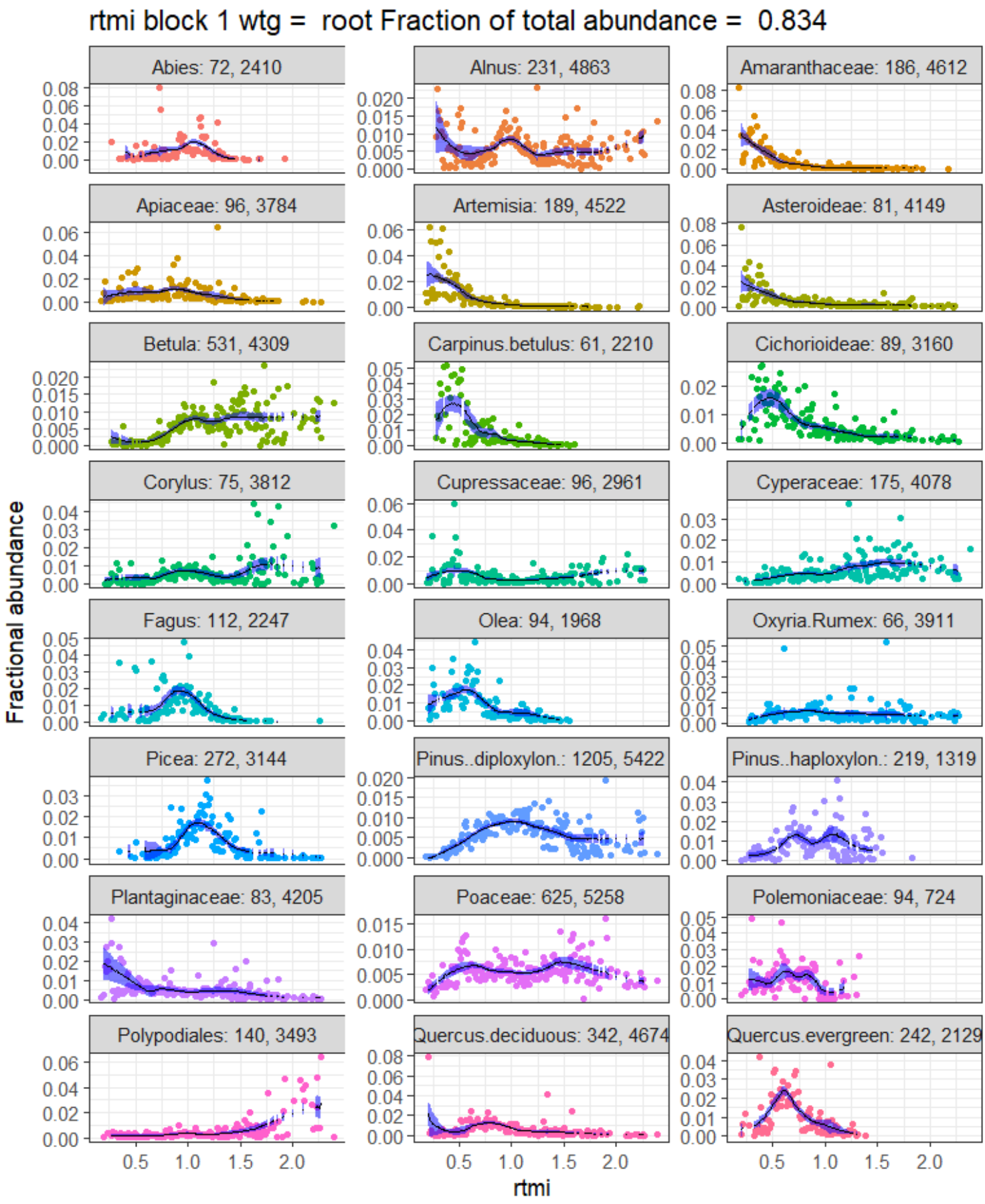
rtmi block 1 wtg = root Fraction of total abundance = 0.834
Abies: 72, 2410
Alnus: 231, 4863
Amaranthaceae: 186, 4612
Apiaceae: 96, 3784
Artemisia: 189, 4522
Asteroideae: 81, 4149
Betula: 531, 4309
Carpinus.betulus: 61, 2210
Cichorioideae: 89, 3160
Corylus: 75, 3812
Cupressaceae: 96, 2961
Cyperaceae: 175, 4078
Fagus: 112, 2247
Olea: 94, 1968
Oxyria.Rumex: 66, 3911
Picea: 272, 3144
Pinus..diploxylon.: 1205, 5422
Pinus..haploxylon.: 219, 1319
Plantaginaceae: 83, 4205
Poaceae: 625, 5258
Polemoniaceae: 94, 724
Polypodiales: 140, 3493
Quercus.deciduous: 342, 4674
Quercus.evergreen: 242, 2129
Fractional abundance
rtmi

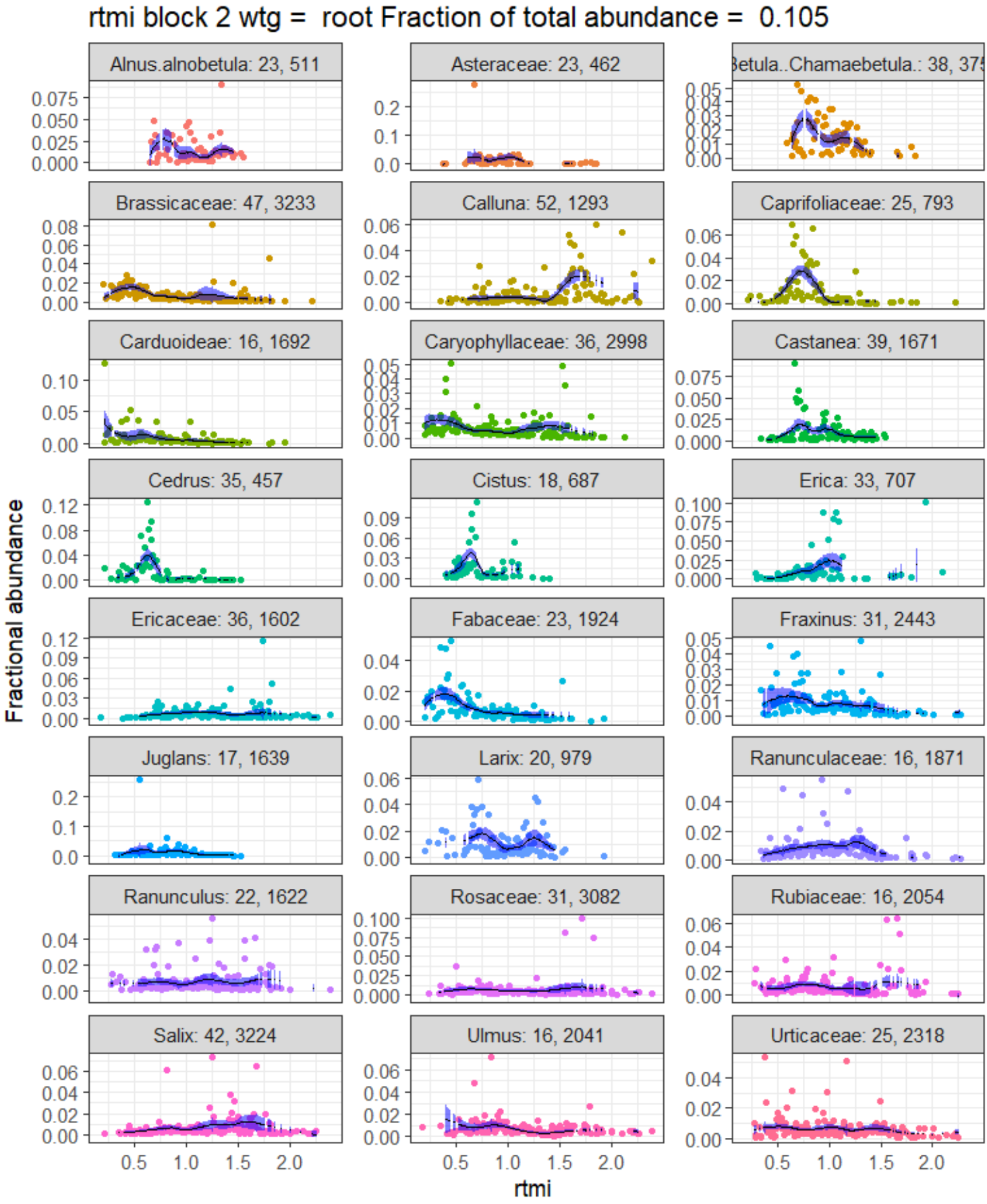
rtmi block 2 wtg = root Fraction of total abundance = 0.105
Alnus.alnobetula: 23, 511
Asteraceae: 23, 462
Betula..Chamaebetula.: 38, 375
Brassicaceae: 47, 3233
Calluna: 52, 1293
Caprifoliaceae: 25, 793
Carduoideae: 16, 1692
Caryophyllaceae: 36, 2998
Castanea: 39, 1671
Cedrus: 35, 457
Cistus: 18, 687
Erica: 33, 707
Ericaceae: 36, 1602
Fabaceae: 23, 1924
Fraxinus: 31, 2443
Juglans: 17, 1639
Larix: 20, 979
Ranunculaceae: 16, 1871
Ranunculus: 22, 1622
Rosaceae: 31, 3082
Rubiaceae: 16, 2054
Salix: 42, 3224
Ulmus: 16, 2041
Urticaceae: 25, 2318
Fractional abundance
rtmi

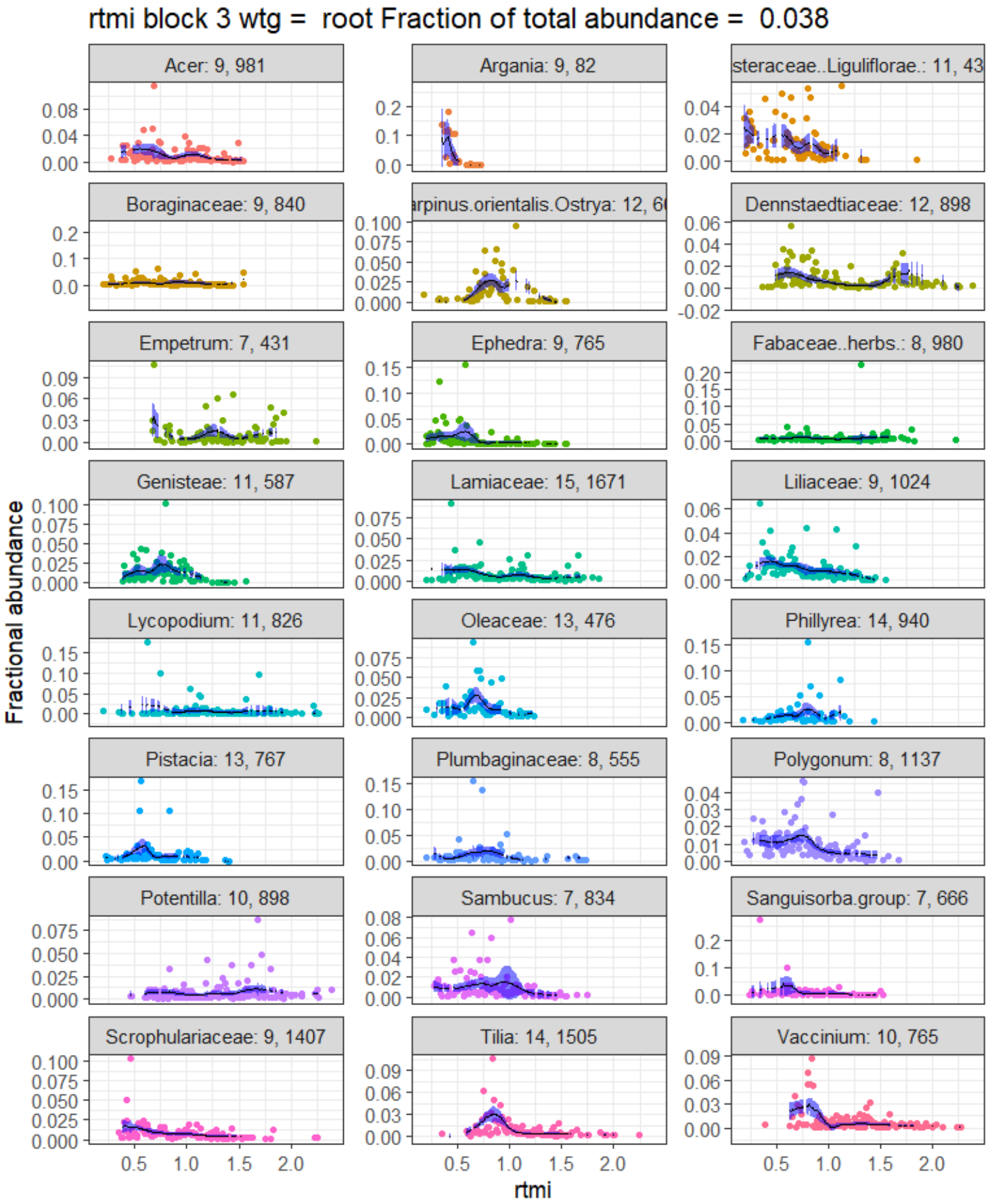
rtmi block 3 wtg = root Fraction of total abundance = 0.038
Acer: 9, 981
Argania: 9, 82
steraceae..Liguliflorae.: 11, 43
Boraginaceae: 9, 840
rpinus.orientalis.Ostrya: 12, 6
Dennstaedtiaceae: 12, 898
Empetrum: 7, 431
Ephedra: 9, 765
Fabaceae..herbs.: 8, 980
Genisteae: 11, 587
Lamiaceae: 15, 1671
Liliaceae: 9, 1024
Lycopodium: 11, 826
Oleaceae: 13, 476
Phillyrea: 14, 940
Pistacia: 13, 767
Plumbaginaceae: 8, 555
Polygonum: 8, 1137
Potentilla: 10, 898
Sambucus: 7, 834
Sanguisorba.group: 7, 666
Scrophulariaceae: 9, 1407
Tilia: 14, 1505
Vaccinium: 10, 765
Fractional abundance
rtmi

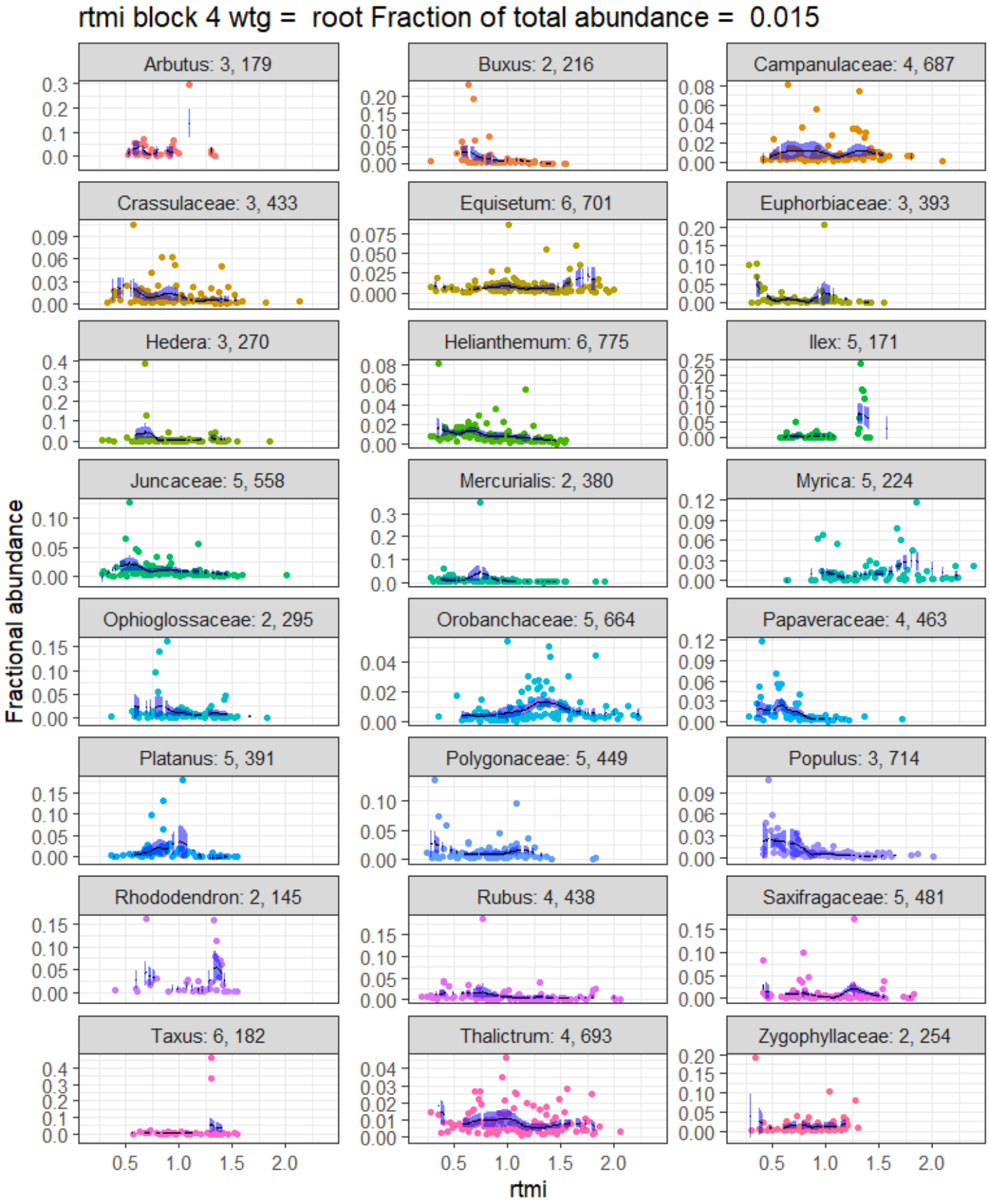
rtmi block 4 wtg = root Fraction of total abundance = 0.015
Arbutus: 3, 179
Buxus: 2, 216
Campanulaceae: 4, 687
Crassulaceae: 3, 433
Equisetum: 6, 701
Euphorbiaceae: 3, 393
Hedera: 3, 270
Helianthemum: 6, 775
Ilex: 5, 171
Juncaceae: 5, 558
Mercurialis: 2, 380
Myrica: 5, 224
Ophioglossaceae: 2, 295
Orobanchaceae: 5, 664
Papaveraceae: 4, 463
Platanus: 5, 391
Polygonaceae: 5, 449
Populus: 3, 714
Rhododendron: 2, 145
Rubus: 4, 438
Saxifragaceae: 5, 481
Taxus: 6, 182
Thalictrum: 4, 693
Zygophyllaceae: 2, 254
Fractional abundance
rtmi

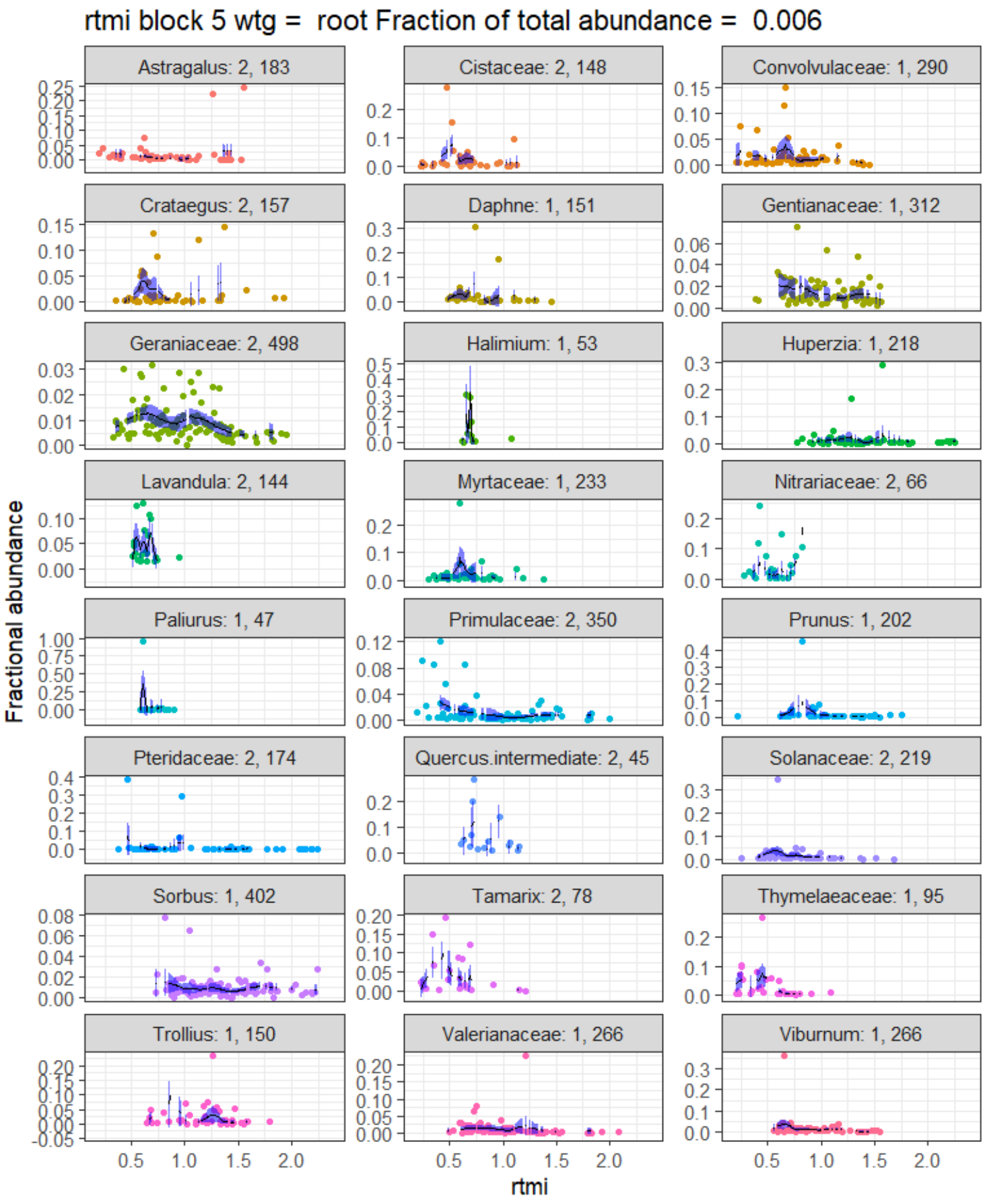
rtmi block 5 wtg = root Fraction of total abundance = 0.006
Astragalus: 2, 183
Cistaceae: 2, 148
Convolvulaceae: 1, 290
Crataegus: 2, 157
Daphne: 1, 151
Gentianaceae: 1, 312
Geraniaceae: 2, 498
Halimium: 1, 53
Huperzia: 1, 218
Lavandula: 2, 144
Myrtaceae: 1, 233
Nitrariaceae: 2, 66
Paliurus: 1, 47
Primulaceae: 2, 350
Prunus: 1, 202
Pteridaceae: 2, 174
Quercus.intermediate: 2, 45
Solanaceae: 2, 219
Sorbus: 1, 402
Tamarix: 2, 78
Thymelaeaceae: 1, 95
Trollius: 1, 150
Valerianaceae: 1, 266
Viburnum: 1, 266
Fractional abundance
rtmi

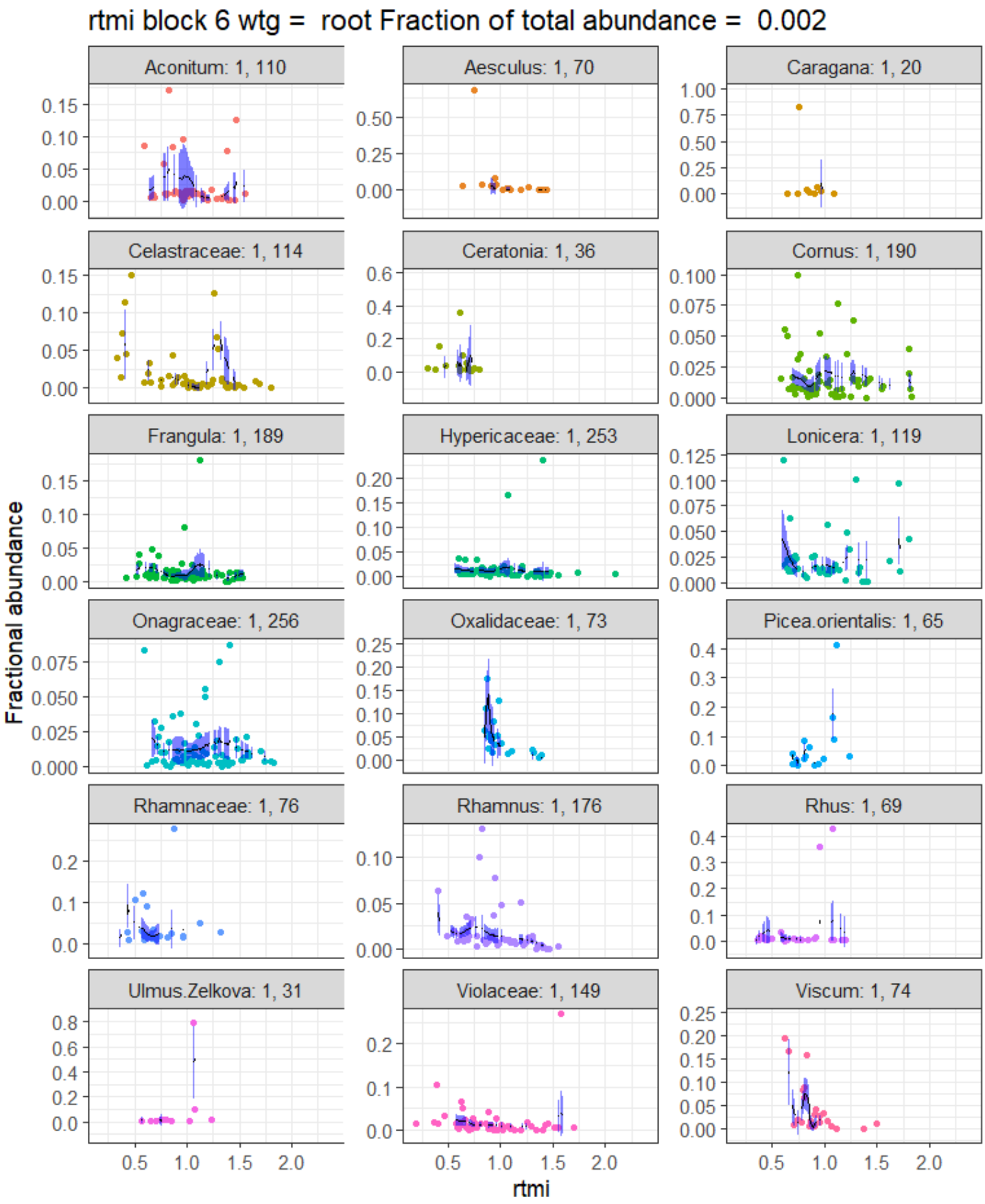
rtmi block 6 wtg = root Fraction of total abundance = 0.002
Aconitum: 1, 110
Aesculus: 1, 70
Caragana: 1, 20
Celastraceae: 1, 114
Ceratonia: 1, 36
Cornus: 1, 190
Frangula: 1, 189
Hypericaceae: 1, 253
Lonicera: 1, 119
Onagraceae: 1, 256
Oxalidaceae: 1, 73
Picea.orientalis: 1, 65
Rhamnaceae: 1, 76
Rhamnus: 1, 176
Rhus: 1, 69
Ulmus.Zelkova: 1, 31
Violaceae: 1, 149
Viscum: 1, 74
Fractional abundance
rtmi

Bootstrapped response curves taxa in the SMPDS, in blocks of 24 in descending order of abundance, to Tmin (MTCO, temperature of the coldest month), gdd (growing degree days > 0 °C), and rtmi (square root of Moisture Index). Numbers in taxon headings are respectively the sum of fractional abundances of the taxon and the number of occurrences of the taxon in SMPDS (number of SMPDS samples = sum of fractional abundances = 6458). Points: fxabf (fractional mean binned abundance). Points: fxabf (mean fractional binned abundance of SMPDS set). Black line: loess curve, span = 0.5, weighting 1/square root of frequency. Blue ribbon: mean ± 2 SD of loess curve resulting from bootstrapping with 500 iterations.

Appendix C: Reconstructions of tmin and gdd for 16 cores

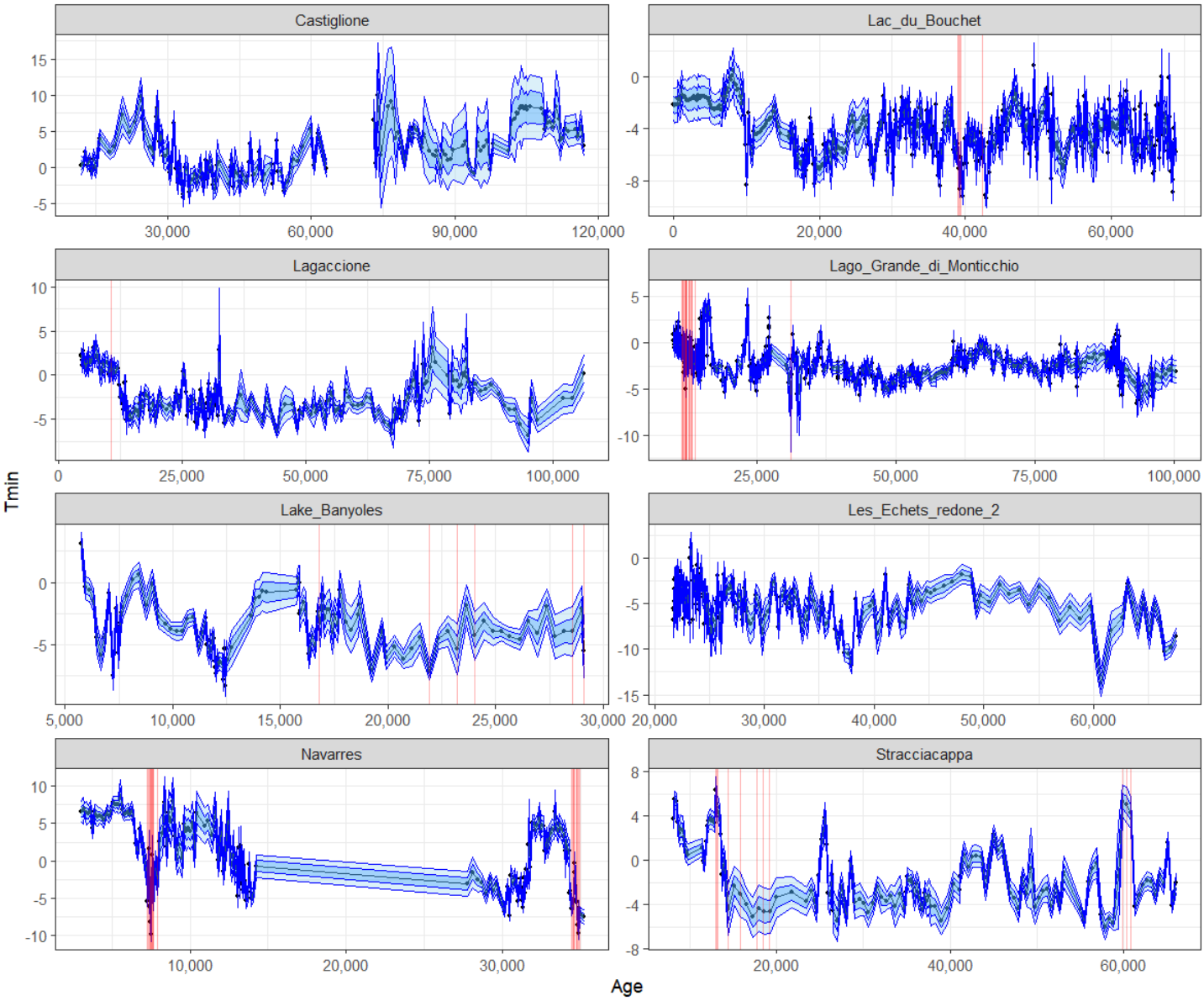

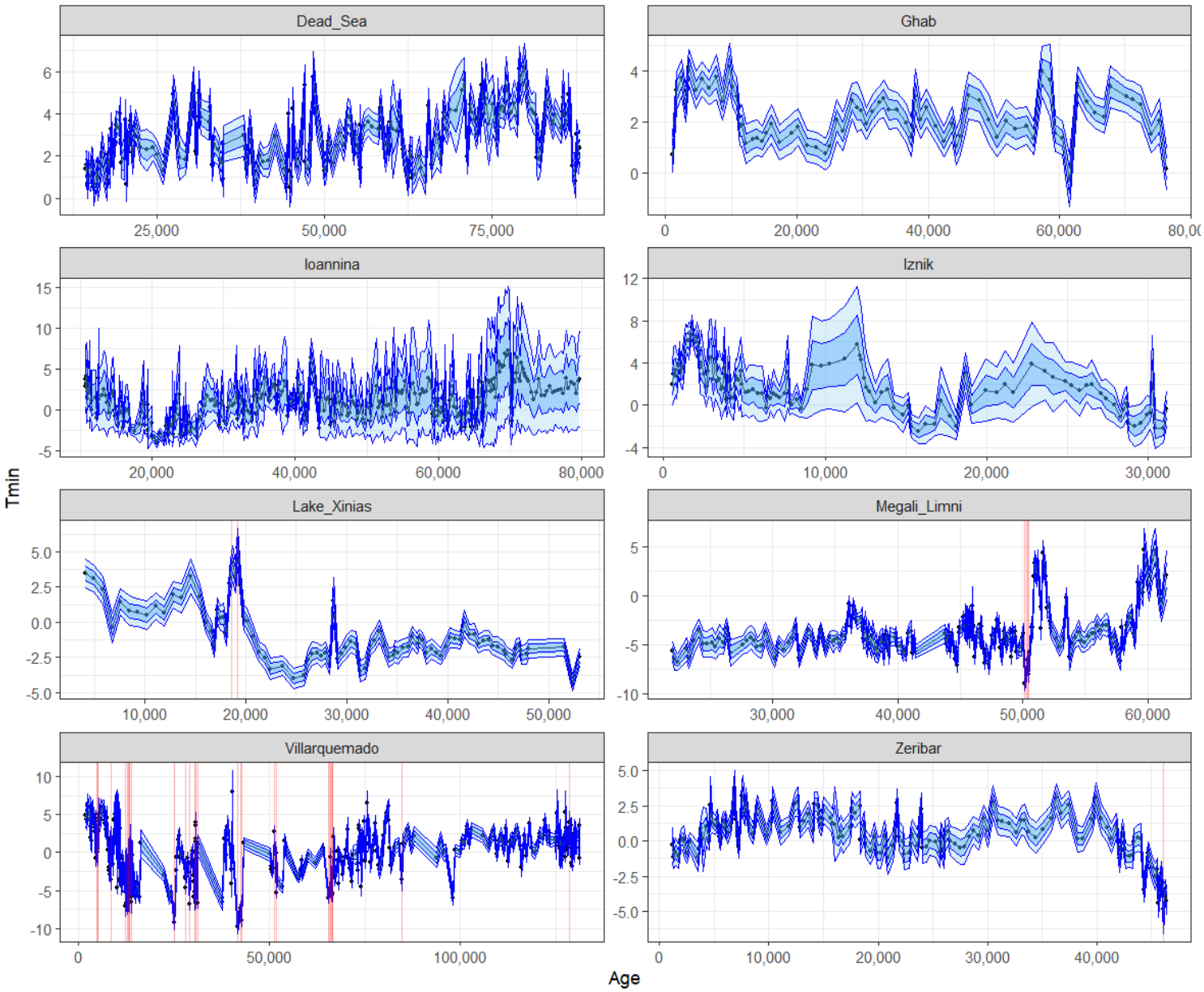

Reconstructed tmin (mean temperature of coldest month) for 16 fossil pollen cores, full SMPDS set. Central black line with black points: fxTWA-PLS reconstruction using Component 3. Mid-blue ribbon: mean bootstrapped reconstruction ± 1 SD derived from bootstrapping ; light blue ribbon: mean bootstrapped reconstruction ± 2 SD. Red vertical lines: samples where Hill's N2 < 2. Ages are the ages provided by the original palynologist, or where available the ACER ages.

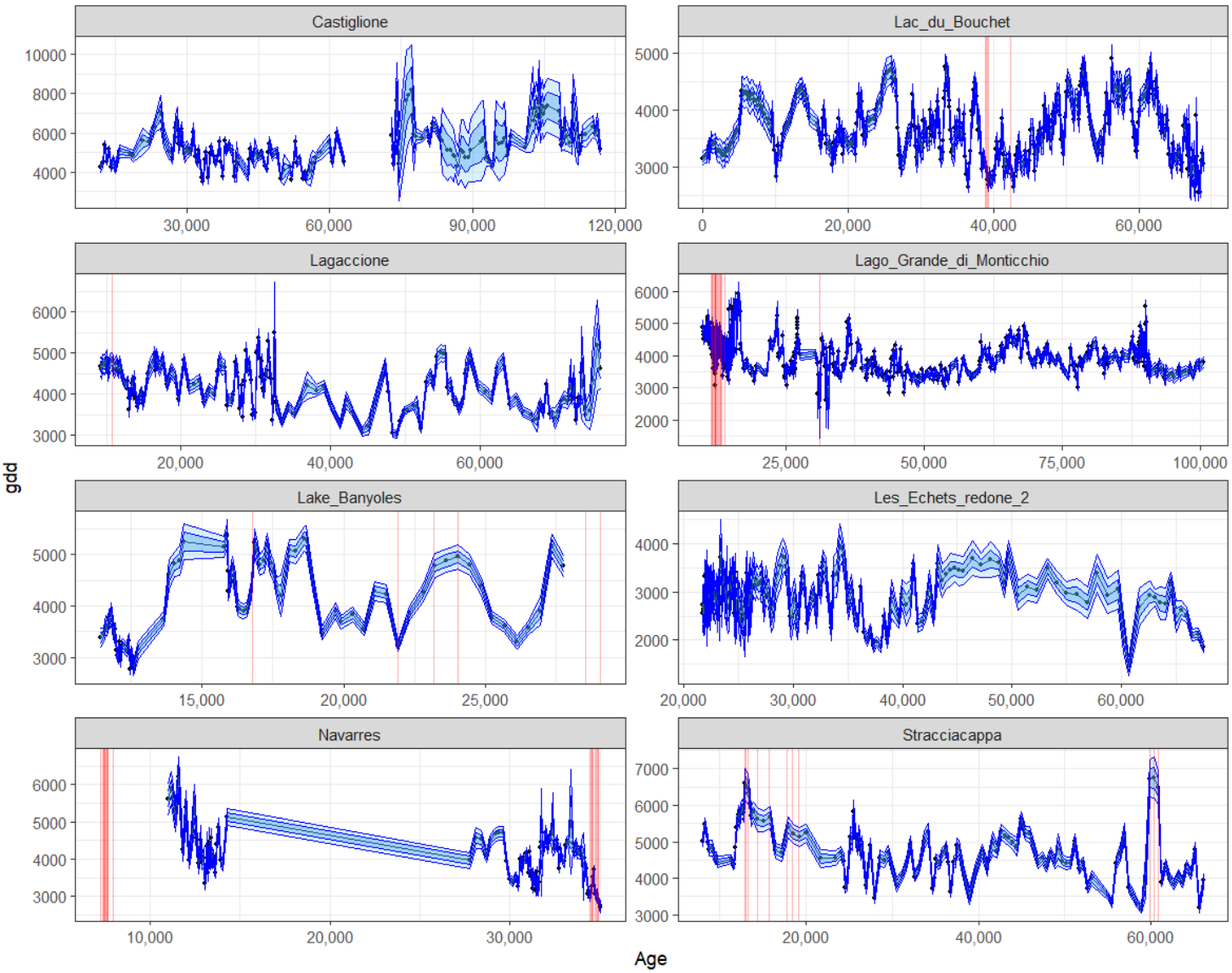
Castiglione
Lac_du_Bouchet
Lagaccione
Lago_Grande_di_Monticchio
Lake_Banyoles
Les_Echets_redone_2
Navarres
Stracciacappa
gdd
Age

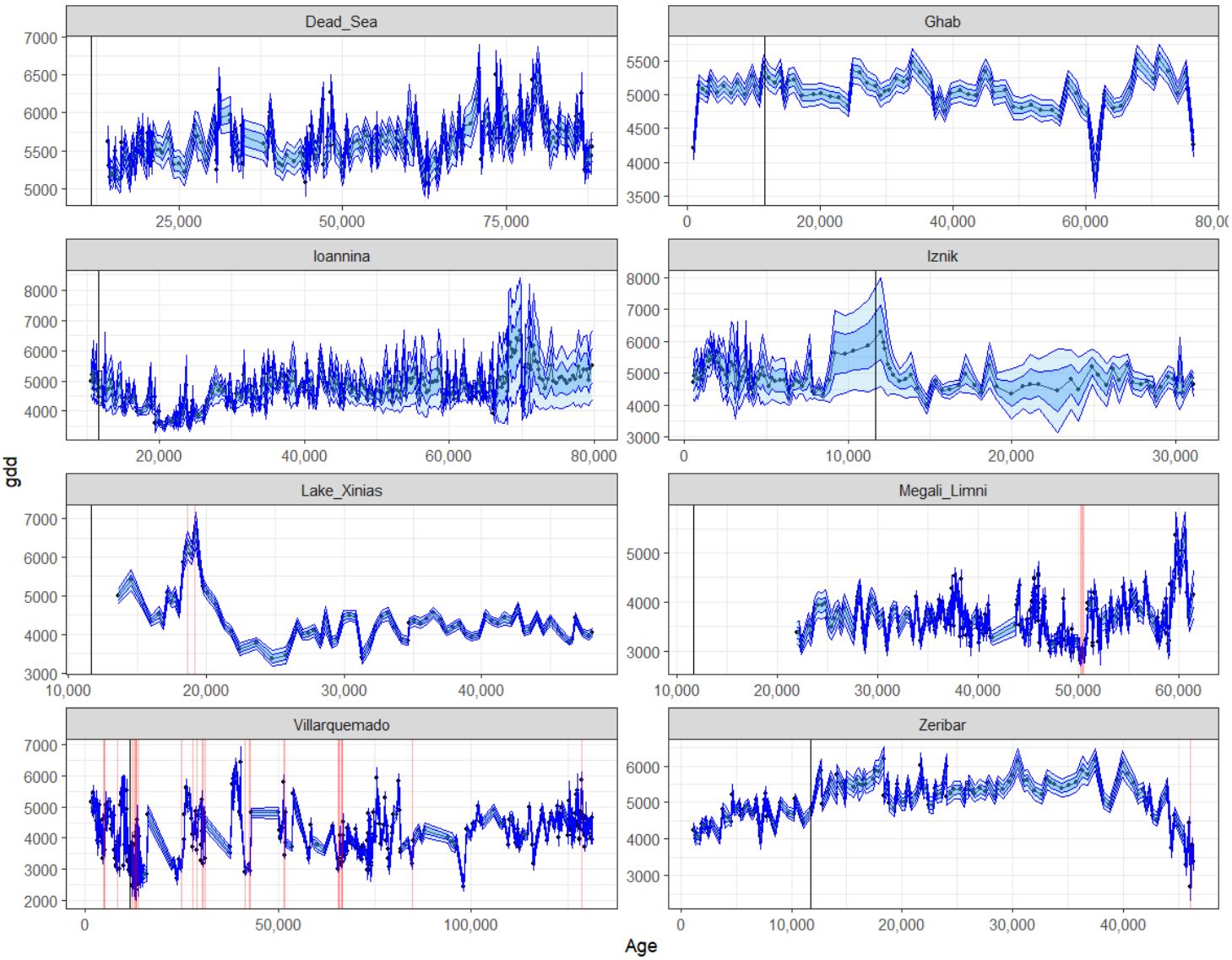

Reconstructed gdd (growing degree days > 0 °C) for 16 fossil pollen cores, full SMPDS set. Central black line with black points: fxTWA-PLS reconstruction using Component 3. Mid-blue ribbon: mean bootstrapped reconstruction ± 1 SD derived from bootstrapping ; light blue ribbon: mean bootstrapped reconstruction ± 2 SD. Red vertical lines: samples where Hill's N2 < 2. Ages are the ages provided by the original palynologist, or where available the ACER ages.

Appendix D: Pattern matching filtering plots for 14 cores

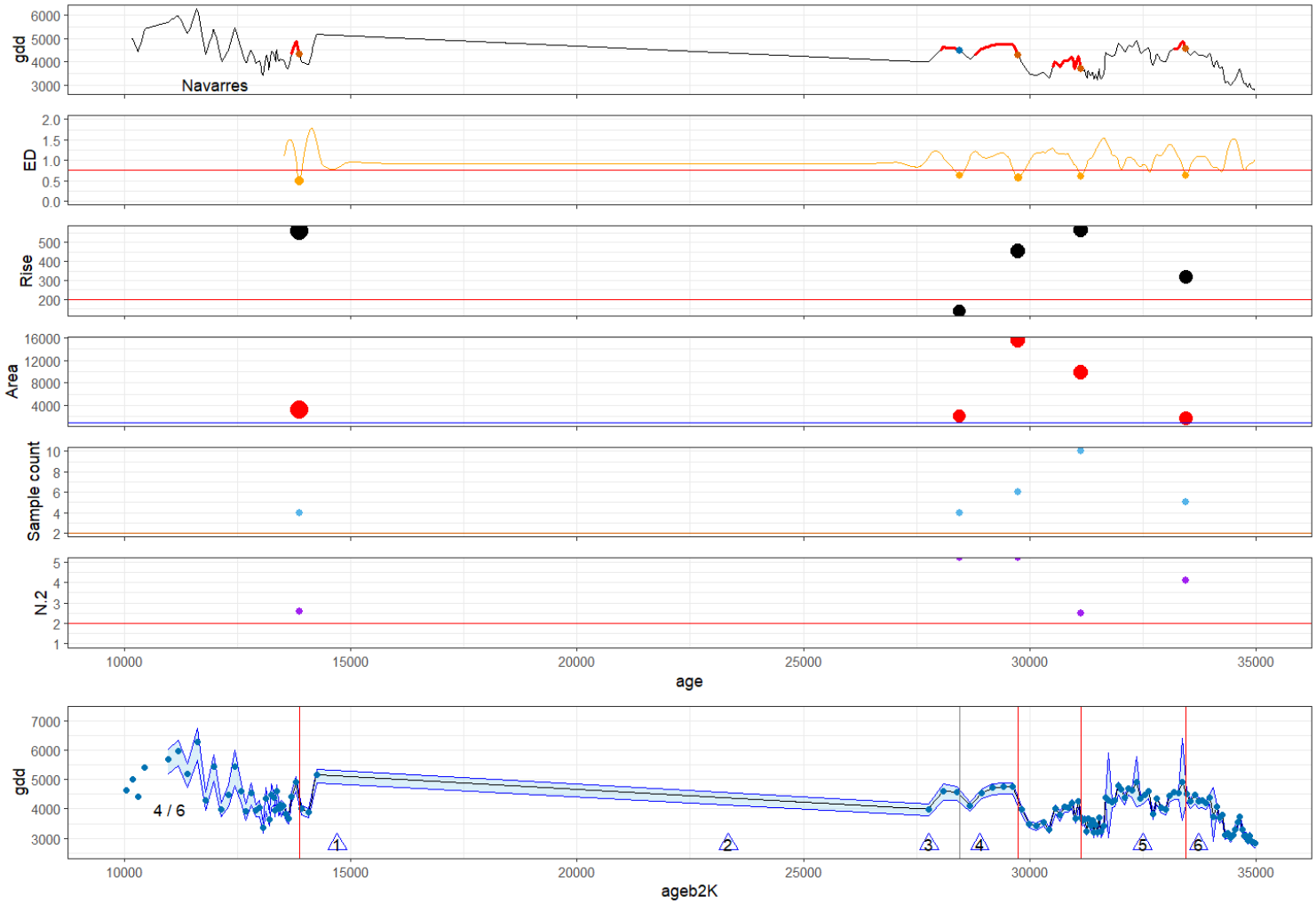

No of GIs in range 6

No of DOLP candidates 5

No of DOLPs left after ED/area/range filtering 4

No of DOLPs left after sample filter 4

No of DOLPs left after N2 filter 4

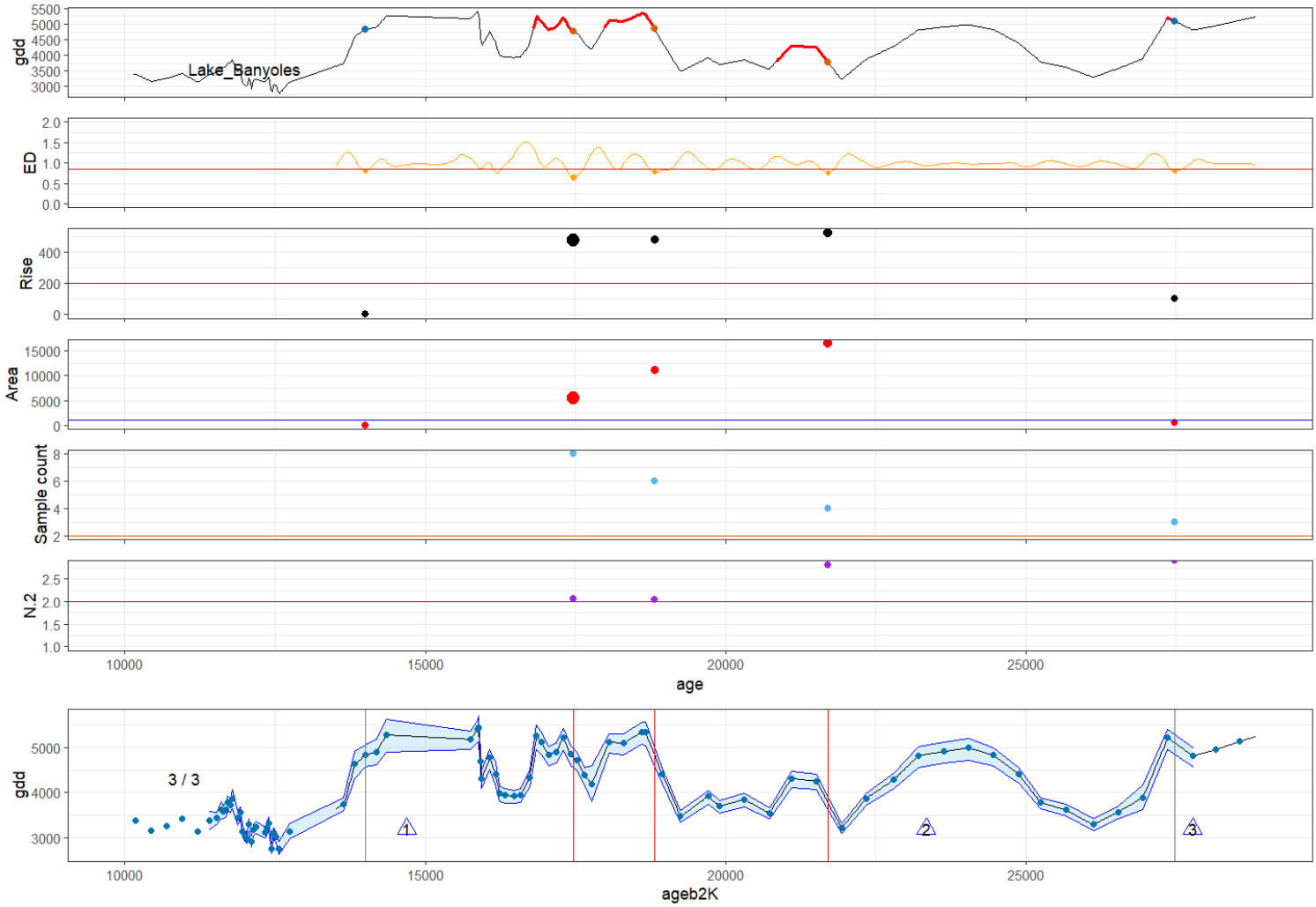

No of GIs in range 3

No of DOLP candidates 5

No of DOLPs left after ED/area/range filtering 3

No of DOLPs left after sample filter 3

No of DOLPs left after N2 filter 3

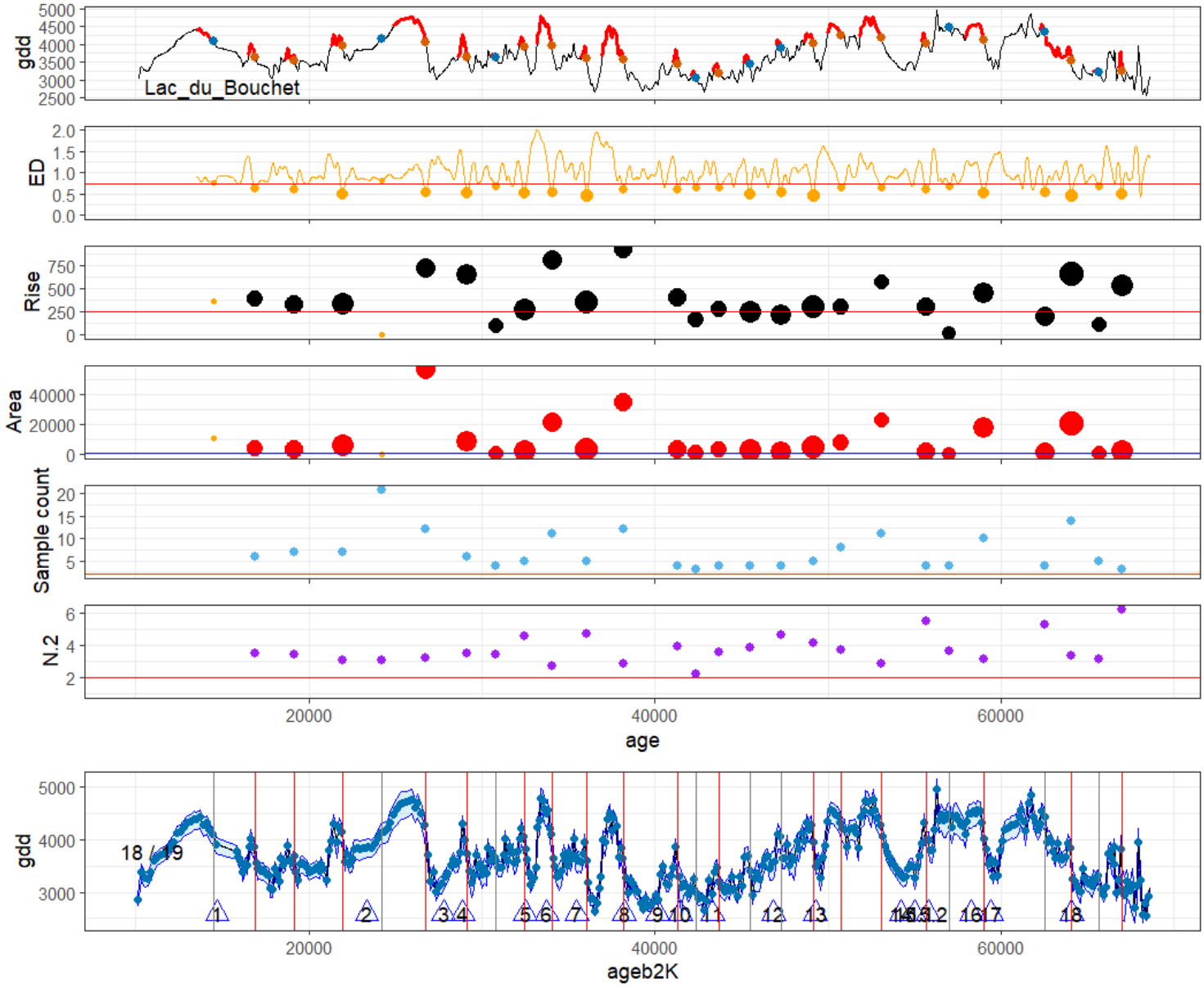

No of GIs in range 19

No of DOLP candidates 27

No of DOLPs left after ED/area/range filtering 18

No of DOLPs left after sample filter 18

No of DOLPs left after N2 filter 18

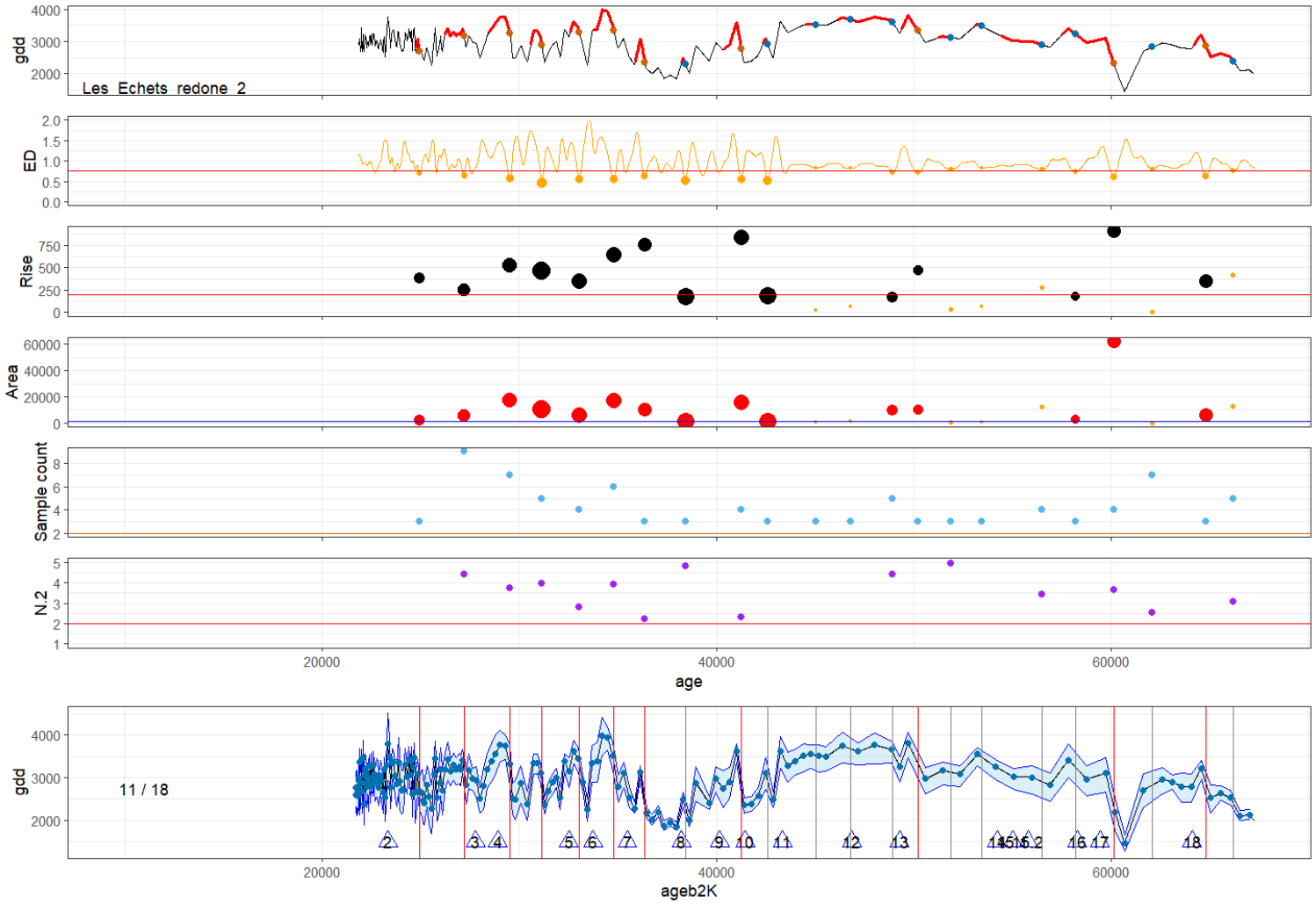

No of GIs in range 18

No of DOLP candidates 22

No of DOLPs left after ED/area/range filtering 11

No of DOLPs left after sample filter 11

No of DOLPs left after N2 filter 11

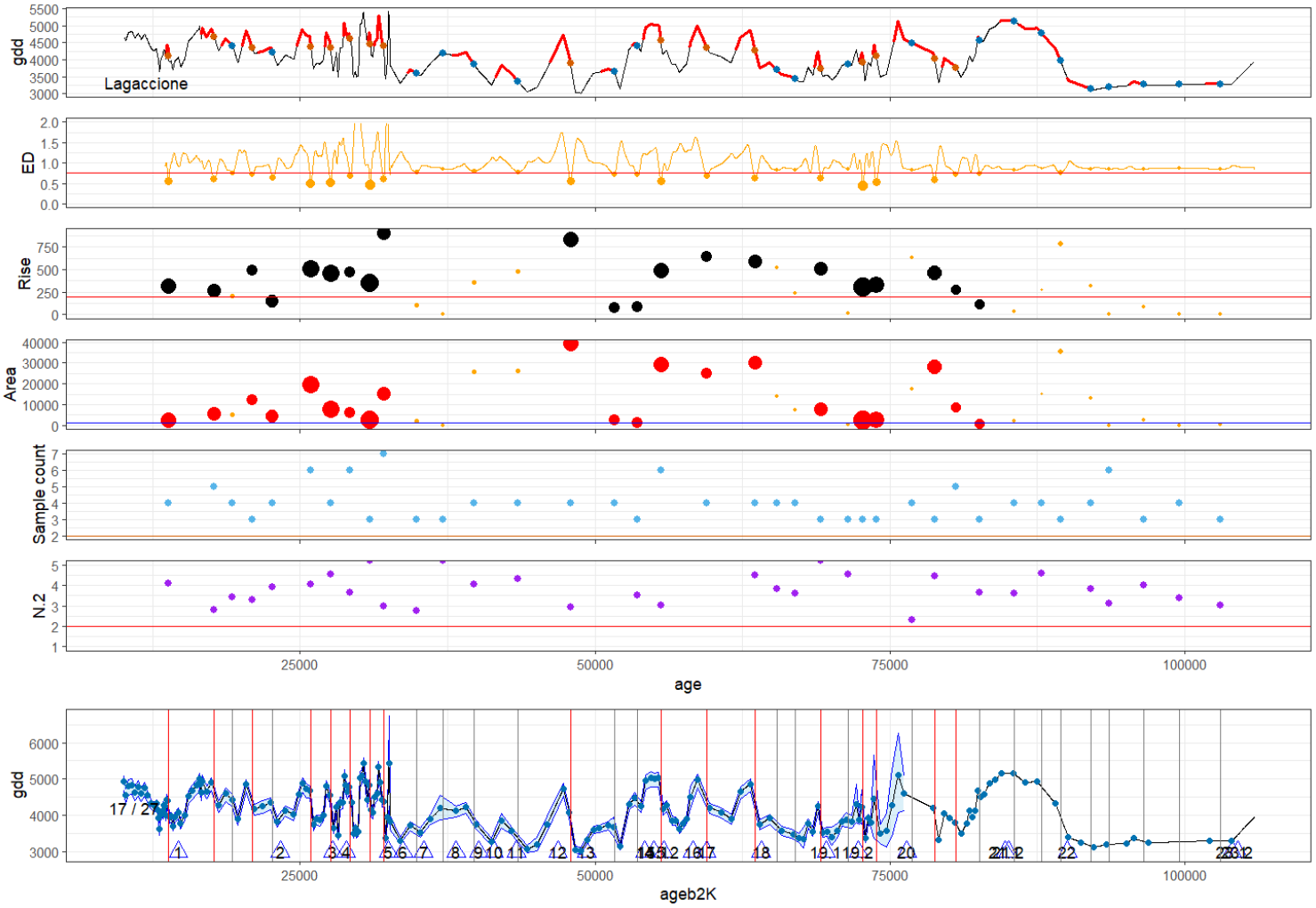

No of GIs in range 27

No of DOLP candidates 38

No of DOLPs left after ED/area/range filtering 17

No of DOLPs left after sample filter 17

No of DOLPs left after N2 filter 17

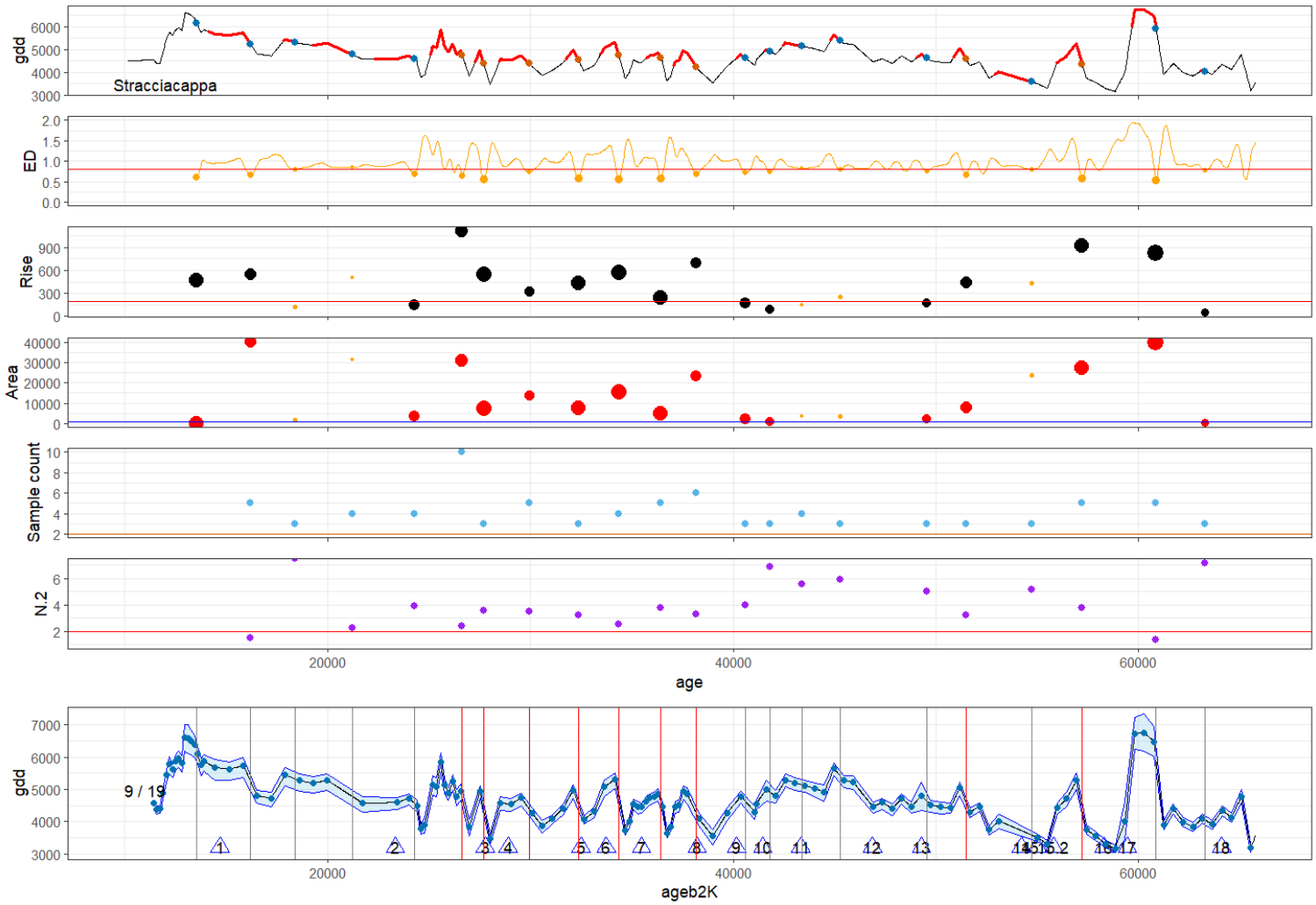

No of GIs in range 19

No of DOLP candidates 22

No of DOLPs left after ED/area/range filtering 11

No of DOLPs left after sample filter 11

No of DOLPs left after N2 filter 9

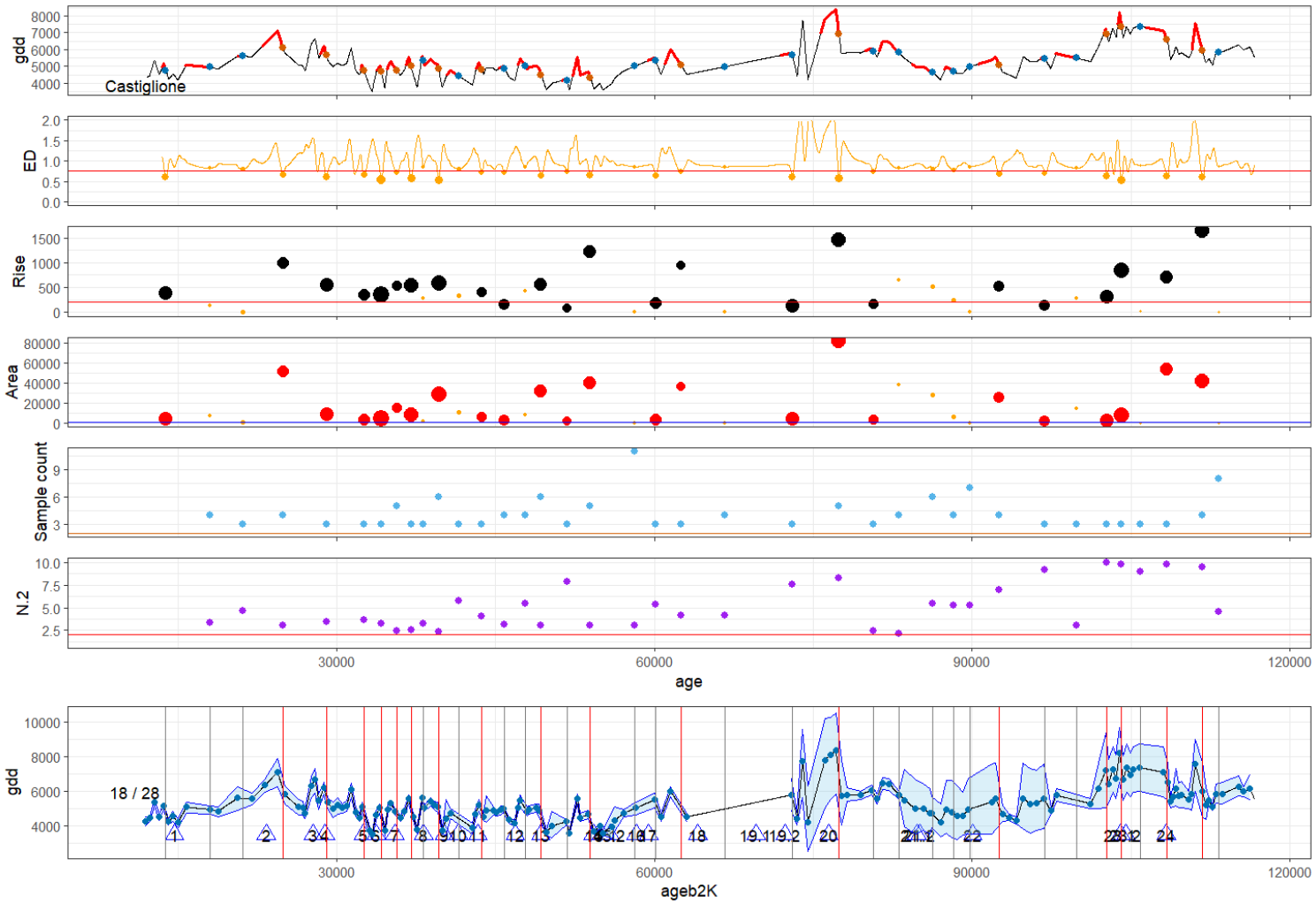

No of GIs in range 28

No of DOLP candidates 38

No of DOLPs left after ED/area/range filtering 18

No of DOLPs left after sample filter 18

No of DOLPs left after N2 filter 18

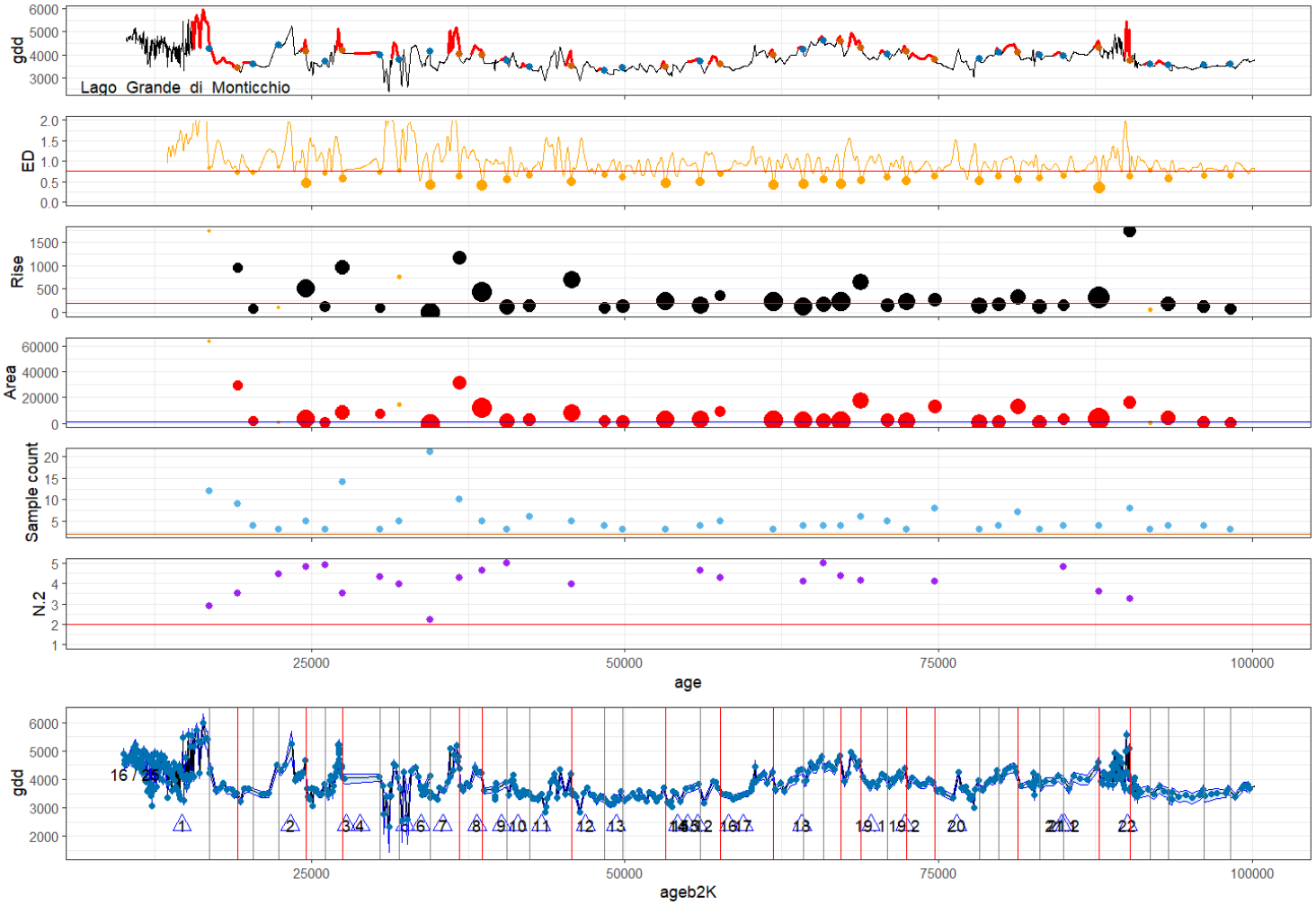

No of GIs in range 25

No of DOLP candidates 39

No of DOLPs left after ED/area/range filtering 16

No of DOLPs left after sample filter 16

No of DOLPs left after N2 filter 16

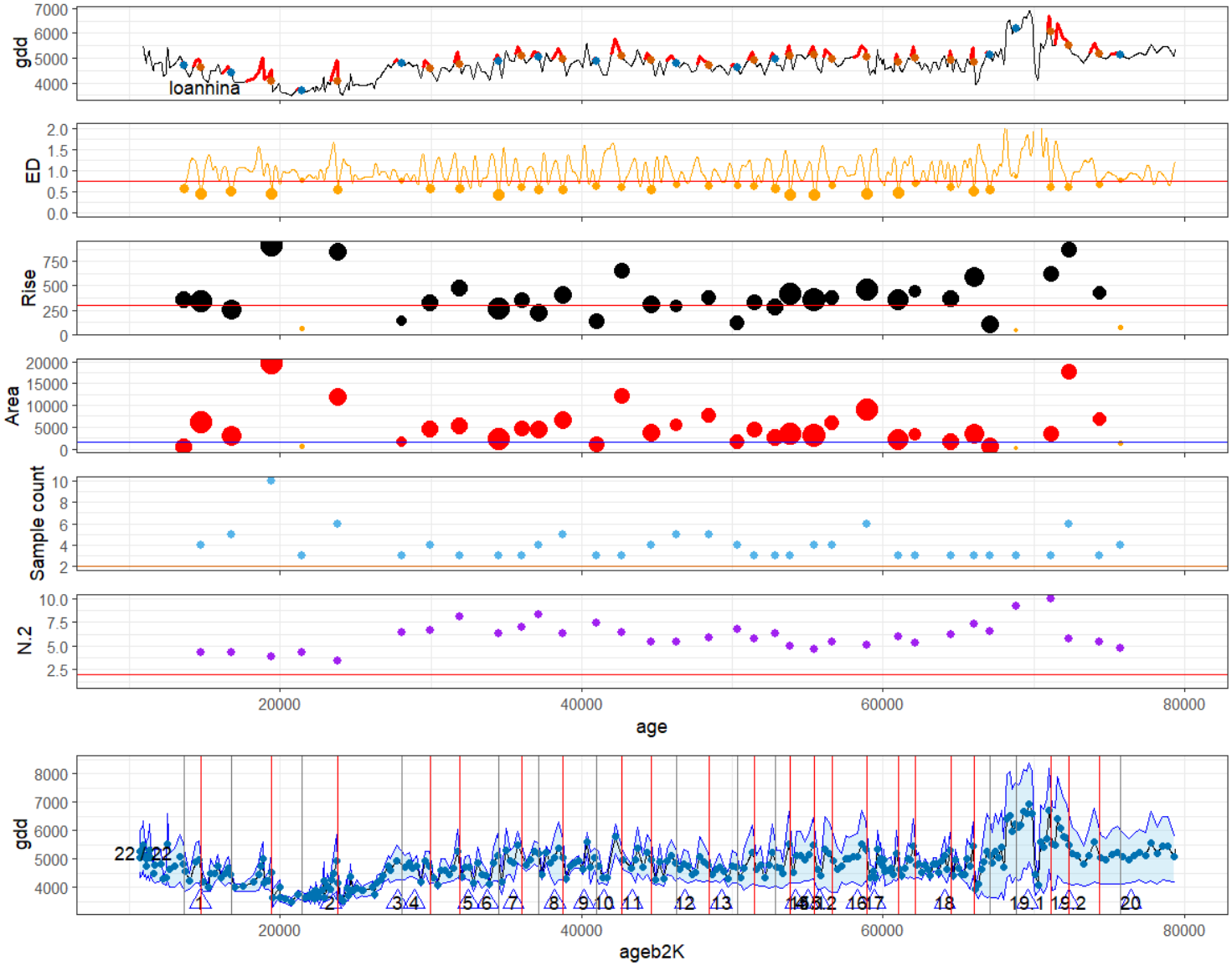

No of GIs in range 22

No of DOLP candidates 35

No of DOLPs left after ED/area/range filtering 22

No of DOLPs left after sample filter 22

No of DOLPs left after N2 filter 22

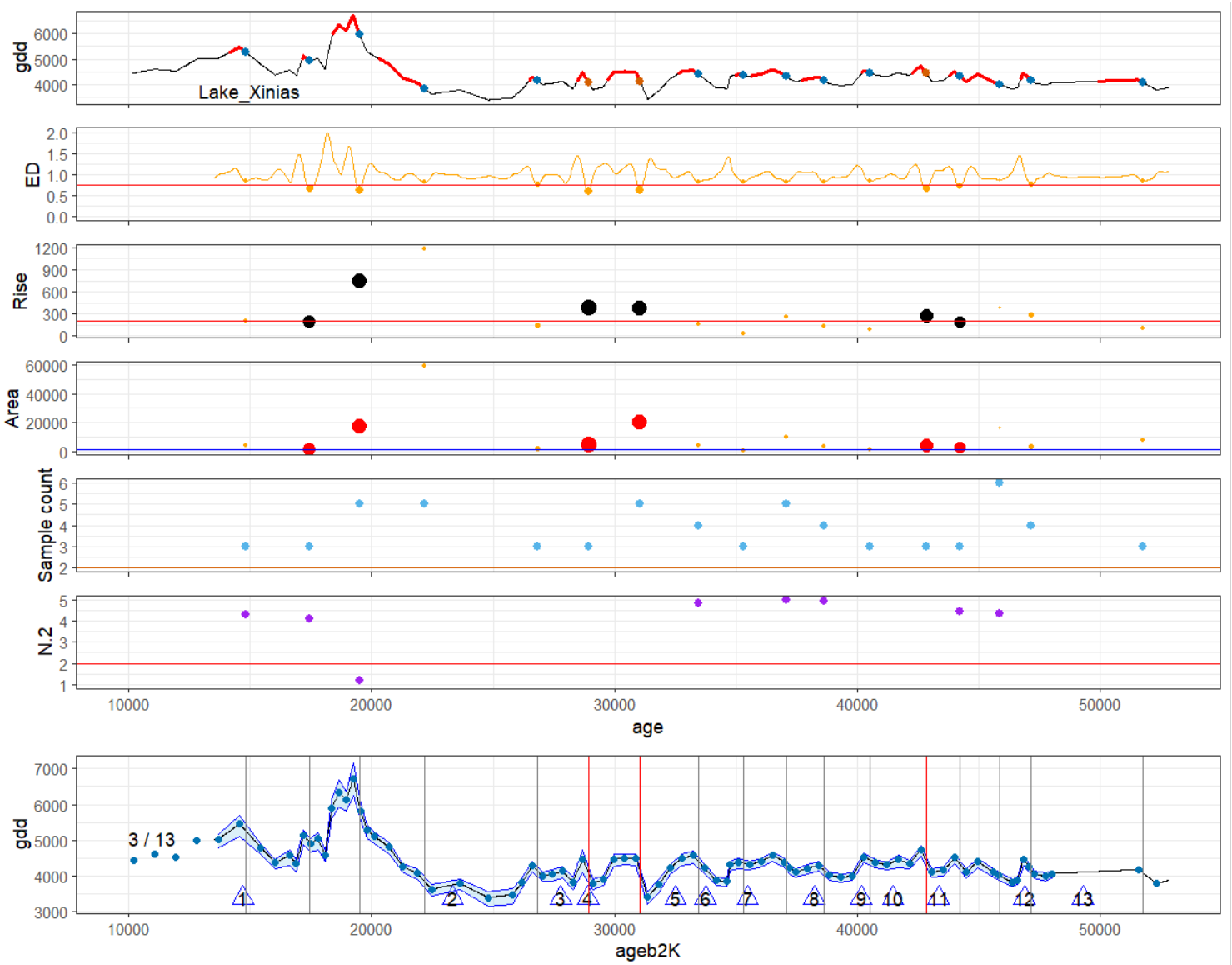

No of GIs in range 13

No of DOLP candidates 17

No of DOLPs left after ED/area/range filtering 4

No of DOLPs left after sample filter 4

No of DOLPs left after N2 filter 3

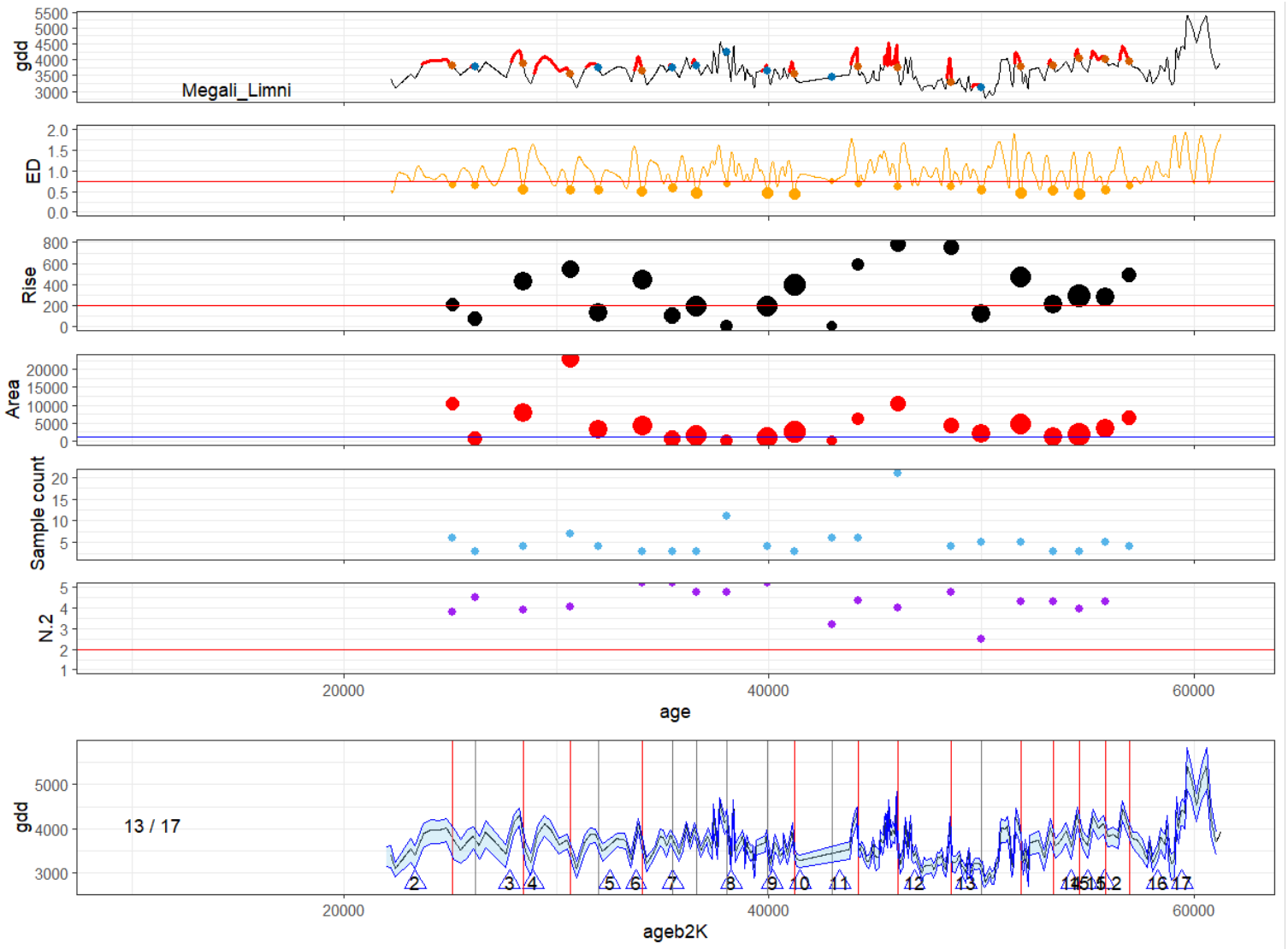

No of GIs in range 17

No of DOLP candidates 21

No of DOLPs left after ED/area/range filtering 13

No of DOLPs left after sample filter 13

No of DOLPs left after N2 filter 13

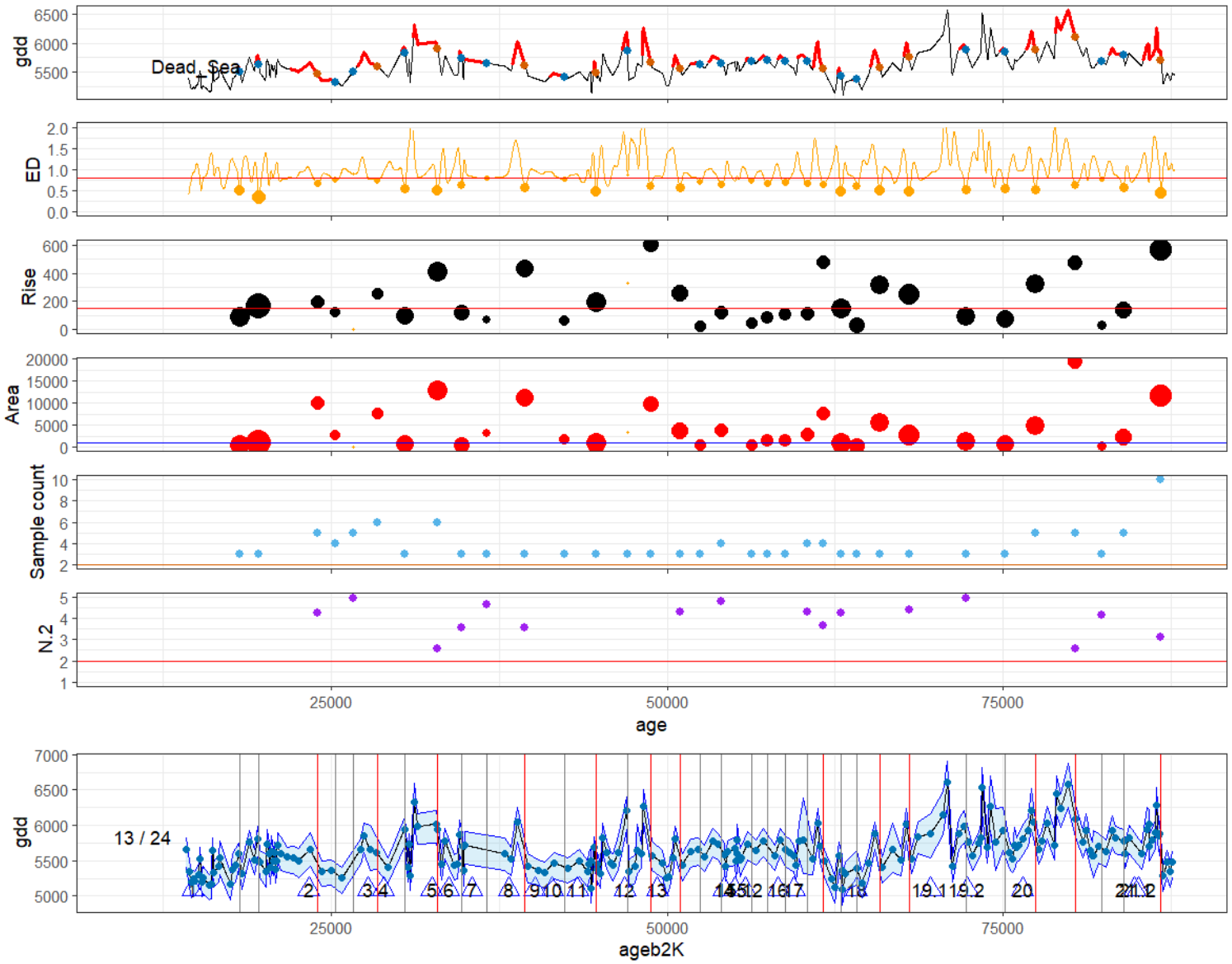

No of GIs in range 24

No of DOLP candidates 34

No of DOLPs left after ED/area/range filtering 13

No of DOLPs left after sample filter 13

No of DOLPs left after N2 filter 13

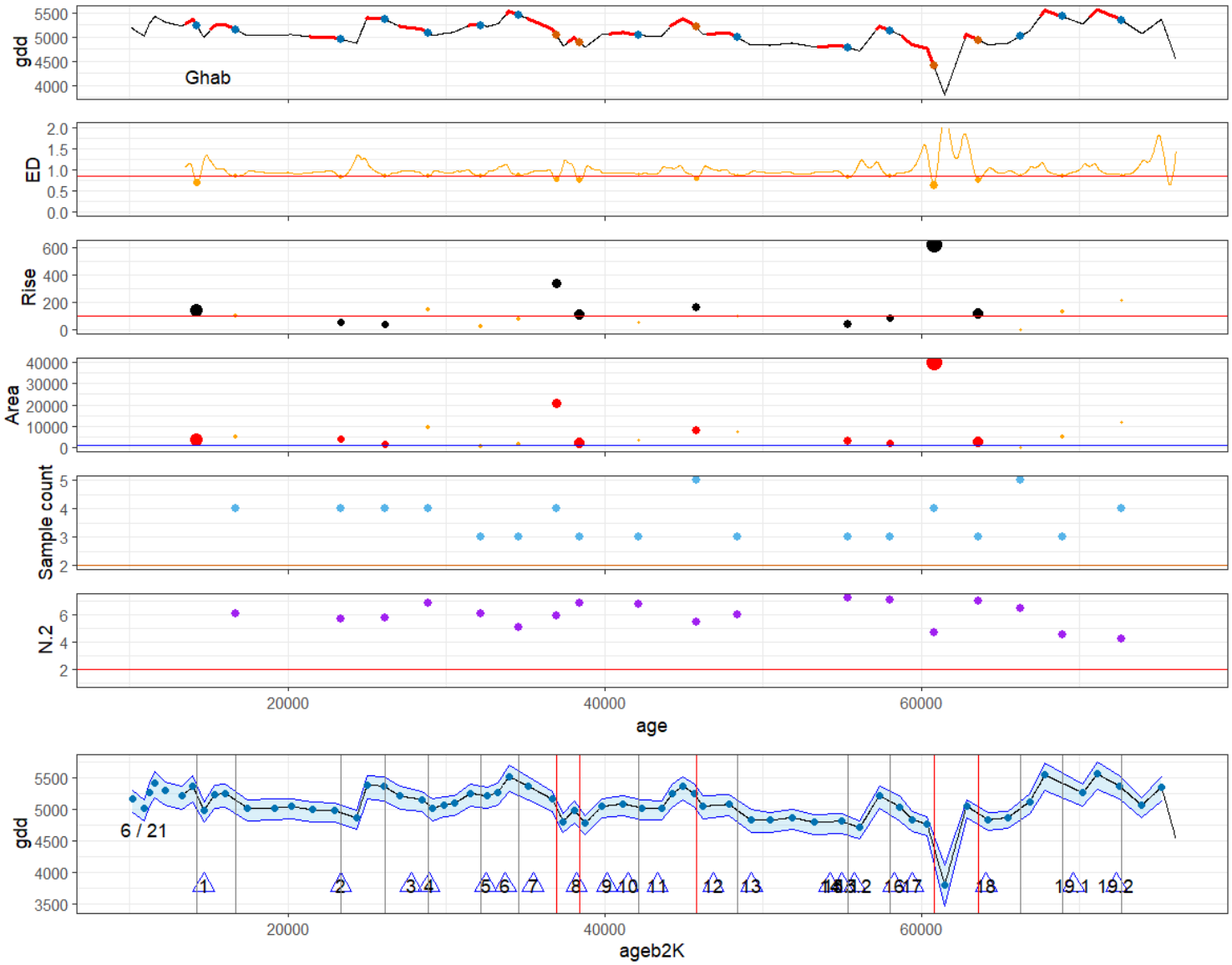

No of GIs in range 21

No of DOLP candidates 19

No of DOLPs left after ED/area/range filtering 6

No of DOLPs left after sample filter 6

No of DOLPs left after N2 filter 6

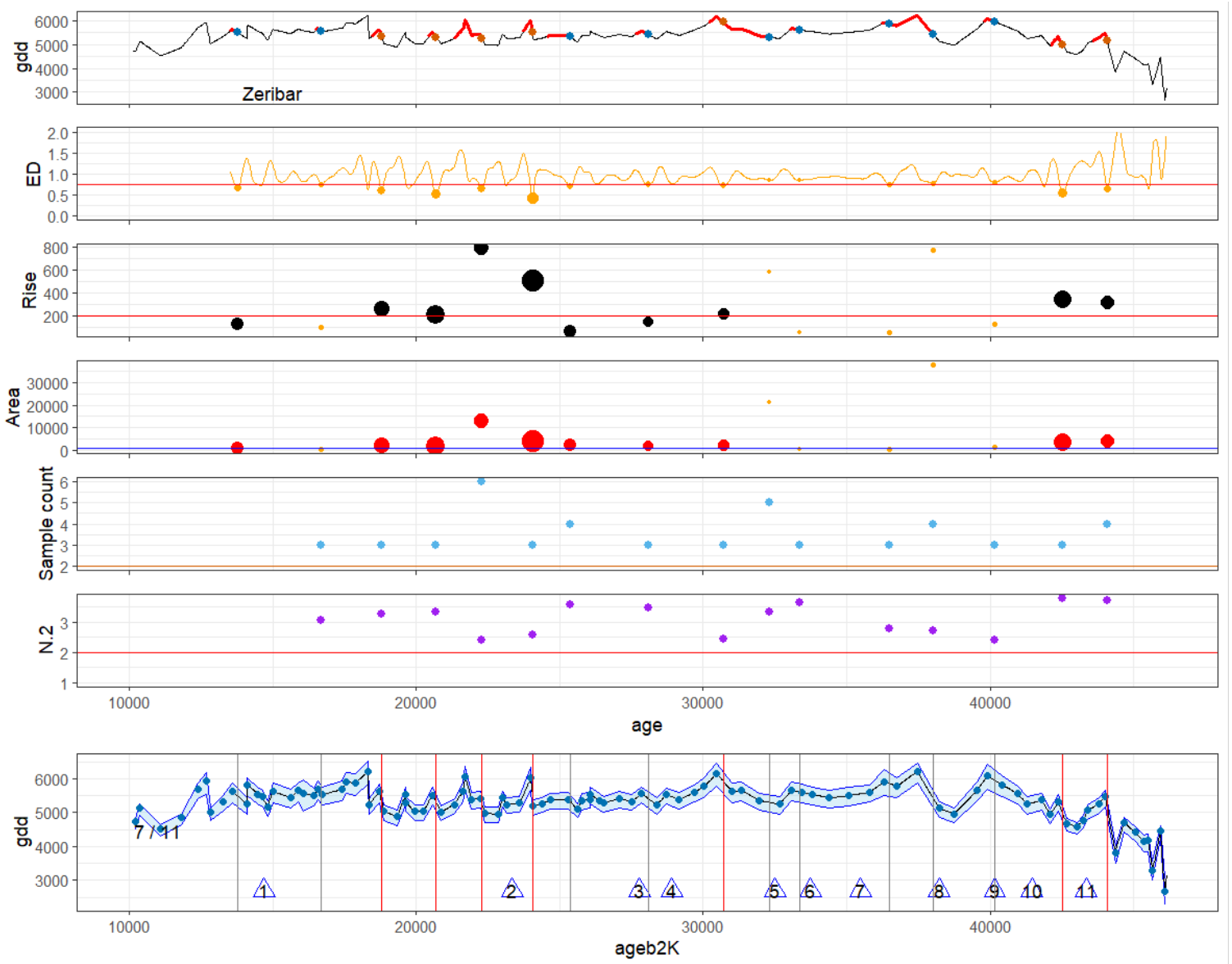

No of GIs in range 11

No of DOLP candidates 16

No of DOLPs left after ED/area/range filtering 7

No of DOLPs left after sample filter 7

No of DOLPs left after N2 filter 7

*Pattern matching filtering process applied to gdd (growing degree days > 0 °C) reconstruction at core named in top panel. Top panel: gdd reconstruction; red points = finally accepted DOLPs; blue points = rejected DOLPs; red segments of reconstruction = warm intervals following all potential DOLPs. Second panel: ED curve with troughs falling below threshold (ED = 0.75) shown as points, size inverse to ED. Third panel: increase in gdd from DOLP value to peak as black points, size inverse to ED; orange points = DOLPs already rejected on grounds of ED; red line: threshold for rise (*rfilta*) = 200 degree days. Fourth panel: area-under-the-curve traced by warm interval; orange points = DOLPs already rejected on ground of ED; blue line: threshold for area (*afilta*) = **1000**. Fifth panel: count of physical samples defining the shape of the warm interval. Sixth panel: mean Hill's N.2 for warm interval; red line = threshold for N.2 = 2 (*n2filt*). Bottom panel: repeat of gdd reconstruction with blue points indicating physical samples, and red vertical lines marking finally accepted DOLPs, grey vertical lines marking rejected DOLP; numbers are number of finally accepted DOLPs / number of GIS in apparent age range; numbers in triangles are GI numbers; GI dates on GICC05modelext scale. In all other panels, age is ACER age model.*